

**Development of a Monolithic Bioreactor:
Design and Application**

Development of a Monolithic Bioreactor: Design and Application

Proefschrift

ter verkrijging van de graad van doctor
aan de Technische Universiteit Delft,
op gezag van de Rector Magnificus prof. dr. ir. J.T. Fokkema,
voorzitter van het College voor Promoties,

in het openbaar te verdedigen op maandag 12 februari 2007 om 15:00 uur

door Karen Mariëlla DE LATHOUDER
scheikundig ingenieur
geboren te Rotterdam

Dit proefschrift is goedgekeurd door de promotoren:

Prof. dr. F. Kapteijn

Prof. dr. J.A. Moulijn

Samenstelling promotiecommissie:

Rector Magnificus, voorzitter

Prof. dr. F. Kapteijn, Technische Universiteit Delft, promotor

Prof. dr. J.A. Moulijn, Technische Universiteit Delft, promotor

Prof. dr. ir. L.A.M. van der Wielen, Technische Universiteit Delft

Prof. dr. A. Linares Solano, Universidad de Alicante

Prof. dr. rer. nat. L. Fischer, Universität Hohenheim

Dr. ir. A.J.J. Straathof, Technische Universiteit Delft

Dr. S.A. Wallin, The DOW Chemical Company

Dit onderzoek is uitgevoerd bij de sectie CE, DelftChemTech, Faculteit Technische Natuurwetenschappen, Technische Universiteit Delft met financiële steun van de Technische Universiteit Delft, the DOW Chemical Company, DSM N.V., de Nederlandse Organisatie voor Wetenschappelijk Onderzoek (NWO), en het Network of Excellence 'Inside Pores'.

Proefschrift, Technische Universiteit Delft

Met samenvatting in het Nederlands / with summary in Dutch

ISBN-10: 90-6464-055-6

ISBN-13: 978-90-6464-055-1

Copyright © 2006 by Karen de Lathouder

All rights reserved

Cover design: ZeroOne

Printed by Ponsen & Looijen B.V., Wageningen, the Netherlands

If we knew what it was we were doing, it would not be called research, would it?

Albert Einstein

Preface

Within the changing chemical industry, public awareness and nationwide agreements on emissions pave the way for sustainable technology and more environmentally friendly solutions. Only using the conventional end-of-pipe techniques (exhaust gas cleaning or wastewater treatment) will not be enough to reduce the rapidly growing industrial pollution. An example of a new approach is the implementation of one or more “green” reaction steps in both existing and future processes. Biocatalysis is such a “green” technology. The application of whole cells or enzymes to carry out selective transformations of commercial importance is the central theme of industrial biocatalysis. Traditionally biocatalysis has been the domain of the life scientist or biochemical engineer, but recent developments in this field have enabled biocatalytic processes to compete with, and in some cases even outperform conventional chemical processing. Biocatalytic reactions can be carried out in water at ambient temperature and neutral pH, without the need for high pressure and extreme conditions. This means that valuable process energy is saved. Reactions that are not easily conducted by classical organic chemistry can be simplified by using a biocatalyst. Sometimes several reaction steps can be replaced by a single enzymatic reaction step. Today, highly chemo-, regio-, and stereoselective biotransformations can simplify manufacturing processes and make them more economically attractive and environmentally acceptable. In some cases, chemo-biocatalytic systems are being developed, combining the most attractive features of enzymes (specificity, selectivity) with those of chemical catalysts (high reactivity, wide specificity). Examples of common products that are made by biocatalysis include fructose, insulin, acrylamide, amino acids, and antibiotics. Even though the selection of a biocatalyst and the design of the process present various problems and restrictions, biocatalysis is expected to play an important role in future technology.

Applications of enzymes are growing rapidly, driven both by a large expansion in the number of enzymes that are available and the increasing need for optically-pure intermediates for the production of pharmaceuticals. Successful examples of commercial enzymatic processes are being reported with greater frequency. Immobilized enzymes already have a wide range of practical applications. Although activity usually decreases slightly upon immobilization, they possess important advantages over dissolved enzymes, e.g. the possibility of recovery and reuse, simple operation, and improved stability. Most conventional enzyme carriers are inorganic particles or porous beads of synthetic polymers, chitosan, agarose or alginate. When used in packed beds, a trade-off must be made between particle size and pressure drop over the bed. To maintain a sufficiently low pressure drop over the bed, particle size usually has a certain minimum value. This can cause internal mass transfer problems. Long diffusion distances inside the particles cause inefficient use of the catalyst. The low mechanical strength can lead to attrition and deactivation upon use in stirred tanks or packed beds. Another frequently encountered problem with particulate carriers is the difficulty to scale up the process. The use of a high mechanical strength, structured support material with a thin coating of active material can circumvent these problems by providing an open structure to allow high flow rates. By combining an increased flowrate with a very thin layer of active material on a

structured support, mass transport problems will be minimized. There are many types of structured reactors; in this study, ceramic monoliths with different microstructures will be applied as structured carriers for different enzymes.

Monolithic catalyst supports, originally developed for use in automotive emission control systems where low pressure drop and high geometrical (external) surface area are required, are an interesting alternative for conventional support materials in heterogeneous catalysis and biocatalysis. The classical honeycomb monolith has square parallel channels on which a catalyst containing ‘washcoat’ can be applied. However, the potential application in biological reaction systems has hardly been explored. The present study is concerned with the application of monolith reactors in the field of (environmental) biotechnology. In order to employ monoliths as support material for biocatalysts, a suitable carrier layer must be applied on the surface of the monolith channels.

Various configurations of the monolith reactor exist, the most commonly used reactor is the monolith loop reactor (MLR). This reactor consists of a vertical monolith section and a storage tank. The reactor can be operated batch-wise or continuously, single or multiphase, and in cocurrent or countercurrent mode. The monolith section can be placed on an existing vessel, which makes it an interesting alternative for conventional reaction systems. Another monolith reactor that can be used in an existing vessel is the monolithic stirrer reactor (MSR), a novel reactor, designed to implement in a convenient way monolithic structures. In this reactor, monolithic structures are used as stirrer blades. By rotating the monoliths through the liquid, both mixing of the reaction medium and contacting the catalyst with reactants by convection through the monolithic channels is facilitated. This reactor is thought to be especially useful in production of fine chemicals and biotechnology, because the stirrer configuration can be implemented relatively easy in existing stirred tanks. In Figure 1, a schematic representation is given an example of the application of enzyme-coated monoliths in the MSR.

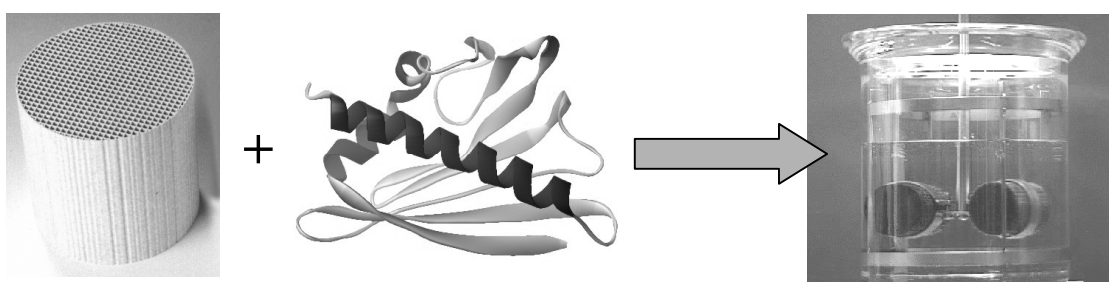


Figure 1. Implementation of structured supports for biocatalysts in the monolithic stirrer reactor.

This work is concerned with the application of ceramic monoliths with different microstructures as catalyst support material in the field of (environmental) biocatalysis. One of the initial incentives of the present research was to use enzyme-coated monoliths for mass transfer measurements in different monolith reactors. Earlier research had already been carried out in our group concerning covalent attachment of trypsin for mass transfer

measurements and sol-gel entrapment of solid acid catalysts. These previous studies were used as a starting point for this work. In order to apply a ceramic monolith as a suitable carrier material for different enzymes, some important questions need to be answered:

- Is it possible to attach different enzymes to the ceramic structure?
- If attached, will the enzyme stay attached within the window of operation?
- Does the catalyst maintain its original activity and stability?
- Is the monolithic bioreactor a feasible alternative for existing biocatalytic processes?

In trying to answer these questions, the current thesis can be divided into three main topics:

- Catalyst preparation; how to successfully immobilize different enzymes to a ceramic support. Different possibilities are explored.
- Catalyst performance; how does immobilization affect activity and stability compared to the free enzyme? Can the catalyst be re-used?
- Application; how does the monolithic bioreactor perform compared to different (commercial) immobilized enzymes, is the monolith a viable alternative for conventional carriers?

Adsorption, ionic adsorption, entrapment and covalent binding have been selected as suitable immobilization protocols to be applied in combination with monolithic backbones. Different industrially relevant enzymes (lactase, lipase, penicillin acylase, and trypsin) are used in the catalyst performance study. By using the monolith-carrier-enzyme combinations in different reactor configurations for industrially relevant reactions, a feasibility study of possible application of a monolithic bioreactor can be performed. The results from the three main topics (preparation, performance, and application) can be combined into a general set of design rules for monolithic biocatalysts. The different topics and the approach are schematically depicted in Figure 2.

The catalyst preparation consists of a comparison of monoliths with different microstructure, in terms of enzyme immobilization. The first step is a conditioning step to prepare the monolith for further treatment. In the conditioning step, the monoliths are washcoated with an inorganic carrier (silica, alumina) to provide additional surface area and anchoring sites for attachment of enzymes or carriers. After application of the carrier (modification), the immobilization conditions for different enzymes are optimized. The performance of these monolithic biocatalysts is assessed in a lab scale set-up, to compare the different immobilization protocols and conditions, including stability and immobilization efficiency. Finally, the optimized immobilization protocols are applied for use in the monolithic stirrer and monolith loop reactor. With the obtained data, a set of design rules is made that takes into account specific process requirements and conditions.

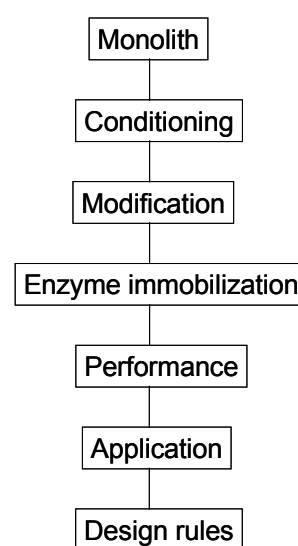


Figure 2. Project layout

Outline

This work was mainly performed as a proof of principle study to investigate the feasibility of monoliths as enzyme support material, and explore the possibilities of application of the monolithic biocatalysts. The different immobilization protocols are integrated with the catalyst performance study; the results of the application studies will be presented separately for the different immobilization protocols/enzymes. Integrated in the preparation and application, a separate study is performed on the microstructure of the monolithic supports. Classic cordierite monoliths are compared with a novel, more open monolith-type. Each chapter of this thesis is partially written based on one or more separate publications, and can be read independently. Therefore, some overlap between the chapters may occur.

Part I of the thesis will provide the background information and will introduce several key concepts that will be used throughout the thesis. **Chapter 1** gives a general overview of the history and current development of biocatalysis. Secondly, the nature and morphology of the different ceramic monoliths and the different types of monolithic reactors will be explained.

In **Chapter 2** conventional enzyme immobilization methods are presented and translated to specific use in combination with monolithic supports. A separate section dealing with enzyme kinetics in both free and immobilized form is added to emphasize the similarities to conventional heterogeneous systems in industrial catalysis.

In **Part II** of this thesis, the preparation and characterization of monolithic biocatalysts is addressed. In order to be able to modify monolithic supports with functional groups for attachment of carrier materials or enzymes, a conditioning step is needed. Moreover, the low specific surface area ($<0.1 \text{ m}^2 \text{ g}^{-1}$) of the bare supports can be increased by adding a coat layer. This layer provides both surface area and surface functionality for the successful binding of chemical linkers. **Chapter 3** covers the washcoating (conditioning) of monoliths with different microstructure. Alumina and silica washcoats are applied, following different preparation methods. By studying different parameters, an optimal approach can be developed for washcoating of monoliths with specific requirements.

In **Chapter 4** the washcoated monoliths are functionalized with two commonly used organo-silane compounds. These compounds can be used to add the desired surface functionalities to the previously applied silica coat layer. Different coating methods are evaluated and the effect of the washcoat layer on final yield and dispersion throughout the monolith is investigated. An optimized method for modification of the silica coat layer is presented, which will be used to modify different monoliths either for direct enzyme binding (**Chapter 5**) or application of a carrier material (**Chapters 6 and 7**)

Chapter 5 starts with an overview of the covalent immobilization techniques that were explored before in order to improve the enzyme loading. Trypsin is covalently attached to different types of monolithic supports. Covalent immobilization proves to have a negative

effect on residual activity of the immobilized enzyme, but a significant increase in enzyme loading has been achieved compared to previous studies. Because chemical immobilization does not yield carriers with a high residual activity, the study has been directed towards more straightforward immobilization methods, including physical and ionic adsorption, and gel entrapment.

In **Chapter 6** ceramic monoliths are functionalized with different gel coatings for entrapment of penicillin G acylase. A study of different gels that are generally used to produce particulate enzyme carriers showed that chitosan and alginate are the most promising materials to apply on the walls of a structured support. The coating procedure for application of a chitosan layer is optimized by using glass plates as a support, and translated for use on monolithic supports. The prepared monoliths are characterized in terms of enzyme adsorption capacity, stability, and activity.

In **Chapter 7** lactase and lipase are immobilized by ionic adsorption on polyethyleneimine, an electrolyte polymer. The immobilization procedure is optimized by comparing different particulate carrier materials in terms of lactase adsorption (capacity, rate) and desorption. Lipase- and lactase-coated monoliths that have been prepared by this method are characterized with respect to the effects of monolith structure, final enzyme loading, activity, enzyme desorption, and reuse.

In **Chapter 8** physical adsorption of lipase and lactase on different carbon coatings is presented. Three types of carbon are used, a sucrose based carbon, a polyfurfuryl based carbon and carbon nanofibers. The carbons are applied on different monoliths and used as a carrier material for lactase and lipase. The carbon coatings have been characterized (both in supported and unsupported form) with respect to porosity, morphology, and surface chemistry. The biocatalysts are compared in terms of enzyme immobilization yield under different conditions, activity, and desorption behavior.

Chapter 9 presents an overview of the application methods, and a summary of the results of the preparation and catalyst performance study. This is generalized in a set of design rules for monolithic biocatalysts.

In **Part III** of the thesis, these design rules are used to apply monolithic biocatalysts in relevant reaction systems. The monolith-carrier system is chosen following the design protocol and tested in different reactor set-ups. At the same time the characteristics of the reactor are studied.

In **Chapter 10** mass transfer measurements are performed in a monolith loop reactor with immobilized trypsin under film flow and Taylor flow conditions. The enzyme has been immobilized via a gel coating and by covalent attachment. The effect of liquid flowrate ($1-8 \text{ cm s}^{-1}$, at 40 cm s^{-1} gas) and cell density (100-400 cpsi) is studied for trypsin on monoliths

with different microstructure. The L-S mass transfer coefficient is determined at the different flow-conditions and the data is compared to theoretical values for flow through a single capillary.

In **Chapter 11** the monolith loop reactor is used as a possible alternative for a slurry reactor in the production of antibiotics. Penicillin G acylases from *E. coli* and *A. faecalis* are entrapped in a gel coating, applied on monolithic supports. The chitosan-coated monoliths are compared with commercially available chitosan beads and with free enzyme in the hydrolysis of penicillin G in different reactors. The concentration-time data is simulated by means of a model that comprises both kinetics and hydrodynamics of the system.

Chapter 12 presents the results of the determination of the L-S mass transfer coefficient in a monolithic stirrer reactor. Trypsin from porcine pancreas is immobilized in chitosan layers and directly onto the monolith-surface by covalent attachment. Catalysts are compared in the hydrolysis of BAEE in the Monolithic Stirrer Reactor.

Chapter 13 describes the application of the polyethyleneimine-coated and chitosan-based supports as support material in the hydrolysis of lactose. Lactase from *Aspergillus oryzae* is adsorbed on the carriers and assessed in the Monolithic Stirrer Reactor. The reaction system is analyzed with respect to kinetics and hydrodynamics.

Chapter 14 presents the application of the immobilized lipase from *Candida antarctica* in the acylation of butanol with vinyl acetate in organic medium in the Monolithic Stirrer Reactor. The effects of temperature and stirrer rate are studied for different monolith-carbon combinations. It has been shown that this system operates in absence of diffusion limitations, and without enzyme deactivation for several weeks.

In **Chapter 15** the main conclusions of this study are presented. Different aspects relevant to the preparation of monolithic biocatalysts are discussed and issues regarding the application of this system are highlighted.

Karen de Lathouder

Delft, November 2006

Table of Contents

Preface

Part I: Introduction

1	General introduction	1
2	Enzyme catalysis and immobilization	19

Part II: Preparation and characterization

3	Preconditioning of monolithic structures	51
4	Functionalization of monolithic structures	75
5	Covalent immobilization of trypsin	95
6	Entrapment of penicillin G acylase	123
7	Ionic adsorption of lipase and lactase	147
8	Physical adsorption of lipase and lactase	179
9	Design rules	215

Part III: Application

10	Liquid-solid mass transfer in a monolith loop reactor	223
11	Hydrolysis of Penicillin G in a monolith loop reactor	259
12	Operation of the MSR with immobilized trypsin under mass transfer limited conditions	293
13	Hydrolysis of lactose in the monolithic stirrer reactor	319
14	Immobilized lipase in organic medium in the monolithic stirrer reactor	347
15	Summary and Evaluation	377

Samenvatting	389
Dankwoord	397
List of publications	401
Curriculum Vitae	407

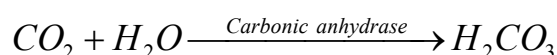
Part I: Introduction

1

General introduction

1 Introduction

While in the last century a great deal of research effort has been made to make organic/inorganic catalysts highly selective, enzymes have evolved over billions of years to their high degree of perfection. Their three-dimensional structures are highly complex, but yet they are formed by spontaneous folding and assembling of a linear polypeptide chain. The catalytic properties of enzymes are far more impressive than the properties of synthetic catalysts that operate under more extreme conditions. Enzymes can catalyze a single reaction on a particular substrate with very high enantioselectivity and enantiospecificity at high rates [1]. The efficiency of enzyme catalysis varies, but most enzymes can enhance the rate of an uncatalyzed reaction by a factor of 10^5 to 10^{14} . One of the most efficient enzymes is carbonic anhydrase:



This enzyme catalyzes the hydration of up to 600000 CO_2 molecules per second under optimal conditions. Carbonic anhydrase is mainly found in red blood cells where it plays a vital role in maintaining the acid-base balance in the body. Apart from the high activity, enzymatic catalysis is more selective than conventional chemical catalysis, and this selectivity is often positional (regioselectivity) or chiral (stereoselectivity). High selectivity has some key benefits, including reduced side reactions, easier separation, and potentially fewer negative environmental effects. Other interesting features that make enzymes an interesting alternative for conventional chemical catalysts are the wide variety of reactions catalyzed, the ability to operate optimally under mild conditions, and the high turnover numbers found in many enzyme-catalyzed reactions. But because enzymes are proteins, they are fragile catalysts. Proteins have a low thermal and chemical resistance, compared to synthetic catalysts. Therefore, factors such as stability, rate of deactivation, and additional downstream processing must also be taken into account when biocatalysis is considered. These factors can be influenced by the form of the catalyst (free or immobilized, cell or enzyme) and the type of reactor (batch or continuous, stirred tank or packed bed) [2]. Despite the many advantages of using enzymes, ultimately economic considerations will determine whether a biocatalytic application will be realized in practice or conventional chemical synthesis wins the competition after all. Experience indicates that only when most or all factors are greatly in favor of biocatalysis, or when there is no chemical alternative, biocatalysis will be the process of choice [3,4]

This chapter will give an introduction into the application of immobilized enzymes, leading to the incentive for application of monolithic bioreactors. A brief history of biocatalysis will be given, followed by some economic aspects of industrial biocatalytic processes. The support structure that was chosen as a carrier for different enzymes, the ceramic monolith, will be introduced and the modes of operation of different monolith reactors will be explained.

2 History of biocatalysis

Throughout history, microorganisms have been of social and economical importance. Without being aware of their existence, man used them in the production of food and beverages. Sumerians and Babylonians practiced beer brewing before 6000 B.C., references to wine making can be found in the Book of Genesis, and Egyptians used yeasts for baking bread. The actual knowledge of the production of chemicals by fermentation is however relatively new. The first reports in literature appeared in the second half of the nineteenth century. Chapman [5] reviewed a number of early industrial processes for organic chemicals. In the course of time it was discovered that not only microorganisms as a whole could be used for fermentation, but also isolated enzymes could be used to perform a single chemical modification. Nowadays these modification processes by single enzymes are called “biotransformations”. Enzymes had already been in use for thousands of years before their nature was gradually understood. It is not known when, for instance, the calf stomach was first used as a catalyst in the manufacture of cheese.

Until about 1950, almost all biological catalysis in industrial processes was accomplished using whole cells or tissues [6]. In recent years there has been an increase in the use of isolated enzyme preparations in industrial, analytical, and medical procedures. The most obvious advantages are greater efficiency of substrate conversion, higher yields, and good product uniformity. However, these advantages must be balanced against the additional costs of enzyme isolation, and the relatively poor stability of purified soluble enzymes. These particular drawbacks have slowed the advancement of enzyme applications. But recent developments in biotechnology, such as recombinant DNA technology, have led to large-scale production of isolated enzymes and new procedures of immobilization. The availability of a great variety of isolated, stable biocatalysts has given momentum to the development of new biocatalytic processes [7].

3 Economy

Industrial pollution (wastes, solvents, cooling water) has been a major concern leading to the development of a whole new mindset based on “green chemistry,” that is, chemistry which is friendly to the environment, minimizes waste, reduces energy utilization, and often favors renewable resources over petroleum-based feedstocks [3]. A major goal for research in chemical industry is the development of “green” processes. The sustainable uses of our resources, whether fossil-based or bio-based renewables, is an important consideration in the chemical industry and enterprise. Chemical or “white” biotechnology is the rapidly growing application of biotechnology to chemical production. It often goes hand-in-hand with green chemistry and the use of renewable feedstocks. Other applications of biotechnology can lead to new products, new manufacturing methods and improved economics. Chemical

biotechnology has made a big impact in the industry structure as firms have been acquired, divested, and restructured around various biochemical innovations. Biotechnology is very pervasive in the food industry - e.g., enzymes for starch manufacturing, beverage production, meat preservatives, etc [6,7].

Even though the incentive to incorporate more “green” process steps into existing processes is growing, immobilized enzyme applications are evolving slowly [8]. In many cases this is because the new application normally requires new process equipment. The use of immobilized enzymes in medical and analytical applications, however, has progressed rapidly [4,6,7]. These areas have been able to make greater use of new developments and the costs involved were very low compared to those for large-scale industrial applications [6]. As was mentioned before, the major advantages of biocatalysts over inorganic catalysts are the high specificity, high reaction rate, nontoxicity, water solubility, biodegradability, and the ability to work under mild conditions. Therefore, the use of immobilized enzymes is firmly established as an effective and economically favorable approach for manufacturing products such as fructose, (semi) synthetic antibiotics, and amino acids [9].

Relatively new applications can be found in the field of biosensors and membrane reactors. Biosensors, used for detection of enzymes or biological compounds such as glucose and urea, are based on immobilized enzymes, antibodies, and receptors. When novel polymeric membranes are used for protein and cell immobilization, the system has the advantages of increased protein stability and the built-in separation and concentration abilities of membranes [3]. The use of membrane bioreactors has led to an increased number of available bioprocess products in the last decades.

The market size for immobilized enzymes is difficult to estimate due to the diversity of applications. Worldwide sales of enzymes in 1987 totaled approximately 445 million \$ [6] and has reached 1.6 billion \$ in 2000 [10].

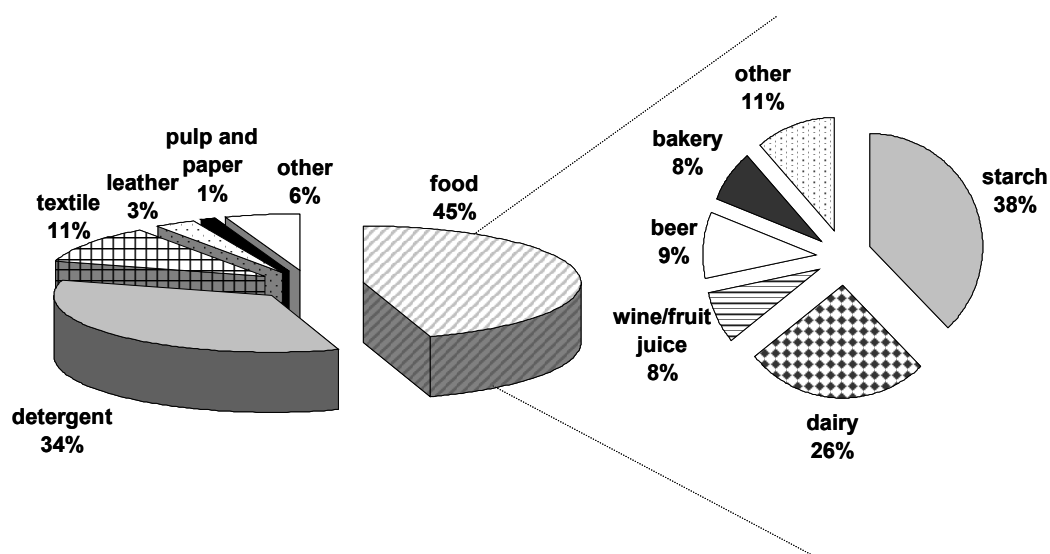


Figure 1. Worldwide sales and specification of the food segment for industrial enzymes in 2000 [10,11]

Volume growth of industrial enzymes is between 4% and 5% AAGR (average annual growth rate), which is accompanied by decreasing prices, due to the increasing number of smaller players on the market. The figure is expected to rise to 3 billion \$ in 2008. A primary factor in this growth is the increased application of immobilized enzymes to new diagnostics, and to biomedical, pharmaceutical, and environmental products. The food industry accounted for almost half the world market for enzymes in 2000, with detergent applications as the second largest segment (Figure 1). Specialty enzyme products (biomedical, diagnostic, and pharmaceutical) currently represent only a small percentage.

4 Enzyme immobilization

If enzymes are actually better catalysts than conventional chemical catalysts in terms of process conditions, reaction rate, and selectivity, why have not all chemical processes been replaced by biocatalytic processes? Although not all chemical processes already have a viable biocatalytic counterpart, the majority of the conventional processes generally have at least one separate step that can be replaced by a biotechnological process. The slow implementation of biocatalysis is a combination of the reluctance of the chemical industry to change anything in a viable process and the drawbacks of using enzymes. Although enzymes can catalyze a reaction up to 10^{14} times faster than the uncatalyzed reaction [1,6] and have a high (stereo)selectivity, they are usually not very stable. The separation of free enzyme from the reaction mixture after reaction is often a very expensive type of downstream processing, and usually does not allow reuse. Moreover, biocatalytic processes are usually operated at low substrate concentrations to prevent inhibition by reactants or products. These diluted systems require a larger reactor volume than the often more intensified chemical counterpart, and moreover an additional concentration step to formulate the product. Another major disadvantage is the price of the catalyst. In order to be cost efficient, enzymes need to be stabilized and reused. Retention of enzyme in the reactor system can provide both. Recirculating the enzyme back into the reactor is expensive and does not increase stability, immobilizing the enzyme onto an insoluble carrier material or membrane retains the catalyst inside the reactor and is usually found to improve operational stability [2].

In the past decades, various types of carrier materials for enzyme immobilization have been studied in combination with the different immobilization methods. Immobilization has been achieved on supports including polymers and resins [12-14], porous glass [15-17], molecular sieves [18-21], silica and silica-alumina composites [22-27], carbonaceous materials [28-30], alginate-based gels [31-34].

The final properties of the immobilized enzyme are not only determined by the carrier material, also the immobilization method influences the catalyst performance. A great variety of different immobilization methods have been developed since immobilization techniques became available. Frequently applied methods include adsorption on different inorganic [35-39] or polymeric [40-43] carriers, entrapment [44], and covalent binding [45,46]. Covalent

immobilization is not as common as adsorption, but avoids the problem of unwanted desorption.

The applied support materials have one thing in common: they are usually in the form of particles, beads or chips [17,47]. Particulate supports can be used in a slurry reactor or in a packed-, fixed-, moving-, or fluidized-bed reactor. The use of these reactor types often leads to particle attrition. Fixed-bed reactors can have additional problems such as maldistribution of reactants and a high pressure drop over the catalyst bed. The solution for these problems can be the use of a structured support. The structure provides a high mechanical strength and the open structure allows for high flowrates and prevents plugging. Finally, a thin layer of carrier material provides shorter diffusion lengths for reactants and products inside the carrier layer compared to the conventional beads. In this study, a ceramic structured support is applied as backbone for the carrier material, in order to produce an improved enzyme support material.

5 Ceramic monoliths

A monolith can be seen as a bundle of small parallel tubes, a continuous unitary structure with straight parallel channels of millimeter size [48,49]. A ceramic monolith is shown in Figure 2. Monolithic supports are usually made of ceramic materials or metals, but also carbon or polymer materials can be used. The wall thickness depends on the channel diameter and geometry. The shape of the channels can be circular, square, rectangular, triangular, hexagonal (honeycomb monoliths), sinusoidal, etc. The shape of the entire block can be adapted to the reactor. The cell density is expressed in cells per square inch (cpsi). Typical values of some important geometric dimensions of ceramic monoliths are listed in Table 1.

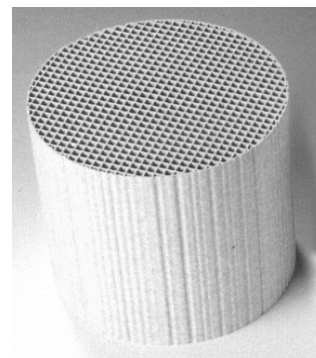


Figure 2. Ceramic monolith

Table 1. Properties of square channel monoliths with different cell density

Cell density [cpsi]	Wall thickness [μm]	Channel diameter [mm]	Geometric surface area [$\text{m}^2 \text{m}^{-3}$]	Void fraction [-]
200 (31 cm^{-2})	270	1.53	1890	0.72
400 (62 cm^{-2})	165	1.11	2740	0.76
600 (93 cm^{-2})	112	0.93	3440	0.80
1100 (170 cm^{-2})	64	0.71	4790	0.84

On the walls of the channels, a catalyst can be applied (Figure 3). The material of this coating layer must have good adherence to the support, but must also be adapted to the particular application (e.g. solvent, temperature, reactants).

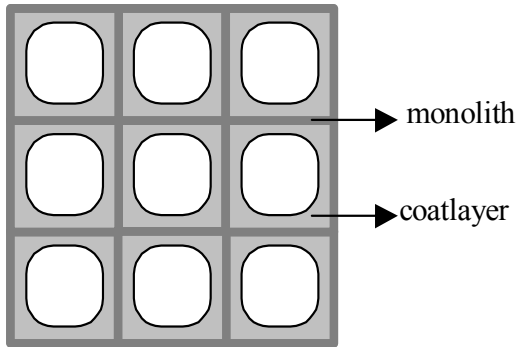


Figure 3. Coated monolith structure

Monoliths were originally designed for decolourisation of nitric acid tail gas and car exhaust emission control [50]. In order to solve the exhaust gas cleaning problem it was necessary to develop a high surface area support with extremely low flow resistance. Developments in producing both ceramic and metallic supports resulted in the industrial production of stable, homogeneous monoliths [51].

Monolithic reactors have some interesting advantages compared to conventional reactors like slurry reactors or fixed bed reactors:

- They are durable, attrition resistant and generally have high thermal, chemical and mechanical strength [49,52].
- They can improve the accessibility of the catalyst, as it is not partially covered by the matrix or binder material. Secondly, the thin catalyst layer provides shorter diffusion path-lengths. This is an advantage for fast reactions [48,52].
- The pressure drop over the length of the reactor is low, due to straight channels and high voidage.
- They have a large external surface.
- The risk of hot-spots is reduced due to the absence of mass transport between the channels, and a better heat distribution, especially with metallic supports in exothermic reactions.
- Taylor flow in the small channels of the monolith results in better plug flow behavior compared to large diameter reactors. This could lead to higher selectivity in reactions where the product is an intermediate.
- Easy separation of catalyst and reactants/products stream,
- They have a low sensitivity to bed plugging, due to the straight, open channels.

There are however also some drawbacks compared to traditional systems:

- The preparation of the monolithic catalyst is more expensive, because special extrusion techniques are needed and the application of the catalyst layer is a time consuming process.
- Replacement of the catalyst requires stopping of the operation, although this also holds true for operation of a packed bed reactor.
- The continuous nature of the monolithic reactor could cause a pH gradient along the reactor length under integral operation. This can be minimized by creating a fast recycle at increased flow rates.

The monolith reactor is proven technology for processes in single-phase flow, for example in the catalytic converter, but also some other applications have recently become of interest. Research is currently directed towards two-phase flow systems. An industrial application

involving gas/liquid operation in a monolith reactor is already in use in the selective hydrogenation of anthraquinones to their corresponding hydroquinones for the production of H_2O_2 [53]. In the 1980s, this process was developed by Eka Nobel (now Akzo Nobel) in Sweden, and is now operational.

5.1 ACM monoliths

The classical honeycomb has square parallel channels with hardly permeable walls: reactants cannot readily enter the wall structure and active material must be deposited on a washcoated egg-shell layer that allows better access to active sites. We have been exploring a new type of structured monolithic support having the same macroscopic geometry as classical cordierite monoliths. This material was developed by The Dow Chemical Company as a new catalyst support. This support is a highly porous acicular mullite. The support material will be indicated in this thesis with Advanced Ceramic Material, ACM. The unique open microstructure of the walls compared to the closed cordierite walls is shown in Figure 4 [54,55].

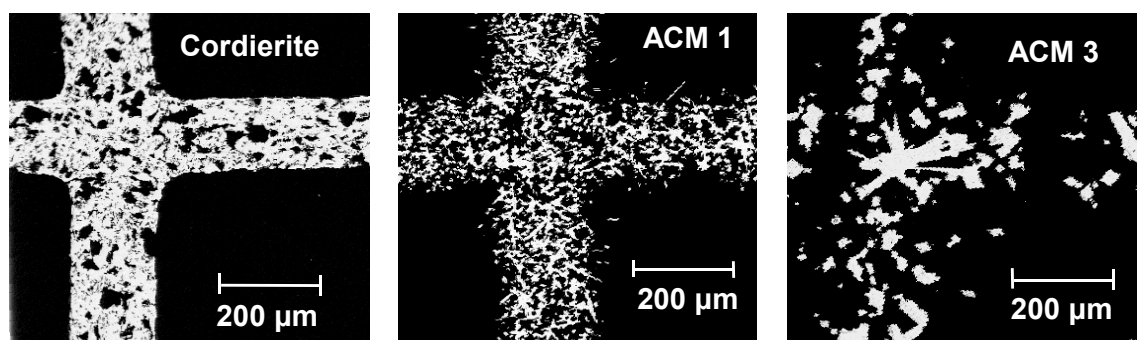


Figure 4. Backscatter electron images of a cross-section of the walls of cordierite, ACM ‘small’ (ACM 1), and ACM ‘large’ (ACM 3) monoliths. Images provided by The DOW Chemical Company

By controlling the synthesis conditions, the mean pore size can be tailored on the micrometer length scale. The open pore structure allows access of reactants to catalysts deposited within the monolith wall [56]. In short, the new ACM supports allow us to further fine-tune the interplay of diffusion and reaction. Elimination of diffusion problems affects reaction time and – more importantly for intensifying fine-chemical processes – reduces the extent of unwanted side reaction: diffusion generally acts as an equalizer that favors the (usually slower) side reactions.

Table 2. Properties of ACM and cordierite monoliths

	ACM 1 ("small")	ACM 2 ("medium")	ACM 3 ("large")	Cordierite
Cell density	200 / 400 cpsi	200 / 400 cpsi	200 / 400 cpsi	200 / 400 cpsi
Wall thickness	0.35 / 0.24 mm	0.35 / 0.24 mm	0.35 / 0.24 mm	0.32 / 0.18 mm
Wall porosity	60%	60%	60%	35%
Pore diameter	5 μm	18 μm	45 μm	7.5 μm

5.2 Monolith reactors

Monoliths can be applied in both single- and multi-phase operation. For co-current gas-liquid flow through a monolith channel, several flow regimes can occur. The preferred regimes for industrial application are film flow and slug flow (Taylor flow) [57,58]. In film flow operation (also possible in counter-current operation), the liquid moves as a thin film over the channel wall. The gas phase moves through the core of the channels. If the liquid velocity is increased or the gas velocity is decreased, the hydrodynamics will change towards Taylor flow, especially for small channels. In Taylor flow operation, the gas phase and liquid phase move through the channels as separate slugs. The gas bubble fills the whole channel diameter and only a thin liquid film separates the gas from the active channel wall (Figure 5).

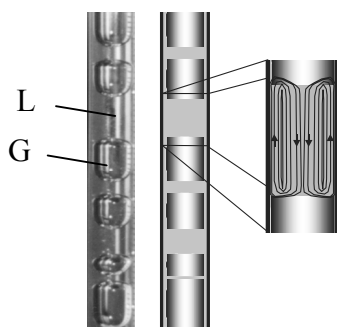


Figure 5. Taylor flow through a single channel

The liquid layer between bubble and catalyst coating is thin, consequently a high gas-solid mass transfer rate through this film is possible. Inside the liquid slugs, an internal recirculation pattern is present (Figure 5). This internal flow increases radial mass transfer. The gas bubbles push the liquid slugs through the channels, yielding a type of plug flow.

Compared to single-phase liquid flow, where the flow in small diameter channels will be laminar (no increased radial transport), mass transfer in multi-phase operation is an order of magnitude larger. Slug flow conditions are easily realized under practical conditions. It can therefore be advantageous for single-phase liquid phase reactions to induce Taylor flow by adding an inert gas component [59].

To operate a monolith reactor, several configurations are possible. In the following paragraphs four options of monolithic reactors that are already used at the lab-scale are introduced; the Screw Impeller Stirred Reactor (SISR), the in-line monolith reactor (ILMR), the monolith loop reactor (MLR), and the monolithic stirrer reactor (MSR).

5.2.1 Screw Impeller Stirred Reactor (SISR) [60,61]

The Screw Impeller Stirred reactor (SISR) consists of a helical screw surrounded by monolith pieces. A mixture of gas and liquid is forced through the monoliths in an internal recirculation mode. The set-up is presented in Figure 6. The reactor can be operated in two- or three-phase mode at elevated pressures. Because of the small volume, this reactor is a very convenient lab scale-reactor to compare monoliths with conventional slurry catalysts.

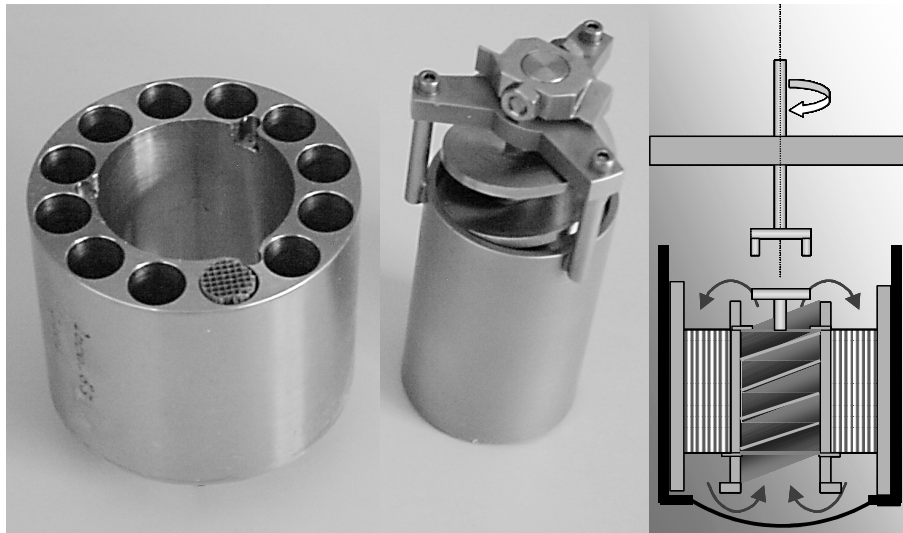


Figure 6. SISR, monolith holder, impeller system and a schematic overview of the set-up

5.2.2 In-line Monolith Reactor (ILMR)

The in-line monolithic reactor is not a separate reactor vessel, but forms an integral part of the pipeline, similar to in-line mixing equipment. The simplest form of an ILMR is presented in Figure 7 and consists of number of horizontally placed modules. The reaction modules contain monoliths that provide a large number of parallel horizontal capillary channels. In these blocks the reaction takes place [62]. In case of a gas-liquid reaction mixing/dispersing modules are placed before each reaction section, to create a uniform dispersion of the gas bubbles over the monolith channels. For strongly endothermic or exothermic reactions, optional heat exchanger blocks can be implemented. Inside the ILMR Taylor flow can easily be realized [63,64]. In this reactor the liquid flow rates can be extremely low, allowing for a high residence time.

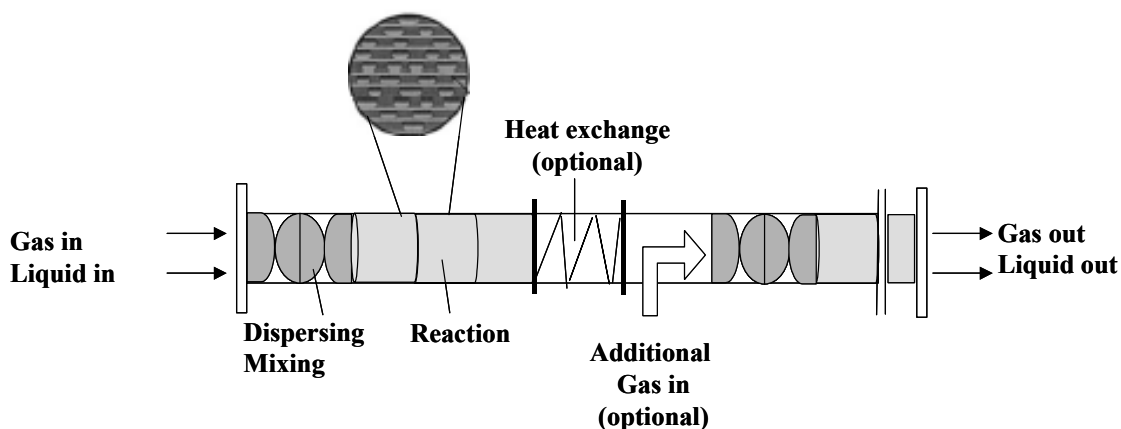


Figure 7. Schematic representation of the in-line monolith reactor [60]

5.2.3 Monolith Loop Reactor (MLR)

As an alternative for conventional three-phase reactors, e.g. slurry stirred tank reactors, trickle bed reactors and bubble column reactors, the monolith loop reactor (MLR) can be used. The monolith is placed vertically in a recycle with a tank. The reactor can be operated in continuous or batch mode. This so-called monolith loop reactor is schematically drawn in Figure 8.

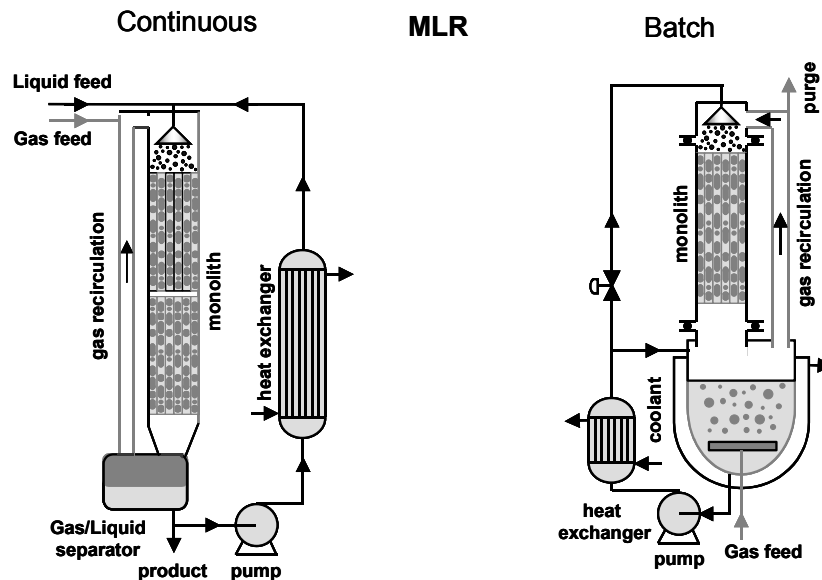


Figure 8. Monolithic loop reactor in two possible configurations [60]

The monolith section can be placed on an existing vessel. The (MLR) consists of a storage tank from which the liquid is pumped towards the liquid distributor. At the distributor the liquid is evenly spread over the monolith cross-section, and subsequently flows back down to the storage tank. The size of this tank depends on the application; for batch operation the tank volume can be large compared to the monolith volume, for continuous operation the tank serves only to separate gas and liquid phases and should be kept small [65]. In this case it can be a retro fit option for a slurry reactor. The suction that is created by the liquid distributor, combined with gravity ensures that the gas is introduced in the channels at the top-section. In this way, no compressor is required. This reactor type was proposed as an alternative to bubble column operation. Compared to a slurry reactor, no stirring or filtration is required. The behavior of the reactor is completely governed by the liquid flow rate. Because of the large liquid circulation flow rate (monolith residence time typically 2-30 s), the conversion per pass is generally low.

5.2.4 Monolithic Stirrer Reactor (MSR)

The Monolithic Stirrer Reactor (MSR), schematically shown in Figure 9, uses monoliths as stirrer blades. When the stirrer is rotated through the liquid, a pressure drop is created over the monolith structures. The pressure drop is the driving force for flow through the monolith

channels. An MSR is a convenient way to transform a slurry reactor into a structured reactor type. This new reactor type can be applied for heterogeneously catalyzed liquid and gas-liquid reactions [66]. This reactor is thought to be especially useful in the production of fine chemicals and in biochemistry and biotechnology. The immobilization of enzymes allows simpler and cleaner routes to many pharmaceutical intermediates, and the monolith system ensures good performance and high enzyme loading in these intensified routes.

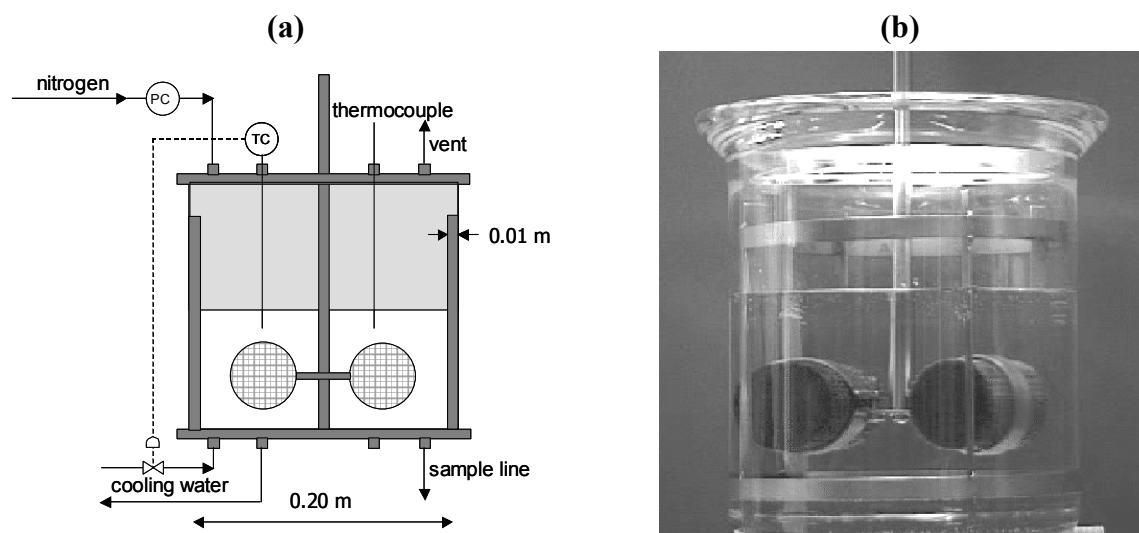
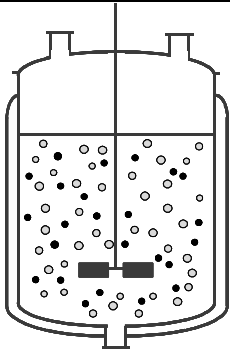
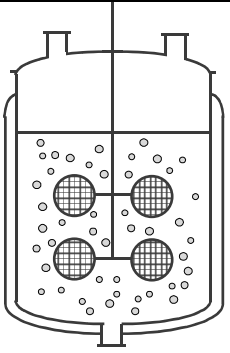


Figure 9. MSR a) schematic overview; b) lab scale reactor, filled with reaction medium

Using a catalytic stirrer that contains structured catalysts as stirrer blades combines the advantages of a structured reactor and a catalytic stirrer, in the sense that the support is a large structure that is readily separated from the liquid medium, and that convenient batch operation and rapid mixing/contacting is facilitated. The wide range of commercially available monolith geometries ensures that a good compromise can be made between the stirring action of the blades and flow through the channels where the reaction occurs on the wall [67]. The main advantage of the MSR is the easy separation of catalyst and reaction medium. Other problems associated with catalyst handling such as attrition and agglomeration are also reduced. Another benefit regarding the safety of operation is that in case of a runaway or emergency a fast shutdown is possible by stopping the impeller. Finally, the stirrer reactor is a versatile tool that can be used for an array of different liquid and gas-liquid reactions by changing monolith-carrier-enzyme combination in the stirrer blades.

Some disadvantages of this reactor include the limited operational experience and the limited catalyst loading of the MSR. The amount of catalyst can be tuned by changing the number, length and cell density of the monoliths. The maximum loading typically is a few wt% of catalyst, similar to commercial reactors. In Table 3 a comparison of the MSR with the slurry reactor is given [67].

Table 3. Comparison of the conventional slurry reactor and the novel monolithic stirrer reactor

Slurry reactor			Monolithic stirrer reactor	
	-	Catalyst separation	++	
	+/-	Catalyst loading	-	
	+	Catalyst preparation	-	
	+/-	Energy input	+/-	
	+/-	Safety	+	
	++	Industrial experience	-	
	+/-	Fast catalyst screening	++	
	-	Scalability	+	
	Commercially available catalyst	Other	Can be applied in existing equipment	

Edvinsson *et al.* [66] showed that the principle of a monolithic stirrer concept works for low viscosity liquids, Hoek *et al.* [67], report successful application of the MSR in both liquid and gas liquid reactions. This study is aimed at immobilizing enzymes onto a monolithic support, and demonstrating applicability of the system. This also includes a study of the hydrodynamic aspects of this novel reactor and the possible application in existing pharmaceutical or biocatalytic processes. The evaluation of the MSR as a convenient laboratory tool for the comparison of monolithic catalyst supports in the absence of mass transfer limitations is an important aspect in the current study.

6 Objectives and outline

Diffusional limitations in conventional carrier beads often result in severely sub-optimal performance [68,69]. Although relatively little research has been done on using monoliths as a support material for enzymes [70,71], the use of structured support materials could be an interesting alternative for conventional enzyme support materials. Monolith-supported enzyme systems present a low flow-resistance, leading to a decreased pressure drop compared to flow through conventional particle-based systems. This low pressure drop allows the use of higher liquid velocities in order to reduce film diffusional effects. Also in case of more viscous media (e.g. starch hydrolysis), the monolithic support with a very thin layer of active material deposited on the walls, can be an interesting alternative for particulate supports in terms of pressure drop and internal diffusion in the carrier material. Finally in case of problems with bed-plugging as can be observed in for example the hydrolysis of lactose in milk [68] this system can present a feasible alternative. In the 1970s, Horvath and Solomon [72] already used slug flow to enhance liquid-solid mass transfer in capillaries. Benoit and Kohler [68] used immobilized catalase on a ceramic monolith and compared this with particulate-supported systems. In 1989, Shiraishi *et al.* [73] used ceramic monoliths in a three-

phase system operating in both film flow and slug flow with immobilized glucose oxidase. Low calorie beer can be prepared by applying a monolith with immobilized glucoamylase [74]. The monolith reactor in this system has covalently bonded glucoamylase and can sustain high flow rates of beer containing yeast and other particulate matter without plugging or fouling.

To effectively attach different enzymes to a monolith, different immobilization protocols are available. These protocols are generally used to produce particulate carriers. To successfully translate these methods for use with structured supports, the methods must first be discussed in more detail. In the following chapter, the immobilization methods will be discussed, followed by a more detailed discussion on enzyme kinetics and industrial application of immobilized enzymes.

7 References

- [1] T. Bugg (1997) An introduction to Enzyme and Coenzyme Chemistry, Blackwell Science Ltd. Oxford, Great Britain
- [2] J. Tramper (1996) *Biotechnology and Bioengineering*; 52: 290-295
- [3] G. Belfort (1989) *Biotechnology and Bioengineering*; 33(8): 1047-1066
- [4] G. Bickerstaff, Ed. (1997) *Immobilization of enzymes and cells, methods in Biotechnology vol.1*, Humana Press, Totowa New Jersey
- [5] J.W. Chapman (1991) *Trends in Food Science & Technology*; 2(7): 176-80
- [6] G.F. Bickerstaff (1987) *Enzymes in Industry and Medicine, New studies in Biology*. Edward Arnold. London, Great Britain
- [7] G.F. Bickerstaff (1995) *Genetic Engineering Biotechnologist*; 15: 13-30
- [8] W.H. Scouten, G. Petersen (1999) Proceedings of the "NEW BIOCATALYSTS: ESSENTIAL TOOLS FOR A SUSTAINABLE 21st CENTURY CHEMICAL INDUSTRY" workshop, November 16-18 1999, Palo Alto, California. CCR Vision 2020 Bioprocessing/Biotechnology Work Group
- [9] *Ullmann's Encyclopedia of Industrial Chemistry*; 5th completely revised edition (1987); VCH Germany; Vol. A9: 199-213
- [10] www.novozymes.com
- [11] T. Godfrey, S. West Eds. (1996) *Industrial enzymology*, 2nd edition; Macmillan Press LTD, Great Britain
- [12] B.C. Koops, E. Papadimou, H.M. Verheij, A.J. Slotboom, M.R. Egmond (1999) *Applied Microbiology and Biotechnology*; 52: 791-796
- [13] W. Warmuth, E. Wenzig (1995) *Bioprocess Engineering*; 12: 87-93
- [14] A.R. Ozdural, D. Tanyolac, I. Boyaci, M. Mutlu, C. Webb (2003) *Biochemical Engineering Journal*; 14: 27-36
- [15] N. Hidaka, T. Matsumoto (2000) *Industrial and Engineering Chemistry Research*; 39: 909-915

-
- [16] L.N. Yee, C.C. Akoh (1995) *Journal of the American Oil Chemists' Society* 72(11): 1407-1408
- [17] R.J. Barros, E. Wehtje, P. Adlercreutz (1997) *Biotechnology and Bioengineering*; 59: 364-373
- [18] J.F. Diaz, K.J. Balkus (1996) *Journal of Molecular Catalysis B: Enzymatic*; 2: 115-126
- [19] E. Dumitriu, F. Secundo, J. Patarin, I. Fechete (2003) *Journal of Molecular Catalysis B: Enzymatic*; 22: 119-133
- [20] F.N. Serralha, J.M. Lopes, F. Lemos, D.M.F. Prazeres, M.R. Aires Barros, J.M.S. Cabral (1998) *Journal of Molecular Catalysis B: Enzymatic*; 4: 303-311
- [21] A.P.V. Goncalves, J.M. Lopes, F. Lemos, J.M.S. Cabral, M.R. Aires Barros (1996) *Journal of Molecular Catalysis B: Enzymatic*; 1: 53-60
- [22] C. Mateo, O. Abain, R. Fernandez-Lafuente, J.M. Guisan (2000) *Biotechnology and Bioengineering*; 68: 98-105
- [23] M. Di Serio, C. Maturo, E. De Alteriis, P. Parascandola, R. Tesser, E. Santacesaria (2003) *Catalysis Today*; 79-80: 333-339
- [24] L. Ferreira, M.A. Ramos, J.S. Dordick, M.H. Gil (2003) *Journal of Molecular Catalysis B: Enzymatic*; 21: 189-199
- [25] M. Ladero, A. Santos, J.L. Garcia, F. Garcia-Ochoa (2001) *Enzyme and Microbial Technology*; 29: 181-193
- [26] N.G. Wilson, T. McCreedy, G.M. Greenway (1999) *The Analyst*; 125: 237-239
- [27] M. Thust, M.J. Schöning, P. Schrot, U. Malkoc, C.I. Dicker, A. Steffen, P. Kordos, P. H. Lüth (1999) *Journal of Molecular Catalysis B: Enzymatic*; 7: 77-83
- [28] Q.Z.K. Zhou, X.D. Chen, (2001) *Biochemical Engineering Journal*; 9: 33-40
- [29] G.A. Kovalenko, O.V. Komova, A.V. Simakov (2002) *Journal of Molecular Catalysis A: Chemical*; 182-183: 73-80
- [30] A.S. Rani, M.L.M. Das, S. Satyanarayana (2000) *Journal of Molecular Catalysis B: Enzymatic*; 10: 471-476
- [31] A. Tanriseven, Y.B. Uludağ, S. Doğan (2002) *Enzyme and Microbial Technology*; 30: 406-409
- [32] N. Munjal, S.K. Sawhey (2002) *Enzyme and Microbial Technology*; 30: 613-619
- [33] T. Coradin, J. Livage (2003) *Comptes Rendus Chimie*; 6: 147-152
- [34] Z. Aksu, G. Bülbül (1999) *Enzyme and Microbial Technology*; 25: 344-348
- [35] C. Marlot, G. Langrand, C. Triantaphylides, J. Baratti (1985) *Biotechnology Letters*; 7: 647-650
- [36] I.C. Omar, H. Saeki, N. Nishio, S. Nagai (1988) *Agricultural and Biological Chemistry*; 52:99-105
- [37] R.A. Wisdom, P. Dunnill, M.D. Lilly (1985) *Enzyme Microbiology and Technology*; 7: 567-572
- [38] C. Brady, L. Metcalfe, D. Slaboszewski, D. Frank (1988) *Journal of the American Oil Chemists' Society*; 65: 917-919
- [39] C. Brady, L. Metcalfe, D. Slaboszewski, D. Frank (1986) US Patent No. 4,629,742
- [40] Y. Kimura, K. Tanaka, K. Sonomoto, T. Nihira, S. Kukui (1983) *European Journal of*

- Applied Microbiology and Biotechnology; 17: 107-112
- [41] S.T. Kang, J.S. Rhee, (1988) *Biotechnology Letters*; 10: 341-346
- [42] T. Gitlesen, M. Bauer, P. Adlercreutz, (1997) *Biochimica Biophysica Acta*; 1345: 188-196
- [43] C.J. Gray, J.S. Narang, S.A. Barker (1990) *Enzyme Microbiology and Technology*; 14: 800-807
- [44] S. Hertzberg, L. Kvittingen, T. Anthosen, G. Skjak-Brack (1992) *Enzyme Microbiology and Technology*; 14: 42-
- [45] F. M. Bautista, M. C. Bravo, J. M. Campelo, A. Garcia, D. Luna, J. M. Marinas and A. A. Romero (1999) *Journal of Molecular Catalysis B: Enzymatic*; 6: 473-481
- [46] J. Kroll, F.R. Hassanien, E. Glapinska, C. Franzke (1980) *Die Nahrung*; 24: 215-
- [47] Y. Yang, H.A. Chase (1998) *Biotechnology and Applied Biochemistry*; 28: 145-154
- [48] J.E. Antia, R. Govind (1995) *Applied Catalysis A: General*; 131: 107-120
- [49] W.B. Kolb, A.A. Papadimitriou, R.L. Cerro, D.D. Leavitt, J.C. Summers (1993) *Chemical Engineering Progress*; 89: 61-67
- [50] A. Cybulski, J.A. Moulijn (1994) *Catalysis Reviews-Science Engineering*; 36 (2): 179-270
- [51] R. Edvinsson, J.A. Moulijn (1996) *Advanced Catalysis engineering Course*; Delft
- [52] F. Kapteijn, J.J. Heiszwolf, T.A. Nijhuis, J.A. Moulijn (1999) *CATTECH*; 3(1): 24-41
- [53] R. Edvinsson Albers, M.Nystrom, M. Siverstrom, A. Sellin, A.-C. Dellve, U. Andersson, W. Herrmann, Th. Berglin (2001) *Catalysis Today*; 69: 247-252
- [54] J.M. Moyer, N.N. Hughes (1994) *Journal of the American Ceramic Society*, 77: 1083-1086
- [55] S.A. Wallin, A.R. Prunier, J.R. Moyer (2001), US Patent 6,306,335
- [56] K.M. de Lathouder, J. Bakker, M.T. Kreutzer, F. Kapteijn, J.A. Moulijn, S.A. Wallin (2004) *Chemical Engineering Science*; 59: 5027-5033
- [57] G. I. Taylor (1960) *Journal of fluid Mechanics*; 10: 161-165
- [58] K.A. Triplett, S.M. Ghiaasiaan, S.I. Abdel-Khalik, D.L. Sadowski (1999) *International Journal of Multiphase Flow*; 25: 377-394
- [59] M.T. Kreutzer, F. Kapteijn, J.A. Moulijn, J.J. Heiszwolf (2005) *Chemical Engineering Science*; 60: 5859-5916
- [60] A.C.J.M. Van de Riet, F. Kapteijn, J.A. Moulijn (1998) *Proceedings of the Second International Symposium on Catalysis in Multiphase Reactors, Toulouse, France* 153–159
- [61] T. Boger, M.M.P. Zieverink, M.T. Kreutzer, F. Kapteijn, J.A. Moulijn, W.P. Addiego (2004) *Industrial and Engineering Chemistry Research*; 43: 2337.
- [62] A. Stankiewicz (2001) *Chemical Engineering Science*: 56; 359-364
- [63] J. Ratulowski, H.-Ch. Chang, (1989). *Physics of Fluids A*; 1: 1642-1655
- [64] T. Fukano, A. Kariyasaki, (1993) *Nuclear Engineering and Design*; 141: 59-68
- [65] J.J. Heiszwolf, L.B. Engelvaart, M.G. vd Eijnden, M.T. Kreutzer, F. Kapteijn, J.A. Moulijn (2001) *Chemical Engineering Science*; 56: 805-812
- [66] R.K. Edvinsson Albers, M.J.J. Houterman, T. Vergunst, E. Grolman, J.A. Moulijn

- (1998) AIChE Journal; 44: 2459-2464
- [67] I. Hoek, T.A. Nijhuis, A.I. Stankiewicz, J.A. Moulijn, (2004) Chemical Engineering Science; 59: 4975-4981
- [68] M.R. Benoit, J.T. Kohler (1975) Biotechnology and Bioengineering; 17: 1616-1626
- [69] T. Zhang, L. Yang, Z. Zhu (2005) Enzyme and Microbial Technology; 36: 203-209
- [70] K. Kawakami, K. Kawasaki, F. Shiraishi, K. Kusonoki (1989) Industrial & Engineering Chemistry Research; 28: 394-400
- [71] N. Papayannakos, G. Markas, D. Kekos (1993) The Chemical Engineering Journal; 52: B1-B12
- [72] C. Horvath, B.A. Solomon (1972) Biotechnology and Bioengineering; 14: 885-914
- [73] F. Shiraishi, K. Kawakami, S. Kono, A. Tamura, S. Tsuruta, K. Kusunoki (1989) Biotechnology and Bioengineering; 33: 1413-1418
- [74] G. Duncombe, W.F. Line, E. Chicoye, US4430348 (1984), to Miller Brewing

2

Enzyme catalysis and immobilization

1 Introduction

This chapter gives an overview of the structure and catalytic activity of enzymes, and introduces some commonly used immobilization methods. Secondly, some thought is given on how to successfully translate these protocols for use with monolithic supports and finally some selected examples of industrial application of different enzymes are discussed.

What are enzymes? What do they do? What kind of environment is suited best to them? These are the sorts of questions that need to be answered first in order to understand the basics of enzyme catalysis and to gain some knowledge on the constraints that are placed on the reaction conditions.

Nature is extremely diverse in terms of the large amount and variety of organic molecules required for life. This diversity is due to the wide catalytic scope of enzymes. Enzymes are giant macromolecules, generally with a molecular weight from 5 to 5000 kDa (1 Da corresponds with the atomic mass of hydrogen, so $1 \text{ Da} = 1 \text{ g mol}^{-1}$), with typical values in the range 20-100 kDa. Enzymes belong to a larger biochemical family of macromolecules; the proteins. All proteins are polypeptides, a linear sequence of α -amino acid building blocks joined together by amide linkages. Proteins consist of 20 different α -amino acid units, only L-amino acids. Consequently enzymes are chiral molecules. To form the polypeptide chain each amino acid is linked to the next via an amide bond, forming a linear sequence of 100-1000 amino acids. This is the primary structure of the protein. The secondary structure of the protein is formed by local regions (10-20 amino acids) that have ordered three-dimensional structures, held together by hydrogen bonds. The tertiary structure arises from packing the elements of secondary structure to form a global conformation. In water, this packing usually involves burying hydrophobic amino acid side chains on the inside and positioning hydrophilic side chains on the surface of the protein. Most enzymes are therefore not soluble in apolar solvents. Larger proteins often consist of more than one tertiary structure, which fit together to form the quaternary structure.

The catalytic properties of enzymes are far more impressive than the properties of synthetic catalysts that operate under more extreme conditions. Under identical conditions, the rate of an enzymatic reaction may be higher by a factor of one million than the rate of the reaction in the absence of the catalyst [1]. As far as selectivity is concerned, enzymes are unambiguously superior to chemical catalysts. The mild process conditions enable the use of (poly)unsaturated substrates, yielding new types of functional or polymer chemicals. The high selectivity results from enzyme substrate complex formation. This is schematically presented in Figure 1. First, the substrate has to fit into the active site of the enzyme and secondly, the enzyme binds only one type of reactive group. This reduces the number of reaction steps, since it is not necessary to protect other reactive groups.

The part of the enzyme that is responsible for the catalytic activity, the active site, is usually a hydrophilic cleft or cavity containing an array of amino acids side chains, which bind the substrate and carry out the enzymatic reaction [1,2].

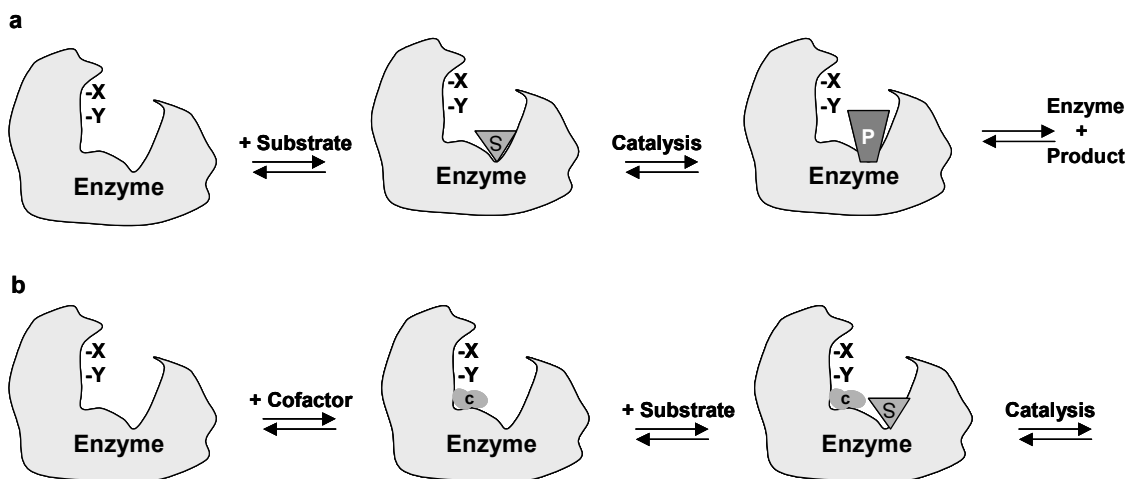


Figure 1. Mechanism of enzyme catalysis following the lock-key model

Concerning stability, enzymes can only be used in a relatively narrow range of physical and chemical conditions, whereas chemical catalysts are much more stable under more extreme conditions. However, in some cases enzymes can be more advantageous than chemical catalysts when comparing the conditions necessary for the highest activity. For example, ambient temperature, suitable for an enzyme process, is more economic than a high or very low temperature necessary for many classical (endothermic) chemical processes. Moreover, it was thought that enzymes could only be active in aqueous solution. But during the last decades, it has been found that most enzymes can work in almost anhydrous solvents [2].

The recent developments in biotechnology have led to several commercially viable applications. Recombinant DNA techniques have been adopted by chemists and enzymologists to investigate structure and function of enzymes. Industrial biotechnology makes use of such techniques for the production of a new generation of enzymes, with specific amino acid changes from the native enzyme. These modified enzymes are used in processes where their native counterparts could not be introduced, especially in the chemical industry [2].

2 Classification of enzymes

Approximately 3500 enzymes have been characterized to some degree, while over 500 are available commercially from enzyme suppliers. All enzymes can be grouped into one of the six distinct classes (Table 1), depending on the reactions they catalyze. Each protein is given an **Enzyme Classification Number**. The method of classification is by the type of reaction the enzyme catalyzes. The EC Number consists of 4 digits corresponding to four levels of classification. Peroxidases, for example, are given the EC Number 1.11.1.X - where X is the digit that represents the particular type of peroxidase in question. The first digit in the EC

Number represents the first level of classification. All enzymes under EC 1 are oxidoreductases.

Table 1. Enzyme classification

Enzyme classification	Subclasses
1. Oxidoreductases	oxidases, oxygenases, peroxidases, dehydrogenases
2. Transferases	glycotransferases, methyltransferases, transaldolases, transketolases, acyltransferases, alkyltransferases, transaminases, sulfotransferases, phosphotransferases, nucleotidyltransferases
3. Hydrolases	esterases, lipases, glycosidases, proteases, sulfatases, phosphatases, aminoacylases, nucleases, halohydrolases
4. Lyases	decarboxylases, aldolases, ketolases, hydratases, dehydratases, polysaccharide lyases, ammonia lyases
5. Isomerases	racemases, epimerases, isomerases
6. Ligases	synthetases, carboxylases

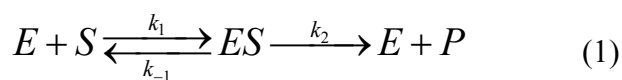
- 1. Oxidoreductases** are divided into several classes. The dehydrogenases and oxidases catalyse oxidation and reduction reactions on the following groups: hydroxyl, aldehyde, ketone, carboxyl, amino, NAD(P)(H). Peroxidases oxidize reduced compounds with H_2O_2 as oxidant, and oxygenases incorporate either one or both oxygen atoms from O_2 into the product.
- 2. Transferases** catalyse the transfer of a functional group of one compound (donor) towards an acceptor. Specifically, methyl, hydroxymethyl, formyl, glucosyl, acyl, alkyl, phosphate, and sulfate groups are transferred.
- 3. Hydrolases** are the most readily commercially available and well studied enzymes. Their primary function is to catalyse the hydrolysis of a variety of compounds, including esters and lipids, thioesters, phosphates and pyrophosphates, sulfates, glycosides, peptides, and proteins.
- 4. Lyases** cleave C-C, C-N, and C-O bonds by elimination to produce double bonds or add groups to double bonds.
- 5. Isomerases** catalyse intramolecular isomerization.
- 6. Ligases** catalyse the linking of two or more molecules, simultaneously hydrolysing ATP. Typical bonds include C-O, C-N, C-S, and C-C.

3 Catalytic activity of enzymes

The stoichiometry of enzymatic reactions is usually well known. In this study several types of reactions will be used, involving one or more different reactants and/or products. The nomenclature is as follows [3]:

Reaction	Name
$A \rightarrow P$	Uni-uni
$A \rightarrow P + Q$	Uni-bi
$A + B \rightarrow P$	Bi-uni
$A + B \rightarrow P + Q$	Bi-bi

The theory of enzyme catalyzed reactions proposed by Michaelis and Menten in 1913 is based on the assumption that the enzymatic reaction occurs in two steps [4]. The simplest realistic form of this kinetic model involves four species: E, S, ES, and P. In the first step, a complex ES is formed by a reaction of the enzyme E and substrate S (k_1 and k_{-1} are rate constants of the forward- and backward reaction, respectively). In the second step, the complex ES dissociates forming the enzyme and product P.



From this it follows that the overall reaction rate is proportional to the concentration of the enzyme-substrate complex [ES]. Therefore [ES] is a parameter that determines the reaction rate. [ES] depends on the concentrations of both enzyme and substrate.

If for example the amount of enzyme remains unaltered and the substrate concentration increases, the concentration of the complex ES also increases.

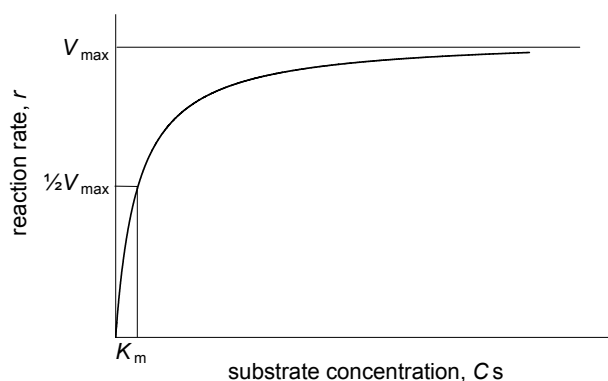


Figure 2. Effect of the substrate concentration on the rate of an enzymatic reaction

Finally all enzyme is present in the form of the complex ES. Under these conditions the reaction rate achieves its maximum value V_{\max} (Figure 2). The enzyme is saturated with substrate. The typical course of such a dependence of reaction rate on substrate concentration is presented in Figure 2. The Michaelis Menten constant K_m is defined as the substrate concentration at half the maximal reaction rate. At the rate of $\frac{1}{2} V_{\max}$, one half of the total amount of enzyme is present in the form of ES, the second half being free so that $[ES] = [E]$.

The concentrations of ES and P are related to the concentrations of E and S, so a set of macroscopic balances can be written for this system:

$$\begin{aligned}\frac{-dC_S}{dt} &= k_1 \cdot C_E \cdot C_S - k_{-1} \cdot C_{ES} \\ \frac{-dC_E}{dt} &= k_1 \cdot C_E \cdot C_S - k_{-1} \cdot C_{ES} - k_2 \cdot C_{ES}\end{aligned}\quad (2)$$

This system can only be solved analytically with certain assumptions:

1. $C_S \gg C_{E,\text{tot}}$
and
2. $k_{-1} \gg k_2$ The pseudo-equilibrium assumption
or
3. $dC_E/dt = 0$ The pseudo-steady state assumption

Applying the equilibrium assumption implies that the equilibrium between ES and the free substrate is very fast. It follows that k_{-1} must be much larger than k_2 . This implies that the product-releasing step is the rate-determining step. This gives for the overall rate:

$$r = k_2[ES] \quad (3)$$

Setting up the equilibrium expression we find:

$$k_1[E][S] = k_{-1}[ES] \rightarrow [E] = [ES] \frac{k_{-1}}{k_1[S]} \quad (4)$$

The total enzyme concentration e must be conserved and all enzyme is present either as free enzyme or in an enzyme substrate complex:

$$e = [E] + [ES] \quad (5)$$

Substituting (4) in (5) and then (5) in (3) yields:

$$r = \frac{k_2 \cdot e \cdot [S]}{\frac{k_{-1}}{k_1} + [S]} \quad (6)$$

In this situation, the Michaelis Menten constant K_m approaches the dissociation constant of the complex ES (substrate constant K_s) defined according to the Guldberg-Waage law [4]:

$$K_s = \frac{[E][S]}{[ES]} = \frac{k_{-1}}{k_1} \approx K_m (= \frac{k_{-1} + k_2}{k_1}) \quad (7)$$

Thus, in this case the Michaelis constant expresses the affinity of the enzyme to the substrate. This only holds if k_2 is much smaller than k_{-1} . But the Michaelis-Menten model is in general too simple for many purposes, although it is still often used. The Briggs-Haldane model, where the less restrictive pseudo-steady state assumption is used, has proven more useful to describe the system after the initial period in which the enzyme substrate complex is formed.

Since k_1 and k_{-1} are constant their ratio is also constant. The Michaelis-Menten constant for fast equilibrium systems, $K_m (= k_{-1}/k_1 =$ dissociation constant for ES), is enzyme specific and also depends on the temperature. $k_2 \cdot e$ is equal to the maximum rate. Thus the constant V_{max} is proportional to the amount of enzyme and the temperature. The Henri-Michaelis-Menten rate expression can now be written as [3,5,6]:

$$r = \frac{V_{max} \cdot [S]}{K_m + [S]} \quad (8)$$

For most typical biochemical substrates the values of K_m range between 10^{-5} and 10^{-8} mol m⁻³. This idealized situation is rarely found in nature. The Michaelis-Menten model was derived for irreversible conversion of a single substrate to a single product (irreversible uni-uni reaction). Usually the enzyme has to deal with multiple substrates and products. Consequently, terms for reverse reactions, inhibition or other reactants are involved. Michaelis-Menten kinetics is valid only during the initial stage of the reaction (where product concentrations are negligible) if the additional substrates are present in excess (for example in hydrolysis reactions). In all other cases, rate equations can be derived using the pseudo-steady state assumption, ($d[E]/dt = 0$), and elimination of unobservable enzyme states (lumping). This assumption means that the concentration of free enzyme (and of any other enzyme state) does not change during the time interval that is considered.

The efficiency of an enzyme-catalyzed reaction is indicated by the molar activity, also called turnover frequency. This number is defined as the number of substrate molecules converted per unit of time by one enzyme molecule under standardized conditions [5]. If the molecular mass of the enzyme is known, this can be calculated from the specific activity of a particular enzyme.

The main factors affecting the rate of enzymatic reactions are [3,5-7]: the enzyme concentration, substrate concentration, and presence of inhibitors, activators or organic solvents, pH, temperature and ionic strength of the medium.

3.1 Effect of organic solvents

Enzymes, like other proteins, maintain their spatial structure with the help of disulphide bonds, electrostatic interactions, hydrogen bonds and also on the basis of hydrophobic interactions between the side chains of the amino acids. Hydrophilic groups are prevalent on the surface of the enzyme molecule and thus, with few exceptions, enzymes are soluble in water and the above hydrophobic interactions are most efficient in an aqueous medium [8,9]. An aqueous medium is, however, not always the optimum for organic reactions. Many organic compounds, which could be used as substrates, are sparingly soluble in water. In addition, excess water in the medium adversely affects the reaction equilibrium of reactions such as esterification [10]. Furthermore, at low water activity, side-reactions that are water dependent can be prevented [11], including the denaturation of enzymes. In absence of water, the synthesis by hydrolases (lipases, proteases) of ester and amide bonds can be favored over hydrolysis. Changing the organic solvent can also influence the substrate specificity and the region- and enantioselectivity of a given enzyme [12]. However, although enzymes in organic media have several advantages, most enzymes show a remarkable decrease in activity, and can even become completely denatured. The nature of this behavior can be ascribed to several factors such as diffusion problems, high saturation substrate concentrations, restricted protein flexibility, low stabilization of the enzyme-substrate complex, and even partial enzyme denaturation. The addition of an organic solvent probably attenuates the hydrophobic interactions, so that relevant parts of the protein molecule are denatured, which becomes irreversible in anhydrous solvents [8].

3.2 Effect of temperature and pH

The temperature dependence of enzyme-catalyzed reactions exhibits an optimum because the thermodynamic increase of reaction rate (known relationships derived by van 't Hoff and Arrhenius hold for enzyme reactions) is followed by a steep drop caused by thermal degradation of the enzyme. An empirical rule suggests that elevating the temperature by 10 K approximately doubles the reaction rate. For temperatures exceeding 323 to 333 K, most enzymes are irreversibly denatured, mainly in aqueous solutions. Increased thermal stability is observed for an enzyme in an organic solvent containing a small amount of water.

The pH value of the medium can also strongly affect the stability and activity of enzymes, due to the dependence of the dissociation state of acid as well as basic functional groups of the active site and of other parts of the enzyme on this value (Figure 3). For most enzymes the optimum pH range is 5 to 9, however, the optimum pH value need not necessarily be constant for a particular enzyme; it may depend on the substrate used.

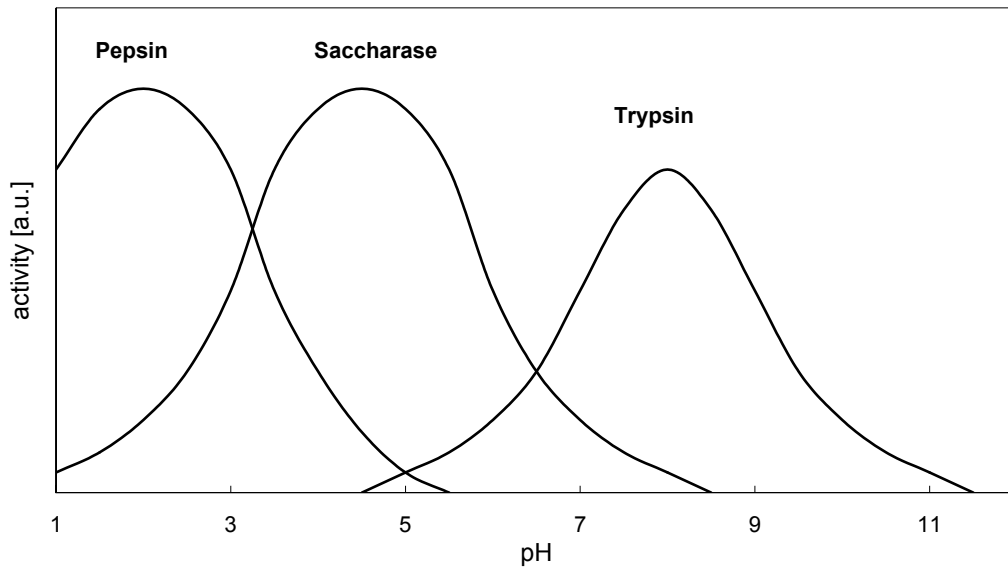


Figure 3. Activity of various enzymes as a function of pH [5]

4 Free versus immobilized enzymes

The main problems that were experienced with the use of enzymes have been both practical and economical [2]. When expensive enzymes are used, the operation costs can be reduced by recovering the catalyst from the solution, provided the biocatalyst retains its activity. This can be done by separation techniques or by immobilising the enzyme. The principle of attaching biocatalysts to an insoluble matrix is relatively simple. In 1953, Grubhofer and Schleith [13] immobilised pepsin, diastase and ribonuclease by using deazotized polyaminopolystyrene resin. In 1969 the first industrial process utilising immobilised enzymes became operative. It was a continuous process for the optical resolution of DL-amino acids, by immobilised aminoacylase [14]. In this section, the benefits of free enzymes versus immobilized ones are compared.

4.1 Free enzymes

Enzymes in aqueous buffer solutions are easily denatured by the action of elevated temperature, extreme pH values and inhibitors [15]. Irreversible changes of the conformation, chemical changes of functional groups in side chains of amino acid units and hydrolysis of peptide bonds may occur. Certain enzymes are also sensitive to atmospheric oxygen. All these factors are important with respect to the reaction conditions. The use of free enzymes also causes the need for complex down-stream processing, because especially in pharmaceutical and food applications no protein residue is allowed in the final product. On the other hand, there are no problems with diffusion, the substrate and product molecules can easily penetrate into the active center of the enzyme and they can also be easily released back into the medium.

4.2 Immobilized enzymes

Immobilization provides long-term stability and high enzyme activity. Enzyme immobilization signifies the capture of the enzyme in a certain space, which is in contact with the liquid phase containing molecules of the substrate and product, which facilitates a free movement of these molecules into and out of the space containing the enzyme. The enzyme however cannot leave this space. This space is typically formed by particles of a solid carrier having the enzyme bound on their surfaces or in pores. Immobilized enzymes are very advantageous as catalysts in comparison with free enzymes, due to the following features:

- Repeated or continuous use
- Increased stability
- Easy separation

The main concern with enzyme immobilization is to obtain a biocatalyst with a stability and activity that have not been affected during the immobilization process in comparison with the enzyme in its free form. Ideally, the immobilized enzyme will exhibit improved catalytic performance. There is no rule to predict the obtained activity and stability of an enzyme upon immobilization. Immobilization may decrease or increase enzyme activity. Most immobilized lipases for example exhibit a higher optimum temperature values than free lipase. This is attributed to the fact that immobilized enzymes are less sensitive to thermal deactivation since their structure is more rigid after immobilization. Upon immobilization, intrinsic properties expressed as the kinetic constants V_{\max} and K_m may be altered. This may be because of conformational changes, induced by the attachment. More often however, there can be a direct influence of the support or the microenvironment. A polymer matrix for example may cause a pH difference between the microenvironment and the bulk fluid. Thus the activity as a function of pH can be quite different for free or immobilized enzyme. Additional attraction or repulsing interactions of the support matrix with the substrates or products may lead to altered values of K_m .

Another important difference between free and immobilized enzyme is the possibility of mass transfer problems. The external mass transfer or film diffusion is determined by the velocity difference between the support and the bulk fluid. External mass transfer problems can be minimized by increasing the flow rate or increased stirring speed. Internal mass transport problems become more dominant with increased layer thickness.

Effects of the support matrix and internal diffusion limitations can be expressed by introducing an effectiveness factor, which yields for the activity of an immobilized enzyme:

$$r_{immob} = r_{free} \cdot \eta \quad (9)$$

In the following paragraphs, different immobilization strategies are discussed and the approach to translate these general methods to a suitable protocol for a monolithic support will be given. Furthermore some examples of industrially important enzymatic conversions will be given.

5 Principles of enzyme immobilization

In solution, enzymes behave as any other solute in that they are readily dispersed in the appropriate solvent and have complete freedom of movement. Enzyme immobilization may be considered as a technique specifically designed to greatly restrict the freedom of movement. There are five general approaches for achieving enzyme immobilization i.e. (ionic) adsorption, covalent binding, crosslinking, entrapment, and encapsulation. These methods are illustrated in Figure 4.

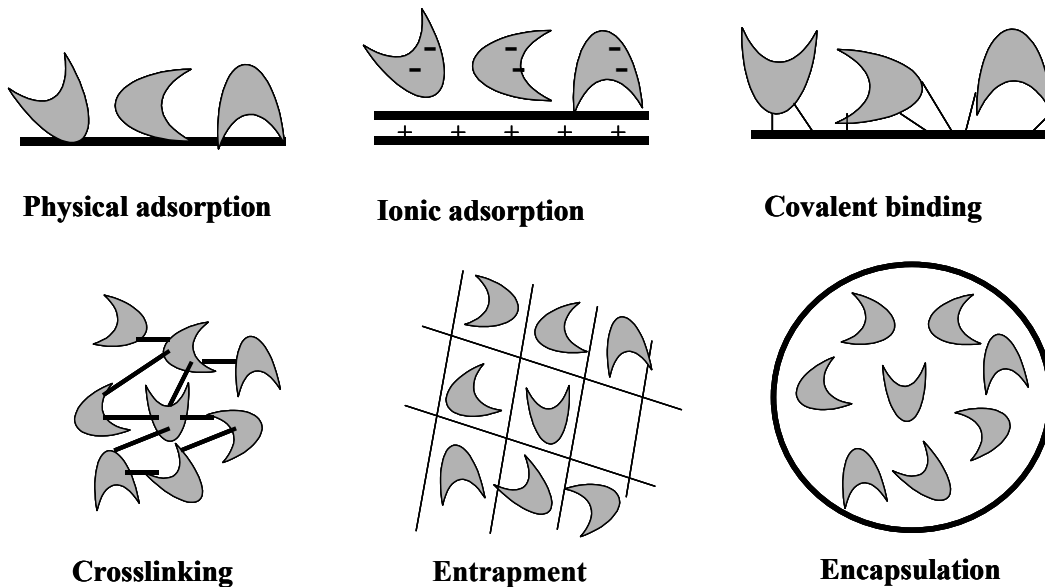


Figure 4. Overview of different immobilization protocols

5.1 Adsorption

Immobilization by adsorption is the most straightforward method and involves reversible surface interactions between enzyme/cell and support material [7]. The forces involved are mostly van der Waals' forces, together with electrostatic forces (ionic interactions and hydrogen bonding). These forces are very weak, but sufficiently large to enable reasonable binding. For example, it is known that yeast cells have a surface chemistry that is substantially negatively charged so that use of a positively charged support will enable immobilization. Existing surface chemistry between the enzymes/cells and support is used; therefore no chemical activation or modification is required.

The adsorption procedure consists of mixing the enzyme and a support with adsorption properties, under suitable conditions (pH, ionic strength, temperature, etc.). After the incubation period, the immobilized material is collected and washed extensively to remove non-bound biological compounds.

5.1.1 Physical adsorption

This method for the immobilization of an enzyme is based on the physical adsorption of enzyme protein on the surface of water-insoluble carriers. Hence, the method causes little or no conformational change of the enzyme or destruction of its active centre. Adsorption tends to be less disruptive to the enzymatic protein than chemical means of attachment because the binding is mainly by hydrogen bonds, multiple salt linkages, and Van der Waals' forces [5,6]. In this respect, the method bears the greatest similarity to the situation found in natural biological membranes and has been used to model such systems.

Various inorganic supports can be used, but also synthetic resins and natural materials (chitosan beads) with a strong adsorption capacity are suitable. Adsorbing materials that are usually employed as filter materials in wastewater treatment and purification of product streams could also be used to deliberately attach biological materials for increased stability and re-use. Regarding the support material, operational characteristics (mechanical strength, hydrodynamics, resistance to degradation) must be good and cost should be low [16]. Carbonaceous materials, widely used in industry and ecology for pollutant removal (active carbon), gas separation (molecular sieves) and chemical reaction (catalysts and catalyst supports), usually meet most of these requirements. Carbonaceous materials are stable in acidic and basic media and the textural properties and chemical characteristics of these materials can easily be tailored.

The most interesting advantages of physical adsorption are that this method is [5-7]

- Not damaging enzymes or cells.
- Simple, cheap, and quick, no chemical changes of the support or enzymes
- Reversible, which allows regeneration with fresh enzymes or cells.

There are, however, some disadvantages to adsorptive immobilization

- Leakage of enzymes from the support, leading to contamination of the product.
- Formation of non-specific bonds between enzyme and support.
- Overload of the support.
- Steric hindrance by the support.

The most significant disadvantage is leakage of biocatalyst from the support, caused by desorption. This can occur under many circumstances, but environmental changes in pH, temperature, and ionic strength will usually promote desorption. Sometimes an enzyme/cell can desorb during reaction as a result of substrate binding, binding of contaminants, product formation, or other conditions leading to changes in protein conformation. Other factors that can lead to desorption are: shear forces or bubble agitation due to changing flows, particle-particle abrasion, and scouring effect of particles on vessel walls. However, desorption can be turned into an advantage if regeneration of the support is built into the operation cycle. In this case, rapid desorption of exhausted biocatalyst can be compensated by replacement with fresh enzyme.

Another problem of adsorption is non-specific binding. This can occur if substrate, product, or residual contaminants are charged, and interact with the support. The presence of these

unwanted substances can lead to diffusion limitations and reaction kinetics problems. Furthermore, binding of protons to the support can result in an altered pH microenvironment. This can pose problems for enzymes with precise pH optimum requirements. The third, frequently encountered problem is the formation of multiple enzyme layers on the support surface. Unless carefully controlled, overloading of the support will lead to decreased catalytic activity. Finally, the absence of a spacer between the enzyme and the support can produce problems related to steric hindrance.

5.1.2 Ionic adsorption

Ionic adsorption uses electrostatic forces to immobilize the enzyme onto a charged support material. Since enzymes consist of amino acids with ampholytic properties, the charge of the enzyme can be influenced by changing the pH. If a support material is used that has the opposite charge at the applied pH, fast and complete desorption will be established. Binding of enzymes with this method is influenced by the type of buffer, pH, ionic strength, and temperature [5,6]. Several derivatives of cellulose and Sephadex, as well as various ion-exchange resins and polyelectrolytes can be used as carrier material.

Compared to physical adsorption, the adsorption is faster and no desorption will occur under the same conditions. Usually, the enzyme activity of the immobilized enzyme is slightly higher than for physical adsorption [5-7].

5.1.3 Adsorption on monolithic supports

Adsorbing materials that are usually employed as filter materials in wastewater treatment and purification of product streams could also be used to deliberately attach biological materials for increased stability and re-use. Obviously, such adsorbent-supports must meet certain criteria. They must have a sufficient adsorption capacity, with respect to the enzyme or microorganism, and hold them firmly on the surface. They must also retain and stabilize the biological activity of the immobilized material at a relatively high level. Finally, operational characteristics (mechanical strength, hydrodynamics, resistance to degradation) must be good and cost should be low [17]. Carbonaceous materials, widely used in industry and ecology for pollutant removal (active carbon), gas separation (molecular sieves) and chemical reaction (catalysts and catalyst supports), usually meet most of these requirements. Carbonaceous materials are stable in acidic and basic media and the textural properties and chemical characteristics of these materials can easily be tailored. Carbon-ceramic composites offer a combination of the good properties of ceramic materials (mechanical strength, cellular structure, etc.) with those of carbon (high surface area, adjustable surface properties) [17]. Carbon coated monoliths can be produced by dipping the supports in a precursor solution [18,19] or by growing carbon filaments over deposited metal particles. The enzyme can be directly adsorbed onto the carbon layer. This method was successfully applied by Kovalenko *et al.* [16,17] to immobilize microorganisms onto carbon-coated monoliths

The practical approach to apply ionic adsorption for enzyme immobilization onto a monolith is slightly more complicated than for physical adsorption, because the polymeric carrier must be chemically attached to the support matrix. The monoliths need to be washcoated to create surface area and anchor sites for attachment of the carrier. The polymeric carriers can be attached via organo silane compounds that provide binding with Si-OH groups on one side and different functional groups (e.g. amine, epoxy, aldehyde) for binding with the enzyme on the other side. For both physical and ionic adsorption, the binding strength is relatively low compared to chemical attachment of the enzyme onto the monolith (covalent binding). In case of high shear forces or extreme reaction conditions (pH, temperature) covalent immobilization is usually the method of choice.

5.2 Covalent Immobilization

Covalent immobilization involves the formation of a covalent bond between the enzyme/cell and a support material. The covalent bond is normally formed between functional groups present on the surface of the support and functional groups belonging to amino acid residues on the surface of the enzyme. The most commonly used functional groups on the enzyme surface are [7]:

- The amino group (NH₂) of lysine and arginine
- The carboxyl group (COOH) of aspartic acid and glutamic acid
- The hydroxyl group (OH) of serine and threonine
- The sulfhydryl group (SH) of cysteine.

Many different types of support materials are available for covalent binding. The extensive range of supports reflects the fact that no ideal support exists. Therefore, the properties of the support must be taken into account when a given immobilization method is considered. An important property of the support material is the hydrophilicity [20]. Higher hydrophilicity of the support leads to higher immobilization efficiency and enzyme activity. Consequently, polysaccharide polymers, which are very hydrophilic, are popular support materials for enzyme immobilization. Also hydroxyl groups create an aqueous (hydrophilic) environment in the support by formation of hydrogen bonds with water molecules. Other popular supports for covalent immobilization are porous silica and porous glass, although these supports are less hydrophilic than the polysaccharide materials. Covalent immobilization is practically unlimited in different support-enzyme interactions. No method of immobilization is restricted to a particular type of support material, and an extremely large number of permutations are possible between methods of immobilization and support material. These variations can be achieved by chemical modification of normal functional groups on a support material to produce a range of derivatives. Thus, chemical modification increases the range of immobilization methods that can be used for a given support material.

It is very important to choose a method that will not inactivate the enzyme by reacting with amino acids at the active site. This will result in a deactivation of the enzyme. Generally, two steps are involved in covalent binding of enzymes to a support material. First, the functional

groups on the support material are activated by a specific reagent. Second, the enzyme is added in a coupling reaction to form a covalent bond with the support. Normally, the activation reaction in the first step is designed to make the functional groups on the support strongly electrophilic (electron deficient). In the following coupling reaction, these groups will react with strong nucleophilic (electron donating) groups of the enzyme, to form a covalent bond.

5.2.1 Reaction procedures of covalent immobilization

There are many different procedures for coupling an enzyme to a support via covalent bonding. Most reactions, however, can be placed in one of the following categories [5]:

- Formation of an isourea linkage
- Formation of a peptide bond
- Formation of a diazo linkage
- Alkylation reactions
- Carrier crosslinking

Examples of the first three methods are given in Figure 5.

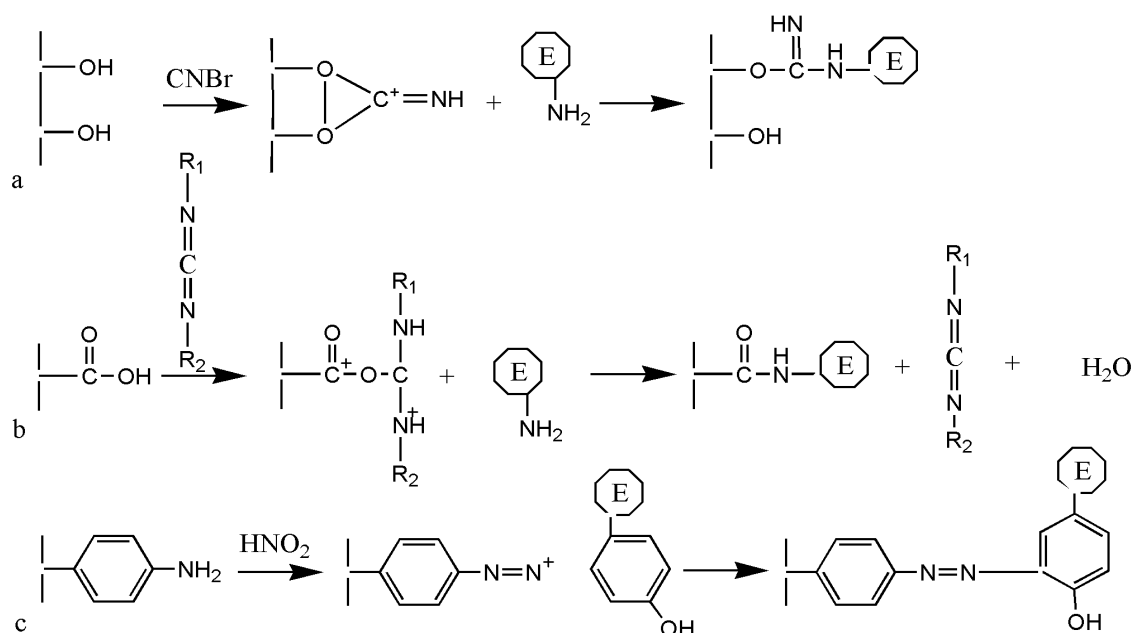


Figure 5. Examples of covalent bonding. a) formation of an isourea linkage, b) peptide bond formation, c) formation of a diazo linkage

If the desired covalent bond is an isourea linkage (Figure 5a), the functional groups on the support material should be the hydroxyl (OH) groups. A commonly used activator for the hydroxyl functional groups in polysaccharide supports is cyanogen bromide (CNBr). In the coupling reaction, enzyme amino groups and activated support groups are joined via an isourea linkage.

In the case of peptide bond formation (Figure 5b), the support should have a carboxyl (COOH) group. This carboxyl group is then activated by reaction with a carbodiimide. Subsequent reaction of the activated groups with NH₂ residues of N-terminal amino acids and/or lysine leads to the peptide bond.

If the support contains an aromatic amino (NH₂) functional group, it can be diazotised using nitrous acid (Figure 5c). Subsequent reaction with the ring structure of an aromatic amino acid, such as tyrosine or histidine, leads to the formation of a diazo linkage. Other amino acids such as lysine and arginine are also known to participate in this reaction.

Alkylation groups (for example (halogenated) cellulose or derivatives of ion exchange resins) on supports can easily react with amino groups, phenolic hydroxyl groups, and sulhydryl groups of the enzyme.

Supports and enzymes can also be crosslinked with bi- or multifunctional reagents. For example, amino groups on a support can be linked to amino groups of the enzyme with glutaraldehyde. Diisocyanates represent another group of crosslinking agents.

Although enzyme activity usually decreases upon chemical bonding and in general toxic chemicals and complicated procedures are involved, this method has some important advantages over other immobilization methods [21]:

- Effective for immobilization of a wide variety of enzymes
- Reproducible
- Strong bond, no enzyme leaching can take place
- Localization on the surface
- Increased (heat) stability [22]

Generally encountered drawbacks include [23]:

- Low immobilized activity due to deactivation as a result of chemical modification
- The strong bond restricts free movement, resulting in a decreased activity
- Usually complicated (expensive) multi-step procedures
- Toxic reagents are usually involved
- Covalent immobilization is not reversible

5.2.2 Covalent immobilization on a monolithic support

This protocol is expected to be convenient for attachment of enzymes onto monolithic supports. In general, covalent binding is used to attach proteins to silica carriers [8,24-30]; therefore the protocol can easily be translated for use with silica-coated monoliths. The enzyme is attached to a spacer that can be placed on a surface with silanol groups. Monoliths can be washcoated with a silica layer to provide surface area and binding sites for different functional organo silane compounds. These organo silanes can be used directly for enzyme attachment or can be chemically activated to utilize a different functional group of the enzyme. The most common approach to couple enzymes to silica surfaces, the α -aminopropyltriethoxysilane (APTES)-glutaraldehyde protocol, was already used in the 70s by

many researchers in an attempt to bind trypsin to controlled-pore glass and capillaries. [23-25,15]. Additionally, some covalent methods were selected that bind the enzyme via another functionalization agent, 3-(glycidopropyl)trimethoxysilane (GPTMS).

5.3 Crosslinking

Crosslinking is the support-free variant of covalent immobilization. This type of immobilization involves joining the cells or enzymes to each other to form a three-dimensional complex structure. Depending on the state of the enzyme before crosslinking, CLEAs (Crosslinked Enzyme Aggregates) or CLECs (Crosslinked Enzyme Crystals) can be made. This method is generally used to prepare highly purified enzyme systems. The most common reagent used for cross-linking is glutaraldehyde. Cross-linking reactions are carried out under relatively severe conditions. These harsh conditions can change the conformation of active centre of the enzyme and so may lead to significant loss of activity. This can be achieved by chemical or physical methods [31]. Chemical methods of crosslinking normally involve covalent bond formation by means of a bi- or multifunctional reagent. Examples of such reagents include glutaraldehyde, and toluene diisocyanate. The toxicity of these reagents is a limiting factor in applying this method to living cells and many enzymes. Both albumin and gelatin have been applied as spacers. The use of spacers minimizes the close proximity problems caused by crosslinking a single enzyme.

Physical crosslinking of cells by flocculation leads to high cell densities, and is therefore a well-known technique in biotechnology industry. Flocculating agents such as polyamines, polyethyleneimine, polystyrene sulfonates, and various phosphates, have been used extensively. Crosslinked enzyme usually is very stable during operation and because it consists of 100% protein a high catalyst productivity and space-time yield can be obtained [32]. An important advantage of this method is that it is relatively simple and cheap. Problems that can be encountered with this method include possible reaction with amine-groups in the active site, possible reduced accessibility, and production of too many crosslinks, which will ultimately minimize conformational freedom of the individual enzymes and thereby reduce the immobilized activity. Furthermore, crosslinking is rarely used as the only means of immobilization, due to poor mechanical stability and the poor stability. Therefore, this method is often used to enhance other methods of immobilization.

5.3.1 Crosslinking onto a monolithic support

Monoliths could in principle be used to increase the stability and mechanical strength of crosslinked enzymes. Because the protein density with this method is relatively high (immobilizations are carried out at high enzyme concentrations) a high immobilization yield should be obtained by attaching crosslinked enzymes onto a monolith. Possible problems could be deactivation due to the presence of chemical reagents. Two possible approaches can be used:

- Direct growth of a layer of crosslinked enzyme on the monolith surface by adding the functionalized support during the crosslinking reaction.
- Attachment of crosslinked enzyme to a monolith by adding the functionalized monolith backbone after crosslinking is completed.

5.4 Entrapment

The entrapment method of immobilization is based on the localization of an enzyme within the lattice of a polymer matrix or membrane. It can be classified into lattice and micro capsule types. Immobilization by entrapment differs from adsorption and covalent binding in that enzymes are free in solution, but restricted in movement by the structure of a gel [33]. Lattice type entrapped enzymes are present in a gel matrix from polysaccharides, proteins or synthetic polymers. Microcapsule type-biocatalysts are entrapped within microcapsules of semi permeable synthetic polymers. To ensure that the structure is tight enough to prevent leakage of enzymes, yet at the same time to allow free movement of substrate and product, the porosity of the gel lattice can be controlled. Inevitably, the support will act as a barrier to mass transfer. This can have a negative effect on reaction kinetics, but can also prevent interaction of the biocatalyst with harmful cells, proteins and enzymes. The advantages of the entrapping methods are that not only single enzymes but also several different enzymes, cellular organs, and cells can be immobilized with essentially the same procedure. The enzymes are not chemically modified, leading to really full utilization of the enzyme activity and the presence of the gel eliminates the effect of proteases and enzyme inhibitors of high molecular mass. However, some important drawbacks are:

- Diffusion problems for substrates of high molecular mass
- Supports are not renewable

5.4.1 Lattice type entrapment

The lattice type immobilization is most widely applied. There are several methods of entrapment in a gel matrix [2,3]:

- Ionotropic gelation of macromolecules with multivalent cations (e.g. alginate).
- Temperature induced gelation (e.g. agarose, gelatin).
- Organic polymerization by chemical/photochemical reaction (e.g. polyacrylamide).
- Precipitation from an immiscible solvent (e.g. polystyrene).

Ionotropic gelation consists of mixing an enzyme with a polyionic polymer material, followed by crosslinking the polymer with multivalent cations in an ion-exchange reaction. In the second step, a lattice structure is formed, that traps the enzymes or cells.

Temperature change is a relatively simple method of gelation by phase transition, using 1-4% solutions of agarose or gelatin. However, the gels are usually soft and unstable. A significant development in this area has been the introduction of κ -carrageenan polymers [34] that can

form gels by ionotropic gelation and by temperature induced phase transition. This has increased the degree of flexibility in gelation systems for immobilization.

Entrapment by organic polymerization proceeds by a chemical polymerization reaction. The enzyme-monomer mixture is polymerized to form a 3-dimensional crosslinked polymeric network. A crosslinking agent is added during polymerization to form the crosslinkages between the polymer chains. The enzyme is trapped in the interstitial spaces of the lattice. The pore size of the gel and its mechanical properties are determined by the relative amounts of monomer and crosslinking agent. It is therefore possible to influence the lattice structure by varying these concentrations. Recently, entrapment in sol-gel matrices has become of interest for immobilization of enzymes for use in organic solvents [35-36].

Precipitation occurs by phase separation rather than by chemical reaction. A major drawback of this method is the need to contact the enzyme with a water-miscible organic solvent. Since most cells/enzymes are not resistant to such solvents, precipitation is limited to highly stable or stabilized enzymes and nonliving cells.

5.4.2 Encapsulation

Microcapsule-type entrapping involves enclosing the enzymes within semi permeable polymer membranes. The advantage of this method compared to lattice type entrapment is the absence of diffusion problems. An important drawback is the difficult separation from the reaction medium. In principle, a reactor system with free enzyme that is contained inside a membrane could be classified as encapsulation at the macro-scale. In this reactor, the separation is less problematic, but these membranes are often sensitive to fouling and/or clogging.

5.4.3 Entrapment in a gel on a monolithic support

Encapsulation requires the free movement of encapsulated enzyme, and can therefore not be used in combination with a monolithic support. Entrapment in a gel layer that is applied following the general procedures for washcoating of a monolithic support could be a very interesting alternative for the conventional particulate carriers for entrapment. Monoliths could be washcoated and functionalized first, to chemically attach the gel layer to the monolith, but gel washcoats could also be directly applied on the monolith channels. If a sufficiently thin gel layer can be applied, diffusion problems can be minimized compared to the generally larger (~1 mm) gel beads. Also mechanical strength and separation efficiency can be improved using a monolithic support for gel entrapment. Since the gel lattice is in general only suitable for immobilization of larger catalysts (whole cells or microorganisms) a chemical modification is needed to retain the enzymes inside the gel. In a preliminary stage of the research, sol-gel entrapment was also studied for use on a monolithic support. The main problems of this technique arise from the two-step procedure that is needed to apply a sol gel-coating on a monolithic support. Poor control over the pH inside the channels leads to a sol-gel that is too dense to provide sufficient accessibility for reactants/products. This did not lead

to active biocatalysts and sol-gel entrapment was not considered a suitable technique for use in combination with monoliths. For immobilization of enzymes onto a monolithic support, a combination of crosslinking and entrapment will be used.

6 Industrial enzyme catalysis

In this paragraph an overview of some important biocatalytic processes will be given with a description of the used enzyme. In addition to final yield, which determines the overall efficiency of the process, systems with enantiomeric products are characterized by an important parameter; *ee* or enantiomeric excess. This parameter is the measure of enantiomeric purity of a mixture of enantiomers, given by:

$$ee = \frac{\text{moles of enantiomer } A - \text{moles of enantiomer } B}{\text{total moles}} \quad (10)$$

6.1 Lipase

Lipases (triacylglycerol ester hydrolase, EC 3.1.1.3) catalyze the breakdown of fats and oils with subsequent release of free fatty acids, diacylglycerols, monoacylglycerols and glycerol [37]. These enzymes are distributed among higher animals, microorganisms and plants in which they fulfill a key role in the biological turnover of lipids. Despite differences in size, sequence homology, substrates, activators, inhibitors, and other properties, most often adopt a similar core topology, known as the α/β hydrolase fold. The interior topology of α/β hydrolase fold proteins is composed largely of parallel β -plated strands (at least five in lipase), separated by stretches of α -helix, and forming an overall super helically twisted-plated sheet. Helical peptide sections packed on both faces of this sheet form much of the outer surface of the protein.

Lipases have been traditionally defined as enzymes “capable of hydrolyzing esters of oleic acid” [38]. The definition of a lipase as a hydrolytic enzyme originated primarily from its physiological function of triglyceride hydrolysis. Later it was recognized that the enzymes are effective catalysts both for ester hydrolysis and the reverse reaction of synthesis. This has resulted in a lot of applications to synthetic organic chemistry. Additionally, lipases are capable of catalyzing transesterification (acidolysis, interesterification, alcoholysis), aminolysis, and thioesterification in anhydrous organic solvents and biphasic systems. The ability of lipases to accept not only water, but also other nucleophiles such as alcohols, amines, thiols, and more, implies a vast synthesis potential with these enzymes. Moreover, lipases are in general also stable and active in organic solvents. Understanding the catalytic cycle of lipases has been of significant importance to their widespread use in different biotechnological applications. The lipase active site is composed of three different residues: serine, histidine and aspartate or glutamate.

The hydrolysis of an ester involves an acyl-enzyme complex. The catalytic cycle starts by nucleophilic attack of the hydroxyl group of the serine side chain on the carbonyl carbon atom of the ester bond (1 in Figure 6) and release of the alcohol (Y-OH). The complex is resolved by the nucleophilic attack of water (or any other nucleophile that is present, see 2 in Figure 6), the product is liberated and the enzyme is regenerated (3).

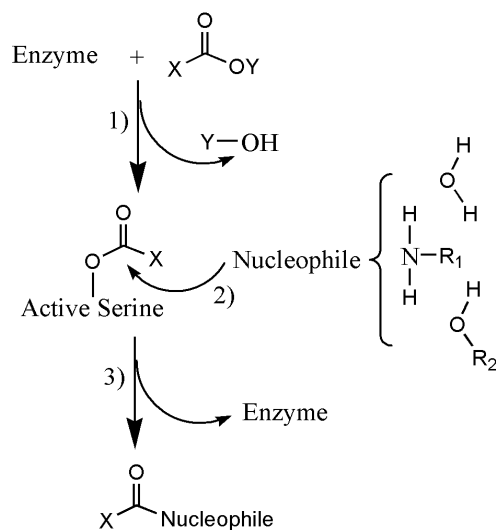


Figure 6. Reaction mechanism of lipase biocatalysis showing (1) the nucleophilic attack of serine on the carbonyl carbon atom of the ester and liberation of the alcohol, (2) a second nucleophilic attack, and (3) regeneration of the enzyme.

As lipases are active in organic solvents, water can be replaced by other nucleophiles such as alcohols. The result of this reaction is a transesterification. For racemic alcohols only one enantiomer may be acylated, thereby leading to enantioselective transformations. Suitable acyl donors are vinyl esters, anhydrides or diketene. The reaction is irreversible and the separation of the remaining alcohol and the newly formed ester is simple. This principle is now used in many reactions to produce enantiomerically pure alcohols.

6.1.1 Industrial application of lipase

BASF (Germany) has several biotechnological processes for the large-scale manufacture of a number of important optically active building blocks and their derivatives. The company has recently extended its chiral synthesis capabilities to the enzymatic resolution of racemic alcohols. A broad range of enantiomerically pure alcohols can now be formed from a mixture of enantiomers (Figure 7a). Only one of the enantiomers is used by the lipase, and subsequently converted. The product can now easily be separated for the unreacted alcohol.

Amines might also be used as nucleophiles. Racemic amines are efficiently resolved using ethylmethoxyacetate as acylating agent (Figure 7b). Excellent yields and selectivity and minimal amounts of enzyme characterize this new process, which has been used by BASF since 1993. The products, the R-amide and the S-amine, can be recovered and separated by distillation and have high chemical and optical purities. This process is applicable to a broad

spectrum of amines, which are of considerable interest as chiral building blocks or as auxiliaries for the syntheses of bioactive ingredients.

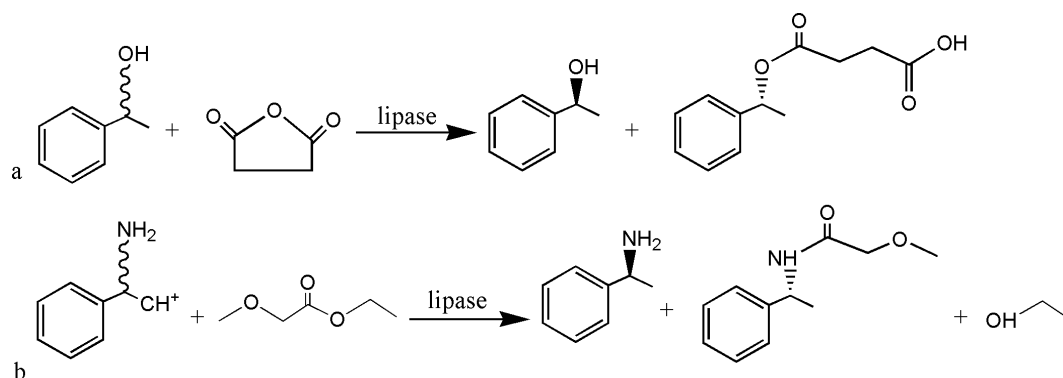


Figure 7. Recently developed biocatalytic systems at BASF. Lipases are successful biocatalysts used in the synthesis of a) enantiomerically pure alcohols, and b) chiral amines by selective reaction of a mixture of enantiomers. One of the enantiomers is converted, giving two different products

As an example, the production of 1-phenylethylamine/phenylethylmethoxyamide at the Ludwigshafen site can be considered. This is a carboxylic ester hydrolysis.

An immobilized lipase (polyacrylate beads) is used at pH 8-9 at 298 K in methyl tert-butyl ether. Final conversion of this 100 t/a process is around 50%, with a yield of >90% and an *ee* of >99%. The products are intermediates for pharmaceuticals and pesticides

6.2 Lactase

Galactosidases (EC 3.2.1.23) catalyze the enzymatic hydrolysis of lactose to glucose and galactose. These enzymes are widely distributed in nature, appearing in micro-organisms, plants and animal tissues [39]. The lactase from *Aspergillus oryzae* has an optimum pH of 4.5 and an approximate diameter of 12 nm. The molecular mass was found to be 126 kDa [40]

The hydrolysis of lactose is a promising process in the food industry for the development of new products without lactose in their composition. Lactose is the main carbohydrate in milk and whey (at a concentration between 50 and 100 g l⁻¹, depending on the source of milk). The consumption of foods with a high lactose content is problematic for almost 70% of the world population, as the enzyme that is naturally present in the human intestine loses its activity during a person's lifetime [41]. Together with the relatively low solubility and sweetness of lactose, this has led to an increasing interest in the development of industrial processes to hydrolyze lactose. Moreover, lactose has a high BOD (Biological Oxygen Demand), its disposal means the pollution of aquatic environments. Hydrolysis of lactose is a way to recycle the whey, using it as a source to obtain additives for human or cattle feeding [39].

6.2.1 Industrial application of lactase

The hydrolysis of lactose can be performed by acids or acid resins or by enzymatic treatment (Figure 8). The use of acids is not adequate to hydrolyze lactose in milk and whey due to the

generation of nasty flavors, odors, and colors during the process and the reduction in nutritional properties of milk. When the enzymatic treatment is performed with β -galactosidases as catalyst, the taste of milk is only changed to a sweeter one (glucose and galactose are four times sweeter than the lactose) and the development of lactose crystals in refrigerated products is avoided.

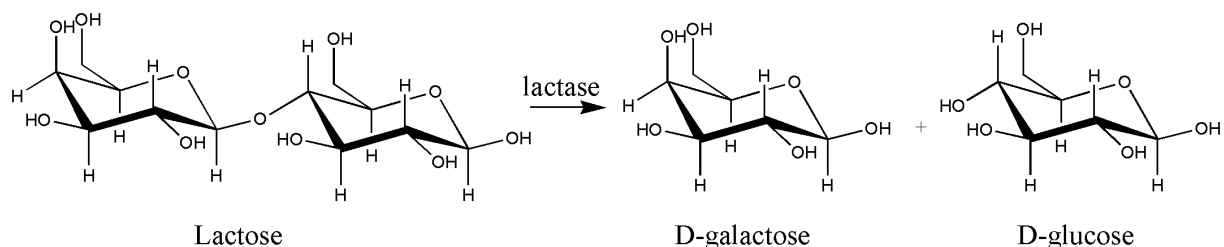


Figure 8. Lactose hydrolysis to D-glucose and D-galactose

A second advantage is the occurrence of a side reaction: the synthesis of galacto-oligosaccharides, which are carbohydrates able to promote the growth of beneficial bacteria in the intestine [42]. However, there are some drawbacks such as the lower hydrolysis rate and the higher cost of the enzyme [43]. The low stability of these enzymes is a technical problem that is usually overcome by injecting an enzyme dose in each brick of milk and letting the hydrolysis proceed between the packing and the consumption of the milk. Continuous processes are still being studied and developed [39]. Large-scale hydrolysis is performed at different sites. Sumitomo, Snow Brand, and Central del Latte run a continuous process in a plug flow reactor. At 308 K, lactose is hydrolyzed by immobilized lactase to 70-80% conversion. The kinetics of this reaction can be described by a Michaelis-Menten model with competitive product inhibition by galactose [44-46]. The reactor volume can be as large as 250 m³. Central de Latte has a production capacity of 8000 l d⁻¹.

6.3 Trypsin

Trypsin (E.C. 3.3.21.4) is a proteolytic enzyme that hydrolyzes peptide bonds on the carboxyl side of the amino acids arginine and lysine. Additionally, the enzyme splits off the amide and ester groups (in case of a terminal position) of both amino acids. Reactivity increases in the order peptide<amide<ester. Trypsin is one of the three principal digestive proteinases, the other two being pepsin and chymotrypsin. The enzyme is produced in the pancreas as an inactive precursor (trypsinogen). After the enzyme arrives in the stomach, the N-terminal part of the pro-enzyme is split off, yielding the active enzyme. Bovine trypsin consists of 223 amino acids and has a molecular mass of 24 kDa. The diameter of this enzyme is around 4-5 nm.

6.3.1 Industrial application of trypsin

Trypsin has a wide range of industrial and scientific uses. Trypsin is used in biotechnological applications, especially in the cultivation of mammalian cells. Trypsin is also used as a

protein-degrading enzyme in the processing of trypsin insensitive biopolymers, in detergent manufacturing, and in leather tanning.

6.4 Penicillin acylase

Penicillin amidohydrolase (E.C. 3.5.1.11) is the official name for penicillin acylase or penicillin amidase [47,48]. Penicillin acylases catalyze the hydrolysis of an amide bond between a carboxylic acid and a β -lactam nucleus while leaving the β -lactam intact (Figure 9).

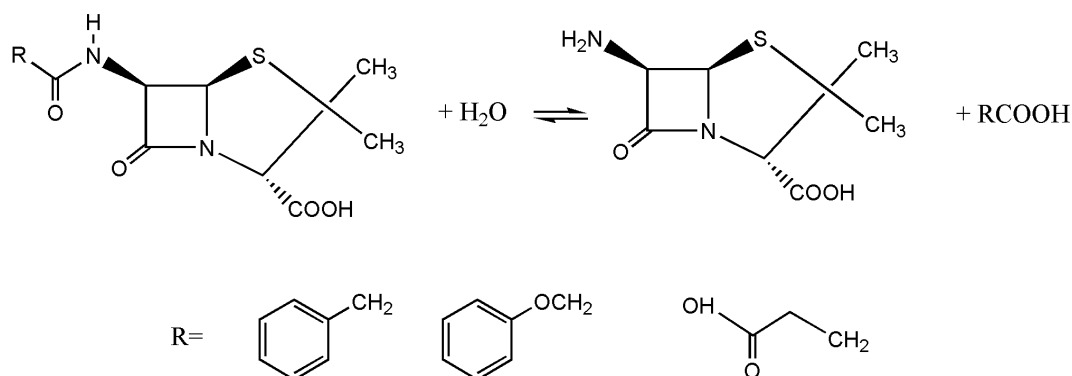


Figure 9. Reaction catalyzed by penicillin G acylases (R=benzyl), penicillin V acylases (R=phenoxyethyl) and glutaryl acylases (R=carboxypropyl). Also cephalosporin nuclei can be accepted in place of 6-APA

Penicillin acylase is an intracellular enzyme produced by several microorganisms, including various bacteria, fungi and yeasts. The biological role of this enzyme is not known, but it has been suggested that it may play a role in metabolism of phenyl acetic acid derivatives as a carbon source. The enzyme produced by *E. coli* is a heterodimer with a small α -subunit of 23 kDa and a large β -subunit of 63 kDa. The protein has approximate dimensions of 7.5·5·5 nm. The isoelectric point for penicillin acylase has been reported to be between pH 6-7.

6.4.1 Industrial application of Penicillin G acylase

Penicillin acylase from *E. coli* is the best-studied penicillin acylase with respect to the synthesis of semi-synthetic antibiotics. The introduction of semi-synthetic β -lactam antibiotics in the early 1960s initiated a development that would make the β -lactam nucleus in the form of 6-aminopenicillanic acid (6-APA) a major pharmaceutical intermediate [49]. Two other very important β -lactam cores were discovered shortly after. These nuclei, 7-ACA and 7-ADCA are presented in Figure 10.

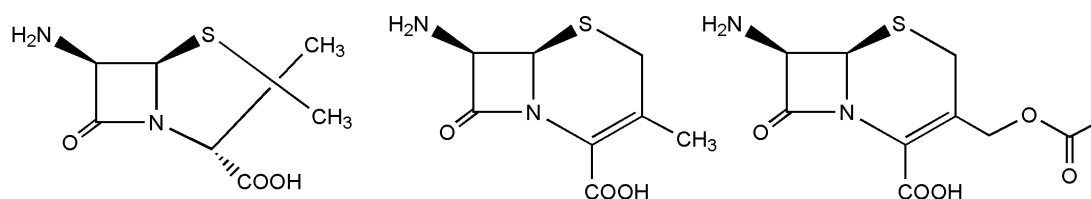


Figure 10. Major nuclei for semi-synthetic antibiotics [47]

6-APA is prepared by direct hydrolysis of Penicillin G, whereas 7-ADCA is prepared from oxidized Penicillin G. 7-ACA can be made from Cephalosporin C (another natural antibiotic). At DSM Anti-infectives, Penicillin G Acylase is used in the production of several antibiotics. The kinetically controlled enzymatic synthesis of β -lactam antibiotics from different β -lactam nuclei is presented in Figure 11.

An important drawback of the kinetically controlled synthesis is the accompanying hydrolysis of the side-chain donor, as well as the product. This can be solved by adding an excess of the side-chain donor, but this leads to more laborious downstream processing [48]. The use of immobilized enzyme preparations tends to increase the hydrolysis rate even further, due to internal diffusion limitations. Inside the carrier, reactant depletion (and subsequent product accumulation) leads to hydrolysis of the product. The combined effect of primary hydrolysis of the side-chain donor and secondary hydrolysis of the product inside the enzyme carrier were initially of such a magnitude that the industrial synthesis of β -lactam antibiotics continued to depend on chemical procedures [47].

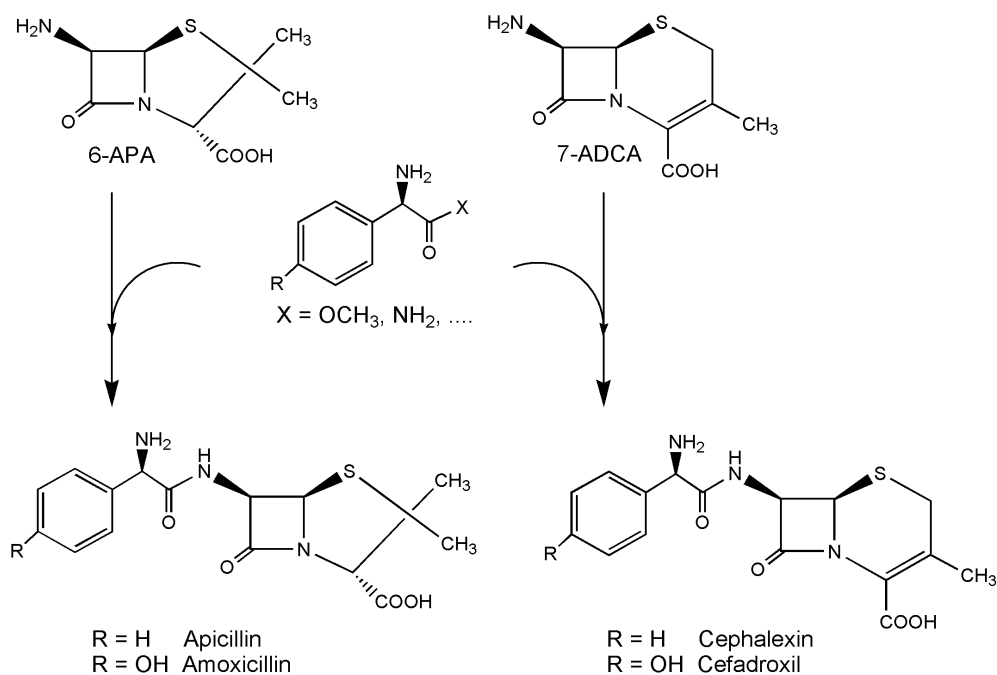


Figure 11. Penicillin G acylase catalyzed synthesis of β -lactam antibiotics [49]

Only after a breakthrough in finding the appropriate carrier material and adjusting the process conditions, the enzymatic yield was drastically improved. In combination with the availability of cheap industrial enzymes, and the acceptance of enzymes by organic chemists as part of their tool box [47], in the mid 1980s biocatalysis became the method of choice for production of several intermediates and products.

6.5 Other industrial immobilized enzymes

The Coca-Cola Company uses a peptide bond hydrolysis for the production of phenylalanine as sweetener in their “light”-products. At pH 7.5, 298 K the solubilized *Subtilisin carlsberg* (hydrolase) is used in a CSTR with a yield of 73% and an *ee* of 95% [50].

The low-calorie sweetener aspartame (L- α -aspartyl-L-phenylalanine methyl ester) is produced on a kiloton scale by Holland Sweetener Company, a joint venture of Tosoh and DSM [50]. The aspartame process uses a proteolytic enzyme, thermolysin, to catalyze the formation of the dipeptide from N-protected L-aspartic acid and D/L-phenylalanine methyl ester.

DSM has a long history in biocatalysis, starting with the enzymatic resolution of D/L-phenylglycinamide into D-phenylglycinamide and L-phenylglycine using hog-leucine aminopeptidase and an L- α aminoacyl-amidase from *Pseudomonas putida*. Currently, DSM uses biocatalysis, biotransformation and fermentation technologies in addition to chemical methods to produce advanced intermediates for the custom manufacturing arena. The oldest biocatalytic process at DSM is propane oxirane production from glycidate. This carboxylic ester hydrolysis is performed in a batch reactor with an immobilized lipase. Propane oxirane can be converted into (S)-beta blockers.

The Swiss custom-manufacturing company Lonza specializes in the production of many chemical compounds, including N-heterocycles. Lonza has developed a series of biocatalytic routes for the production of certain functionalized N-heterocycles where chemical synthesis is inefficient.

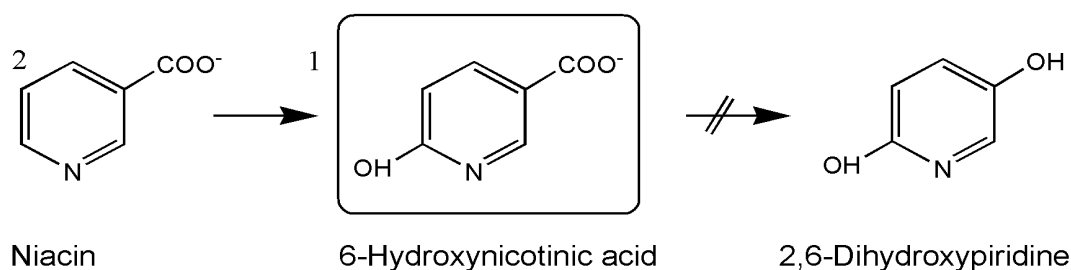


Figure 12. Catabolic pathway for the production of 6-hydroxynicotinic acid with *Achromobacter xylosoxidans* LK1 [50].

6-Hydroxynicotinic acid (1 in Figure 12), a derivative of niacin (2 in Figure 12), serves as a versatile building block predominantly in the synthesis of modern insecticides. The chemical synthesis of 6-substituted niacin results in the formation of by-products, which make the cost prohibitively high. Lonza has detected microorganisms growing on niacin capable of accumulating up to 65 g l⁻¹ 6-hydroxynicotinic acid at an overall yield of 90%. Remarkably, at niacin concentrations greater than 10 g l⁻¹ the second enzyme of the pathway (6-hydroxynicotinate hydroxylase) is strongly inhibited, whereas the niacin hydroxylase remains unaffected. This means that the second reaction does not proceed (Figure 12).

7 Symbols

C_i	concentration component i	[mol m ⁻³]
e	total enzyme concentration	[-]
ee	enantiomeric excess	[-]
k_i	reaction rate constant of reaction i	[mol s ⁻¹]
K_m	Michaelis Menten constant	[mol m ⁻³]
K_s	substrate constant	[mol m ⁻³]
r	reaction rate	[mol m ⁻³ s ⁻¹]
r_{free}	reaction rate of the free enzyme	[mol m ⁻³ s ⁻¹]
r_{immob}	reaction rate of the immobilized enzyme	[mol m ⁻³ s ⁻¹]
t	time	[s]
V_{max}	maximum rate	[mol m ⁻³ s ⁻¹]

Greek symbols

η	efficiency	[-]
--------	------------	-----

Compounds

E	enzyme
ES	enzyme-substrate complex
P	product
S	substrate

8 References

- [1] T. Bugg (1997) An introduction to Enzyme and Coenzyme Chemistry. Blackwell Science Ltd, Oxford, Great Britain
- [2] P. Gemeiner (1992). In Enzyme Engineering: Immobilized Biosystems; Gemeiner, P., Ed.; Ellis Horwood Limited
- [3] S. de Vries, A.J.J. Straathof, J.A. Jongejan (2000) Enzyme Technology, Kluwer Laboratory for Biotechnology, Faculty of Applied Sciences, Delft, the Netherlands.
- [4] U. Kragl, W. Kruse, W. Hummel, C. Wandrey (1996) Biotechnology and Bioengineering; 52: 309-319
- [5] T. Sato, T. Tosa (1999) Encyclopedia of Bioprocess Technology, Wiley and Sons, Inc. Vol 2: 1062-1064
- [6] Ullmann's Encyclopedia of Industrial chemistry (1987) 5th, completely revised Edition Vol A9, VCH, Germany: 344-505
- [7] J. Woodward (1985). Immobilised enzymes: Adsorption and covalent coupling, ed. J.Woodward, IRL Press Ltd, Oxford, Great Britain

- [8] A.M. Klibanov (1997) *Trends in Biotechnology*; 15: 97-101
- [9] E. Katchalski-Katzir (1993) *Trends in Biotechnology*; 11: 471-478
- [10] K. Faber, M.C.R. Franssen (1993) *Trends in Biotechnology*; 11: 461-477
- [11] F. Secundo, G. Carrea (2002) *Journal of Molecular Catalysis B: Enzymatic*; 19: 93-102
- [12] G. Carrea, G. Ottolina, S. Riva (1995) *Trends in Biotechnology*; 13: 63-70
- [13] N. Grubhofer, L. Schleith (1953) *Naturwissenschaften*; 40: 508
- [14] Ullmann's Encyclopedia of Industrial chemistry (1987) 5th, completely revised Edition Vol A9, VCH, Germany: 199-213
- [15] J. Halgas, *Studies in Organic Chemistry* 46; *Biocatalysts in Organic Synthesis*, 1st ed., Amsterdam, (1992) pp. 7-33
- [16] G.A. Kovalenko, E.V. Kuznetsova, Yu.I. Mogilnykh, I.S. Andreeva, D.G. Kuvshinov, N.A. Rudina (2001) *Carbon* 39; 1033-1043
- [17] G.A. Kovalenko, O.V. Komova, A.V. Simakov, V.V. Khomov, N.A. Rudina (2002) *Journal of Molecular Catalysis A: Chemical*; 182-183: 73-80
- [18] E. Crezee (2003) PhD thesis, Delft University of Technology, The Netherlands
- [19] Th. Vergunst, F. Kapteijn, J.A. Moulijn (1998) *Studies in Surface Science and Catalysis*; 118: 175-183
- [20] G. Bickerstaff, Ed. (1997) *Immobilization of enzymes and cells, methods in Biotechnology* vol.1, Humana Press, Totowa New Jersey
- [21] J.M. Bolivar, L. Wilson, S.A. Ferrarotti, J.M. Guisan, R. Fernandez-Lafuente, C. Mateo (2006) *Journal of Biotechnology*; in press
- [22] T. Godjevargova, R. Nenkova, N. Dimova. (2005) *Macromolecular Bioscience* 5: 760-766
- [23] M. Arroyo, J.M. Sanchez-Montero, J.V. Sinisterra (1999) *Enzyme and Microbial Technology*; 24: 3-12
- [24] H.H. Weetall (1969) *Science* 166: 615-616
- [25] M. Ladero, A. Santos, F. Garcia-Ochoa (2000) *Enzyme and Microbial Technology* 27: 583-592
- [26] M. Narshima Rao, A.A. Kembhavi, A. Plant (2000) *Biotechnology Letters* 22: 1557-1559
- [27] H.H. Weetall, G. Baum (1970) *Biotechnology and Bioengineering*; 12: 399-407
- [28] J. Rogalski, J. Szczodrak, M. Pleszcynska, J. Fiedurek (1997) *Journal of Molecular Catalysis B: Enzymatic* 3:271-283
- [29] H.H. Weetall, N.B. Havewala. (1972) *Biotechnology and Bioengineering Symposium* nr 3 241-266
- [30] C. Horvath, B.A. Solomon (1972) *Biotechnology and Bioengineering*; 14: 885-914
- [31] G.H. Broun, G. Manecke, and L.B. Wingard, Jr. eds. *Enzyme engineering*, Vol. 4, Plenum Publishing Corp. New York, United States
- [32] R.A. Sheldon, F. van Rantwijk (2004) *Australian Journal of Chemistry*; 57: 281-89
- [33] G.F. Bickerstaff (1995) *Genetic Engineering Biotechnologist*; 15: 13-30
- [34] K.H. Jang, S.J. Jung, H.S. Chang, U.H. Chun, (1996) *Journal of Microbiology and*

- Biotechnology; 6; 36-carrageenan
- [35] M.T. Reetz (2002) *Current Opinion in Chemical Biology*; 6: 145-150
- [36] J-P. Chen and W-S. Lin (2003) *Enzyme and Microbial Technology*; 32: 801-811
- [37] P. Villeneuve, J.M. Muderhwa, J. Graille, and M.J. Haas (2000) *Journal of Molecular Catalysis B: Enzymatic*; 9: 113-148
- [38] J.S. Dordick (1991) *Biocatalysts for Industry*, 1st ed., New York 193-213.
- [39] V. Gekas, M. Lopez-Leyva (1985) *Process Biochemistry*; 20: 2-12
- [40] F. Widmer, J-L. Leuba (1979) *European Journal of Biochemistry*; 100: 559-567
- [41] M. Richmond, J. Gray, C. Stime (1981) *Journal of Dairy science*; 64: 1759-1771
- [42] R.R. Mahonay (1998) *Food Chemistry*; 63: 147-154
- [43] G. Mooser, in P.D. Boyer (ed) *The Enzymes* (1992), Academic Press, New York, United States: 187-233
- [44] N. Papayanakos, G. Markas, D. Kekos (1993) *Chemical Engineering journal*; 52: B1-B12
- [45] A. Santos, M. Ladero, F. Garcia-Ochoa (1998) *Enzyme and Microbial Technology*; 22: 558-576
- [46] C.R. Carrara, A.C. Rubiolo (1996) *Process Biochemistry*; 31: 243-248
- [47] A. Bruggink (ed) *Synthesis of β -lactam antibiotics: Chemistry, biocatalysis & Process Integration* (2001) Kluwer Academic Publishers, Dordrecht, the Netherlands
- [48] A. Parmar, H. Kumar, S.S. Marwaha, J.F. Kennedy (2000) *Biotechnology Advances*; 18: 289-301
- [49] A.I. Kallenberg, F. van Rantwijk, R.A. Sheldon (2005) *Advanced Synthesis and Catalysis*; 347: 905- 926
- [50] A. Tanaka, T. Tosa, T. Kobayashi (1993) *Industrial Application of Immobilized Biocatalysts*, Marcel Dekker, Inc. New York, United States

Part II: Preparation and characterization

Preconditioning of monolithic structures

Abstract

Two commonly used washcoating methods were assessed for two types of monoliths with a different microstructure. The influence of several parameters on the final washcoat properties was studied. Silica and alumina washcoats were applied by the slurry coating method and by dipcoating in colloidal solutions.

Application of these methods on monoliths with different microstructure, yields support-washcoat combinations with significantly different properties. On cordierite, slurry coating mainly produces a layer that covers the channels, whereas pore filling provides a layer that actually adheres to the complete surface of the monolith microstructure. No severe effects of washcoat hold-up were observed for cordierite carriers. By using α -alumina as an intermediate layer, internal diffusion problems inside the washcoat layer can be prevented. The open frontal area however, decreased by this method.

For Advanced Ceramic Material (ACM) supports, slurry coating fills the highly porous wall. The loading capacity increases in the order ACM-S < ACM-M < ACM-L. Pore filling with concentrated solutions also led to the plugging of the walls of ACM monoliths. With lower concentrations, a homogeneous thin layer was observed, covering the micrograins. Different carrier-washcoat combinations were explored. Application of a specific method to deposit an active material depends on the kinetics, the applied conditions in the final process and the mode of operation for ACM monoliths.

1 Introduction

The monolithic reactor is the most widely used catalytic system for environmental applications [1]. Compared to other structured materials, such as the Sulzer packing, the industrial experience with Sulzer-packings may surpass that of monoliths, but monoliths definitely have some important advantages [2]. The porous ceramic material for instance is easier to apply as catalyst support than the conventional metallic packings and in general ceramic monoliths are more attractive with respect to production costs (due to large scale production for automotive industry). For application of a ceramic honeycomb, the requirements for the support depend on the type of application. In this study, two different ceramics are used: cordierite (magnesia, silica, and alumina, 2:5:2) and mullite (mixed oxide of silica and alumina, 2:3). Cordierite is commonly used for automotive catalysts, because it has a high mechanical strength, high temperature resistance and can endure large temperature shocks. The main disadvantages of these ceramic materials are their low specific surface area (typically $0.7\text{-}2\text{ m}^2\text{ g}^{-1}$) and the low catalyst-support interaction. For industrial application, carbon, silica or alumina honeycombs would be much more attractive with respect to surface area ($200\text{ m}^2\text{ g}^{-1}$) and surface functionality. However, the mechanical strength of these materials is significantly lower. To combine the advantages of monolithic supports (open structure, high mechanical strength) with those of conventional catalyst supports (high surface area, higher support-catalyst interaction) thin coat layers can be deposited on the monolith channel walls. Commonly used washcoats include silica [3,7,8], α -alumina [9] γ -alumina [9,10] and carbon [10-14]. Ready-made catalysts that do not need a specific support material, such as zeolites can be deposited directly onto the monolith wall [4,5].

For gas phase application, the washcoat layers have a thickness in the order of tens of microns. For liquid phase application, the optimum might be different. To avoid concentration gradients in the catalyst, thin, porous layers are required [10].

In this study, two commonly used washcoating methods will be used for the preparation of various monolith-washcoat combinations [3]. The macroporous structure of the ceramic supports provides anchoring for the washcoat. Two different approaches can be used. The support can be (partly) filled with a washcoat material (pore filling) or a thin layer can be applied on the pore structure (slurry coating). Pore filling is usually done with a colloidal solution of the washcoat material, and because it will also be applied to coat non-porous material it will be referred to in this work as washcoating with colloidal solutions. This method results in a strong interaction between monolith and coat layer, due to anchoring inside the pores. The amount of coating that can be deposited is limited to the macro pore volume of the support. In case of a non-porous carrier, a thin layer will be deposited on the surface. Slurry coating is generally done by coating with a suspension of particles (typically $5\text{ }\mu\text{m}$). This method has the advantage that relatively high loadings can be achieved.

In Figure 1, SEM images of the bare support materials are depicted. Cordierite is a dense material with large macro pores throughout the walls. These macro pores vary in size from $1\text{-}20\text{ }\mu\text{m}$ (Figure 1a). At higher magnification (Figure 1b) a layered structure is visible.

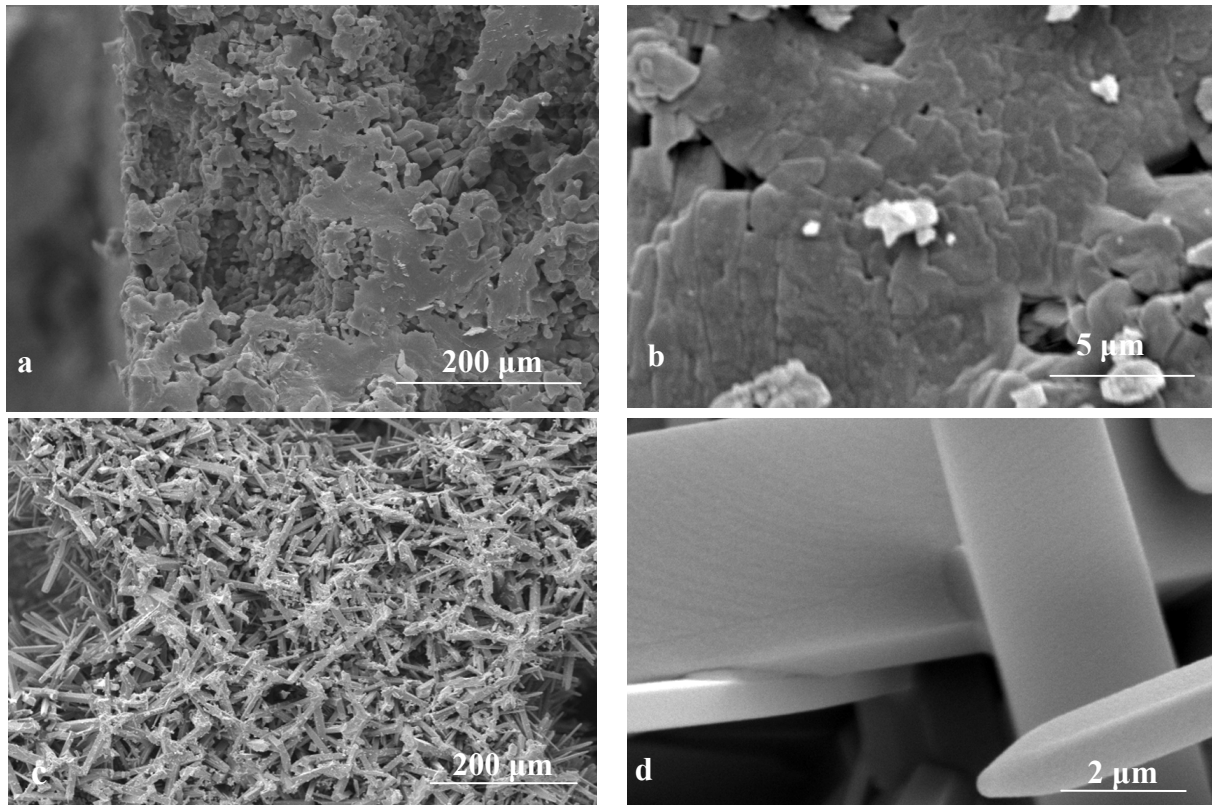


Figure 1. SEM micrographs at different magnifications of bare monoliths, a) and b) cordierite, c) and d) ACM

ACM monoliths consist of non-porous mullite “needles”. The walls of these monoliths are highly porous as can be seen in Figure 1c. This new type of monolith was synthesized by the Dow Chemical Company and consists of high-porosity acicular mullite ACM. The ACM monolith distinguishes itself from a cordierite monolith by the permeability of the microstructured walls. In contrast to the cordierite walls, the walls of the ACM monoliths are made up of an open network of interlocking elongated ceramic grains with lengths and diameters in the micrometer range. The ceramic grain size and the pore diameter size are tunable [15, 16]. At a higher magnification (Figure 1d), the non-porous surface of the separate micrograins can be observed.

1.1 Washcoating with slurries

This method has the advantage that diffusional distances of the reactant to the active phase are minimized and that washcoat loading is not limited by the monolith macropore volume. Slurry coating with different materials is discussed in more detail by Addiego et al [17]. Typically, the washcoat material is wet-milled to adjust the particle size to the size of the macro pores of the support. Alumina slurry requires a low pH, typically 3.5 at 40% solid concentration [6], while silica slurries are usually prepared at pH 8 [3]. The pH is very important to control viscosity and to minimize the dissolving of alumina/silica. The relatively large particles of the coating are present in the slurry, together with smaller binder particles [3]. Commonly used binders include colloidal alumina or pseudo Boehmite for alumina

slurries and waterglass or colloidal silica for silica washcoats. Upon drying, the binder provides sufficient contact area between the larger washcoat particles. In some cases, binder materials can also influence the active phase. Zamaro *et al.* [2] found a catalytic effect of the binder in NO_x reduction over deposited CoZSM5. The final characteristics of a washcoat are usually a function of the monolith type, slurry properties, and preparation conditions [1,2,17]. The final shape and yield of the washcoat are normally determined by the concentration and the number of immersions [9]. Also the withdrawal rate was found to affect the washcoat [19]. The dip time does not significantly influence the washcoat yield. Agrafiotis and Tsetsekou [6] give a detailed description of the effect of slurry properties in coating with γ -alumina. They optimize the solids content (up to 45%) while retaining viscosity between 50-150 mPa·s. Viscosity can be adjusted with inorganic electrolytes or organic deflocculants. In this way an efficient coating (>20 wt%) can take place with a minimum amount of immersions.

1.2 Washcoating with colloidal solutions

This is the most straightforward method to coat a ceramic honeycomb. A sample is placed in a colloidal solution of the washcoat material. For both silica and alumina, these are commercially available. This method has the important advantage that the open frontal area of the monoliths, which determines the pressure drop, is not altered. An important disadvantage is that the yield depends on the macropore volume of the support material, since most of the material will end up in the pores. In case of a non-porous support (ACM for example) a thin layer will be deposited on the surface. Beausigneur [20] applied this method for different systems. Different parameters influence the washcoat properties, when coating with colloidal solutions. Layer thickness and distribution are strongly influenced by the applied pressure during cleaning of the channels and the following drying process. The total immersion time must be sufficient to allow penetration of the solution into the smaller pores. Finally, the type and amount of functional groups and the resulting surface area can be influenced by the calcination temperature.

1.3 Drying and calcining

The use of a liquid phase to deposit the washcoat is not without difficulties. Drying is a critical process [13,21] step that often leads to problems with dimension control, cracking and segregation [22]. In general the washcoating process has a low reproducibility and commonly encountered problems include formation of non-uniform layers, and the accumulation of washcoat at the exit/entrance of the monolith due to capillary effects during drying. In practice, during drying and temperature treatment of washcoated monoliths in ambient atmosphere, without air circulation through the channels, the extensive evaporation of the solvent takes place from the external surface. As a result, the solution containing the precursor or the active component is driven to the external surfaces of the sample by capillary forces. This results in a non-uniform distribution [13]. For the open mullite structure, this

accumulation in the walls and on the outside of the support is much stronger due the highly porous walls. This is schematically depicted in Figure 2. Ismagilov *et al.* [23], have studied the drying profile in monoliths under varying conditions, and observed the same trend.

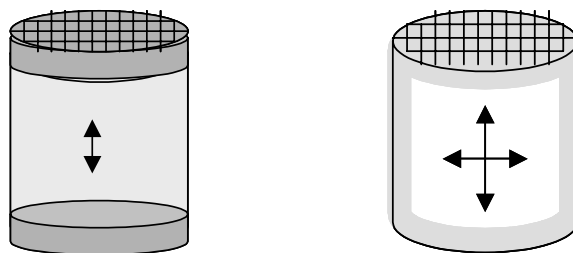


Figure 2. Drying effect during washcoating step in a) cordierite and b) ACM

Solutions proposed to solve this problem include drying under rotation [3], freeze-drying [24-26], and microwave drying [27]. During calcination, heating/cooling rate can affect the final properties of the washcoat. High rates can cause the layer to crack due to shrinkage or expansion.

1.4 Outline

In this work, monoliths with different microstructures are used in various washcoating procedures. The effect of the deposition method, washcoat material, precursor concentration, and monolith type on loading, porosity, and morphology of the washcoat will be determined. In this study, monolithic supports will be the backbone of the enzyme carriers. To apply a certain immobilization strategy, the backbone (i.e the washcoated monolith) must meet certain requirements. Carbon materials are promising materials for enzyme adsorption, especially carbon nanofibers were found to be very effective [7,11,28]. To prevent the growth of carbon filaments inside the cordierite backbone and to provide sufficient surface area for deposition of the growth catalyst, a washcoat layer must be applied. For cordierite, slurry coating seems to be the preferred method [10], but for ACM, this method possibly plugs the open structure of the walls [7]. For covalent binding and ionic adsorption, the monolith surface should be functionalized via its Si-OH groups. In this case a colloidal washcoat provides both surface area and functionality to the backbone.

The open structure of the ACM monoliths can be exploited in two ways [7,16]:

- If high catalyst loadings are desired (e.g. for reactions where mass transfer is not a limiting factor), the high porosity of the monolith wall allows the catalyst loading per unit volume to be maximized while still retaining a low pressure drop through the reactor and good accessibility of the catalyst inside the wall. For these applications slurry coating could be a suitable preparation method.
- When fast reactions impose diffusional limitations, the deposition of a thin conformal catalyst layer on the acicular grains minimizes diffusional limitations while permitting significant catalyst loadings and ensuring bulk diffusional properties within the monolith wall. In this case, coating with colloidal solution would be preferred.

In this chapter different washcoating methods and materials will be explored in order to be able to tune the washcoat to specific needs with respect to later steps in enzyme immobilization and/or catalyst application.

2 Experimental

Colloidal and slurry coatings were applied on the monolith structures following the general procedures proposed by Nijhuis *et al.* [3]. Also combinations of different coatings were prepared by subsequent dipcoating in different precursors.

2.1 Materials

Ludox AS-30 (30% colloidal silica in water with ammonium counter ion) Ludox AS-40 (40% in water with ammonium counter ion), Ludox HS-30 (30% in water with sodium counter ion), Ludox HS-40 (40% in water with sodium counter ion), and Ludox SM-30 (30% in water with sodium counter ion), Silica gel (Davisil grade 643, 200-425 mesh, 99⁺%) were from Aldrich. Colloidal aluminium oxide (20% in water) was from Alfa Aesar, γ -alumina (Puralox SBA 200) from Condea, and α -alumina (AKP-30, with an average particle diameter of 0.4 μm and a surface area of 6.5 $\text{m}^2 \text{g}^{-1}$) was provided by Sumitomo Chemical Company, Ltd, Japan. Nitric acid (65%) was purchased at Baker. In Table 1 some properties of the different washcoat materials are summarized.

Table 1. Properties of washcoat precursors

Precursor	BET surface area [$\text{m}^2 \text{g}^{-1}$]	Particle size [nm]
γ -alumina	250	(10-100) $\times 10^3$
α -alumina	6.5	400
Silica	290	(36-75) $\times 10^3$
Colloidal alumina	45	50
Ludox SM-30	345	7
Ludox AS-40	135	20
Ludox AS-30	230	11
Ludox HS-30	220	12
Ludox HS-40	220	12

Honeycomb monoliths of ACM having cell densities of 200 and 400 cells/inch² (31 and 62 cells/cm²) were prepared by a proprietary Dow process [15,16]. They have a wall porosity of 60%, but differ in the wall macropore size. Cordierite monoliths with cell densities of 200 and 400 cells inch⁻² (31 and 62 cells cm⁻²) were used for comparison. The key properties of these monoliths are given in Table 2.

Table 2. Nominal values of the key properties of monoliths employed in this study.

	ACM 1 (“small”)	ACM 2 (“medium”)	ACM 3 (“large”)	Cordierite
Cell density	200 / 400 cpsi	200 / 400 cpsi	200 / 400 cpsi	200 / 400 cpsi
Wall thickness	0.35 / 0.24 mm	0.35 / 0.24 mm	0.35 / 0.24 mm	0.3 / 0.18 mm
Wall porosity	60%	60%	70%	35%
Specific surface area	>10000 m ² m ⁻³	>10000 m ² m ⁻³	>10000 m ² m ⁻³	1945 / 2788 m ² m ⁻³
Pore diameter	5 μm	18 μm	45 μm	7.5 μm

2.2 Washcoating

2.2.1 Washcoating with slurries

Different alumina layers were prepared with the slurry coating method; a γ -alumina layer and an α -alumina covered with γ - or colloidal alumina/Si.

Washcoating with a γ -alumina layer (particle size 1 μm, thickness ~15 μm) was done according to the method described by Nijhuis *et al.* [3]. Alumina (300 g) and colloidal alumina (170 g) were mixed in 400 ml water, to obtain a 35 wt% alumina solution. The pH was adjusted to 4.5, using nitric acid. To create the desired particle size, this slurry was ball-milled for 24 h. The pH was again adjusted to 4.5 with nitric acid. Monoliths were dipped in the alumina slurry for 5 min and cleaned with an air knife, followed by horizontal drying overnight. The carriers were calcined at 723 K for 4 h (heating rate 5 K min⁻¹).

The α -alumina layers were prepared by dipping the supports in a suspension of AKP-30 in water (15-30 wt%) for 5 min and cleaned with pressurized air, followed by horizontal drying overnight and calcining at 723 K for 4 h (5 K min⁻¹). Viscosity of the slurry was varied by adding a surfactant. Different volumes of Teepol (an alkylarylsulfonate type surfactant) or ethanol (96%) were added before dipcoating.

A silica washcoat was prepared similar to the γ -alumina layer by mixing silica (125g, 18 wt%) and colloidal silica (50 g) in water (500 g), followed by adjusting the pH to 8.0 with concentrated NaOH. The slurry was ball-milled overnight, and the pH adjusted to 8.0. Monoliths were dipped for 5 min and dried horizontally (room temperature) rotating overnight. Finally the supports were calcined at 723 K for 4 h.

2.2.2 Washcoating with colloidal solutions

Silica coatings were alternatively prepared by dipping the monoliths in a colloidal (Ludox) suspension for 5 min, followed by horizontal rotating overnight and calcination at 673 K for 4 h (heating rate 2 K min⁻¹). Alternatively, microwave drying was used instead of horizontal drying; samples were heated 4x5 min at 50W, with intermediate turning of the monoliths. The concentration of the different Ludox solutions was adjusted by diluting with water. Alumina coatings were prepared in a similar manner with a colloidal Al₂O₃ solution.

2.3 Characterization

Mercury intrusion porosimetry was performed on a CE Instruments Pascal 140 and 440 (thermo group). N₂ adsorption isotherms were measured on a Quantachrome Autosorb-6B at 77 K. Samples were outgassed under vacuum at 623 K. Surface area was calculated from nitrogen adsorption using the BET equation (S_{BET}). Total pore volume was determined from N₂ adsorption isotherms at $P/P^0 = 0.95$ ($V_{\text{tot N}_2}$). For the calculation of the pore size distribution, the BJH method has been applied, using the desorption branch of the nitrogen isotherms. The amount of coating was determined by measuring the sample weight before and after the various preparation steps. The total amount of coat layer was calculated as:

$$Y_C = \left(\frac{w}{w_s + w} \right) \cdot 100 \quad (1)$$

where w_s is the mass of the support and w is the washcoat mass.

To obtain qualitative information about the texture and distribution of the washcoats in the monolith, Scanning Electron Microscopy was performed using a Philips XL-20 scanning electron microscope.

2.4 Nomenclature

Samples names are coded depending on the monolith type and the washcoat layer. The first letter of the samples is used to distinguish the monolith type, “C” is used for cordierite, “A” for ACM. A second letter is used in the case of ACM to determine the microstructure of the ACM; “S” for small micrograins, “M” for medium needles and “L” for the most open structure with large micrograins. The washcoats are abbreviated with α for an α -alumina, γ for γ -alumina, Si for slurry silica, Lx for Ludox and Al for colloidal alumina. In some occasions, combinations of washcoats are made; the second washcoat is placed at the end. This is summarized in Table 3. Additional comments such as the type of Ludox are added directly behind the component in question.

Table 3. Nomenclature

Position	Component	Code
1	Monolith type	C or A
2	Micro grain structure ACM	S, M, or L
3	Slurry washcoat	α , γ , or Si
4	Colloidal washcoat	Lx or Al

3 Results and Discussion

3.1 Washcoating with slurries

The slurry method was used to apply different alumina and silica washcoats. The loading varies with cell density; different 200 and 400 cpsi samples were analyzed with respect to porosity. In Table 4 the washcoat yield, measured surface areas and pore size are given. The surface area of the precursor materials was determined by N₂ adsorption

Table 4. Results of washcoating with the slurry method

Sample	Cpsi	Yield [wt%]	BET _{precursor} [m ² g ⁻¹]	BET surface area [m ² g ⁻¹ _{washcoat}]	Pore size [nm]
C		-	-	<0.1	>1000
AM		-	-	<0.3	>1000
C- γ	200	6.2	180 (250*)	179	7
C- γ	400	8.0	180	170	8
AS- γ	400	23	180	174	8
AM- γ	200	25	180	170	8
AM- γ	400	25	180	196	8
AL- γ	400	30	180	180	8
C- α	400	7.4	6.9 (6.6*)	5.1	-
AS- α	400	20	6.9	4.5	-
C-Si	200	2.9	290	276	9
C-Si	400	3.6	290	270	9
AM-Si	200	16	290	262	11
AM-Si	400	17	290	250	9

* From manufacturer

The bare monoliths show negligible adsorption, resulting in a low BET surface area. Since no contribution in surface area and porosity is expected from the bare monoliths, all measured BET surface areas and pore volumes can be ascribed to the washcoat. The obtained values for α -alumina and γ -alumina are slightly lower than the surface area that was provided by the manufacturer (see Table 4), but in the same order of magnitude as the value that was obtained by N₂ adsorption measurements on the crude alumina. For the silica washcoat, the value for S_{BET} is in agreement with the value that was found for the precursor material.

In general, the washcoat loading on 200 cpsi cordierite samples is slightly lower than for 400 cpsi cordierite samples. This is in agreement with the decreased specific surface area for 200 cpsi samples (see Table 2). The total wall volume increases (200 cpsi monoliths have thicker channel walls, so more washcoat can be deposited inside the channel walls), but not enough to cancel out the decrease in surface area. For ACM monoliths, there is hardly any decrease in available surface area, due to the individual needles inside the wall. So for these monoliths, the wall porosity is a very important parameter. The decreased channel surface area of 200 cpsi samples is cancelled out by a relatively large increase in wall thickness. This can be the explanation for the similar loading of 200 and 400 cpsi AM samples.

In Figure 3, a selection of nitrogen isotherms and BJH pore size distribution of the different slurry coatings is plotted. Isotherms (normalized for washcoat yield) for cordierite and ACM are identical; only the isotherms of the cordierite samples are shown in Figure 3. Apparently the monolith microstructure does not influence the properties of the coating. The γ -alumina and silica coated monoliths (curve 1 and 2, Fig. 3a) all show a type IV isotherm, characteristic for mesoporous materials. The α -alumina coated samples (3) show a low uptake at low relative pressures, followed by a nearly horizontal line in the mesoporous range and a large uptake at high relative pressures. This indicates a type II isotherm, indicative for non- or macroporous materials.

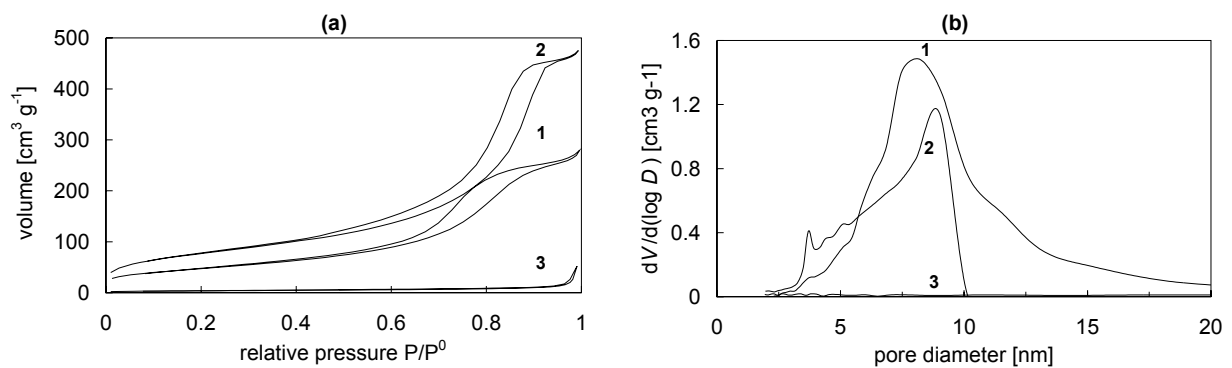


Figure 3. a) nitrogen adsorption isotherms and b) BJH pore size distribution for slurry coatings with different precursor materials. 1) C- γ , 2) C-Si, and 3) C- α

The pore size distribution as calculated with the BJH method from the desorption branch corresponds nicely to the pore sizes that were found for the precursor materials. The α -alumina particles are non-porous, and for silica and γ -alumina a mean pore size of 8-10 nm was found.

3.1.1 Alumina washcoats

Applying a washcoat of γ -Al by means of slurry coating on 400 cpsi monoliths, in general leads to a loading of 8 wt% (cordierite) or 23-30 wt% (ACM). Depending on the cell density, this value can slightly change. SEM images of cordierite with a γ -alumina washcoat (Figure 4) show a coat layer (50-100 μm) that completely covers the channel walls.

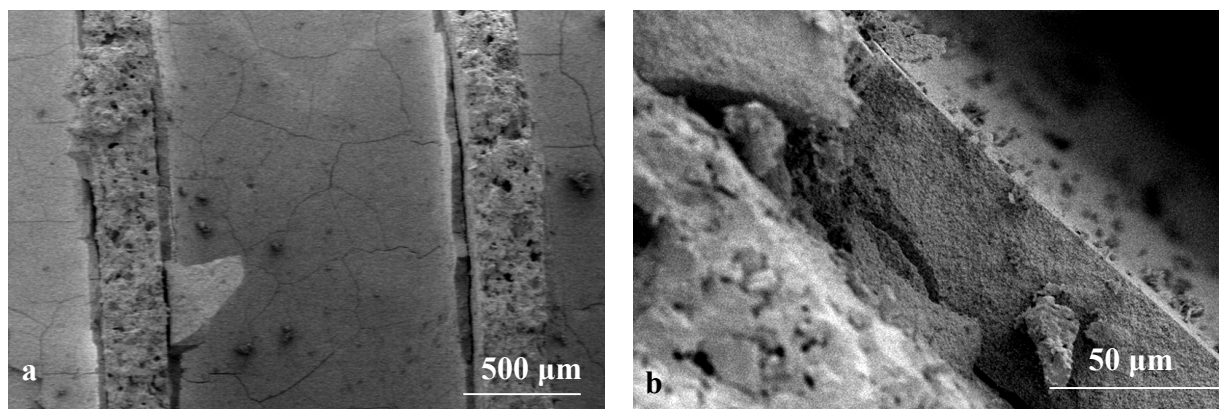


Figure 4. SEM micrographs of γ -alumina washcoats on 400 cpsi cordierite monoliths. a) cross-section of a channel, b) washcoat layer on the monolith wall

On ACM monoliths, the coating completely plugs the open structure (Figure 5). This is caused by the high viscosity of the slurries that were used. As can be seen in the pictures, the needle size influences the final properties of the carriers. Samples with small needles will be almost completely covered, only in some areas the tips of the needles can be seen on top of the layer. The corners of the samples are rounded, as is usually seen for cordierite samples. The samples with large needles will hold most of the washcoat inside the wall and on the needles.

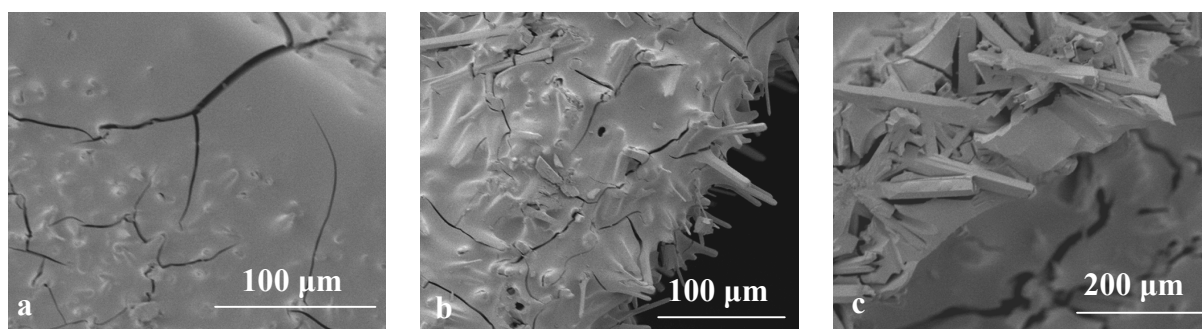


Figure 5. SEM images of γ -alumina washcoats on ACM monoliths a) AS- γ , b) AM- γ , and c) AL- γ

If high catalyst loadings are desired (e.g. for reactions where mass transfer is not a limiting factor), the high porosity of the monolith wall allows the catalyst loading per unit volume to be maximized while still retaining a low pressure drop through the reactor. For these applications slurry coating could be a suitable preparation method. However, when fast reactions impose diffusional limitations, the deposition of a thin conformal catalyst layer on the acicular grains minimizes diffusional limitations while permitting significant catalyst loadings and ensuring bulk diffusional properties within the monolith wall. In this case, a very thin layer must be deposited and coating with a colloidal solution would be preferred. But decreasing both viscosity and/or the precursor concentration of the slurry can also lead to a thin, more uniform coatlayer on the ACM monoliths. However, the large particles in the slurry (see also paragraph 3.4) will influence the thickness and the smoothness of the layer. These parameters were not studied here; the effect can only be speculated.

For α -alumina washcoats, a similar behavior is observed, although the layers are generally much thinner. On cordierite, a very uniform layer of 5-10 μm is present on the surface (see Figure 6). The washcoat loading is around 7 wt% on 400 cps cordierite monoliths. On ACM, the walls are completely plugged as was seen for γ -alumina.

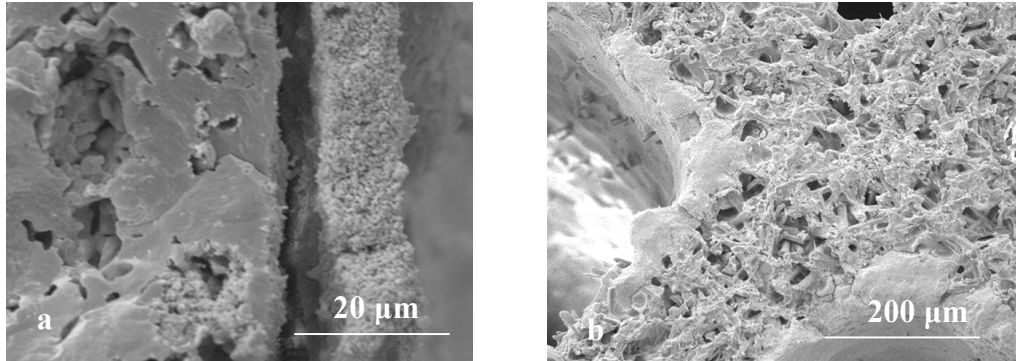


Figure 6. SEM images of α -alumina slurry coatings. a) C- α and b) AS- α

The yield on ACM supports depends on the needle size and varies between 20-30 wt%. As was observed for γ -alumina washcoats, there is a large holdup of washcoat material inside the porous walls. The small needles are almost covered, whereas the large needles are covered with a thin layer of washcoat. This strongly influences the hydrodynamic properties of the ACM monoliths, and diminishes the advantages of the open wall structure. Moreover, an α -alumina washcoat does only lead to a minor increase in total available surface area, another deposition step is needed (e.g. with silica or γ -alumina). This washcoat type is not suitable for use with ACM carriers. For Cordierite supports this method can be used to completely fill the macropores of the support and change the rounding of the channels, before applying the final washcoat with active material.

3.1.2 Effect of a surfactant on α -alumina coating on cordierite

To influence the final properties of the α -alumina washcoat layers, a surfactant can be added. Different volumes of Teepol and ethanol were added to the slurry and the effect on yield and morphology of the coatings was studied. In Table 5, the results are summarized. The yield slightly decreases after adding a surfactant. A surfactant leads to a decrease in surface tension of the slurry, resulting in a slightly thinner coatlayer.

Table 5. Effect of a surfactant on α -alumina coatings on 200 cps cordierite samples

Sample	Yield wt%
C- α	7.4
C- α , 1.5 ml Teepol	6.6
C- α , 3 ml Teepol	4
C- α , 1.5 ml ethanol	7.0
C- α , 3 ml ethanol	4.5
C- α , 4.5 ml ethanol	5.3

The slurry tends to spread out more over the surface of the monolith. Together with the additional effect of slightly reduced viscosity, this leads to a lower final yield. From SEM analysis however, it seems that the thickness of the washcoat does not decrease significantly. SEM micrographs of α -alumina layers that were prepared with surfactant (Figure 7) reveal that adding a surfactant leads to the formation of “bubbles”.

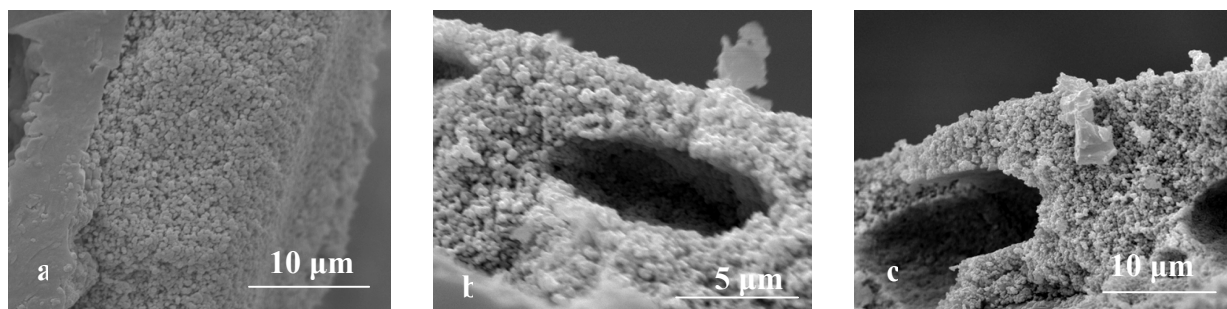


Figure 7. SEM images of different C- α samples. a) no surfactant, b) with 3.5 ml Teepol, c) with 4.5 ml ethanol

This effect is thought to have a negative effect on the mechanical strength of the coating. The bubbles are probably caused by the high airflow rate that was used to clean the channels after dipcoating. Comparable to a solution of a detergent, the slurry starts foaming when mixed vigorously, causing the formation of air bubbles in the coating.

3.2 Silica washcoats

The silica-coated monoliths prepared by the slurry method typically have a loading of 3.6 wt% (C-Si) or 17 wt% (AM-Si). The morphology of the coat layers was investigated using SEM. A selection of images at different magnifications is given in Figure 8.

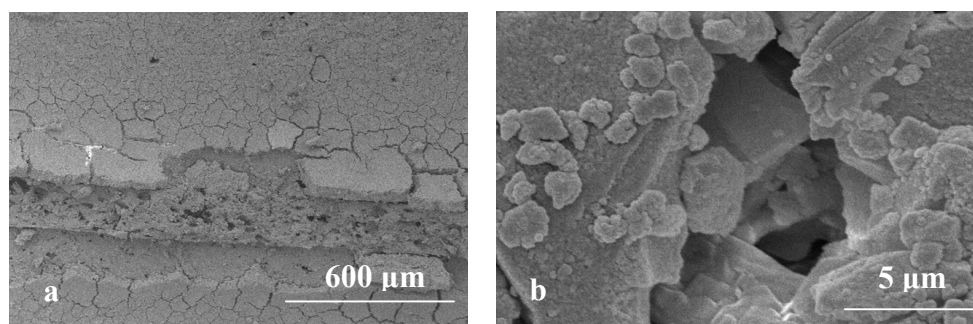


Figure 8. SEM images of C-Si at different magnifications

A uniform layer was found throughout the channels, completely closing off the macropores of the carrier. It seems that the silica layer is cracked (Figure 8a). This is probably caused by cutting the sample for SEM analysis. Most of the cracked surface is positioned along the channel wall that was removed in order to get a cross-sectional view. In the middle of the channel, the washcoat looks smooth, only a little damage is observed, probably caused by shrinkage during drying/calcining. The average layer thickness in the center of the channel is around 7 μm . The size of the ground silica particles varies from 1-10 μm (Figure 8b). Silica

washcoats on ACM (not shown) have a similar appearance to those of γ -alumina washcoats, with a completely filled wall. Again the Si-yield can be influenced by lowering the viscosity of the precursor solution. The effect of viscosity was not quantified in the present study.

3.3 The effect of multiple dipcoating steps

As was observed previously [9], the α -alumina layer is very suitable to be used as a “base” layer on cordierite to fill the macropores and change the shape of the channels. Rounded channels facilitate the deposition of a thin homogeneous catalyst layer. This often leads to improved selectivity, because internal mass transfer limitations are minimized. The parameter that is often used to express the ratio of the surface reaction rate and the diffusion through the catalyst layer is the Thiele modulus ϕ . For an irreversible n^{th} order reaction, the Thiele modulus can be written as:

$$\phi = L \sqrt{\frac{r_{v,obs}}{D_{eff}} \cdot \frac{(n+1)}{2} \cdot C_s^{n-1}} \quad (2)$$

When the Thiele modulus is large, diffusion usually controls the overall rate of reaction; when ϕ is small, the surface reaction is controlling. Since ϕ is proportional to the layer thickness L , a thin homogeneous layer of active material can improve diffusion through the catalyst layer. This is schematically depicted in Figure 9.

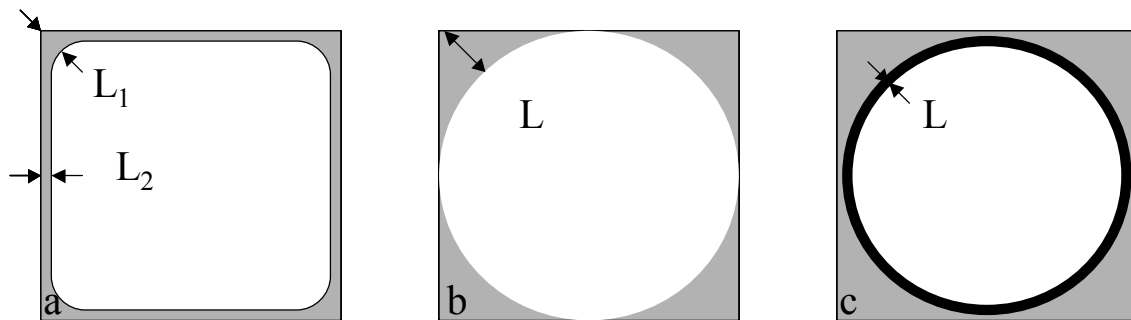


Figure 9. Washcoat geometries on a square monolith channel with a) single layer, b) multiple layers, and c) a base material with a final coating of the active material.

In Figure 9a and b, the active material is deposited directly onto the monolith wall. This leads to increased layer thickness in the corners, whereas the little active material is deposited in the center of the channel. In Figure 9c a non-porous base material (e.g. α -alumina) is used to change the shape of the channel, on which the active material is deposited. This creates a homogeneous layer with equal diffusion distances anywhere in the channel [9]. This geometry can be obtained by subsequent slurry washcoats with α -alumina.

In Figure 10, SEM images of multi-layer washcoats on cordierite are given, at different magnifications. With two layers (Figure 10a), the corners of the channels are already rounded, but the center of the channel wall remains flat. Total loading for this washcoat was

approximately 20%. In Figure 10b it can be seen that the first layer is not visible in the center of the channel, the washcoat material is preferentially deposited in the corners during the first immersion. After a second coating step a 50 μm thick layer is visible on the center of the walls. After 4 subsequent washcoats, the channel has become completely round (Figure 10c), with a final washcoat yield of 50 wt%. An example of the deposition of a separate high surface layer on the rounded channels is given in Figure 10d. A 10-20 μm thick silica layer was deposited on 3 subsequent α -alumina layers. Although selectivity can be significantly improved by this approach, the pressure drop over the monolith is increased dramatically due to reduction of the open frontal area.

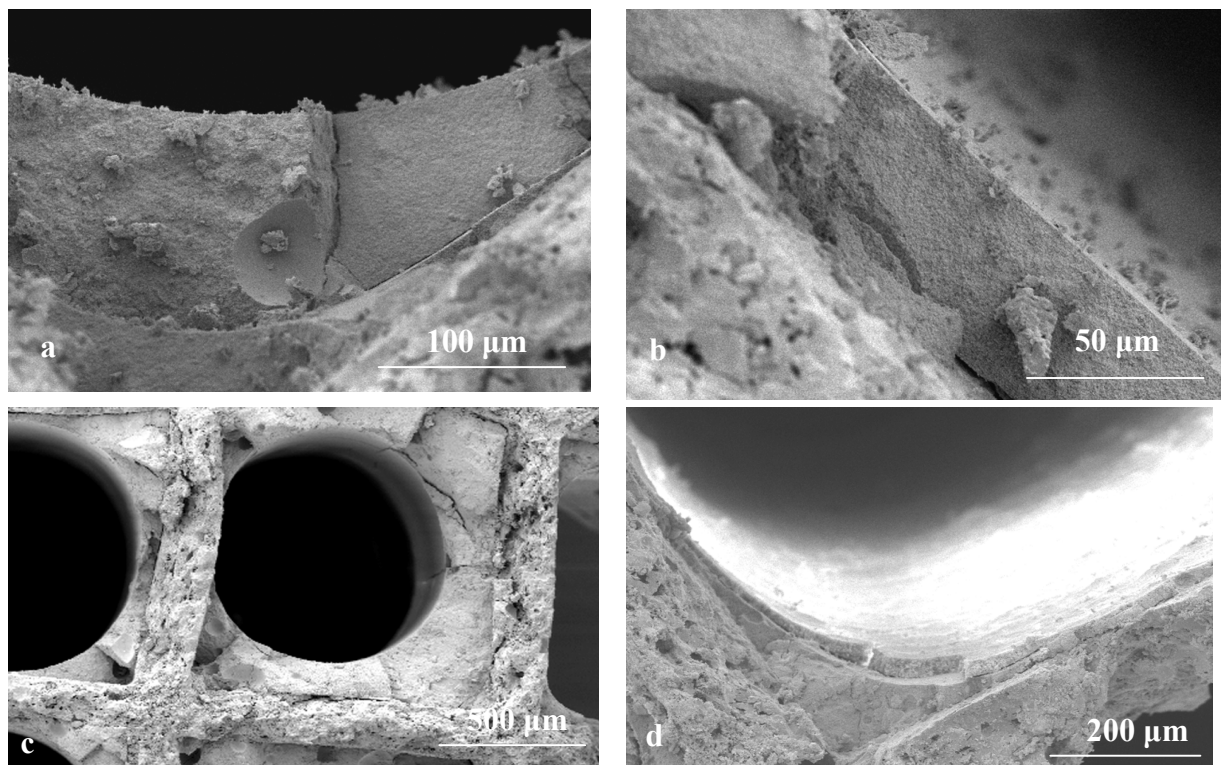


Figure 10. SEM images of 400 cpsi C- α samples containing multiple coatlayers. a) corner with 2 layers, b) center with 2 layers, c) whole channel with 4 layers, and d) corner with 3 layers and a silica washcoat on top

A more appropriate way to benefit from a homogeneous washcoat on a rounded channel would be to directly produce monolith supports with rounded channels by extrusion. As long as these supports are not commercially available, the channels can be rounded by balancing the solids content and the viscosity in order to achieve a homogeneous washcoat with a minimum number of steps. A suitable solution for this problem is the use of monoliths with hexagonal channels that are commercially available, and rounding the channels with α -alumina.

3.4 Washcoating with colloidal solutions

The results of applying the washcoat via colloidal solutions on 200 cpsi ACM and cordierite carriers are summarized in Table 6. Again, no contribution in porosity is expected from the

bare monoliths, all measured BET surface areas and pore volumes can be ascribed to the washcoat.

Table 6. Results for washcoatings prepared with the colloidal method on 200 cpsi monoliths

Sample	Washcoat yield [wt%]	$S_{\text{BET,precursor}}$ [m ² g ⁻¹]	S_{BET} [m ² g ⁻¹]	Hg intrusion volume [cm ³ g ⁻¹]
C-LxAS30	8.4	230	190	0.143 (0.22*)
C-LxAS40	10.5	135	136	0.121
C-LxHS30	8.5	220	198	-
C-LxHS40	12.9	220	187	0.111
C-LxSM30	9.3	345	250	0.126
AS-LxAS40, 10%	5.3	135	118	0.5 (0.57*)
AM-LxAS40, 10%	5.0	135	140	0.46 (0.59*)
AL-LxAS40, 40%	30	135	122	0.36 (0.79*)
C-Al	5.2	-	200	-
AS-Al	16	-	190	-

*Hg intrusion volume of bare carrier

The obtained values for total surface area are in the same order of magnitude as the values that were supplied by the precursor (as supplied by the manufacturer). The loading for the 200 cpsi colloidal silica-coated cordierite monoliths is approximately 3 times higher than for the slurry-coated monoliths (average loading 2.9 wt%, see table 4). This can be explained by the combination of a higher concentration, smaller particle size, and lower viscosity of the colloidal solutions compared to the slurries. The solution of lower viscosity / smaller particles enters the macroporous walls of the cordierite monoliths more easily and can penetrate also the smaller pores. The higher concentration in the Ludox solutions (40 wt%) compared to the slurry (18 wt%) also contributes to a higher washcoat yield for these samples.

For 200 cpsi ACM monoliths, the yield using undiluted colloidal Ludox solutions is approximately 2 times higher (30 wt% for AL-LxAS40) than when an 18.5 wt% silica slurry is used (average loading 16 wt%, see Table 4). Although these ACM-samples have a highly porous wall, the separate mullite needles are non-porous. So the only parameters that define the final washcoat loading for ACM monoliths are the wall porosity (AM, AS, or AL) and the concentration of the slurry/colloidal solution. At comparable wall porosity (AM / AL = 60 / 70 %), the higher silica concentration in the Ludox precursor that was used for AL-LxAS40 leads to a higher washcoat yield than can be obtained with a less concentrated slurry.

No effect of needle size was observed. The washcoat yield for Ludox-coated ACM samples seems to stay constant with increasing needle size (thus with increasing wall porosity, see Table 2), this is in agreement with the results for slurry coating, see Table 4. This was also observed for other Ludox types (not shown).

For alumina, the yield of the colloidal coating is slightly lower than for slurry coating. In this case the concentration of the colloidal solution (20 wt%) is lower than for the slurry (35%), and secondly the difference in particle size between slurry and colloidal solution is less pronounced.

The total mass increase after colloidal coating with silica for a selection of 200 cpsi monoliths is presented in Figure 11.

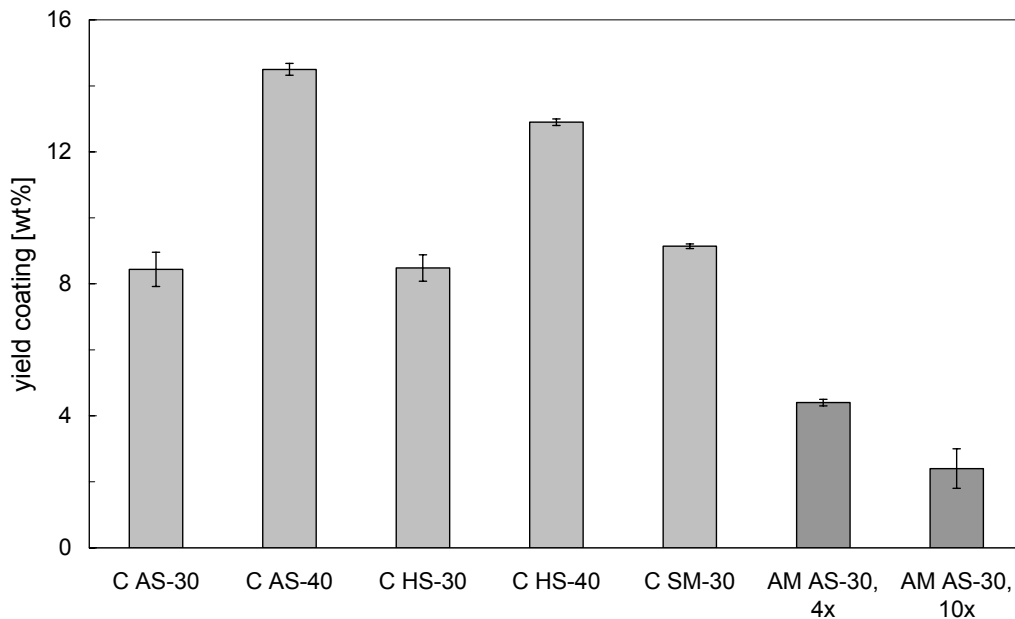


Figure 11. Ludox loading on 200 cpsi monoliths. Lines represent the 95% confidence interval from replicates. For ACM monoliths, the Ludox solution was diluted; the dilution factor is indicated below the sample.

The effect of precursor concentration is clearly visible for the cordierite samples and in the same order of magnitude for the different Ludox types (AS-30/40 and HS-30/40). For the ACM samples, the Ludox solution was diluted (4x and 10x respectively), resulting in a lower silica yield at lower concentration. The effect of dilution is discussed in more detail in paragraph 3.4.1.

The porosity of the washcoated monoliths was studied with nitrogen adsorption. A selection of nitrogen isotherms and BJH pore size distributions is given in Figure 12. The isotherms for the bare monoliths are not included since they show no significant adsorption.

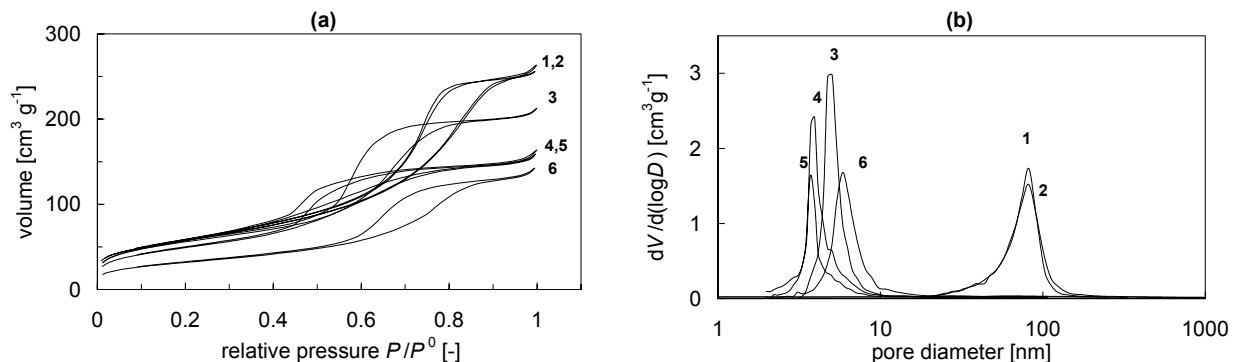


Figure 12. a) nitrogen adsorption isotherms and b) BJH pore size distribution of washcoat layers prepared with colloidal solutions. 1) C-Al, 2) AM-Al, 3) C-LxSM30, 4) C-LxHS40, 5) C-LxAS30, and 6) C-LxAS40

All samples that were coated with colloidal solutions show a type IV isotherm, indicating the mesoporous character of the washcoat. The BJH pore size distributions have a similar shape with a pore size between 4 and 10 nm. Small deviations are observed due to the different particle sizes of the precursors. This mean pore size probably corresponds to the intraparticle voids of the 12-20 nm silica particles of the different colloidal solutions. For colloidal alumina (curve 1 and 2 in Fig. 12b), the particles are relatively large; the intraparticle voids are therefore also an order of magnitude larger than for the silica washcoats. No differences are observed between the isotherms of washcoated ACM and cordierite (see curves 1 and 2 in Figure 12a).

The results of the SEM analysis of the colloidal silica-coated monoliths are shown in Figures 13 a-c. All figures are top-view of the silica layer. This washcoating method leads to the deposition of a very thin layer on both cordierite and ACM. In Figure 13c, it can be seen that the small silica particles (~20 nm) form a densely packed layer on the carrier material.

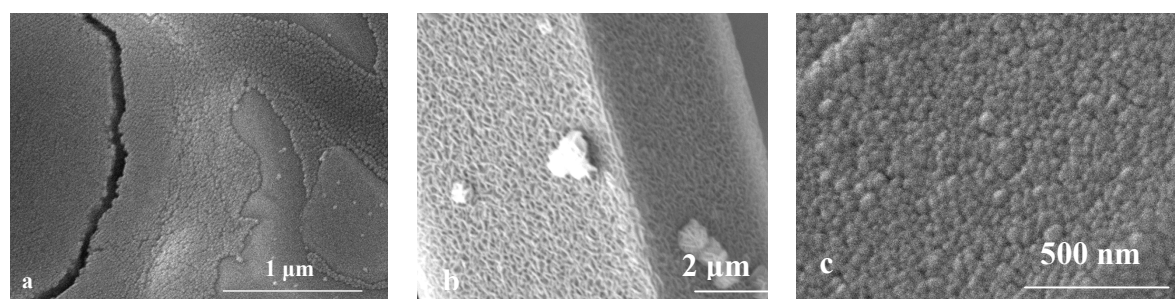


Figure 13. SEM images of colloidal Ludox AS-30 washcoats a) C-LxAS30 b) AM-LxAS30. c) magnification of the washcoat on AM-LxAS30

In the ACM monoliths, large areas were found where the porous wall was (partly) plugged with silica. Apparently, the cleaning/drying steps are not optimal for this new type of monolith. For ACM monoliths, the effect of precursor concentration and drying method were studied in more detail to prevent plugging of the walls during washcoating.

SEM micrographs of monoliths, washcoated with colloidal alumina solutions are presented in Figure 14.

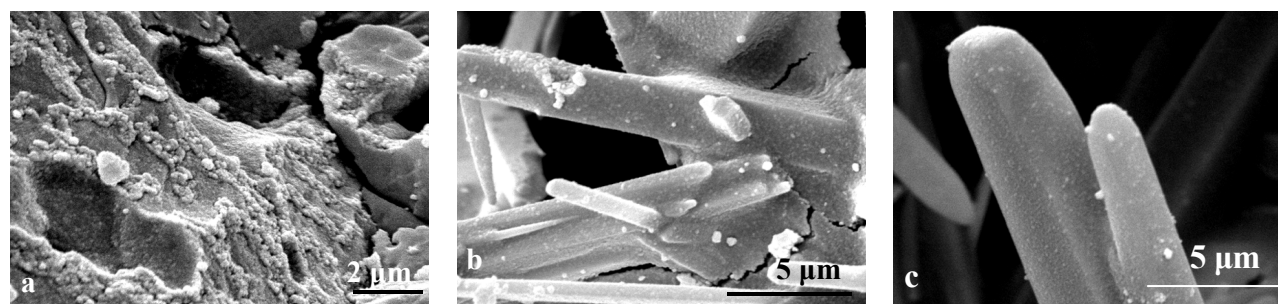


Figure 14. SEM images of colloidal alumina washcoats a) channel wall of C-Al, b and c) AM-Al at different positions in the channel wall.

On cordierite (Figure 14a) no separate layer is visible, as was seen for slurry washcoats. Inside the wall, the macropores are filled with alumina. On ACM, the alumina is mostly

concentrated inside the channel walls and at the base of the needles (Figure 14b). There also seems to be a thin layer covering the needles, in Figure 14c a thin washcoat is present on the needles. It is expected that the concentration of the precursor solution influences the morphology and yield of the washcoat on ACM. With decreasing concentration, the wall will become less filled. In the following section the effect of silica concentration on final yield and morphology of different AM-LxAS30 samples will be discussed.

3.4.1 Effect of the precursor concentration

Different 200 cpsi ACM monoliths (medium grain size) were coated with Ludox AS-30, with different silica concentrations. Ludox AS-30 was diluted in water to obtain the desired concentration. The silica yield after dipcoating versus concentration is plotted in Figure 15. The yield is proportional to the precursor concentration. To determine the optimal concentration for washcoating ACM monoliths, the morphology of the washcoat was studied with electron microscopy. Samples were taken from the outside of the monoliths, because most of the holdup is usually found there due to drying effects. SEM images of the monoliths with different final loading are presented in Figure 16.

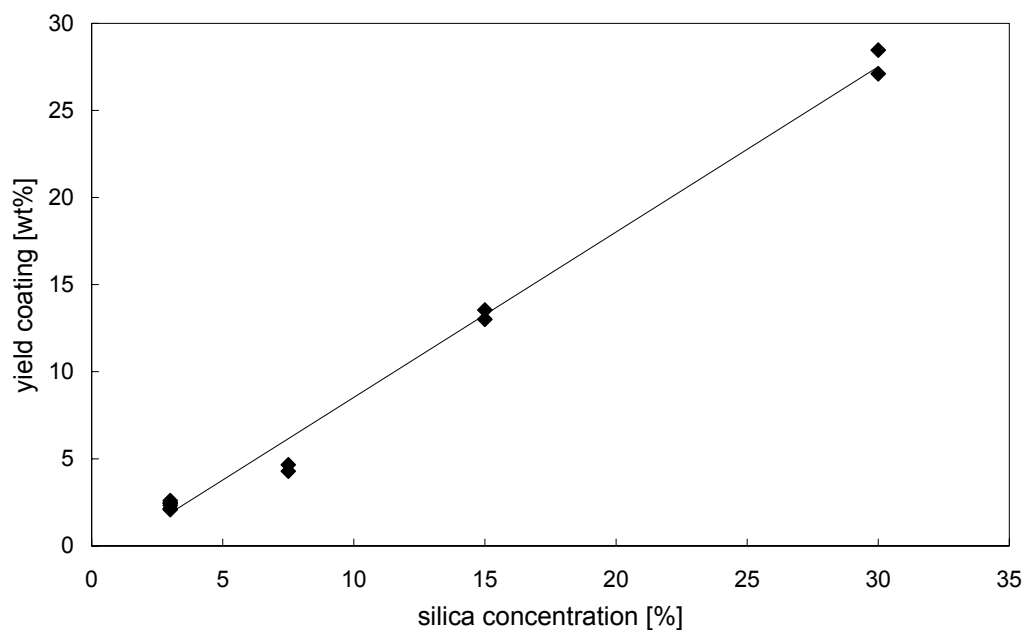


Figure 15. Effect of silica concentration in water on the final washcoat yield for AM-LxAS30

In Figure 16a, it can be seen that the wall is filled with the 30 wt% Ludox solution. A 50 % decrease of precursor concentration leads to a large improvement in accessibility of the porous wall (Figure 16b). At concentrations below 5 wt%, no plugging is observed, although the silica content in the centre of the porous wall is always slightly higher than on the needle tips.

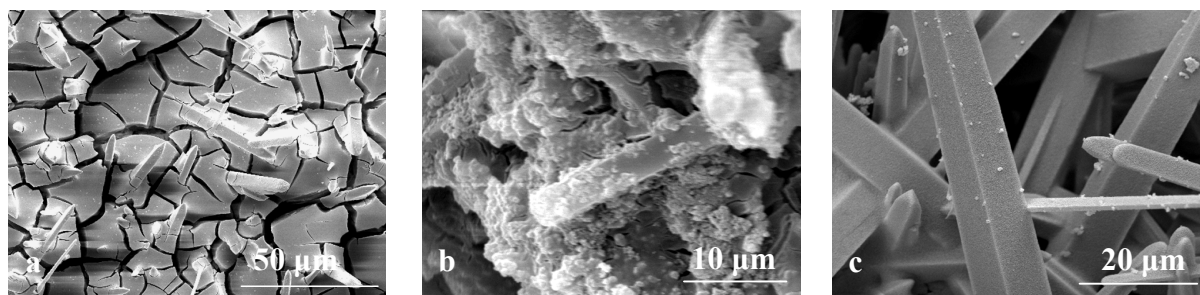


Figure 16. Ludox AS-30 washcoats on ACM. a) AL-LxAS30, 30 wt%, b) AL-LxAS30, 15 wt%, and c) AL-LxAS30, 3 wt%

The final yield (~ 1 g) is around 3 times lower than for cordierite monoliths. This is caused by the absence of macropores in the ACM needles. A significant quantity of the silica enters the macropores of the cordierite, thereby filling the wall. The actual colloidal silica layer, present *on* the cordierite surface can sometimes be very difficult to detect (see also [5]). For the ACM all washcoat material is deposited on top of the surface of the needles, in the form of a very thin layer. It is not known if the surface is completely coated. From these results it seems that there are areas of silica hold-up inside the wall and large areas of washcoat on the surface of the needles. Elemental analysis over a cross section of a coated monolith (not shown) shows that silica is present throughout the structure. More research is needed to determine the silica deposition on the separate micrograins. Even if the washcoat is present as a hold-up between the needles instead of a complete coating, the accessibility of the catalyst (that will be deposited on the washcoat) will be much higher than for cordierite. For carbon-washcoated cordierite monoliths [29] it was shown that the active material was present throughout the channel wall, causing severe internal diffusion limitations. Using an ACM monolith with the washcoat partly present between the micrograins can be an interesting alternative.

3.4.2 Effect of the drying method on the silica distribution in ACM monoliths

The effect of drying was followed by SEM analysis of different 200 cpsi ACM monoliths, coated with a 3 wt% Ludox AS-30 colloidal solution. In figure 17, the micrographs of samples dried in air, in a microwave, and by freeze-drying respectively are presented.

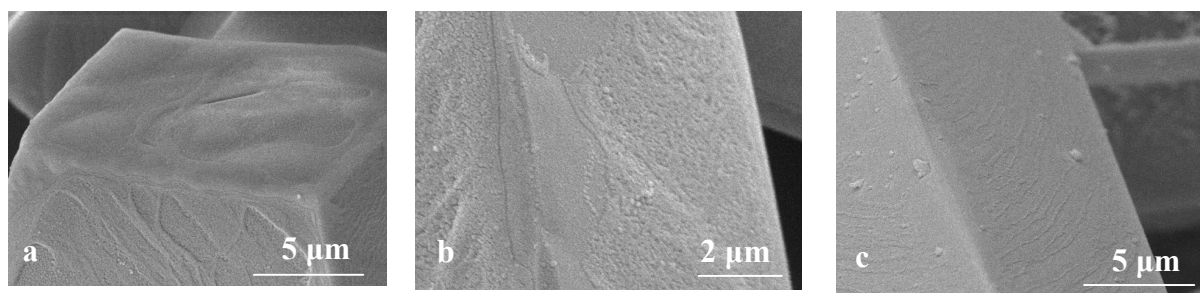


Figure 17. Ludox AS-30 washcoats on ACM_L. a) air b) microwave and c) freeze-drying

If the precursor concentration is sufficiently low, air-drying does not impose large problems regarding silica distribution throughout the monolith. The concentration inside the wall will

be slightly higher than on the needle-tips. But from Figure 17a, it seems that a thin washcoat layer is present on the needles. The problem that arises when analyzing the SEM images of these samples is that the gold-particles that were used to coat the samples (for improved conduction) are of the same size as the silica particles of the coating. It is possible that the coatings that are visible in Figure 17 are a combination of SiO₂ and gold. Therefore, no conclusions can be drawn on the silica distribution *on* the micrograins. The only clear differences between the drying methods can be found in the distribution of the washcoat throughout the monolith. Microwave drying and freeze-drying should provide a better silica distribution due to faster local drying (less agglomeration of the washcoat on the outside of the samples). Indeed, a better SiO₂ distribution in the walls was observed. But at higher magnification, no large differences were found with respect to air-drying (Figure 17b,c). Freeze drying produces a film layer on top of the walls (not shown) due to extremely rapid drying. This layer can easily be removed by ultrasonic treatment. A homogeneous layer remains on the needles (Figure 17c). The disadvantages of this method are the need for expensive equipment and the need for an extra ultrasonic treatment step. Considering the silica distribution at the macro level and the complexity of the different drying methods, microwave drying is suggested as the optimal drying method for ACM monoliths. For cordierite less distribution problems are present during drying, but to decrease accumulation of washcoat material on the outer surface of the cordierite samples, microwave drying can be used.

4 Conclusions

Two different methods were studied to prepare washcoated monoliths; coating with slurries and coating with colloidal solutions. Application of these methods on monoliths with different microstructure, yields support-washcoat combinations with significantly different properties. On cordierite, alumina and silica washcoats were successfully deposited with both methods. The final yield is determined by the precursor concentration and the particle size. For the macroporous cordierite loading can be increased by using smaller (~10-20 nm) particles that can enter the pores. Slurry coating mainly produces a layer that covers the channels, whereas pore filling provides a layer that actually adheres to the complete outer surface of the monolith microstructure. No severe effects of washcoat hold-up were observed for cordierite carriers. Addition of a surfactant leads to the formation of bubbles in the washcoat, this is expected to have a negative effect on mechanical strength. By using α -alumina as a base layer, internal diffusion problems inside the washcoat layer can be prevented. The open frontal area however, decreased by this method. All washcoats were found to increase the total available surface area of both cordierite and ACM monoliths; from less than 0.3 m² g⁻¹ for the bare monoliths to more than 100 m² g⁻¹ after washcoating.

For ACM supports, slurry coating fills the highly porous wall. The loading capacity increases in the order ACM_S < ACM_M < ACM_L. If high catalyst loadings are required,

washcoating with an active material yields significantly higher loadings than can be obtained for cordierite carriers, without increasing the pressure drop over the monolith. The advantages of the open wall are partially lost when using this washcoat procedure. The active material is much more accessible than if applied on cordierite. ACM monoliths can be an interesting alternative for monolithic supports that suffer from internal diffusion limitations. It is expected that by decreasing the concentration and viscosity of the slurry, also thin layers can be deposited on the needles thereby preserving the open structure.

Washcoating with concentrated colloidal solutions also led to filling of the macroporous cordierite channel walls. Loading and surface area can be influenced by varying the particle size and concentration of the sol. For ACM monoliths, the use of concentrated solutions leads to complete plugging of the open wall. When lower concentrations were used a more homogeneous, thin layer was observed, covering the micrograins. The hold-up between the needles in the centre of the wall is always slightly higher than the amount of silica present on the needle tips. The drying method was found of little influence on the final washcoat properties. To increase the available surface area for deposition of an active component, washcoating is an essential process step in the preparation of monolithic catalysts that can have a substantial influence on final catalyst performance. It is therefore very important to survey the support requirements before a suitable washcoating protocol can be designed.

5 Acknowledgements

Corning Inc. is acknowledged for supplying the monoliths. The Dow Chemical Company is acknowledged for supplying the ACM monoliths and funding part of this research. Sander Brouwer and Johan Groen of PAS&BR are acknowledged for performing the nitrogen adsorption and Mercury intrusion porosimetry.

6 Symbols

C_s	Surface substrate concentration	$[\text{mol m}^{-3}]$
D_{eff}	Effective diffusion coefficient	$[\text{m}^2 \text{s}^{-1}]$
L	Layer thickness	$[\text{m}]$
n	Reaction order	$[-]$
$r_{v,\text{obs}}$	Observed reaction constant	$[\text{mol m}^{-3} \text{cat s}^{-1}]$

Greek symbols

ϕ	Thiele modulus	$[-]$
--------	----------------	-------

7 References

- [1] A. Cybulski, J.A. Moulijn (1994) *Catalysis Reviews - Science and Engineering*; 36(2): 179-270
- [2] J.M. Zamaro, M.A. Ulla, E.E. Miro (2005) *Catalysis Today*; 107-108: 86-93
- [3] T.A. Nijhuis, A. Beers, T. Vergunst, I. Hoek, F. Kapteijn, J.A. Moulijn (2001) *Catalysis Reviews*; 43(4): 345-380
- [4] A.E.W. Beers, T.A. Nijhuis, F. Kapteijn, J.A. Moulijn (2001) *Microporous and Mesoporous Materials*; 48: 279-284
- [5] I. Hoek (2004) PhD thesis, Delft University of Technology, The Netherlands, 53-66
- [6] C. Agrafiotis, A. Tsetsekou (2000) *Journal of Materials Science*; 35: 951-960
- [7] K.M. de Lathouder, J. Bakker, M.T. Kreutzer, F. Kapteijn, J.A. Moulijn, S.A. Wallin (2004) *Chemical Engineering Science*; 59: 5027-33
- [8] M.F.M. Zwinkels, S.G. Järås, P.G. Menon, K.I. Åsen (1996) *Journal of Materials Science*; 31: 6345-6349
- [9] A.F. Perez-Cadenas, M.M.P. Zieverink, F. Kapteijn, J.A. Moulijn (2005) *Catalysis Today*; 105: 623-628
- [10] N. Jarrah, J.G. van Ommen, L. Lefferts (2003) *Catalysis Today*; 79-80: 29-33
- [11] G.A. Kovalenko, E.V. Kuznetsova, Yu.I. Mogilnykh, I.S. Andreeva, D.G. Kuvshinov, N.A. Rudina (2001) *Carbon*; 39: 1033-43
- [12] E. Crezee, A. Barendregt, F. Kapteijn, J. A. Moulijn (2001) *Catalysis Today*; 69: 83-290
- [13] T. Vergunst, F. Kapteijn, J.A. Moulijn (2001) *Applied Catalysis, A: General*; 213(2): 179-187
- [14] Th. Vergunst, F. Kapteijn, J.A. Moulijn (2002) *Carbon*; 40(11): 1891-1902
- [15] S.A. Wallin, A.R. Prunier, J.R. Moyer (2001) US Patent 6,306,335
- [16] J.J.W. Bakker, M.T. Kreutzer, K. de Lathouder, F. Kapteijn, J.A. Moulijn, S.A. Wallin (2005) *Catalysis Today*; 105: 385-390
- [17] W.P. Addiego, I.M. Lachman, M.D. Patil, J.L. Williams, M.R. Williams, K.E. Zaun (1993), US Patent 5,212,130
- [18] A.V. Boix E.A. Lombardo, E.E. Miro (2005) *Catalysis Today*; 107-108: 330-337
- [19] E. Tronconi (1997) *Catalysis Today*; 34: 421-427
- [20] P.A. Beauseigneur, I.M. Lachman, M.D. Patil, S.H. Swaroop, R.R. Wusirika (1994) US 5,334,570
- [21] A. Lekhal, B.J. Glasser, J.G. Khinast (2001) *Chemical Engineering Science*; 56(15): 4473-4487
- [22] J. Jiyoun Guo, J.A. Lewis (1999) *The Journal of the American Ceramic Society*; 82 (9) 2345-2358
- [23] Z.R. Ismagilov, S.A. Yasnik, A.A. Matveev, I.V. Koptuyug, J.A. Moulijn (2005) *Catalysis Today*; 105: 484-491
- [24] S. Jiansirisomboon, K.J.D. MacKenzie, S.G. Roberts, P.S. Grant (2003) *Journal of the*

- European Ceramic Society; 23: 961-976
- [25] A.B. Bashaiwoldu, F. Podczeck, J.M. Newton (2004) *European Journal of Pharmaceutical Sciences*; 21: 119-129
- [26] M. Murru, A. Prabowo, A. Gavriilidis (2005) *Journal of Membrane Science*; 248: 27–36
- [27] D. Fino, N. Russo, G. Saracco, V. Specchia, (2004) *Chemical Engineering Science*; 59: 5329 – 5336
- [28] K.M. de Lathouder, T. Marques Flo', F. Kapteijn, J.A. Moulijn (2005) *Catalysis Today*; 105: 443–447
- [29] E. Crezee (2003) PhD thesis, Delft University of Technology, Delft, the Netherlands, 71-82

Functionalization of washcoated monoliths

Abstract

The silanization of monoliths with different microstructure was studied. To provide anchor sites on the monolith surface, the monoliths were washcoated with different colloidal silicas. (3-Aminopropyl)triethoxysilane (APTES) and (3-glycidoxypropyl)trimethoxysilane (GPTMS), were used to apply amino and epoxy-functionalities on the monolith surface.

Functionalization of the washcoated supports with APTES or GPTMS leads to a sharp decrease in available specific surface area and porosity of the SiO₂. After treatment in GPTMS, the samples become practically non-porous in the range 0.5-200 nm. The distribution of the silane through the monolith channels was found to fluctuate significantly, whereas the total weight increase of the sample was found to be within 10% error for different batches. The type of colloidal silica does not influence the final silane yield. Silanization in toluene at ambient conditions leads to the highest yield. Increasing the silane concentration during silanization leads to a higher yield. For ACM monoliths, the silanization yield per gram of silica is higher than for cordierite supports for both organo silanes. This is due to the higher accessibility of the silica in the open structure of the ACM monoliths. The silane loading only seems to depend on the type of silane and on the microstructure of the monolith. DRIFT-IR could be used to follow changes in the surface chemistry as a result of the chemical modification. After silanization, the typical silica bands disappear and are replaced by the typical vibrations of the silanes' functional groups. No apparent changes on the surface were observed with SEM after silanization.

1 Introduction

Inorganic materials are very suitable for enzyme immobilization in many respects. They possess good mechanical properties, high thermal stability and resistance to microbial attack and organic solvents. Different enzymes were immobilized on various types of inorganic carriers such as silica gel [1], sol-gel materials [2], and siliceous molecular sieves [3,4]. Silica-based materials modified by inorganic and organic functional groups have been a subject of considerable interest due to many possible applications [park14]. These materials are composed of siloxane groups (Si-O-Si) in the inward region and silanol groups (Si-OH) distributed on the surface. The silanol groups allow chemical modification of this carrier [5-7] to facilitate effective enzyme immobilization and adjust the properties of the carrier to the required reaction conditions.

The use of particulate supports however, can lead to several problems. First a trade off between mechanical properties and internal diffusion problems must be made. For packed bed operation, particle size generally has a lower limit due to rising pressure drop and problems with mechanical strength. Inside the porous particles, intraparticle limitations are bound to occur [8]. An alternative to large beads in a fixed-bed reactor is a stirred slurry of smaller beads that can be as small as 100 μm [9]. However, the generally soft support-material lacks the mechanical strength for high intensity contacting. Also, the density of the support material is often close to that of the solvent and, as a consequence, an (often cumbersome) separate filtering step is required. The use of structured support materials could provide an interesting alternative for conventional enzyme support materials. A washcoat of inorganic carrier material can easily be applied onto monolith backbones. As was discussed in chapter 3, different washcoating strategies are available. In combination with ionic adsorption or covalent binding, the monolith surface should be functionalized via its Si-OH groups. In this case a colloidal silica washcoat provides both surface area and functionality to the backbone.

The application of organic-inorganic hybrid materials in various fields of chemistry, is a growing research area [10]. Different inorganic carriers such as $\gamma\text{-Al}_2\text{O}_3$, $\alpha\text{-Al}_2\text{O}_3$, and various molecular sieves can be functionalized with organo silane compounds. In this variety of materials, the organically modified silicas have recently attracted considerable attention because they combine the structural characteristics of mesoporous silicas with with the chemical functionality of organic materials [11]. Organo silane compounds were first applied to improve interfacial strength between organic and inorganic phases in composite materials [10]. Now they are also used to change the surface chemistry of membranes [12,13], for immobilization of transition metal complexes [14], immobilization of DNA [15], peptides [16], and proteins [17], and as coating to protect from scratches and/or cracking. A very interesting new approach is to use organic-inorganic hybrid materials to improve physico/chemical properties of biomaterials [18]. Introduction of silica into biomaterials can increase oxygen permeability, biocompatibility and biodegradability.

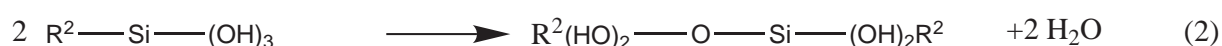
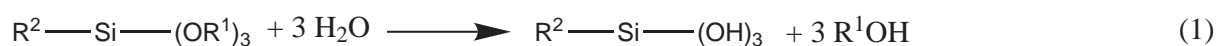
Organo silanes can be described by the general formula $(R^1O)_3\text{-Si-R}^2$, in which R^1 usually is an alkyl group and R^2 a short hydrocarbon with the aimed surface functionality. The most commonly used functionalities are the amine, the epoxy, and the chloride. But also -CN, -SH, -COOH, and phenyls or longer alkyl chains are possible [3]. The surface properties of organo silane coatings have been studied extensively [19-23]. Surface modifications are usually achieved through silanization by using an appropriate organo silane agent [24-27]. Two common methods are available:

- Co-condensation (direct synthesis)
- Grafting (post-synthesis)

Co-condensation is a one step process of tetraalkoxysilanes such as tetraethyl orthosilicate (TEOS) with organosilanes. This method usually results in high loadings and a uniform distribution of functional groups. The carrier cannot be calcined thermally, as the functional group may decompose at high temperature. Also the accessibility for large proteins is expected to be low, these type of carriers should be produced already containing the enzyme. Previous studies on using this method to apply uniform sol-gel coatings on monolith backbones resulted in severe distribution problems, low enzyme activity due to denaturation, and highly irreproducible carriers (unpublished results).

Grafting consists of reaction of an organo silane compound with surface silanol groups using an appropriate solvent. Grafting can be done from both liquid phase (wet chemical method) and gas phase (vapour phase deposition method) [14,28]. The latter improves silane distribution through the support, but requires a special set-up. Also the pre-treatment of the silica surface before grafting influences the final grafting process and was studied extensively [1].

In water, hydrolysis of the alkoxide groups produces silanols (1) and through condensation, the hydrolyzed molecules form siloxane bonds (2):



Since each monomer has three functional groups, large crosslinked polymers are possible. In addition the hydrolysed molecules (or formed oligomers) can bond with the silica surface, either through condensation or by formation of hydrogen bonds with surface hydroxyls. This is depicted in Figure 1 [29]. If surface silanol groups are abundant and in a suitable configuration, double or triple bonds between silane and surface result in a stronger binding (see also Figure 2). Results from several studies show that the molecules adsorb, condense and interact in a variety of ways with silica surface silanols [29,30]. The adsorption configuration changes with concentration. At low silane concentrations, the molecules tend to spread out and cover a large area, often adopting a configuration in which the molecule lies

down on the surface. At higher concentrations they tend to pack closely together on the surface with the hydrocarbon tails extending away from the surface.

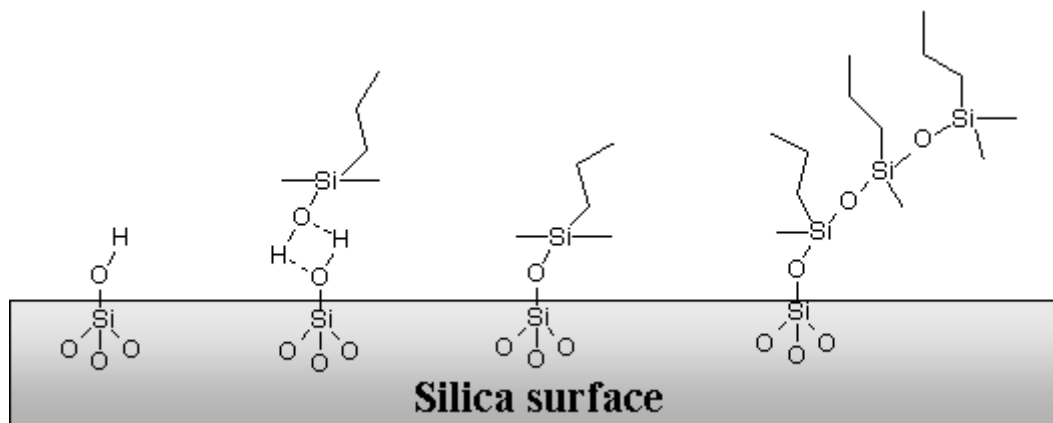


Figure 1. Possible adsorption configurations for a silane coupling agent on a silica surface

When not enough silane is present to cover the complete surface, the molecules form patches on the surface rather than adsorbing as random isolated molecules [31].

In organic solvents (generally toluene, ethanol or acetone are used), surface silanol groups react with the silane to form a layer of covalently coupled surface functional groups. This is schematically represented in Figure 2 for a compound with $R = C_2H_5$.

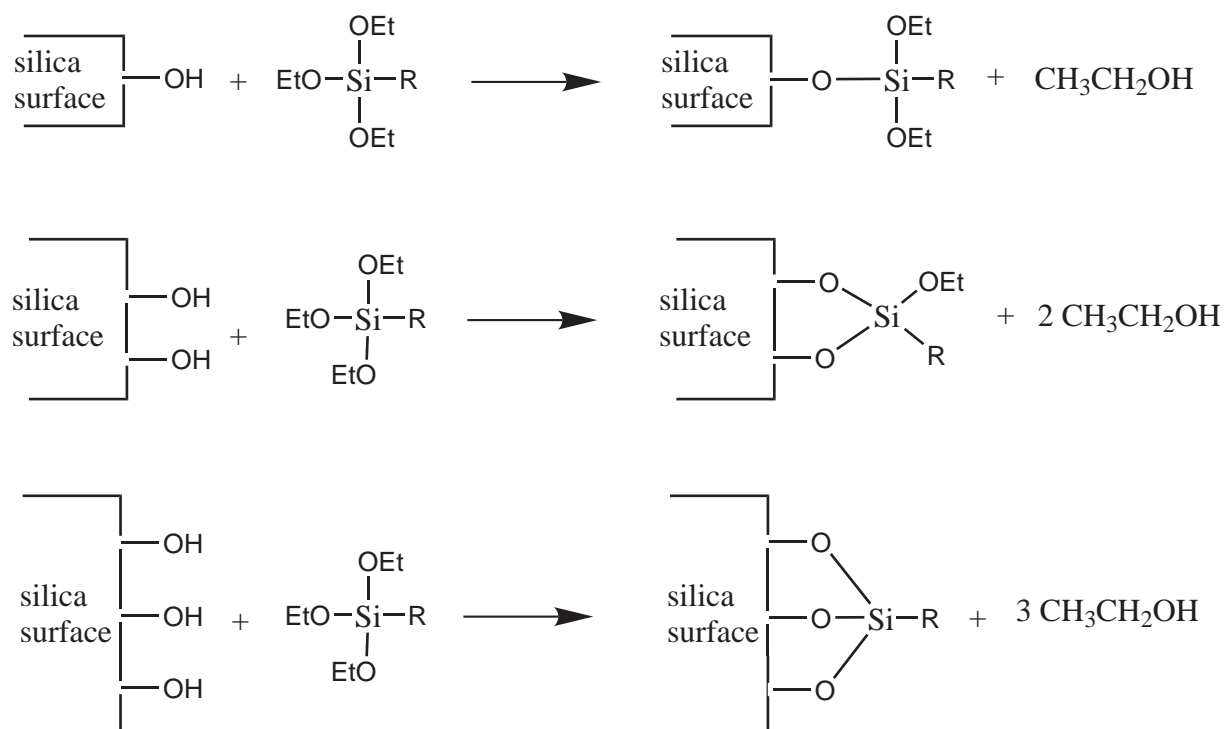


Figure 2. Organo silane coupling to silica surface via surface hydroxyl groups [28]

Depending on the configuration and abundance of silanol groups on the surface, the silane can form one, two or three bonds. The most apparent advantage of grafting is the good preservation of the mesostructure after modification. However, this method often leads to

reduced pore size and pore volume [10,32] and final silane loading is limited. But since a ready-made silica washcoat is available on the monolith backbone, grafting is the preferred method to functionalize monoliths.

The most common approach to couple enzymes to silica surfaces, the (3-aminopropyl)triethoxysilane (APTES)-glutaraldehyde protocol, was already used in the 70s by many researchers in an attempt to bind trypsin to controlled-pore glass and capillaries. [33-35]. Nowadays, this method is still used [36] although many alternatives have been developed. Modified silica surfaces, covered by a monolayer of aminopropyl groups (chemically grafted through interaction with (3-aminopropyl)triethoxysilane (APTES)), are used in many fields of modern chemistry and technology [37,38]. It was recently discovered that APTES functionalized carriers are not only effective as catalyst support, but can be quite effective as catalyst in Knoevenagel condensations, Michael additions and nitroaldol reactions [39].

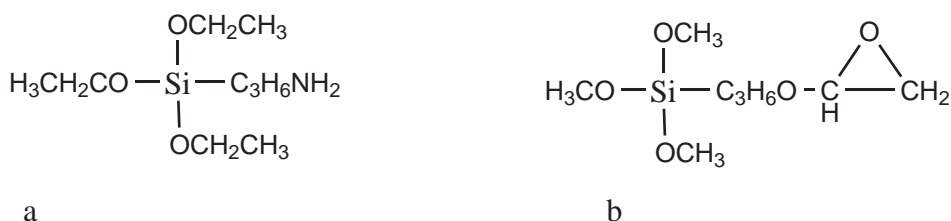


Figure 3. Molecular structures of a) APTES and b) GPTMS

For bio-applications, (3-glycidoxypropyl)trimethoxysilane (GPTMS) is often used, because the use of APTES usually involves activation with glutaraldehyde. In most cases the use of glutaraldehyde leads to deactivation of the bioactive component [40]. Functionalization with this organo silane generally leads to the formation of extremely stable O-C and N-C bonds after reaction with the epoxy group [24]. GPTMS was for instance used to improve the properties of chitosan-silica hybrid membranes [18]. The structures of APTES and GPTMS are presented in Figure 3.

1.1 Layout

In chapter 3, different silica precursors were successfully deposited onto monolith backbones. The effective functionalization of washcoated monoliths with different organosilanes is a vital step in many different enzyme immobilization protocols. In this study, the functionalization of washcoated monoliths with different microstructure is studied with respect to functionalization method, type of functionalization agent, and type of monolith backbone. Washcoats of colloidal silica are applied following the procedure that was developed in chapter 3. The washcoats are treated with (3-aminopropyl)triethoxysilane (APTES) and (3-glycidoxypropyl)trimethoxysilane (GPTMS). The modified silica layers will be studied in terms of coating yield, porosity, and surface chemistry.

2 Experimental

2.1 Materials

Ludox AS-30 (30% silica in water with ammonium counter ion), Ludox AS-40 (40% in water with ammonium counter ion), Ludox HS-30 (30% in water with sodium counter ion), Ludox HS-40 (40% in water with sodium counter ion), and Ludox SM-30 (30% in water with sodium counter ion) were from Aldrich. (3-aminopropyl)triethoxysilane (APTES) and triethylamine were from Fluka. (3-glycidoxypropyl)trimethoxysilane (GPTMS, 97%), was from Sigma. ACM monoliths of mullite with a cell density of 200 cells inch⁻² (31 cells cm⁻²) were prepared by a proprietary Dow process. Cordierite monoliths with cell densities of 200 and 400 cells inch⁻² (31 and 62 cells cm⁻²) were used for comparison. The key properties of these monoliths are given in Table 1.

Table 1. Structural properties of the used monoliths

Cell density	ACM 1 (“small”)	ACM 2 (“medium”)	ACM (“medium”)	Cordierite
	200 cpsi	200 cpsi	200 cpsi	200 / 400 cpsi
Wall thickness	0.35 mm	0.35 mm	0.35 mm	0.3 / 0.18 mm
Wall porosity	60%	60%	70%	35%
Pore diameter	5 μm	18 μm	45 μm	7.5 μm

2.2 Support preparation

2.2.1 Washcoating

Monoliths with a cell density of 200 and 400 cpsi and a length of 5 cm are used. The monoliths were calcined (10 K min⁻¹, 1273 K, 4 h) and washcoated with a colloidal silica solution. Optimization of the washcoating with different silicas was described in Chapter 3. Cordierite monoliths were dipped in the Ludox solution as received. ACM monoliths were washcoated with a 3-4% silica (10 times diluted in water) solution. After dipcoating the channels were cleaned with pressurized air and the monoliths were dried in a microwave oven for 20 min at 150 W. Samples were subsequently calcined at 673 K (5 K min⁻¹, 4 h).

2.2.2 Functionalization

Many different methods are available to functionalize inorganic materials with organo silane compounds via the wet chemical method [41]. A selection of methods was used to functionalize the washcoated monoliths with both (3-aminopropyl)triethoxysilane (APTES) and (3-glycidoxypropyl)trimethoxysilane (GPTMS).

Toluene under reflux conditions

The monoliths were treated in a 10% (v/v) solution of APTES or GPTMS in toluene. The solution was refluxed through the monolith for 5 h in a glass monolith loop reactor, with nitrogen as an inert gas to create liquid flow. The samples were washed with toluene and dried at 393 K for 4 h.

Toluene at ambient conditions

Alternatively, washcoated monoliths were treated in 250 ml of a 2.5-10 wt% solution of silane in toluene with 0.1 % (v/v) tetraethylamine. The monolith was mounted on glass pins that were present on the sides of the glass reactor to allow space for the magnetic stirrer. The mixture was stirred at 293 K for 24 h. Supports were washed with toluene and acetone and dried at 393 K for 4 h (2 K min⁻¹).

Ethanol at ambient conditions

Ethanol (250 ml, 96%) was acidified to pH 4.5 with acetic acid and 2.5-10 wt% silane was added. The samples were treated in a glass reactor with a magnetic stirrer for 24 h at room temperature, washed with ethanol and dried at 393 K for 4 h.

Water at ambient conditions

Distilled water (250 ml), acidified to pH 4.5 with acetic acid was used as a solvent to prepare a 2.5-10 wt% solution of the different silanes. The monoliths were treated in a glass reactor with magnetic stirrer for 24 h, washed with water and dried at 393 K for 4 h.

2.3 Characterization

The amount of coating was determined by measuring the sample weight before and after the various preparation steps. The coating yield was calculated as:

$$Y_C = \left(\frac{w}{w_s + w} \right) \cdot 100 \quad (3)$$

where w_s is the mass of the support and w is the mass of the corresponding coatlayer. Thermogravimetric analysis (TGA) was performed on a Mettler Toledo TGA/SDTA851. The samples were heated in air (100 ml min⁻¹) to 1273 K (heating rate 10 K min⁻¹) to follow the oxidation and decomposition of the applied organo silane compound.

N₂ adsorption isotherms were measured on a Quantachrome Autosorb-6B at 77 K. Samples were outgassed under vacuum at 623 K. Surface area was calculated from nitrogen adsorption using the BET equation (S_{BET}). Total pore volume was determined from N₂ adsorption isotherms at $P/P^0 = 0.95$ ($V_{\text{tot N}_2}$). For the calculation of the pore size distribution, the BJH method has been applied, using the desorption branch of the nitrogen isotherms.

Scanning Electron Microscopy was performed using a Philips XL-20 scanning electron microscope, to obtain qualitative information about the texture and distribution of the

washcoats and organo silane in the monolith. FTIR spectra were recorded on a Thermo Nicolet spectrophotometer (Nexus with an MCT detector) equipped with a diffuse reflectance accessory model (COLLECTOR from SpectraTech). Samples were dried overnight and heated to 373 K during analysis.

2.4 Nomenclature

Samples names are coded depending on the monolith type and the immobilization protocol. The first letter of the samples is used to distinguish the monolith type, “C” is used for cordierite, “A” for ACM. A second letter is used in the case of ACM to determine the microstructure of the ACM; “S” for small micrograins, “M” for medium needles and “L” for the most open structure with large micrograins. The Ludox type will be denoted as ‘Lx’, followed by the name of the colloidal solution. The two different organo silanes will follow after the washcoat. This is summarized in Table 2.

Table 2. Nomenclature

Position	Component	Code
1	Monolith type	C or A
2	Micro grain structure ACM	S, M, or L
3	Ludox type	LxAS30, LxAS40, LxHS40, or LxSM30
4	Silane type	APTES or GPTMS

3 Results and Discussion

3.1 Yield and specific loading

The yield of silanization with APTES and GPTMS was determined by following the weight increase of the whole sample and by cutting samples from different parts of the monolith for Thermogravimetric analysis. In this way the overall yield from sample weight and the local yield from TGA can be compared, and the distribution of the silane throughout the monolith channels can be obtained.

3.1.1 TGA

In Figure 4 the TGA profiles of different ACM-based composites are presented. Samples were prepared in toluene at ambient conditions. In Figure 4a, the relative weight decrease (in wt%) is given and In Figure 4b the absolute weight decrease and the DTG curve of AM-LxAS30-GPTMS are given. No weight loss was recorded for the pure ACM (curve 1). AM-LxAS30 (curve 2) has some adsorbed water on the surface. At 400 K, a weight decrease of 0.1% is measured, at higher temperatures no additional weight decrease was observed. For AM-LxAS30-GPTMS, the same initial weight loss of 0.1% is found up to 400 K. This

corresponds with the small endothermal peak in the DTG curve, representing the evaporation of adsorbed water. At 500 K, the silane starts to decompose, resulting a total weight loss of 1.2 %. Total weight loss by decomposition of the silane was calculated by integrating the endothermal peak.

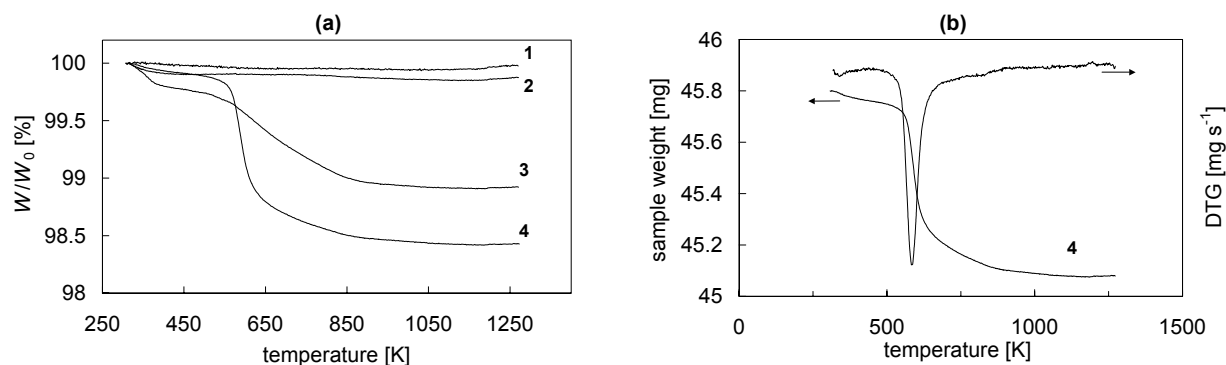


Figure 4. a) thermogravimetric TG and b) absolute waste loss combined with the first derivative of the weight loss (DTG). Oxidation profiles in air of 1) AM, 2) AM-LxAS30, 3) AM-LxAS30-APTES, 4) AM-LxAS30-GPTMS.

For AM-LxAS30-APTES (curve 3), the initial weight loss (300-400K) is much higher than for the GPTMS sample. Where in the DTG curve of AM-LxAS30-GPTMS, a small water evaporation step can be seen, the DTG curve of the APTES-sample (not shown) clearly shows two steps. This could be caused by the higher water content; the aminosilane readily picks up moisture from the air, through hydrogen bonding.

3.1.2 Effect of solvent

To study the effect of the silanization method, cordierite samples were silanized with APTES from different solvents. The weight increase of the whole sample and the range of local weight loss at different positions in the sample are presented in Table 3.

Table 3. Effect of solvent during silanization for C-Lx-AS30_APTES. Silane yield by weight increase of the total sample and from TGA analysis in different parts of the monolith (local samples by random check).

Solvent	Monolith [wt%]	Ranges found for 4 local samples by TGA [wt%]
Toluene reflux (10 wt%)	0.59	0.25-0.85
Toluene ambient (5 wt%)	1.51	1.23-1.72
Ethanol ambient (5 wt%)	1.24	0.72-1.52
Water ambient (10 wt%)	0.5	0.83-1.21

For all solvents, the distribution of the silane along the length of the monolith channels was found to vary significantly, whereas the total weight increase of the sample was reproducible within 10% for different batches. Silanization in toluene at ambient conditions leads to the highest yield (1.5 wt%). These results are in agreement with the results obtained by Ramos *et al.* [30] for comparing the silanization with APTES from toluene solutions under reflux conditions and at room temperature. Since this was also the most convenient method (no extra

steps to set the desired pH are needed) silanization in toluene under ambient conditions was chosen as the standard method. It is expected that the fluctuations in silane yield are actually caused by inhomogeneous silica distribution. It seems likely that the silane concentrates at the positions in the monolith where the highest silica content is found. For ACM monoliths this is inside the porous wall, for cordierite, this would be inside the macropores of the cordierite. The distribution of the silica through the monolith was only studied qualitatively with SEM, and was found to be good. This also explains the high reproducibility of the total weight increase of each sample after silanization; the weight increase of the sample after washcoating was found to be reproducible within 10% (see chapter 3).

3.1.3 Silane concentration

The effect of organo silane concentration on final yield was studied for silanization with GPTMS in toluene at ambient conditions. The results for ACM and Cordierite samples are presented in Figure 5. The concentration of the silane was converted to mmol APTES g^{-1} SiO_2 , present in the reactor. This immediately gives rise to a difference in effective concentration between ACM and cordierite; since the washcoat yield on cordierite is significantly higher, cordierite samples are silanized at lower effective concentration.

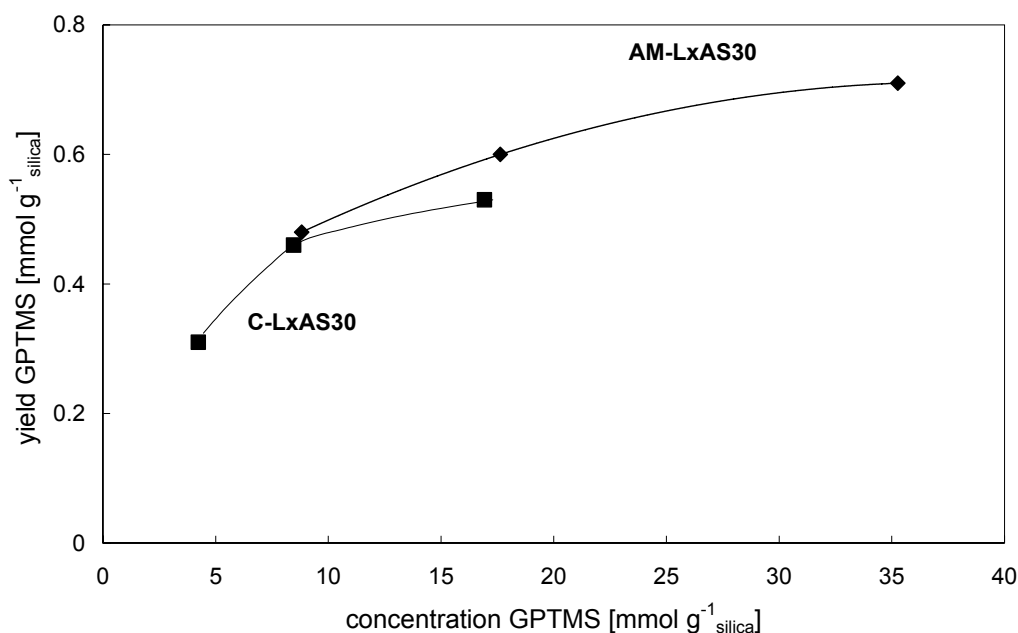


Figure 5. Effect of organo silane concentration on final GPTMS yield for silanization in toluene at ambient conditions. ♦AM-LxAS30-GPTMS and ■ C-LxAS30-GPTMS

Above 10 mmol g^{-1} the yield per g of silica for ACM and cordierite starts to differ. Until 10 mmol g^{-1} enough silica surface is available for silanization. At higher concentrations, it seems that ACM-samples have a better accessibility, resulting in more efficient silanization. Probably, part of the silica that is present inside the cordierite macropores is not accessible to the silane. Although for ACM the silica is more concentrated inside the porous wall (as was

shown in Chapter 3), it is completely accessible to the silane. This leads to a higher silane yield per g of washcoat. An increased silane concentration leads to a higher yield. The maximum value was not reached, although the slope of the curve is approaching 0 between 40 and 80 mmol g⁻¹.

3.1.4 Effect of colloidal silica on APTES loading

The results for silanization with APTES from a 5 wt% solution in toluene on Ludox AS-30 and AS-40 are given in Table 4.

Table 4. Silanization with APTES from a 5 wt% solution in toluene

Monolith	Ludox	Washcoat loading [wt%]	Silane loading [mmol g ⁻¹ _{silica}]	Silane loading [mmol g ⁻¹ _{monolith}]
AS	AS-30	4.9	1.68	0.32
AS	AS-40	5.5	1.36	0.30
AM	AS-30	2.5	1.83	0.18
AM	AS-40	3.4	1.51	0.21
AL	AS-30	2.4	1.92	0.18
C	AS-30	7.6	0.95	0.24
C	AS-40	10.5	0.71	0.25

As was observed in Figure 5 for GPTMS, silane loading on ACM is higher than for cordierite. The APTES-loading on AS-40 samples is lower than on those with AS-30 for both cordierite and ACM monoliths. This could be caused by the higher washcoat loading for these samples. As a result of the higher washcoat content, the effective ratio silane: SiO₂ is lower for samples with a higher silica content. As can be seen in figure 4, this leads to a decreased silane loading. It is therefore assumed that the Ludox type does not influence the final silane yield for equal washcoat loadings. Due to differences in washcoat loading, the ratio silane/silica is not the same for all samples, leading to an apparent effect of the washcoat material. This also accounts for the lower loading on cordierite.

Silanization with APTES in toluene leads to a final yield of around 0.85 mmol g⁻¹_{silica} for cordierite and 1.8 mmol g⁻¹_{silica} for ACM backbones. The same results were found for silanization with APTES in dry toluene on silica gel by Etienne and Walcarius [10]. They observed a maximum of 1.75 mmol g⁻¹_{silica}. This is in good agreement with the value of 1.8 mmol g⁻¹ that was found for ACM monoliths (see Table 4). The amount of APTES in this study is in the same order of magnitude as was used in [10] (around 15 mmol APTES g⁻¹ silica and 8 mmol g⁻¹ silica for cordierite). For cordierite, the silane yield is significantly lower due to the higher washcoat yield and the fact that the washcoat is mostly present inside the macropores.

The total silane yield per monolith seems to be slightly higher for AS samples, probably due to the higher washcoat yield. For all other ACM monoliths, the final loading is constant at 0.2 mmol g⁻¹_{monolith}. The loading on cordierite monoliths is higher at 0.25 mmol g⁻¹_{monolith}. The small differences are caused by differences in washcoat loading.

3.1.5 Effect of colloidal silica on GPTMS loading

To validate the influence of the Ludox type, ACM and cordierite samples with a comparable silica loading of different colloidal silica sources were silanized with GPTMS in toluene. The results are presented in Table 5. The small differences in washcoat loading lead to differences in silane yield, but in general it can be concluded that the silane yield is constant on the different washcoats. Around $0.4 \text{ mmol g}^{-1}_{\text{silica}}$ for cordierite and $0.75 \text{ mmol g}^{-1}_{\text{silica}}$ for ACM was deposited on the washcoated monoliths.

Table 5. Silanization with GPTMS

Monolith	Ludox	washcoat loading [wt%]	Silane loading [mmol g ⁻¹ _{silica}]	Silane loading [mmol g ⁻¹ _{monolith}]
AS	AS-30	4.9	0.59	0.12
AM	AS-30	3.1	0.70	0.09
AM	AS-40	3.3	0.84	0.11
C	AS-30	8.4	0.41	0.11
C	AS-40	9.8	0.35	0.13
C	SM-30	9.3	0.39	0.11
C	HS-30	8.5	0.43	0.11
C	HS-40	12.9	0.29	0.18

The total GPTMS loading per monolith is constant for all samples (0.11 mmol g^{-1}), due to the higher washcoat loading of the cordierite. Applying different effective concentrations for ACM and cordierite, eventually leads to the same total GPTMS yield.

The silane loading only seems to depend on the type of silane (compare Tables 4 and 5) and on the microstructure of the monolith (see Figure 4). Silanization with GPTMS leads to a significantly lower final silane yield compared to APTES. The two times lower yield for GPTMS can be partially explained by the lower molarity that was used for GPTMS; due to the 10% lower Mw for GPTMS the concentration is also 10% lower. Another explanation could be the difference in binding strength. If GPTMS preferably forms three bonds with the silica and APTES only two (APTES is known to form internal and external hydrogen bridges [37,39], thereby inhibiting the formation of at least one more Si-O-Si), the loading of both organo silanes would differ significantly. No proof for this speculation was found in literature. The effect can be investigated with solid state NMR [13,32] and/or FTIR by monitoring the amount of single, double, and triple Si-O bonds and the amount of free hydroxyl groups on the surface at equal silane loading. Since adsorption in solution is a complex process, influenced by many parameters (molecular size, solubility, etc.), a clear explanation of the differences in final silane yield can not be given here.

Silane yield can also be influenced by the amount of silanol groups on the surface. The calcination temperature that was used for washcoating with colloidal solutions was 623 K. For calcination above 473 K [10], the amount of surface silanol groups decreases. Total silane yield can be increased further by calcination at lower temp or by rehydration in acidic medium after calcination [1].

3.2 Porosity

The yield and surface area of different Ludox AS-40 carriers that were treated in 5 wt% silane solutions in toluene are presented in Table 6. Series of 4-6 samples were washcoated and silanized with APTES and GPTMS. Table 6 presents the mean values for yield and surface area per group of samples. After silanization, a sharp decrease in surface area was observed. This is in accordance with findings of Ramos *et al.* [30] and Etienne and Walcarius [10].

Table 6. Results for silanization from 5 wt% solution in toluene on Ludox-AS40

Sample group (4-6 samples)	SiO ₂ yield [wt%]	S_{BET} [m ² g ⁻¹ _{washcoat}]	Silane yield [mmol g ⁻¹ _{washcoat}]	S_{BET} [m ² g ⁻¹ _{washcoat}]
C-LxAS40, APTES	10.5	136	0.71	10.2
AM-LxAS40, APTES	3.4	140	1.51	15.8
C-LxAS40, GPTMS	9.8	134	0.35	33.5
AM-LxAS40, GPTMS	3.3	128	0.84	24.0

In Figure 6 the nitrogen adsorption isotherms at 77 K and BJH pore size distributions (desorption branch) of the functionalized monoliths are presented. The silica-coated cordierite has a type IV isotherm, pointing out the mesoporous character of the silica. The pore size of 4 nm is caused by the intraparticle voids. After treatment with GPTMS, the voids become filled with silane, and access of nitrogen becomes limited. At lower silane loadings (not shown) the samples show both high-pressure hysteresis and low-pressure hysteresis, caused by diffusion limitations of the nitrogen. This effect increases with increasing silane loadings.

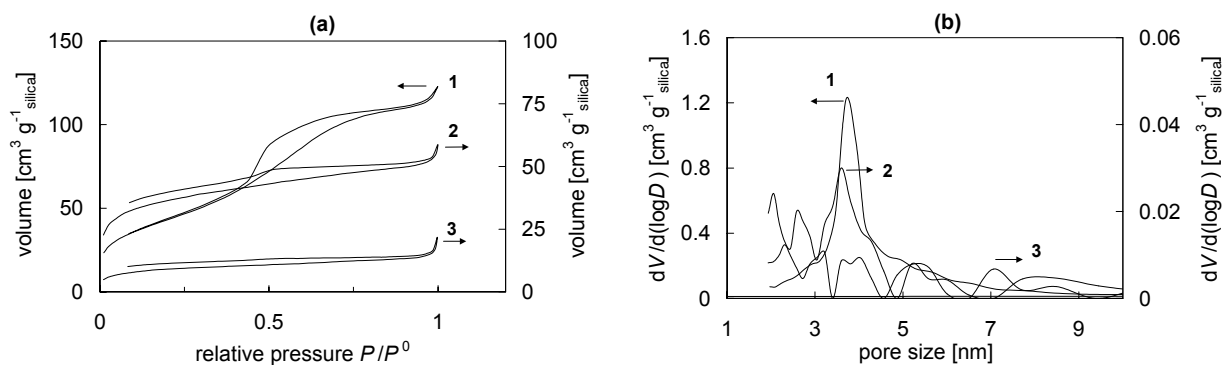


Figure 6. a) nitrogen adsorption isotherms at 77 K and b) pore size distributions for 1) C-LxAS40, 2) C-LxAS40-GPTMS, and 3) C-LxAS40-APTES

After silanization the samples become practically non-porous in the range 0.5-200 nm (curve 3 in Figure 6a). In the pore size distributions in Figure 6b it can be seen that the intraparticle voids have been filled up or closed off by the silane. The washcoated precursor C-LxAS30 has a mean pore size of 4 nm (curve 1 in Figure 6b), but the material becomes non-porous after silane coating (curve 2 and 3). These results correspond to the findings of Ramos [30] and Daniels and Francis [29]. They also observed a decrease in surface area and porosity for increased silane loading. At a silane/washcoat weight ratio (R) of approximately 0.4 during silanization, Daniels and Francis [29] already observe a completely non-porous material. The

silane solutions of APTES and GPTMS that were used in the present work are much higher ($R=5$ for cordierite and $R=10$ for ACM).

After silanization, the accessible surface area is reduced to the outer surface of the silica washcoat. Despite the significant drop in surface area, the available surface area remains higher (Table 6) than the surface area of the bare monolith supports ($<0.3 \text{ m}^2 \text{ g}^{-1}$, see also Chapter 3). The isotherms of the bare monolith materials are not given in Figure 5, because N_2 adsorption is negligible. Depending on the application, an optimum between silane loading and loss of porosity can be found by changing the silane concentration. In case internal diffusion limitations must be excluded (see Chapter 10 and 12, a high silane loading creates a virtual nonporous carrier with a high density of functional groups. If a higher surface area is required, the silane loading can be slightly decreased without significant loss of functional sites.

3.3 Surface chemistry

To study the surface chemistry of the coated monoliths, DRIFT-IR spectra were recorded. DRIFT-IR spectra of functionalized ACM monoliths are presented in Figures 7 and 8. Due to specular reflections of the ceramic samples when used with a KBr background, bare cordierite and ACM were used as to record the background spectrum that was subtracted from the spectra of the coated monoliths.

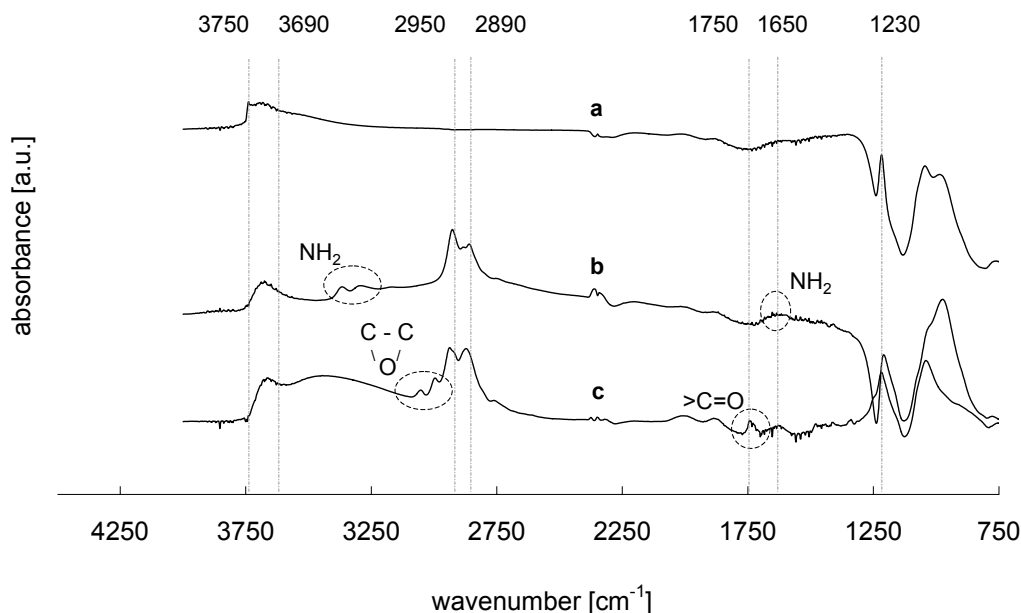


Figure 7. DRIFT-IR spectra of functionalized ACM samples, against an ACM background. a) AM-LxAS40 b) AM-LxAS40-APTES c) AM-LxAS40-GPTMS

The spectra of ACM and cordierite samples are identical at wavelengths above 1250 cm^{-1} (not shown, in Figures 7 and 8 these spectra are set as background). Apparently the backbone-material does not influence the surface chemistry of the washcoated samples. No specific

interactions can be observed with FTIR. The bare ACM and Cordierite (not shown) typical bands at 801 cm^{-1} (Si-O-Si silica) and 1110 cm^{-1} (Si-O-Si silica) [30,42]. After washcoating with Ludox AS-40, two bands appear; an Si-OH stretching vibration of isolated silanols (3750 cm^{-1}) and a hydrogen bonded silanol band (3690 cm^{-1}) [29,30].

After silanization, the typical silica bands disappear and are replaced by the typical vibrations of the silanes' functional groups. Part of the band at (3690 cm^{-1}), representing hydrogen-bonded silanols remains visible, while no more typical Si-OH stretching vibrations are observed at 3750 cm^{-1} .

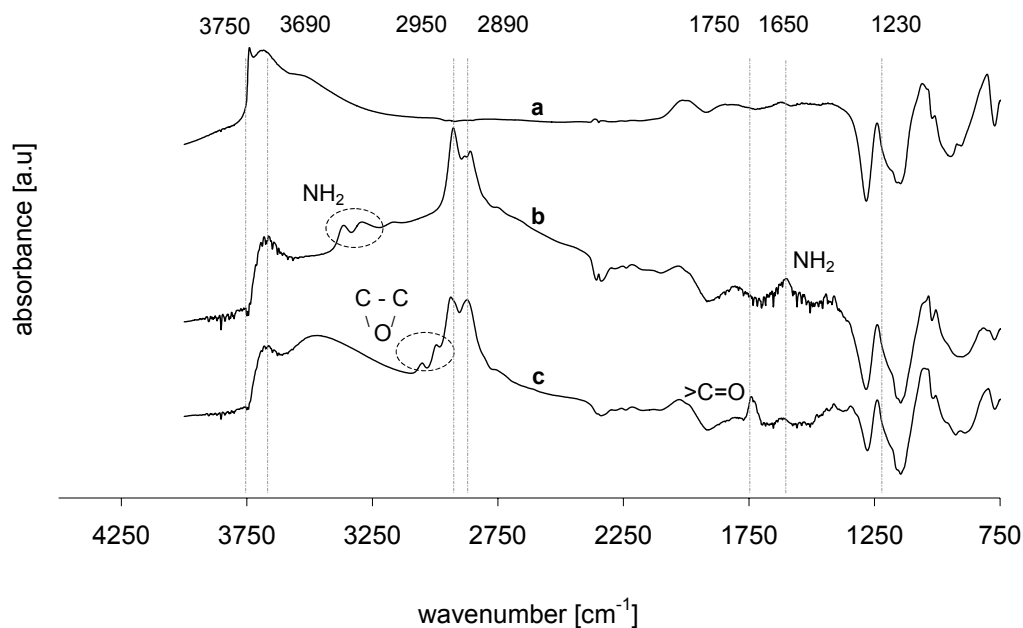


Figure 8. DRIFT-IR spectra of functionalized cordierite samples, against a cordierite background. a) C-LxAS40, b) C-LxAS40_APTES, c) C-LxAS40_GPTMS

For both silanes the carbon backbone can be observed at $2890\text{--}2950$ and 1460 cm^{-1} . For the epoxysilane (GPTMS, curve c in Figures 7 and 8), a doublet at 1700 cm^{-1} is observed, this band is generally ascribed to $>\text{C}=\text{O}$ stretching [42], the presence of these carbonyl groups in the GPTMS-samples cannot be explained. Storage of the sample under air could possibly lead to reaction with the epoxygroup or with the ether group in the backbone of the molecule.

Epoxy ring compounds adsorb at $1280\text{--}1230\text{ cm}^{-1}$ as a result of the ring breathing vibration (C-C, C-O, and C-O bonds all stretching in phase) The CH and CH₂ groups in the ring adsorb either at $3050\text{--}3029$ or $3004\text{--}2990\text{ cm}^{-1}$. In the spectra for GPTMS functionalized monoliths, two bands are visible around $3000\text{--}3060\text{ cm}^{-1}$ (dashed ellipse in curve c), indicating the absorbance of the CH₂ groups in the epoxyring. For the aminosilane (APTES, curve b in Figures 7 and 8), typical bands at 1650 and $3330\text{--}3380\text{ cm}^{-1}$ (see dashed ellipse in Figure 7 and 8) appear, indicating amine groups. The NH₂ group generally gives rise to absorption at $3550\text{--}3330\text{ cm}^{-1}$ (asymmetric stretch) and at $3450\text{--}3250$ (symmetric stretch). Both stretching vibrations are visible in Figures 7 and 8. The band at 1650 cm^{-1} is caused by deformation of the NH₂ group [42]. DRIFT-FTIR can be used to follow the changes in surface chemistry

upon silanization with different organo silane compounds. The different silanes can be clearly distinguished, and binding is confirmed by the disappearance of typical Si-OH bands for the washcoat. Results are in agreement with several studies on silanization of siliceous materials [14,18,29,30,39]. No differences in interaction with the support can be observed in between ACM and cordierite.

3.4 SEM

In Figure 9, SEM images of silanized AM-LxAS30 samples are presented. In Figure 9a, the smooth silica surface of a washcoated ACM monolith is shown (the picture was taken from a silica hold-up between the micrograins). On cordierite the same smooth surface can be observed (not shown, see also Chapter 3).

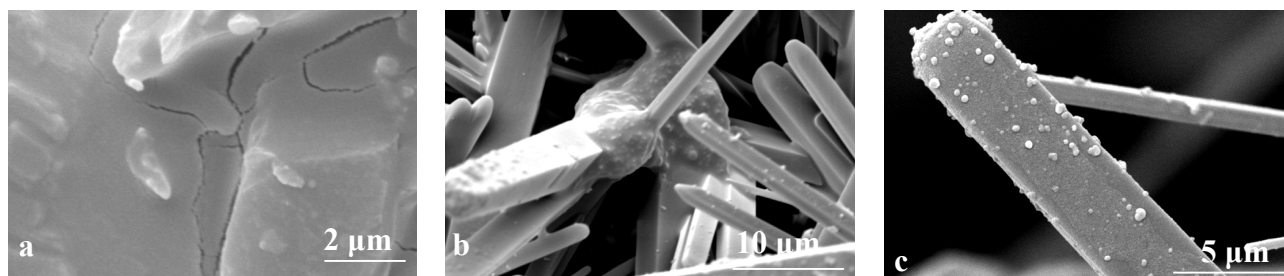


Figure 9. SEM micrographs of (silanized) ACM monoliths. a) AM-LxAS30, b,c) AM-LxAS30-GPTMS

Figure 9b shows a general overview of some micrograins after silanization. At higher magnification, the silica layer can be seen on the needle. The larger agglomerates that can be seen are probably part of the original ACM structure; these larger bubbles can sometimes be seen on different batches of ACM monoliths. At even higher magnification it is more likely to encounter surface effects caused by silanization [29,43].

4 Conclusions

Silanization of cordierite and ACM monolith backbones with different microstructure was studied. The monoliths were washcoated with different colloidal silicas. The yield of silanization with APTES and GPTMS was determined by following the total weight increase of the sample and by determining the local loading with TGA. For all employed silanization methods, the distribution of the silane through the monolith channels was found to fluctuate significantly, probably due to inhomogeneous washcoat distribution. Total weight increase was found to be within 10% error. From the different solvents, silanization in toluene at ambient conditions leads to the highest yield and a better distribution throughout the monolith than other methods. By changing the silane concentration, the final yield can be tuned to find a balance between loss of surface area and functional sites.

On ACM monoliths, the silane yield per g of silica is higher than on cordierite monoliths for both APTES and GPTMS. Probably, part of the silica that is present inside the cordierite macropores is not accessible to the silane. The open structure of the ACM provides better accessibility of the washcoat.

The Ludox type does not influence the final silane yield. The silane loading only seems to depend on the type of silane and on the microstructure of the monolith. Silanization with GPTMS leads to a significantly lower final silane yield compared to APTES. Silanization with APTES in toluene leads to a final yield of around $0.85 \text{ mmol g}^{-1}_{\text{silica}}$ for cordierite and $1.8 \text{ mmol g}^{-1}_{\text{silica}}$ for ACM backbones. Silanization with GPTMS yields around $0.4 \text{ mmol g}^{-1}_{\text{silica}}$ for cordierite and $0.75 \text{ mmol g}^{-1}_{\text{silica}}$ for ACM.

After silanization, a sharp decrease in surface area was observed. After treatment with GPTMS, the samples become practically non-porous in the range 0.5-200 nm.

DRIFT-IR was used to confirm the presence of the washcoat and the organo silane compounds on the monolith surface. After silanization, the typical silica bands disappear and are replaced by the typical vibrations of the silanes' functional groups. No apparent changes at the surface were observed by SEM after silanization.

5 Acknowledgements

Dirk van Benthem is gratefully acknowledged for performing part of the experiments. Corning Inc. is acknowledged for supplying the monoliths. The Dow Chemical Company is acknowledged for supplying the ACM monoliths and funding part of this research. Sander Brouwer and Johan Groen of PAS&BR are acknowledged for performing the nitrogen adsorption measurements.

6 References

- [1] S.W. Park, Y.I. Kim, K.H. Chung, S.I. Hong, S.W. Kim (2002) *Reactive & Functional Polymers*; 51: 79–92
- [2] A.S. Maria Chong, X.S. Zhao (2004) *Applied Surface Science*; 237: 398-404
- [3] H.H.P. Yiu, P.A. Wright, N.P. Botting (2001) *Journal of Molecular Catalysis B: Enzymatic*; 15: 81-92
- [4] H.H.P. Yiu, P.A. Wright, N.P. Botting (2001) *Microporous and Mesoporous Materials*; 44-45: 763-768
- [5] A.S. Maria Chong, X.S. Zhao (2004) *catalysis Today*; 93-95: 293-299
- [6] L. Ferreira, M.A. Ramos, J.S. Dordick, M.H. Gil (2003) *Journal of Molecular Catalysis B: Enzymatic* 21:189-199
- [7] M. Narshima Rao, A.A. Kumbhavi, A. Plant (2000) *Biotechnology Letters* 22: 1557-

- 1559
- [8] M.R. Benoit and J.T. Kohler (1975) *Biotechnology and Bioengineering*; 17: 1616-1626
- [9] R.J. Barros, E. Wehtje and P. Adlercreutz (1997) *Biotechnology and Bioengineering*; 59: 364-373
- [10] M. Etienne, A. Walcarius (2003) *Talanta*; 59: 1173-1188
- [11] W. Cheng, Z. Zhou, W. Miao, H. Chen, B. Huang, T. Tang (2006) *Materials Letters*; 60: 1843-1846
- [12] T. Van Gestel, B. Van der Bruggen, A. Buekenhoudt, C. Dotremont, J. Luyten, C. Vandecasteele, G. Maes (2003) *Journal of Membrane Science*; 224: 3–10
- [13] R.P. Singh, J.D. Way, S.F. Dec (2005) *Journal of Membrane Science*; 259: 34-46
- [14] H. Juvaste, E.I. Iikola, T.T. Pakkanen (1999) *Journal of Molecular catalysis A: Chemical*; 150: 1-9
- [15] J.J. Storhoff, C.A. Mirkin (1999) *Chemical Reviews*; 99: 1849-1862
- [16] S.R. Whaley, D.S. English, E.L. Hu, P.F. Barbara, A.M. Belcher (2000) *Nature*; 405: 665-668
- [17] W.C.W. Chan, S. Nie (1998) *Science*; 281: 2016-2018
- [18] Y-L. Lui, Y-H. Su, J-Y Lai (2004) *Polymer*; 45: 6831-6837
- [19] C-H Chiang, J.L. Koenig (1980) *Polymers and Composites*; 1: 88-92
- [20] M.W. Daniels, J. Sefcik, L.F. Francis, A.V. McCormick (1999) *Journal of Colloid and Interface Science*; 219(2): 351-356
- [21] E.R. Pohl, F.D. Osterholtz (1985) in “Molecular Characterization of Composite Interfaces” (H. Ishida, and G. Kumar, Eds.), Plenum, New York: 157
- [22] H-J. Kang, W. Meesiri, F.D. Blum (1990) *Materials Science and Engineering A*; 126: 265-270
- [23] D.J. Hook, T.G. Vargo, J.A. Gardella, K.S. Litwiler, F.V. Bright (1991) *Langmuir*; 7: 142-151
- [24] S.W. Park, S.Y. Choi, K.H. Chung, S.I. Hong, S.W. Kim (2002) *Journal of Bioscience and Bioengineering*; 94(3): 218-224
- [25] F.S. Vieira, A.R. Cestari, J.A. Simoni, C. Airoidi (1999) *Thermochimica Acta*; 328: 247-252
- [26] A.W. Flounders, D.L. Brandon, A. Bates (1995) *Applied Biochemistry and Biotechnology*; 50: 265-283
- [27] A.R. Cestari, E.F.S. Vieira, J.A. Simoni, C. Airoidi (2000) *C. Thermochemica Acta*; 348: 25-31
- [28] C. Leger, H.D.L. Lira, R. Paterson (1996) *Journal of Membrane Science*; 120: 187–195
- [29] M.W. Daniels, L.F. Francis (1998) *Journal of Colloid and Interface Science*; 205: 191-200
- [30] M.A. Ramos, M.H. Gil, E. Schacht, G. Matthys, W. Mondelaers, M.M. Figueiredo (1998) *Powder Technology*; 99: 79-85
- [31] N. Nishiyama, T. Asakura, K. Horie (1988) *Journal of Colloid and Interface Science*;

- 124: 14-21
- [32] A.S. Maria Chong, X.S. Zhao, A.T. Kustedjo, S.Z. Qiao (2004) *Microporous and Mesoporous Materials*; 72: 33-42
- [33] B.J. Rovito, J.R. Kittrel (1973) *Biotechnology and Bioengineering*; 15: 143-161
- [34] H.H. Weetall (1969) *Science* 166: 615-616
- [35] C. Horvath, B.A. Solomon (1972) *Biotechnology and Bioengineering*; 14: 885-914
- [36] U. Brand, B. Reinhardt, F. Ruther, T. Scheper, K. Schugerl (1991) *Sensors and Actuators B*: 4: 315-318
- [37] A.A. Golub, A.I. Zubenko, B.V. Zhmud (1996) *Journal of Colloid and Interface Science*; 179: 482-487
- [38] G.S. Caravajal, D.E. Leyden, G.E. Maciel, (1986) “Silanes, Surfaces, and Interfaces” (D. E. Leyden, Ed.), Gordon and Breach, New York:383.
- [39] X. Wang, Y-H. Tseng, J.C.C. Chan, S. Cheng (2005) *Journal of catalysis*; 233: 266-275
- [40] S. Wang, M. Yoshimoto, K. Fukunaga, K. Nakao (2003) *Biotechnology and Bioengineering* 83(4): 444-453
- [41] A. Simon T. Cohen-Bouhacina, M.C. Porte, J.P. Aime, C. Baquey (2002) *Journal of Colloid and Interface Science*; 251: 278-283
- [42] N.B. Colthup, L.H. Daly, S.E. Wiberly (1990) *Introduction to Infrared and Raman Spectroscopy*, third edition Academic press
- [43] J. Bouchet, G. Rochat, Y. Letterier, J. A.E. Manson, P. Fayet (2006) *Surface and Coating Technology*; 200: 4305-4311

Covalent immobilization of trypsin

Abstract

Covalent immobilization of trypsin onto cordierite and ACM monoliths with different microstructure was studied with the purpose to produce highly active biocatalysts to be used for Liquid-Solid mass transfer studies in monolith reactors. For this purpose, biocatalysts with high enzyme loading and absence of enzyme leaching and internal diffusion problems are needed. Covalent immobilization usually provides stable, active catalysts. To provide anchor sites on the monolith surface, the monoliths were washcoated with Ludox AS-40 colloidal silica. (3-aminopropyl)triethoxysilane (APTES) and (3-glycidoxypropyl)trimethoxysilane (GPTMS) were used to attach the trypsin to the monolithic supports. The immobilization protocols that use GPTMS yield a higher enzyme loading and a higher activity per g of enzyme. For the APTES-glutaraldehyde method, both enzyme loading and activity are lower than for the GPTMS-based methods. Attachment of enzyme crystals (CLEAs) or Nylon to the monolithic carriers does not yield suitable biocatalysts. Moreover, preparation via these methods is a time-consuming, multi-step process, and therefore less attractive. The best carrier material was obtained by immobilization via the ALD/IM protocol. This method uses an aldehyde group for enzyme immobilization, created by hydrolyzing an epoxysilane and subsequently attaching it to a washcoated monolith. The use of ACM monoliths leads to an additional increase in trypsin loading. Specific activity of the enzyme is not influenced by the monolith-microstructure. ALD/IM is a reproducible method, and the catalysts show only a slow deactivation during storage at 278 K. This deactivation is accelerated at higher temperatures.

1 Introduction

Immobilized enzymes are increasingly employed in life sciences and technology as novel heterogeneous biocatalysts [1] or specific biosorbents [2]. Enzyme immobilization provides long-term stability and high enzyme activity. The main concern is to obtain a biocatalyst with high stability and activity that have not been affected during the immobilization process. Ideally, the immobilized enzyme will exhibit improved catalytic performances. There is no rule to predict a priori the obtained activity and stability of an enzyme upon immobilization. Various types of carrier materials for enzyme immobilization have been studied in combination with different immobilization methods. [3-12]. The carrier materials are usually used in the form of particulates. Although very attractive in many respects, the use of particulate-supported enzyme systems has one inherent disadvantage: these systems are often severely diffusion limited, leading to a considerable fraction of unused enzymatic activity [8]. In this respect, the honeycomb monolith support offers several advantages over particulate supports, including a high geometric external surface, structural durability, easy catalyst separation, a low pressure drop, and uniform flow distribution within the matrix [13]. However, the application in biological reaction systems has hardly been explored. A thin layer of carrier material on a monolithic support could be an interesting alternative for particulate carriers by increasing mechanical stability and decreasing diffusion distance.

Covalent immobilization is expected to be a convenient protocol for attachment of enzymes onto monolithic supports. This protocol was already studied extensively during the pioneering phase of enzyme immobilization [14]. In general, covalent binding is used to attach proteins to silica carriers [15-20], therefore the protocol can easily be translated for use with silica-coated monoliths. Although enzyme activity usually decreases upon chemical binding and in general toxic chemicals and complicated procedures are involved, this method has some important advantages over other immobilization methods:

- It has been well studied
- Very effective for immobilization of a wide variety of enzymes
- Stable and selective [21]
- Reproducible [16]
- No enzyme leaching can take place

Covalent immobilization can be divided into crosslinking (without support) and binding onto prefabricated carriers. Crosslinking generally leads to materials with low mechanical and hydrodynamic stability [14], but is still used extensively [22-27]

Chemical attachment of enzymes onto carrier materials is currently applied on a large scale for the production of biosensors [16, 17, 28] and selective protein/antibody separation and purification [49,50]. This method is very suitable to couple different enzymes onto silica surfaces [16, 19, 29], and can therefore easily be translated for use with washcoated monoliths.

The most common approach to couple enzymes to silica surfaces, the (3-aminopropyl)triethoxysilane (APTES) -glutaraldehyde protocol, was already used in the 70s by many researchers in an attempt to bind trypsin to controlled-pore glass and capillaries. [30-32,15]. Even the first experiments with immobilization on ceramic honeycomb date from this decade [1]. Nowadays, this method is still used [33] although many alternatives have been developed. In previous studies, enzyme coated monoliths were applied to determine L-S mass transfer characteristics of monolith reactors [34]. The enzyme was covalently attached to the monolith support by the (APTES)-glutaraldehyde protocol. A fast enzymatic reaction and the absence of internal diffusion limitations, make the monolithic bioreactor very suitable to operate in the mass transfer limited regime. After performing the initial hydrodynamics measurements in a monolith loop reactor and a monolithic stirrer [34], it was concluded that enzyme loading needed to be improved in order to remain in the mass transfer limited regime during measurement. To this purpose this is done by optimizing the existing protocol and exploration of other covalent procedures.

1.1 Immobilization protocols

Research was initially focused on increasing the amount of functionalization agent on the cordierite surface. But from numerous studies on this immobilization protocol [35-37] it was concluded that more glutaraldehyde leads to decreased activity. This is caused by multipoint covalent attachment of the enzyme to the glutaraldehyde linkers, limiting the conformational freedom of the enzyme during reaction, or by steric hindrance. Although multi-point attachment has been reported to lead to improved stability at elevated temperatures [37], the optimal immobilization method would be through a strong single point covalent link, not in or near the active site of the enzyme. Different immobilization strategies are available. A selection of some common methods includes:

- APTES-glutaraldehyde
- indirect aldehyde
- p-nitrofenylchloroformate
- carbonyl-diimidazole
- CLEAs
- nylon

A short description of the different methods is presented here. In Figure 1, the APTES-glutaraldehyde route is depicted. Glutaraldehyde is a bifunctional reactive agent that has been extensively used for fast protein immobilization. It is inexpensive, readily available and easy to use.

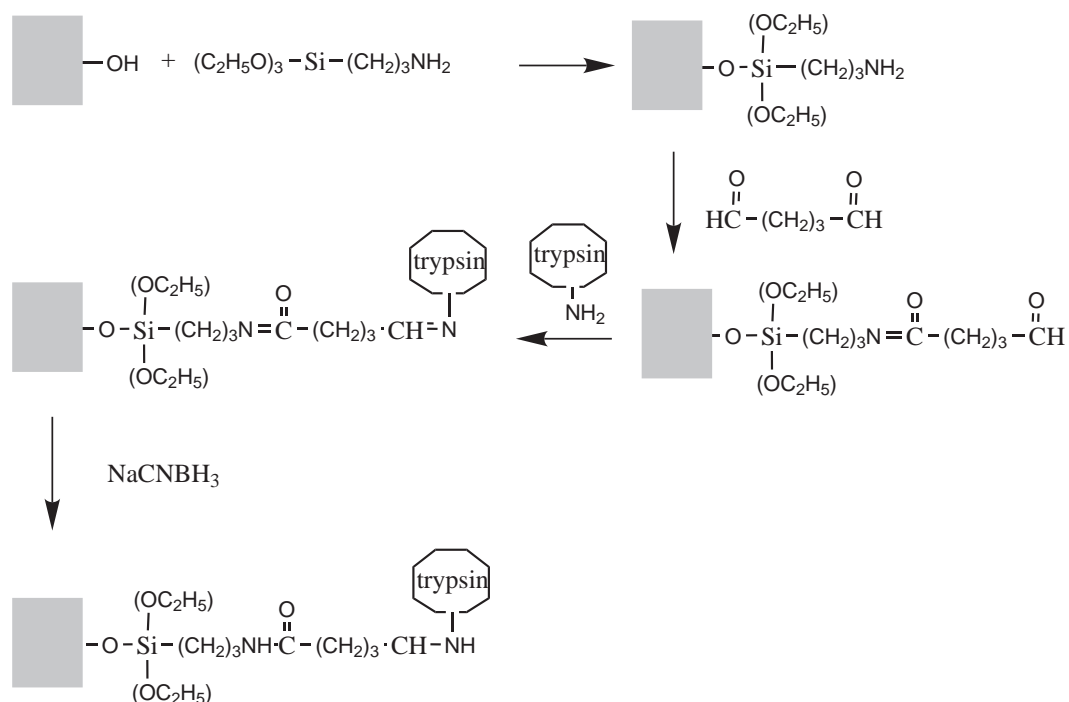


Figure 1. Covalent coupling of trypsin through the APTES-glutaraldehyde route

Glutaraldehyde exists in different forms depending on the solution conditions. Under acidic and neutral conditions glutaraldehyde exists as a monomer in its free aldehyde form, hydrate or hemiacetal. At higher concentrations it polymerizes to oligomeric hemiacetals [38].

All of these forms can react with proteins in different ways and lead covalent bonding. Under basic conditions glutaraldehyde undergoes aldol condensation to form α,β -unsaturated aldehyde polymers. These products can react with proteins either via stabilized Schiff's base formation or by Michael adduct formation. The Schiff's base can be reduced to a stable secondary amine by a mild reducing agent.

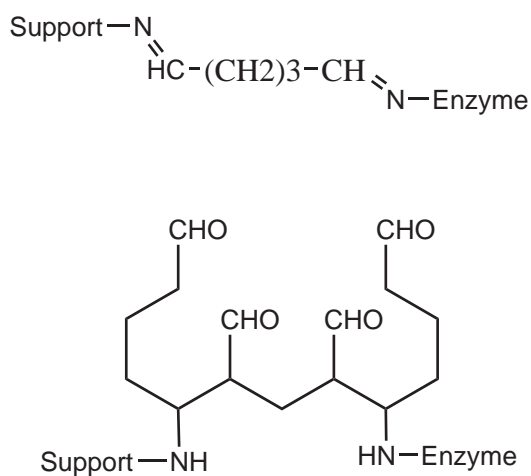


Figure 2. Reactions of glutaraldehyde with NH_2 groups. Formation of a Schiff's base (top) and Michael adduct formation (bottom) [39]

The following 3 protocols (indirect aldehyde, p-nitrophenylchloroformate, and carbonyl-diimidazole) use 3-glycidyloxy-trimethoxysilane (GPTMS) to activate the carrier. These methods are represented in Figure 3. In the indirect aldehyde method, the epoxy group of the silane is converted to an aldehyde to which the enzyme can be attached. Cyanoborohydride is used to reduce the imine-bond. For the other methods the aldehyde group is reduced to a hydroxyl group, to facilitate acylation of carboxyl-diimidazol or p-nitrophenylchloroformate. In this way, no cyanoborohydride is needed.

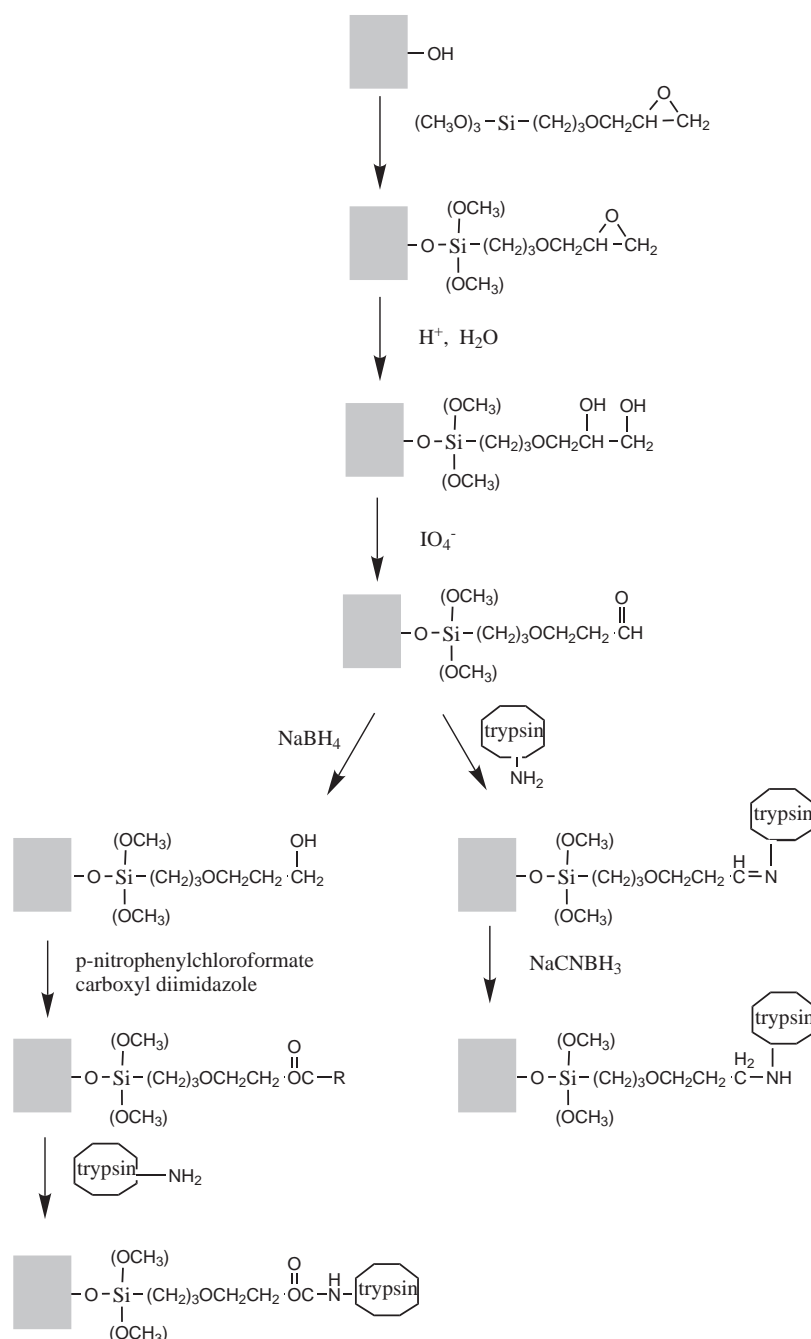


Figure 3. Covalent coupling via GPTMS functionalization.

Cross-linked enzyme crystals (CLECs) were developed in the 1990s [40, 41], and represented a significant advance in enzyme immobilization technologies. CLECs are very stable during

operation and because they consist of 100% protein they have high catalyst productivities (mass protein/(mass cat·time)) and space-time yields. An important drawback of CLECs is the need to purify the enzyme in order to successfully crystallize the protein. Sheldon and coworkers [42] developed a method to prepare aggregates from precipitated enzyme. To produce these crosslinked enzyme aggregates (CLEAs), no pure enzyme is needed. Furthermore the method is simple and cheap. The preparation of both CLECs and CLEAs is schematically drawn in Figure 4. Enzyme aggregates can be formed by precipitation (with ammoniumsulfate) and the addition of a crosslinking agent. CLECs [25, 26] are formed after crystallization of the enzyme. CLEAs can also be attached to a carrier material, for instance a membrane [24]. If a monolith is functionalized with aldehyde groups, CLEAs can also be attached to ceramic supports.

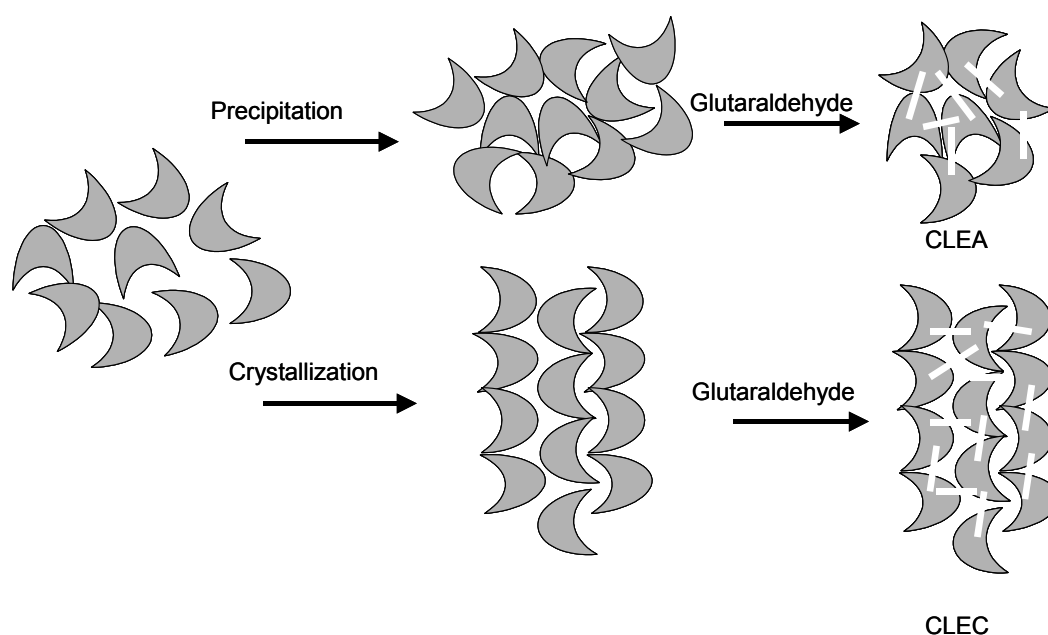


Figure 4. Schematic overview of the formation of CLECs and CLEAs

Glutaraldehyde is a vital component in the formation of CLEAs. This component influences the final particles size of the aggregates. If the reaction proceeds too long, unwanted side reactions will drastically decrease residual enzyme activity:

- Reaction with amine-groups in the active site
- Too many crosslinks, which will ultimately minimize conformational freedom of the individual enzymes and thereby reduce the immobilized activity.

Nylon is a relatively cheap material, with good mechanical properties and is available in many different forms. Nylon can be an attractive matrix for enzyme immobilization [43], involving inexpensive and relatively non-toxic chemicals. An array of different enzymes has been successfully immobilized onto nylon [44-47]. A Nylon coating can also be applied on a silica surface. Nylon can then be hydrolyzed to create amino groups, which can be coupled to proteins via glutaraldehyde.

1.2 Trypsin

Trypsin (E.C. 3.3.21.4) is produced in the pancreas as an inactive precursor (trypsinogen). After the enzyme arrives in the stomach, the N-terminal part of the pro-enzyme is split off, yielding the active enzyme. Bovine trypsin consists of 223 amino acids and has a molecular mass of 23 kDa. Trypsin is a globular enzyme with a size of 3.8 nm [60]. The natural function of the enzyme is to hydrolyze the peptide bonds next to lysine and arginine, in other words to digest proteins. Additionally the enzyme splits off the amide and ester groups (in case of a terminal position) of both amino acids. Reactivity increases in the order peptide<amide<ester. The enzyme has the highest activity around pH 8, but the highest stability around pH 2. Heavy metals, organic phosphates, and several natural inhibitors deactivate the enzyme [48]. The active site of trypsin consists of aspartic acid, histidine and serine residues, with COOH, imidazole, and –OH side groups respectively. The surface of the enzyme possesses –S-S-, amines and thiol groups, which present suitable sites for attachment via both physical adsorption and covalent binding [60]. Since no amine groups are present in the active site, the enzyme is suitable to be immobilized via aldehyde-functionalized surface groups.

A generally used assay to follow trypsin-activity is the hydrolysis of n-benzoyl-L-arginine ethyl ester (BAEE). The reaction scheme is presented in Figure 5. Both reactant and product molecules are relatively large, the absence of diffusion problems should be verified for different enzyme-support systems. For the current system, with the enzyme directly attached to the support, no internal diffusion limitations are expected. This reaction takes place in aqueous environment at pH 8 at 296 K, and can easily be followed by UV-VIS at 253 nm.

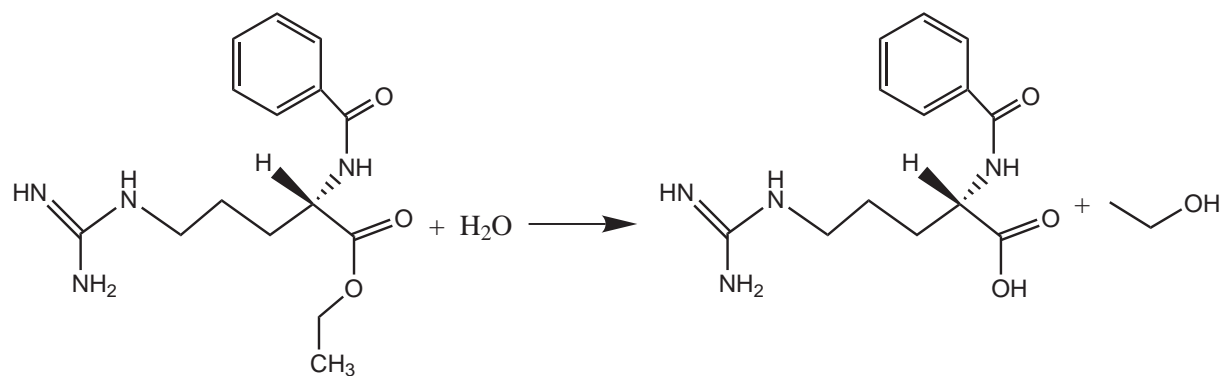


Figure 5. Hydrolysis of n-benzoyl-L-arginine ethyl ester

1.3 Layout

This study was aimed to improve the immobilization efficiency and residual activity of trypsin, immobilized by covalent attachment to monoliths with a different microstructure. The development of the protocol is focused on the monolith-activation step and the enzyme-immobilization step. The activation step is defined as the reaction step in which the enzyme or carrier is chemically modified to facilitate covalent binding. This was done by optimizing the conventional APTES-glutaraldehyde protocol and by investigating other frequently used covalent procedures on cordierite monoliths. Because of the recent interest in enzyme

aggregates, it was also attempted to attach the enzyme to the monolith via the simultaneous growth and attachment of CLEAs. The prepared biocatalysts are tested in the hydrolysis of n-benzoyl-L-arginine ethyl ester in a stirred vessel. In this way, the different immobilization protocols can be compared in terms of immobilized activity and (storage) stability.

2 Experimental

2.1 Materials

(3-aminopropyl)triethoxysilane (APTES), glutaraldehyde (25% in water), n-benzoyl-L-arginine ethyl ester (BAEE), NaIO_4 , triethylamine, NaBH_4 and NaCNBH_4 (purity >96%) were purchased from Fluka. (3-glycidioxypropyl)trimethoxysilane (GPTMS, 97%) and dimethyl aminopyridine were from Sigma. THF, p-nitrophenyl chloroformate (97%), diethylamide, carbonyl diimidazole, and melamine (99%) were from Aldrich. Buffer salts were of analytical grade and purchased at Baker. Novo pancreatic trypsin, type 6 salt free, was kindly supplied by Novozymes. ACM monoliths of mullite having cell densities of 200 and 400 cells inch^{-2} (31 and 62 cells cm^{-2}) were prepared by a proprietary Dow process. Cordierite monoliths with cell densities of 200 and 400 cells inch^{-2} (31 and 62 cells cm^{-2}) were used for comparison. The key properties of these monoliths are given in Table 1.

Table 1. Properties of the monoliths

	ACM ("medium")		Cordierite	
Cell density	200 cpsi	100 cpsi	200 cpsi	400 cpsi
Wall thickness	0.35 mm	0.43 mm	0.30 mm	0.18 mm
Wall porosity	60%	35%	35%	35%
Specific surface area	>10000 $\text{m}^2 \text{m}^{-3}$	1394 $\text{m}^2 \text{m}^{-3}$	1945 $\text{m}^2 \text{m}^{-3}$	2788 $\text{m}^2 \text{m}^{-3}$
Pore diameter	18 μm	7.5 μm	7.5 μm	7.5 μm

2.2 Catalyst preparation

2.2.1 Washcoating

Monolith samples with a cell density of 100, 200 and 400 cpsi and a length of 5 cm were used.

The monoliths were calcined (10 K min^{-1} , 1273 K, 4 h) and washcoated with a colloidal silica solution (Ludox AS-40). Optimization of the washcoating with different silicas was described in Chapter 3. Cordierite samples were dipped in the Ludox solution as received. ACM monoliths were washcoated with a 4% Silica (10 times diluted Ludox AS-40 in water) solution. After dipcoating the channels were cleaned with pressurized air and the monoliths were dried in a microwave oven for 20 min at 150 W. Samples were subsequently calcined at 673 K (5 K min^{-1} , 4 h).

2.2.2 Functionalization and Trypsin immobilization

Monoliths were functionalized following the different protocols. After enzyme immobilization and during stability tests, the catalysts were stored in a 1 g l^{-1} NaN_3 solution in 10 mM phosphate buffer pH 8 at 278 K. This was done to prevent the growth of microorganisms on the biocatalysts.

APTES-Glutaraldehyde (GLU)

The pH of a 400 ml 5-wt% water ethanol mixture was lowered to 4.5 with acetic acid. 8.8 g (3-aminopropyl)triethoxysilane (APTES) was dissolved and the monoliths were treated for 4 h, rinsed with ethanol and dried at 393 K (5 K min^{-1} to 323K, 1 h and 5 K min^{-1} to 393 K, 1 h). For treatment at high glutaraldehyde concentrations (GLU/H), the functionalized samples were treated in a 1 M glutaraldehyde solution in 0.1 M acetate buffer pH 5 for 2.5 h at 278 K. At low glutaraldehyde concentrations (GLU/L), a 10 mM glutaraldehyde solution was used. After reaction, the monoliths were washed with buffer solution. Subsequently, 100 ml 3 g l^{-1} trypsin in 0.1 M phosphate buffer pH 8 was circulated over the carrier for 5 h at 278 K. Then, 50 ml NaBH_4 was added to yield a final borohydride concentration of 1 mM.

Indirect aldehydegrou (ALD)

Two variations are possible. In one approach, the sequential method (SM), 3-glycidoxytrimethoxysilane (GPTMS) is first coupled to the washcoat and subsequently reacted with acid to form a diol [53]. The other approach, the indirect method (IM), starts with reaction of the GPTMS with acid to form a diol before the silane is actually coupled to the silica washcoat [54].

▪ Sequential Method (ALD/SM)

As described in chapter 4, monoliths were functionalized with GPTMS from a 5 wt% solution at room temperature. Monoliths were treated in this solution for 24 h at 293 K to attach the silane to the washcoat. After drying under vacuum, monoliths were immersed for 1 h in 250 ml HCl (pH 2) at 363 K to create a diol. The product was then oxidized for 2 h with 400 ml of a 70 mM NaIO_4 solution in 0.1 M acetate buffer pH 4.5 to form the aldehyde groups.

▪ Indirect Method (ALD/IM)

Before coupling the organo silane to the monolith, the epoxy-group was reduced by treating 3 g GPTMS in 300 ml HNO_3 (pH 2) at 363 K for 1 h. The pH of the solution was raised to 7 by adding 0.5 M sodium acetate and contacted with a monolith for 6 h. Oxidation of the diol was done as described above.

Trypsin was immobilized on the carriers from a 2 g l^{-1} solution in 0.1 M phosphate buffer pH 7.5. Cyanoborohydride (3 g l^{-1}) was added to reduce the imine bonds.

p-Nitrophenylchloroformate (NFCF)

An aldehyde group was created with the indirect method and reduced with 100 mM sodiumborohydride in ethanol for 1 h. Monoliths were washed with ethanol and dried under vacuum. 2 g p-Nitrophenylchloroformaat (NFCF) was dissolved in 100 ml acetone and the carrier was added. 50 ml 0.3 M solution of dimethylaminopyridine in acetone was added dropwise over a period of 2 h. Monoliths were washed with acetone and dried under vacuum. Trypsin was immobilized at 278 K from a 0.1 M phosphate buffer pH 7.5.

Carbonyl-diimidazole (CDL)

An aldehyde group was created with the sequential method and reduced with 100 mM sodiumborohydride in ethanol for 1 h. Monoliths were washed with ethanol and dried under vacuum. The acylation of carbonyl-diimidazole (1.63 g, 10 mmol) was performed in 150 ml acetone. After 1 h the monoliths were washed with acetone and dried under vacuum. Trypsin was immobilized at 278 K from a 0.1 M phosphate buffer pH 7.5.

Nylon (Ny)

Monoliths were treated with APTES as described above. Nylon was coated from adipoyl chloride (Cl-CO-C₄H₈-CO-Cl) and melamine (C₃N₆H₆). Melamine has 3 amine groups, to create a 3D polymer network. The problem with this combination of monomers is their different polarity. Adipoyl chloride is hydrophobic, melamine is only soluble in water. Two different coating methods were explored:

1. Water method

Monoliths were immersed in 200 ml 10 mM melamine solution in water. 1 mmol Adipoyl chloride was slowly added to this solution. To neutralize the reaction product HCl, NaOH was used to maintain neutral pH. After reaction, monoliths were washed with water and dried at 333 K for 2 h.

2. Two-phase method

100 ml 10 mM melamine in water and 100 ml 10 mM adipoyl chloride in tetrahydrofuran were prepared in separate beakers. Monoliths were dipped in the adipoyl chloride solution and dried in air. Subsequently, monoliths were dipped in the melamine solution and dried in air. This sequence was repeated 4 times.

After deposition of the Nylon, samples were treated for 4 h in 10 mM glutaraldehyde solution in 0.1 M acetate buffer pH 4.5 and washed with water. After drying at 333 K, trypsin (3 g l⁻¹) in 0.1 M phosphate buffer pH 8 was circulated over the carrier for 5 h at 278 K. Then, 50 ml sodium borohydride was added to yield a final 1 mM solution. Carriers were washed with water and dried under vacuum.

Enzyme aggregates (CLEAs)

Monoliths were functionalized with aldehyde groups through the APTES-glutaraldehyde protocol as described above. Trypsin (10 g) was added to 200 ml of a 500 g l⁻¹ (NH₄)₂SO₄ in 50 mM phosphate buffer pH 8. A milky solution was formed. 8.1g of 25 wt% glutaraldehyde

was added to start the crosslinking. The resulting imine-bonds were reduced by adding 0.66 g cyanoborohydride. Monoliths were immersed in this solution for 17 h.

2.3 Catalyst performance

The activity of the immobilized trypsin was followed spectrophotometrically for the hydrolysis of N-Benzoyl-L-arginine ethylester at 298 K in aqueous environment. Initial substrate concentration was 0.3 g l^{-1} in a 50 mM phosphate buffer pH 8. Total reaction volume was 0.16 l. The absorbance was measured at 253 nm. Catalysts were compared for their initial activity (0-30 min), calculated from the initial linear part of the concentration/time plot. The experimental set-up consisted of a glass reactor with a stirrer and a recycle mechanism to force the liquid circulation through the monolith channels. A schematic overview of the experimental set-up is presented in Figure 6.

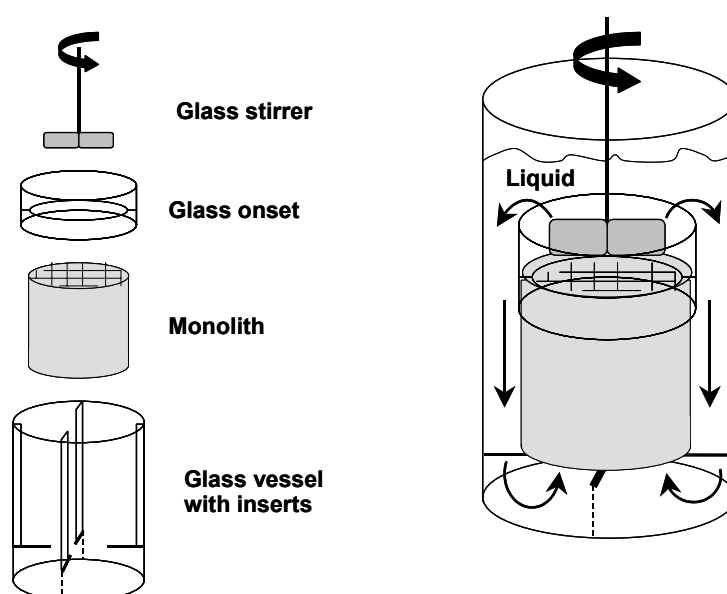


Figure 6. Experimental set-up with glass reactor, onset, and stirrer

Before starting the test sequence in order to compare the different biocatalysts, the system was tested for the presence of mass transfer limitations by varying the stirrer rate. A stirrer rate of 1000 rpm was selected for all experiments. Catalyst stability was tested by storage at 278 and 313 K and by repetitive activity testing. A 1 cm quartz cuvette was used to measure the absorbance. During activity tests samples of 2.5 ml were withdrawn from the reactor and returned to the reaction mixture after measurement. To establish the optimal wavelength, several scans were performed from 240-300 nm. In Figure 7 the absorbance of reaction mixtures with different composition are plotted. The arrow indicates increasing conversion. The maximal difference in absolute absorbance between 0 and 100% conversion was found at 253 nm. This is in accordance with earlier observations [30,32,34].

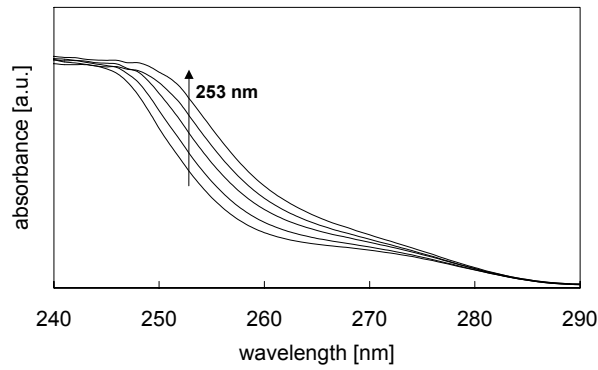


Figure 7. Selection of the wavelength for the BAEE assay

Both reactant (BAEE) and the product (N-benzoyl-L-arginine, BA) of the enzymatic reaction absorb light at 253 nm, but the intensity is different. There is no interaction between BA and BAEE that influences the total absorption intensity (the sum of the individual adsorption intensities). The total adsorption intensity can be expressed as a function of conversion (ξ), A_{BAEE} , and A_{AA} (1). And conversion can be expressed as a function of the product concentration (2)

$$A = A_{BAEE} + (A_{BA} - A_{BAEE}) \cdot \xi \quad (1)$$

$$\xi = \frac{C_{0,BAEE} - C_{t,BAEE}}{C_{0,BAEE}} \quad (2)$$

By calibrating the system for A_{BAEE} and A_{AA} at $C_{0,BAEE}$ and measuring total absorption during the course of the reaction, the product concentration can be determined using equations 1 and 2. In Figure 8a, calibration results at 253 nm are given for product and reactant. The calibration curve was verified by comparing the calculated concentrations (solid lines in Figure 8b) with the absolute concentrations (dots in Figure 8b) at different conversion levels. It is concluded that the measured absorbance can be used to calculate the conversion level by using equations 1 and 2 and the calibration of Figure 8a.

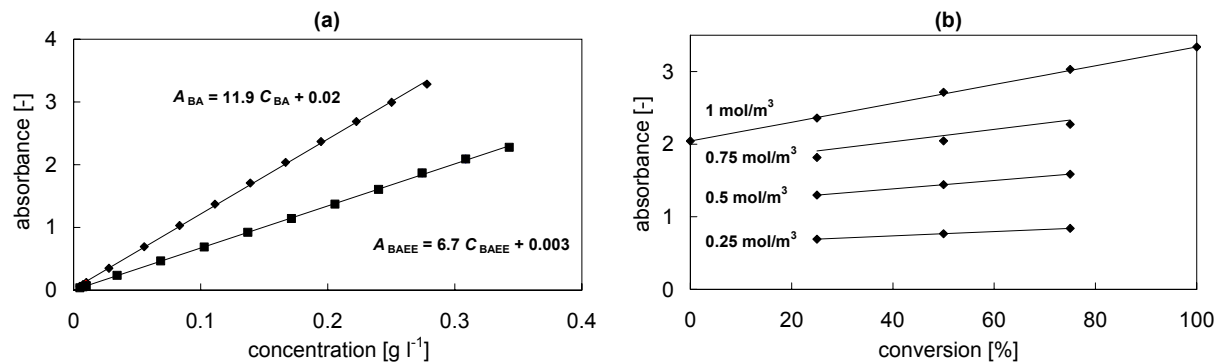


Figure 8. a) Calibration of the UV-cell and b) comparison of measured (dots) and calculated values (lines) after calibration

With this calibration, data from the enzyme assay was converted to concentration/time data in order to follow initial activity of the monolithic biocatalysts.

2.4 Nomenclature

Samples names are coded depending on the monolith type and the immobilization protocol. The first letter of the samples is used to distinguish the monolith type, “C” is used for cordierite, “A” for ACM. A second letter is used in the case of ACM to determine the microstructure of the ACM; “S” for small micrograins, “M” for medium needles and “L” for the most open structure with large micrograins. The methods are abbreviated with a code. This is summarized in Table 2.

Table 2. Nomenclature

Position	Component	Code
1	Monolith type	C or A
2	Micro grain structure ACM	S, M, or L
3	Method of immobilization:	
	Glutaraldehyde high concentration	GLU/H
	Glutaraldehyde low concentration	GLU/L
	Indirect aldehyde/ sequential method	ALD/SM
	Indirect aldehyde/ indirect method	ALD/IM
	p-Nitrofenylchloroformate	NFCF
	Carboxyl-diimidazole	CDL
	Nylon	Ny
	Enzyme aggregates	CLEA

3 Results and Discussion

All immobilization protocols yielded active biocatalysts, but the differences in immobilization yield and activity were relatively large. In the following sections, the immobilization efficiency and catalyst performance of all prepared biocatalysts will be compared.

3.1 Trypsin immobilization

Immobilization of trypsin by applying the different methods leads to carriers with different final enzyme yield. Since the trypsin preparate is not completely pure, the measured calibration curve represents the total protein loading. This value is not corrected for impurities, but will nevertheless be indicated as total trypsin loading. The trypsin loading is presented for the used methods in Figure 9. See section 2.5 for the explanation of the codes. ACM monoliths were only used for the method with the best result for cordierite supports (ALD/IM protocol). The trypsin loading for CLEA and Ny are not known, due to severe disturbance of the UV-VIS adsorption by residual chemicals in the solution.

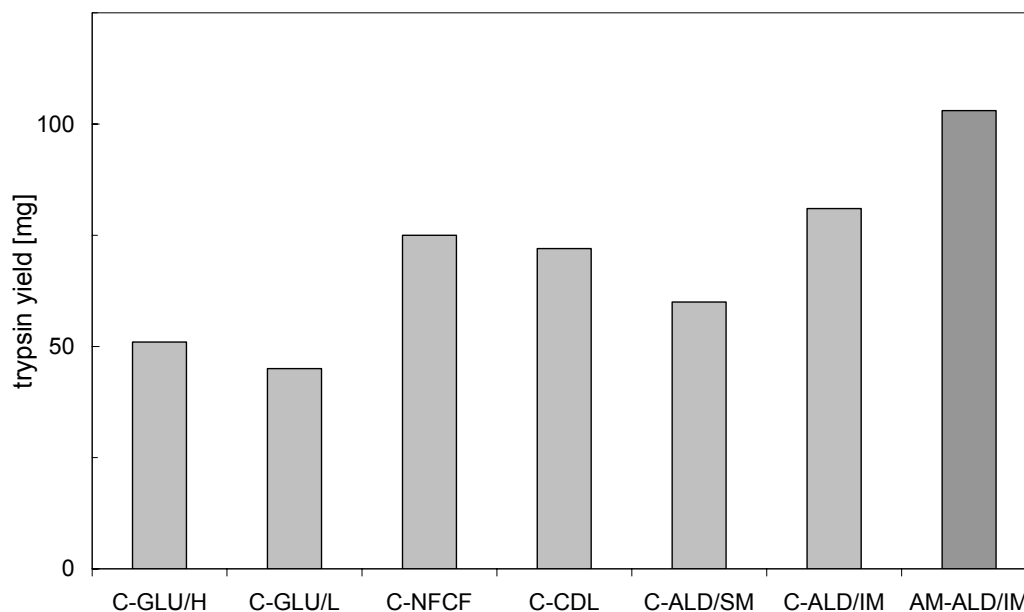


Figure 9. Final trypsin loading on 200 cps cordierite samples for the different immobilization protocols. Trypsin was immobilized from a 3 g l^{-1} aqueous phosphate buffer. 200 cps ACM was used in combination with the ALD/IM method.

The highest enzyme loading for cordierite monoliths was achieved with the ALD/IM method. When this method was applied for immobilization on ACM monoliths, the trypsin loading could be further increased. The enzyme loading for GLU/L and GLU/H are in the same order of magnitude, as are the results for the three GPTMS-based methods ALD/SM, NFCF, and CDL.

3.1.1 Immobilization via APTES

Initially, the objective was to optimize enzyme loading by increasing the amount of aldehyde groups on the surface. It was found that the pH during activation of the monolith with glutaraldehyde (GA) significantly influences the final glutaraldehyde loading. The concentration of GA in solution can be determined by UV-VIS at 280 nm. At pH 5, around 7 mg GA was attached to the surface of a cordierite sample, at pH 9 this value decreased to 4 mg. But the higher GA loading, obtained at pH 5, did not result in a significant increase in enzyme loading (not shown). The excess glutaraldehyde is probably only used in multi-point attachment of the enzyme, instead of providing for new binding sites. This could affect the activity of the enzyme [37]. An increase in GA on the surface can therefore not be used to increase trypsin loading. Since no difference in enzyme loading was observed for GA treatment at higher pH this step was only performed at pH 5.

However, enzyme loading could be increased by varying another important parameter, the pH during immobilization. The effect of pH on trypsin immobilization was studied, in combination with post-immobilization crosslinking with GA. The results are presented in Figure 10. The immobilized activity of different samples (GLU/H-pH5, GLU/H-pH9, and crosslinked after immobilization) is plotted at two different immobilization-pH's.

Additionally, the results of the GLU/L protocol (decreased GA concentration) are given for immobilization at pH 8. For all used GA concentrations and post-immobilization crosslinking the enzyme loading remained constant at 50 mg. So apparently, the different protocols affect the final activity of the biocatalyst. It is known that trypsin is in its most active form at pH 8, this is clearly supported by the data in Figure 10; adsorption at pH 8 leads to a higher activity, compared to immobilization at pH 6. A similar effect of pH on immobilized activity was also observed for urease in various studies [44, 51,52]

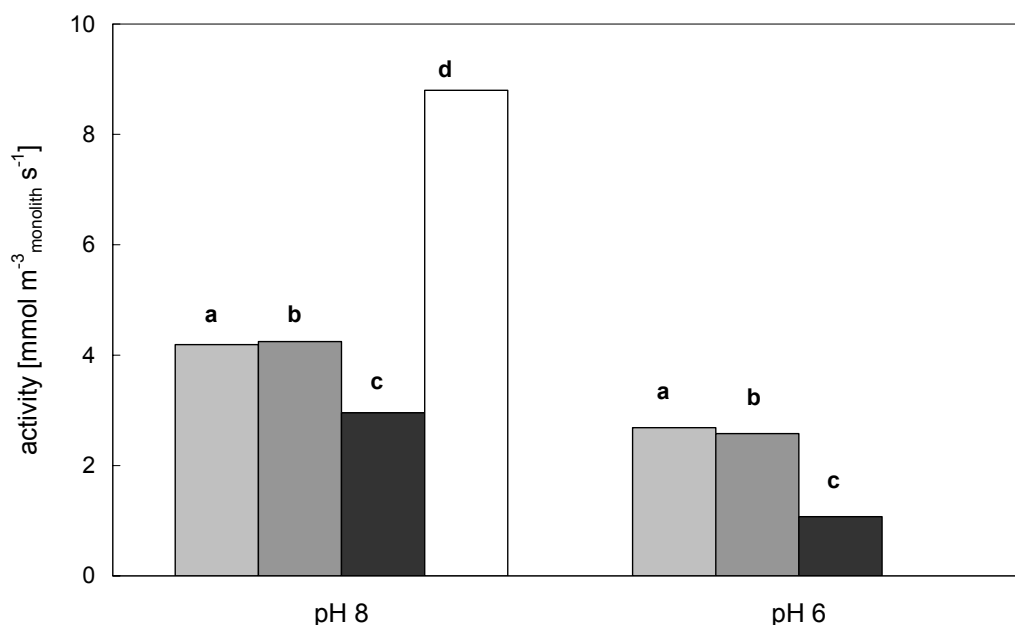


Figure 10. Optimization of the GLU protocol for immobilization of trypsin on cordierite monoliths. Initial activity in the hydrolysis of BAEE for a) GLU/H, 7 mg GA, b) GLU/H, 4 mg GA, c) GLU/H, 7 mg GA crosslinked after immobilization, d) GLU/L

At both pH 6 and 8, a higher glutaraldehyde loading (compare bars a and b) does not influence the enzyme loading or change final activity after trypsin adsorption. Apparently the immobilization conditions are more important for immobilized activity than a high glutaraldehyde content of the carrier. At very low GA concentration however, activity significantly increases (d). The initial reactions with GA (a at pH 9 and b at pH 7) were done with a glutaraldehyde concentration of 0.1 M. Since an increase in bound glutaraldehyde did not affect the final activity of the immobilized trypsin, it was investigated if a decrease in aldehyde groups could minimize the deactivating effect [35-39] of this component. The concentration could be decreased to 10 mM at pH 5 (the GLU/L protocol) to optimize residual activity (d). The exact GA loading of samples prepared with the GLU/L protocol is not known. The lower glutaraldehyde concentration did not influence final trypsin loading (see Figure 9 GLU/H and GLU/L), but resulted in a doubling of the immobilized activity of the biocatalyst (Figure 10 a and d).

In order to try to retain more enzyme on the monolith, samples were treated a second time with GA, after immobilization (crosslinking with a 10 mM GA solution). There is a clear negative effect of crosslinking (c). This can be caused by deactivation of the enzyme due to

high glutaraldehyde concentrations and strong multi-point attachment that limits conformational changes.

3.1.2 Immobilization via GPTMS

When the GPTMS-based methods are compared, it can be seen that immobilization via ALD/IM leads to a slight increase in enzyme loading compared to ALD/SM (Figure 9). By hydrolyzing the epoxygroup before attachment of the silane to the silica surface, the enzyme loading increases with 25%. Since aldehyde formation and enzyme immobilization are the same for both methods, the difference should be caused by the activation step of the support. A possible explanation can be the more efficient functionalization at elevated temperature in the ALD/IM protocol. Another important difference between ALD/SM and ALD/IM is the solvent. In ALD/SM toluene is used, whereas water is used in ALD/IM. It has been observed [53] that the use of an organic solvent leads to the formation of a mono-layer of silane and aqueous medium leads to formation of polymerized network of silane. Bogart and Leyden [54] found that during silanization in aqueous solution, the mixture becomes turbid during the reaction (due the formation of polymerized silane) and then transparent again (binding of the polymer to the silica surface). When the ALD/IM protocol was applied, this was not observed, the solution remained clear. It is possible that polymerization does not occur at the low pH that is required to simultaneously hydrolyze the epoxygroup. This would imply that for both methods a monolayer of silane is deposited on the monolith surface. The increase in enzyme loading for ALD/IM however does indicate that the silanization step in aqueous medium is more efficient. When ACM monoliths are used, the total enzyme loading can be further increased. As was shown before (Chapter 4), the silane yield on ACM is higher than on cordierite. This is probably the reason for a higher final trypsin loading on ACM. The more open structure of the ACM monoliths provides more binding sites for silanization and can therefore bind a higher amount of protein.

Bonding through NFCF and CDL leads to comparable enzyme loadings with yields after immobilization with ALS/SM. This is in agreement with earlier work by Ernst-Cabrera *et al.* [55], who found no difference in enzyme loading for immobilization via ALD/SM, NFCF, and CDL.

If we assume a cordierite backbone (with a LudoxAS-40 washcoat) with a total surface area of $10 \text{ m}^2 \text{ g}^{-1}_{\text{silica}}$ for APTES and $30 \text{ m}^2 \text{ g}^{-1}_{\text{silica}}$ for GPTMS and a washcoated ACM support with $25 \text{ m}^2 \text{ g}^{-1}_{\text{silica}}$ for GPTMS, the surface coverage after immobilization can be calculated (see Chapter 4 for details on surface area and pore volume of silanized monoliths). If trypsin is assumed to be a flat circle with a diameter of 4 nm and a mass of 23 kDa, the corresponding loading and coverage of the different methods are given in Table 3. It follows that for all employed protocols, the enzyme is present below a monolayer coverage with a coverage of 22-50% for cordierite and 87 % for AM-ALD/IM.

Table 3. Trypsin loading on 200 cpsi monoliths, expressed in surface area and total coverage.

Method	Trypsin loading		
	mg	mg m ⁻²	% surface
C-GLU/L	45	1.5	53
C-ALD/SM	60	0.72	22
C-ALD/IM	81	0.94	30
AM-ALD/IM	103	3.4	82
C-NFCF	75	0.83	26
C-CDL	70	0.78	24

3.2 Catalyst Performance

When the activity of the biocatalysts is regarded, two important parameters should be taken into account:

- The activity of the biocatalyst per monolith volume
- The specific activity, per g of enzyme

In Table 4, immobilization yield and initial activity per reactor volume is presented for the different protocols in combination with 200 cpsi monoliths.

Table 4. Immobilization and initial activity for immobilized trypsin at 298 K

Catalyst	Total adsorption	Volumetric activity	Specific activity
	mg	mmol m ⁻³ _{monolith} s ⁻¹	mmol g ⁻¹ _{protein} s ⁻¹ *
Free trypsin	-	-	23 x 10 ⁻²
C-GLU/H	51	4.2	0.5 x 10 ⁻²
C-GLU/L	45	9	1.2 x 10 ⁻²
C-ALD/SM	60	15.7	1.5 x 10 ⁻²
C-ALD/IM	81	21.3	1.6 x 10 ⁻²
AM-ALD/IM	103	26.7	1.5 x 10 ⁻²
C-NFCF	75	17.1	1.3 x 10 ⁻²
C-CDL	72	15.2	1.1 x 10 ⁻²
C-Ny	-	7.7	-
C-CLEA	-	1.6	-

* Trypsin content in the crude protein is estimated to be 10%

If a trypsin content of 10% is assumed, the specific activity of the free and immobilized enzyme can be used to estimate the turnover frequency (TOF), defined as the number of converted substrate molecules per site per second. For free trypsin, a TOF of 55 s⁻¹ was found, for immobilized trypsin (AM-ALD/IM) this number is 4 s⁻¹. The value for free trypsin is in the same order of magnitude as the general value of 100 given by Bickerstaff [56]. Covalent immobilization apparently leads to a relatively large decrease in specific enzyme activity. Covalently attaching the proteins chemically alters the molecules, thereby limiting the conformational freedom and possibly altering the structure of the enzyme or the chemistry in the active site (in the case of reactions with glutaraldehyde all amino acids with free amine groups can be chemically altered or connected). This leads to a recovered enzyme activity of

only 7%. Similar values were obtained for immobilization via the GLU protocol in various studies [1,57-59]

In Figure 11 the activity per monolith volume (bars) and the specific activity of the immobilized trypsin (symbols) are presented for the different immobilization protocols.

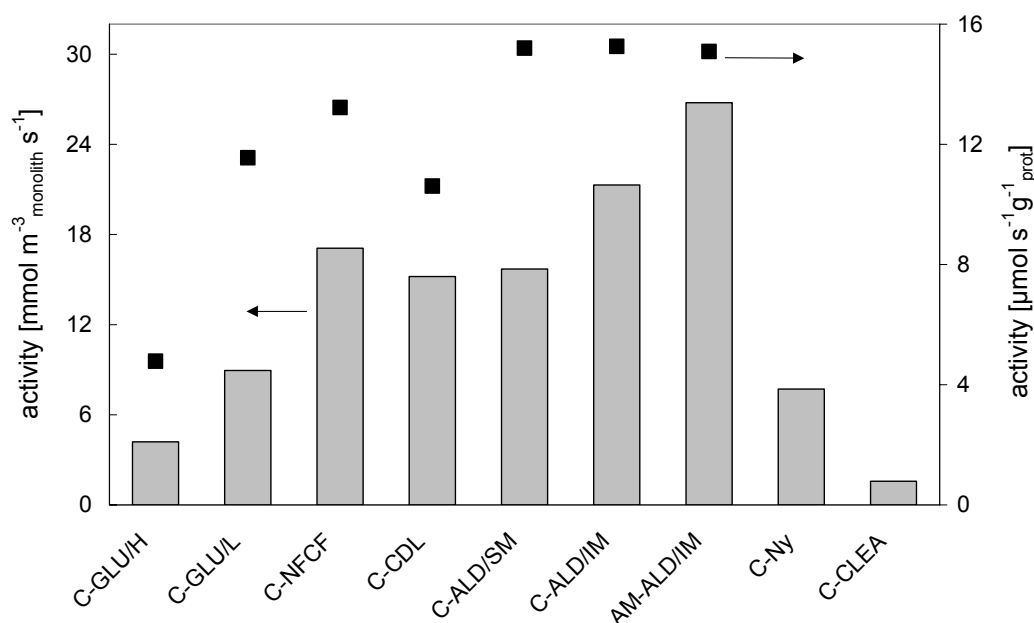


Figure 11. Initial activity (bars, left axis) and specific activity (symbols, right axis) of the prepared 200 cpsi cordierite biocatalysts in the hydrolysis of BAEE at 298 K. 200 cpsi ACM was used in combination with the ALD/IM protocol.

There is a large difference in immobilized activity for GLU/H and GLU/L. The glutaraldehyde concentration clearly negatively affects the final activity of the biocatalyst. It was stated before that a high concentration negatively influences specific enzyme activity [37], by limiting the conformational freedom of the immobilized enzyme. In Figure 9 it was shown that final enzyme loading does not change significantly when the glutaraldehyde concentration is decreased. It seems that a large part of the trypsin is deactivated in the case of GLU/H. This can also be seen by comparing the specific activity of both biocatalysts.

The biocatalysts prepared by ALD/SM and ALD/IM also differ significantly in activity. This is only caused by increased enzyme loading for ALD/IM (Figure 9), the specific enzyme activity is the same. When ACM monoliths are used, the activity increases further, but again the specific activity does not change with microstructure. The other GPTMS-based methods that use an acylation (NFCF and CDL) were found to have an equal enzyme loading (Figure 9), but from Figure 11 it follows that specific activity is lower for these methods. It is possible that reactants and/or side products that are formed during the activation and immobilization steps have a negative effect on enzyme activity.

3.2.1 CLEAs

Although CLEAs were prepared from a concentrated enzyme solution, final activity was low compared to the other biocatalysts. To prepare the CLEAs, cyanoborohydride, glutaraldehyde and high salt concentrations are needed. This probably has a strong deactivating effect on the immobilized trypsin. Although enzyme density on the surface is much higher than for the other carriers, this protocol does not lead to an interesting performance. Cyanoborohydride forms a precipitate with the CLEAs, preventing effective attachment of the aggregates to the monolith surface.

3.2.2 Nylon

The low activity for nylon-coated monoliths can be explained by the low nylon yield during functionalization of the washcoated support. Results for the different process steps in nylon deposition on the monolith surface are presented in Table 5. For each component the total yield per gram monolith is given, as well as the yield per mol of silane (to check the percentage of organo silane and glutaraldehyde groups molecules that have reacted).

Table 5. Final yield for the different preparation steps of the two methods to attach nylon onto cordierite monoliths as determined by TGA

Component	2-phase method		water-method	
	Yield		Yield	
	mg g ⁻¹ _{total}	mol mol ⁻¹ _{silane}	mg g ⁻¹ _{total}	mol mol ⁻¹ _{silane}
Water	2.7	-	4.3	-
Glutaraldehyde	1.4	0.27	3.3	0.43
Silane	6.8	1	10.0	1
Nylon	3.1	0.26	4.7	0.27

The carrier that was used in the 2-phase method, has a silane yield of 0.68 g g⁻¹_{monolith} and the carrier for the water method has a silane content of 1 g g⁻¹_{monolith}. Polymerization with the 2-phase method leads to a slightly lower total nylon yield (0.31 g g⁻¹) than the water method. This is caused by the lower silane yield on this carrier. The relative yield per mol silane is identical for both methods. Based on the initial concentrations, these coatings were acquired at 44% and 70% conversion for the 2-phase method and the water method respectively. Taking into account the practical aspect of the water method, this would be the preferred method to apply a nylon coating on a monolith surface.

If attachment of CLEAs is compared to attachment of Nylon, CLEA seems a suitable method to create a high enzyme density on the monolith surface. This method however, was originally developed to facilitate catalyst separation, not to optimize specific activity. The use of glutaraldehyde severely deactivates the trypsin. The formation of a tightly connected enzyme layer could also cause substrate/product diffusion problems inside this catalyst layer. Deactivation could be minimized by using a dialdehyde with a longer backbone. This would

increase the flexibility of the connections and therefore the conformational freedom of the enzyme.

Nylon can be attached to the monolith, but if it actually leads to a significant increase in binding sites remains unclear. The very low polymer to silane ratio indicates incomplete coating. Secondly, it remains unclear if glutaraldehyde binds with the present amino-groups of the silane (following the GLU method) or the amino groups of the polymer. If we assume a specific activity in the same order of magnitude as GLU/L (see Figure 11), the enzyme loading would be around 4 times lower for Ny. If the polymer yield on the monolith surface could be increased, in theory, more aldehyde groups would be available compared to GLU/L. this would lead to a higher enzyme loading. Although Ny seems the preferred method over CLEA for use with monoliths, this protocol also uses glutaraldehyde. Therefore it is not expected that this method can outperform the GPTMS-based methods. This method could still be a very interesting option if Nylon monoliths could be fabricated by extrusion. Extensive research [45-47] on immobilization of enzymes on nylon cloth and tubes has shown that this method leads to active and stable biocatalysts.

Based on practical considerations, all methods need to be performed in fume hoods due to toxic chemicals involved and consisting of one or more consecutive activation/drying steps. The methods that used cyanoborohydride are not favored due to handling the extremely toxic reducing agent. The same argument holds true for the protocols that involve the use of glutaraldehyde. The complicated CLEA and Nylon procedures are also unattractive because they involve production of a carrier material and a subsequent step to attach the carrier to the monolith. Based on the enzyme yield and specific activity the ALD/IM protocol would be the preferred method to maximize the activity per monolith volume.

3.2.3 Application as a biocatalyst for L-S mass transfer measurements

To verify if the increased enzyme immobilization by optimizing the protocol that was aimed for is sufficient for application of these biocatalysts in mass transfer studies of monolith reactors, the activity of the monoliths should be compared to the observed mass transfer coefficient in earlier studies [34]. From [34], a mass transfer coefficient k_s of $6 \cdot 10^{-6} \text{ m s}^{-1}$ was found for 400 cpsi monoliths with a length of 5 cm at 319 K. From this value an apparent rate constant $k_{r,obs}$ can be calculated by using the geometrical surface area of a 400 cpsi monolith (0.157 m^2) and a reactor volume of 2.1 l by equation (3)

$$k_s = k_{r,obs} \frac{V_L}{A_m} \quad (3)$$

From equation (3), $k_{r,obs}$ was found to be $5 \cdot 10^{-4} \text{ s}^{-1}$. For C-ALD/IM (400 cpsi), an apparent rate constant of $38 \cdot 10^{-4} \text{ s}^{-1}$ was determined (not shown) under kinetically limited conditions at 298 K. So $k_{r,obs}$ for C-ALD/IM is much larger than the previously determined $5 \cdot 10^{-4} \text{ s}^{-1}$. The difference is actually even stronger considering the temperature of both experiments; the rate

constant for C-ALD/IM was determined at 298 K, whereas the experiments in [34] were performed at 319 K. Apparently the activity per monolith volume has increased significantly after optimizing the immobilization protocol and it is therefore expected that the monolithic biocatalysts can be applied to measure L-S mass transfer coefficients in the monolithic stirrer reactor and the monolith loop reactor. The use of C-ALD/IM-catalysts should lead to further increase in the range of stirrer rates that can be used, due to the increased enzyme loading capacity.

3.2.4 Effect of cell density

Cordierite samples with different cell densities (100, 200, and 400 cpsi) were used in combination with the ALD/IM protocol. The results are presented in Figure 12.

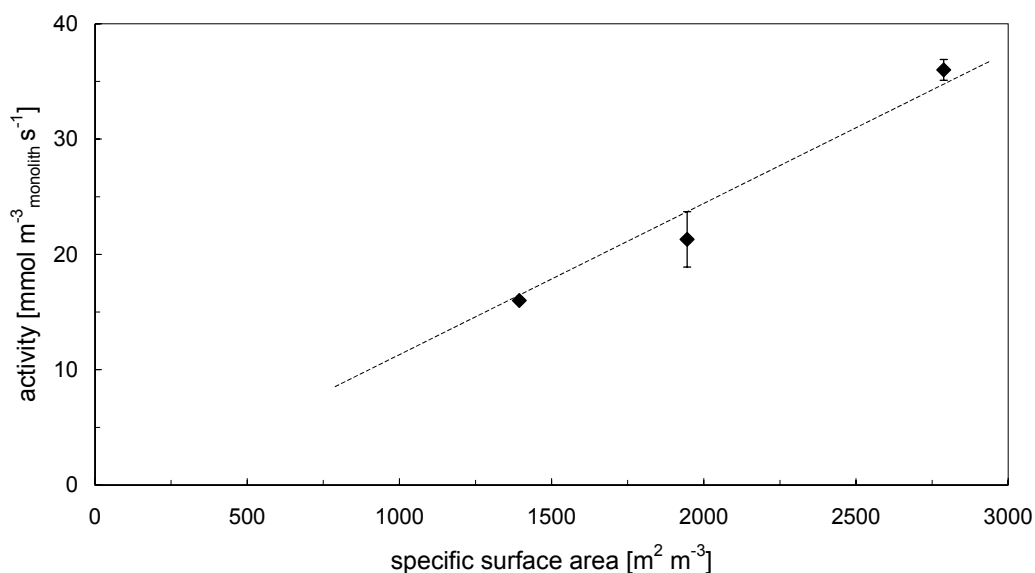


Figure 12. Effect of cell density on the initial activity per monolith volume in the hydrolysis of BAEE at pH 8, 298 K, expressed in geometrical surface area. Bars represent the 95% confidence interval

The activity per monolith volume (which depends on enzyme loading, as was seen in Table 4) corresponds to the surface area of the used monoliths. The cell density does not influence the specific activity of the enzyme. As expected, the enzyme loading increases proportionally with the available surface area. The fact that the loading on ACM monoliths with a 25 times higher specific surface area (Table 1) is not proportional to the data that is presented here, is most likely caused by plugging of the wall by the washcoat material, decreasing the available surface area. From Table 4, the activity of the ACM sample is $26.7 \text{ mmol m}^{-3} \text{monolith s}^{-1}$. This corresponds to specific surface area of around 2300 in Figure 12. The specific surface area of the ACM monolith has decreased by a factor 20 due to filling up the porous wall during washcoating.

3.3 Reproducibility with ALD/IM

Five different batches of biocatalysts were prepared with the ALD/IM method. Immobilization via the ALD/IM protocol is reproducible, as is demonstrated in Figure 13. The activity for different batches of 200 cpsi C-ALD/IM and AM-ALD/IM is compared at 298 K.

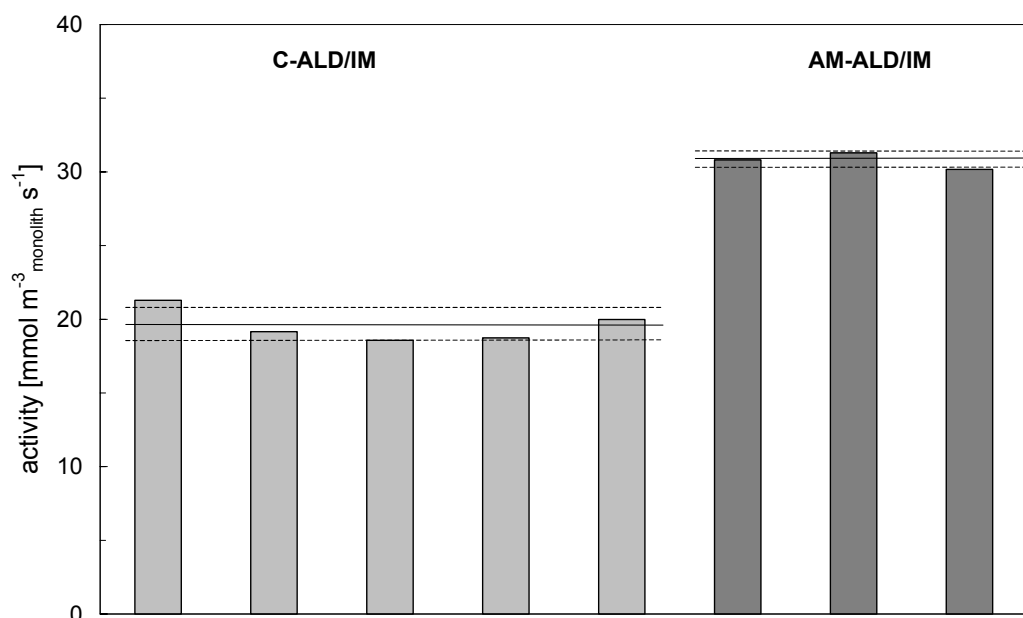


Figure 13. Reproducibility of the ALD/IM method on cordierite (light colored bars) and ACM (dark colored bars), expressed in terms of activity per monolith volume in the hydrolysis of BAEE at 298 K. The solid lines indicate the average value. The dashed lines represent the 95% confidence interval.

3.4 Stability of ALD/IM biocatalysts

The stability of the monolithic biocatalysts was studied with respect to storage for prolonged periods of time at different temperatures and by a sequence of activity tests at 312 K.

3.4.1 Consecutive testing

After a sequence of 11 consecutive activity tests (with storage overnight between test 5 and 6) with C-ALD/IM, the activity had gradually decreased to 80%. Apparently repetitive use at 312 K, leads to a deactivation. It is likely that use at elevated temperatures deactivates the immobilized trypsin, this enzyme has a low temperature stability above 315 K [48]. It is assumed that both the use at 312 K and storage slowly deactivate the biocatalyst.

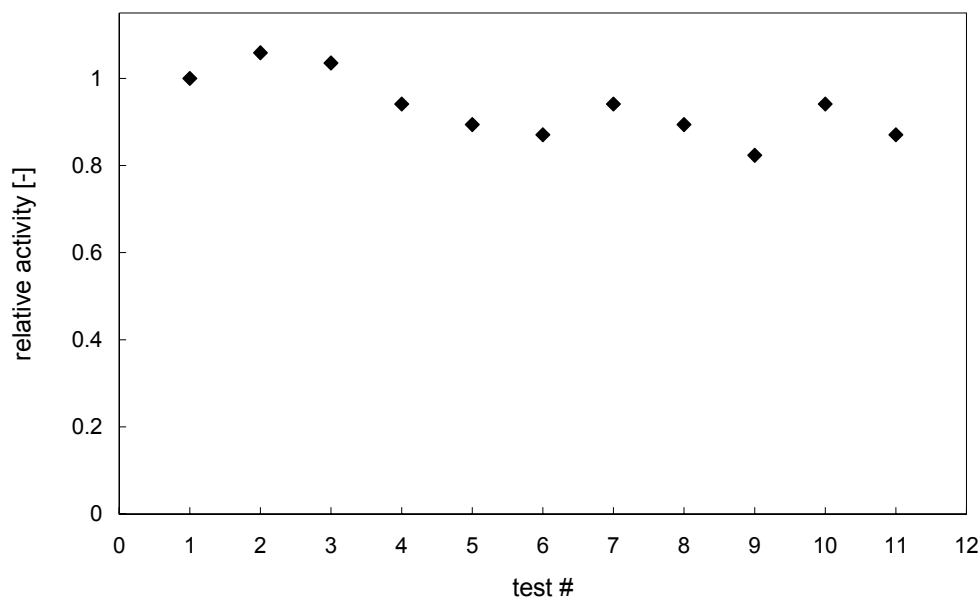


Figure 14. Stability of C-ALD/IM (400 cps) during subsequent tests in the hydrolysis of BAEE at pH 8, 312 K

3.4.2 Storage stability

The effect of storage at 278 K and at 315 K on the initial activity of the biocatalysts at 312 K is presented in Figure 15. Over a period of 20 days, the activity decreases with around 1% per day when the monolith is stored at 278 K. At a storage temperature of 315 K, a deactivation of 8% was observed after 42 h. Since no NaN_3 was used during storage at higher temperature, it was expected that additional deactivation would occur due to growth of microorganisms on the protein rich monolithic supports.

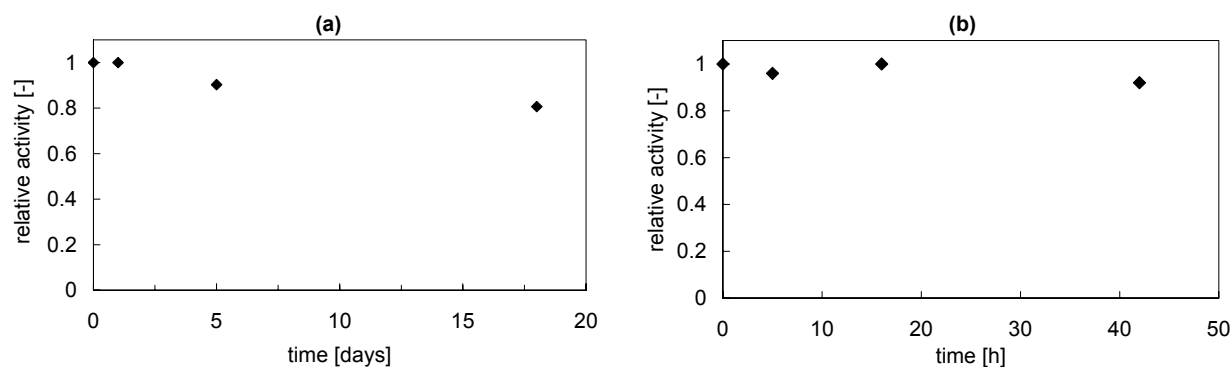


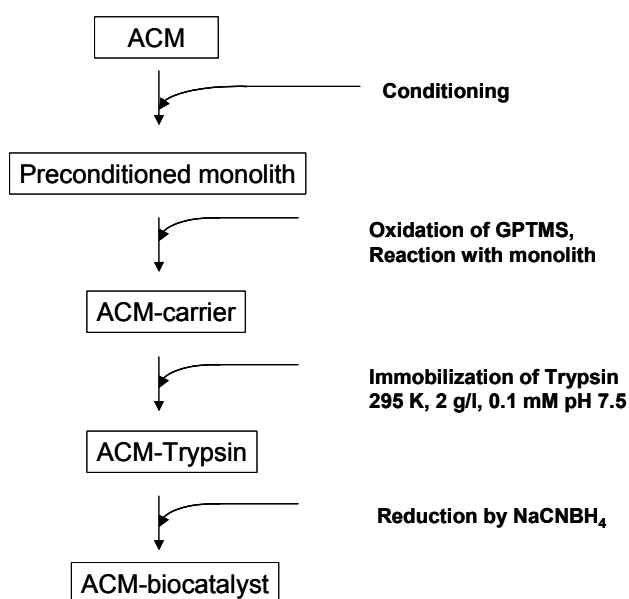
Figure 15. Initial activity (relative) of a 200 cps C-ALD/IM sample in the hydrolysis of BAEE at 298 K. a) after storage in 1 g l^{-1} sodiumazide at 278 K, b) after storage in 10 mM phosphate buffer pH 7 at 315 K for several hours

The ALD/IM protocol can be used to prepare active and stable biocatalysts. Although the immobilized activity seems low at only 7% compared to the free enzyme, this is a typical value for covalent immobilization. To increase the immobilized activity, another less destructive protocol is suggested, such as adsorption or entrapment. The main advantage of covalent binding with respect to L-S mass transfer measurements is the strong bond between

enzyme and support in case of high shear forces at higher flow rates. Secondly, the enzyme is attached on the outer surface of the silanized washcoat (note the decreased surface area of the washcoat after silanization that was observed in chapter 4). This results in absence of internal mass transfer limitations that are often found in biocatalysts prepared by entrapment or adsorption. And since the present loading that can be achieved with the ALD/IM method is sufficient to proceed with L-S mass transfer experiments, the ALD/IM method is recommended as the immobilization protocol for mass transfer studies in different types of monolithic bioreactors. In Chapters 10 and 12, this system will be used to determine L-S mass transfer coefficients in different reactor systems.

4 Conclusions

Trypsin can be covalently attached to monolithic supports with different microstructure. Several protocols, either based on (3-aminopropyl)triethoxysilane (APTES) or (3-glycidoxypropyl)trimethoxysilane (GPTMS) were studied. The immobilization protocols that use GPTMS generally result in a higher enzyme loading and a higher activity per g of enzyme. The APTES-glutaraldehyde method could be optimized by varying pH and glutaraldehyde loading, but both enzyme loading and activity are lower than for the GPTMS-based methods. Attachment of enzyme crystals (CLEAs) or Nylon monoliths does not yield very active biocatalysts. Moreover, preparation via these methods is a time-consuming, multistep process, and therefore less attractive. The best carrier material was obtained by immobilization via the ALD/IM protocol in which the epoxygroup of GPTMS is hydrolyzed before reaction of the silane with the silica support. This leads to higher enzyme loading than hydrolysis after binding to the silica (ALD/SM). To maximize the activity per monolith volume, the biocatalyst should be prepared according to the following scheme:



The use of ACM monoliths leads to an additional increase in trypsin loading and in volumetric activity. The specific enzyme-activity is not influenced by the monolith-microstructure, and remains constant around 7% compared to the free enzyme (for the ALD/IM method). Both the enzyme loading and the activity per monolith volume are proportional to the monolith surface area, changing the cell density does not influence specific activity.

The reproducibility of the preparation of monolithic biocatalysts, prepared via the ALD/IM method is high. The catalysts show a slow deactivation during storage at 278 K. This deactivation is faster at higher temperatures. Deactivation occurs during both storage and testing. From a comparison with previous results, it is expected that the ALD/IM biocatalysts have a sufficient enzyme loading and activity to be successfully used in L-S mass transfer experiments in the monolith loop and the monolithic stirrer reactor. To minimize the effect of deactivation, catalysts should be used in no more than 10 subsequent tests over a maximum period of 5 days.

5 Acknowledgements

Nico Hinskens is gratefully acknowledged for performing the immobilization studies. Rob Schoevaart and dr. Hanefeld are thanked for their useful input during these studies. Corning Inc. is acknowledged for supplying the monoliths. The Dow Chemical Company is acknowledged for supplying the ACM monoliths and funding part of this research.

6 Symbols

A_i	absolute absorption of component i	[-]
A_m	geometric surface area	[m ²]
$C_{0,i}$	initial concentration of component i	[mol m ⁻³]
$C_{t,i}$	concentration of component i	[mol m ⁻³]
$k_{r,obs}$	observed reaction rate constant	[s ⁻¹]
k_s	mass transfer coefficient	[m s ⁻¹]
V_L	liquid volume	[m ³]

Greek symbols

ζ	conversion	[-]
---------	------------	-----

Components

BAEE	n-benzoyl-L-arginine ethyl ester
BA	n-benzoyl-L-arginine

7 References

- [1] M.R. Benoit, J.T. Kohler (1975) *Biotechnology and Bioengineering*; 17: 1616-1626
- [2] E.A. Grovendera, C.L. Cooney, R.S. Langer, G.A. Ameer (2001) *Chemical Engineering Science* 56: 5437-5441
- [3] B.C. Koops, E. Papadimou, H.M. Verheij, A.J. Slotboom, M.R. Egmond (1999) *Applied Microbiology and Biotechnology*; 52: 791-96
- [4] W. Warmuth, E. Wenzig (1995) *Bioprocess Engineering*; 12: 87-93
- [5] A.R. Ozdural, D. Tanyolac, I. Boyaci, M. Mutlu, C. Webb (2003) *Biochemical Engineering Journal*; 14: 27-36
- [6] N. Hidaka, T. Matsumoto (2000) *Industrial Engineering and Chemistry Research*; 39: 909-15
- [7] L.N. Yee, C.C. Akoh (1995) *The Journal of the American Oil Chemists' Society*; 72(11): 1407-8
- [8] R.J. Barros, E. Wehtje, P. Adlercreutz (1997) *Biotechnology and Bioengineering*; 59: 364-73
- [9] J.F. Diaz, K.J. Balkus (1996) *Journal of Molecular Catalysis B: Enzymatic*; 2: 115-26
- [10] E. Dumitriu, F. Secundo, J. Patarin, I. Fecete (2003) *Journal of Molecular Catalysis B: Enzymatic*; 22: 119-33
- [11] F.N. Serralha, J.M. Lopes, F. Lemos, D.M.F. Prazeres, M.R. Aires Barros, J.M.S. Cabral (1998) *Journal of Molecular Catalysis B: Enzymatic*; 4: 303-11
- [12] A.P.V. Goncalves, J.M. Lopes, F. Lemos, J.M.S. Cabral, M.R. Aires Barros (1996) *Journal of Molecular Catalysis B: Enzymatic*; 1: 53-60
- [13] F. Kapteijn, J.J. Heiszwolf, T.A. Nijhuis, J.A. Moulijn (1999) *CATTECH*; 3(1): 24-41.
- [14] W. Tischer, V. Kasche (1999) *TIBTECH* 17: 326-335
- [15] B.J. Rovito, J.R. Kittrel (1973) *Biotechnology and Bioengineering*; 15: 143-161
- [16] A. Subramanian, S.J. Kennel, P.I. Oden, K.B. Jacobson, J. Woodward, M.J. Doktycz (1999) *Enzyme and Microbiology* 24: 26-34
- [17] M. Thust, M.J. Schoning, P. Schroth, U. Malkoc, C.I. Dicker, A. Steffen, P. Kordos, H. Luth (1999) *Journal of Molecular Catalysis B: Enzymatic* 7: 77-83
- [18] M. Ladero, A. Santos, F. Garcia-Ochoa (2000) *Enzyme and Microbial Technology* 27: 583-592
- [19] M. Narshima Rao, A.A. Kembhavi, A. Plant (2000) *Biotechnology Letters* 22: 1557-1559
- [20] H.H. Weetall, G. Baum (1970) *Biotechnology and Bioengineering*; 12: 399-407
- [21] T. Godjevargova, R. Nenkova, N. Dimova. (2005) *Macromolecular Bioscience* 5: 760-766
- [22] L. Cao, L. van Langen, R. A. Sheldon (2003) *Current Opinion in Biotechnology* 14(4): 387-394
- [23] L. Cao, L. M. van Langen, F. van Rantwijk R. A. Sheldon (2001) *Journal of Molecular Catalysis B: Enzymatic* 11(4-6): 665-670

- [24] N. Hilal, R. Nigmatullin and A. Alpatova (2004) *Journal of Membrane Science* 238(1-2): 131-141
- [25] J.F. Amorim Fernandes, M. McAlpine P.J. Halling (2005) *Biochemical Engineering Journal* 24(1): 11-15
- [26] J.J. Roy, T.E. Abraham, K.S. Abhijith, P.V. Sujith Kumar and M.S. Thakur *Biosensors and Bioelectronics* (2005) 21(1): 206-211
- [27] C.P. Govardhan (1999) *Current Opinion in Biotechnology* 10(4): 331-335
- [28] W. Gopel (1991) *Sensors and Actuators B, Chemical*; 4:7-21
- [29] J. Rogalski, J. Szczodrak, M. Pleszcynska, J. Fiedurek (1997) *Journal of Molecular Catalysis B: Enzymatic* 3:271-283
- [30] H.H. Weetall (1969) *Science* 166: 615-616
- [31] H.H. Weetall, N.B. Havewala. (1972) *Biotechnology and Bioengineering; Symp nr3* 241-266
- [32] C. Horvath, B.A. Solomon (1972) *Biotechnology and Bioengineering*; 14: 885-914
- [33] U. Brand, B. Reinhardt, F. Ruther, T. Scheper, K. Schugerl (1991) *Sensors and Actuators B*: 4: 315-318
- [34] I. Hoek (2004) PhD thesis, Delft University of Technology, The Netherlands, 21-38
- [35] S. Wang, M. Yoshimoto, K. Fukunaga, K. Nakao (2003) *Biotechnology and Bioengineering* 83(4): 444-453
- [36] L. Ferreira, M.A. Ramos, J.S. Dordick, M.H. Gil (2003) *Journal of Molecular Catalysis B: Enzymatic* 21:189-199
- [37] W.S. Adriano, E.H.C. Filho, J.A. Silva L.R.B. Goncalves (2005) *Biotechnology and Applied Biochemistry* 41: 201-207
- [38] D.R. Walt, V.I. Agayn (1994) *Trends in Analytical Chemistry*; 13: 425-430
- [39] C. Tual, E. Espuche, M. Escoubes and A Domard (2000) *Journal of Polymer Science, part B: Polymer Physics*; 38: 1521-1529
- [40] R.A. Sheldon, F. van Rantwijk (2004) *Australian Journal of Chemistry* 57: 281-89
- [41] L. Cao, F. van Rantwijk R. A. Sheldon (2000) *Organic Letters* 2: 1361-1364
- [42] R.A. Sheldon, R. Schoevaart, L. van Langen (2003) *Speciality Chemicals Magazine*; 7-8: 40
- [43] F.H. Isgrove, R.J.H. Williams, G.W. Niven, A.T. Andrews (2001) *Enzyme and Microbial Technology* 28: 225-232
- [44] A. Anita, C.A. Sastry, M.A. Hashim (1997) *Bioprocess Engineering* 17: 241-245
- [45] L. Amaya-Delgado, M.E. Hidalgo-Lara, M.C. Montes-Horcasitas (2006) *Food Chemistry*; 99(2): 299-304
- [46] M. Portaccio, M. El-Masry, N. Rossi Diano, A. De Maio, V. Grano, M. Lepore, P. Travascio, U. Bencivenga, N. Pagliuca, D.G. Mita (2002) *Journal of Molecular Catalysis B: Enzymatic*; 18: 49-67
- [47] G.M. Escandar, D. González Gómez, A. Espinosa Mansilla, A. Muñoz de la Peña, H.C. Goicoeche (2004) *Analytica Chimica Acta*; 506: 161-170
- [48] H.P. Kasserra, K.J. Laidler, (1969) *Canadian Journal of Chemistry* 47: 4031-4039
- [49] A. Borchert, E.O. Larsson, K. Mosbach (1982) *Journal of Chromatography*; 244: 49-56

- [50] H.E. Swaisgood, I.M. Chaiken, (1985) *Journal of Chromatography*; 327: 193-204
- [51] A. Anita, C.A. Sastry, M.A. Hashim (1997) *Bioprocess Engineering* 16:375-380
- [52] A. Anita, C.A. Sastry, M.A. Hashim (1997) *Bioprocess Engineering* 17:355-359
- [53] P.O. Larsson, M. Glad, L. Hansson, M.O. Månsson, S. Olshon, K. Mosbach, (1982) *Advances in Chromatography*; 244: 41-44
- [54] G.R. Bogart, D.E. Leyden, (1989) *Journal of Chromatography*; 483: 209-219
- [55] K. Ernst-Cabrera, M. Wilchek (1986) *Analytical Biochemistry*; 159: 267-272
- [56] G.F. Bickerstaff (1987) *Enzymes in Industry and Medicine*. Edward Arnold, London Great Britain
- [57] C. Suan, M.R. Sarmidi (2004) *Journal of Molecular Catalysis, B: Enzymatic*; 28: 111-119
- [58] G.K. Lee, R.A. Lesch, P.J. Reilly (1981) *Biotechnology and Bioengineering*; 23: 487-497
- [59] F. Ayhan, H. Ayhan, E. Piskin, A. Tanyolac (2002) *Bioresource Technology*; 81: 131-140
- [60] H.H.P. Yiu, P.A. Wright, N.P. Botting (2001) *Journal of Molecular Catalysis B: Enzymatic*; 15: 81-92

Entrapment of penicillin G acylase

Abstract

The objective of this work was to develop a hydrogel coated monolith for the entrapment of different penicillin G acylases, Assemblase[®] (PGA I) and Separase[®] (PGA II). Different biopolymers, including agarose, gelatin, alginate and chitosan were evaluated for their gel formation properties and the ability for immobilization of penicillin acylase. All polymers could form hydrogels that might be applicable on a monolithic structure. The immobilization parameters for covalent bonding of Assemblase were optimized using thin (200 μm) gel layers on glass plates. Based on enzyme loading capacity, chitosan cross-linked with glutaraldehyde was selected to be used as the carrier material on the monolith. For this gel, the effects of chitosan concentration, Assemblase concentration, glutaraldehyde concentration, and pH were studied to optimize immobilization capacity.

The optimized immobilization protocol was used to immobilize penicillin G acylase on chitosan-coated monoliths. The preparation of chitosan-coated monolithic structures immobilized with penicillin G acylase leads to active biocatalysts for the enzymatic hydrolysis of penicillin G. The storage stability is at least a month without loss of activity.

1 Introduction

The use of natural polymers in the biomedical [1] or industrial fields is interesting because of their biocompatible character and their possible biodegradation [2] into molecules easily assimilated by living organisms. And at present, public health and environmental regulations urge people to use non-toxic materials. For instance, the use of alginate, κ -carrageenan and other biopolymers as support materials for immobilization of various molecules, proteins, and cells have received considerable attention in recent years. Biopolymer supports have certain advantages over other polymeric materials such as low cost, ease of enzyme accessibility, hydrophilic character, and presence of hydroxyl groups on the surface capable of interaction with proteins. Enzyme immobilization on these supports is quick and apparently irreversible and provides nontoxic and biocompatible microenvironment conducive to the catalytic activity and stability of the enzyme. Hydrogels of natural polymers such as gelatin, chitosan, xanthan, and agarose can be used conveniently in both wet and dried states, although, these supports suffer from low mechanical strength and ease of microbial degradation. Also the particulate nature of these carriers usually leads to severe diffusion problems inside the carrier beads. The use of a thin layer of hydrogel on a monolith support can strongly reduce the problems associated with mechanical strength and diffusion of substrate/product.

Hydrogels can be defined as watersoluble, three-dimensional network of polymer chains able to swell but do not dissolve in aqueous environment. The high water content is responsible for high diffusivity of molecules. They provide ideal aqueous conditions for bioactive materials such as proteins [1]. The formation of a 3D network structure increases the mechanical and chemical stability. The term hydrogels refers to a range of polysaccharides and proteins that are nowadays widely used [2,3]. Applications include thickening and gelling of aqueous solutions, use as super absorbents [4], the use in stabilizing foams, emulsions and dispersions [5], inhibiting ice and sugar crystal formation, the controlled release of flavors and drugs [6,7], and enzyme immobilization [8,9]. Hydrocolloids, a separate group of hydrogels, are formed through physical interaction, for example by hydrogen bonding, hydrophobic association, cation-mediated cross-linking, etc. They differ from synthetic polymer gels, which normally consist of covalently cross-linked polymer chains. The most remarkable property of physical gels is the reversible gelation. Some hydrocolloids form thermally reversible gels where gelation occurs under cooling or heating. Other form non-thermally reversible gels; in such cases cross-linking polymer chains with divalent cations or a pH shift may induce gelation. In this study, different hydrogel forming agents were investigated to explore their gelling properties. Gelatin and agarose form thermally reversible hydrogels, alginate and chitosan gelate independent of temperature (see Table 1).

Table 1. Hydrocolloid gelling agents used in this study.

Gel	Gelation	Remarks
Gelatin	Temperature	Coil helix transition, followed by aggregation
Agarose	Temperature	Coil helix transition, followed by aggregation
Alginate	Addition of polyvalent cations or pH	Molecules cross-linked by polyvalent ions
Chitosan	pH	pH higher than 6.5, amino salt formation

1.1 Agarose

Agarose is a strongly gelling hydrocolloid from marine algae [10]. It is a linear structure of repetitive units of D-galactose and 3-6, anhydro-L-galactose. Gelation produces physical gels, which means that the polymer molecules of these aqueous gels maintain their structure so the process is not a polymerization but an electrostatic attraction. Agarose is frequently mentioned in literature as a carrier for protein adsorption; penicillin acylase was covalently bound to different types of agarose using different binding techniques, for instance on glyoxyl agarose using multipoint attachment [11,12].

1.2 Alginate

Alginates are quite abundant in nature as structural components in marine brown algae and as capsular polysaccharides in soil bacteria [10]. Alginate is a block copolymer composed of homopolymeric regions of α -L-guluronic acid (G) and β -D-mannuronic acid (M).

The blocks vary in size and alternating M and G segments as well as random blocks may also be present. The ion-binding properties of alginates are the basis for their gelling properties. The affinity of alginates for alkaline earth metals increases in the order $Mg << Ca < Sr < Ba$. Alginate gels gelate independent of temperature, although the kinetics of the gelling process are strongly influenced by temperature. Calcium alginate gel has been widely used in cell entrapment and encapsulation and is a well-known technique. The immobilization method is not toxic and inert, inexpensive and practical. Calcium alginate is normally not used for enzyme entrapment as the large pore sizes of these beads result in enzyme leakage, even in the case of large enzymes with molecular weights over 300.000. However, individually entrapped glucoamylase and pullulanase in calcium alginate beads for the hydrolysis of starch are known [13]. The same technique was also reported for the immobilization of tyrosinase [14]. Another option is immobilization in fibers and beads treated with glutaraldehyde and isocyanate, which was done for glucoamylase [15]. A rather different approach is the immobilization of lipase in a beads composed of a blend of alginate with gelatin cross-linked with glutaraldehyde [16].

1.3 Gelatin

Gelatins do not exist in nature but are derived from collagen, isolated from animal skin and bones. Gelatin contains a number of amino acids that contain amino-, carboxyl-, and hydroxyl groups. At temperature above 308-313 K gelatins in solutions behave as random coils, upon

cooling aggregation occurs and a clear transparent gel will form. These gels are thermally reversible. On dehydration however, irreversible conformational changes take place. Standard techniques for immobilization of biomolecules in gelatin include entrapment and cross-linking. Entrapment in gelatin gels was used for the immobilization of tyrosinase [14]. While the immobilization of pectinmethylesterase was realized in gelatin gels cross-linked with glutaraldehyde [17]. Natural gelling agents such as gelatin and agar have been tested for the formation of lecithin micro-emulsion-based gels as well as hydrogels (without surfactant and oil). Lipase keeps its catalytic function after being entrapped in these gels.

1.4 Chitosan

Chitin is a highly ordered copolymer of 2-acetamido-2-deoxy- β -D-glucose and 2-amino-2-deoxy- β -D-glucose that is isolated from invertebrates [10]. Different from other abundant polysaccharides, chitin contains nitrogen. Chitosan indicates a family of deacetylated chitins (Figure 1).

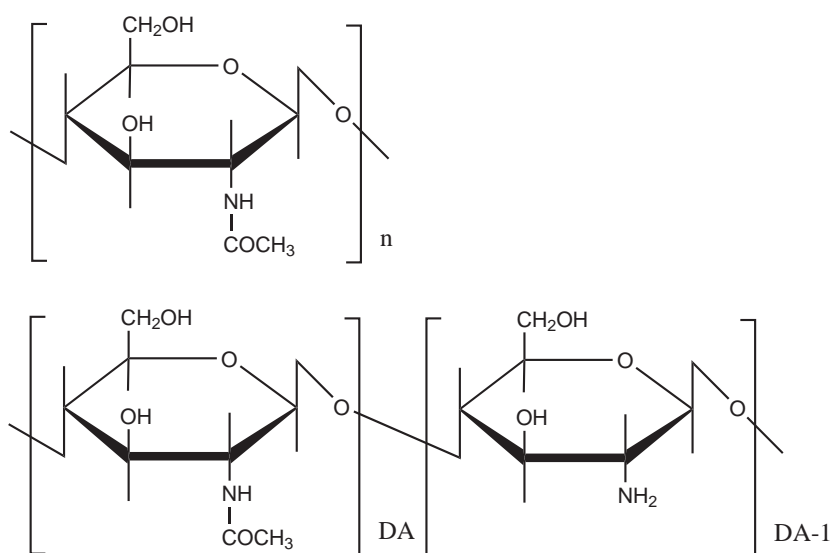


Figure 1. Structures of Chitin and chitosan. DA is the degree of deacylation

The average molecular weight for chitosan can reach values of 500,000 or more. Commercial chitosans may contain insoluble highly acetylated fractions that come from the core of the granules that were submitted to heterogeneous deacetylation. Chitosan is insoluble in organic solvents, in acids at high concentrations and in alkali. It is also insoluble in aqueous solution at $\text{pH} \geq 6$, except for low molecular weight samples. Chitosan is soluble in aqueous acidic media, due to protonation of amino groups in the repeating unit. Under certain conditions chitin and chitosan can give hydrophilic highly swellable hydrogels: cross-linking agents or organic solvents also promote gel formation. Chemical and physical gels are produced, both thermally reversible and not reversible. A very popular cross-linking agent for chitosan is glutaraldehyde. When glutaraldehyde is used, covalent bonds are formed between glutaraldehyde and chitosan macromolecules [18]. Chitosan is a promising support material

for enzyme immobilization because it is cheap, hydrophilic, biocompatible, biodegradable, and has anti-bacterial properties. Upon dehydration however, severe shrinkage and deformation occurs. The immobilization of penicillin acylase on chitosan powder, particles and beads was investigated in 1989 [19]. The immobilization of catalase into chitosan beads prepared by cross-linking with glyoxyl hydrate and reinforcement with glutaraldehyde was reported [20]. Cross-linking of chitosan beads with carbodiimide is also an option. The technique was used for the immobilization of lipase [21]. Recently glucose oxidase was immobilized in porous gels of chitosan-SiO₂, cross-linked with formaldehyde [22].

1.5 Penicillin G acylase

Since the discovery of penicillin G in the 1940s, penicillin and its derivatives have become the most important class of antibiotics, because of their low toxicity and their effectiveness against bacterial infection. The commercial success of the semi-synthetic antibiotics has quickly resulted in a worldwide cost based market [23]. Presently Western-Europe, India and, especially, China are world leader in industrial production. Penicillin amidohydrolase (E.C. 3.5.1.11) is the official name for penicillin acylase or penicillin amidase [23,24]. Penicillin acylases catalyze the hydrolysis of an amide bond between a carboxylic acid and a β -lactam nucleus while leaving the β -lactam intact. Penicillin acylase is produced by several microorganisms, including various bacteria, fungi and yeasts. This enzyme is usually applied as an immobilizate, which allows easy separation and recycling. Penicillin acylase from *E. coli* is the best-studied penicillin acylase with respect to the synthesis of semi-synthetic antibiotics. The enzyme is a heterodimer with a small α -subunit of 23 kDa and a large β -subunit of 63 kDa. The two monomer chains consist of 209 and 557 amino acid residues, respectively [25]. The protein has approximate dimensions of 7.5·5·5 nm. The isoelectric point for *E. coli* penicillin acylase has been reported as pH 6.8 [24] and pH = 6.3 [26].

1.6 Outline

The objective of this project is to develop and test a hydrogel coating on the interior walls of a monolithic structure for the immobilization of *E. coli* penicillin G acylase. Different hydrogels will be compared in terms of handling, gel formation and enzyme immobilization capacity. The most promising hydrogel material will be applied on the walls of cordierite¹ monoliths and the carrier application method is optimized. The properties and distribution of the gel are studied. Finally, the monolith-carrier combination is used for the immobilization of two commercial penicillin G acylases. The biocatalysts will be characterized in terms of activity and stability in the hydrolysis of penicillin G.

¹ ACM monoliths were not considered here, because the work was performed at the DSM facilities in Delft. The patent for ACM monoliths was still pending at this time.

2 Experimental

The experimental work is divided into the evaluation of the gel formation properties of several natural polymers, followed by the optimization of the coating method on glass plates, and finally the application of chitosan coatings on monoliths.

2.1 Materials

Colloidal silica solution (Ludox AS-40), agarose type I, gelatin A (from porcine skin), bloom strength of 300 was purchased from Sigma. Sodium alginate was obtained from Ashland Chemicals. γ -(aminopropyl)triethoxysilane (APTES) and low viscous chitosan with viscosity < 200 mPa s were purchased from Fluka. Acetic acid, glutaraldehyde and CaCl_2 of analytical grade were purchased from Merck. Sodium periodate was obtained from Acros. Separase[®] (pen G acylase from *A. faecalis*), Assemblase[®] (from *E. coli*) Assemblase[®] stock solution (Batch nr: ASM 031302, 10 g l⁻¹), Assemblase[®] Immob (batch nr: D576010), Separase[®] solution (batch nr: SEP 032616) and Separase[®] Immob (batch nr: D572154) were all kindly supplied by DSM Anti-Infectives, Delft, The Netherlands.

2.2 Catalyst preparation

2.2.1 Hydrogel preparation for screening

Gels were prepared on a glass plate and either used as such or cut into smaller pieces (2-5-5 mm). The concentration of the gel was varied, but for immobilization experiments a concentration of 1.0 % (w/v) was used. Only for gelatin, a higher concentration was needed to get a solid gel.

Agarose

Agarose gels were formed by heating a 1% (w/v) solution to 253 K and subsequent cooling to ambient temperature. For some gels, NaIO_4 was added to the agarose solution to obtain a concentration of 3.0 / 6.0 mM periodate. The solution was gently stirred for 3 h before cooling. The gel was washed to remove unreacted periodate.

Alginate

A glass microfibre filter (Whatman GF/A, 90 mm \varnothing) placed on a petridish was soaked in 0.25 mol l⁻¹ CaCl_2 for 60 min to saturate the filter with calcium. The calcium chloride solution was poured of and replaced with a sodium alginate solution (alginate concentration 0.5 and 1.0 % w/v). Gel formation started at the surface of the filter, where sodium ions in the alginate mixture were exchanged for calcium ions.

Gelatin

Gelatin powder was dissolved in water (3 % w/v) and heated to 333 K. Subsequently the solution was cooled to ambient temperature to form the gel. For enzyme binding, a cross-linked gel was prepared by adding 0.05 % (v/v) glutaraldehyde to the gelatin solution. The gel was washed with demiwater to remove free glutaraldehyde.

Chitosan

Chitosan powder 1% (w/v) was added to 1% (v/v) acetic acid and gently stirred (100 rpm) for 3h at room temperature. Undissolved matter was removed by filtration over a 100 µm filter. Three different methods were used to induce gel formation:

- pH shift; by adding NaOH to the chitosan solutions.
- Cross-linking; glutaraldehyde (5% v/v) was added
- Evaporation; in a petridish.

2.2.2 Optimization of the coating method

In order to control layer thickness, a thin layer of gel was coated onto glass plates.

About 75-100 mg of chitosan gel, prepared as described above was coated on glass plates, resulting in a gel layer of 175-225 µm thickness. All calculations of enzyme loading are based on the amount of chitosan filtrate that is coated on the glass plates, because at this point both gel mass and chitosan concentration can be exactly determined. The average thickness of the chitosan gel layer was also calculated on the basis of the initial amount of gel present on the plates according to equation 1.

$$L_{chitosan} = \frac{m_{chitosan}}{A \cdot \rho_{chitosan}} \quad (1)$$

Where $m_{chitosan}$ and $\rho_{chitosan}$ are the mass and density of chitosan filtrate and A is the coated surface area of the glass plate. The density of 1.0 % chitosan filtrate is assumed to be equal to the density of water. Optimization parameters are summarized in Table 2.

Table 2. PGA II immobilization on chitosan layers

Parameter	Range
Chitosan concentration	0.5-2.0 % w/v
Glutaraldehyde concentration	0.25-2.20 %w/v
PH	5-9
Enzyme concentration	5-10 mg ml ⁻¹

2.2.3 Monolith coating

Monoliths (400 CPSI, $L_m = 4$ cm, $\varnothing=2$ cm) were coated with chitosan gel by dip-coating. Monoliths were held in a 1.0 % w/v chitosan solution containing 1.1 % w/v glutaraldehyde

for 60 sec. After cleaning the channels, samples are air dried for 90 min. The average thickness of the chitosan gel layer was calculated by:

$$L_{chitosan} = \frac{m_{chitosan} / \rho_{chitosan}}{\frac{\pi}{4} \cdot d_m^2 \cdot L_m \cdot a'} \quad (2)$$

Where $m_{chitosan}$ and $\rho_{chitosan}$ are the mass and density of chitosan filtrate, d_m and L_m are the diameter and height of the monolithic structure and a' is the specific surface area. Density of 1.0 % chitosan filtrate is assumed to be equal to the density of water. Optionally a second dipcoating step can be introduced, after the first round of dip-coating. The monolith was air dried for 60 min, then coated and dried for another 60 min. Also APTES/GA functionalized samples were coated, washcoating and functionalization with APTES was done as described in Chapters 3 and 4, by dip-coating in colloidal silica solutions (Ludox HS-40).

2.2.4 Enzyme immobilization

Gels were suspended in 20-40 ml enzyme solution. Immobilization was done at ambient temperature during 24 hours while gently stirring. After washing, 20 ml of phosphate buffer (25 mM pH 7.0) was added to the gel. Desorption of non-bonded protein took place at ambient temperature during 24 hours, while gently stirring.

Immobilization on chitosan-coated monoliths was performed in a continuous set-up, consisting of a chromatography column with a diameter of 26 mm. Enzyme solution was pumped bottom-up through the column (Figure 3).

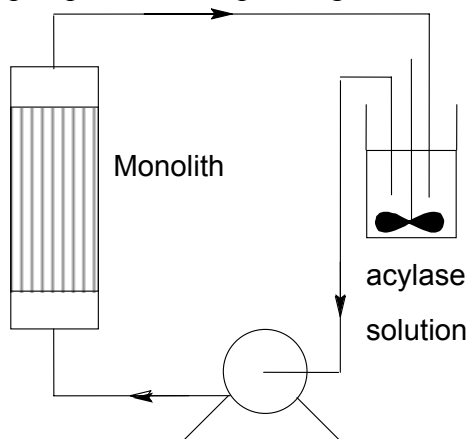


Figure 2. Continuous set-up for acylase immobilization.

Immobilization was performed by recycling a total volume of 30 ml through the monolith (flow rate 2 ml min^{-1}) at room temperature during 24 hours. The monolith was washed with demineralized water to remove unbound enzyme. Biocatalysts were stored in a solution of 30 % w/w 1,2-propanediol at 277 K until further use.

2.2.5 Penicillin G hydrolysis

The hydrolysis of penicillin G is presented in Figure 3.

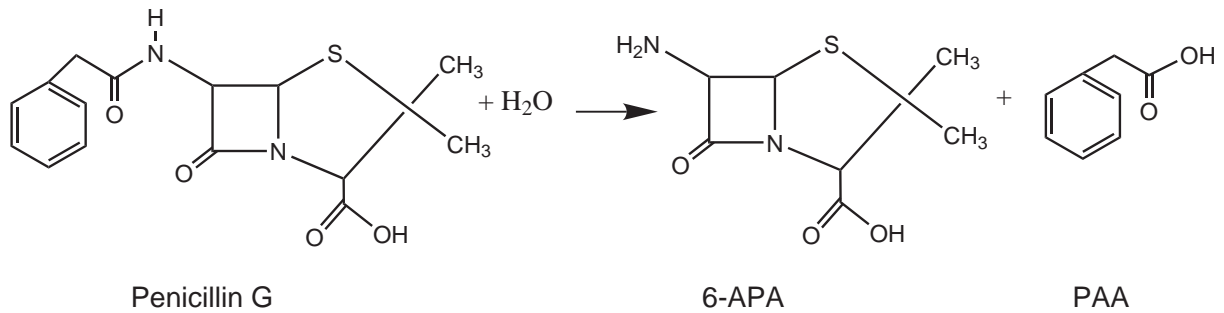


Figure 3. Hydrolysis of penicillin G to 6-aminopenicillic acid (6-APA) and phenyl acetic acid (PAA)

Conversions with free enzyme and Immob were carried out in 80 ml penicillin solution (initial Pen G-ammonia salt concentration 250 mM), to which the equivalent of 50 mg enzyme ($[E_0] = 7.8 \times 10^{-3} \text{ mmol l}^{-1}$) was added. Conditions were pH=8.50 and T= 304 K. The conversion was measured by titration with 1.0 M NaOH of released phenylacetic acid (PAA) by:

$$\zeta = \frac{V_{NaOH} \cdot [NaOH]}{V_{L,t=0} \cdot [PenG_{t=0}]} \quad (3)$$

The continuous set up (Figure 3) was used for penicillin G hydrolysis with monolithic biocatalysts.

2.3 Characterization

2.3.1 Gel morphology and distribution

Scanning Electron Microscopy (SEM) was applied to investigate the distribution of the chitosan gel over both the length of the monolith and over the cross-section of the channels. Samples were analyzed on a Philips XL-20 scanning electron microscope operated at 12 kV.

2.3.2 Protein concentration

During immobilization and washing the protein concentration in solution was determined by measuring the absorbance at 280 nm. Samples were analyzed on a Unicam UV300 UV/VIS Spectrophotometer.

2.3.3 Penicillin G decomposition

During storage at 277 K a slow decomposition of penicillin G in solution occurs. HPLC has been used to determine the penicillin concentration in the stock solution at the start of each conversion experiment. The decomposition of penicillin G appears to follow the first-order

decay. The inactivation rate constant k_{inact} was calculated at 0.009 day^{-1} , i.e. 9 ‰ penicillin decomposition per day.

2.3.4 Penicillin concentration

Initial Pen G concentration was determined by HPLC. The chromatographic experiments were performed on a Spectra Physics AS1000 HPLC with a Spectra Physics UV100 detector connected to a RP-18 column (5 μm particle diameter). The mobile phase used was water-acetonitril-phosphate buffer of pH 3.0, with the column flow rate set at 1.0 ml min^{-1} . The UV trace was followed at 214 nm. Retention times of 6-APA, PAA and Pen G are < 1 min, 2.84 and 3.91 minutes respectively. To validate the use of NaOH consumption to follow conversion, samples were withdrawn at regular intervals to measure the Pen G and PAA concentrations by HPLC. Conversion was calculated by:

$$\zeta = \frac{[PAA_{t=x}] - [PAA_{t=0}]}{[PenG_{t=x}] + [PAA_{t=x}] - [PAA_{t=0}]} \quad (4)$$

The highest deviation with conversion calculation from the NaOH consumption was 2.3 ‰. As this is within the margin of error in dilution and analysis of the HPLC samples, NaOH consumption data can be used to calculate the conversion.

Time [min]	Conversion NaOH [%]	Conversion HPLC [%]	Deviation [%]
20	31.0	31.6	1.9
45	60.4	61.8	2.3
80	89.2	89.6	0.4
135	99.8	98.1	1.7

2.3.5 Protein in reaction mixture

HPSEC (high performance size exclusion chromatography) was used to detect traces of protein in samples taken from the reaction mixture. Measurements were performed on a Dionex ASI100 HPLC with a Dionex 170V UV-detector connected to an TSK gel G3000SWXL column (ID = 7.8 mm, L = 30 cm). The mobile phase was a 25 mM phosphate buffer of pH 7.0, with the column flow rate set at 1.0 ml min^{-1} . The UV trace was followed at 280 nm. Retention times of PGA II and PGA I are 8.92 min and 8.03 minutes respectively.

3 Results and Discussion

3.1 Gel formation and immobilization

For application on monoliths, the gel should be stable and easily applicable inside the channels. Selection of a suitable hydrogel for the immobilization of PGA II should ideally be based on the recovered enzyme activity. This activity however, depends on enzyme loading, enzyme distribution and substrate/product diffusion. Therefore, only the final enzyme loading is used as a selection criterion here. Immobilization can be done during gelation by adding a cross-linker to the gelling agent or by enzyme addition to the solid gel. Simultaneous gelation and immobilization often leads to deactivation [14], therefore immobilization after gel formation was used. An overview of enzyme loading for each gel is displayed in Figure 4.

Agarose

At higher agarose concentrations, an insoluble mass was formed. After dilution and heating to 353 K the agarose slowly dissolved. Strong stiff gels are easily formed within 1 hour. These gels were very susceptible to dehydration, but shrinkage can be partially reversed by addition of water. Addition of NaIO_4 did not increase the finale loading. For this gel the enzyme loading depends on the thickness of the gel layer and the external surface area. A 5 mm layer on a glass plate can immobilize 4 mg ml^{-1} gel. Cutting the gel into smaller pieces ($\pm 2.5 \cdot 5$ mm) reduces the layer thickness and increases external surface area. This doubled the enzyme loading. Using a 0.5 mm thick layer on a glass plate yielded the same result; a PGA II loading of 7.5 mg ml^{-1} was reached.

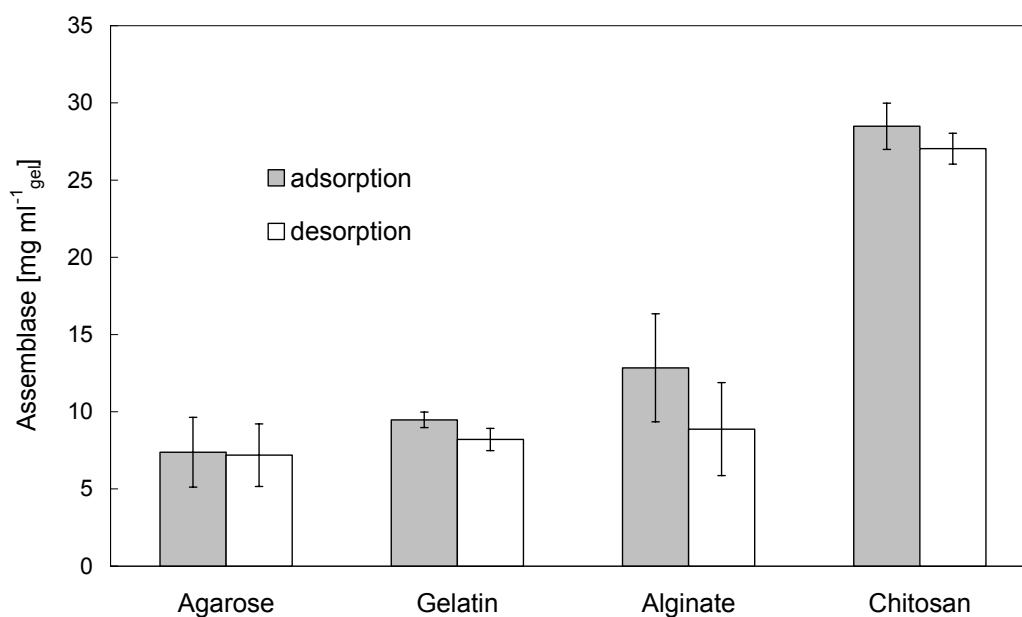


Figure 4. PGA II loading on each type of hydrogel, cut into 5·5·5 mm blocks. Lines represent the 95% confidence interval.

Gelatin

At high gelatin concentrations (10 % w/v) elastic gels were easily formed upon cooling. Gelatin gels are sensitive to dehydration. Solutions of 1.0 % gelatin do not gelate at ambient temperature. 2 % gelatin is the lower boundary for gel formation. Gel formation in a gelatin solution is a thermally reversible process. Therefore gelatin can only be used at ambient temperature. Addition of a suitable cross-linking agent can extend the temperature range to elevated temperatures. In a 4 mm layer, 3.7 mg ml⁻¹ gel PGA II could be bound. By cutting the gel (5·5·5 mm), this could be doubled to 8.0 mgml⁻¹ gel. Both chitosan and gelatin are crosslinked via amine groups with glutaraldehyde. The enzyme is then bound to free glutaraldehyde groups via lysine amino groups. The loading on gelatin gel is much lower than on chitosan. Since gelatin contains less free amino groups (about 27 lysine residues per 1000 amino acids) than chitosan (1 amino group per repeating unit, 75-80 wt% of which are deacetylated), enzyme loading on gelatin probably provides less room for improvement.

Alginate

A colorless, transparent gel was formed within 45 min. In NaCl solution it remained intact. This means no exchange of Ca²⁺ and Na⁺ occurs, gel formation was irreversible. It is known [27] that Ca²⁺ alginate gels are not stable against chelating agents such as phosphate ions, and therefore less suitable for PGA II immobilization under these conditions. Also there are some reports in literature that suggest a decreased activity of immobilized enzyme in Ca²⁺ alginate due to interaction between the protein and Ca²⁺ [28]. Alginate is less suitable for entrapment of small sized molecules such as enzymes because proteins tend to leach out. No cross-linking agent was used here, thus all enzymes are physically bound to the gel matrix. To prevent the leakage of acylase out of the gel, it is possible to cross-link the gel and the enzyme. An important drawback of this method is the presence of two-phase liquid system. Both a solution of alginate (e.g. Na-alginate) and a solution of cations (e.g. CaCl₂) are required. Using a 5 mm alginate layer on a glass plate, an enzyme loading of 12.5 mg ml⁻¹ alginate gel was reached. There is ample room for improving the loading by decreasing the layer thickness, but considering the drawbacks this was not attempted.

Chitosan

The results for the different methods of gelation are given in Table 3.

Table 3. Gelation of chitosan

Method	Gel formation
pH shift	+/-
Evaporation	+/-
Cross-linking	+

The method of pH shift does not provide stable chitosan gels. Direct injection of NaOH leads to formation of aggregates. Gelation on the surface of a NaOH saturated glass filter gives slightly better results. However, this process is reversible, therefore pH shift is not useful as a method to induce gelation. The evaporation method might be applicable to form ultra thin chitosan films. A small amount of chitosan filtrate, cast on a petridish had completely evaporated after 24 hours. When the gel was rehydrated, it was not clear if the film layer was

continuous or a spreading of smaller gel areas. Moreover, immobilization of biocatalysts will only occur on the surface of the film layer, thus limiting the final loading.

The preferred method to form chitosan gels is the addition of glutaraldehyde. Flexible, yellow and transparent gels are formed in 1 hour. The pH of the solution plays a fundamental role on the swelling degree of the matrix. Chitosan is a basic carbohydrate with amino groups (pK_a is 6.3) [28]. Chitosan is positively charged at pH below 6.3. This means a higher concentration of amino groups as salt (NH_3^+). Due to electrostatic repulsion between carbohydrate chains, swelling is observed. Neutralizing the gels that are formed in an alkaline solution can reduce the swelling of chitosan films. Fixing the polymer chains by cross-linking is also an effective tool to decrease swelling [29]. When cut into 2.5·5 mm blocks, this gel has the highest immobilization capacity (27.2 mg ml⁻¹ gel). Gel formation can easily be controlled and the gelation occurs gradually. This would make chitosan a very suitable gel to apply on monolithic structures.

All biopolymers provide physically stable hydrogels. The effect of enzyme loading as a function of layer thickness was observed for all hydrogels. This is in agreement with other studies [6,30] that report this effect. The application of alginate within the monolith channels seems possible, but a two-step coating is needed. Gelatin can only be used at ambient temperatures, and has a significantly lower loading capacity than chitosan. Loading on agarose could not be increased significantly by modifying the gel, final loading is only 25% of final loading on chitosan. The highest enzyme loading (27 mg ml⁻¹ gel) by far was achieved on a chitosan hydrogel. The enzyme loading in chitosan is 3-4 times higher than the enzyme loading in agarose and gelatin gels. Chitosan was selected as a carrier for acylase.

3.2 Optimization of the coating method

3.2.1 Chitosan concentration

Chitosan filtrate 0.5 %w/v, 1.0% w/v and 2.0 %w/v were used with different degrees of glutaraldehyde cross-linking. Chitosan filtrate of 2.0 %w/v chitosan was a very viscous solution. Gel formation occurred immediately after addition of only a small amount (± 0.25 % v/v) of glutaraldehyde. This concentration is too high for use within a monolith.

From the results (Figure 5a) it can be seen that a positive relation exists between the chitosan concentration and the amount of immobilized PGA II.

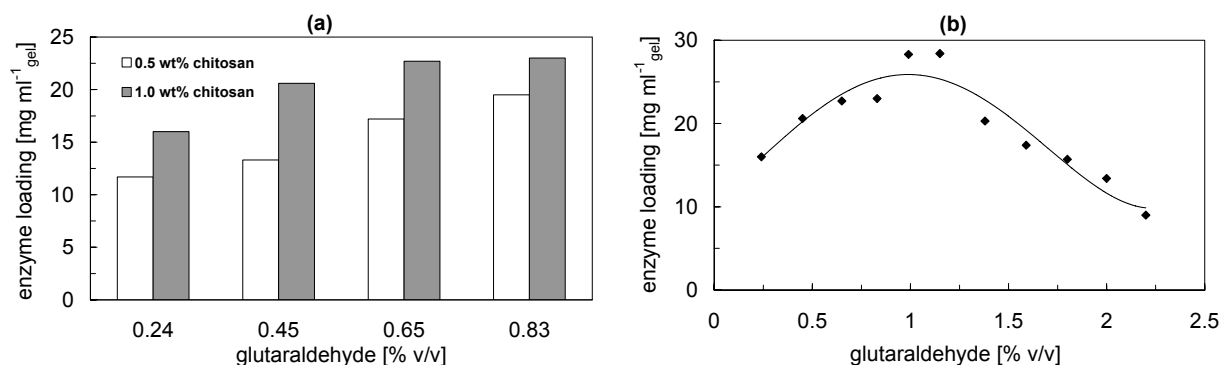


Figure 5. Optimization of the chitosan protocol. a) chitosan concentration. Glutaraldehyde indicates the glutaraldehyde concentration in the chitosan/ glutaraldehyde mixture before gelation. b) glutaraldehyde concentration. Immobilization was performed with an initial concentration of 5 g l⁻¹.

For all glutaraldehyde concentrations, more enzyme can be bound to the more concentrated gel. An increase of the chitosan concentration doubles the amount of amino groups present in the gel. After reaction with glutaraldehyde more binding sites will be available for protein binding leading to an increase in enzyme loading. Secondly, gel density is increased, resulting in a more crosslinked gel with smaller pores. This negatively affects enzyme loading. An advantage of a more dense gel structure at higher chitosan concentration would be reduced swelling and shrinking effects [29].

3.2.2 Glutaraldehyde concentration

The optimum glutaraldehyde concentration for the immobilization of PGA II in a 1.0 %w/v chitosan gel is 1.1 %v/v glutaraldehyde (Figure 5b). This value represents the amount of glutaraldehyde in chitosan/glutaraldehyde mixture before gelation. Two opposing mechanisms seem to determine the position of the maximum. At low concentrations both aldehyde groups in each glutaraldehyde molecule are involved in network formation. As the glutaraldehyde concentration increases an increasing number of free aldehyde groups will be present for binding with a lysine residue in PGA II. But at higher glutaraldehyde concentrations the enzyme loading is restricted by the accessibility of the polymer network. As glutaraldehyde concentration increases, the cross-linking density also increases and a more rigid gel is formed. This leads to a lower in enzyme loading. Glutaraldehyde concentration of around 1 % in chitosan filtrate before gelation was found to be optimal.

3.2.3 PGA II concentration

The effect of enzyme concentration is depicted in Figure 6a. An increase in the PGA II concentration has a positive effect on the enzyme loading. With increasing glutaraldehyde concentration it can be observed that the difference in enzyme loading slightly diminishes, due to deactivation and higher crosslinking degree. At a concentration of 10 g l⁻¹, the highest loading can be achieved. To increase sensitivity in the analysis of the protein content, a

solution of 5 g l^{-1} PGA II was adopted in this study. In this way, the relative decrease in concentration is much higher than for a starting concentration of 10 g l^{-1} .

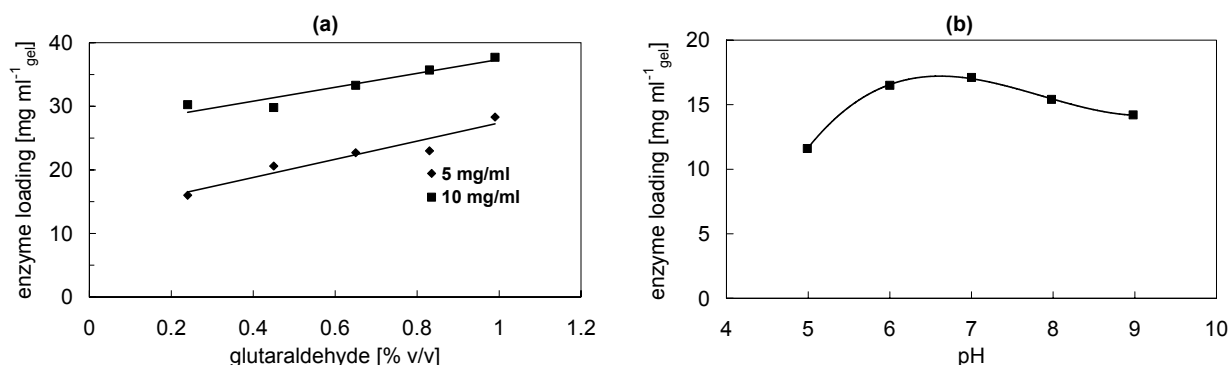


Figure 6. Optimization of the chitosan coating. a) initial PGA II concentration, ‘glutaraldehyde’ indicates the glutaraldehyde concentration in the chitosan / glutaraldehyde mixture before gelation. b) pH, initial enzyme concentration was 5 g l^{-1} .

3.2.4 PH during immobilization

The optimum pH for the immobilization of PGA II into a chitosan hydrogel is near pH 7 (Figure 6b). This corresponds nicely to the optimum found for the immobilization of penicillin acylase on nylon particles via glutaraldehyde activation [32]. The maximum activity was recovered when using enzyme solutions with pH in the range 7.0-8.0. Braun et al. reported no significant increase in enzyme loading when using immobilization solutions of pH 6, pH 7 and pH 8. They did observe an increase in activity retention with increasing pH [6]. The immobilization reaction takes place between aldehyde groups and neutral $-\text{NH}_2$ groups. No bonding occurs with positively charged $-\text{NH}_3^+$ groups. PGA II has an isoelectric point of 5.4. Below $\text{pH} = 5.4$ the enzyme is positively charged. The pK_a value of the amino group is reported as 6.3 [28]. Thus at $\text{pH} < 6.3$ the majority of amino groups is positively charged. Initially an increase in enzyme loading is observed with increasing pH, which corresponds to a decrease in the level of ionization of NH_3^+ -groups. An explanation for the decrease in immobilization at $\text{pH} > 7$ could be related to the ionic strength of the immobilization solution. A negative correlation between enzyme activity and phosphate concentration has been reported [32]. Although the effect of salt concentration was not incorporated in this study, it is advised to use only a minimal amount of phosphate to control the immobilization solution at the desired pH.

3.2.5 PGA I immobilization

PGA I was immobilized at pH 8.0. The final loading of PGA I is in the same order of magnitude (around $30 \text{ mg ml}^{-1} \text{ gel}^{-1}$). This can be expected due to the similar structure and size of both acylases.

3.3 Chitosan coated monoliths

By weighing, and assuming a homogeneous gel layer throughout the channel, the average layer thickness is calculated to be around 77 μm . This number varied between 95 μm and 65 μm for different samples. The chitosan layer thickness as calculated is an average over the entire monolith structure. In practice the gel film in a square channel will not be uniform. As a result of the surface tension during gelation, it will have a rounder shape, as depicted in Figure 7, with a greater thickness in the corners than in the middle of the channels. Not that the layer thickness is calculated assuming a smooth channel surface. The roughness of the gel layer (with pits and bumps of 5-10 μm) can result in a thicker average gel film in practice.



Figure 7. Schematic representation of actual layer thickness compared to a uniform film layer (left); thicker film in monolith channel corners due to surface tension (middle); thicker gel layer due to uneven surface (right).

The introduction of a second coating step does not increase the thickness of the gel layer. The extra coating only compensates for dehydration during gelation. This is probably caused by the shorter drying time that is used when two layers are applied. The gel is still wet after the first coating and swells directly when the monolith is dipped in the aqueous gel mixture for the second cycle. The re-wetted gel can be blown out when the channels are cleaned with pressurized nitrogen. The overall result is a layer with the same thickness as a single coating. If a silane coating is applied on the cordierite before gel application, the average gel layer thickness increases to 90 μm . This is an increase of 16 %.

3.3.1 Scanning electron microscopy

Scanning electron microscopy (SEM) was performed to investigate the distribution of the chitosan layer in the monolith. Due to the vacuum the gels are completely dehydrated, it is therefore not possible to quantify the layer thickness from the SEM micrographs. In monolith structures without pretreatment the gel is more or less evenly distributed along the length of the channels, as can be seen in Figure 8a and b. A cross-sectional view shows that most of the gel is concentrated in the corners of each channel (Figure 8c). This effect is usually observed for coated square channels, as was described in chapter 3. Although in Figure 8c it seems that the layer is not much thicker in the corners than on the wall. It might seem surprising, but this visible layer of dry material comprises only 1-5 % of the total gel. As a result of the drying step, it is very difficult to quantify layer thickness based on these SEM images.

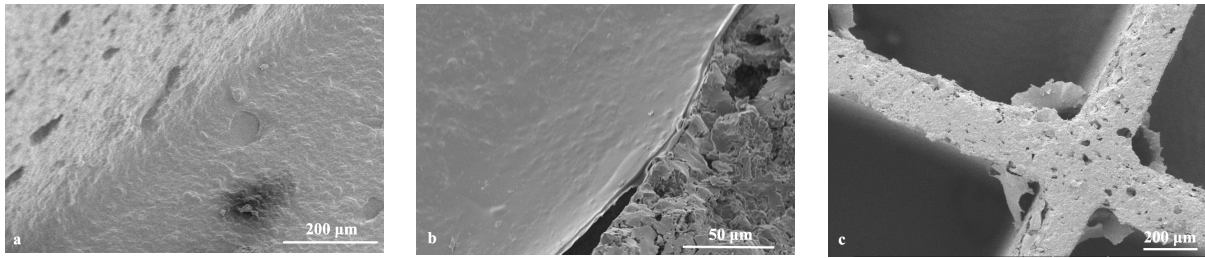


Figure 8. SEM micrographs of chitosan layers on cordierite. a) gel distribution inside a channel, the image shows an even gel-distribution in a corner of the channel. b) indication of layer thickness at the edge of a channel wall. c) cross sectional view of monolith sample showing the gel in the corners of the channels

After washcoating and functionalization with APTES/GA, the channels become more rounded and gel distribution improves. Average layer thickness increases to 95 µm. But the macro pores in the cordierite remain (partially) open (Figure 9a,b). Chitosan forms a gel layer over the silica coating both in the center and in the corners of the monolith channels. A gel layer is also found on silica dispersed in the cordierite macro pores, but the pores are not completely filled.

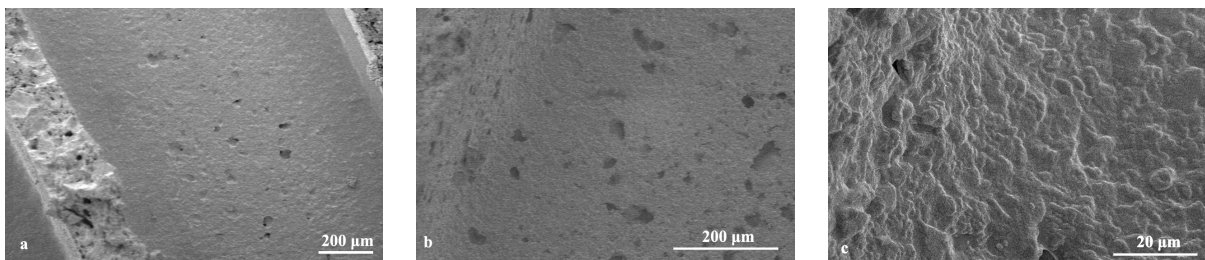


Figure 9. SEM micrographs of chitosan layers on washcoated and functionalized cordierite. a and b) gel distribution through a functionalized monolith channel, most of the macro pores are filled c) corner of a channel, showing an accumulation of gel.

3.3.2 Immobilization of penicillin G acylase on cordierite monoliths.

Results for enzyme immobilization on monoliths are plotted in Figure 10. On chitosan coated-glass plates the PGA I/II loadings are equal, but when a chitosan-coated monolith is used, enzyme loading is different. PGA I loading increased with 22% compared to glass plates, whereas PGA II loading on the monoliths shows a 50% decrease. The reason for this remains unclear. Immobilization was followed during 24 hours to establish the time necessary to reach “steady-state” loading. In 2 hours, 80 % of the equilibrium loading is reached while in the remaining 22 hours the last 20 % is immobilized. Initially, the chitosan network is more accessible to the enzyme. The biocatalyst diffuses into the gel and is bound mostly in the top region. The accumulation of proteins in the top layer of the gel network hinders further diffusion of free enzyme from the bulk solution into the gel. The average diffusion rates within the gel network decrease with diffusion length and with time. An immobilization time of 2 hours, in which 80 % of equilibrium is reached, matches reasonably well with the current industrial immobilization process for Immo particles (with a similar diffusional distance $d_p/6$ as the layers that are used in this study), which is also based on a loading time of two hours.

The same trend was also found [31] for the immobilization of penicillin acylase onto nylon-grafted particles.

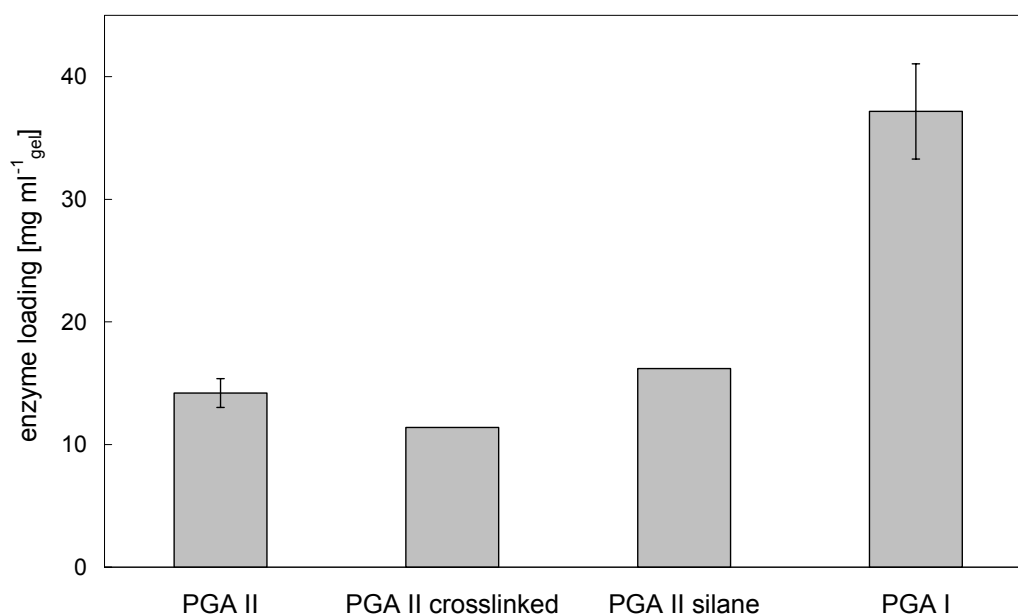


Figure 10. Immobilization on 400 cpsi cordierite monoliths. Lines represent the 95% confidence interval.

Effect of post treatment with glutaraldehyde

In order to create more anchors in the chitosan gel to bind amino groups in PGA II, monolith structures were treated with a glutaraldehyde solution after the gel formation and aging step. During immobilization aggregate formation was observed in the PGA II bulk solution, indicating the release of free glutaraldehyde from the chitosan gel. The aggregates of cross-linked enzymes are unable to diffuse into the gel pores. Aggregate formation within the gel leads to blocking of pores, preventing additional enzyme binding. Total loading did not improve.

Effect of silanization on enzyme loading

Although functionalization with APTES/GA improved the gel distribution and total loading (a 16% increase in layer thickness was observed), with a loading of 15.9 mg PGA II ml⁻¹ gel the total enzyme loading did not increase significantly (Figure 10). Since only a single immobilization experiment was done on a functionalized monolith, the positive effect of APTES/GA on enzyme loading can only be speculated here. A positive effect should be expected, due to higher gel loading. It is possible that the increased gel-thickness requires longer immobilization time to fully benefit from the better distribution through the channels.

3.4 Hydrolysis of Pen G

Catalyst performance tests were used to compare the free enzyme with the monolithic biocatalysts.

3.4.1 Effect of immobilization

The initial rate per gram of enzyme of penicillin hydrolysis was compared in a batch reactor, the total amount of enzyme, the total volume, and the penicillin G concentration was the same for free enzyme and the monolith. The initial reaction rate for free enzyme is higher than the reaction rate for immobilized enzyme (Figure 11).

The immobilization process affects the apparent activity of the enzyme. Note that the initial reaction rate of free PGA II is lower than for PGA I. This might be caused by fast denaturation of the enzyme during the initial stage of the experiment. The addition of 1.0 M NaOH as a titrant is likely to cause local hotspots of extreme alkaline pH leading to a denaturation of free enzyme. Apparently free PGA I is more stable against these local high pH levels than PGA II. Both immobilized enzymes, are shielded from the pH hotspots by the gel

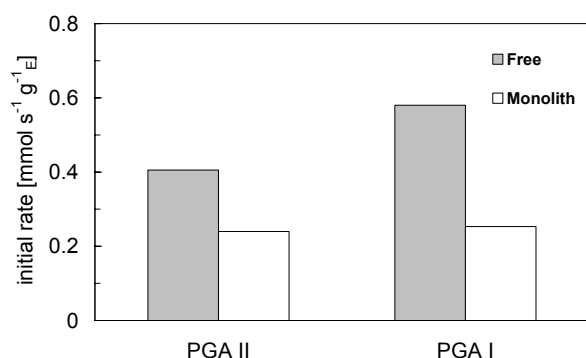


Figure 11. Initial rate of 50 mg free and a monolith with 50 mg enzyme, at 304 K and pH = 8.50

layer, thus can retain their activity. It seems however from Figure 11 that the enzyme loses activity upon immobilization. Although immobilization generally leads to an apparent deactivation, it was found that for this type of matrix the reaction rate does not significantly decrease after immobilization [33]. This was validated by grinding commercial PGA II particles and comparing the initial rate. The initial rate for the smaller particles was the same as for the free enzyme. With intact particles, the reaction rate was significantly lower than for free enzyme, as is shown in Figure 11.

The lower activity after immobilization is probably caused by diffusion limitation in the gel matrix of the carrier. The reaction rate for fast reactions in carriers with high enzyme loading becomes limited by diffusive transport of the reactive species (internal diffusion limitation). For this enzyme system an additional problem is present; in the hydrolysis of penicillin G an acid (phenylacetic acid) is produced. In heterogeneous biocatalysts this gives rise to pH gradients due to the coupling of reaction and diffusion of substrates and products within the carrier. As the kinetics of the penicillin hydrolysis reaction are strongly dependent on pH, a pH gradient within the biocatalyst particle is expected to have a strong additional influence on the observed reaction rate.

3.4.2 Stability

The operational stability of PGA I on a chitosan coated monolith system was investigated by repeated use of the same monolith structure under equal reaction conditions (80 ml 250 mM penicillin solution, pH = 8.5, 304 K, flow rate 15 ml min⁻¹). From the results in Figure 12 it is clear that activity drops initially, probably due to loss of unbound enzyme. Activity remains constant from the 2nd cycle onwards during 4 successive conversions.

The structure was stored at 277 K for 35 days between the 3rd and 4th conversion cycle without notable loss of activity. This shows that the storage stability of penicillin G acylase on a chitosan coated monolithic structure is at least a month without loss of enzyme activity. This is in good agreement with a literature report concerning the immobilization of lipase onto chitosan beads. Lipase retained an activity of 92 % after 6 cycles [13]. The presence of proteins was only detected by HP-SEC in the reaction mixture of the first cycle. No free protein was detected in the following experiments. The enzyme loss amounted 5.4 mg (7.7%). Rinsing with water does not remove enzyme bound by ionic interactions, but increased ionic strength in the Pen G reaction mixture removes this loosely bound enzyme. Therefore the introduction of a washing step with a suitable salt solution is suggested.

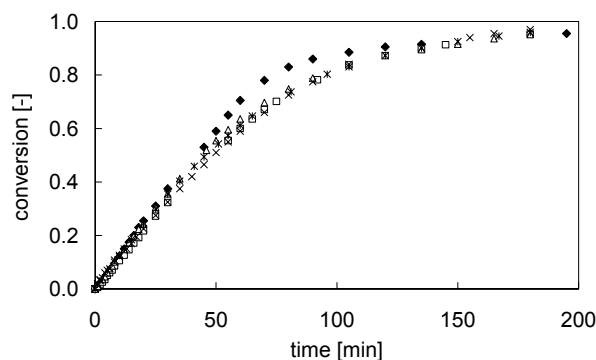


Figure 12. Conversion (top) of a monolith with immobilized penicillin G acylase (PGA I) after repeated use, at 304 K and pH=8.50.

4 Conclusions

Penicillin G acylase from *E. coli* (Assemblase[®], PGA II) has been immobilized in agarose, alginate, chitosan and gelatin hydrogels. The highest enzyme loading, 27 mg ml⁻¹ gel, was achieved on a chitosan gel. Agarose and gelatin gels proved less successful in the immobilization of penicillin G acylase. The methods of pH shift, cross-linking and evaporation were investigated for the formation of chitosan hydrogels. Evaporation and pH shift were found unsuitable for the formation of stable gels. The cross-linking method resulted in a stable gel that is suitable for the immobilization of penicillin G acylase.

The immobilization parameters have been optimized, using thin (200 μm) chitosan layers coated on a glass surface. The optimal conditions for the immobilization process are:

- 10 g l⁻¹ enzyme
- 1.0 %w/v chitosan
- 1.1 %v/v glutaraldehyde (GA)
- pH 7.0.

The same conditions apply for PGA I, except that pH of the immobilization solution should be pH 8.0.

Coating of 400 cpsi monoliths with a chitosan layer yields a smooth layer with an average layer thickness of 77 μm . With an extra washcoating and silanization step, the layer thickness can be increased to 95 μm .

Several strategies have been employed to enhance the immobilization efficiency on chitosan-coated monoliths. Increasing the layer thickness of the coating by second coating cycle and

functionalization with APTES GA, does not increase the final enzyme loading, although the application of a silane coating resulted in a 16 % increase in layer thickness. Scanning electron microscopy revealed that the gel is evenly distributed along the length of the monolith structures, but most of the chitosan has been accumulated in the corners of the channels. Application of a silane coating provides anchors for chitosan binding, improving the distribution through the channel. The covalent bonding of PGA I on chitosan-coated monoliths is $35.9 \text{ mg ml}^{-1} \text{ gel}$, which is in the same order of magnitude as the enzyme loading achieved on chitosan coated glass plates. PGA II loading on the chitosan-coated monoliths is only $14.2 \text{ mg ml}^{-1} \text{ gel}$, which is 50 % below the level that was realized on chitosan coated glass. The reason for this remains unclear.

An immobilization time of two hours is sufficient to reach 80 % of the equilibrium loading, which was found to be comparable to current industrial carriers. It has been shown that the catalyst system is active in the hydrolysis of penicillin G. The operational stability was tested in 5 reaction cycles. The catalyst lost 7% of its activity after the first cycle. The chitosan-monolith system is stable for at least 35 days while stored in 1,2-propanediol at 277 K.

5 Acknowledgements

Mike Smeltink is gratefully acknowledged for performing all experiments. Dr. ir. E. van de Sandt and M. Paasman of DSM Anti-Infectives, Delft are acknowledged for their valuable contribution to this work. DSM Anti-Infectives is gratefully acknowledged for funding part of this research. Corning Inc. is acknowledged for supplying the monoliths. Adrie Straathof is acknowledged for his input during the study.

6 List of Symbols

a'	specific surface area monolith	$[\text{m}^2 \text{ m}^{-3}]$
A	surface area coating	$[\text{m}^2]$
d_m	monolith diameter	$[\text{m}]$
$[E_0]$	initial enzyme concentration	$[\text{mol m}^{-3}]$
k_{cat}	catalytic constant	$[\text{s}^{-1}]$
k_{inact}	rate constant of penicillin G decomposition	$[\text{day}^{-1}]$
$K_{c,app}$	apparent equilibrium constant	$[\text{mol m}^{-3}]$
$K_{i,j}$	inhibition constant component j	$[\text{mol m}^{-3}]$
$K_{m,j}$	Michaelis-Menten constant component j	$[\text{mol m}^{-3}]$
$L_{chitosan}$	layer thickness	$[\text{m}]$
L_m	monolith length	$[\text{m}]$
m	mass	$[\text{kg}]$

r	reaction rate	[mol s ⁻¹]
V_L	reaction volume	[m ³]
V_i	volume of component i	[m ³]

Greek symbols

ρ	density	[kg m ⁻³]
ζ	conversion	[-]

Components

6-APA	6 amino penicillanic acid
E	enzyme
PAA	phenyl acetic acid
PenG	Penicillin G
PGA I	Penicillin G acylase from <i>A. faecalis</i> , Separase [®]
PGA II	Penicillin G acylase from from <i>E. coli</i> , Assemblase [®]

7 References

- [1] D. Magnin, J. Lefebvre, E. Chornet and S. Dumitriu (2004) Carbohydrate Polymers; 55: 437-453
- [2] J.G. Prichard (1970) Poly(vinyl alcohol) Basic Properties and Uses, Gordon and Breach, London
- [3] C.A. Finch (1973) Poly (vinyl alcohol) Properties and Applications, Wiley, London
- [4] Y. Zhao, H. Su, L. Fang, T. Tan (2005) Polymer; 46(14): 5368-5376
- [5] I. Capek (2002) Advances in Colloid and Interface Science; 99(2): 77-162
- [6] C. Tang, C. Yin, Y. Pei, M. Zhang, L. Wu (2005) European Polymer Journal; 41(3): 557-562
- [7] A. Abhijit, A. Date and V.B. Patravale (2004) Current Opinion in Colloid & Interface Science; 9: 222-235
- [8] K. Martinek, A.M. Klibanov, V.S. Goldmacher, I.V. Berezin (1977) Biochimica et Biophysica Acta; 485: 1-12
- [9] A. Bodalo, E. Gomez, J.L. Gomez, J Bastida, M.F. Maximo, F. Diaz (1991) Process Biochemistry; 26: 349-353
- [10] G.O. Philips Ed. (2000) Handbook of hydrocolloids: 21-40, 67-86, 366-395
- [11] J.M. Guisan (1988) Enzyme and Microbial Technology; 10: 375-382
- [12] S. Rocchietti, A. San Vicente Urrutia, M. Pregnolato, A. Tagliani, J.M. Guisan, R Fernandez-Lafuente, M. Terrini (2002) Enzyme and Microbial Technology; 31: 88-93
- [13] I. Roy, M.N. Gupta (2004) Enzyme and Microbial Technology; 34: 26-32
- [14] N. Munjal, S.K. Sawhney (2002) Enzyme and Microbial Technology; 30: 613-619
- [15] A. Tanriseven, Y.B. Uludag, S. Dogan (2002) Enzyme and Microbial Technology; 30:

- 406-409
- [16] N.W. Fadnavis, G. Sheelu, B.M. Kumar, B.U. Bhalerao, A.A. Deshpande (2003) *Biotechnology Progress*; 19: 557-564
- [17] S.A. de Assis, B.S. Ferreira, P. Fernandes, D.G. Guaglianoni, J.M.S. Cabral, O.M.F. Oliveira (2004) *Food chemistry*; 86: 333-337
- [18] E.A. Merkovich, M.L. Carruete, V.G. Babak, G.A. Vikhoreva, L.S. Galbraikh, V.E. Kim (2001) *Colloid Journal*; 63: 350-354
- [19] J. Braun, P. le Chanu, F. le Goffic (1989) *Biotechnology and Bioengineering*; 33: 242-246
- [20] S.A. Cetinus, H.N. Öztop (2003) *Enzyme and Microbial Technology*; 32: 889-894
- [21] S.H. Chiou, W.T. Wu (2004) *Biomaterials*; 25: 197-204
- [22] Y.M. Yang, J.W. Wang, R.X. Tan (2004) *Enzyme and Microbial Technology*; 34: 126-131
- [23] A. Bruggink Ed. (2001) *Synthesis of β -lactam Antibiotics*, 1st ed., Dordrecht, the Netherlands: 13-54
- [24] A. Parmar, H. Kumar, S.S. Marwaha, J.F. Kennedy (2000) *Biotechnology Advances*; 18: 289-301
- [25] H.J. Duggleby, J.P. Tolley, C.P. Hill, E.J. Dodson, G. Dodson, P.C.E. Moody (1995) *Nature*; 373: 264-268.
- [26] C.B. Patel, V.G. Gaikar, (2004) *Separation Science and Technology*; 39: 2655-2675
- [27] C. Mateo, O. Abian, R. Fernandez-Lafuente, J.M. Guisan (2000) *Enzyme and Microbial Technology*; 26: 509-515
- [28] E. Taqieddin, M Amiji (2004) *Biomaterials*; 25: 1937-1945
- [29] E. Calleri, C. Temporini, G. Massolini, G. Caccialanza (2004) *Journal of Pharmaceutical and Biomedical Analysis*; 35: 243-258
- [30] J.L. van Roon, M. Joerink, M.P.W.M. Rijkers, J. Tramper, C.G.P.H. Schroën, H.H. Beftink (2003) *Biotechnology Progress*; 19: 1510-1518
- [31] M.H. Janssen, L.M. van Langen, S.R.M. Pereira, F. van Rantwijk, R.A. Sheldon (2002) *Biotechnology and Bioengineering*; 78: 425-432
- [32] M.S. Mohy Eldin, C.G.P.H. Schroën, A.E.M. Janssen, D.G. Mita, J. Tramper (2000) *Journal of Molecular Catalysis B: Enzymatic*; 10: 445-451
- [33] C.G.P.H. Schroën, C.B. Fretz, V.H. de Bruin, W. Berendsen, H.M. Moody, E.C. Roos, J.L. van Roon, P.J. Kroon, M. Strubel, A.E.M. Janssen, J. Tramper (2002) *Biotechnology and Bioengineering*; 80:331-340

Ionic adsorption of lipase and lactase

Abstract

Cordierite and acicular mullite (ACM) monoliths, having a more open structure, were used as support material for ionic adsorption of a lactase from *Aspergillus oryzae* and a lipase from *Candida rugosa*. Monoliths were functionalized with polyethyleneimine (PEI), by adsorption or via functionalization of the monolith surface. Two spacers were used, (3-glycidoxypropyl)trimethoxysilane (GPTMS) and (3-aminopropyl)triethoxysilane (APTES). The open structure of the ACM allows for a higher carrier deposition, and results in a higher protein loading. Immobilization via a GPTMS-functionalized ACM-monolith yields the best enzyme carrier. At pH 7, 200 mg lipase g⁻¹ SiO₂ and 150 mg lactase g⁻¹ SiO₂ can be deposited. These PEI systems provide an optimal environment for the lactase, 92% of the free enzyme activity is retained after immobilization. For the lipase, only 14% of the activity is retained. Immobilization at varying pH influences both enzyme yield and specific activity, immobilization at pH 5 was found to be optimal. The enzymes could be completely desorbed to facilitate reuse of the monolith-carrier combination. The molecular weight of the polymer also influenced the adsorption behavior and stability of the biocatalysts with respect to increasing ionic strength. In general, a higher polymer loading provides a more stable environment for the enzyme, and this stabilizing effect increases with polymer size. Therefore, the open walls of the ACM monoliths provide an important advantage when used in this immobilization protocol.

1 Introduction

Immobilization of enzymes or microorganisms often involves the irreversible covalent binding between the enzyme and a preexisting support. This is done to ensure a strong catalyst-support interaction. Usually, when the biocatalyst becomes deactivated during its application, both enzyme and support should be eliminated as waste [1]. In this perspective, the conventional covalent immobilization protocols have some important drawbacks:

- A relatively high cost due the use of expensive supports and the performance of complex immobilization reactions.
- The use and production of generally toxic compounds and waste, involved in the covalent immobilization methods and upon deactivation of the enzyme.

Other methods, based on physical adsorption of the enzyme on inorganic carriers, although reversible, are mostly suitable to prepare biocatalysts for use in organic solvents. A relatively large amount of enzyme would desorb when used in aqueous environment. From this point of view, reversible enzyme immobilization through ionic adsorption could be a convenient protocol for production of industrial biocatalysts. Reversible in this context means the possibility to promote complete desorption of the enzyme from the support. The supports can then be recovered fully intact and enzyme-free, and become ready to be used again for immobilization of fresh enzyme. In this way, even a relatively expensive support can be used infinitely, and the only waste is a solution of deactivated enzyme.

A number of protocols for reversible immobilization have been reported in the last decade, enzymes were adsorbed onto supports including polymers and resins [1-4], molecular sieves [5-8], silica and silica-alumina composites [9-13], and carbonaceous materials [14-16]. A method that is becoming increasingly popular is adsorption on ionic exchange resins (mainly anionic exchangers). Although ionic adsorption significantly decreases enzyme leakage in aqueous environment, the electrostatic binding forces are not very strong and most proteins are already fully desorbed at moderate ionic strength (0.2-0.3 M NaCl) or if a pH shift occurs due to reaction. In this way, the reaction itself or possible high concentrations of ionizable substrates can promote undesirable leakage of enzyme from the carrier. This leads to an apparent inactivation of the enzyme and contamination of the product [17]. Different remedies have been offered such as the addition of cations during immobilization [18], and multipoint attachment [19]. Since the conventional carriers consist of rigid supports, it has been suggested that the relatively fast desorption is caused by the lack of flexibility of the support; the enzyme is not stabilized sufficiently when attached on the surface of a rigid particle. Composites consisting of porous rigid supports, covalently coated with flexible polymers with a high density of ion exchange moieties can be used as alternative supports for enzyme immobilization. Adsorption of proteins on this flexible polymer coating should promote minimal conformational distortion, because the polymer can adapt to the protein during multipoint attachment.

The use of particulate supports can sometimes be unwanted due to a relatively low mechanical strength and a low mass transfer efficiency [20]. Decrease of the particle size to increase mass transfer efficiency can cause high pressure drops over fixed bed reactors or settling problems in slurry reactors. The use of a thin layer of carrier material (minimizing diffusional distances) on structured monolithic support materials could be an interesting alternative for existing particulate carriers, in terms of mechanical stability and diffusion distances in the carrier. The more open structure of the ACM monoliths [21,22] can be used to increase the carrier loading and accessibility of the catalyst [23].

1.1 Deposition of a polymeric carrier on monoliths

The present study is concerned with the application of monolith reactors in the field of biotechnology. In order to employ monoliths as a support material for ionic adsorption of enzymes, a suitable carrier layer must be applied on the surface of the monolith channels. Different hydrophilic polymers can be used to create a suitable environment for enzyme immobilization [24]. The size of the polymer molecules influences the binding strength of the enzyme-carrier interaction and the stability of the enzyme. Large polymer molecules form a stabilizing (protective) environment for the enzyme and the stronger bonds makes these biocatalysts more resistant against desorption of the enzyme in high-ionic strength environment. Examples of cheap, readily available polymers for ionic adsorption are depicted in Figure 1.

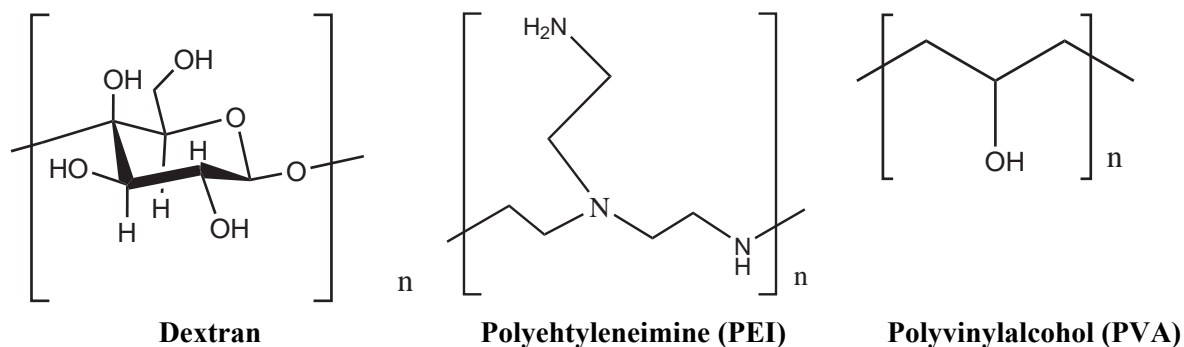


Figure 1. Examples of polymers for ionic adsorption

In order to function as a carrier material or to be attached to a ceramic monolith, the polymer should be easy to handle and relatively reactive. Dextran can be functionalized by oxidation of the -OH groups. Aldehyde dextran can be obtained via periodate oxidation of commercial dextrans with varying molecular weight. These functional polymers can react with primary amine groups in enzymes, supports or other polymers. The low solubility and the extra activation step make Dextran less favorable. Polyvinyl alcohol (PVA) is one of the few high molecular weight polymers that is water-soluble. PVA forms a tough, clean film with high tensile strength and abrasion resistance. PVA can be functionalized with aldehyde-groups by reaction with glutaraldehyde at pH 1. The extreme reaction conditions and large amounts of glutaraldehyde that are needed for this reaction also make PVA less favorable.

Polyethyleneimine (PEI) is commercially available in a range of different molecular weights and concentrations in water. Branched PEI is readily soluble, whereas linear PEI is practically insoluble in water. PEI contains a high concentration of primary, secondary, and tertiary amine groups. Most of these groups are already ionized at neutral pH; hence this polymer can be used for adsorption of proteins or other polyanionic polymers. In addition, the presence of non-ionized primary amine groups allows for the covalent attachment of the polymer onto aldehyde- and epoxy-supports. The polymer can also be adsorbed directly onto a washcoated support material. The availability of ready-made PEI solutions in water and the possibility to react PEI directly with GPTMS or APTES/glutaraldehyde supports, makes this polymer a favorable carrier material for application on monoliths.

To provide surface area and binding sites for the polymer, the monolith must be washcoated with silica and, if necessary functionalized with an organo-silane compound. As was discussed in Chapter 3, different washcoating strategies are available. In combination with ionic adsorption, the monolith surface should be functionalized via its Si-OH groups. In this case a colloidal silica washcoat provides both surface area and functionality to the monolith. Different methods of PEI-modification and ionic adsorption on silica surfaces are presented here:

1.1.1 Ionic adsorption on physically adsorbed PEI

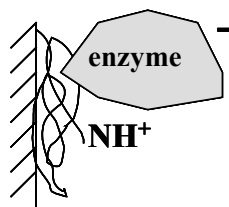


Figure 2. Physical adsorption-ionic adsorption

The ionic adsorption of a protein on adsorbed PEI is schematically drawn in Figure 2. The polymer is adsorbed onto the silica surface, with all amino groups available for ionic adsorption of. Linear or branched PEI can be used. In theory, this method allows for reuse of both the support material and the carrier. In practice desorption of polymer from the carrier can be observed.

1.1.2 Ionic adsorption on GPTMS-PEI surface and APTES/GLU-PEI surface

In Chapter 4, functionalization of washcoated monoliths was discussed. For immobilization via PEI, both (3-aminopropyl)triethoxysilane (APTES) and (3-glycidoxypropyl)-trimethoxysilane (GPTMS) can be used, see Figure 3.

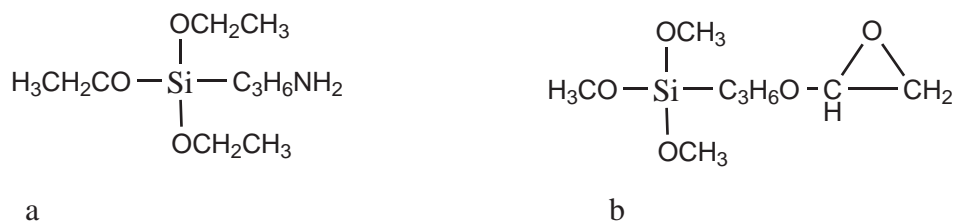


Figure 3. Molecular structures of a) APTES and b) GPTMS

This covalent attachment of PEI via an organo-silane with subsequent enzyme adsorption is depicted in Figure 4. In case of the silanization with GPTMS the epoxy-groups of GPTMS can react directly with the amino groups of PEI (Figure 4a). In case of functionalization with APTES, a second step is needed before the polymer can be attached. A bifunctional reagent is needed to connect the amino groups of APTES with the amino groups of the polymer. Usually, glutaraldehyde is used for this type of reaction.

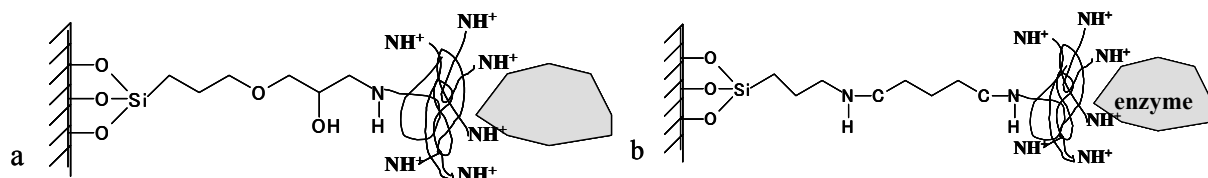


Figure 4. Covalent attachment-ionic adsorption system with a) GPTMS, b) APTES

The aldehyde groups of glutaraldehyde react with the amino groups of the polymer on one side, and with the amine groups of the silane on the other side (Figure 4b).

After the polymer has been deposited on the monolith backbone, the enzyme is attached to the monolith-PEI carrier by means of ionic adsorption. Polyethyleneimine is a weak electrolyte. A polyelectrolyte consists of a “macro-ion”, i.e., a macromolecule carrying covalently bound anionic or cationic groups, and low-molecular “counterions” securing electro neutrality. PEI forms a polyion-counterion system only in a limited pH range, and is present as an undissociated polybase in the alkaline range. Enzymes can be either positively or negatively charged due to the terminal amine $-NH_2$ and carboxyl ($-COOH$) groups and the groups on the side chain of the individual amino acids in the primary structure of the protein. They are positively charged at low pH and negatively charged at higher pH. The intermediate pH at which an enzyme molecule has a net charge of zero is called the isoelectric point.

If the immobilization is carried out above the isoelectric point of the enzyme (which makes it negatively charged) and below the pH where the PEI becomes dissociated (the polymer will be positively charged), the enzyme will be attracted to the support and remain immobilized (Figure 5).

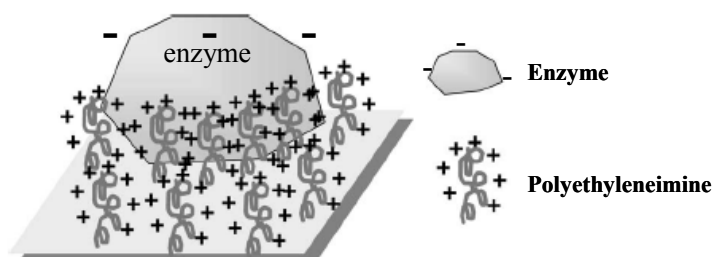


Figure 5. Immobilization of enzymes on PEI-activate supports [1], at a pH above the iso electric point of the enzyme and below the dissociation pH of PEI.

1.1 Layout

The aim of the present work is to compare ACM monoliths with classical cordierite monoliths as support material for different enzymes through ionic interaction with polyethyleneimine (PEI). The coating procedure of PEI on the support is optimized. PEI can be attached to the backbone by covalent binding and by physical adsorption, and enzymes can then be reversibly immobilized on the carrier. Adsorption of PEI on a washcoated monolithic support is a straightforward method, which allows both carrier (desorption/adsorption of enzymes) and the support (desorption/adsorption of PEI) to be reused. Possible problems with this approach can be the desorption of the polymeric carrier from the monolith backbone in aqueous medium.

Covalent attachment of PEI can be done via attachment of aldehyde or epoxy groups. The first step is the silanization of the monolith i.e. the introduction of an organic amino group or an organic epoxy group on the inorganic support. After optimizing the deposition of the polymer, lactase and lipase will be adsorbed. The biocatalysts are compared in terms of activity, stability and ease of reuse.

2 Experimental

2.1 Materials

Ludox AS-40 (40% colloidal silica in water), and polyethyleneimine (high molecular weight (MW = 60000-1000000), water free; MW = 750000, 50% in water; low molecular weight MW = 60000 or MW = 25000) were from Aldrich. β -Galactosidase from *Aspergillus oryzae* (E.C. 3.1.2.23), lipase from *Candida rugosa* (E.C. 3.1.1.3, type VII), p-nitrophenyl propionate (pNPP), 3-[(trimethoxysilyl)propyl]polyethyleneimine hydrochloride solution, o-nitrophenyl- β -galactopyranoside (oNPG), and (3-glycidoxypropyl)trimethoxysilane (GPTMS) were purchased from Sigma. (3-aminopropyl)triethoxysilane (APTES), CPC-silica carrier (mesh size 50), glutaraldehyde (25% in water) and NaBH₄ (>96%) were purchased from Fluka. Analytical grade buffer salts were obtained from Baker. Square channel monoliths of ACM, 200 cells inch⁻² (62 cells cm⁻²) were prepared by a proprietary Dow process to produce honeycombs with “small”, “medium”, and “large” pores. Cordierite monoliths with a cell density of 200 cells inch⁻² were used for comparison. The key properties of these monoliths are given in Table 1.

Table 1. Nominal values of the key properties of square channel monoliths employed in this study

	ACM 1 (“small”)	ACM 2 (“medium”)	ACM 3 (“large”)	Cordierite
Cell density	200 cpsi	200 cpsi	200 cpsi	200 cpsi
Wall thickness	0.24	0.24	0.24	0.3 mm
Wall porosity	60%	60%	70%	35%
Pore diameter	5 μ m	18 μ m	45 μ m	7.5 μ m

Monolith samples with a length of 5 cm and a diameter of 4.3 cm were calcined for 4 h at 1273 K in static air (10 K min^{-1}) to remove possible contaminants.

2.2 Support preparation

Particulate carriers and monolithic carriers were prepared from CPC-silica carrier and monolithic backbones respectively. Crushed monoliths were also employed as particulate carrier. Polyethyleneimine (PEI)-functionalized supports were prepared by the method of Mateo *et al.* [1] and Fernandez-Lafuente *et al.* [25], either with a 2-step approach via γ -aminopropyltriethoxysilane (APTES) and glutaraldehyde or through coupling to (3-glycidoxypropyl)trimethoxysilane (GPTMS). In order to provide sufficient silanol groups on the support surface, the monoliths were coated with a colloidal silica layer before reacting with the silane. PEI was also directly deposited on SiO_2 -washcoated supports and the particulate CPC-support.

2.2.1 Washcoating and silanization

A Silica washcoat was applied on the monolith backbones by dipcoating for 5 min in a Ludox AS-30 solution. For dipcoating of ACM samples, the Ludox solution was diluted to a final concentration of 4%. The supports were dried horizontally in air at ambient conditions under continuous rotating for 12 h. The samples were calcined for 2 h at 673 K (heating rate 2 K min^{-1}). Washcoated monoliths and CPC-carrier were submerged in a 5-10 wt% solution of silane in toluene or with 0.1 %v/v tetraethylene amine. The mixture was stirred at 293 K for 24 h. Supports were washed with toluene and acetone and dried at 393 K for 4 h (2 K min^{-1}).

2.2.2 Formation of aldehyde groups

Monoliths or CPC-carrier, silanized with APTES were treated with a 5%v/v solution of glutaraldehyde in 50 mM phosphate buffer pH 7 at 278 K for 24 h.

The epoxy groups of the GPTMS can also be converted into aldehyde groups by hydrolysis with sulfuric acid. GPTMS coated monoliths were stirred at room temperature for 1 h with 1 M H_2SO_4 . The supports were washed with water and subsequently treated at room temperature for 1 h. in a 1 M solution of NaIO_3 to create aldehyde groups.

2.2.3 Polyethyleneimine addition

PEI was attached to both functionalized and SiO_2 -washcoated supports from a 10 wt% PEI solution in water at pH 10. Alternatively, washcoated monoliths were treated with a pre-made silane-PEI composite (diluted to 10 wt% in 2-propanol). Reaction was allowed to proceed for 24 h at 293 K. After reaction with washcoated monoliths, samples were washed with water. The GPTMS-coated monoliths were washed with 1 M NaCl and water. In case of reaction with glutaraldehyde functionalized supports, excess glutaraldehyde groups were quenched

with NaBH_4 after reaction. The carriers were reduced by adding 2.4 g solid borohydride, and the reaction was left to proceed for 2 h. The monoliths were washed alternately with 50 mM acetate buffer pH 5, 50 mM borate buffer pH 9 and 1 M sodium chloride and finally with an excess of distilled water.

2.2.4 Enzyme adsorption

Immobilizations on particulate supports were carried out at room temperature in plastic bottles. The enzyme was dissolved in a 5 mM phosphate buffer at pH 7. 1 Gram of support material was mixed continuously with 10 ml of enzyme solution for 20 h. Different 0.05 M buffer solutions were used, ranging from pH 5-9. The enzyme concentration was varied between 1-4 g l^{-1} . During immobilization, samples were withdrawn and the enzyme concentration was determined using UV-VIS (with the oNPG assay on a Thermo Optek UV-540). After immobilization the samples were washed with phosphate buffer, dried under vacuum or at 278 K and stored under air at 278 K. Immobilizations on monolithic supports were carried out in up-flow operation, using a glass reactor and a peristaltic pump. The liquid was recycled over the support in upflow. Different 5 mM buffer solutions were used, ranging from pH 5-9. Enzyme concentration was varied between 1-4 g l^{-1} . During immobilization, samples were withdrawn and the enzyme concentration was determined using UV-VIS (on a Thermo Optek UV-540 with a 1 cm cuvette) or by the Bradford method. After immobilization, the samples were washed with 50 mM phosphate buffer pH 7 and 5 mM acetate buffer pH 4.5, dried under vacuum overnight, and stored in 5 mM acetate buffer pH 4.5 with 1 g l^{-1} sodium azide at 278 K.

2.3 **Characterization**

The amount of coating, mass increase, and mass decrease were determined by measuring the sample weight before and after the various preparation steps.

Thermogravimetric analysis (TGA) was performed on a Mettler Toledo TGA/SDTA851^e. The samples were heated in air (100 ml min^{-1}) to 1273 K (heating rate 10 K min^{-1}).

2.3.1 Surface chemistry

Diffuse reflectance IR spectra were recorded on a Thermo Nicolet spectrophotometer model Nexus with an MCT detector coupled with a diffuse reflectance accessory model COLLECTOR from SpectraTech. Samples were diluted in KBr and measured against a KBr background.

2.3.2 Electron Microscopy

To obtain qualitative information about the texture and distribution of the silica washcoat in the monolith, Scanning Electron Microscopy was performed using a Philips XL-20 scanning electron microscope.

2.3.3 Stability and activity of immobilized lactase and lipase

Desorption of the enzyme from the carrier was studied by increasing the ionic strength in an aqueous solution. The prepared biocatalysts were placed in 150 ml 50 mM phosphate buffer (pH 7), with increasing concentrations of NaCl. Enzyme concentration was followed by UV-VIS, and checked by the Bradford method.



Figure 6. Experimental set-up with glass reactor, onset, and stirrer

The activity and stability of the biocatalysts were compared by performing activity assays, with intermediate storage of the catalysts at 278 K. Total reaction volume was 160 ml. Catalysts were compared for their initial activity (0-10 min), calculated from the initial linear part of the concentration/time plot. The experimental set-up consisted of a glass reactor with a stirrer and a recycle mechanism to force the liquid circulation through the monolith channels. A schematic overview of the experimental set-up is presented in Figure 6. A stirrer rate of 500 rpm was selected for all experiments. A 1 cm quartz cuvette was used to measure the absorbance. During the activity tests 2.5 ml samples were withdrawn from the reactor and returned to the reaction mixture after measurement.

β -Galactosidase activity was followed spectrophotometrically by the increase in absorbance at 405 nm, promoted by the hydrolysis of oNPG in aqueous medium (Figure 7). Experimental conditions were 1-2 mM oNPG in 0.05 M Tris buffer pH 7 and 293 K.

Table 2. Nomenclature

Position	Component	Code
1	Support type	CPC, C or A
2	Micro grain structure ACM	S, M, or L
3	Washcoat	LxAS30, LxAS40
4	Silane	APTES or GPTMS
5	Polymer,Mw	PEI,Mw

Some additional comments can be added in the code such as the acid treatment of the epoxysilane to produce indirectly aldehyde groups, which will be noted as (ox) with the silane. For the pre-fabricated silane-polymer compound, “silane-PEI” will be used

3 Results and Discussion

Washcoating and silanization were already discussed in Chapter 3 and 4. The monolith backbones that are used for application of a polyethyleneimine coating are washcoated and silanized with the optimized methods. To prevent complete plugging of the open walls of the ACM monoliths, a diluted (10x) Ludox solution was used. Some important parameters are presented in Table 3.

Table 3. Results preparation of supports for PEI attachment

Support	Ludox AS-30 loading wt%	APTES loading mmol g ⁻¹ _{silica}	GPTMS loading mmol g ⁻¹ _{silica}
Cordierite	7.6	0.95	0.41
ACM-S	4.9	1.78	0.59
ACM-M	2.8	1.83	0.70
ACM-L	2.4	1.92	-

As was already observed in Chapter 4, the higher porosity of the open wall of ACM and the lower washcoat loading for large-grain ACM give a better accessibility during silanization. This results in a higher silane loading on ACM monoliths compared to classical cordierite and a slight increase in silane yield on ACM samples with a larger micrograin size.

3.1 PEI addition

The polymer (unless noted otherwise, high molecular weight branched PEI with a Mw of 25000 was used) was either attached via the addition of glutaraldehyde or directly onto the GPTMS coating. PEI was also adsorbed onto the silica surface. The yield was measured by following the weight increase of the total support and by taking small samples from different parts of the monoliths for TGA analysis.

3.1.1 TGA

The monolith backbones with physically adsorbed PEI were checked for polymer desorption by stirring in water for 5 h. After each cycle a TGA was performed. The results for a washcoated ACM monolith with small needles, AS-LxAS40-PEI, are presented in Figure 9. Because the samples were used directly after overnight drying in air, the water content is still relatively high as can be seen from the large weight decrease at 300-400 K. Initially, 2.5 wt% PEI was loaded onto the backbone. After 2 desorption steps, part of the polymer has desorbed from the monolith.

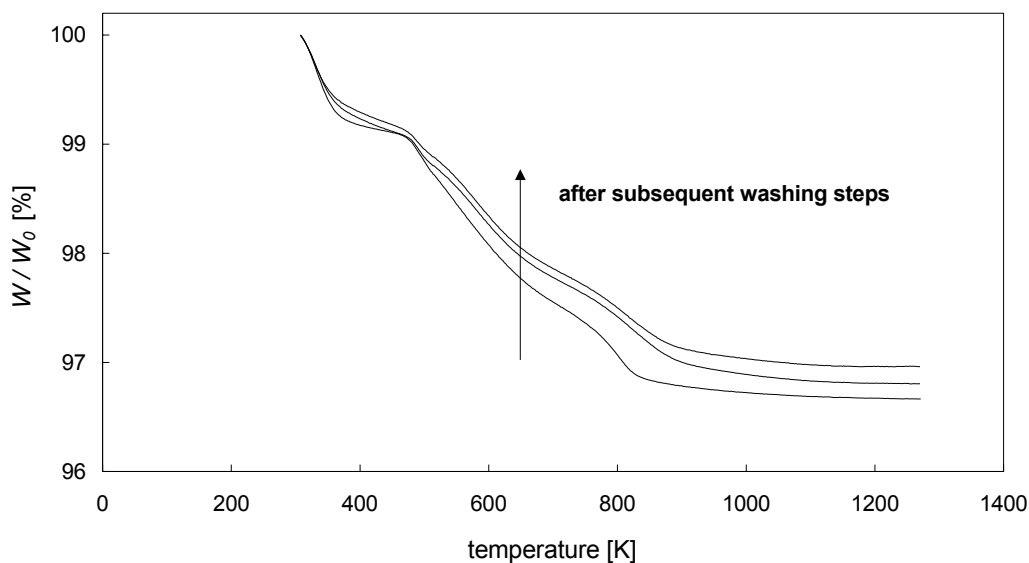


Figure 9. Thermogravimetric oxidation profiles of AS-LxAS40-PEI as a function of temperature. As prepared and after 2 subsequent desorption steps in water for 5 h, with intermediate vacuum drying.

Although the direct adsorption of PEI is very simple and only requires one preparation step, the significant desorption when applied in aqueous environment does not make this the preferred preparation method for polymer-ceramic composites. Covalent attachment of the polymer is recommended. In Figure 10, TGA results for C-GPTMS-PEI after each preparation step are presented. As was already observed in Chapter 4, the washcoated monoliths only show a small weight loss due to physisorbed water. GPTMS decomposes around 550 K. The polymer decomposes in 2 steps, first a large step where water is evaporated, and then a mixed decomposition of both polymer and organo silane.

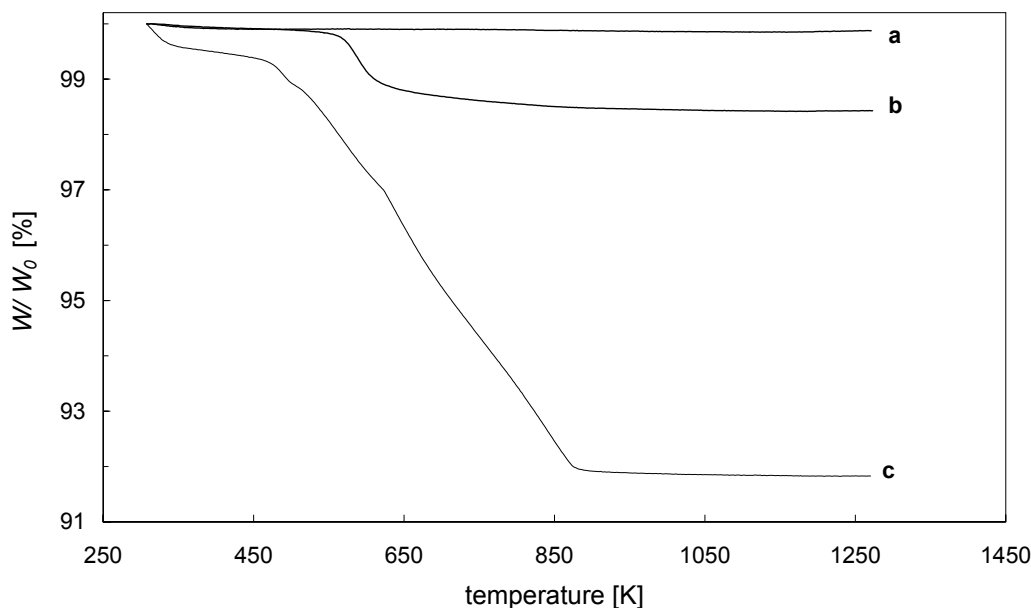


Figure 10. Thermogravimetric oxidation profiles of C-LxAS40-GPTMS-PEI. a) C-LxAS40, b) C-LxAS40-GPTMS, c) C-LxAS40-GPTMS-PEI. Relative mass after each preparation step

The loading that was established from TGA (from different parts of the monoliths) was found to be in good agreement with weight increase of the whole samples. Apparently the distribution throughout the channels can be considered to be homogeneous. The results for the different coating methods are given in Table 4.

Table 4. PEI yield for coating on C-LxAS30, AS-LxAS30, and AM-LxAS30

Method	Y_{PEI} cordierite wt%	Y_{PEI} ACM-S wt%	Y_{PEI} ACM-M wt%
GPTMS	7.9	9.5	12.1
APTES-Glutaraldehyde	4.7	6.1	6.3
PEI ads	2.3	2.5	3.2

The PEI loading is higher for ACM monoliths than for cordierite monoliths. Based on the higher washcoat and silane loadings, combined with the better accessibility a higher polymer loading could be expected for ACM backbones. The increased wall porosity and surface area of the AM-samples lead to a slight increase in polymer loading compared to the AS-samples. As was observed in chapter 3, the washcoat loading of the AM samples was 20-30% lower. The better accessibility of the washcoat for silanization leads to a higher density of functional groups compared to cordierite. The combination of a higher loading capacity and better accessibility for the PEI molecules inside the open wall, explains the increase in PEI loading on ACM monoliths.

3.1.2 Surface chemistry

To investigate the effect of surface chemistry of the different coatings, ACM and cordierite samples were analyzed with DRIFT-FTIR. The spectra of washcoated and functionalized ACM samples are given in Figure 11.

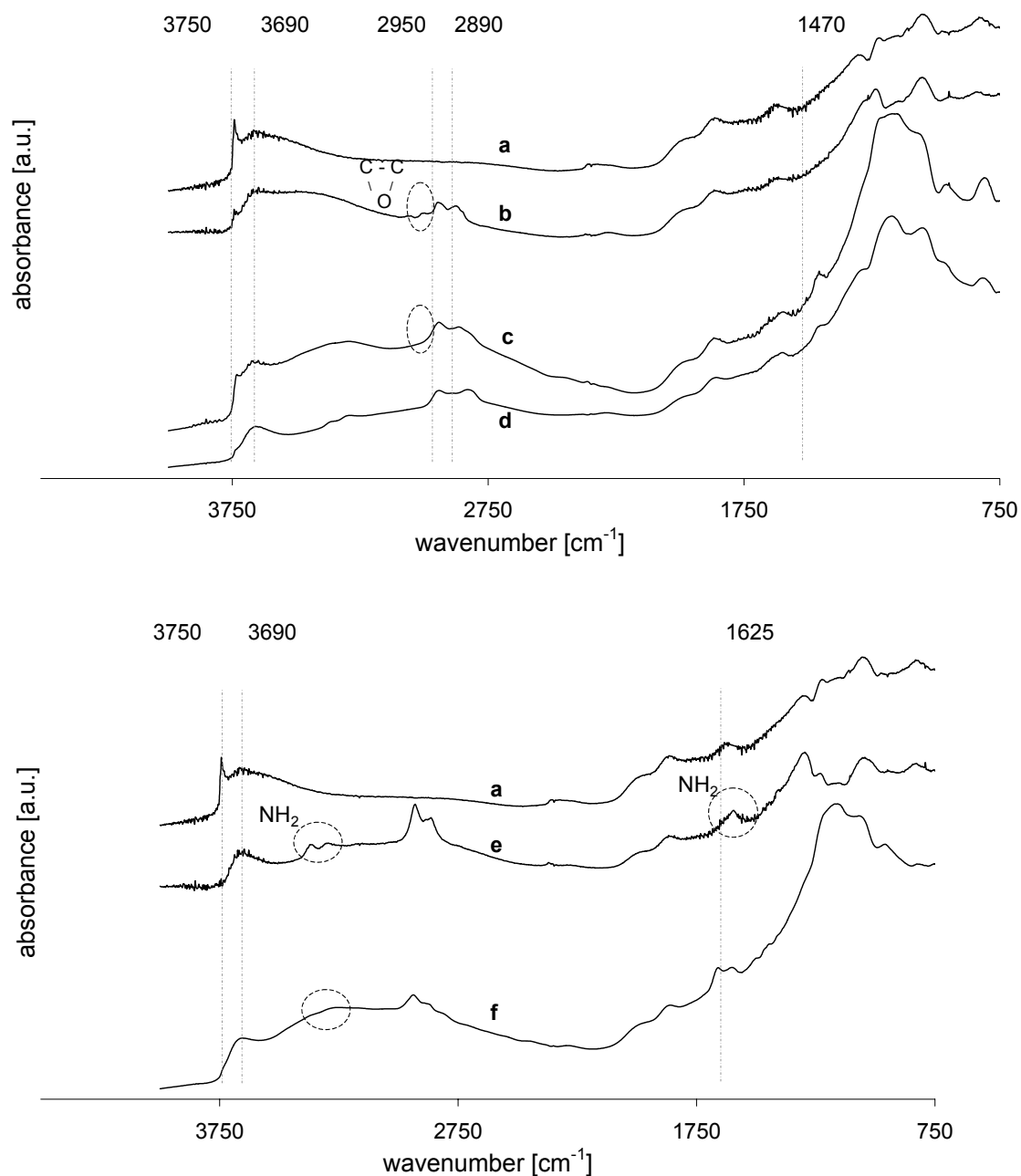


Figure 11. Drift-FTIR spectra for coated ACM monoliths. a) AM-LxAS30, b) AM-GPTMS, c) AM-GPTMS-PEI, d) AM-silane-PEI, e) AM-APTES, f) AM-APTES-PEI

The bare ACM (not shown) shows typical bands at 801 cm^{-1} (Si-O-Si silica) and 1110 cm^{-1} (Si-O-Si silica) [26,27]. After washcoating with Ludox AS-30 (a), two bands appear at 3750 and 3690 cm^{-1} ; an Si-OH stretching vibration (3750 cm^{-1}) and a hydrogen bonded silanol

band (3690cm^{-1}) [26,28], although the latter is difficult to identify because of the strong contribution of the broad feature of the O-H stretching vibration of physisorbed water. The presence of physisorbed water in various samples is also apparent by the bending mode at around $1625\text{-}1650\text{ cm}^{-1}$.

After silanization with GPTMS (b), the characteristic silica bands disappear and are replaced by the vibrations of the silanes' typical bands (epoxy ring and amino groups) at $3000\text{-}3060\text{ cm}^{-1}$. After addition of the polymer (c), these vibrations disappear. The vibrations of the carbon backbone at $2890\text{-}2950\text{ cm}^{-1}$ remain visible because the polymer also has a CH_2 backbone. The presence of the polymer can also be confirmed by the vibrations for amine groups at $3000\text{-}3550\text{ cm}^{-1}$ and 1625 cm^{-1} , whereas the intensity of the physisorbed water vibrations has also decreased, in agreement with the more apolar character of the material. The band at 1470 is most likely also associated with the CH_2 backbone (bending mode). When a washcoated monolith is reacted directly with a silane-PEI composite (d), a similar spectrum is observed with slightly lower intensities in the specific range where the organo-silane can be observed. This is due to the stoichiometric ratio in which GPTMS and PEI are added to this sample. In sample c, an excess of GPTMS was already present on the surface, whereas for sample d the surface is reacted with silane-PEI molecules. For functionalization via APTES, a similar result is obtained. After silanization with APTES the carbon backbone and the typical amine stretching vibrations (1625 cm^{-1} and $3250\text{-}3550\text{ cm}^{-1}$) are observed. If the polymer is deposited on APTES (curve f), the spectrum of the composite is almost identical to that of PEI attached to GPTMS (curve c). This indicates good polymer coverage; the underlying silane coating is not visible after reaction with PEI.

In Figure 12, a selection of FTIR spectra of functionalized cordierite monoliths is presented.

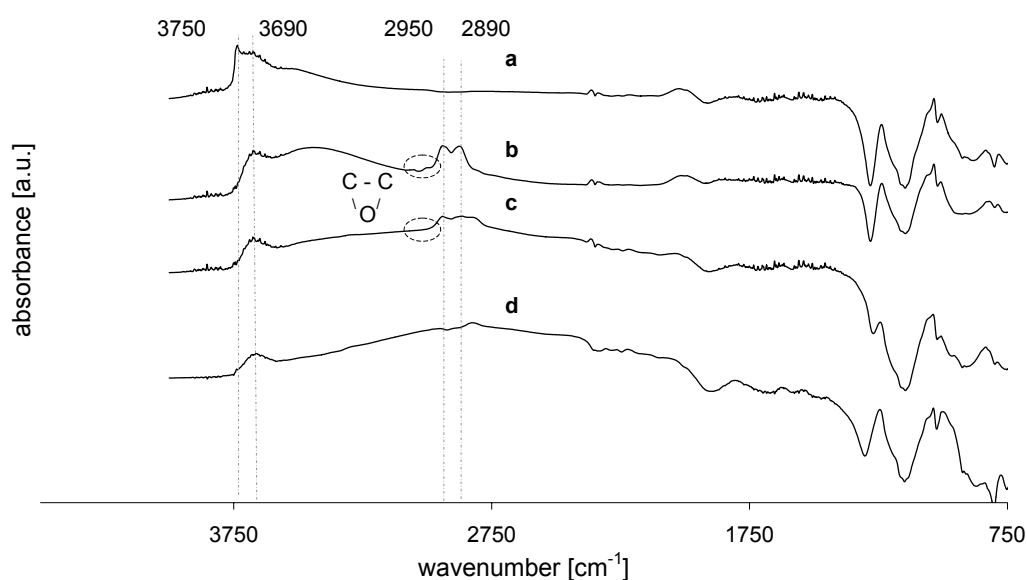


Figure 12. Drift-FTIR spectra for coated cordierite monoliths with a cordierite background. a) C-LxAS30, b) C-GPTMS, c) C-GPTMS-PEI, d) C-PEI

Due to interference of the cordierite, washcoated and functionalized samples were measured against a cordierite background. In accordance with the washcoated ACM sample (Figure 11, spectrum a) two bands appear at 3750 and 3690 cm^{-1} as a result of free and hydrogen-bonded silanols in the washcoat.

After silanization with GPTMS (b), the typical silica bands disappear and are replaced by the vibrations of the silanes' functional groups. Because the samples were diluted in KBr, the typical vibrations of the organo-silane compounds are not very pronounced. After addition of the polymer (c) the spectrum is similar to that for silane-PEI addition on ACM monoliths. The presence of the polymer is confirmed by the vibrations for amine groups at 3000-3550 cm^{-1} and 1625 cm^{-1} , although again these vibrations might also have spectral contributions due to the presence of physisorbed water. When PEI is adsorbed directly on a washcoated monolith (d), a similar spectrum is observed.

3.2 Enzyme immobilization

After preparation of the PEI-functionalized monoliths, lactase and lipase were adsorbed on the carriers. Since the lyophilized protein powders are not of the highest grade, the exact enzyme content is not known. Enzyme content usually ranges between 5-10%. Since the used protein powders were relatively cheap and assumed to be of a lower grade, an enzyme content of 5% was assumed for both lipase and lactase. The analysis methods that are used (UV-VIS and the Bradford method) cannot distinguish between different proteins, therefore the adsorption results are given in total amount of immobilized protein. The immobilization results are expressed in lipase/lactase immobilization yield, the values were not corrected for possible impurities. Possible effects of selective adsorption of specific proteins are not taken into account because the exact composition of the enzyme lyophilizates was not known. In an adsorption curve, the enzyme concentration (in g l^{-1}) as a function of time is represented. Figure 13 is an example of a lipase adsorption on a C-GPTMS-PEI sample at 278 K. Unless mentioned otherwise, adsorption measurements take place at pH 7 and 278 K, from a 2 g l^{-1} solution in water.

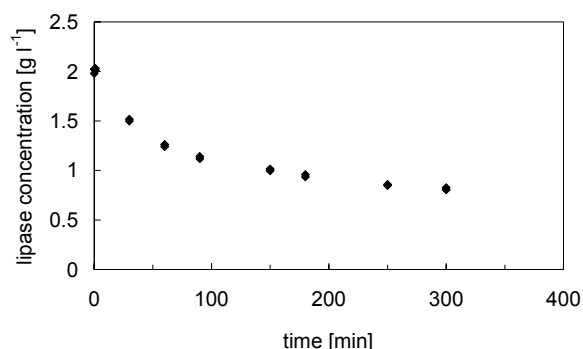


Figure 13. Concentration-time plot during lipase adsorption on C-GPTMS-PEI sample in batch operation (2 g l^{-1} , 278 K, $V_L = 0.4$ l) from aqueous phosphate buffer pH7

3.2.1 Lactase adsorption

Lactase was adsorbed from a 2 g l^{-1} solution in a 5 mM phosphate buffer pH 7, at 278 K. The results for adsorption on different carriers are presented in Figure 14. The carriers that have the polymer adsorbed on the washcoated monolith were not used for enzyme adsorption due

to desorption of the polymer. The highest adsorption capacity was measured for carriers with a GPTMS linker (dark bars). As was observed before (see chapter 5), the use of APTES and glutaraldehyde leads to a lower enzyme adsorption capacity (light bars). The pre-made silane-PEI composite (white bars) did not result in improved performance. Beforehand, the use of a single reaction step was expected to be more efficient than separate steps to bind the silane and the polymer, because every silane molecule that is bound already contains a PEI tail. Probably, silanization is less efficient with the bulky silane-PEI molecules. Adsorption on ACM monoliths leads to higher total enzyme loading, because of the higher PEI loading (see Table 4) on these monoliths.

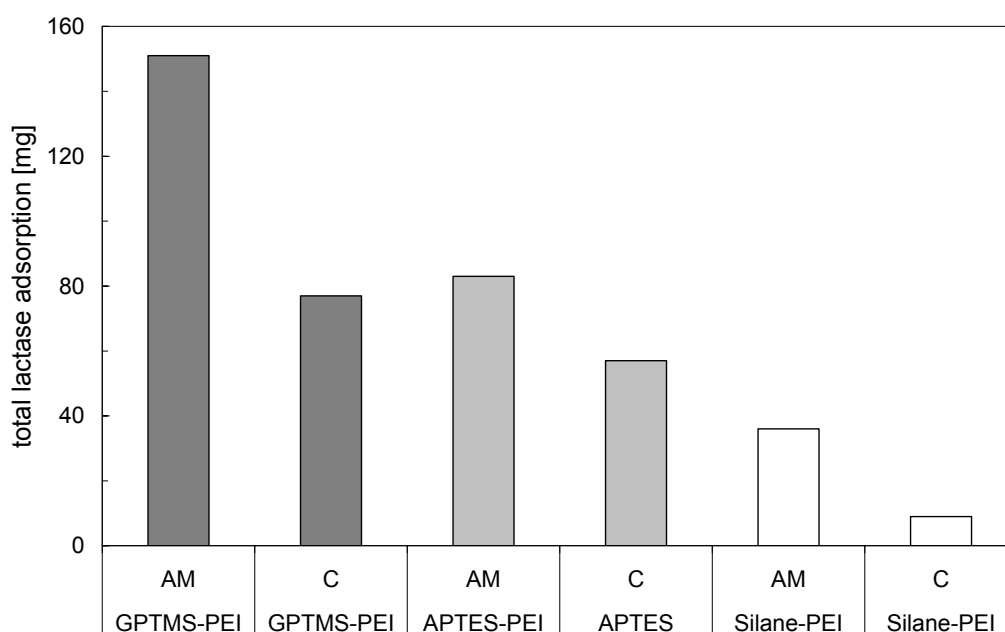


Figure 14. Lactase adsorption on 200 cpsi cordierite and ACM samples with PEI carrier

3.2.2 Lipase adsorption

Lipase was adsorbed from a 2 g l^{-1} solution in a 5 mM phosphate buffer pH 7, at 278 K. The results for adsorption on different carriers are presented in Figure 15. The carriers with adsorbed PEI on the washcoated monolith were not used for enzyme adsorption due to desorption of the polymer. In accordance with lactase adsorption (Figure 14), the highest adsorption capacity was measured for carriers with a GPTMS linker (dark bars). The effect of more efficient silane coating at higher GPTMS concentration, as was observed in chapter 4, is clearly visible; lipase yield is doubled with increased silane loading for cordierite. The standard concentration of 5 wt% silane was used for all other samples in Figure 15. Adsorption on APTES-functionalized samples is significantly lower (lighter bars). Adsorption of lipase on pre-fabricated GPTMS-PEI carriers is much higher than lactase adsorption, but yields a similar picture of total enzyme adsorption.

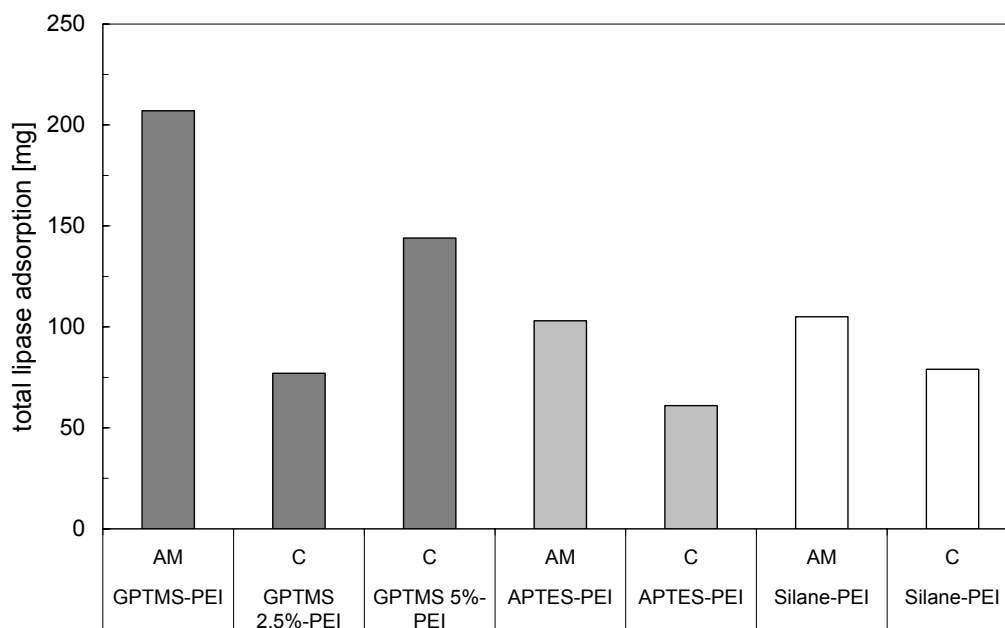


Figure 15. Lipase adsorption on 200 cpsi cordierite and ACM samples with PEI carrier. For silanization of cordierite with GPTMS, 2.5 and 5 wt% silane were used

Also for lipase, the best carrier was the AM-GPTMS-PEI monolith. Similar to what was observed in Chapter 5, the use of GPTMS leads to higher enzyme adsorption compared to APTES-GA.

3.3 Reuse of the monolith-carrier combination

In Table 5, the amounts of lactase adsorbed and desorbed in repeated adsorption-desorption cycles with an AM-Silane-PEI sample using a 2 g l^{-1} solution at pH 7 are presented. Partial desorption by increasing the ionic strength will be discussed elsewhere.

Table 5. Reuse of AM-Silane-PEI for lactase adsorption

Run	Lactase adsorbed mg	Enzyme desorbed mg
1	35	32
2	30	30
3	24	25
4	37	12
5	23	50

In general, all adsorbed enzyme is desorbed upon treatment in guanidine. Only in run 4 not all enzyme was desorbed, the remaining lactase was desorbed in run 5. The reason for the ineffective desorption in run 4 is not known, possibly an experimental error is responsible. Apparently the maximum loading of the carrier is around 45-50 mg. After run 4, approximately 25 mg lactase remained at the surface, to which another 23 mg was added in run 5. Because the adsorptions are usually stopped after 5 h, this value was not obtained in run 1-4. When used with lipase, the same complete adsorption-desorption cycles can be

obtained. Guanidine is generally used to completely denature proteins. The PEI coated-supports can be reused by removing the enzyme with guanidine, the total amount of adsorption sites is not influenced by this desorption method, so apparently no protein residues are left behind on the carrier.

3.4 Catalyst performance

After enzyme immobilization, the catalysts were tested in colorimetric assays in aqueous medium, performed in a glass reactor as described in chapter 5.

3.4.1 Immobilized lactase

The activity of the immobilized lactase in the hydrolysis of oNPG at 295 K is presented in Figure 16. Lactase was immobilized from a 2 g l^{-1} lactase solution at pH 7, 278 K.

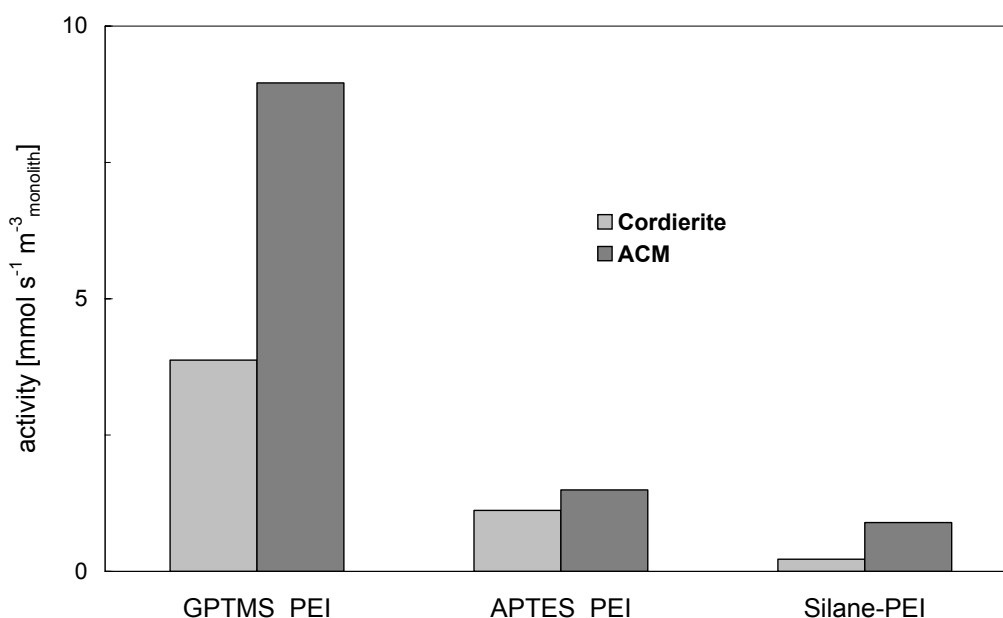


Figure 16. Comparison of ACM and cordierite in terms of activity per monolith volume of immobilized lactase in the hydrolysis of oNPG at 295 K, pH7

Figure 16 shows a similar trend to the one that was observed for enzyme immobilization in Figure 14. It can be concluded that the activity per monolith volume is proportional to the amount of immobilized protein. ACM monoliths have a higher activity per monolith volume, because the open wall allows for more PEI to be deposited. This results in a higher protein yield and a higher activity. In Table 6, the protein loading and the specific activity per gram of protein are presented for the immobilized lactase. The activity of the free enzyme under the same conditions is included. The GPTMS-PEI-samples have the highest enzyme loading, and the highest specific activity. The reason for the lower activity of the silane-PEI samples that actually consist of the same components (only the sequence of the reaction steps has been

different) is not clear. The samples are of the same batch and also have a much lower enzyme loading than the same samples that were used for lipase adsorption (see Figures 14 and 15).

Table 6. Lactase immobilization: Immobilization yield and catalyst performance in the hydrolysis of oNPG at 295 K

Catalyst	Total adsorption mg	Enzymatic activity	
		$\text{mmol m}^{-3} \text{monolith s}^{-1}$	$\text{mmol g}^{-1} \text{lactase s}^{-1} *$
Free lactase			3.25×10^{-3}
C-silane-PEI	9	0.2	1.4×10^{-3}
C-GPTMS-PEI	77	3.9	2.9×10^{-3}
C-APTES-PEI	57	1.1	1.1×10^{-3}
AM-Silane-PEI	36	1.5	2.1×10^{-3}
AM-GPTMS-PEI	150	9.0	3.0×10^{-3}
AM-APTES-PEI	83	0.9	5.4×10^{-4}

* Actual lactase content in the crude protein is estimated to be only 5%

The specific activity of the lactase is comparable to that of the lactase on GPTMS-PEI carriers (see Table 6), although based on the absence of free epoxy groups that could cause deactivation of the enzyme by covalent binding a slightly higher immobilized activity was expected for the silane-PEI samples. In general, the specific activity depends on the immobilization protocol. This was already observed for covalent immobilization in Chapter 5. In accordance with the results for covalent immobilization via APTES-glutaraldehyde, the specific activity of the APTES-PEI-samples is relatively low compared to the GPTMS-containing carrier materials. Only 15-30% of the free lactase activity is retained after immobilization via APTES. This is probably caused by the presence of free aldehyde groups, which result in chemical modification of the enzyme and a lower specific activity. The GPTMS-PEI-samples have the highest activity, 92 % of the free lactase activity is retained after immobilization. For all methods, the immobilized activity of lactase is significantly higher than for covalent immobilization of trypsin (only 2% of the free trypsin activity was retained after covalent immobilization). For lactase adsorption on GPTMS-PEI samples, the immobilized activity is higher than on different carbon carriers (Chapter 9, 50-70% of the activity was retained after adsorption). For lactase adsorption on silane-PEI the immobilized activity (65%) is comparable to that of the carbon-bound lactase. If a lactase content of 5 wt% is assumed, a turnover frequency of 7 s^{-1} is found for the biocatalyst with the highest specific activity (based on the GPTMS-PEI system). This is close to the value of 8 s^{-1} observed for the free enzyme. The optimum activity of the enzyme is found at pH 5, this assay was performed at pH 7, leading to a relatively low TOF.

3.4.2 Immobilized lipase

The activity of lipase coated monolithic biocatalysts in the hydrolysis of pNPP is presented in Figure 17. Lipase was immobilized from a 2 g l^{-1} solution at pH 7, 278 K. The activity correlates with enzyme loading. So the trend that was seen in Figure 15 for the amount of immobilized lipase can be seen again in Figure 17 for the activity per monolith volume.

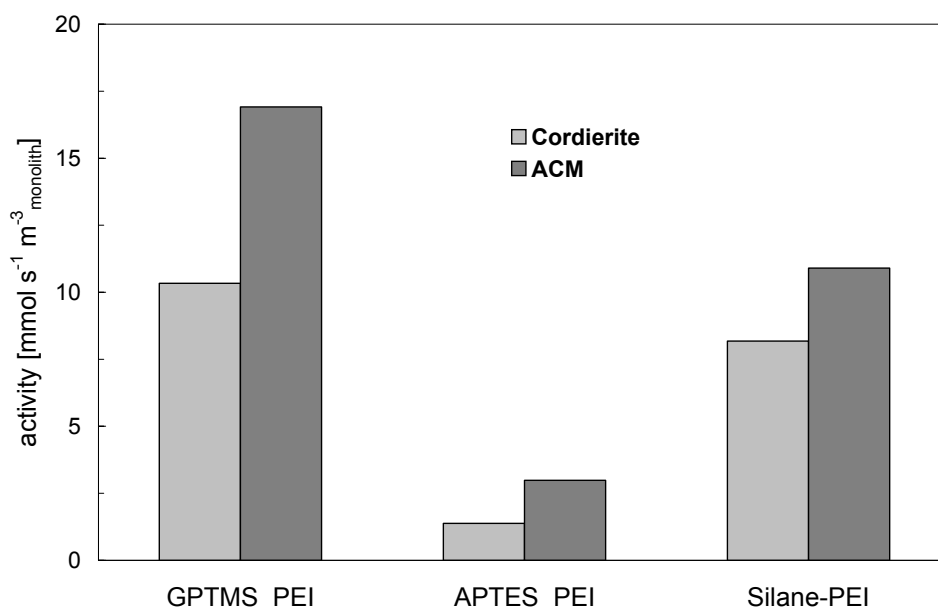


Figure 17. Comparison of ACM and cordierite in terms of initial activity per monolith volume of immobilized lipase in the hydrolysis of pNPP at 295 K, pH7

Immobilization via GPTMS-PEI leads to the highest activity per monolith volume. Comparing cordierite and mullite monoliths (light and dark bars), for all different preparation protocols the ACM monoliths have a higher activity. This corresponds with the higher loading for this carrier (Figure 15), but the specific activity differs strongly. Table 7 presents the quantitative data of protein adsorption, volumetric and specific activity, together with that of the free enzyme.

Table 7. Lipase immobilization: Immobilization yield and catalyst performance in the hydrolysis of pNPP at 295 K

Catalyst	Total adsorption		Enzymatic activity	
	mg	mmol m ⁻³ monolith S ⁻¹	mmol g ⁻¹ lipase S ⁻¹ *	
Free lipase				3.0x10 ⁻²
C-silane-PEI	79	8.2		6.1 x10 ⁻³
C-GPTMS-PEI	144	10.3		4.2 x10 ⁻³
C-APTES-PEI	61	1.4		1.3 x10 ⁻³
AM-Silane-PEI	105	10.9		5.2 x10 ⁻³
AM-GPTMS-PEI	207	16.9		4.1 x10 ⁻³
AM-APTES-PEI	103	4.0		1.5 x10 ⁻³

* Actual lipase content in the crude protein is estimated to be only 5%

In contrast to the results for immobilized lactase, the specific activity of the silane/PEI samples is slightly higher than for the GPTMS-PEI samples. The reason for increased activity with the pre-fabricated silane-PEI component is not clear. It is possible that the unreacted epoxygroups in the GPTMS-PEI-samples influence the protein stability or form covalent bonds with the enzyme, resulting in a lower activity per gram of enzyme. The specific activity of the APTES-PEI samples is significantly lower, probably due to the negative influence of

the glutaraldehyde used (presence of unreacted aldehyde groups) or due to the reducing agent used to stabilize the glutaraldehyde-PEI bond.

The specific immobilized lipase activity for the silane-PEI-samples is 20% of that of the free lipase at the same conditions. Compared to the specific activity of lipase that was adsorbed onto carbon-ceramic composites (Chapter 9), this is in the same order of magnitude. The immobilized activity of the GPTMS-PEI sample is only 14%, and slightly lower than for adsorption on carbon. A possible explanation for this lower activity is the presence of unbound epoxy-groups that may chemically alter the lipase (covalent bonding occurs) upon adsorption, leading to a lower immobilized activity. If a lipase content of 5 wt% is assumed, a turnover frequency of 21s^{-1} is found for free *Candida rugosa* lipase. The immobilized lipase has a TOF of 3 s^{-1} . The relatively low TOF of this lipase can be explained by the reaction conditions; the assay is performed at pH 7, while the optimum activity should be around pH 5.

For both enzymes the highest enzyme loading and hence the highest activity per monolith volume is achieved by immobilization via the GPTMS-PEI method on ACM monoliths. The specific activity of the lactase from *Aspergillus oryzae* is slightly higher than for adsorption on carbon-ceramic composites. The large, hydrophilic enzyme is readily adsorbed onto the PEI-carrier, retaining 92% of its free enzyme activity. The hydrophobic lipase from *Candida rugosa* tends to form aggregates [29-30] in solution that lead to adsorption of inactive protein. The surface chemistry of the support matrix strongly influences the cleavage of the protein aggregates. This can be a reason for the higher specific activity when adsorbed onto carbon layers with different oxygen containing surface complexes. If the charged groups on the polymer matrix do not split the lipase-complex, but adsorb the whole aggregate in its inactive form, specific activity may be lower. Therefore, the immobilization yield and specific activity are slightly lower than for adsorption onto hydrophobic carbon coatings. About 15-20% of the free enzyme activity is retained.

3.4.3 Effect of the pH on lipase adsorption and activity

To further improve the performance of the lipase-coated monoliths, the pH during adsorption was varied. An AM-GPTMS-PEI sample was used as a carrier material at different pH from a 2 g l^{-1} solution at 278 K. Due to the nature of the ionic adsorption process, the pH has a strong influence on final adsorption. At pH 5, the highest adsorption capacity was observed (Figure 18), and because this pH is close to the isoelectric point of the lipase, specific activity also increases significantly, to 20 % of the free enzyme activity. Apparently this is the preferred adsorption pH. Due to instability of the enzyme at pH 11, the specific activity becomes very low, although deactivated protein is still adsorbed onto the PEI-carrier.

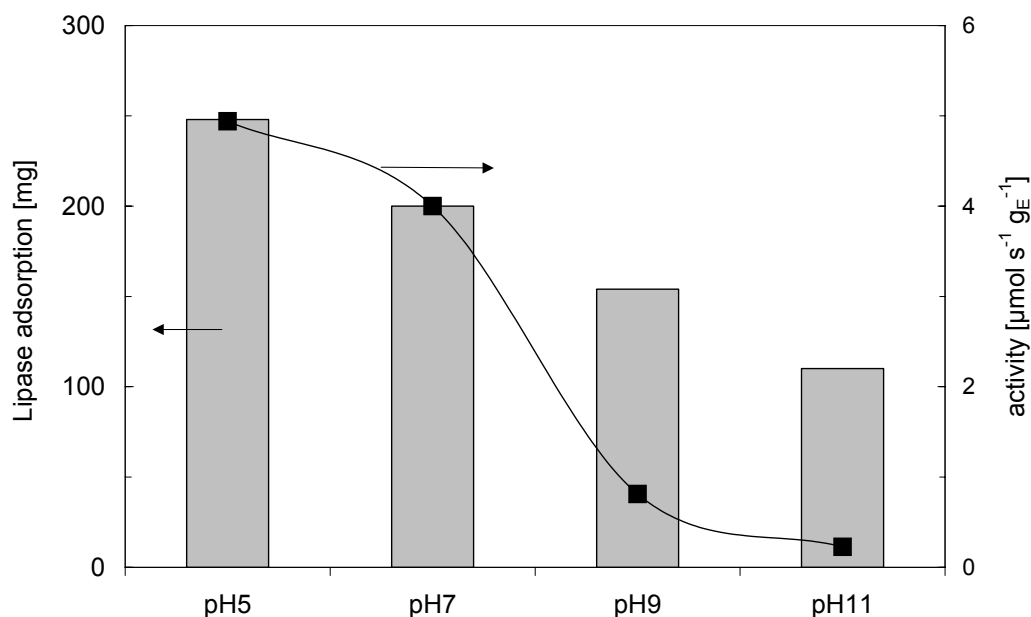


Figure 18. Effect of pH on total adsorption and specific activity on AMLxHS40-GPTMS-PEI

3.5 Stability of the biocatalysts

To study the stability of the immobilized lactase, a C-GPTMS_PEI-sample was assayed several times during a period of 15 days. Between the subsequent tests, the sample was washed and stored under air at 278 K. The enzyme was adsorbed onto the carriers from a 2 g l^{-1} lactase solution at 278 K, pH 5.

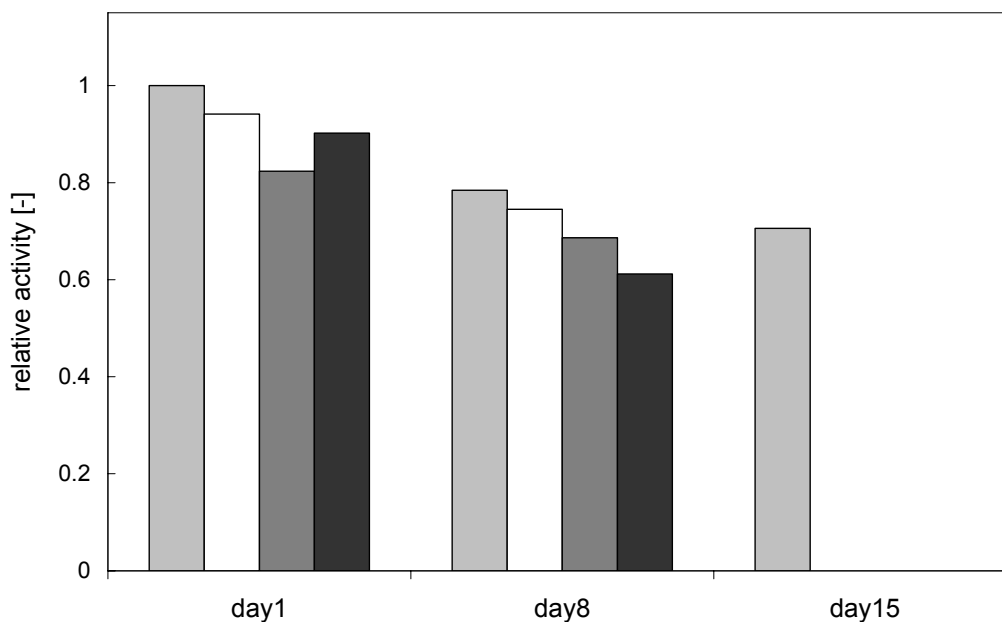


Figure 19. Stability of a CLxHS40-GPTMS-PEI sample over 15 days. The catalyst sample was tested regularly –day 1, day 8, day 15- in the hydrolysis of oNPG at 295 K, pH7. On all other days, the samples were stored at 278 K under air.

During a series of tests on the same day, a slight activation is observed (Figure 19). After storage at 278, the activity also decreased slightly. In general, slow deactivation of the biocatalysts is observed during both testing and storage. The deactivation in consecutive tests indicates product sensitivity. This could be irreversible, because activity does not completely return after washing and storing. Total deactivation seems to be the sum of deactivation by reaction and storage in air. Since storage under air generally leads to accelerated deactivation and no desorption should occur at low ionic strength, storage in phosphate buffer with NaN_3 is recommended to stabilize the performance of the PEI-based biocatalysts.

Due to the low immobilization yield and low specific activity of the APTES-based carriers, this method is not further optimized. The silane/PEI method consists of a one-step attachment of the carrier and is also not considered further, although the specific activity of lipase is still good, but the total enzyme loading less than for the GPTMS protocol. In the following section, the GPTMS protocol is studied in more detail with respect to the preparation method, possible mass transfer problems during polymer attachment, and the influence of the microstructure of the monolith.

3.6 Optimization of GPTMS protocol

Cordierite monoliths were used crushed, and coated with PEI by using various methods. To investigate any mass transport limitations in the macroporous monolithic system during preparation, a particulate CPC-silica carrier with a controlled pore size (CPC) was used as comparison. To investigate the influence of the type of surface functionality present on the carrier surface, GPTMS coated supports with epoxy groups or with aldehyde groups were used to react with low molecular weight ($\text{MW}=25000$) PEI. The influence of the molar weight of the polymer was studied by using 25000, 750000 and 60000-1000000 g mol^{-1} grades of branched PEI.

3.6.1 Polymer loading on particulate carriers

To compare the PEI loading on different carriers in the absence of mass transfer limitations, crushed cordierite (1-2 mm) was used and compared with CPC-carrier. In addition to the general PEI attachment to the epoxy groups, an indirect aldehyde group was created for binding of the polymer by acid treatment and subsequent oxidation with NaIO_4 of the silanized carriers. Agarose-PEI, a generally used enzyme support [17,31] was used as control reference. The polymer was also directly adsorbed onto CPC and washcoated monolithic carrier. After addition of the polymer, the polymer content was followed by determining the nitrogen content. The polymer content increases with increasing nitrogen content. The results are presented in Table 8. Washcoated cordierite contains practically no nitrogen. PEI coating of this support by adsorption leads to a nitrogen content of 0.21 wt%. If GPTMS is used to covalently link the polymer to the support, the same total yield was obtained. Based on these results, adsorption of PEI would be the most straightforward one-step coating procedure, but

in this case the support-carrier combination is not stable (see section 3.1.1 on TGA analysis of the composites).

Table 8. Carbon and nitrogen content for particulate carriers

Sample	Carbon content wt%	Nitrogen content wt%
CLxAS40	0.2	0.011
CLxAS-40-PEI	0.35	0.21
CLxAS40-GPTMS-PEI	0.58	0.18
CLxAS40-GPTMS(ox)-PEI	0.52	0.19
CPC-PEI	2.41	1.25
CPC-GPTMS-PEI	2.34	1.23
CPC-GPTMS(ox)-PEI	2.65	1.06
Sepabeads EP3 (agarose + PEI)	56.7	0.88

Polymer adsorption on controlled pore glass leads to a nitrogen content of 1.25 wt%. If PEI is attached via epoxy or aldehyde groups, this value decreases slightly. The difference in PEI loading between CPC-carrier and cordierite could be caused by the lower content of silanol groups on the crushed monolith. The carriers were crushed after silanization, a substantial part of the cordierite is therefore not coated (material from the inside of the monolith wall never has been contacted with the washcoat material). In addition, the surface area of the relatively large cordierite pieces is much lower, resulting in a much lower total silanol content for the crushed cordierite. This leads to lower GPTMS and PEI yields. With 0.88 wt% nitrogen, the agarose support lies in between.

3.6.2 Enzyme adsorption and desorption on particulate carriers

All particulate carriers were used for the adsorption of a lactase (1 g l^{-1}) from *Aspergillus oryzae* from a 5 mM phosphate buffer pH 7 at 295 K. To check the adsorption on bare support materials, silica coated monolith and pure CPC-carrier were also included. The results for enzyme adsorption over 21 h are presented in Figure 20.

No adsorption is observed for the bare CPC and the washcoated monolith. The CPC carriers reach the maximum adsorption already after 5 h, adsorption on crushed cordierite is slower. The final total amount of adsorbed lactase was 100 mg g^{-1} carrier for all supports. The lactase adsorption process corresponds to the results in Table 8; the silica carriers with high PEI loading bind the lactase at a higher speed than the agarose carrier with lower PEI loading. The cordierite supports, with the lowest PEI yield, display a (s)lower lactase adsorption. This could be expected because the silica content of the monolithic carriers is much lower (on 1 gram of support approximately 10% silica washcoat is present. The available amount of PEI is therefore significantly lower (see Table 8), resulting in a slower and less effective adsorption. The same enzyme loading must be accomplished on a smaller amount of carrier. On monoliths, the effective loading is 1 g g^{-1} silica carrier. It is therefore expected that the less tight bound enzyme on the crushed cordierite will desorb faster after addition of NaCl. Since all lactase was adsorbed, no conclusions on loading capacity of the different supports can be

drawn from these results. The PEI loading and adsorption speed of the agarose carrier are found at an intermediate level.

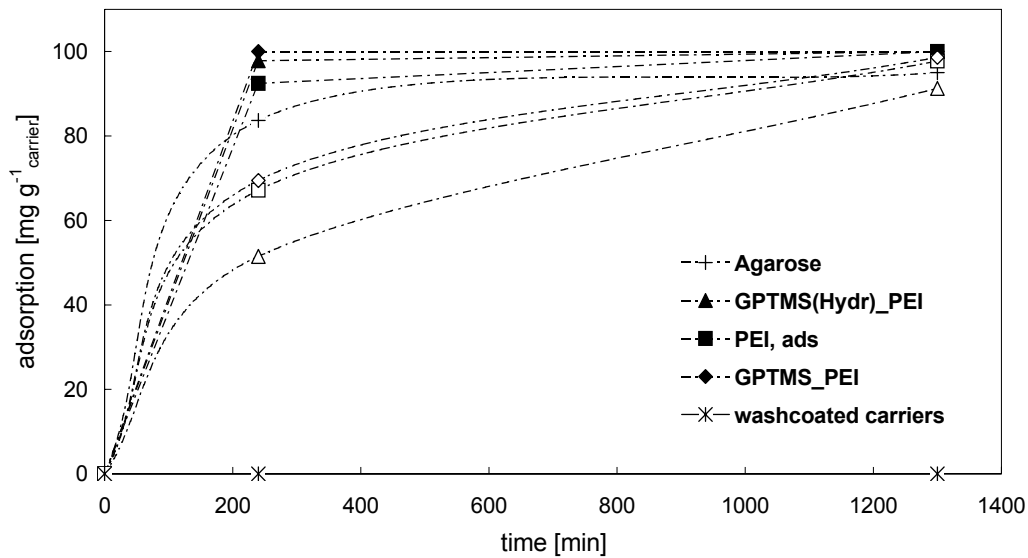


Figure 20. Adsorption of lactase on particulate carriers from a 1 g l^{-1} lactase solution at 295 K. The closed symbols represent the CPC-carriers and the open symbols represent the crushed cordierite

The carriers with 100 mg of adsorbed lactase were mixed with solutions of increasing concentrations NaCl. The relative amount of desorbed protein is presented in Figure 21. The agarose-PEI carrier is very stable with respect to desorption at higher ionic strength. The desorption of adsorbed lactase from crushed cordierite already takes place at lower ionic strength, due to a weaker enzyme-support interaction on this carrier.

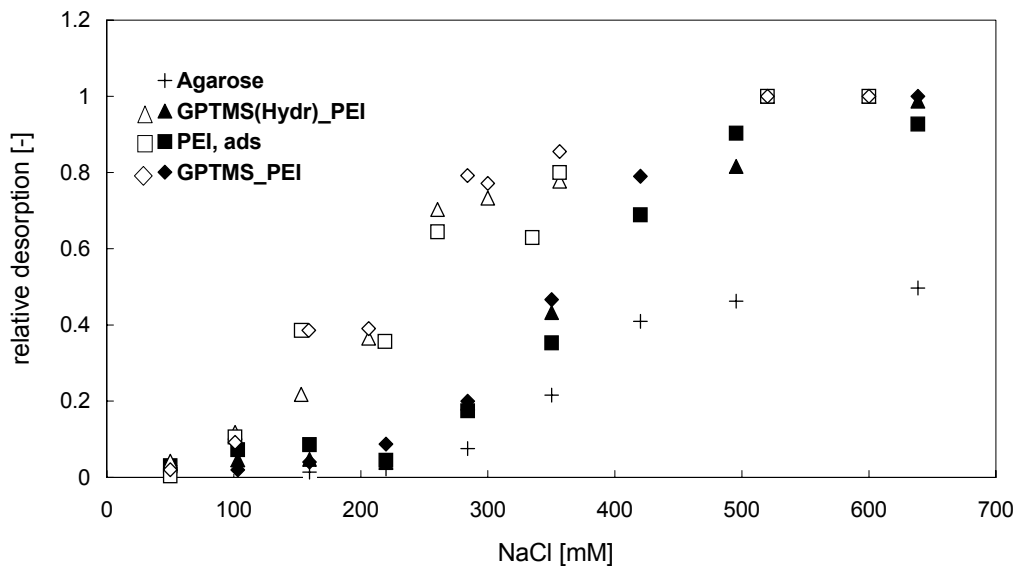


Figure 21. Desorption of lactase at increasing ionic strength in 10 ml NaCl mixtures. The closed symbols represent the CPC-carriers; the open symbols represent the crushed cordierite.

This was already expected based on the lower binding strength that is the result of a 10 times increased enzyme loading compared to the CPC-carriers. No significant differences are observed between the different immobilization methods. Above 0.6 M NaCl all lactase is desorbed from the CPC- and cordierite-carriers. For agarose-PEI, a 1-1.5 M concentration was needed for complete desorption of lactase [17] (not shown).

3.6.3 Effect of PEI size on adsorption on particulate carriers

To study the effect of PEI-size, crushed cordierite was prepared with via the GPTMS_PEI method with different polymer size. It is expected that larger PEI molecules provide a more stable environment and a stronger PEI-lactase bond. If mass transfer problems are present during polymer attachment, the polymer yield will be lower and the enzyme adsorption/desorption behavior will be distinctive. For the crushed carriers the adsorption (a) and desorption (b) curves of lactase are presented in Figure 22.

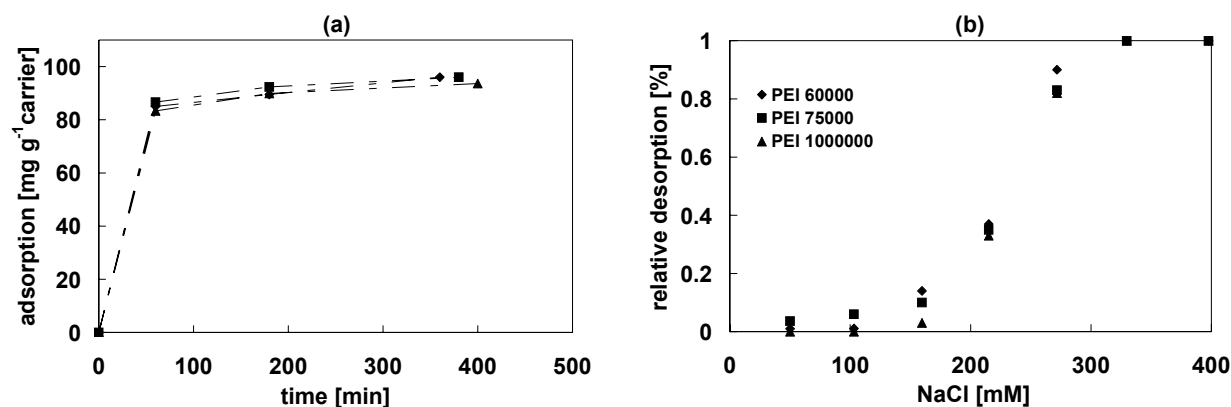


Figure 22. Adsorption (a) and desorption (b) behavior of lactase on crushed cordierite with a PEI coating applied via the GPTMS-PEI method. Symbols represent different MW PEI

No effect of PEI size was observed for adsorption on crushed cordierite. For desorption a marginal effect of polymer size can be observed. The larger polymer provides a more stable environment against higher ionic strength, and shows a slower desorption until 160 mM NaCl. The smaller polymer (MW 750000) is less effective, and the smallest polymer molecules provide the least stable environment, both resulting in a faster lactase desorption. From these results it can be concluded that no large differences in polymer loading are present for the different carriers and that apparently no diffusion limitations are present inside the cordierite matrix during PEI attachment.

3.6.4 Effect of PEI size on adsorption on monolithic supports

The molecular weight of the polymer strongly influences the viscosity of the PEI solution. It is expected that for whole monoliths the mass transport problems will be more pronounced if different PEI-size is used. In Figure 23 the adsorption on ACM and cordierite monoliths, coated with different polymer size is presented.

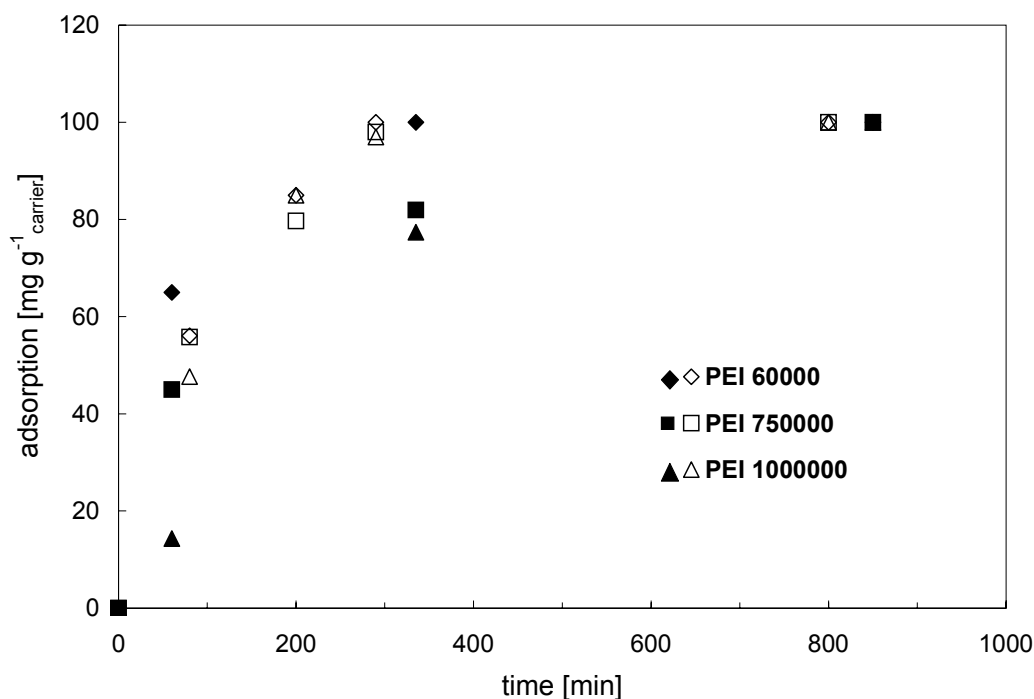


Figure 23. Lactase adsorption from a 1 g l⁻¹ solution at 295 K, pH 7 on ACM (open symbols) and cordierite (closed symbols) on carriers coated with different molar weight PEI

In general, the ACM monoliths display a faster lactase adsorption. The open symbols are found above the closed symbols after the same time interval, immobilization on ACM monoliths is faster than on cordierite for all Mw's. But this process is still slower than for CPC-beads (see Figure 22). This is caused by the higher relative concentration of PEI in the case of CPC (1 g of sample CPC-PEI contains more PEI than 1 g of sample monolith-silica-PEI). It therefore difficult to compare the results of both experiments in a quantitative way. Compared to cordierite, the open wall of the ACM allows for a higher polymer yield, which results in a more efficient enzyme immobilization. For cordierite monoliths, the smallest PEI has no problems to cover the whole silica layer by relative fast diffusion through the channels. The samples that were coated with the larger polymers have a slower enzyme adsorption, probably caused by a lower PEI loading (due to diffusion problems in the more viscous solution). After 20 h all lactase is completely adsorbed onto the supports.

From these results it can be expected that the cordierite-PEI samples have a weaker enzyme-carrier bond, causing faster desorption in high ionic strength environment than ACM monoliths. The desorption results are presented in Figure 24. As expected, desorption from the cordierite samples is faster than from the ACM samples. Two different effects can be observed in Figure 24. AM-GPTMS-PEI,1000000 is very stable with respect to increasing ionic strength compared to the lower Mw polymers. Up to 0.2 M NaCl, no desorption takes place. Secondly, a higher polymer loading provides a stronger enzyme-polymer interaction. The higher PEI-loading of the C-GPTMS-PEI-60000 provides a more stable basis against forced desorption. For cordierite monoliths, the positive effect of the polymer size is not observed (see also Figure 23). This is probably caused by distribution problems of the viscous polymer solutions during PEI-coating. Apparently, the open structure of the ACM monoliths

allows for a better polymer distribution of the higher Mw PEIs and a also for a higher PEI-loading than can be obtained for cordierite samples. This results in a stronger enzyme-carrier bond.

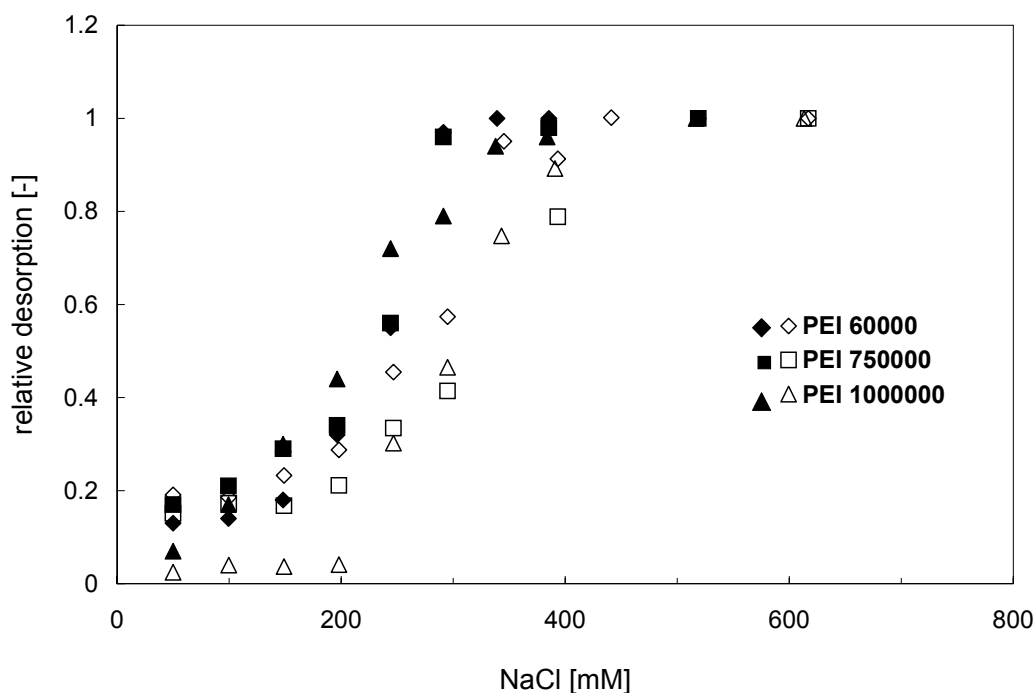


Figure 24. Lactase desorption at 295 K from ACM (open symbols) and cordierite (closed symbols) carriers with different molecular weight PEI

Compared to agarose carriers, the monolith-PEI system has sufficient enzyme adsorption capacity. A higher PEI loading results in a stabilizing effect for the enzyme, this was concluded from slower desorption at increasing ionic strength. Increasing polymer size also increases the stability of the enzyme. For silica particles no diffusion problems for addition of larger polymers were observed. The polymer with larger MW showed a delayed desorption at increasing ionic strength. For cordierite monoliths, transport problems during PEI addition lead to decreased enzyme adsorption efficiency. Also the stabilizing effect of the larger polymer molecules had decreased for these samples. For ACM monoliths the diffusion problems during polymer addition are minimized, resulting in a faster enzyme adsorption and increased stability against desorption.

4 Conclusions

Cordierite and ACM monoliths with different microstructure were used as support material for a lactase from *Aspergillus oryzae* and a lipase from *Candida rugosa*. Enzymes were immobilized via ionic adsorption on a polyelectrolyte polymer, polyethyleneimine (PEI). The open structure of the ACM provides a larger carrier deposition capacity, and results in a

higher protein loading. Immobilization via a GPTMS-functionalized ACM-monolith yields the best enzyme carrier. At pH 7, 200 mg lipase and 150 mg lactase can be deposited.

These PEI systems provide an optimal environment for the lactase, nearly the full (92%) activity of the free enzyme is retained after immobilization. For the more hydrophobic lipase, only 14% of the activity is retained. Immobilization at varying pH influences both enzyme yield and specific activity. Immobilization at pH 5 was found to be optimal.

The enzymes can be completely desorbed in consecutive adsorption-desorption cycles to facilitate reuse of the monolith-carrier combination.

The catalyst deactivates slowly during both storage and use. The deactivation in consecutive tests is probably caused by product sensitivity.

The molecular weight of the polymer also influences the adsorption behavior and stability of the biocatalysts with respect to increasing ionic strength. In general, a higher polymer loading provides a more stable environment for the enzyme and this stabilizing effect increases with polymer size. On ACM monoliths, more carrier can be deposited. This was concluded from TGA measurements and increased enzyme adsorption on ACM monoliths. With increasing molecular weight of the polymer, the ACM monoliths show an increased enzyme adsorption speed. This indicates a higher polymer loading. Therefore, the open walls of the ACM monoliths provide an important advantage when used in this ionic adsorption protocol.

5 Acknowledgements

The Netherlands Organization for Scientific Research (NWO) is acknowledged for funding of this research by means of a grant, filenumber R74-68. Cesar Mateo, Roberto Fernandez-Lafuente and Jose Miguel Guisan of the Department of Biocatalysis of the Institute of Catalysis and Petroleum Chemistry of the Spanish Council for Scientific Research (CSIC-ICP) in Madrid are acknowledged for their contribution to this work. Dirk van Benthem is acknowledged for performing the FTIR measurements and the study on immobilization on monolithic supports.

6 Symbols

V_L	liquid volume	[m ³]
w	weight of the carrier	[kg]
w_s	weight of the support	[kg]
W_0	weight of the carrier at starting point TGA	[kg]
W_r	weight of the carrier during TGA	[kg]
Y_i	yield of component i	[%]

7 References

- [1] C. Mateo, O. Abain, R. Fernandez-Lafuente, J.M. Guisan (2000) *Biotechnology and Bioengineering*; 68: 98-105
- [2] B.C. Koops, E. Papadimou, H.M. Verheij, A.J. Slotboom, M.R. Egmond (1999) *Applied Microbiology and Biotechnology*; 52: 791-796
- [3] W. Warmuth, E. Wenzig (1995) *Bioprocess Engineering*; 12: 87-93
- [4] A.R. Ozdural, D. Tanyolac, I Boyaci, M. Mutlu, C. Webb (2003) *Biochemical Engineering Journal*; 14: 27-36.
- [5] J.F. Diaz, K.J. Balkus (1996) *Journal of Molecular Catalysis B: Enzymatic*; 2:115-126
- [6] E. Dumitriu, F. Secundo, J. Patarin, I. Fechete (2003) *Journal of Molecular Catalysis B: Enzymatic*; 22: 119-133
- [7] F.N. Serralha, J.M. Lopes, F. Lemos, D.M.F. Prazeres, M.R. Aires Barros, J.M.S. Cabral (1998) *Journal of Molecular Catalysis B: Enzymatic*; 4:303-311
- [8] A.P.V. Goncalves, J.M. Lopes, F Lemos, J.M.S. Cabral, M.R. Aires Barros (1996) *Journal of Molecular Catalysis B: Enzymatic*; 1: 53-60
- [9] M. Di Serio, C. Maturo, E. De Alteriis, P. Parascandola, R. Tesser, E Santacesaria (2003) *Catalysis Today*; 79-80: 333-339
- [10] L. Ferreira, M.A. Ramos, J.S. Dordick, M.H. Gil (2003) *Journal of Molecular Catalysis B: Enzymatic*; 21: 189-199
- [11] M. Ladero, A. Santos, J.L. Garcia, F. Garcia-Ochoa (2001) *Enzyme and Microbial Technology*; 29: 181-193
- [12] N.G. Wilson, T. McCreedy, G.M. Greenway (1999) *The Analyst*; 125: 237-239
- [13] M. Thust, M.J. Schöning, P Schrot, U. Malkoc, C.I. Dicker, A. Steffen, P. Kordos, H. Lüth (1999) *Journal of Molecular Catalysis B: Enzymatic*; 7: 77-83
- [14] Q.Z.K. Zhou, X.D. Chen (2001). *Biochemical Engineering Journal*; 9: 33-40
- [15] G.A. Kovalenko, O.V. Komova, A.V. Simakov, (2002) *Journal of Molecular Catalysis A: Chemical*; 182-183: 73-80
- [16] A.S. Rani, M.L.M Das, S. Satyanarayana (2000) *Journal of Molecular Catalysis B: Enzymatic*; 10: 471-476
- [17] B.C.C. Pessela, R. Fernandez-Lafuente, M. Fuentes, A. Vian, J.L. Garcia, J.L, A.V. Carrascosa, C. Mateo, J.M. Guisan (2003) *Enzyme and Microbial technology*; 32: 369-374
- [18] B.C.C. Pessela, L. Betancor, F. Lopez-Gallego, R. Torres, G.M. Dellamora-Ortiz, N. Alonso-Morales, M. Fuentes, R. Fernandez-Lafuente, J. M. Guisan, C. Mateo (2005) *Enzyme and Microbial Technology*; 37: 295–299
- [19] B.C.C. Pessela, M. Fuentes, C. Mateo, R. Munilla, A.V. Carrascosa, R. Fernandez-Lafuente, J. M. Guisan (2006) *Enzyme and Microbial Technology*; 39: 909-915
- [20] Y. Yang, H.A. Chase (1998) *Biotechnology and Applied Biochemistry*; 28: 145-154
- [21] J.M. Moyer and N.N. Hughes (1994) *Journal of the American Ceramic Society*; 77: 1083-1086

- [22] S.A. Wallin, A.R. Prunier and J.R. Moyer (2001) US Patent 6,306,335
- [23] K. De Lathouder, J.J.W. Bakker, M.T. Kreutzer, F. Kapteijn, J.A. Moulijn and S.A. Wallin (2004) *Chemical Engineering Science*; 95: 5027-5033
- [24] J. Yakovleva, R. Davidsson, M. Bengtsson, T., J. Emneus (2003) *Biosensors and Bioelectronics*; 19: 21-34
- [25] R. Fernandez-Lafuente, V. Rodriguez, J.M. Guisan (1998) *Enzyme and Microbial Technology*; 23: 28-33
- [26] M.A. Ramos, M.H. Gil, E. schacht, G. Matthys, W. Mondelaers, M.M. Figueiredo (1998) *Powder Technology*; 99: 79-85
- [27] N.B. Colthup, L.H. Daly, S.E. Wiberly (1990) *Introduction to Infrared and Raman Spectroscopy*, third edition Academic press
- [28] M.W. Daniels, L.F. Francis (1998) *Journal of Colloid and Interface Science*; 205: 191-200
- [29] M.L. Foresti, A. Errazu, M.L. Ferreira (2005) *Biochemical Engineering Journal*; 25: 69-77
- [30] C.I. Lopez-Amaya, A.G. Marangoni (2003) *Colloids and Surfaces B: Biointerfaces*; 32: 263-274
- [31] R. Torres, B.C.C. Pessela, M. Fuentes, C. Mateo, R. Munilla, R. Fernandez-Lafuente and J. M. Guisán (2006) *Enzyme and Microbial Technology*; 39: 167-171

Physical adsorption of lipase and lactase

Abstract

Tuneable carbon-coated monoliths as carriers for enzyme adsorption are presented. Depending on the enzyme properties and reaction conditions, the carrier can be adjusted to optimize the enzyme loading. Carbon-ceramic composites were prepared by sucrose carbonization, polyfurfuryl alcohol (PFA) carbonization, and by growth of carbon nanofibers (CNFs) over deposited Ni. Monoliths with different microstructure were used as backbone for the carbon carriers. The composites were applied as a carrier for lipase from *Candida rugosa* and lactase from *Aspergillus oryzae*. The CNFs proved to be the best carrier, with respect to enzyme loading. Untreated fibers could adsorb 115 mg lactase g⁻¹_{carbon}. After air/HNO₃ treatment this value increased to 360 mg g⁻¹. Porosity was not affected by air and air/HNO₃ treatment, implying that lactase adsorption mainly depends on surface chemistry. A clear correlation was observed between oxygen content of different CNFs and lactase adsorption. Optimal conditions for both enzymes are pH 5 and 4 g l⁻¹ enzyme. The open wall of ACM monoliths allows for a higher carrier loading, and leads to a higher total enzyme loading. The monolithic biocatalysts were compared with respect to enzymatic activity and stability in a model test reaction. After immobilization, lipase maintains 30% of its original activity, for lactase this value is higher at 50-70%. The use of high porosity ACM monoliths leads to more stable and more active bioreactors. The open microstructure of ACM affords good access to catalysts deposited within the walls of a monolith. In combination with CNFs and subsequent oxidation treatment, this would be the optimal enzyme carrier.

1 Introduction

The development of effective adsorbents for biologically active substances, including enzymes and microorganisms, is relevant. Adsorbing materials for use as filter materials are required for processes such as wastewater treatment and purification of product streams. These adsorbents could also serve as support materials in biotechnology and the pharmaceutical industry to deliberately attach biological materials for increased stability and re-use [1]. Obviously, such adsorbents-supports must meet certain criteria. They must have a sufficient adsorption capacity, with respect to the enzyme or microorganism, and hold them firmly on the surface. They must also retain and stabilize the biological activity of the immobilized material at a relatively high level. Finally, operational characteristics (mechanical strength, hydrodynamics, resistance to degradation) must be good and cost should be low. Supports that are often used for immobilization of bacteria include silicate materials (sands, clays, glass, minerals) and micro-porous activated carbons.

The success and efficiency of the physical adsorption of an enzyme on a solid support depends on several parameters. The size of the protein to be adsorbed, the specific surface area of the carrier and the nature of its surface (porosity, pore size) are crucial. Typically the use of a porous support is preferred since the enzyme will not be adsorbed only at the outer surface of the material but within the pores as well. An efficient adsorption also depends on the enzyme concentration. The amount of adsorbed enzyme per amount of support increases with the enzyme concentration reaching a plateau at the saturation of the carrier. This operation is usually carried out at constant temperature, and consequently, adsorption isotherms are obtained which follow Langmuir or Freundlich equations [1]. The pH at which the adsorption is conducted is equally important since ionic interactions can either increase or decrease final enzyme loading and can also influence residual activity. Usually, the maximum adsorption is observed at a pH close to the isoelectric point of the enzyme. Finally, addition of water miscible solvents during the immobilization process favors the adsorption by reducing the solubility of the enzyme in the aqueous phase. The most commonly used additive to improve immobilization efficiency is probably glutaraldehyde, which stabilizes the interaction of the enzyme with the support. Regeneration of the immobilized biocatalyst is often possible. Once the enzyme has lost a significant amount of its original activity, desorption is possible by changing of the pH or the ionic strength of the reaction medium, followed by binding of a fresh enzyme. However, desorption can also be a major drawback of this immobilization technique if it occurs during the catalyzed reaction. Unfortunately, there are no empirical rules to predetermine the strength of adsorption. In some cases, the simple addition of the substrate will be sufficient to induce a significant desorption, whereas, in other cases no desorption will be observed, even under drastic conditions.

Carbon materials are well-known in adsorption and catalytic processes. Advantages of using carbonaceous materials include the stability in acidic and basic media and the fact that both

textural properties and chemical characteristics can easily be tailored. Hence, these materials have a wide range of applications in different areas, such as pollutant removal (active carbon), gas separation (molecular sieves) or chemical reaction (catalysts and catalyst supports). Nevertheless, only a few large-volume catalytic processes currently use carbon-supported catalysts [2, 3]. Problems regarding mechanical properties, reproducibility and quality control in large-scale production processes of carbons limit the physical form to granules or extrudates. The use of these structures in trickle bed reactors is associated with potential channeling, high pressure drops, and decreased catalyst efficiency. These problems can be overcome by using structured carbon-ceramic composite materials. Macrostructured supports such as honeycomb monoliths are very suitable to apply thin coat layers of various materials.

Monolith reactors have proven to be an interesting alternative for conventional three phase slurry reactors and trickle bed reactors [4]. Compared to these systems, monoliths offer a low pressure drop over the reactor, resistance to plugging, high mechanical strength, low axial dispersion, and high mass transfer rates.

Carbon based monoliths can be of the integral or coated type [5,6]. The integral monoliths are prepared by extrusion of the carbon precursor, mixed with various additives. The function of the additive (in general organic or inorganic powders or cellulose fibers) is to make the resin extrudable. Carbon coated monoliths are mainly produced by dipping the supports in a polymeric solution. To remove excess polymer efficiently from the channels, low viscosity polymer solutions are preferred as carbon precursors. The most straightforward method is the dipcoat method [6]: the honeycombs are dipped in a precursor solution and then dried and/or cured. Subsequently, the precursor is carbonized and if needed activated. Many different carbon precursors have been used such as saccharides [2, 7], polyfurfuryl alcohol [5, 8], and phenolic [9] or furanic [10] resins.

Another way to apply carbon on a ceramic surface is the growth of carbon filaments over deposited metal particles. Carbon nanofibers have been known for a long time as a nuisance that often emerges during catalytic conversion of carbon containing gases [11]. These graphitic materials are chemically similar to fullerenes and carbon nanotubes, and have a large potential for a range of applications. In 1899 [12] the first patent concerning carbon filaments, grown from carbon containing gases over a metallic crucible, was published. Over the following decades, these filaments were considered a nuisance. In the nickel catalyzed conversion of methane to synthesis gas for instance, the growth of carbon nanofibers deactivates the catalyst [11, 13] Not only destruction of the catalyst micro-structure was observed, also complete destruction of catalyst pellets, attack and rupture of reactor walls were encountered [14, 15]. In the 1980s, the use of carbon nanofibers as additives for polymers and as catalyst support materials were explored. At present, carbonaceous fiber structures are widely studied because of their use as catalyst support materials [16-18], selective adsorption agents [1, 19, 20], energy storage [21], composite materials, nanoelectric devices [22], field emission devices [11, 23, 24], and as filter materials [25]. Therefore,

studying the structure [26, 27], the growth of nanofibers [28, 29], and the parameters that influence the growth [30, 31] is an important research topic.

The aim of this study is the preparation of carbon-ceramic composites for adsorption of different enzymes. These carrier materials serve as a functional enzyme carrier, combining the properties of ceramic materials (mechanical strength, cellular structure, etc.) with those of carbon (adjustable surface properties, high adsorption capacity for biological substances). Three different carbons are used; a heat-treated sucrose (SUC), a carbonized polymer (polyfurfuryl alcohol, PFA), and carbon nanofibers (CNF) grown over deposited Ni. Carriers were activated by different treatments. Because the detailed characterization of the carbon carriers is outside the scope of this thesis, the carriers were studied in more detail elsewhere [32, 44]. The cordierite supports are relatively difficult to handle, especially when small amounts of carrier are needed, therefore all carbon carriers were also prepared in unsupported form. Finally, the ceramic composites are applied as support material for a lactase from *Aspergillus oryzae* and a lipase from *Candida rugosa*.

2 Experimental

2.1 Materials

Nitric acid (65%) was purchased at Baker. γ -alumina (Puralox SBA 200) was from Condea. Silica gel (Davisil grade 643, 200-425 mesh, 99⁺%) and Ludox AS-30 (colloidal silica in water) were from Aldrich. Saccharose was from Merck. Furfuryl alcohol (99%) and pyrrole (98%) were from Sigma. β -Galactosidase from *Aspergillus oryzae* (E.C. 3.1.2.23) and Lipase from *Candida rugosa* (E.C. 3.1.1.3, type VII), p-nitrophenyl propionate (pNPP), and o-nitrophenyl- β -galactopyranoside (oNPG) were purchased from Sigma. Analytical grade buffer salts were obtained from Baker.

ACM monoliths of mullite, 400 cells inch⁻² (62 cells cm⁻²) were prepared by a proprietary Dow process to produce honeycombs with “small”, “medium”, and “large” pores. Cordierite monoliths with cell densities of 200 and 400 cells inch⁻² (31 and 62 cells cm⁻²) were used for comparison. The key properties of these monoliths are given in Table 1.

Table 1. Nominal values of the key properties of monoliths employed in this study

	ACM (“small”)	ACM (“medium”)	ACM (“large”)	Cordierite
Cell density	400 cpsi	400 cpsi	400 cpsi	200 / 400 cpsi
Wall thickness	0.24 mm	0.24 mm	0.24 mm	0.3 / 0.18 mm
Wall porosity	60%	60%	70%	35%
Pore diameter	5 μ m	18 μ m	45 μ m	7.5 μ m

The samples had a length of 5 cm and a diameter of 4.3 cm. Prior to coating the monoliths were calcined for 4 h at 1273 K in a static air oven to remove possible contaminants. When a carbon is deposited using the dipcoating method, monoliths can be used directly. When carbon nanofibers are grown on the monolith walls, deposition of a washcoat layer is needed. In order to prevent fiber growth inside the ceramic structures and to provide sufficient surface area for deposition of the growth catalyst, a washcoat is applied on the monolith channels. As was described in chapter 3, washcoats were prepared by coating with an alumina slurry or with a colloidal silica solution.

2.2 Carbon deposition

2.2.1 Formation of carbon from a sucrose (SUC) coating [7, 19]

Monoliths were dipped for 5 min at room temperature in a 65% sucrose solution in water. After impregnation, excess solution was removed from the channels by blowing air through the channels. Samples were dried under continuous rotation for 24 h at room temperature, followed by drying at 393 K for 3 h. Subsequently they were carbonized in a tubular quartz reactor, placed in a horizontal furnace (Figure 1). The samples were heated (10 K min^{-1}) in a N_2 stream up to 823 K and carbonized for 2h under different N_2/H_2 mixtures (total volume 500 ml min^{-1}).

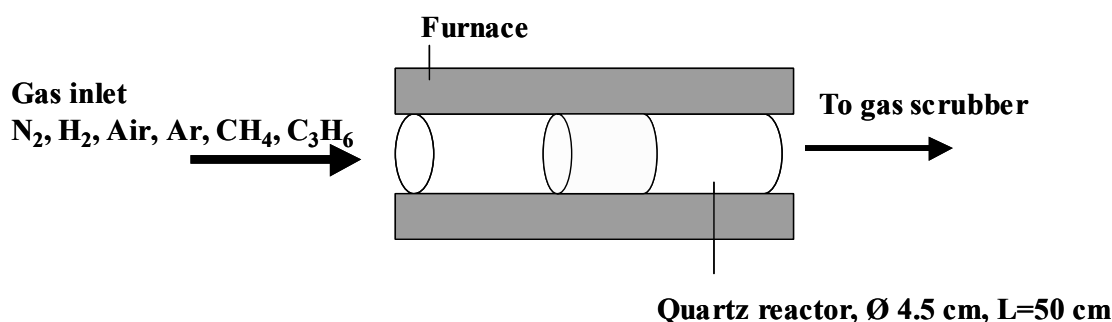


Figure 1. Quartz reactor for carbon formation

2.2.2 Carbonization of a polyfurfuryl alcohol (PFA) coating [8]

Furfuryl alcohol (90 ml) and pyrrole (27 ml) were stirred at 293 K. Acid catalyst (7 ml 65% HNO_3) was added stepwise over a period of 45 min. During this exothermic reaction, temperature was kept constant at 293 K by using an ice bath. Polymerization was continued for 1 h at 293 K. Monoliths were dip coated for 5 min in the partially polymerized mixture. Excess liquid was blown out with nitrogen and the dip coating was repeated after 5 min. The polymer was solidified for 4 h at ambient conditions, and polymerization was continued overnight at 353 K. Carbonization of the polymer was performed in a quartz reactor at 823K (heating rate 10 K min^{-1} , 300 ml min^{-1} , 100% Ar) for 2 h.

2.2.3 Growth of carbon nanofibers (CNF) over deposited nickel

Washcoating with a γ -alumina layer (particle size 1 μm , thickness $\sim 15 \mu\text{m}$) was done according to the method described by Nijhuis *et al.* [33]. Alumina (300 g) and colloidal alumina (170 g) were mixed in 400 ml water, to obtain a 35 wt% alumina solution. The pH was adjusted to 4.5, using nitric acid. To create the desired particle size, this slurry was ball-milled for 24 h. The pH was again adjusted to 4.5 with nitric acid. Monoliths were dipped in the alumina slurry for 5 min and cleaned with an air knife, followed by horizontal drying overnight. The carriers were calcined at 723 K for 4 h (heating rate 5 K min^{-1}).

Silica coatings were prepared by dipping the monoliths in a colloidal (Ludox) suspension for 5 min, followed by horizontal rotating overnight and calcination at 673 K for 4 h (heating rate 2 K min^{-1}). For ACM samples, the Ludox solution was diluted to a final concentration of 4%.

Nickel was deposited from a 0.5 M urea solution by homogeneous deposition precipitation (HDP) [34, 35]. For silica washcoated monoliths, the solution was acidified to pH 2 with nitric acid. For alumina a neutral environment was used. Monoliths were added to 300 ml 30 mM $\text{Ni}(\text{NO}_3)_2$ solution (to get a final Ni loading of 0.15 g $\text{g}^{-1}_{\text{washcoat}}$ or 0.55 g per monolith = 2 wt%) and kept at 363 K for 6 h. After washing, the samples were dried at 393 K for 10 h (heating rate 2 K min^{-1}) followed by 673 for 2 h (heating rate 5 K min^{-1}).

Carbon fiber growth was carried out in a quartz reactor, placed in a horizontal furnace. The sample was heated (10 K min^{-1}) in a N_2 stream to 823-973 K [19]. Then Ni was reduced for 1 h in 20% H_2 in N_2 (total flowrate 150 ml min^{-1}). After cooling to 773-873 K carbon fibers were grown in a flow of methane/propene (120 ml min^{-1}) and H_2 (10 ml min^{-1}) in N_2 (70 ml min^{-1}).

2.3 Oxidation of the carbons

Partial oxidation in air/Ar was performed in a horizontal furnace at 603 K (10K min^{-1} , 300 ml min^{-1} , 10% O_2 in Ar) for 3 h. After 1.5 h, samples were switched and turned to facilitate homogeneous oxidation treatment through the sample.

After oxidation in air, carriers were stirred in 1 M HNO_3 at 293 K for 1 h. Samples were washed with water until neutrality of the filtrate, and dried overnight at 253 K.

2.4 Enzyme immobilization

Immobilizations were carried out in up-flow operation, using a glass reactor and a peristaltic pump. Different 0.05 M buffer solutions were used, ranging from pH 5-9. Enzyme concentration was varied between 1-4 g l^{-1} . During immobilization, samples were withdrawn and the enzyme concentration was determined using UV-VIS. A 1 cm quartz cuvette was used (on a Thermo Optek UV-540). The concentration was checked with the Bradford method. The effect of temperature, enzyme concentration and pH was investigated. After immobilization the samples were washed with buffer, dried under vacuum or at 278 K and stored at 278 K.

2.5 Nomenclature

In this study, the samples are named depending on the monolith type, the carbon type, and the treatment. The first letter of the samples is used to distinguish the monolith type, “C” is used for cordierite, “A” for ACM. A second letter is used in the case of ACM to determine the microstructure of the ACM; “S” for small micrograins, “M” for medium needles and “L” for the most open structure with large micrograins. The carbons are added with “SUC” for sucrose, “PFA” for polyfurfuryl alcohol, and “CNF” for carbon nanofibers. In some occasions, additional oxidation treatment of the carbon is indicated with the addition of “air” for air treatment and “air/HNO₃” for subsequent acid treatment. This is summarized in Table 2.

Table 2. Nomenclature

Position	Component	Code
1	Monolith type	C or A
2	Micro grain structure ACM	S, M, or L
3	Carbon type	SUC, PFA, or CNF
4	Treatment	Air or air/HNO ₃

Following this procedure, a sucrose-based support prepared from medium grain ACM, treated in air and HNO₃ will be noted as: AM-SUC-air/HNO₃.

2.6 Characterization.

The amount of coating, mass increase, and mass decrease were determined by measuring the sample weight before and after the various preparation steps. The carbon amount was calculated as:

$$Y_C = \left(\frac{w}{w_s + w} \right) \cdot 100 \quad (1)$$

where w_s is the mass of the support and w is the carbon mass.

Thermogravimetric analysis (TGA) was performed on a Mettler Toledo TGA/SDTA851^e. The samples were heated in air (100 ml min⁻¹) to 1273 K (heating rate 10 K min⁻¹).

2.6.1 Porosity

The texture of the prepared carriers was analyzed using N₂ (at 77 K) and CO₂ (at 273 K) adsorption on an AUTOSORB-6B. Samples were outgassed during 4 h at 523 K. Surface area was calculated from nitrogen adsorption using the BET equation (S_{BET}). Total pore volume was determined from N₂ adsorption isotherms at $P/P^0 = 0.95$ (V_{tot} N₂). Total Micropore volume (V_{DR} (N₂)) and narrow micropore volume (V_{DR} (CO₂)) were calculated applying the

Dubinin Radushkevich (DR) equation to the N₂ adsorption data at 77 K and the CO₂ adsorption data at 273 K, respectively.

2.6.2 Surface chemistry

TPD-MS measurements were performed on TGA-DSC 2960 from TA INSTRUMENTS and a mass spectrometer THERMOSTAR from Pfeiffer. The samples were heated in He (120 ml min⁻¹) to 1223 K (heating rate 20K min⁻¹). Oxygen content per g of sample was determined by integration of the CO and CO₂ signals.

FTIR spectra were recorded on a Mattson spectrophotometer model Infinity with an MCT detector coupled with a diffuse reflectance accessory model COLLECTOR from SpectraTech. Samples were diluted in KBr and measured against a KBr background.

XPS spectra were obtained with a VG-Microtech Multilab electron spectrometer, by using the Mg K_α (1253.6 eV) radiation of twin anode in the constant analyzer energy mode with pass energy of 50 eV. Pressure of the analysis chamber was maintained at 5·10⁻¹⁰ mbar.

Boehm titrations were performed with NaOH, NaHCO₃, Na₂CO₃ to neutralize all acidic groups, carboxylic groups, and lactones respectively. Samples were mixed with 0.1 N basic solutions and kept at 298 K overnight. 20 ml of the supernatant was titrated with 0.05 N HCl. EDX elemental analysis was performed on a Hitachi S-3000N scanning electron microscope.

2.6.3 Electron microscopy

To obtain qualitative information about the texture and distribution of the carbon in the monolith, Scanning Electron Microscopy was performed using a Philips XL-20 scanning electron microscope. Transmission electron microscopy (TEM) was performed using a Philips CM30T electron microscope with a LaB₆ filament as the source of electrons operated at 300 kV. Bulk sample were grinded in a mortar. Ethanol was added in order to obtain a suspension. Samples were mounted on Quantifoil® microgrid carbon polymer supported on a copper grid by placing some drops of the suspension on the grid.

2.6.4 Stability and activity of immobilized lactase and lipase

Desorption of the enzyme from the carrier was studied by increasing the ionic strength in an aqueous solution by adding NaCl. The activity and stability of the biocatalysts was compared by performing activity assays in aqueous medium during a period of time, with intermediate storage of the catalysts at 278 K under air.

β-Galactosidase activity was followed spectrophotometrically by the increase in absorbance at 405 nm, promoted by the hydrolysis of o-Nitrophenyl-β-galactopyranoside (oNPG) (Figure 2). A 1 cm quartz cuvette was used, 2.5 ml samples were withdrawn regularly and returned to the reaction mixture after measurement. Experimental conditions were 1-2 mM oNPG in 0.05 M Tris buffer pH 7 and 293 K.

During heat treatment the precursor solution that is present inside the cordierite mesopores will shrink and form a thin layer over the pore.

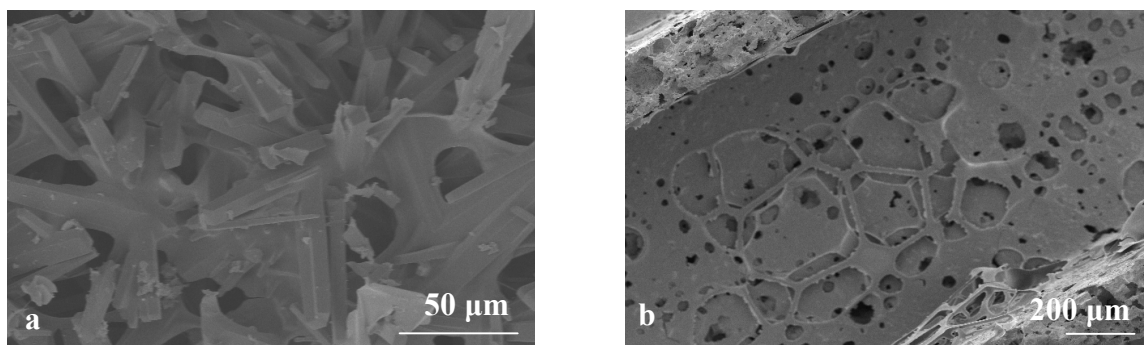


Figure 4. SEM micrographs of supported sucrose-based carbon a) AM-SUC, b) C-SUC

For AM-SUC (Figure 4a), the carbon is present on and between the needles. The channel walls are not completely filled with carbon. The open structure can be used to increase the loading of the carbon carrier, without affecting the hydrodynamic properties of the monolith. By decreasing the viscosity, a thin layer of sucrose can be deposited without plugging the wall. This carbon can therefore be used in the two modes of operation as discussed in chapter 3:

- High catalyst loading for reactions where mass transfer is not a limiting factor, while still retaining a low pressure drop through the reactor and good accessibility of the catalyst inside the wall.
- A thin conformal catalyst layer on the acicular grains to minimize diffusional limitations for fast reactions that impose diffusional limitations.

The PFA-coating (Figure 5) forms a very dense layer, almost completely covering the cordierite surface and filling the porous walls of the ACM. Some pores can be seen in Figure 5b, however when the inside of these pores is studied, a large amount of carbon can be found inside. The pores are probably formed by shrinking of the precursor during carbonization. This carbon is very similar to the slurry washcoats that were discussed in chapter 3. On a cordierite support, carbonized PFA will form a thin layer of approximately 5-10 μm , with rounded corners. As was observed for the sucrose coated cordierite samples, the mesopores are not completely filled, although to a greater extent than was observed for the sucrose coating. The carbon layer is present inside the larger pores. On ACM, the carbon completely plugs the wall. The precursor material is a relatively viscous solution. To create a conformal, thin coating with this carbon, the viscosity must be decreased drastically. This can be done by decreasing the pre-polymerization temperature or time.

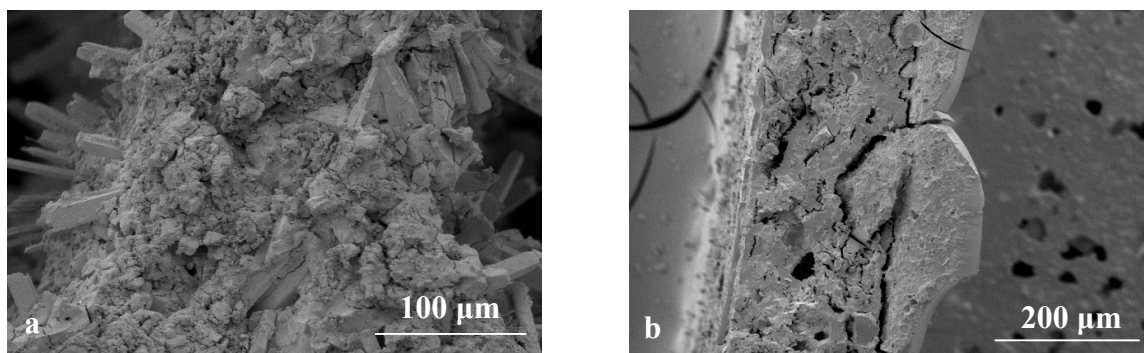


Figure 5. SEM micrographs of supported PFA-base carbon a) AM-PFA, b) C-PFA

Carbon fibers (Figure 6) form a homogeneous layer that covers the washcoat surface. For cordierite, a thick non-porous washcoat is needed to prevent growth of CNF inside the wall. In many occasions, the monoliths were deformed or cracked after too much carbon deposition (see Figure 7a and c). Adjusting the concentration of the growth catalyst and the growth conditions could prevent the destruction of the backbone in the case of cordierite. In the case of less extreme growth conditions, it is possible that the CNF are only partially covering the monolith (Figure 7b), For ACM supports, cracking did not occur, due to the large open space inside the wall. These supports are therefore very attractive to obtain a high carbon yield. Depending on the type of washcoat (slurry or colloidal), the fibers will either fill or cover the monolith wall. In the case of AM-CNF (Figure 6a), a slurry washcoat was used, allowing for a high carbon yield. The open structure of the channel walls is not completely preserved.

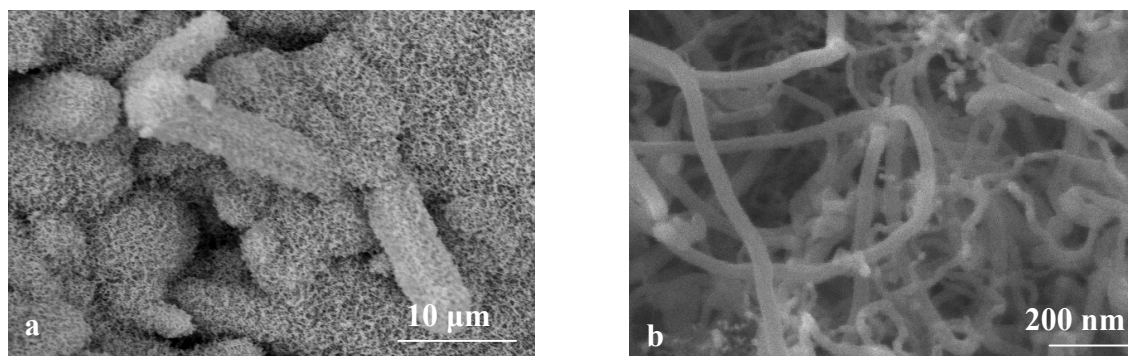


Figure 6. SEM micrographs of supported CNF on γ -alumina washcoat a) AM-CNF, b) C-CNF

The CNFs form a uniform layer of fibers up to 1 μm length. In comparison to the sucrose-derived samples and the PFA-derived samples, less carbon was deposited for the carbon nanofibers, while the open connected pore structure is still maintained. Further, there is always a risk of cracking the support when growing fibers on a macroporous support such as monoliths. The very high porosity of the ACM supports makes them very favorable in this respect. At this point it is not completely clear how the fibers are attached to the monolith surface. It seems that the fibers are somehow rooted in the washcoat layer. The washcoat “swells” and becomes filled with fibers, as was described elsewhere [36].

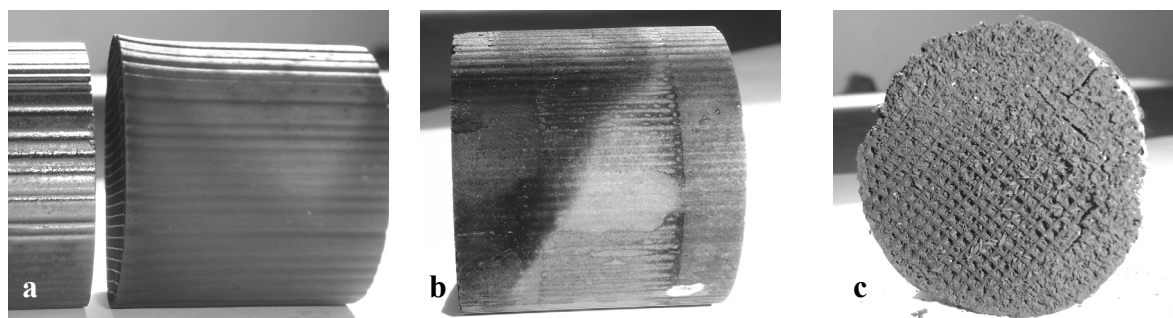


Figure 7. Cordierite monoliths after CNF growth. a) deformed, b) partly covered, and c) completely filled

When the fibers are grown on controlled pore glass, it seems that the pellets are completely cracked by the fibers, which also form large agglomerations. When the fibers are removed from the monolith surface (by scraping with a razor blade), elemental analysis (not shown) reveals traces of cordierite and washcoat at the roots of the fibers. Apparently the fibers are attached firmly onto the monolith.

In Figure 8, TEM images of CNFs are presented. Part of the fibers was present as carbon nanotubes (CNT), a tube with parallel graphite sheets as the wall and a hollow core (Figure 8b). In Figure 8a, the Ni crystallite can be seen in the fiber-tip. More detailed studies on the morphology and alignment [25] and the removal of the growth catalyst [32, 52] are published elsewhere.

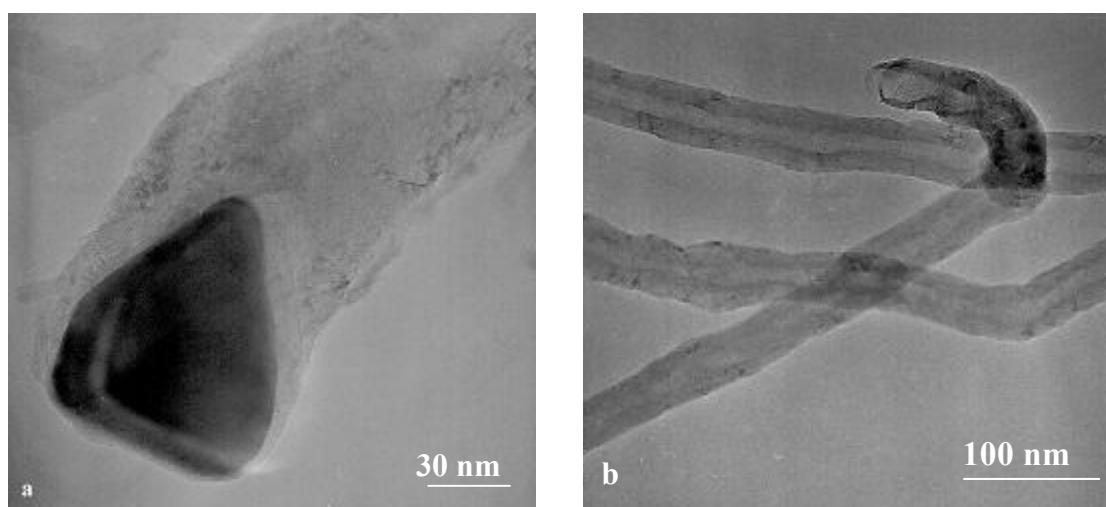


Figure 8. TEM micrographs of unsupported CNFs a) fiber-tip with Ni crystallite, b) CNT with hollow core

3.1.2 Carbon yield and porosity

The preparation of carbon-coated monoliths with different precursors leads to composites with a different carbon loading and texture. The carbon-yield (Figure 9) is not only influenced by the type of monolith, but also by the monolith-micro structure. Different trends can be observed for the direct dipcoating methods (SUC and PFA) and the growth of CNF on a silica washcoat. For the SUC and PFA methods, the carbon loading on ACM is significantly higher than on cordierite. This is direct result of the high viscosity of the precursor solutions and the

large difference in wall porosity (see Table 1). Consistent with the results for washcoating (see Chapter 3), there seems to be no difference in yield for ACM-S and ACM-M. The wall porosity of these samples was found to be equal for these samples (see Table 1), explaining the similar loading. The higher wall porosity of the ACM-L leads to more precursor deposition, and a higher yield.

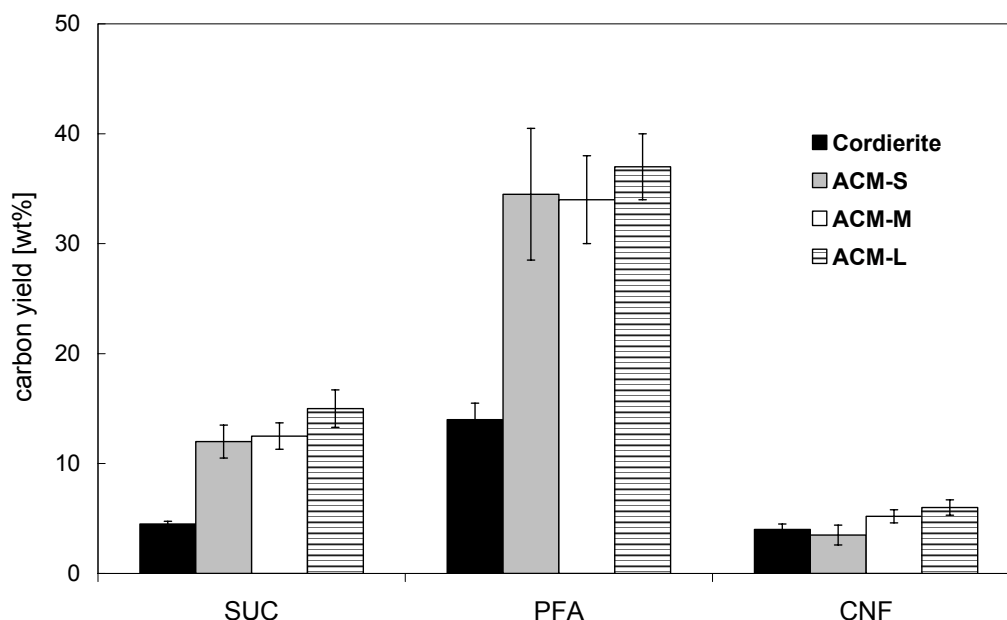


Figure 9. Carbon yield for different 400 cpsi cordierite and ACM backbones. CNFs were deposited on a SiO₂ washcoat.

For the monolith-CNF composites the carbon loading on ACM is comparable to that on cordierite. In case of growing CNF, washcoating and the deposition of Ni are also important preparation steps. For CNF, the increases in carbon yield can be explained by the higher accessibility of the silica washcoat for Ni deposition and secondly the better accessibility for the carbon source during pyrolysis. The more open large-needle supports should have the highest carbon loading from this point of view.

In terms of reproducibility, the PFA-samples have a relatively large 95% confidence interval. This is due to the fact that polymerization of the precursor continues during dipcoating. It is therefore very difficult to exactly reproduce the conditions. Factors such as the total volume and amount of monoliths that need to be coated and the needle size have a large influence on the final carbon loading. For complete reproducibility, the time from the first dipcoat and the type of monolith that is used at every time-slot needs to be the same. Very different results were obtained for 4 identical small-needle samples that were coated from the same batch of precursor. This effect can be minimized by cooling all containers during dipcoating or working at lower viscosity (lower degree of polymerization).

The sucrose-based carriers have a moderate carbon yield of 4 wt% (cordierite) and 12 wt% (ACM). This can be influenced by changing the viscosity of the precursor or perform multiple coating steps. The PFA carriers have a large carbon loading, caused by the high viscosity of

the polymer precursor. This yield can be adjusted by changing the viscosity of the precursor solution (shorter polymerization time/ lower temperature). The yield of the CNFs can be influenced by varying the temperature, the carbon source and the reaction time. Because this lies outside of the scope of this thesis, it will not be discussed here.

3.1.3 Porosity

From N₂ and CO₂ adsorption, it was found that for all carbon layers the specific surface area of the composite material increases compared to bare monoliths (<0.2 m²/g). The preparation of carbon coated monoliths yields carbon carriers with different properties. The surface characteristics and carbon loading depend on the preparation method. In Table 3, the results for unsupported carbons are presented [32]. These samples were prepared without a monolithic support.

Table 3. Results unsupported carbons, prepared without a monolithic support

Carrier	S_{BET} m ² g ⁻¹	$V_{\text{DR}}(\text{N}_2)$ cm ³ g ⁻¹	$V_{\text{DR}}(\text{CO}_2)$ cm ³ g ⁻¹	$V_{\text{tot}}\text{N}_2$ cm ³ g ⁻¹
PFA	8*	0*	0.12	0*
PFA-air	3*	0*	0.12	0*
PFA-air/HNO ₃	3*	0*	0.13	0*
SUC	15-30	0.01	0.06	0.02
SUC-air	160-240	0.08	0.17	0.14
SUC-air/HNO ₃	10-25	0.01	0.15	0.01
CNF	59	0.02	0.01	0.19
CNF-air	63	0.03	0.02	0.18
CNF-air/HNO ₃	60	0.03	0.02	0.21

*obtained from N₂ adsorption at 77 K, although equilibrium was not reached

Among the three different carriers, PFA and S presented diffusional problems for N₂ adsorption at 77 K, easily deduced from much higher CO₂ adsorption at 273 K [37]. This is characteristic for carbon samples with narrow microporosity. Long equilibration times were required for these measurements, and in the case of PFA samples the values assessed from these experiment were estimated from the unequilibrated system. The existence of narrow micropores in these samples is confirmed from the values of $V_{\text{DR}}(\text{CO}_2)$ (0.12 cm³ g⁻¹ and 0.16 cm³ g⁻¹ for the PFA and S, respectively).

To see whether the presence of a monolithic support influences the porosity of the carbons, the same characterization was done for supported carbons. In Figure 10, a selection of isotherms and the BJH pore-size distribution is presented for carbon-ceramic composite materials (SUC and PFA). The results are normalized for carbon content. The N₂ isotherms of the CNF based composites, could not be normalized for carbon content because they are a mixture of the isotherm of the washcoat and the CNF. Therefore, the results for CNF-based composites will be presented separately in Figure 11. In Figure 10, the isotherm and BJH pore-size distribution of unsupported CNFs is included to give an indication of the properties of the CNFs.

No differences were observed between the N_2 and CO_2 adsorption isotherms for cordierite- or ACM-based composites. The sharp peaks (4-7 nm) in the pore size distribution derived from the N_2 desorption isotherm are artifacts that can be attributed to the ‘Tensile Strength Effect’ of the adsorbate [38].

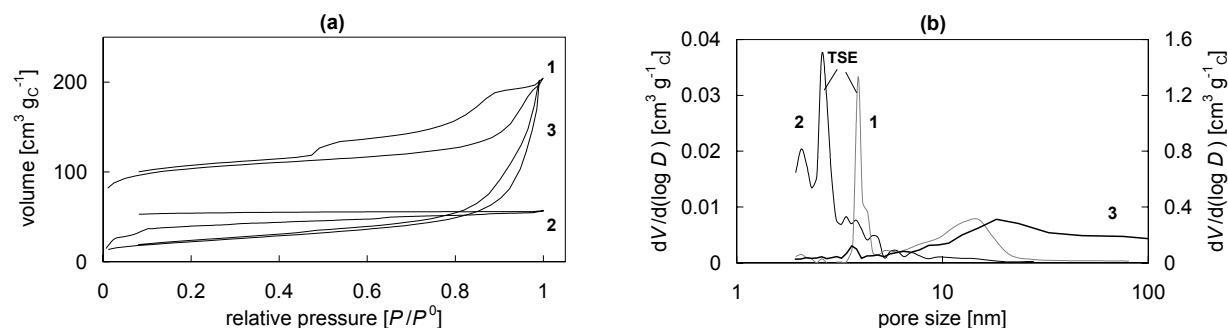


Figure 10. N_2 Isotherms (a) and BJH pore size distribution (b) for 1) C-SUC, 2) C-PFA, 3) unsupported CNFs

The nitrogen isotherm (Figure 10a) for PFA shows a large effect of hysteresis, the adsorption and desorption branch do not close at low relative pressure. This behavior is generally caused by the presence of small or blocked pores in the sub-micropore region (<1 nm) or strong surface interaction of nitrogen. From CO_2 adsorption (not shown, see Table 3) it follows that the carbon has a mainly microporous nature. This was also observed in other studies concerning this carbon type [5, 8, 39].

The sucrose-based carbon shows a type IV isotherm, indicative for mesoporous materials. The large uptake at low relative pressure also indicates the presence of micropores. This is confirmed by the non-closing of the isotherm, caused by delayed ad- or desorption. The possible effect on the calculated BET surface area is less than 2%. The pore size distribution (Figure 10b) shows a local maximum around 14 nm.

In Figure 11 the nitrogen isotherms and BJH pore size distributions of pure CNF, the CNF-composite on a γ -alumina washcoat and the washcoated cordierite monolith are given. The isotherm for pure CNF is corrected for the amount of carbon (right axis) and the isotherms for the coated monoliths are normalized for cordierite content (left axis)

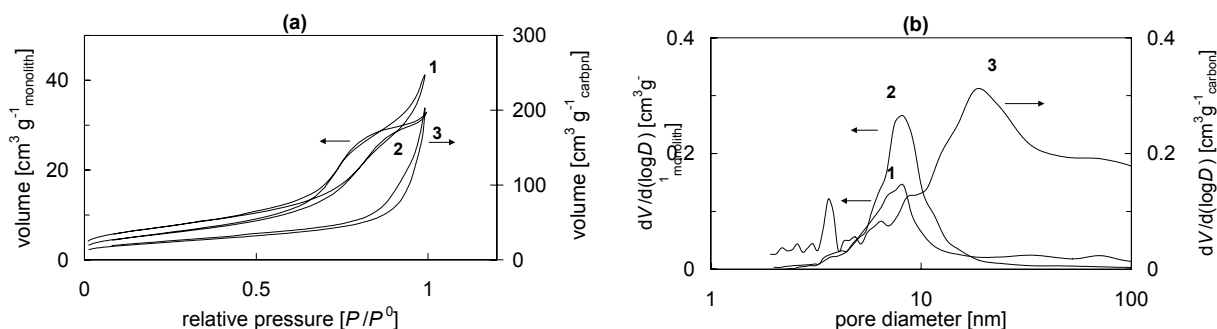


Figure 11. Nitrogen isotherms (a) and BJH pore-size distribution (b) of cordierite composites. 1) C- γ -CNF, 2) C- γ , and 3) CNF (unsupported). Curve 1 and 2 are represented on the left axis per g monolith, curve 3 on the right axis per g carbon

The CNF-coated monolith shows a type IV isotherm, characteristic for mesoporous materials. The shape of the isotherm is different from the type IV isotherm of the washcoat (curve 2) at higher relative pressures. This can be explained by combining the isotherms of the carbon fibers and the washcoated monolith. The isotherm for the washcoated monolith is a type IV isotherm. The isotherm for the pure CNFs (curve 3) shows a low uptake at lower and medium relative pressure. Towards a relative pressure of 1, a steep uptake is observed, pointing out the presence of large meso- and macropores, surface roughness and/or interparticle porosity. At this high pressure good reversibility of the adsorption and desorption isotherm is observed, indicating good accessibility of the pores or voids. If the type II isotherm of the CNF is combined with the type IV isotherm of the washcoat, curve (1) is observed.

The pore size distribution of the CNF-composite (curve 1) has a maximum around 8 nm. This corresponds to the mean pore size of the γ -alumina washcoat (as determined from C- γ , curve 2). The pore size of the fibers has a maximum between 20-100 nm, probably caused by open space between the fibers and the open inner core of the fibers (after removal by mechanical force from the support, the inside of the fibers becomes accessible). The presence of the CNF (curve 3) leads to a broad band from 20-100 nm in the pore size distribution of the composite (curve 1). Due to the low carbon loading, the contribution of this band is relatively low. An identical comparison of the isotherms and BJH pore size distributions of composite, CNF, and washcoat can be made for CNFs grown on silica washcoats (not shown).

In Table 4 a summary of the N₂ and CO₂ adsorption data for carbon-ceramic composites is given. The carbon content that was calculated from the mass changes in general corresponds well with the TGA results. Since TGA is more sensitive for local differences in loading, the yield from weight increase was used to normalize all results with respect to total amount of carbon.

Table 4. Porosity data on 400 cpsi monoliths with supported carbons (composite materials)

Carrier	Y_C wt%	Y_C (TGA) wt%	S_{BET} comp $m^2 g^{-1}$	S_{BET} carbon $m^2 g_C^{-1}$	Pore size nm	V_{DR} (CO ₂) $cm^3 g_C^{-1}$	V_{DR} (N ₂) $cm^3 g_C^{-1}$	V_{tot} (N ₂) $cm^3 g_C^{-1}$
C-PFA	12	15	8	57	<2	0.11	0.01	0.02
AM-PFA	34	31	20	59	<2	0.14	0.02	0.03
C-SUC	4.5	4.2	20	442	14	0.26	0.12	0.30
AM-SUC	15	11	68	546	11	0.28	0.23	0.27
C-CNF	4.3	4.7	26	139	8	0.008*	0*	0.06*
AM-CNF	5.2	6.1	64	142	7	0.009*	0*	0.14*

*Values are in $cm^3 g^{-1}_{monolith}$. The total contribution of the CNF is not known, due to the washcoat

The PFA-based carbon ceramic composites were measured with longer equilibration times than for the unsupported carbon (see Table 3), to get a better indication for the available surface area. Diffusional problems for N₂ adsorption at 77 K were still present; the values are estimated from the unequilibrated system. The values for $V_{DR}(CO_2)$ are in good agreement with the values for $V_{DR}(CO_2)$, found for unsupported PFA-based carbon (see Table 3, $0.13 cm^3 g_C^{-1}$). The results presented here are not in agreement with the values found by Crezee for

comparable PFA-samples [39]. This could be caused by differences in equilibration time at each relative pressure, lab procedures, and external conditions.

The micro pore volume and total pore volume of the PFA-based composites is in general agreement with the values found for the pure carbons (compare Tables 3 and 4). Surface area and porosity of the sucrose-based supported carbon do agree with the values found in earlier work for sucrose-coated monoliths [7, 19], but are very different from the values for unsupported sucrose. Possibly, the carbon is not homogeneously distributed throughout the monolith, leading to local deviations in carbon content. Another explanation of the large differences for unsupported and supported sucrose can be the stabilizing effect and the homogeneous layer thickness on a monolith. While the data on porosity of unsupported sucrose was not reproducible, the results for carbon-coated monoliths were reproducible within a 10 % interval. The exact reason for the large differences between supported and unsupported sucrose based carbon is not clear, it was not observed for carbonized PFA. The sucrose samples display a large increase in volume during carbon formation, due to the escape of volatile components. The carbon yield depends on the escape of volatile material. The pure sucrose is unconfined and will expand in all directions, leading to a lower carbon yield than when applied to a monolith backbone. Therefore, also porosity and morphology will be different. The high oxygen content of the sucrose precursor compared to the final carbon leads to a different behavior than for carbon formation from PFA (this polymer has already a much higher C-content in the precursor and will be less affected by experimental differences). Another important difference between PFA and SUC carbon formation is that during heat treatment of the SUC-precursor, the precursor melts before forming the final carbon. This melting process influences the formation of porosity; the more melting, the less porous the resulting carbon will be. It is possible that applying the precursor onto a monolith prevents or decreases melting. This stabilizing effect can be used to explain the formation of a more porous carbon when supported on a monolith and also explains the better reproducibility of the supported carbon.

Growing of CNF on a washcoat, leads to an increase in surface area. The surface area of the fibers was calculated assuming that the contribution of the washcoat is unaltered after fiber growth. For C-CNF, a contribution of $20 \text{ m}^2 \text{ g}^{-1}_{\text{monolith}}$ was found for the γ -alumina washcoat (see chapter 3). So the increase of $6 \text{ m}^2 \text{ g}^{-1}_{\text{monolith}}$ is caused by $0.043 \text{ g}_{\text{CNF}} \text{ g}^{-1}_{\text{monolith}}$. This gives a BET surface area for the fibers of $139 \text{ m}^2 \text{ g}^{-1}_{\text{C}}$. For all CNF-composites, the specific surface area of the fibers varied between 100 and $140 \text{ m}^2 \text{ g}^{-1}_{\text{C}}$. The differences are probably caused by the local differences in carbon yield inside the monolith channel. This is in agreement with earlier research [34, 36].

The values for fibers that were removed from the support (Table 3) however, are very different from the supported CNFs with respect to surface area and porosity. The differences in porosity can be explained by the presence of a washcoat for the supported fibers. For the free CNF, the space between the fibers and the hollow core are included in the total pore volume, whereas for the composites the hollow core is not accessible (CNF are attached to the washcoat) and the washcoat has a significant contribution. Therefore the pore volume of the

free CNFs is significantly larger than for the supported CNF, the correction with respect to carbon content is not possible and the values in Table 4 are per g of composite.

The differences in surface area between supported and unsupported fibers (Tables 3 and 4) were not expected. The support that was used to produce CNFs for removal by mechanical force was prepared with a doubled Ni-content to ensure good fiber growth. It is possible that the fiber diameter was influenced by Ni loading and dispersion, an important parameter that governs fiber morphology [36,40]. The much higher value for S_{BET} of the composites with CNFs could also be caused by the presence of fibers with a smaller diameter on the support. It is possible that removing the fibers from the support by mechanical force leaves the very small fibers on the surface and only removes the thicker larger fibers. Perhaps the pores of the washcoat are filled with small fibers that can have a relatively large contribution to the measured surface area, new pores have been created by growing CNFs inside the washcoat/cordierite. Some indication for a possible cause can be found by studying the porosity of a monolith/washcoat after all carbon has been burned of. Then it would become clear if extra porosity was formed by growing CNFs (note that growing CNFs can destroy a monolith, see Figure 7), or if the existing pores were just filled with CNFs. This experiment was unfortunately not performed.

For the CNF-based composites, $V_{\text{DR}}(\text{N}_2)$ approaches 0. Compared to γ -alumina washcoats, the total pore volume slightly decreases, and pore size remains unaltered after fiber growth. It seems that the fibers have completely filled the micropore volume. It seems logical that the solid fibers are non-porous, but provide enough external surface area for enzyme adsorption. The fishbone type carbon fibers that are normally produced with Ni under the used conditions [40] have a BET surface area of around $60 \text{ m}^2 \text{ g}^{-1}_{\text{carbon}}$ (see Table 3). This value can also be estimated from carbon yield during the CVD process and the fiber diameter that can be seen in the TEM micrographs (Figure 8). If we assume a single cylinder shaped, solid fiber and a carbon density of 2.25 g cm^{-3} , we can derive a diameter and carbon yield dependent equation:

$$\text{Surface area} = \frac{Y_c \cdot 889}{r_f \text{ (nm)}} \quad (2)$$

with Y_c is the carbon yield (g) during CVD and r the radius of the CNFs (nm).

It follows that for a carbon yield of 1 g that was observed for CNFs, and an average diameter of 29 nm (as was observed with TEM), the estimated surface area would be $61 \text{ m}^2 \text{ g}^{-1}$. This is in good agreement with the values that were found for unsupported CNFs. Apparently the presence of the smaller CNFs in the pores of the washcoat or the (partly) hollow structure lead to a much larger surface area for the monolith carriers.

3.1.4 Surface chemistry

The total oxygen content per gram of carbon was calculated from TPD-MS experiments, by analyzing both CO and CO₂ evolution. Since the fibers still contain growth catalyst, the

oxygen content for CNFs was normalized for the carbon content that was found by burning the CNFs in a TGA. In Figure 12 the CO and CO₂ evolution patterns of the supported carbon carriers are presented, normalized for carbon content.

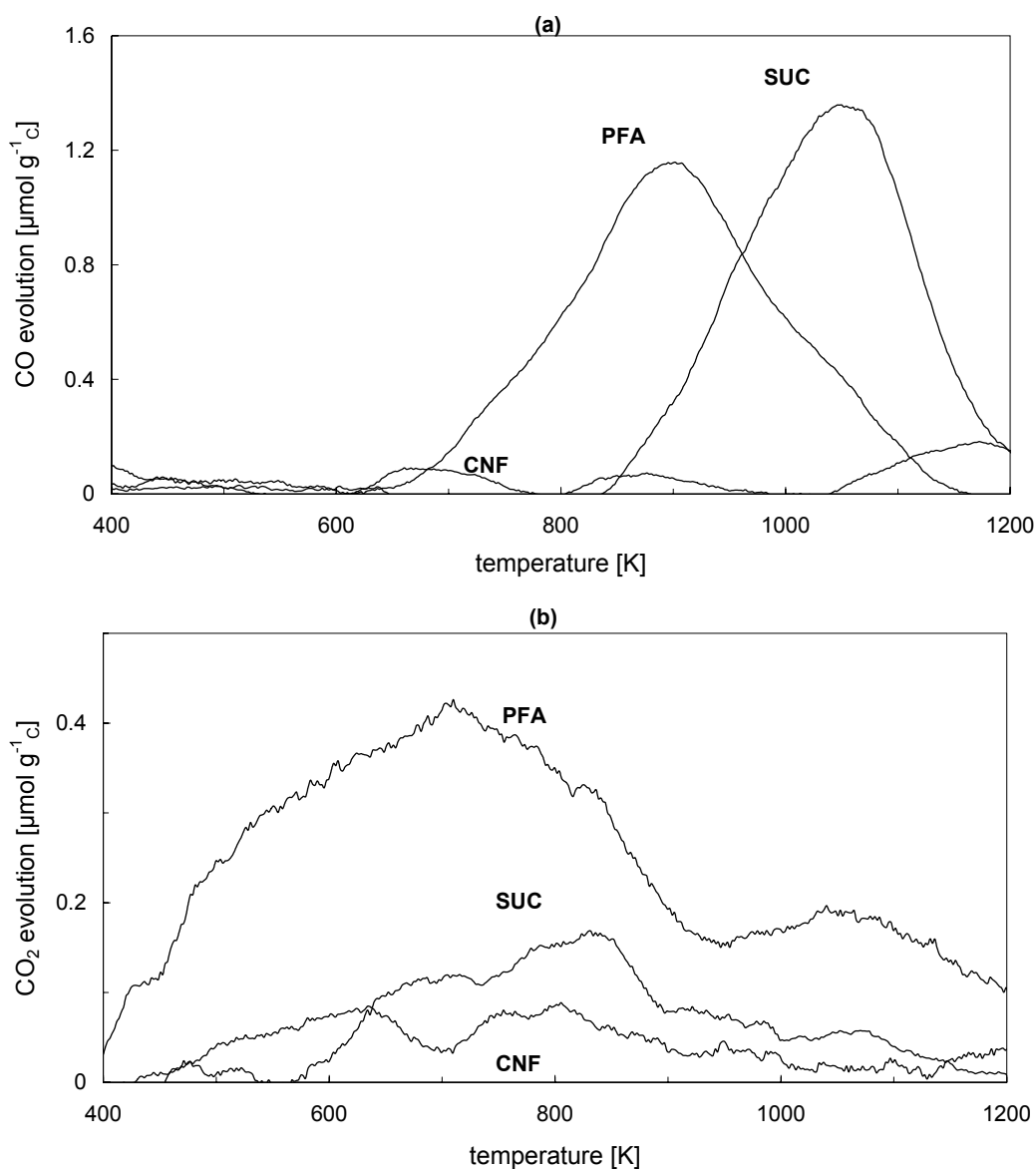


Figure 12. CO (a) and CO₂ (b) evolution of supported carbon carriers as determined by TPD-MS

Apparently carbon formation under was not complete, because a substantial part of both SUC and PFA carriers is still present in the form of oxygen containing components. The CNFs display a modest CO evolution from 650-1100 K. A small band can be seen at 873 K, indicating phenolic groups [41], and a band at higher values around 1150 K, indicating the presence of carbonyl groups.

The sucrose-based carbon has a large peak around 1050 K, indicating the presence of quinones and carbonyl groups. For PFA the largest CO evolution is observed at lower temperature, indicating the presence of phenolic groups, but this carbon most likely also contains quinones and carbonyl groups. CO₂ evolution (Figure 12b) is much lower than CO

evolution for all carbons. CO₂-generating groups are decomposed at lower temperature, with the maximum rate around 700-850 K. The CNFs have a small band around 600-800 K, indicating the presence of lactones [41]. The evolution at lower temperatures usually means that carboxylic groups are present. Sucrose-based carbon displays the same pattern, only with a slightly higher total evolution. For PFA a broad band at 673 K indicates the presence of carboxylic groups and lactones.

In Figure 13, the calculated total oxygen content corresponding to the three different carbons before and after treatment in air and air/HNO₃ is presented. A correction for the presence of oxidized growth catalyst (all Ni in the fiber tips was assumed to be present in the form of NiO in the oxidized samples) was included. Initially PFA based carbon has the highest content of oxygen containing groups; sucrose was found to have a slightly lower oxygen content. Because the carbon nanofibers were prepared by CVD from a methane/H₂ mixture, it could be expected that the CNFs have a very low oxygen content. Air and nitric acid treatment considerably increase the amount of oxygen containing groups per gram of carbon. Oxidation in air and subsequent acid treatment with HNO₃, leads to a doubled oxygen content for CNFs, whereas a five-fold increase in total oxygen content was observed for sucrose based carbon.

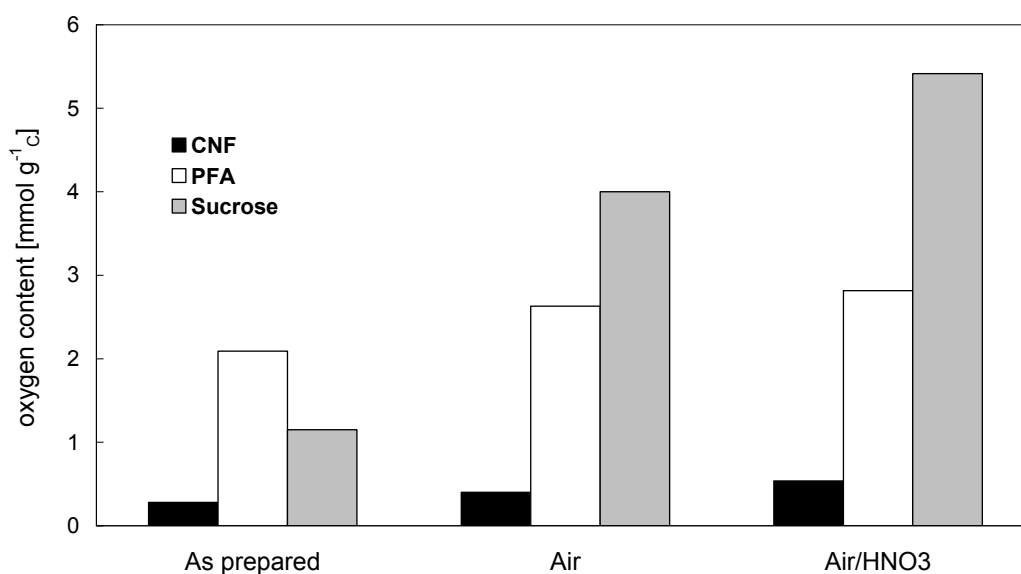


Figure 13. Overview of the effect of oxidation on supported carbon carriers

The relative increase in oxygen content after more severe treatment is also a measure for the reactivity of the carbon. The CNFs are difficult to oxidize, as follows from Figure 13. PFA-based carbon is more reactive; the oxygen content increases significantly after the oxidation treatments. As expected, the sucrose-based carbon has the highest reactivity (the highest relative increase in oxygen content in Figure 13) in these oxidation methods, a result of the nature of the carbon. These results were confirmed by determining the surface oxygen concentration in the (sub)surface (2-3 nm) with XPS. The same trend in total oxygen content that can be seen in Figure 13 was also observed in the O/C atomic ratio as determined by XPS

(not shown); the effects of oxidation treatment on (surface) oxygen content that were observed with both techniques are in the same order of magnitude.

Another way to obtain information on surface chemistry is to perform Boehm titration.

NaOH (pK_a 15.74) neutralizes carboxylic groups, lactones and phenols, $NaHCO_3$ (pK_a 6.37) neutralizes only carboxylic groups and Na_2CO_3 (pK_a 10.25) reacts with carboxylic groups and lactones. In Table 5 the values for different PFA-based carbons are presented.

Table 5. Number of oxygen surface complexes determined by titration

Sample	Total acidity mmol g ⁻¹	Carboxylic mmol g ⁻¹	Phenols mmol g ⁻¹	Lactones mmol g ⁻¹
PFA	5.5	1.0	1.6	0.9
PFA_ox	9.3	4.2	4	1.1
PFA ox_acid	11.8	5.4	4.5	1.9

The increase in phenolic groups was confirmed by the TPD results (not shown). From CO_2 evolution at 673-873 K, the presence of lactones [41], and the increase after oxidation could be concluded. Carboxylic groups are formed both by air and acid treatment. Titration can be used to give a qualitative indication of the effect of oxidation treatment on surface chemistry. However, the method is not very reproducible, especially with the low quantities of material that were used here. And because the values poorly correlated with quantitative data obtained by TPD-MS and XPS, and the procedure is very laborious, no titrations were performed for the other carbon types. Similar findings were reported by Crezee [39].

3.2 Enzyme adsorption

Enzyme adsorption on the different carbons results in typical concentration profiles. An enzyme concentration plot is presented in Figure 14. This concerns the adsorption of lactase on a CNF-based support from a 2 g l⁻¹ solution at 278 K.

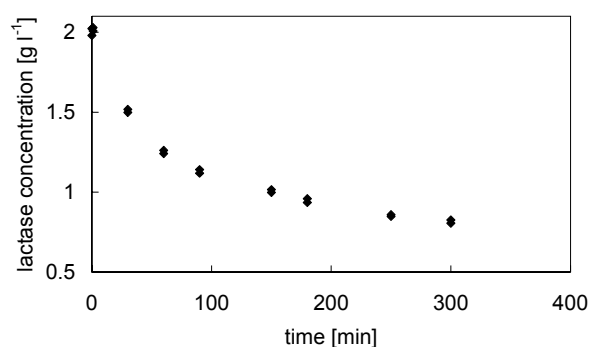


Figure 14. Typical enzyme concentration vs time curve for lactase adsorption on CNF (2 g l⁻¹, 278 K, pH 7)

In general, 80% of the final loading is already deposited after 5 h. After 20 h the adsorption process should be complete. To compare the different backbones, carriers, and adsorption conditions, enzyme loading was measured after 5 h. All adsorptions were carried out at 278 K for 5 h. In this section, the effect of carrier type, monolith microstructure, pH, enzyme type, and enzyme concentration will be discussed.

Unless mentioned otherwise, adsorption measurements take place at pH 7 and 278 K, from a 2 g l⁻¹ solution. The used lyophilized protein powders are not highly purified. Enzyme content usually varies between 5-10%. Since the used protein powders were relatively cheap and assumed to be of a lower grade, an enzyme content of 5% was assumed for both lipase and lactase. Since the analysis methods

that are used (UV-VIS and the Bradford method) cannot distinguish protein type, adsorption results are given in total amount of immobilized protein. Possible effects of selective adsorption of specific proteins are not taken into account because the exact composition of the enzyme lyophilizates was not known.

3.2.1 Lactase adsorption on different carbon carriers

In Figure 15, the different carbons are compared in terms of lactase loading per gram of carbon. The CNF-based carbons are clearly the best carrier for this enzyme. This was also observed for different lipases [42-43]. Apparently, air/HNO₃ treatment has a significant positive influence on adsorption capacity of the CNFs. Treatment in air followed by acid treatment (CNF_{air}/HNO₃) results in an optimal carrier (Figure 15, right hand side).

There is a large difference between the supported (curve 1) and the unsupported (curve 4) sucrose-based carbon. When applied onto a monolith backbone, enzyme adsorption capacity increases significantly. This can be explained by the large difference in porosity between the supported and the unsupported carbon. In unsupported form, the yield and texture of the carbon was highly irreproducible for different batches of thermally treated sucrose. Almost no adsorption of N₂ at 77K was observed. The supported carbon has a type IV isotherm, indicating a mesoporous material. Apparently this carbon is stabilized by the monolith backbone.

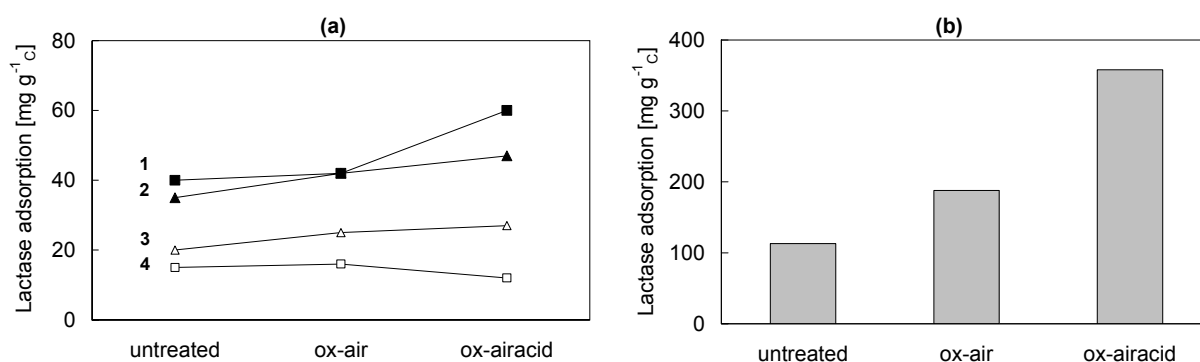


Figure 15. Lactase adsorption at pH 7 and 278 K. a) Supported (solid markers) and unsupported (open markers) PFA and sucrose-based carbons (1) C-SUC, (2) C-PFA, (3) PFA, (4) SUC), b) supported CNF.

For PFA a similar effect was observed, although less pronounced. The porosity of the carrier was not influenced by applying the carbon to a monolith, but an increase in enzyme adsorption was seen for this carbon (curve 2), compared to the unsupported carbon (curve 3). The unsupported carbon was used as small mm-scale particles, whereas a sub mm-scale carbon layer was formed on the monolith support. This probably results in a higher lactase adsorption for the supported PFA-based carrier, due to a higher available surface area.

The CNFs have a completely different structure than the other carriers. Whereas the sucrose- and PFA-based carbons have a dense structure with a network of pores (mainly micro pores), the CNFs can be visualized as the negative image. Considering that lactase is a globular

protein with a diameter of 12 nm, it is therefore expected that lactase adsorption in the open CNF-structure is much higher than in the mainly microporous structure of the other two carriers. Lactase cannot enter the micro pores of sucrose and PFA based supports, and will therefore be present only on the outer surface. On the other hand, for CNFs, adsorption can take place anywhere on and between the carbon fibers. This is schematically depicted in Figure 16.

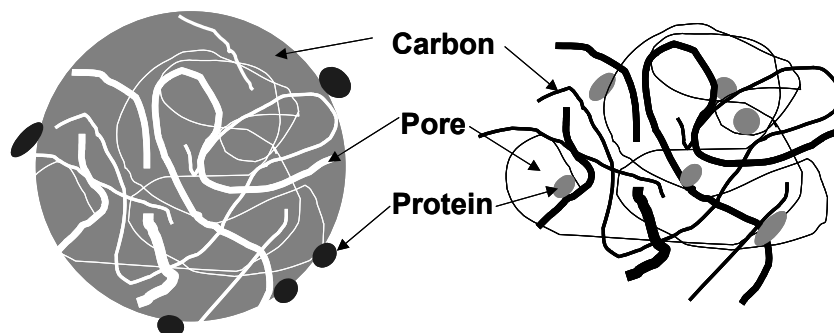


Figure 16. Schematic representation of enzyme adsorption on microporous carbons (left) and on CNFs (rights).

This structural difference between the different carriers results in the large difference in total enzyme adsorption, as shown in Figure 15. It is expected that for smaller enzymes with a similar surface chemistry, such as trypsin (~5 nm), the effect of micro-porosity will be greater. Smaller enzymes will probably show increased adsorption on the sucrose-based carbon, because the larger pores around 8 nm become accessible to the enzyme. The completely microporous PFA will still only have adsorption on the outer surface.

Lactase adsorption can also be influenced by oxidizing the carbons in air and subsequent HNO_3 treatment (Figure 15). Oxidation treatment does not affect the narrow microporosity of the samples. For both PFA and CNFs, the N_2 isotherms (not shown) of the carbons also did not differ significantly after oxidation. A more extreme treatment is necessary to alter the porosity of these carbons. For sucrose however, the N_2 adsorption isotherms were very different after application on a ceramic support and/or oxidation with air and HNO_3 . Apparently the mesoporous structure of the sucrose-based carbon is affected by the monolith backbone and the different treatments. The porosity of the sucrose based carriers shows an initial decrease after air treatment and a subsequent increase after air/ HNO_3 treatment. From the increased lactase adsorption capacity after oxidation, it can be concluded that surface chemistry is an important parameter in the total lactase adsorption capacity of the carriers. Only for the sucrose based carriers there is also an effect of the changing porosity on final lactase loading.

To investigate the effect of surface chemistry on lactase adsorption, CNF-based cordierite supports were treated with different oxidizing agents. For the hydrophilic lactase that was used in this study, it was assumed that oxygen containing surface groups would have a positive effect on lactase adsorption. Therefore, lactase adsorption in mg/g carbon was plotted against total oxygen content as calculated from CO and CO_2 evolution in TPD-MS (Figure

13). A detailed study of the surface chemistry of the carriers is given elsewhere [32]; the results for lactase adsorption on oxidized CNFs are presented in Figure 17.

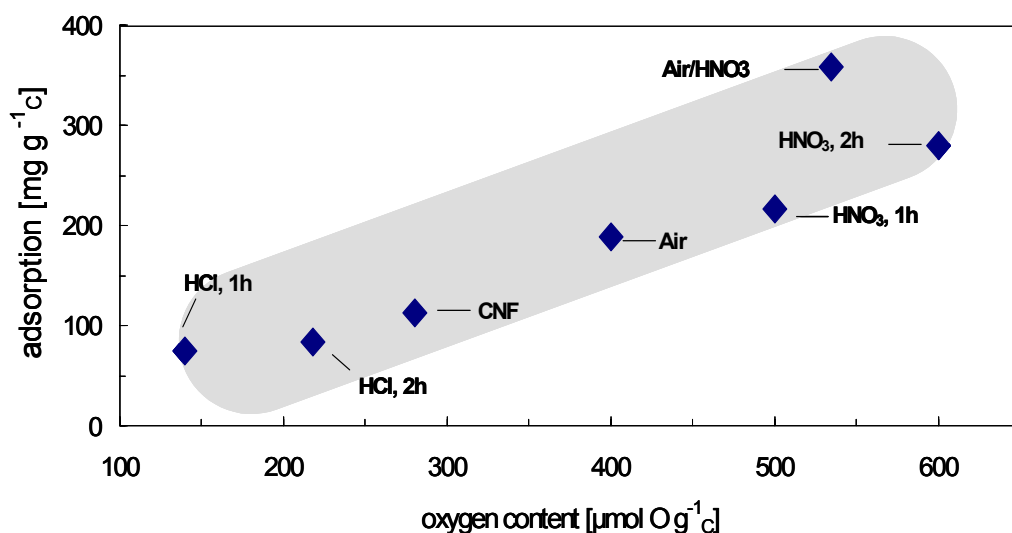


Figure 17. Adsorption of lactase on 200 cpsi CNF-based cordierite composites

A clear trend in total adsorption can be seen. The untreated fibers, labeled CNFs, have a total oxygen content of $280 \mu\text{mol g}^{-1}$. Treatment in HCl has a negative effect on lactase adsorption, because the oxygen content is decreased. After treatment in air, enzyme adsorption is improved. Treatment in HNO_3 has a further positive effect on lactase adsorption.

3.2.2 Optimization of the immobilization procedure

To be able to compare ACM and cordierite monoliths (in combination with the different carbon carriers) in terms of enzyme adsorption capacity, the optimal conditions for adsorption of both lactase and lipase should first be found. Since the optimal pH for both enzymes is near 5, it is expected that enzyme loading will be maximal at this pH. At pH 11 the lactase is not stable, no adsorption experiments were performed at this pH. The effect of pH on enzyme adsorption on CNF and sucrose-based cordierite monoliths is presented in Figure 18.

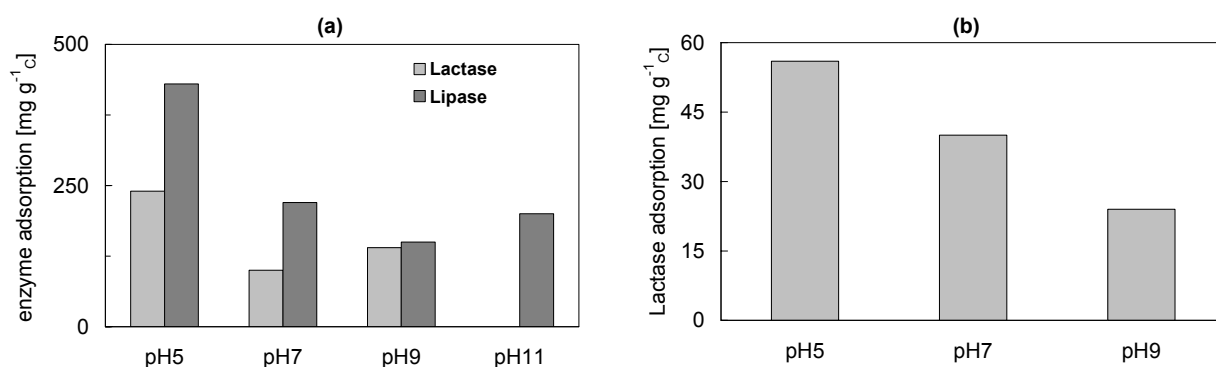


Figure 18. Enzyme immobilization at 278 K from a 2 g l^{-1} solution on cordierite samples. a) lipase and lactase adsorption on C-CNF, b) lactase adsorption on C-SUC at different pH from aqueous solution

The general trend on both C-CNF and C-SUC is a decreased adsorption at higher pH. Also for PFA-based supports pH 5 proved to be optimal. For ACM backbones, a similar trend was observed, only at a higher total adsorption (see also Figure 19). The exact reason for the pH dependency is not known, probably the charges of both the enzyme and the carbon surface influence the final loading. At pH 5 these enzymes are uncharged (lactase and lipase have an isoelectric point around pH 5), if the carbon surface is also uncharged (which seems likely for taking into account the surface complexes that were identified using Boehm titration), adsorption would be optimal. At increasing pH the enzymes become negatively charged, resulting in a decreased adsorption, because the acidic groups on the carbon surface are deprotonated and also become negatively charged. Theoretically, adsorption at pH 4 should give equally high loadings, this value is also close to the isoelectric point of the enzymes and the overall charge of the carbon surface will not be very different. At lower pH the enzyme will be positively charged or become unstable and the carbon surface will become positively charged, resulting in repulsion.

The effect of enzyme concentration on the final loading was studied by using solutions of 1, 2, and 4 g l⁻¹. As could be expected, an increase in final loading was observed for higher concentrations (not shown). This effect was also observed for immobilization on alginate gels in Chapter 6.

3.2.3 Adsorption capacity of functionalized monoliths

The optimal conditions to compare cordierite and ACM backbones with different carriers were found to be pH 5, 4 g l⁻¹ enzyme solution, and 5 h adsorption at 278 K. In Figure 19 this comparison is presented for lipase (a) and lactase (b), normalized for the amount of carbon carrier that was deposited on the monolith.

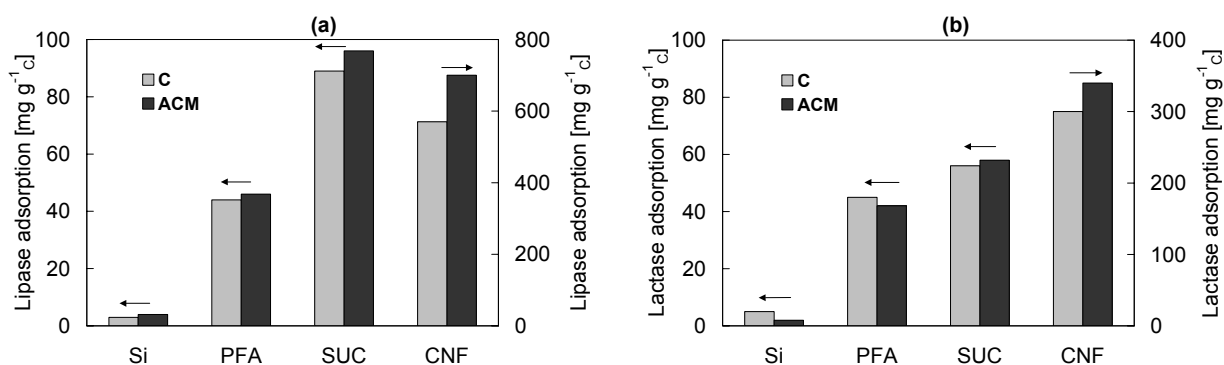


Figure 19. Comparison of cordierite (grey bars) and ACM (black bars) monoliths in combination with different carbon carriers at pH 5, from a 4 g l⁻¹ aqueous enzyme solution. a) lipase, b) lactase

Adsorption on bare monoliths (not shown) and washcoated (“SiO₂“ in Figure 19) monoliths is negligible. Based on the higher carbon loading on ACM, a higher total enzyme loading could be expected. Indeed, in general the total enzyme loading on carbon-coated ACM monoliths is higher than on carbon coated cordierite (not shown). But apparently there is another difference between the ACM-carbon and the cordierite-carbon carriers that leads to a

difference in adsorption capacity per gram of carbon carrier (Figure 19). ACM-composites have a higher enzyme adsorption capacity per gram of carbon than cordierite-composites. In the more open channel wall of the ACM monoliths, the carbon is more accessible than on the closed cordierite walls. For the even more open composite consisting of ACM + CNFs this effect increases, resulting in the largest relative difference between ACM and cordierite. Therefore, AM-CNF carriers have the highest enzyme loading capacity for both enzymes under the present conditions.

3.3 Catalyst performance

3.3.1 Activity of immobilized lipase from *Candida rugosa*

The activity of lipase coated monolithic biocatalysts in the hydrolysis of pNPP is presented in Figure 20. Lipase was immobilized from a 4 g l^{-1} aqueous solution at pH 5.

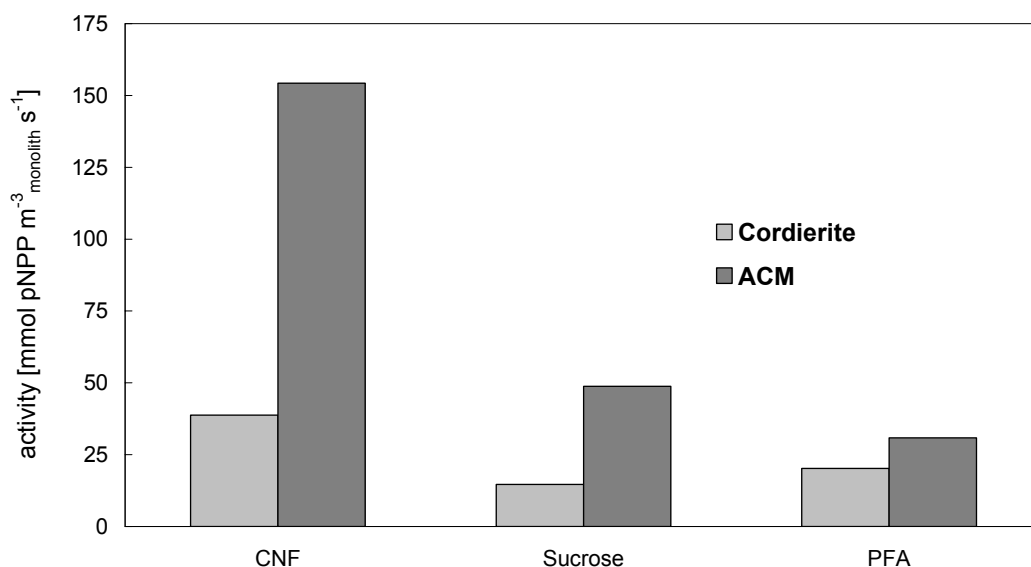


Figure 20. Initial rate per monolith volume in the lipase catalyzed hydrolysis of pNPP at 293 K in aqueous medium (DMSO/tris buffer pH 7 1:9) for different carbon-ceramic composites. $C_b = 0.4 \text{ mM}$

ACM-based biocatalysts have a significantly higher activity than biocatalysts with a cordierite backbone, due to the higher total enzyme loading. The amount of adsorbed lipase and the activity in the hydrolysis of pNPP are shown in Table 6 for a series of carbon/ACM and carbon/cordierite samples. These samples were not oxidized in air or air/HNO₃. Were the oxidized samples to be used, enzyme loading and resulting activity could increase significantly.

In general the carbon/ACM supports have a higher adsorption capacity than the similarly prepared carbon/cordierite supports, because the ACM supports allow more carbon to be deposited. As was shown before, the open structure of the ACM monoliths also yields a better accessibility (higher surface area) for enzyme deposition, see Figure 19. The resulting higher enzyme loading gives a higher activity per unit monolith volume. For all monoliths, the

activity per unit monolith volume corresponds to the amount of adsorbed enzyme (Table 6). This implies that the activity per unit mass of enzyme is constant for all carbon types ($9 \cdot 10^{-3} \text{ mmol s}^{-1} \text{ g}^{-1}_{\text{protein}}$). Small differences between the different carbon carriers can be the result of the nature of the surface groups that can influence enzyme binding.

Table 6. Carbon-ceramic carriers for lipase immobilization: Immobilization and initial rate in the hydrolysis of pNPP at 298 K in DMSO/tris buffer pH 7 (1:9). $C_b = 0.4 \text{ mM}$

Catalyst	Enzymatic activity	
	Total adsorption mg	$\text{mmol m}^{-3}_{\text{monolith}} \text{ s}^{-1}$
Free lipase		30×10^{-3}
C-SUC	81	15
C-PFA	127	20
C-CNF	312	39
AM-SUC	340	49
AM-PFA	170	31
AM-CNF	1000	154

* Lipase content in the crude protein is estimated to be 5%

To compare the catalyst performance, free lipase was also tested. The results of the activity per g of protein are presented in Table 6. The specific activity of immobilized lipase is lower than that of the free enzyme. It is known that residual activity of an enzyme after immobilization usually decreases significantly. Also the carrier has a substantial influence on both residual activity and kinetic constants [45]. A decrease in the observed rate per g enzyme can usually be ascribed to conformational changes, steric effects or denaturation. Ayhan *et al.* [46], report a residual activity of 1% after coupling via glutaraldehyde immobilization in polymer microbeads. Lee *et al.* [47] report a residual activity of 2% after covalent immobilization of glucoamylase onto controlled pore glass. When physical or ionic adsorption is employed, the enzymes maintain their natural configuration and residual activity is usually around 30% of free enzyme activity [48]. This corresponds with our results; the immobilized activity of *Candida rugosa* lipase was found to be 15-30%.

If we assume a lipase content of 5% in the crude protein mixture, a turnover frequency of 21 s^{-1} can be calculated for the free lipase and 6 s^{-1} for the immobilized lipase. A value of around 200 s^{-1} was observed by Blackberg and Hernel [46], for a similar (free) lipase in a different assay. The low turnover frequency is probably due to the reaction conditions in the p-NPP model reaction. The optimum pH for this lipase is 4.5-5, while the assay is performed at pH 7. And in general enzymatic reactions are performed at slightly elevated temperatures (308 K), whereas this reaction proceeds at 295 K. The combination of solvent, temperature, and pH can apparently lead to strong deviations in turnover frequency.

3.3.2 Activity of immobilized lactase from *Aspergillus Oryzae*

The activity of monolithic biocatalysts with adsorbed lactase in the hydrolysis of oNPG is presented in Figure 21. The enzyme was immobilized from a 4 g l^{-1} aqueous solution at pH 5. The carriers consist of monolith-carbon combinations that were not oxidized to increase

enzyme loading. For oxidized samples, immobilization yield and resulting activity would be significantly higher.

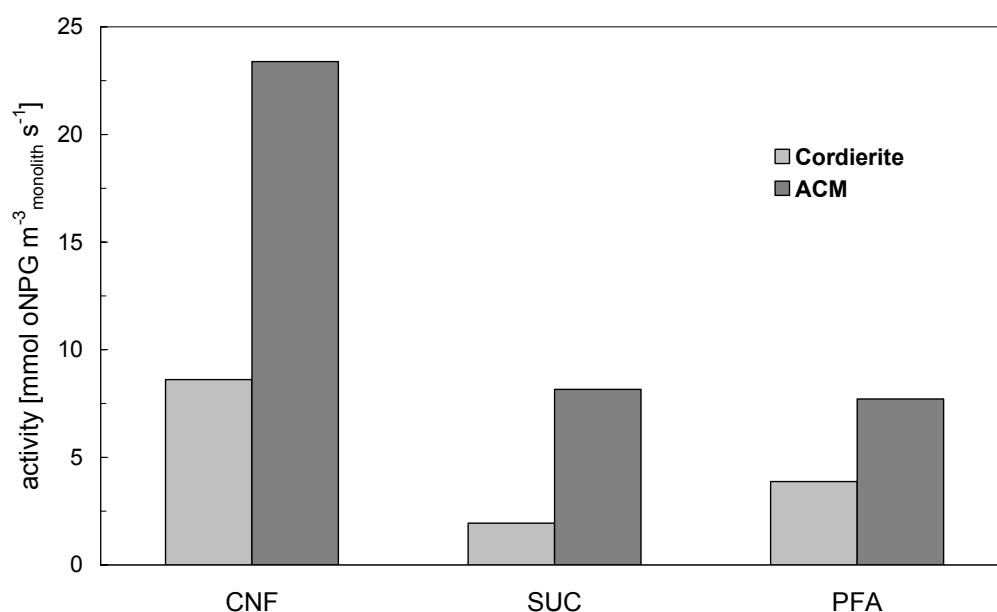


Figure 21. Initial rate per monolith volume in the lactase catalyzed hydrolysis of oNPG at pH 7 for different carbon-ceramic composites at 293 K, $C_b = 2$ mM

For immobilized lactase, the same trends in the results are observed. AM-CNF and C-CNF outperform the other composites. The amount of adsorbed lactase and the activity in the hydrolysis of oNPG are shown in Table 7.

Table 7. Carbon-ceramic carriers for lactase immobilization: Immobilization and initial rate in the hydrolysis of oNPG at 293 K in aqueous medium at pH 7. $C_b = 2$ mM

Catalyst	Total adsorption mg	Enzymatic activity	
		$\text{mmol m}^{-3} \text{ monolith s}^{-1}$	$\text{mmol g}^{-1} \text{ protein s}^{-1} *$
Free lactase			3.3×10^{-3}
C-SUC	60	1.9	1.9×10^{-3}
C-PFA	130	3.9	2.4×10^{-3}
C-CNF	210	8.6	2.0×10^{-3}
AM-SUC	197	8.2	2.1×10^{-3}
AM-PFA	155	7.7	2.5×10^{-3}
AM-CNF	510	23.4	1.8×10^{-3}

* Lactase content in the crude protein is estimated to be 5%

Also for this enzyme, the activity per unit monolith volume corresponds to the amount of adsorbed enzyme. This implies that the activity per unit mass of enzyme is constant for all carbon types ($2 \times 10^{-3} \text{ mmol s}^{-1} \text{ g}^{-1} \text{ protein}$). Small differences between the different carbon carriers can be the result of the nature of the surface groups that can influence enzyme binding. Free lactase was included in Table 7 to address the effect of immobilization on the specific enzyme activity. If we assume a lactase content of 5% in the crude protein mixture a

turnover frequency of 8 s^{-1} can be calculated for the free lactase. Bickerstaff [47] reports a TOF of 200 s^{-1} , but the enzyme source is not known in this case, neither are the substrate type or the reaction conditions. The relatively low turnover frequency could be expected for this model reaction. In the o-NPG assay as conducted here, the activity of the enzyme is followed at pH 7 and 295 K, far from its optimum pH of 5 and temperature of 309 K.

The specific activity of immobilized lactase is lower than that of the free enzyme. For the monolithic biocatalysts, the immobilized activity of *Aspergillus oryzae* lactase was found to be 52-76 %. The immobilized enzyme has a turnover frequency of around 4 s^{-1} .

Because both enzymes have a very different nature (size, molecular weight and surface chemistry) it is not useful to directly compare the activity. What can be said is that the residual activity of the immobilized lactase is significantly higher than for the lipase. The reason for the large decrease in activity of the lipase is not clear. It is possible that this hydrophobic enzyme tends to “spread” out over the hydrophobic carbon surface, thereby losing its conformation. The larger, hydrophilic lactase retains its globular conformation. To check if there is sufficient surface area for the enzyme to form a nice coating layer, or if the enzyme is actually present in multiple layers, the surface coverage of both enzymes can be calculated in $\text{m}^2_{\text{enzyme}}$ per $\text{m}^2_{\text{carbon}}$ carrier.

The coverage of the cordierite based composites of Tables 6 and 7 are given in Table 8. Only values of non-oxidized carbons are used, assuming globular proteins with a radius of 2.5 nm and 6 nm respectively for lipase and lactase and using the S_{BET} values of the untreated carbon-ceramic composites from Table 4.

Table 8. Surface coverage for lactase/lipase on carbon ceramic composites

Carrier	Adsorption $\text{g g}^{-1}_{\text{C}}$	Surface area $\text{m}^2 \text{g}^{-1}_{\text{C}}$	% surface coverage
C-SUC_lip	0.055	500	6
C-PFA_lip	0.090	60	33
C-CNF_lip	0.570	175	95
C-SUC_lact	0.044	500	7
C-PFA_lact	0.057	60	47
C-CNF_lact	0.300	175	70

For the sucrose-based catalysts, less than 10% of the surface is covered. In the case of lactase, this can be explained by the mean pore size of 14 nm (Figure 10) that was found for this carrier. The pore size of the carrier is only slightly larger than the size of the enzyme (12 nm). For lipase, this can be caused by the surface chemistry of the carbon, which is slightly different from the surface chemistry of PFA. This could influence binding of the lipase [51]. For this carrier, ‘spreading’ of the enzyme is possible due to a low enzyme density on the carbon surface. For PFA-based carbons, almost 50% of the surface is covered with enzyme. Also for this carrier no overload (multiple layers of enzyme) is observed. For C-CNF however, total coverage approaches 100%, possibly multilayers are present at these high loadings. If the enzyme is present in layers, this leads to decreased efficiency. This can be an explanation for the slightly lower specific activity of the CNF-based biocatalysts. For both

lipase and lactase (see Tables 6 and 7) the activity per g of enzyme is lower than for the other carbon carriers. For the CNF, also the globular shape of the enzyme is taken into account, because the protein molecules are assumed to be present surrounding the fibers. The actual diameter of the fiber is corrected for the size of the enzyme (2.5 nm on both sides for lipase and 6 nm on both sides for lactase), because enzymes are assumed to be packed around the fibers as perfect spheres (Figure 22).

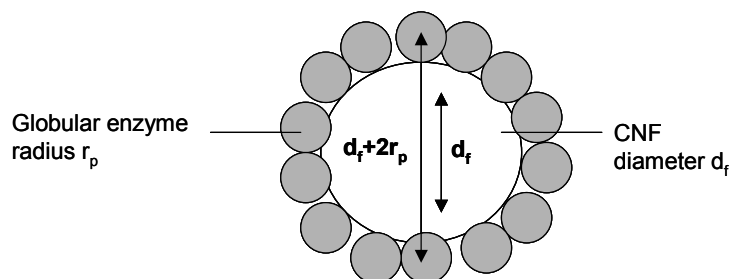


Figure 22. Schematic representation for calculation of the available surface area for CNF samples

For a mean diameter of 28 nm, this is an increase in available surface area of 20% for lipase and 40% for lactase.

3.3.3 Stability of the biocatalysts

The storage stability of lipase-based catalysts was evaluated by the following approach. The activity was measured on a freshly prepared catalyst. The catalyst was washed with clean water, air-dried and stored in a refrigerator in a sealed container, usually overnight, before the activity was measured again. This was repeated using the same sample for the duration of each stability measurement. The results for the different supported carbon carriers with immobilized lipase are presented in Figure 23.

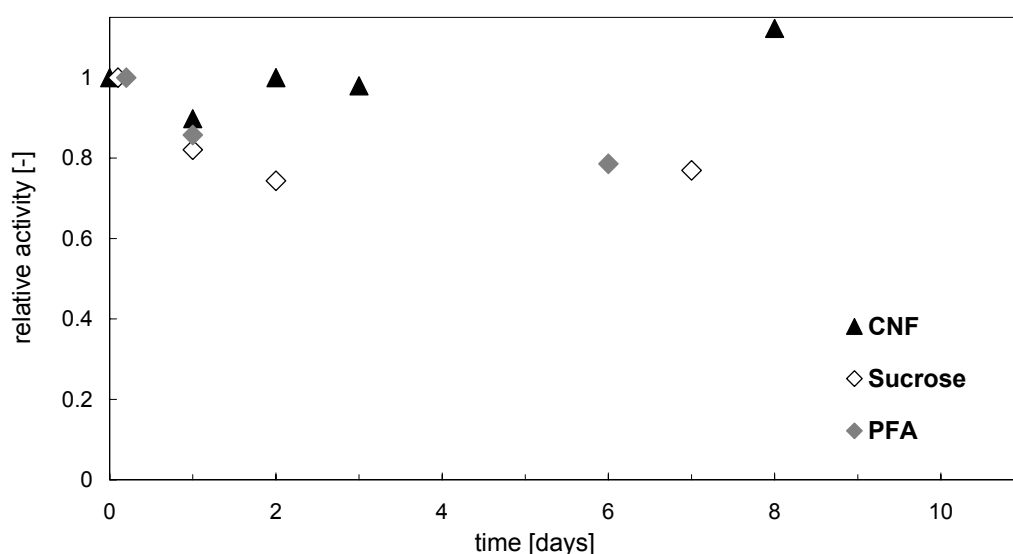


Figure 23. Stability of immobilized lipase on carbons with an ACM backbone in the hydrolysis of pNPP ($C_b = 0.4$ mM) in aqueous medium (DMSO/tris buffer pH 7 1:9) at 293 K.

The AM-SUC-lip and AM-PFA-lip catalysts initially lose 20% of the initial activity after 2 days, but remain stable after that. The AM-CNF-lip remains stable for at least 8 days. It was expected that activity would decrease faster due to extensive desorption in the aqueous reaction mixture. However, only a small initial desorption was observed during the first activity assay. During subsequent tests, the activity in solution was followed by removing the monolith from the reaction mixture halfway the assay. No free enzyme activity could be detected. Figure 24 shows the activity as a function of storage time for a C-PFA-lip and AM-PFA-lip sample. Both samples had a comparable amount of enzyme per gram of carrier and the same initial activity.

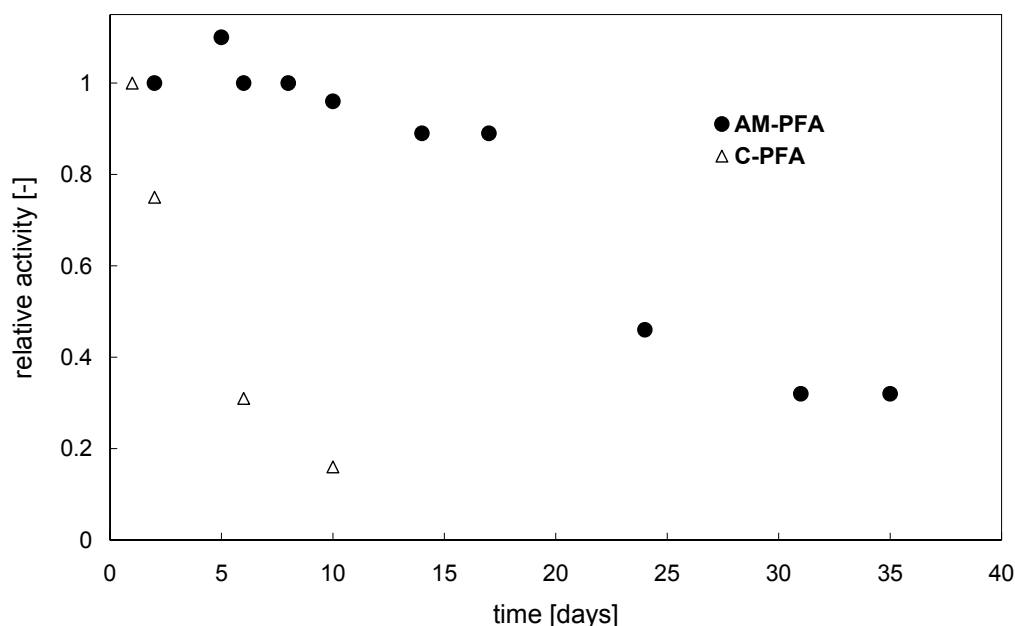


Figure 24. Stability comparison for AM-PFA-lip and C-PFA-lip in the hydrolysis of pNPP ($C_b = 0.4$ mM) in aqueous medium (DMSO/tris buffer pH 7 1:9) at 293 K.

The activity of the cordierite-based catalyst decreased faster than the ACM-based catalyst. After 10 days, the ACM catalyst still retained more than 90% of its original activity, while the cordierite sample has less than 20% of its original activity. Similar observations (although less pronounced) were made for sucrose-derived samples. The CNF-based composites did not show any difference in stability for ACM and cordierite. It remains unclear whether the morphology or the chemical composition of the mullite leads to the improved stability of the ACM biocatalysts. The open structure of the ACM could affect the water content inside the monolith wall. ACM walls usually hold significantly more water than cordierite. For sucrose and PFA, the carbon coating does not absorb any water. The higher moisture content in the ACM composites could have a stabilizing effect on the immobilized enzyme. For the CNF, the cordierite composite can also retain water inside the fiber coating, improving the stability. This can explain the higher stability of the C-CNF catalysts compared to the other carbon carriers (Figure 23).

4 Conclusions

Characteristics of a new monolith catalyst support with a very open wall structure are compared with those of classic cordierite monoliths. Different carbon materials, deposited on a ceramic honeycomb monolith support are suitable carriers for the immobilization of different enzymes. Composites with different morphology, porosity, and surface chemistry were prepared. Mild treatment in air and subsequent treatment with HNO₃ did not affect the porosity of the carbons, but significantly improved enzyme adsorption capacity. Carbonized sucrose and polyfurfuryl alcohol coated monoliths yielded enzyme carriers with a low enzyme adsorption capacity. This is attributed to the microporous nature of these carbons. The CNF-based supports showed a large adsorption capacity due to the open structure between the fibers. Oxidation treatment was used to further improve enzyme adsorption of the CNFs, by increasing the amount of surface oxygen complexes. The adsorption capacity for lactase correlates well with the amount of oxygen containing surface groups.

For lactase and lipase, optimum loading was obtained at pH 5, from a 4 g l⁻¹ enzyme solution. With respect to catalysis, the open wall structure of ACM monoliths allows high and well-accessible catalyst loadings. More carbon could be deposited per unit wall volume, thus more enzyme was immobilized, and more active honeycomb biocatalyst were prepared with the ACM monoliths.

To compare the performance of the carbon-ceramic supports as carriers for different enzymes, three different preparation methods were used for cordierite and ACM monoliths. Untreated carbons were used in the activity tests. For each preparation method, the activity per gram of enzyme was essentially independent of the ceramic support used. For immobilized lipase, the activity was 30% of the free activity, for lactase this value was slightly higher at 50-70%.

Catalysts were stable for at least 10 days, stored at 278 K with intermediate performance testing. The general design rules for the carbonaceous enzyme carrier can also be applied for the adsorption of other enzymes and can be summarized as:

- The texture of the carbon must be in accordance with the size of the enzyme.
- The surface chemistry of the carrier must be adapted to match the nature of the enzyme

The preferred method to produce a carbon-ceramic composite for immobilization of different enzymes would be an ACM backbone with a CNF coating. The enzyme should be immobilized from a 4 g l⁻¹ solution at 278 K at pH 5.

5 Acknowledgements

Mike Smeltink is gratefully acknowledged for his value contribution to the experimental work. The Netherlands Organization for Scientific Research (NWO) is acknowledged for funding of this research by means of a grant, filenumber R74-68. Ugo Lafont and Patricia

Kooyman of the National Centre for High Resolution Electron Microscopy (NCHREM) of the Faculty of Applied Sciences, Delft University of Technology are acknowledged for recording the TEM micrographs. Eduardo Villaplana-Ortego of the Materiales Carbonosos y Medio Ambiente (MCMA) group at the department of Inorganic Chemistry, University of Alicante is acknowledged for recording the adsorption isotherms. Dolores Lozano Castelló and Angel Linares Solano of the Materiales Carbonosos y Medio Ambiente (MCMA) group at the department of Inorganic Chemistry, University of Alicante are acknowledged for their contribution to this work. Corning Inc. is acknowledged for supplying the cordierite monoliths. The Dow Chemical Company is acknowledged for supplying the ACM monoliths. Part of this work was done in the framework of the Network of Excellence 'Inside Pores'.

6 Symbols

C_b	bulk substrate concentration	[mol m ⁻³]
d_f	diameter of the CNF	[m]
r_f	radius of the CNF	[m]
r_p	radius of the protein	[m]
w	weight of the carbon	[kg]
w_s	weight of the support	[kg]
Y_i	yield of component i	[%]

7 References

- [1] G.A. Kovalenko, E.V. Kuznetsova, Yu.I. Mogilnykh, I.S. Andreeva, D.G. Kuvshinov, N.A. Rudina (2001) *Carbon* 39; 1033-1043
- [2] L.R. Radovic, C. Sudhakar, in H. Marsh, E.A. Heintz, F. Rodriguez-Reinoso (Eds.) (1997) *Introduction to Carbon Technologies*, Universidad de Alicante, Secretariado de Publicaciones: 103
- [3] F. Rodriguez-Reinoso (1998) *Carbon*; 36:159-175
- [4] M.T. Kreutzer, F. Kapteijn, J.A. Moulijn, J.J. Heiszwolf (2005) *Chemical Engineering Science*; 60: 5859-5916
- [5] Th. Vergunst, M.J.G. Linders, F. Kapteijn, J.A. Moulijn (2001) *Catalysis Reviews*; 43: 291-314
- [6] K.P. Gadkaree (1998) *Carbon*; 36: 981-989
- [7] T. Valdés-Solís, G. Marbán, A.B. Fuertes (2001) *Microporous and Mesoporous Materials*; 43: 113-26
- [8] Th. Vergunst, F. Kapteijn, J.A. Moulijn (1998) *Studies in Surface Science and Catalysis*; 118: 175-183

- [9] E.M. DeLiso, K.P. Gadkaree, Mach, Streicher. US 5,451,444 (1995)
- [10] K.P. Gadkaree (1996) US 5,487,917
- [11] K.P. de Jong, J.W. Geus (2000) *Catalysis Reviews Science and Engineering*; 42(4): 481-510
- [12] T.V. Hughes, C.R. Chambers (1899), US Patent 405,480
- [13] Y. Zhang, K. J. Smith (2005) *Journal of Catalysis*; 231(2): 354-364
- [14] C.H. Bartolomew, (1982) *Catalysis Reviews- Science and Engineering*; 24: 67-112
- [15] D.L. Trimm (1977) *Catalysis Reviews- Science and Engineering*; 16: 155-89
- [16] J.H. Bitter, M.K. van der Lee, A.G.T. Slotboom, A.J. van Dillen, K.P. de Jong (2003) *Catalysis letters*; 89(1-2): 139-42
- [17] H.C. Foley (1995) *Microporous Materials*; 4: 407-433
- [18] N.M. Rodriguez, A. Chambers, R.T.K. Baker (1995) *Langmuir*; 11:3862-3866
- [19] G.A. Kovalenko, O.V. Komova, A.V. Simakov, V.V. Khomov, N.A. Rudina (2002) *Journal of Molecular Catalysis A: Chemical*; 182-183: 73-80
- [20] H. Suda, K. Haraya (1997) *Journal of Physical Chemistry B*; 101: 3988-94
- [21] B.T. Hang, M. Eashira, I. Watanabe, S. Okada, J-L. Yamaki, S-H.Yoon, I. Mochida (2005) *Journal of Power Sources*; 143:256-264
- [22] S. Flandrois, B. Simon (1999) *Carbon*; 37: 165-180
- [23] E. Ochoa-Fernandez, D. Chen, Z. Yu, B. Totdal, M. Ronning, A. Holmen (2004) *Surface Science*; 554: L107-L112
- [24] F. Salman, C. Park, R.T.K. Baker (1999) *Catalysis Today*; 53: 385-394
- [25] S.J. Park, D.G. Lee, (2005) *Fabrication of nano-filters by direct synthesis of carbon nanotubes onto micron filters*, Abstracts of the European Aerosol Conference 2005: 18
- [26] Y-M. Shyu, F. Chau-Nan Hong (2001) *Diamond and Related Materials*; 10: 1241-45
- [27] A.V. Melechko, V.I. Merkulov, D.H. Lowndes, M.A. Guillorn, M.L. Simpson (2002) *Chemical Physics Letters*; 356: 527-33
- [28] S-H. Yoon, S. Lim, S-H. Hong, W. Qiao, D.D. Whitehurst, I. Mochida, B. An, K. Yokogawa (2005) *Carbon*; 43: 1828-38
- [29] Y. Wang, N. Shah, G.P. Huffmann (2005) *Catalysis Today*; 99: 359-64
- [30] S. Lim, S-H. Yoon, Y. Korai, I. Mochida (2004) *Carbon*; 42: 1765-81
- [31] R.T. Baker (1989) *Carbon*; 27: 315-323
- [32] K.M. de Lathouder, D. Lozano-Castelló, A. Linares-Solano, F. Kapteijn and J.A. Moulijn (2006) *Carbon*; 44: 3053-3063
- [33] T.A. Nijhuis, A. Beers, T. Vergunst, I. Hoek, F. Kapteijn, J.A. Moulijn (2001) *Catalysis Reviews*; 43(4): 345-380
- [34] M.L. Toebes, J.H. Bitter, A.J. van Dillen, K.P. de Jong (2002) *Catal Today*; 76: 33-42
- [35] M.S. Hoogenraad, R.A.G.M.M. van Leeuwarden, G.J.B. van Breda Vriesman, A. Broersma, A.J. van Dillen, J.W. Geus (1995) *Studies in Surface Science and Catalysis*; 91: 263
- [36] N. Jarrah, J.G. van Ommen, L. Lefferts (2003) *Catal today*; 79-80: 29-33
- [37] D. Lozano-Castello, D. Cazorla-Amoros, A. Linares-Solano (2004) *Carbon*; 42: 1233-42

-
- [38] J.C. Groen, J. Perez-Ramirez, L.A.A. Pfeffer (2002) *Chemistry Letters*; 1: 94-99
- [39] E. Crezee (2003) PhD thesis, Delft University of Technology, The Netherlands
- [40] M. Toebes (2004) PhD thesis, University of Utrecht, The Netherlands
- [41] J.L. Figueiredo, M.F.R.Pereira, M.M.A. Freitas, J.J.M. Órfão (1999) *Carbon*; 37(9): 1379-89
- [42] K.M. de Lathouder, J. Bakker, M.T. Kreutzer, F. Kapteijn, J.A. Moulijn, S.A. Wallin (2004) *Chemical Engineering Science*; 59: 5027-5033
- [43] K.M. de Lathouder, T. Marques Flo', F. Kapteijn, J.A. Moulijn (2005) *Catalysis Today*; 105: 443-47
- [44] C. van Gulijk, K.M. de Lathouder and R. Haswell (2006) *Carbon*; 44: 2950-2956
- [45] C. Suan, M.R. Sarmidi (2004) *Journal of Molecular Catalysis B: Enzymatic*; 28: 111-119
- [46] F. Ayhan, H. Ayhan, E. Piskin, A. Tanyolac (2002) *Bioresource Technology*; 81: 131-140.
- [47] G.K. Lee, R.A. Lesch, P.J. Reilly (1981) *Biotechnology and Bioengineering*; 23: 487-497
- [48] C. Marzadori, S. Miletta, C. Gessa, S. Ciurli (1998) *Soil Biology and Biochemistry*; 30: 1485-1490
- [49] L. Blackberg, O. Hernell (1981) *European Journal of Biochemistry*; 116: 221-225
- [50] G.F. Bickerstaff (1987) *Enzymes in Industry and Medicine*. Edward Arnold, London Great Britain
- [51] M.L. Foresti, A. Errazu, M.L. Ferreira (2005) *Biochemical Engineering Journal*; 25: 69-77
- [52] K.M. de Lathouder, D. Lozano-Castelló, A. Linares-Solano, S.A. Wallin, F. Kapteijn and J.A. Moulijn (2006) *Microporous and Mesoporous Materials*; in Press

Design rules for monolithic biocatalysts

Abstract

To be able to suggest the optimal immobilization protocol for a given application, the separate parameters need to be identified. The final properties of the immobilized enzyme are determined by the properties of both the support and the enzyme. After addressing different protocols, a set of general designrules is presented based on the following parameters:

1. Monolith microstructure
2. Support preconditioning
3. The nature and chemistry of the enzyme.
4. Process parameters and conditions.

Other practical considerations and requirements include translating the method to be used with monoliths, the chemistry of the (preparation of) carrier, and the price and the preparation time of the support.

1 Introduction

The development of robustly immobilized enzymes is a major challenge in industrial biocatalysis, many studies have been performed in this field [1-4]. The selection of an immobilization strategy or a modification procedure is based on the process specifications for the biocatalyst, which include such parameters as overall enzymatic activity, effectiveness of enzyme utilization, deactivation and regeneration characteristics, cost of the immobilization procedure, toxicity of immobilization reagents, and the desired final properties of the immobilized enzyme.

Many factors have an influence on the final properties of enzyme-carrier systems. These factors concern morphology of the carrier (type, porosity, concentration) and support chemistry as well as activation and immobilization procedures. Moreover, the relative importance of all of these parameters is different for different enzymes.

Enzymes can be fixed onto a support by physical forces such as hydrophobic interaction, van der Waals binding or ionic interactions. These are generally too weak to prevent desorption under industrial conditions in aqueous phase, but this method is cheap and simple and can be sufficient for application in organic medium. In contrast, covalent binding of enzymes to a support is stable, but this method is irreversible and often leads to deactivation. In combination with cheap supports that do not require reuse, this method is very convenient in terms of enzyme loss during operation. Therefore this protocol has been favored in some occasions [5-7]. Although the activity is generally high, entrapment in hydrogels is generally associated with loss of enzyme, unless the enzyme is crosslinked onto the matrix. But this can result in internal mass transport problems. Polyelectrolytes for ionic adsorption, have the advantage of a high retained activity and reversibility. Complicated preparation and enzyme loss however, make this protocol less advantageous for some applications.

To be able to suggest the optimal immobilization protocol for a given application, the separate parameters need to be identified. The properties of the immobilized enzyme are determined by the properties of both the support and the enzyme. In some occasions, the support material can influence the kinetics of the enzyme [8] or lead to improved activation of an enzyme [9]. The interaction between carrier and enzyme can lead to very specific chemical, biochemical, mechanical and kinetic properties for different support materials. This is schematically depicted in Figure 1 [10]. A very important factor that influences the final performance of the biocatalyst is the reactor. Conditions such as pH, ionic strength, substrate concentration, temperature should be known before selecting a carrier material/immobilization strategy. Once the enzyme-carrier combination and reactor type have been selected, the resulting performance can be expressed in enzyme yield, activity, and stability. These factors can then be translated to productivity and economic performance.

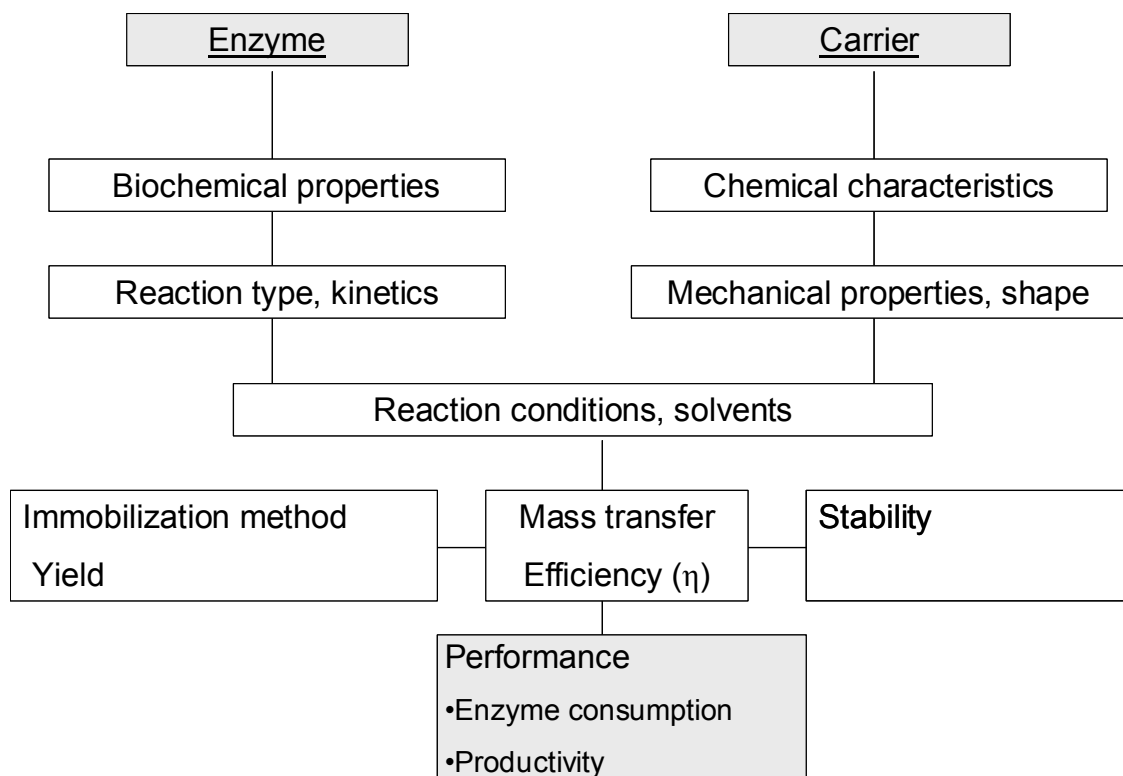


Figure 1. The properties of the biocatalyst are determined by several factors

In this study, adsorption, ionic adsorption, entrapment and covalent binding have been selected as suitable immobilization protocols to be applied in combination with monolithic backbones. Different industrially relevant enzymes (lactase, lipase, penicillin acylase, and trypsin) are used in the catalyst performance study. The results from the preparation and performance can be combined into a general set of design rules for monolithic biocatalysts. Monoliths are suitable as enzyme support material, but a suitable carrier layer is required. The immobilization methods (physical and ionic adsorption, entrapment, and covalent binding) must first be translated for use with monolithic supports. Two types of monoliths are used; classical cordierite monoliths and a new material “Acicular Ceramic Monolith” (ACM), with a more open, porous nature of the channel walls.

2 Results

This work is concerned with the application of ceramic monoliths with different microstructures as catalyst support material in the field of biocatalysis. In order to apply a ceramic monolith as a suitable carrier material for different enzymes, some important questions need to be answered:

- Which method of immobilization?
- Within which window of operation will the enzyme stay attached?

- Does the catalyst maintain its original activity, or is there a decrease after immobilization? The work was therefore divided into separate studies, depicted in Figure 2.

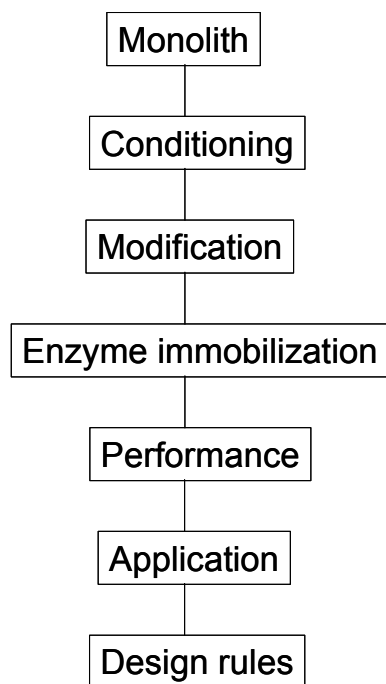


Figure 2. Project-scheme

The catalyst preparation consisted of a comparison of cordierite and ACM monoliths in terms of enzyme immobilization and performance. The monoliths were either washcoated directly with different enzyme carrier materials (hydrogels or carbon carriers) or washcoated with an inorganic carrier (Silica, Alumina) to provide additional surface area and anchor sites for attachment of enzymes or carriers. After application of the carrier, the immobilization conditions for different enzymes were optimized. The monolithic biocatalysts were assessed in a lab scale set-up, to compare the different immobilization protocols and conditions. Also stability and immobilization efficiency have been studied. With the obtained data, a set of design rules can be made that takes into account specific process requirements and conditions. The design rules are comprised of the different parameters that can be encountered in the scheme in Figure 1.

3 Design rules for monolithic biocatalysts

The generalized set of design rules that can be formulated can also be used for other methods than the ones described in the previous chapters. Following this scheme, also new protocols can be developed.

1. Monolith microstructure

If high catalyst loadings are desired (e.g. for reactions where mass transfer is not a limiting factor), the high porosity of the ACM monolith wall allows the catalyst loading per unit volume to be maximized while still retaining a low pressure drop through the reactor and good accessibility of the catalyst inside the wall.

2. Washcoating

When fast reactions impose diffusional limitations, the deposition of a thin conformal catalyst layer minimizes diffusional limitations. To obtain such a layer on a cordierite monolith, a nonporous base-layer is recommended. The disadvantage of this strategy is that these coatings are not very reproducible and strongly decrease the channel size. On ACM monoliths a thin layer of washcoat on the needles already minimizes diffusional problems while permitting significant catalyst loadings and ensuring bulk diffusional properties within the monolith wall.

For washcoating ACM monoliths with a slurry, the viscosity of the precursor is very important, to prevent plugging of the wall. If high catalyst loadings are required and the distribution of the carrier is not very important, ACM is the support of choice, but when thin, homogeneous layers are needed cordierite monoliths are recommended.

3. The nature of the enzyme.

Size, shape and surface chemistry must be compatible with the carrier material. Some lipases for instance need a hydrophobic/hydrophilic interface to be activated. For immobilization inside a porous material, the pore size must be substantially larger than the enzyme diameter. For a fast deactivation of a cheap enzyme, the immobilization should be reversible, whereas for an expensive enzyme that deactivates fast, the carrier should offer increased stability. In some cases the kinetics (inhibition/deactivation) of the enzyme can be influenced by the chemistry of the support material.

4. Process parameters and conditions.

In certain applications, high flow rates can lead to high shear forces. In this case stronger binding (ionic/covalent) is recommended over adsorption. The carrier material to be applied on the monolith should also be stable depending on reaction conditions (solvent, reactants, temperature). Hydrogels and polymeric carriers can be unstable under certain conditions, whereas inorganic carriers such as carbon and silica/alumina are usually more stable.

For very fast reactions, the use of a carrier with a longer diffusion path should be avoided, but in some occasions no diffusion problems arise when using the same carrier in a different system. These mass transport problems can be indicated by calculating the Carberry number and the Wheeler-Weisz criterion.

5. Practical considerations and requirements

The selected immobilization protocol should be translated to be used with monoliths. For some protocols such as sol-gel formation, this can be very difficult. Another important consideration is the chemistry of the (preparation of) carrier. For some applications e.g. food or pharmaceuticals, certain compounds should not be present in the support matrix. Metals and for instance glutaraldehyde are usually not allowed. Closely related to this are the price and the preparation time of the support. Expensive chemicals and multi-step procedures are not preferred.

4 Application

In part III of this work, the 4 different enzymes that were used before in the preparation of the monolithic biocatalysts will be used in different reaction systems. After a short description of the reaction system, the reactor, and the enzyme a carrier/protocol combination will be

chosen. In some occasions also less suitable carrier/enzyme combinations will be used to verify the use of the set of design rules.

5 References

- [1] S.W. Carleymith, P. Dunnill, M.D. Lilly (1980) *Biotechnology and Bioengineering*; 22; 739-756
- [2] W. Tischer V. Kasche (1999) *Trends in Biotechnology*; 17: 326-335
- [3] A. Subramanian, S.J. Kennel, P.I. Oden, K.B. Jacobson, J. Woodward, M.J. Doktycz (1999) *Enzyme and Microbial Technology*; 24: 26-34
- [4] G. Bickerstaff, Ed. (1997) *Immobilization of enzymes and cells, methods in Biotechnology vol.1*, Humana Press, Totowa New Jersey
- [5] D.A. Self, G. Kay, M.D. Lilly, P. Dunnill (1969) *Biotechnology and Bioengineering*; 11; 337-348
- [6] D. Warburton, K. Balashingham, P. Dunnill, M.D. Lilly (1972) *Biochimica Biophysica Acta*; 284: 278-284
- [7] E. Lagerlof, L. Nathorst-Westfelt, B. Eckstrom, B. Sjoberg (1976) *Methods in Enzymology*; 44: 759-769
- [8] C. Mateo R. Monti, B.C.C. Pessela, M. Fuentes, R. Torres, J.M. Guisan, R. Fernandez-Lafuente (2004) *Biotechnology Progress*; 20: 1259-1262
- [9] M.L. Foresti, A. Errazu, M.L. Ferreira (2005) *Biochemical Engineering Journal*; 25: 69–77
- [10] A.I. Kallenberg, F. van Rantwijk, R.A. Sheldon (2005) *Advanced Synthesis and Catalysis*; 347: 905– 926

Part III: Application

Liquid-solid mass transfer in a monolith loop reactor

Abstract

The trypsin-catalyzed hydrolysis of n-benzoyl-L-arginine ethyl ester (BAEE) was used to determine the liquid-solid mass transfer coefficient in the monolith loop reactor. Trypsin was immobilized by gel entrapment and by covalent bonding on monoliths with different cell density and microstructure. On the more porous ACM monoliths the carrier loading is higher, resulting in a higher total trypsin loading. The kinetics of the free trypsin can be described by a Michaelis-Menten expression with $V_{\max} = 0.44 \text{ mmol s}^{-1} \text{ g}_{\text{enz}}^{-1}$, and $K_m = 55 \text{ mmol m}^{-3}$. For the immobilized trypsin V_{\max} and K_m are $0.04 \text{ mmol s}^{-1} \text{ g}_{\text{enz}}^{-1}$ and 130 mmol m^{-3} respectively. An apparent activation energy, E_a , of 53 kJ mol^{-1} was found for the hydrolysis reaction. The conversion per pass in the monolith loop reactor varied between 0.05 and 0.4 for the different experiments. The system is however not completely mass transfer limited ($Ca \neq 1$). The observed mass transfer coefficient, k_{eff} , is not affected by the gas flow rate, but increases proportionally with liquid velocity. Also an increased surface area results in a higher k_{eff} . The use of catalysts with entrapped trypsin leads to significant internal diffusion limitations and therefore to a large underestimation of k_{eff} . Monoliths with covalently immobilized trypsin are suitable catalysts for mass transport measurements in the MLR. The obtained data for cordierite monoliths correlates well with previously derived models for mass transfer in square channels. The mass transfer under the present conditions has improved considerable compared to single-phase flow. Compared to earlier work with Taylor flow in single channels however, the mass transfer is still relatively low. In the ACM monoliths (where the open wall can also participate in the reaction) the gas bubbles “press” the liquid into the catalytic wall, resulting in enhance mass transfer.

1 Introduction

A wide variety of multiphase reactors are used in the chemical, pharmaceutical, and bio-industry. Regular and irregular catalyst packings are commonly used to enhance mass transfer and chemical reaction between catalysts and reacting fluids. Recently, structured supports are considered for use, because of the potential improvements they offer with respect to decoupling of heat and mass transfer phenomena, reduced pressure drop, resistance to attrition, and higher liquid/gas flow rates [1-3]. Monoliths, consisting of small parallel channels, are an example of such structured supports. Monoliths are proven technology for processes with single-phase flow [1,4], hence research is currently directed towards multiphase systems.

The hydrodynamics in a monolith channel are governed by the distribution of the fluid phases over the channels and the velocity of the fluids inside the channels. The use of appropriate distributors is very important, to prevent maldistribution [3,5]. Only if an even distribution of the fluid phases is accomplished, one can describe the entire column with a model for a single channel. On a macroscopic level the distribution of the fluids over the entire cross section of the support is of interest. At the microscale the gas and liquid phase distribution inside a single channel determine the flow regime. Gas-liquid flow in single capillaries has been studied extensively [5-8]. Depending on the mode of operation (co- or countercurrent), the liquid and the gas flow rate, different flow patterns can occur (Figure 1).

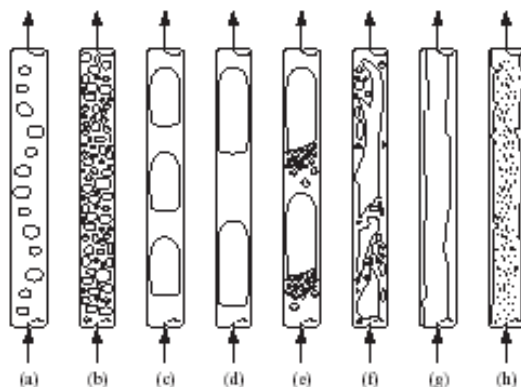


Figure 1. Flow regimes in monolith channels [3]. a,b): bubble flow, c,d) segmented flow (bubble train flow, Taylor flow capillary slug flow), e) transitional slug/churn flow, f) churn flow, g) filmflow (downflow only), h) annular flow

Most interesting for industrial applications are the segmented flow (Taylor flow) and the annular flow condition. In film flow operation (Figure 1g), the liquid moves as a thin film over the channel wall. The gas phase moves through the core of the channels. Film flow allows for both co- and countercurrent operation. The channel diameter is usually smaller than 5 mm and a gas to liquid ratio up to 20 can be used with superficial liquid velocities smaller than 5 cm s^{-1} . If the liquid velocity is increased or the gas velocity is decreased, the hydrodynamics will change towards Taylor flow, especially for small channels. In Taylor

flow operation (Figure 1c,d), the gas phase and liquid phase move through the channels as separate slugs. The gas bubble fills the whole channel diameter and only a thin liquid film separates the gas from the active channel wall. The layer between bubble and catalyst coating is thin, consequently a high gas-solid mass transfer rate through this film is possible. Inside the liquid slugs, an internal recirculation pattern is present [9]. This internal flow increases radial mass transfer. The gas bubbles push the liquid slugs through the channels, yielding a type of plug flow. Compared to single-phase liquid flow, where the flow in small diameter channels will be laminar (no increased radial transport), mass transfer in multi phase operation is an order of magnitude larger. Slug flow conditions are easily realized under practical conditions. It would therefore be advantageous for single-phase liquid phase reactions to induce Taylor flow by adding an inert gas component. Taylor flow monolith reactors can be operated in cocurrent upflow and downflow mode [10]. Usually monoliths with a channel diameter smaller than 2 mm are applied with a gas to liquid ratio of 1-3 and superficial liquid velocities ranging from 5-15 m s⁻¹ [11].

To further increase mass transfer rates, the wall morphology can be tuned using an ACM monolith. This monolith was developed by the Dow Chemical Company [12] and has a porous wall consisting of small micrograins. The grain size and the pore size are tunable [13]. It was concluded that multiphase fluid mechanics under Taylor flow conditions are different for cordierite and ACM monoliths [14]. The fluid flow inside the walls of the ACM monoliths is influenced by the hydrodynamics in the channel. This enhances the accessibility of the catalyst in the monolith walls, because convection is expected to have a positive effect on the reactor performance.

Flow distribution is a general concern in multiphase reactors, due to the negative influence of maldistribution on reactor performance. Flow distribution in trickle beds [15,16], packed columns [17], and structured packings has been studied extensively. For a monolith reactor, liquid distribution is even more important [1,5,10] due to the absence of mass transport perpendicular to the flow direction.

1.1 Description of the system

In this study, the trypsin-catalyzed hydrolysis of n-benzoyl-L-arginine ethyl ester (BAEE) is used to measure liquid-solid mass transport in a monolith reactor. The reaction scheme is presented in Figure 2. This reaction takes place in aqueous environment at pH 8, and can easily be followed by UV-VIS at 253 nm. This assay has already been used to study covalent immobilization of trypsin in Chapter 5. This enzyme is suitable to be used in mass transfer studies because of its high activity and selectivity. The turnover frequency of enzymes is usually much higher than that of the conventional inorganic catalyst, and the system can be operated under mild conditions with a high energy efficiency. However, as mentioned before enzymes are sensitive for high temperatures and extreme pH. This implies that the biodegradable nature of the enzyme must be considered when performing a series of experiments. Without proper measures, bacterial growth inside the reactor would cause enzyme loss and product contamination.

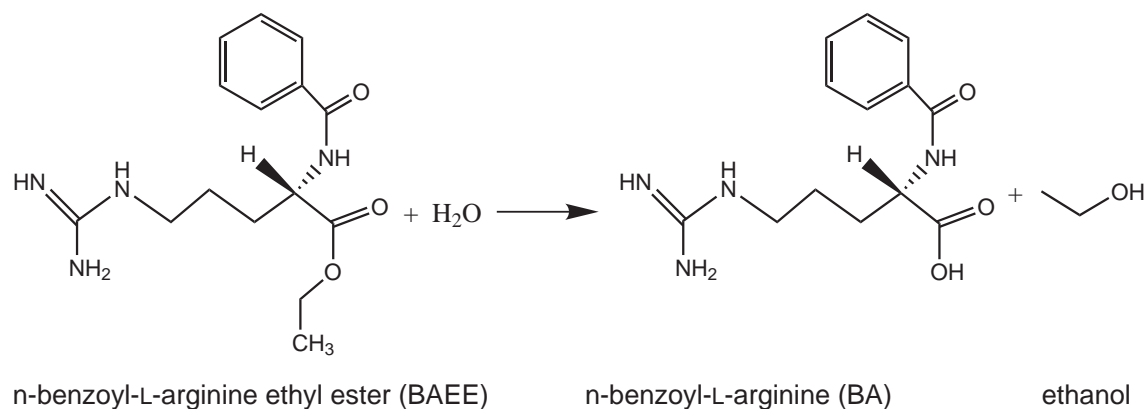


Figure 2. Trypsin catalyzed hydrolysis of n-benzoyl-L-arginine ethyl ester

1.1.1 Trypsin

Trypsin (E.C. 3.3.21.4) is a proteolytic enzyme that hydrolyzes peptide bonds on the carboxyl side of the amino acids arginine and lysine. Additionally the enzyme splits off the amide and ester groups (in case of a terminal position) of both amino acids. Trypsin is one of the three principal digestive proteinases, the other two being pepsin and chymotrypsin. Bovine trypsin consists of 223 amino acids and has a molecular mass of 24 kDa. The diameter of this enzyme is around 4-5 nm. Trypsin has a wide range of industrial and scientific uses, including biotechnological applications (cultivation of mammalian cells), as a protein-degrading enzyme in the processing of trypsin insensitive biopolymers, in detergent manufacturing, and in leather tanning.

1.1.2 Trypsin catalysis

The active site of trypsin is presented schematically in Figure 3. The enzyme belongs to the class of serine proteases that also includes lipase and subtilisin. All serine proteases contain a catalytic triad that has approximately the same configuration and works according to the same mechanism.

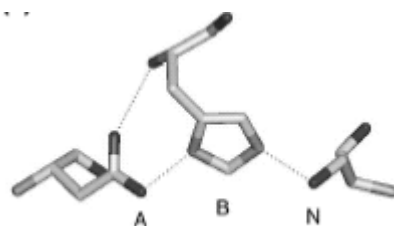


Figure 3. Catalytic triad of trypsin (from [18]). H-bonds are indicated by dotted lines. The base (B) is shown in the center; the acid (A) is shown on the left; the residue that contains the nucleophilic atom (N) is shown on the right. For trypsin, the base B is the imidazole group of Histidine 46, The nucleophile N is the oxygen in Serine-183, and the acceptor A is the oxygen in Asparagine-90

In Figure 4, the series of events that occurs during catalysis of a hydrolysis reaction by a serine protease such as trypsin is presented. First, a Michaelis-Menten complex is formed

between the substrate and the enzyme. Subsequently, the Serin183 is acylated and the imidazol ring transfers a proton from ser-183 to the amine (or alcohol in case of hydrolysis of an ester), which leaves the enzyme-substrate complex. In the last step, the imidazole at his-46 again transfers a proton, this time from a water molecule back to the oxygen at ser-183. The OH^- from the water is added onto the remaining substrate to complete the ester hydrolysis and create the carboxyl-group.

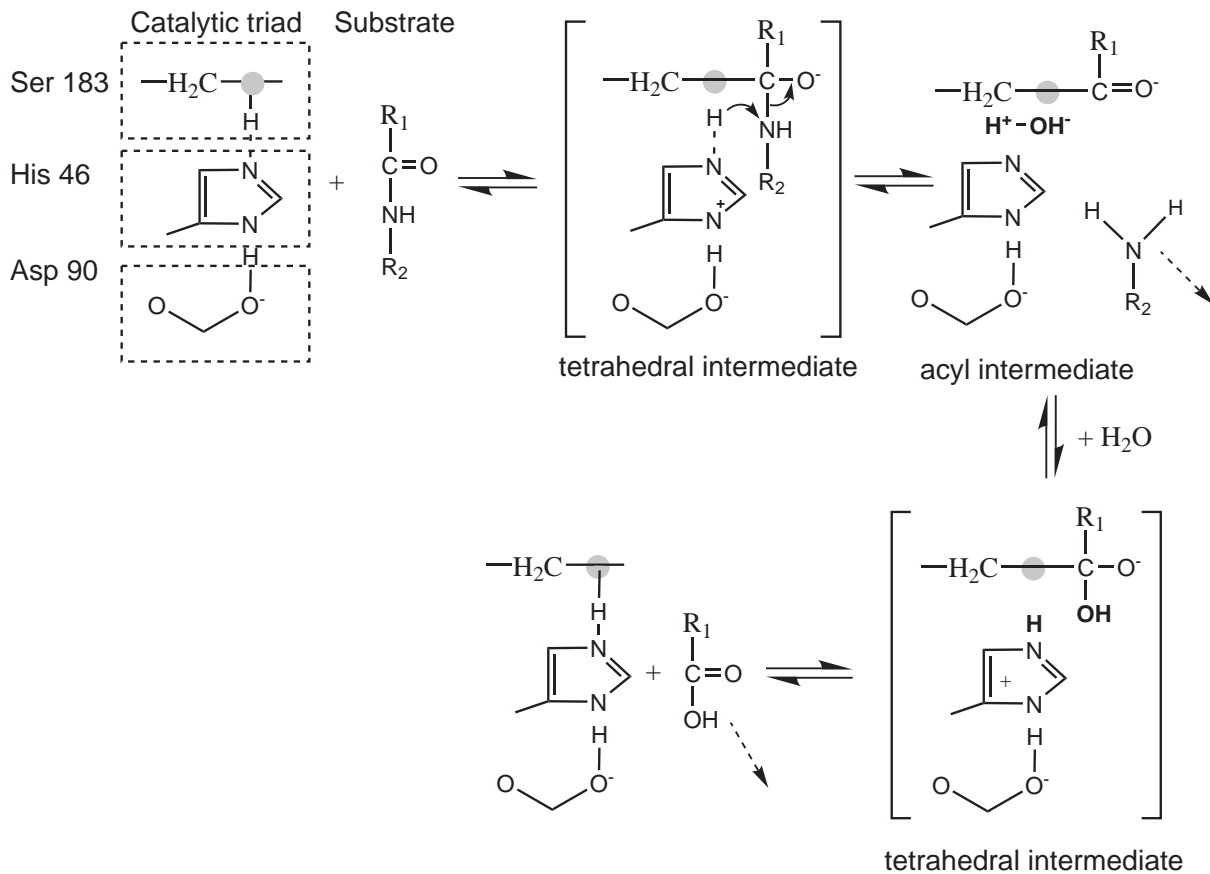
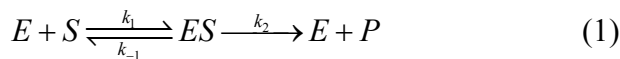


Figure 4. Nucleophilic attack by the catalytic triad of serine proteases on the peptide bond of an amide substrate [18]

The kinetics of trypsin can be described by Michealis-Menten kinetics. For an enzymatic reaction involving a single substrate the general scheme can be represented by:



To analytically solve the macroscopic mass balances, the Michaelis Menten approach assumes a low enzyme concentration compared to [S] and an equilibrium between free and substrate bound enzyme ($k_{-1} \gg k_2$) [19]. This results in the following rate expression:

$$r = \frac{k_2 \cdot e \cdot [S]}{\frac{k_{-1}}{k_1} + [S]} \quad (2)$$

that complies to the general Michaelis-Menten rate expression:

$$r = \frac{V_{\max} \cdot [S]}{K_m + [S]} \quad (3)$$

See also Chapter 2 for a more detailed description. In reality the equilibrium assumption is not always valid, but it is often used because it is easily handled. Equation 3 could also have been derived following the Briggs-Haldane approach [19], by using a less restrictive steady-state assumption for the formation of ES (the rate of formation of ES equals its rate of breakdown in *any* direction, including product formation). The rate expression will now become:

$$r = \frac{k_2 \cdot e \cdot [S]}{\frac{k_2 + k_{-1}}{k_1} + [S]} \quad (4)$$

If the assumption is made that $k_{-1} \gg k_2$, K_m still equals k_{-1}/k_1 and reflects the enzyme's affinity for the substrate. However, this frequent assertion that K_m determines the substrate affinity is dubious in the way that when $k_2 \gg k_{-1}$, K_m becomes k_2/k_1 , and K_m is then bound to be much larger than the dissociation constant. The ideal procedure would be to verify the Michaelis-Menten assumption (fast equilibrium) by measuring K_m and the dissociation constant for ES and comparing them. Experimentally this is unfortunately not possible for a one-substrate system (S and E cannot be mixed without a reaction occurring). So in this study, K_m is regarded as an empirical constant equal to the substrate concentration that gives $\frac{1}{2} \cdot V_{\max}$ under defined experimental conditions. Both V_{\max} and K_m can be determined by conducting a series of experiments at different initial substrate concentrations.

1.1.3 The Monolith Loop Reactor (MLR)

The mass transfer experiments are performed in a monolith-loop reactor. The monolith is placed vertically in a recycle with a tank. The reactor can be operated in continuous or batch mode. The MLR consists of a storage tank from which the liquid is pumped towards the liquid distributor (Figure 5). At the distributor the liquid is evenly spread over the monolith cross-section, and subsequently flows back down to the storage tank. The size of this tank depends on the application; for batch operation the tank volume can be large compared to the monolith volume, for continuous operation the tank serves only to separate gas and liquid phases and should be kept small [4]. The suction that is created by the liquid distributor, combined with gravity ensures that the gas is introduced in the channels at the top-section. In this way, no compressor is required. Compared to a slurry reactor, the MLR has some interesting advantages [4,8]:

- The catalyst and product remain separated
- No catalyst attrition
- Separate heat transfer system from the reaction section
- High gas-liquid mass transfer rates
- Relatively simple construction
- High energy efficiency

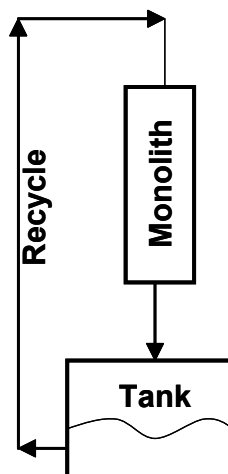


Figure 5. Schematic image of the monolith loop reactor

Because of the large liquid circulation flow rate (monolith residence time typically 2-30 s), the conversion per pass is generally low.

1.2 Immobilization of trypsin

Trypsin has been immobilized on different supports by adsorption [20-22], crosslinking [23], entrapment [24-25], and covalent bonding [26-28]. For application in a monolith loop reactor, a stable carrier is required that can withstand high shear forces and provide a sufficiently high activity to operate in the mass transfer limited regime. Reversibility of the immobilization is not of paramount importance in this study. A very important requirement however, is that internal mass transfer problems should be avoided when measuring L-S mass transfer coefficients. The enzyme should preferably be attached directly onto the monolith surface and not inside the macroporous structure. Adsorption of trypsin would not be a suitable protocol for this application due to expected desorption. Ionic adsorption on polyethyleneimine could improve the enzyme-support bond, but for this typical enzyme, the surface chemistry of the enzyme does not match that of the carrier; trypsin has a high iso-electic point, and in order to become negatively charged the pH must be relatively high. This would result in a weak enzyme support interaction and possible deactivation of the enzyme.

Covalent immobilization has been shown to lead to good results in mass transport measurements [26]. This method provides a strong binding between enzyme and carrier, in combination with a sufficiently high loading. However, the use of glutaraldehyde-based protocols is not recommended due to chemical deactivation of the enzyme, resulting in a

limited window of operation in the MSR under mass transfer limited conditions [29]. In previous studies, enzyme coated monoliths were applied to determine mass transfer characteristics of monolith reactors [26,29]. The enzyme was covalently attached to the monolith support by the (APTES)-glutaraldehyde protocol. After performing the initial hydrodynamics measurements in a monolith loop reactor and a monolithic stirrer [29], it was concluded that enzyme loading needed to be improved in order to remain in the mass transfer limited regime during measurement. The covalent method that was optimized in Chapter 5 yields carriers with a higher enzyme loading and residual activity, and is expected to be suitable for this application.

To investigate the effect of introducing a catalyst with internal diffusion problems, a “Fuzzy wall” monolith is included in the study. This term was introduced by Horvath and Solomon [26], who used coated capillaries with immobilized trypsin to determine mass transfer coefficients. The chitosan-coated monoliths that were developed in Chapter 6, have the same characteristics as the fuzzy wall channels in [26]. They have a high enzyme loading capacity to ensure operation in the mass transfer controlled regime, and a strong enzyme-support bond, so no leaching should take place. But as was already observed by Horvath and Solomon, these catalysts have a high contribution of internal mass transport problems. A schematic cross-sectional view of the monolith channels of both catalysts is given in Figure 6.

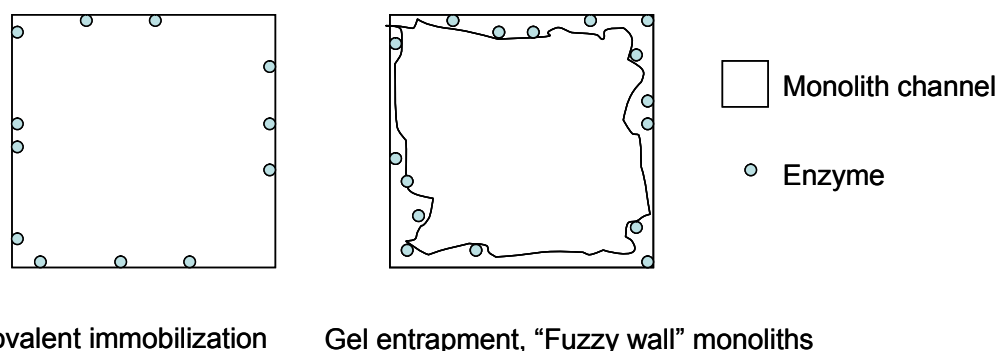


Figure 6. Schematic representation of the two types of monolithic catalysts that are used in the present work

1.3 Layout

The objective is to study in the liquid-solid mass transfer in the monolith loop reactor. First some theory regarding the liquid and gas distribution in monolith channels and mass transfer over the liquid film is given. In the experimental part, the influence of the liquid velocity ($0.5 - 5 \text{ cm s}^{-1}$), the gas velocity ($0-40 \text{ m s}^{-1}$) and the cell density of the monolith (100, 200 and 400 cpsi) are studied for monoliths with different microstructure. After optimization of the covalent protocol (Chapter 5) the same enzyme carrier materials are now applied in the MLR to measure L-S mass transfer coefficients. Chitosan coatings are included in the study to see the effect of internal diffusion limitations on the observed mass transfer coefficient.

2 Hydrodynamics and catalysis in the MLR

2.1.1 Liquid velocity in a single channel

In the monolith loop reactor, the liquid is distributed at the top of the monolith and flows down as a falling film. For a falling film different flow regimes can exist from smooth film flow to turbulent wavy flow [30]. An important dimensionless group that is used as a criterion for flow patterns is the Reynolds number, which can be written for flow through a monolith channel:

$$Re = \frac{\rho \cdot v_L \cdot d_{ch}}{\eta} \quad (5)$$

This correlation describes the level of turbulence. The onset of large disturbance waves in a falling film occurs for values of Re_L above 400 [31]. Also the effect of the liquid distributor on the development of a liquid film can cause some disturbance waves [30].

For a falling film on a vertical plane, the maximum interfacial liquid velocity (v_{Lmax}), the average liquid velocity ($\langle v_L \rangle$), and the film thickness (d_F) can be expressed as a function of liquid velocity [32]:

$$v_{Lmax} = \frac{\rho \cdot g \cdot d_F^2}{2 \cdot \mu} \quad (6)$$

$$\langle v_L \rangle = \frac{\rho \cdot g \cdot d_F^2}{3 \cdot \mu} \quad (7)$$

$$d_F = \sqrt{\frac{3 \cdot \mu \cdot \langle v_L \rangle}{\rho \cdot g}} \quad (8)$$

For the film inside a monolith channel the situation is more complicated because the shape of the liquid film changes with flow rate [30]. The distribution of a falling liquid film in the channels in the presence of a co-current gas phase is not uniform around the wall of a square channel. With MRI imaging, it was shown that for film flow the liquid is primarily located at the corners of the channels [1,5,33]. For a square channel geometry the accumulation of liquid in the corners (Figure 7a) has been reported [7,33]. The resulting meniscus is dependent on the corner angle of the channel (2θ), the distance between the liquid solid contact points ($2l_{wet}$), and the contact angle at the contact line (α) [34]:

$$C_{wet} = \frac{\cos(\theta + \alpha)}{l_{wet}} \quad (9)$$

For square channels and complete wetting $\theta=45^\circ$ and $\alpha=0^\circ$, the liquid distribution in the corner can be described by a quarter of a circle in the channel corner.

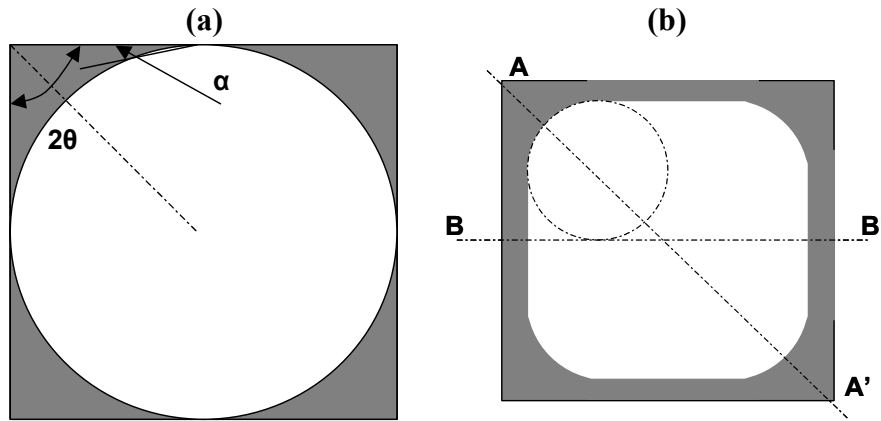


Figure 7. Schematic representation of a monolith channel with the liquid mainly present in the corners. a) film flow with complete wetting of the channel, b) Taylor flow

For Taylor flow, the liquid film is “pressed” into the corners by the passing gas bubbles. The thickness of the film can be described in terms of the capillary number (Ca), the ratio of viscous and internal forces. Strictly, Ca is based on the bubble velocity, but only a small error is introduced by replacing the bubble velocity by the sum of the gas and liquid superficial velocity [9]:

$$Ca = \frac{\eta \cdot (v_L + v_g)}{\sigma} \quad (10)$$

For round channels, Bretherton’s scaling law [35] was established:

$$\frac{d_F}{d_{ch}} \sim Ca^{\frac{2}{3}} \quad (11)$$

For square channels or square channels with rounded corners the effect of the shape is much more important than inertial effects, so the shape of the film can be estimated based on the Capillary number [9]. Kolb and Cerro [36] measured the shape of the liquid film for different Ca over the direction A-A’ and B-B’ (see Figure 7b). For $Ca > 0.04$, the bubble diameter in both directions is the same, while for $Ca < 0.04$ the bubble diameter in the B-B’ direction is independent of Ca [9]. In the A-A’ direction, the dimensionless bubble diameter approaches 1.2 for $Ca \rightarrow 0$. An effective film thickness was calculated for square channels by Kreutzer [9]. From these calculations it can be approximated that:

$$d_{F,eff} = \frac{d_{ch}}{50} \quad (12)$$

2.1.2 Liquid-solid mass transfer

In this study, the liquid solid mass transfer characteristics of the monolith loop reactor are studied. In order for a reaction to take place, the reactants need to be transported to the catalyst layer. For a reaction at a solid catalyst in a three-phase reaction system with an inert gas phase, the following steps can be distinguished:

1. Mass transfer from the bulk liquid to surface of the active catalyst support
2. Diffusion of the reactant in the pores of the support
3. Adsorption of the reactant to the active sites on the support
4. Reaction at the active site of the reactant to the product
5. Desorption of the product from the active site
6. Diffusion of the product to the surface of the active catalyst support
7. Mass transfer of the product from the surface of the active support to the bulk liquid

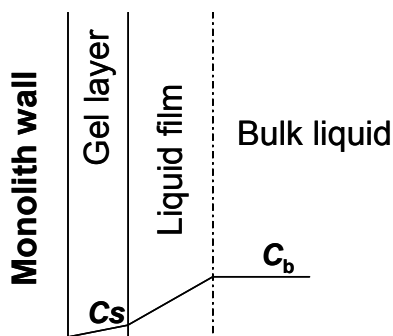


Figure 8. Concentration profile for a liquid phase reactant over the liquid film layer and the carrier material.

Liquid-solid mass transfer takes place from the bulk flow in the monolith channels to the thin catalyst layer on the wall. In case of covalently bonded enzyme, reaction takes place immediately at the wall, whereas for fuzzy wall monoliths the reactants diffuse into the gel layer before reacting with the entrapped trypsin. The concentration profile of the reactant over the film layer is schematically represented in Figure 8 for a gel-coated monolith.

For a liquid phase reactant three different situations can be distinguished:

- **Kinetic limitation.** In this case the rate is determined by the activity of the catalyst. The surface substrate concentration is not zero. This situation occurs if the enzyme loading at the wall is too low. For this situation the reaction rate at the wall is calculated in the model using the Michealis-Menten kinetic equation.
- **Internal diffusion limitation.** In this case the diffusion of the reactant in the active support is rate limiting. This situation is expected to exist for the “fuzzy wall” chitosan-based catalysts.
- **External diffusion limitation.** In this case the mass transfer of the reactant from the liquid bulk to the surface of the active support is rate limiting. In such a case the concentration of the reactant at the surface of the monolith approaches zero. The catalytic activity of the enzyme at the surface is therefore not fully used.

Kinetic limitation

The intrinsic rate is independent of concentration at higher substrate concentration (if $C_b \gg K_m$, $r \approx V_{max}$), but becomes a function of concentration at low C_b . If the system is kinetically controlled (Figure 9a) the supply of substrate from the bulk towards the monolith wall is larger than the rate of conversion. When the catalyst loading on the wall is increased, or the substrate concentration is lowered, a transition regime occurs (Figure 9b).

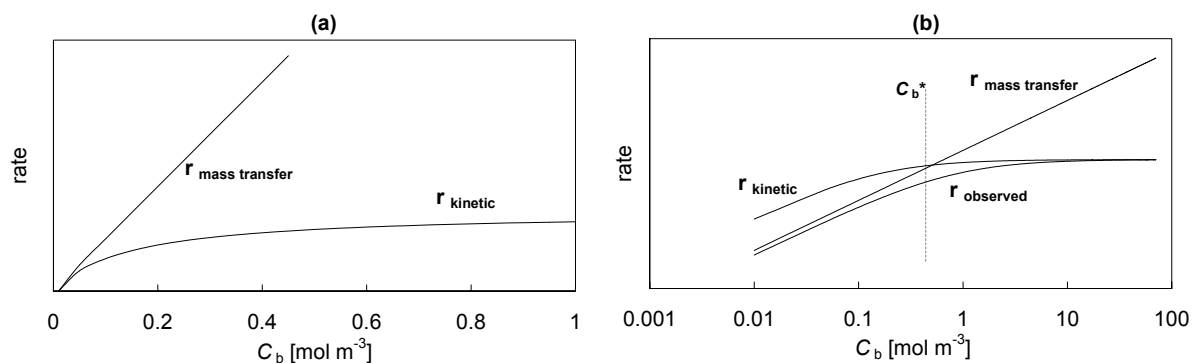


Figure 9. Rate controlling processes during a catalytic reaction. a) kinetically limited, b) transition regime

In this system the reaction rate is kinetically controlled at high substrate concentrations, but at higher conversion (lower C_s), the mass transfer rate becomes limiting. At first, there is a large concentration gradient between the bulk fluid and the wall, resulting in a high flux towards the monolith wall. With decreasing concentration, the transport rate also decreases due to the lower driving force. The reaction is still a zero order reaction at these relatively high substrate concentrations, independent of C_b . At substrate concentration C_b^* , the supply rate becomes limiting and all reactant that is delivered to the enzyme is directly converted. The observed reaction rate is however lower than the mass transfer controlled rate, since this concerns two processes in series. The observed reaction rate can be found by plotting:

$$\frac{1}{r_{obs}} = \frac{1}{r_{mass\ transfer}} + \frac{1}{r_{kinetic}} \quad (13)$$

The observed reaction rate is then a measure for the mass transfer rate. But only if the mass transfer rate is very low compared to the reaction rate, the observed reaction rate equals the mass transfer rate (see Figure 9b). Figure 9 was constructed with the kinetic parameters that were observed in earlier work [29]. C_b^* is found around 0.5 mol m^{-3} . The experiments are performed at a C_b in the transition regime ($0.3\text{-}0.44 \text{ mol m}^{-3}$), to avoid measuring in the kinetically limited regime or at limiting substrate concentrations. Mass transfer is a first order reaction for all concentrations while the reaction is a zero order process at high C_s , but becomes first order at concentrations smaller than K_m . In earlier research [29,37], K_m for immobilized trypsin was found to be around 0.15 mol m^{-3} . It is therefore assumed that for concentrations above K_m first order behavior is an indication for a mass transfer limited situation. Since the enzyme loading capacity of the monoliths has been significantly improved

compared to [29] (Chapter 5), it can be expected that r_{kinetic} in Figure 9b is significantly higher in the present study. This results in a larger difference between r_{kinetic} and $r_{\text{mass transfer}}$, so that $r_{\text{obs}} \approx r_{\text{mass transfer}}$ in the chosen concentration interval.

External diffusion limitations

For a completely mass transfer limited situation the concentration profile of the reactant is primarily located in the inner region of the corners of the monolith. At the walls of the channels depletion of the reactant is observed. The reason for this depletion is the low liquid velocities in these areas. The existence of a kinetically controlled situation can be determined by calculating the Carberry number, Ca , the ratio of the observed rate (in $\text{mol s}^{-1} \text{m}^{-3}$) and the maximal mass transfer rate:

$$Ca = \frac{r_{v,obs}}{a' \cdot k_s \cdot C_b} \quad (14)$$

If a sufficiently high trypsin loading is used, the reactants are converted immediately when they reach the catalyst surface. In this way, the reactant concentration at the catalyst surface approaches zero, so the reaction is completely externally mass transport limited. The observed reaction rate then equals the transport from the bulk to the catalyst layer. Ca is 1 for a completely mass transfer limited situation and 0 for a completely kinetically controlled situation. Based on earlier preliminary experiments and the assumption that this system was mass transfer limited (this means that the observed k_s is also the maximal k_s), Ca is probably between 0.7 and 1 in the present work, so the system will still be in a transition regime. A good indication that the reaction is not kinetically limited is the absence of zero order behavior. In the preliminary experiments, no zero order concentration profile (a straight line) was observed in the chosen concentration interval. But as can be seen in Figure 9b, there is a very broad intermediate regime before the system becomes completely mass transfer limited. These kind of criteria to verify that the measurements are actually performed in the mass transfer limited regime are based on theoretical mass transfer coefficients or intrinsic surface reaction rates (such as the Damköhler number [38,39]). These parameters are exactly the ones we set out to measure, so one ends up calculating in a circle. The most reliable way to use these criteria to verify measuring in the mass transfer limited regime would be to first perform measurements in the kinetically limited regime to determine the intrinsic reaction rate in absence of mass transfer limitations (i.e. at high substrate concentration, see Figure 9b) so Da can be used or to increase the enzyme loading until no further increase in the observed mass transfer coefficient can be measured. Unfortunately, the solubility of BAEE is a limiting factor in this system (maximum substrate concentration is around 1 mol m^{-3} , and the enzyme loading on monoliths can (at this time) not be increased above the optimized loading of Chapter 5. Normally one would also change the temperature or the pH to increase the intrinsic reaction rate. However, in this particular case, a different pH would lead to acid hydrolyzed hydrolysis and an increased temperature would lead to fast deactivation of the enzyme.

Internal diffusion limitations

For the chitosan-coated monoliths, an extra diffusion boundary is present. Reactants and product also have to enter/leave the gel coating in order for the enzymatic reaction to take place. To check whether the internal diffusion of reactants/products through the gel is the rate determining step, the Wheeler-Weisz modulus, the ratio between the observed reaction rate and the diffusion rate through the carrier, can be estimated:

$$\Phi = \eta\phi^2 = \frac{(n+1) \cdot r_{v,obs} \cdot L^2}{2 \cdot D_{eff} \cdot C_b} \quad (15)$$

In the absence of internal diffusion limitations, the Weisz-Prater criterion is valid:

$$\Phi = \eta\phi^2 < 0.15 \quad (16)$$

It is expected that will be $\Phi \gg 0.15$ for the fuzzy wall monoliths, leading to a decreased observed reaction rate and hence an underestimation of the calculated L-S mass transfer coefficient. For the covalently immobilized trypsin no internal diffusion limitations are expected since the enzyme is attached on the outer surface of the channel walls. No enzyme is present inside the non-porous mullite grains nor in the cordierite structure. The macropores of the cordierite monoliths are first filled with a washcoat layer and in the next step all remaining porosity is filled with the organo silane (see also Chapter 4).

Solid-liquid mass transfer measurements in the MLR

During a catalytic reaction, the mass transfer between the liquid and solid phase can be described by equation 17.

$$\phi_{mol} = k_s \cdot a' \cdot (C_b - C_s) \quad (17)$$

The mass transfer per volume of catalyst is determined by the liquid-solid mass transfer coefficient (k_s), the specific surface area (a') and the concentration difference between the bulk liquid (C_b) and the surface of the active support (C_s). For a fast catalyst and low concentrations the surface concentration will be much smaller than the concentration in the liquid bulk. In this case equation 17 can be simplified by the following equation.

$$\phi_{mol} = k_s \cdot a' \cdot C_b \quad (18)$$

The liquid-solid mass transfer coefficient (k_s) for a uniform film layer of thickness $d_{F,eff}$ can be calculated by applying the solution of Fick's law for a stationary film layer.

$$k_s = \frac{D}{d_{F,eff}} \quad (19)$$

The film thickness in a monolith channel, however, is not uniform [5] as was shown before. Therefore, catalyst performance and mass transfer will be expressed in terms of an overall mass transfer coefficient ($k_{eff} = k_s \cdot a'$).

From the concentration profile in the storage tank ($= C_{b,in}$) and the liquid flow rate, the conversion per pass and $C_{b,out}$ can be calculated. The overall average liquid-solid mass transfer coefficient of the monolith is then calculated from the single pass conversion with [30]:

$$k_s a' = \frac{v_L}{L_m} \ln \left(\frac{C_{b,in}}{C_{b,out}} \right) \quad (20)$$

3 Experimental

3.1 Materials

Glutaraldehyde (25% in water), low viscous chitosan (< 200 mPa s), n-benzoyl-L-arginine ethyl ester (BAEE), triethylamine, and NaCNBH₄ (purity $>96\%$) were purchased from Fluka. (3-glycidoxypropyl)trimethoxysilane (GPTMS, 97%) was from Sigma. High molecular weight polyethyleneimine (MW = 60000-1000000), water free was from Aldrich. Buffer salts were of analytical grade and purchased at Baker. Acetic acid ($>95\%$) was from Merck. Novo pancreatic trypsin, type 6 saltfree was kindly supplied by Novozymes. Honeycomb monoliths of ACM (200 cells inch⁻², 31 cells cm⁻²) were prepared by a proprietary Dow process. Cordierite monoliths with cell densities of 100, 200 and 400 cells inch⁻² were supplied by Corning Inc. The length of the monoliths was 22.5 cm. Some important properties are given in Table 1.

Table 1. Key properties of the different monoliths

Monolith	Cell density [cells inch ⁻²]	Wall thickness [mm]	Void fraction [-]	Specific surface area [m ² m ⁻³]	Channel diameter [mm]
C	100	0.43	0.689	1394	2.12
C	200	0.30	0.689	1945	1.49
AM	200	0.35	0.640	>10000	1.44
C	400	0.18	0.740	2788	1.10

3.2 Catalyst preparation

3.2.1 Washcoating

Silica coatings were prepared by dipping the monoliths in a colloidal (Ludox-AS40) suspension for 5 min, followed by horizontal rotating overnight and calcination at 673 K for 4

h (heating rate 2 K min⁻¹). For ACM monoliths a diluted (10 x) Ludox solution was used to prevent filling of the porous wall.

3.2.2 Immobilization of trypsin in chitosan layers

Chitosan powder 1% (w/v) was added to 1% (v/v) acetic acid and gently stirred for 3 h at room temperature. Undissolved matter was removed by filtration over a 100 µm mesh filter. Monoliths were coated with chitosan gel by dip-coating. Monoliths were held in a chitosan solution containing 1.1 % w/v glutaraldehyde for 60 sec. After cleaning the channels, samples were air dried under ambient conditions for 90 min. Gels were washed with water and 10 mM phosphate buffer pH8. Trypsin was immobilized on the carriers from a 3 g l⁻¹ solution in 0.1 M phosphate buffer pH 7.5.

3.2.3 Covalent immobilization of trypsin via ALD/IM

Functionalization of the monolith starts with reaction of the GPTMS to form a diol and subsequent coupling to the silica washcoat [3]. The epoxide-group was reduced by treating 4.5 ml GPTMS in 300 ml HNO₃ (pH 2) at 363 K for 1 h. The pH was raised to 7 by adding 0.5 M sodium acetate and a monolith was kept in this solution for 6 h. The product was then oxidized with 400 ml of a 70 mM NaIO₄ solution in 0.1 M acetate buffer pH 4.5 to form the aldehyde groups. Trypsin was immobilized on the carriers from a 3 g l⁻¹ solution in 0.1 M phosphate buffer pH 7.5. Cyanoborohydride (1 g l⁻¹) was added to reduce the imine bonds.

The protein concentration during immobilization was determined using UV-VIS at 260 nm. Samples were measured in a 1 cm quartz cuvette with a Thermo Electron Unicam 540 spectrophotometer. After immobilization, the samples were washed with phosphate buffer pH 7 and excess distilled water, and stored in 0.1 M phosphate buffer pH 8 with 1 g l⁻¹ sodium azide at 278 K.

3.3 **Characterization**

The amount of coating, mass increase, and mass decrease were determined by measuring the sample weight before and after the various preparation steps. The carrier yield was calculated as:

$$Y_C = \left(\frac{w}{w_s + w} \right) * 100 \quad (21)$$

where w_s is the mass of the support and w is the carrier mass.

The average thickness of the chitosan gel layer was calculated by:

$$L_{chitosan} = \frac{m_{chitosan} / \rho_{chitosan}}{\frac{\pi}{4} \cdot d_m^2 \cdot L_m \cdot a'} \quad (22)$$

Where $m_{chitosan}$ and $\rho_{chitosan}$ are the mass and density of chitosan filtrate, d_m and L_m are the diameter and height of the monolithic structure and a' is the specific surface area. Because the monoliths are washocoated with SiO_2 and subsequently silanized, it is assumed that the chitosan gel will be present only on the outside of the channel walls in case of cordierite. For ACM monoliths the gel is assumed to fill the wall. The density of 1.0 % chitosan filtrate is assumed to be equal to the density of water.

3.3.1 Kinetic measurements

The activity of the free and immobilized trypsin was followed spectrophotometrically for the hydrolysis of n-benzoyl-L-arginine ethylester in an aqueous phosphate buffer at 290-318 K. Kinetics were studied with smaller (length 5 cm, diameter 4.3 cm) cordierite monoliths, free enzyme and crushed monolith. Initial substrate concentration was 0.3 g l^{-1} in a 50 mM phosphate buffer pH 8. Total reaction volume was 0.16 l. The absorbance was measured at 253 nm. Catalysts were compared for their initial activity (0-30 min), calculated from (the initial linear part, $t = 1$ to $t = 5$ min) of the concentration/time plot. The experimental set-up consists of a glass reactor with a stirrer and a recycle mechanism to force the liquid circulation through the monolith channels. A schematic overview of the experimental set-up is presented in Figure 10. To prevent operation with external mass transfer limitations, the maximum possible rate (without the formation of a vortex that disturbs the liquid circulation) of 500 rpm was selected for all experiments with monolithic biocatalysts. For free trypsin and crushed monolith, 650 rpm was used. A 1 cm quartz cuvette was used to measure the absorbance at 253 nm. The system was calibrated for both reactant (BAEE) and the product (n-benzoyl-L-arginine, BA), as described in Chapter 5. With this calibration, absorbance data from the enzyme assay was converted to concentration/time data in order to follow the activity of the monolithic biocatalysts.



Figure 10. Experimental set-up with glass reactor, onset, and stirrer

3.3.2 Liquid-solid mass transfer in the MLR

The set-up for the measurements in the monolith loop reactor is schematically presented in Figure 11. The liquid flow through the monolith section is adjusted by varying the pump speed and by opening the bypass valve. The gas flow rate is set by controlling the N_2 mass flow controller. A gear pump (micropump) was used to circulate the liquid through the set-up. A filter was installed to protect the pump. Liquid flows of $0.83\text{--}3\text{ l s}^{-1}$ were used. Gas flow was fixed at 0.36 l s^{-1} , the lower limit for adequate operation (10% of the maximum throughput) of the mass flow controller. Monoliths were placed inside a glass tube with an inside diameter of 44 mm and a length of 0.25 m. The gap between the top of the monolith and the glass tube was sealed with gasket tape to prevent bypass. The liquid coming from the liquid container was sprayed on the monolith with a nozzle (Spraying Systems Fulljet nozzle with a conical spraying pattern). The nozzle height was adjusted for the different flow rates to get optimal liquid distribution in the monolith. The total liquid volume was 4 l, with a substrate concentration of $0.25\text{--}0.3\text{ g l}^{-1}$. The inlet concentration in the reaction section was followed in-line by a UV-VIS spectrophotometer (Thermo Electron Unicam 540) equipped with a 1 cm quartz flow cell and a peristaltic pump (12 ml min^{-1}).

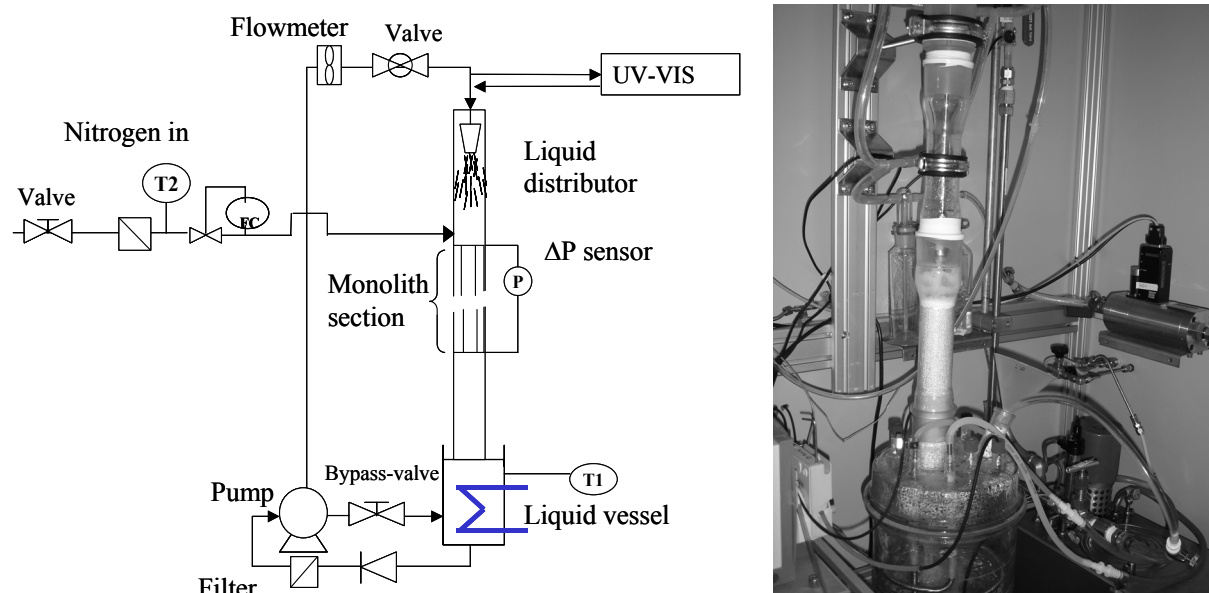


Figure 11. The Monolith Loop Reactor (MLR)

3.4 Nomenclature

Samples names are coded depending on the monolith type and the washcoat layer. The first letter of the samples is used to distinguish the monolith type, “C” is used for cordierite, “A” for ACM. A second letter is used in the case of ACM to determine the microstructure of the ACM; “M” for medium needles. Finally the applied immobilization protocol is defined with “Chit” for chitosan coatings and “ALD/IM” for covalent immobilization. This is summarized in Table 2.

Table 2. Nomenclature

Position	Component	Code
1	Monolith type	C or A
2	Micro grain structure ACM	M
3	Immobilization method	Chit or ALD/IM

4 Results and Discussion

4.1 Yield and layer thickness

The loading of the different carrier materials on the 200 and 400 cpsi monoliths is in the same order of magnitude as was seen before for the different methods when smaller monolith pieces were used. The mean yield and layer thickness on cordierite and ACM monoliths are presented in Table 3. The chitosan loading on the monoliths is in agreement with earlier results (see Chapter 6). The layer thickness on 400 cpsi cordierite monoliths is slightly lower than for the 2 cm monoliths that were used in Chapter 6 for the hydrolysis of penicillin G.

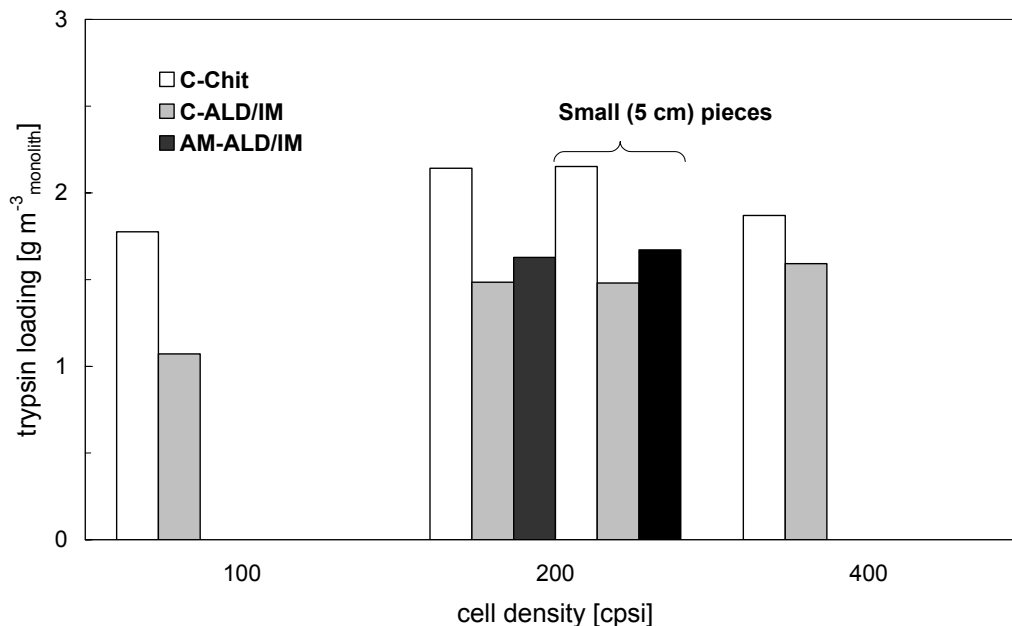
Table 3. Support preparation with different 100, 200 and 400 cpsi monoliths.

Support	Cell density	Y_{carrier} (total carrier volume)	Layer thickness (L)
C-Chit	100 cpsi	22% (45 ml)	96 μm
	200 cpsi	26% (48 ml)	75 μm
	400 cpsi	30% (50 ml)	60 μm
AM-ALD/IM	-	-	-
C-ALD/IM	-	-	-

The gel application on the long monolith pieces did not lead to visible maldistribution inside the channels, but it is possible that the gel layer is not completely homogeneous throughout the monolith. Especially for the small channels of the 400 cpsi samples this can lead to slight deviations in the coating yield. From TGA analysis (not shown) over different sections (top, middle, bottom) of the monolith only small deviations (below 5 wt%) were observed.

4.2 Enzyme immobilization

The immobilization of trypsin via the proposed methods leads to carriers with different final enzyme yield. To get an indication of the distribution of the enzyme throughout the monoliths, the enzyme loading per monolith volume is compared with the loading of the smaller monoliths that were prepared in Chapters 5-6. The results for the different carrier materials are present in Figure 12.

**Figure 12.** Trypsin immobilization on monoliths with different cell densities and enzyme carrier materials

The values are corrected for a subsequent 90 min washing step to remove loosely bound enzyme. The monoliths have a length of 22.5 cm, which is five times longer than the monolith pieces that were used before. The total trypsin loading is in the same order of magnitude as roughly 5 times the values that were observed in Chapter 5 for covalent immobilization and in

Chapter 6 for gel entrapment. Thus, the immobilization method did not seem to be affected by an increased monolith length. As could be expected, the chitosan carrier has the highest immobilization capacity. Immobilization on AM-ALD/IM seems slightly lower than for C-ALD/IM, but the diameter of this sample is slightly smaller. Per monolith volume, the trypsin loading on ACM is 10% higher than for cordierite. This was also observed for lipase and lactase in combination with carbon carriers (Chapter 8). For PEI-monoliths (Chapter 7) this difference was larger due to the cumulating effect of better PEI binding and the higher immobilization yield when more PEI is present.

4.3 Kinetic experiments with free and immobilized trypsin

Although for monolithic catalysts the operation in the MLR is probably outside the kinetically limited regime, crushed monolith and free enzyme can be tested in a stirred vessel without mass transfer limitations. The initial reaction rate of was followed at a substrate concentration of 0.3 g l^{-1} for different amounts of free trypsin and crushed monolith (C-ALD/IM). The effect of catalyst concentration on the initial rate of hydrolysis of BAEE is presented in Figure 13.

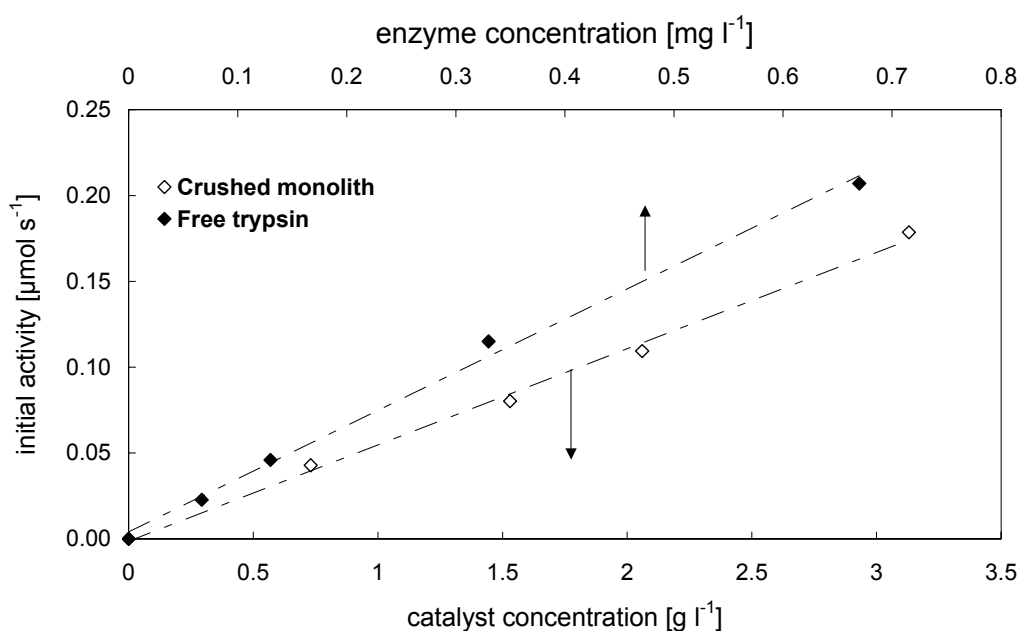


Figure 13. Effect of catalyst concentration on the initial reaction rate in the hydrolysis of BAEE with free and immobilized trypsin. Experiments were performed in a glass reactor ($V=150 \text{ ml}$) at 306 K , 650 rpm with a substrate concentration of 0.3 g l^{-1}

The initial reaction rate increases with catalyst concentration. When there is no catalyst, no reaction takes place. The linear trend indicates a first order dependency of the enzyme. Furthermore it follows from Figure 13 that no mass transfer limitations are present under the current conditions. The kinetic measurements were performed with a free trypsin concentration of 6.7 mg l^{-1} and a crushed monolith concentration of 1.5 g l^{-1} .

To determine K_m and V_{\max} , a series of experiments was performed at different substrate concentrations. In Figure 14a, the initial rate is plotted as a function of the substrate

concentration. This curve becomes asymptotic to a horizontal line that represents V_{\max} . The Michaelis constant, K_m , is defined as that concentration of substrate that gives "half-maximal activity". If the curve is extrapolated to negative values, it becomes asymptotic to a vertical line at $-1/K_m$ (not shown). However, presentation of kinetic data as in Figure 13a is not especially useful. Such data may be better presented in a different form. A frequently used alternative presentation is the double reciprocal or Lineweaver-Burk plot. In double reciprocal plots the y-intercept represents $1/V_{\max}$, while the x-intercept represents $1/K_m$. The down-side of double reciprocal plots is that low concentrations of substrate contribute unevenly to errors with these plots. Much of this problem is avoided if one plots C_b versus $C_b/\text{initial rate}$ (Hanes plots) or initial rate versus initial rate/ C_b (Hofstee plot). In Figure 14b, the Hofstee plots of free and immobilized trypsin are given. The Hofstee plot was constructed to transform the Michaelis-Menten equation into a linear equation:

$$r = -K_m \frac{r}{C_s} + V_{\max} \quad (23), \text{ with intersect } V_{\max} \text{ and slope } K_m.$$

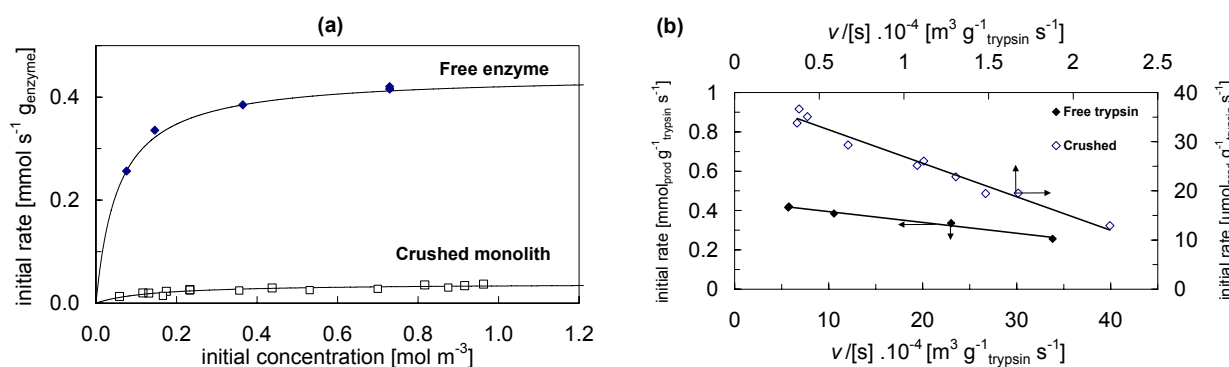


Figure 14. Determination of the kinetic parameters of free and immobilized trypsin. a) Michaelis Menten plot, b) Hofstee plot. Experiments were performed in a glass reactor ($V=150$ ml) at 306 K, 650 rpm with a substrate concentration of 0.05-0.3 g l⁻¹

The kinetic parameters that follow from Figure 14b are given in Table 4.

Table 4. Values of V_{\max} and K_m for free and immobilized (crushed C-ALD/IM) trypsin at 306 K in batch reactor, 150 ml 650 rpm

	Free trypsin	Crushed monolith (C-ALD/IM)
K_m [mol m ⁻³]	0.055	0.13
V_{\max} [mol s ⁻¹ g _{enz} ⁻¹]	4.4×10^{-4}	3.6×10^{-5}

The values for K_m and V_{\max} under these conditions are in good agreement with earlier research [29,37]. After immobilization, K_m increases by a factor 2. The increase in K_m after covalent trypsin immobilization has been reported to be around 1.5-3 [40,41]. This increase is attributed to conformational changes of the enzyme during immobilization, which limit the freedom of movement during reaction. These authors also report a similar 10 times decrease of V_{\max} .

In Figure 14a, the solid lines represent a simulation of the initial rate as a function of substrate concentration. As was mentioned before, if a reaction is mass transfer controlled, the concentration is a natural logarithm of reaction time (first order). But for concentrations below K_m , the kinetically controlled reaction rate also shows this logarithmic dependence. Since K_m was found to be around 0.13 for the immobilized enzyme, possible first order behavior in the chosen concentration interval of 0.3-0.44 mol m⁻³ should be due to mass transfer limitations.

The effect of temperature on the initial reaction rate was studied in the interval 298-318 K. The observed rate constant, k , for a given reaction changes with temperature. The plot of $\ln k$ versus $1/T$ gives a linear plot with a negative slope. E_a represents the activation energy for the reaction, in kJ mol⁻¹. The equation of the line for the graph is:

$$\ln\left(\frac{k}{k_0}\right) = \frac{E_a}{R} \left(\frac{1}{T_2} - \frac{1}{T_1}\right) \quad (24)$$

The observed reaction rate constant (k) was normalized for the rate constant (k_0) at 298 K. From the slope of the trend line ($=-E_a/R$) in Figure 15, an apparent activation energy of 53 kJ mol⁻¹ can be calculated. This is in agreement with values found in other studies [42] (55 kJ mol⁻¹).

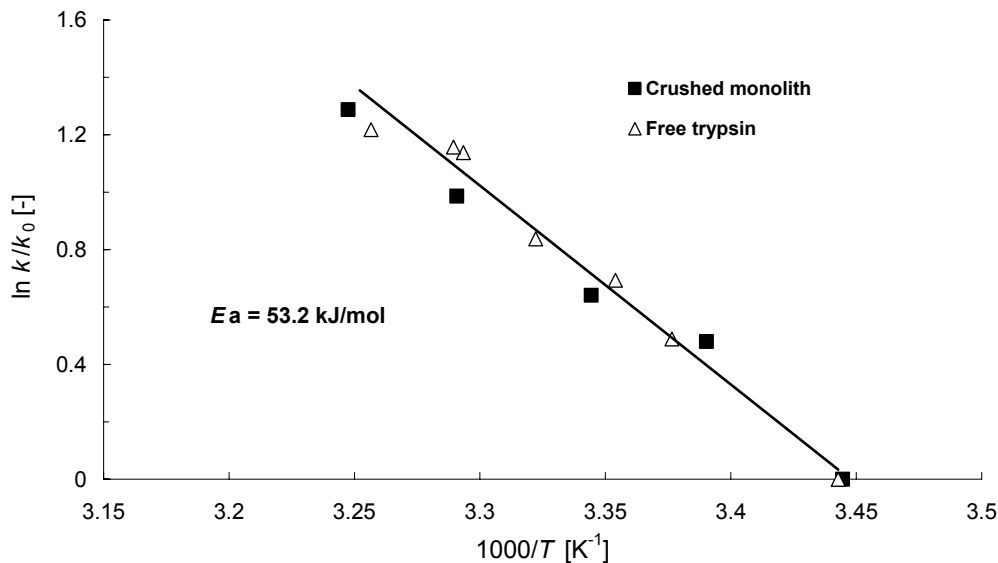


Figure 15. Arrhenius-plot for free enzyme (Δ), and crushed C_{ALD}/IM (\blacksquare) in batch reactor at 650 rpm, $C_b = 0.3$ g l⁻¹

4.4 Liquid-solid mass transfer in the MLR

To determine the liquid solid mass transfer coefficient (k_{eff}) in the monolith loop reactor, a monolith with immobilized trypsin was used for the hydrolysis of BAEE under different conditions. Trypsin was immobilized on monoliths (diameter = 4.3 cm, length = 22.5 cm)

with different cell density and via different methods. Trypsin was attached directly onto the monolith channel to ensure the absence of internal diffusion limitations. Some important parameters of the reaction mixture are presented in Table 5.

Table 5. Used parameters

Parameter	Value
Density, ρ	995 kg m ⁻³
Viscosity, η	7.86 x 10 ⁻⁴ Pa s
Diffusivity, D	6 x 10 ⁻¹⁰ m ² s ⁻¹
Effective Diffusivity, D_{eff} in chitosan	4 x 10 ⁻¹⁰ m ² s ⁻¹

The effective diffusion coefficient (D_{eff}) of the reactant in the chitosan gel was estimated to be 4x10⁻¹⁰ from the diffusivity (D):

$$D_{eff} = \frac{D \cdot \varepsilon_{gel} \cdot \sigma}{\tau} \quad (25)$$

with σ (constriction factor) taken as unity. The gel has a very high water content and has almost the same properties as water, ε_{gel} is assumed to be 0.8. The tortuosity of the gel (the ratio of the actual distance a molecule travels between two points and the shortest distance between those points, τ) is therefore assumed to be very close to unity and taken as 1.2.

This gives $D_{eff} = 2/3 D$ for diffusion inside the chitosan layer.

To verify operation in the external mass transfer limited regime, the temperature was chosen to be 308 K. This temperature was indicated to be sufficiently high in preliminary experiments. During use at higher temperatures for a series of experiments, the enzyme starts to deactivate (see Chapter 5). Furthermore, the total enzyme loading has been significantly improved compared to earlier studies [29], see also Chapter 5. This assumption was verified by calculating Ca for the monolith with the lowest reaction rate (100 cpsi, C-Chit and 100 cpsi C-ALD/IM) at the highest flowrate ($v_L = 5.7 \text{ m s}^{-1}$):

$$Ca = \frac{r_{v,obs}}{a' \cdot k_s \cdot C_b} \quad (14)$$

To estimate the mass transfer coefficient, the maximal k_s (1.5x10⁻⁵) that was found in preliminary experiments was used in equation 14. If mass transfer is slower than conversion in the case of the lowest reaction rate, it will also be slower for increased enzyme loading and decreased liquid flowrate. For C-Chit and C-ALD/IM, Ca becomes 0.6 and 0.7 if the initial substrate concentration is used in equation 14. It can be assumed that for operation in the chosen substrate concentration interval (0.3-0.44 mol m⁻³), all experiments were operated in the mass transfer limited regime. Indeed, $Ca \gg 0.05$ for all experiments.

For ACM monoliths however, the available surface area is much higher, leading to enhanced mass transfer. Assuming the same surface area as for cordierite, Ca varies between 0.5 and 0.6 for AM-ALD/IM. For these samples, the system will probably not be completely mass transfer limited, especially at the higher flow rates.

Chitosan-coated “fuzzy wall” monoliths were included in the study to see if it would be possible to distinguish catalysts with severe internal diffusion problems from the externally limited-only situation and prevent the generation of erroneous data.

4.4.1 Single pass conversion

To get an indication of the conversion per pass during operation of the MLR, a 200 cpsi AM-ALD/IM sample was used at a liquid flowrate of 50 l h^{-1} under single pass operation (the reaction mixture was not allowed to circulate, but was directly transferred into a second vessel after passing the monolith section). This process was repeated several times. The concentration profile is presented in Figure 16. The concentration of the in- and outgoing mixture increases stepwise. Due to the decreased substrate concentration, the conversion per pass decreases significantly above 0.2 g l^{-1} of product. The catalyst used in this experiment shows the highest initial rate of all tested catalysts, and therefore the highest conversion per pass just in the chosen interval for measuring mass transfer. A conversion per pass of around 0.6 was observed. For C-ALD/IM and C-Chit samples, the conversion per pass varied between 0.05 and 0.4. To prevent the pump from running dry, not all liquid could be passed through the monolith.

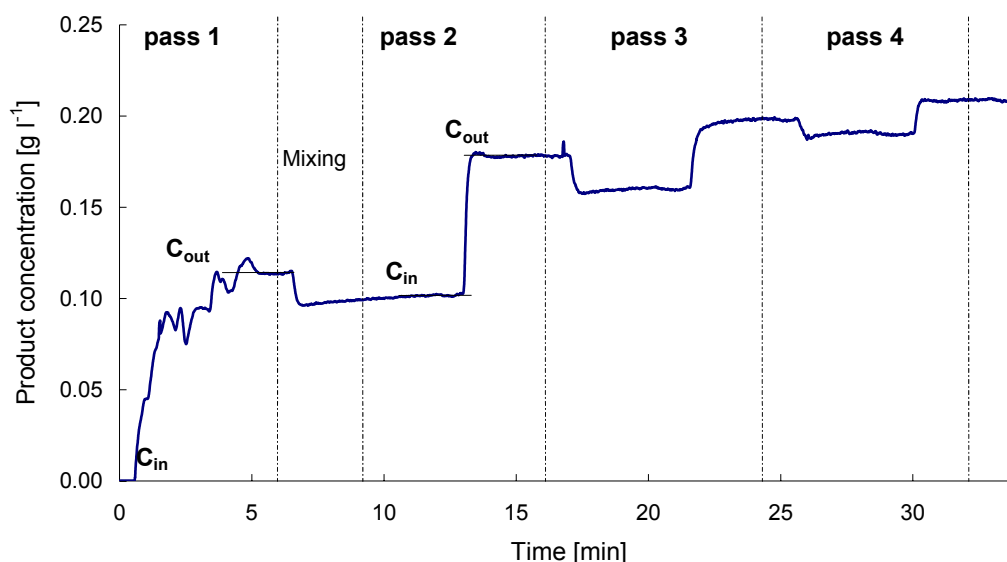


Figure 16. Single-pass run with 200 cpsi AM-ALD/IM. The experiment was performed at $C_b = 0.25 \text{ g l}^{-1}$, 306 K , $v_g = 40 \text{ cm s}^{-1}$ and $v_L = 2.1 \text{ cm s}^{-1}$.

Around 0.5 l of reaction medium remained in the recycle line. Before starting the second pass, this was mixed with the liquid that had reacted in the previous pass. This mixing process causes a small step in the product concentration, as indicated in Figure 16.

The stability of the catalysts at high shear force was studied by performing a second experiment at the conditions of the first experiments after completing the whole series. No differences in initial reaction rate were observed. Apparently the catalysts are stable and can be used several times in the MLR without deactivation.

4.4.2 Effect of cell density for cordierite monoliths

The effect of cell density on the observed effective mass transfer coefficient ($k_s a^?$) was studied by using 100, 200, and 400 cpsi cordierite monoliths. The results for chitosan-based and ALD/IM monoliths are given in Figure 17 for different superficial liquid velocities.

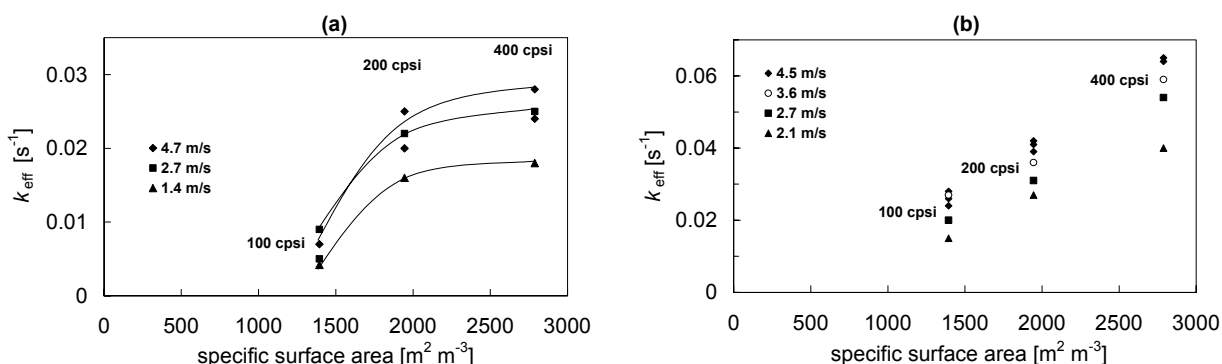


Figure 17. Effect of cell density on the effective mass transfer coefficient in the MLR for a) C-Chit samples, b) C-ALD/IM. Experiments were performed with $C_b = 0.25 \text{ g l}^{-1}$, $v_g = 40 \text{ cm s}^{-1}$, at 308 K.

The different cell densities are expressed in terms of specific surface area (m² m⁻³). For the chitosan-based catalysts (Figure 17a), there is a clear upward trend with increasing cell density. At lower liquid velocity however, there is an initial increase in k_{eff} , but above 2000 m² m⁻³ only a marginal effect is observed.

Since the fuzzy wall monoliths probably have an uneven distribution of chitosan throughout the channels and also a large contribution of internal diffusion limitations, the combination of these factors results in a different behavior. On 400 cpsi samples the enzyme loading is higher (Figure 12), and the gel loading (layer thickness) is lower (Table 3) for these samples. It seems that the opposite effects of increased conversion rate and decreased layer thickness cancel each other out, therefore the internal diffusion limitations do not decrease. No positive effect on k_{eff} compared to 200 cpsi is observed for using 400 cpsi samples. To quantify the internal diffusion limitations, the Wheeler-Weisz modulus was estimated for the C-Chit samples from equation 15:

$$\Phi = \eta \phi^2 = \frac{(n+1) \cdot r_{v,obs} \cdot L^2}{2 \cdot D_{eff} \cdot C_b} \quad (15)$$

As was seen in Table 3, the gel loading is constant for the C-Chit samples with increasing cell density. This results in a decreased layer thickness at higher cell density. Therefore the

estimated Φ and thus the internal diffusion problems decrease at higher cell density. For 100 cpsi samples Φ is around 3, whereas for 200 and 400 cpsi Φ is around 1.5.

For these gel-coated samples, the internal mass transport becomes the limiting step at higher specific surface area.

Compared to earlier studies [37] the measured k_{eff} is a factor 10 higher. The enzyme loading in the previous work was significantly lower; it is possible that the results in [37] were acquired under kinetically limited conditions. But since the present study is performed at significantly higher liquid flow-rates and thus probably in a different flow regime, it is not useful to compare the results from the different experiments.

4.4.3 Effect of gas velocity

The effect of the gasflow rate is expected to be very small at these high gas flowrates of 40 cm s^{-1} . The gas velocity was varied between 10 and 40 cm s^{-1} , at a liquid velocity of 5 cm s^{-1} . For the cordierite samples with different carrier materials the gas velocity does not seem to affect the observed k_{eff} . For AM_ALD/IM however, a slight increase is observed. This could be caused by the gas flow “pushing” the liquid more inside the wall, resulting in an increased participation in the hydrolysis reaction of the enzyme that is present inside the porous wall.

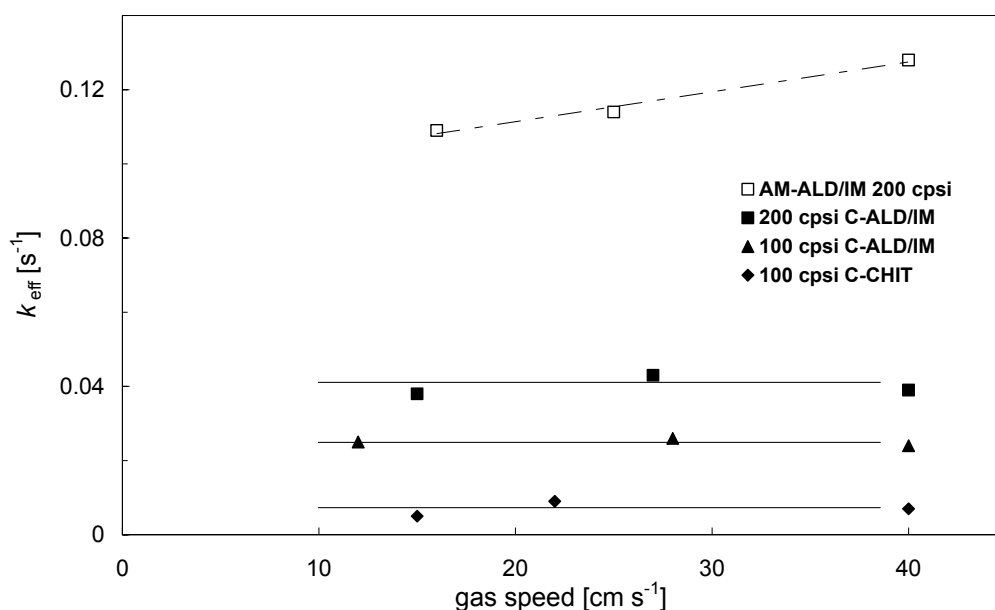


Figure 18. Effect of gas flow rate on the effective mass transfer coefficient in the MLR. Experiments were performed with $C_b = 0.25 \text{ g l}^{-1}$, $v_L = 5 \text{ cm s}^{-1}$, at 308 K .

4.4.4 Effect of liquid velocity

The effect on k_{eff} of the superficial liquid velocity, v_L , is presented for fuzzy wall monoliths and ALD/IM catalysts in Figure 19.

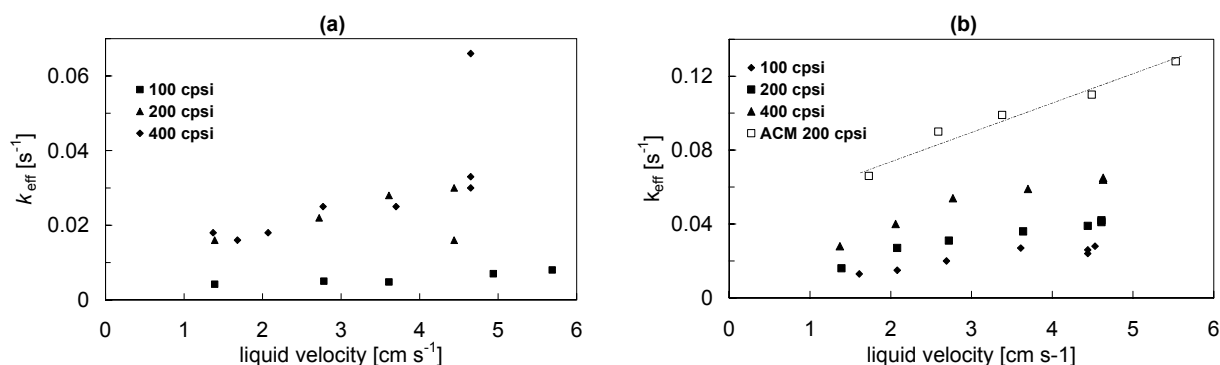


Figure 19. Effect of liquid flow rate on the effective mass transfer coefficient in the MLR. a) C-Chit, b) C-ALD/IM and AM-ALD/IM. Experiments were performed with $C_s = 0.25 \text{ g l}^{-1}$, $v_g = 40 \text{ cm s}^{-1}$, at 308 K.

If we compare the values for k_{eff} that are observed with samples that suffer from internal diffusion limitations (Figure 19a) to the values that were observed with covalently attached enzyme (Figure 19b), it becomes clear that the presence of internal diffusion limitations leads to a significant underestimation of the effective L-S mass transfer coefficient. For all C-Chit samples, a slight increase in k_{eff} (Figure 19a) is observed with increasing liquid velocity. A five-fold increase in liquid flow-rate leads to a 50% increase in k_{eff} . This moderate effect of liquid velocity is an indication that the measurements are performed near or in the Taylor flow regime. For the 400 cpsi samples, k_{eff} does not increase compared to 200 cpsi. As was seen before, these samples have a $\Phi > 1$. These internal diffusion limitations can explain why in Figure 19a the data for 200 and 400 cpsi are in the same order of magnitude. Apparently the transport of the reactant towards the catalyst (through the gel layer) is the rate-limiting step at higher cell density.

For the C-ALD/IM samples, also a moderate effect of liquid velocity on k_{eff} was observed (Figure 19b). Only for AM-ALD/IM the effect of v_L on k_{eff} is more pronounced, because here also the open monolith wall can participate in the reaction. So at higher liquid flow-rates, the wall becomes more filled with liquid and the observed L-S mass transfer is increased.

Apparently, the use of fuzzy wall monoliths leads to an underestimation of the observed mass transfer coefficient. It is very important to analyze the system before measuring, to prevent the generation of incorrect data. This analysis should include possible internal diffusion problems and an estimation of the conditions in terms of flow regime and mass transfer. In the following paragraph, the present system is analyzed and compared with earlier studies. Since the chitosan-based samples suffer from internal mass transfer limitations, they are not included.

4.4.5 Hydrodynamics

To verify the operation of the system in the Taylor flow regime, the flow in the monolith channels is analyzed in more detail in this section.

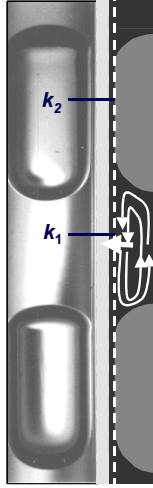


Figure 20. Schematic presentation of L-S mass transfer

$$Sh = \frac{k_s \cdot d_{ch}}{D} \quad (26)$$

The total Sh in the monolith channel is a combination of the two Sherwood numbers:

$$Sh_{tot} = \left(\frac{1}{Sh_1} + \frac{1}{Sh_2} \right)^{-1} \quad (27)$$

From the experimental data values for Sh_1 were found to vary between 30-50.

With these data the film thickness can be estimated by combining equation 19 with an expression for k_s :

$$k_s = \frac{D}{d_F} \quad (28)$$

For all experimental data points, d_F was found to be around 30-60 μm . Considering the varying channel diameter for the different monoliths and comparing with equation 12:

$$50 \approx \frac{d_{ch}}{d_{F,eff}} \quad (12)$$

was found to be true for all measurements with C-ALD/IM and AM-ALD/IM. Apparently all measurements have been performed in the Taylor flow regime. However, to determine the exact flow regime, a more detailed analysis was performed. Sh_{tot} values were plotted against Gz for all experiments. The Graetz number is a function of Re (equation 5) and the Schmidt number, Sc :

$$Gz = \frac{L_m}{Sc \cdot Re \cdot d_{ch}} \quad (29)$$

Sc is defined as the ration between the hydrodynamic boundary layer and the mass transfer boundary layer:

$$Sc = \frac{\delta_h}{\delta_m} = \frac{\eta}{\rho \cdot D} \quad (30)$$

In Figure 21, the results for Sh as a function of Gz are presented together with the data of Horvath and Solomon [44], translated to the present conditions. For this plot, the model value of Sh_1 was calculated according to [9]. From Figure 21, it seems that the experimental data are in good agreement with the model values that are expected for a system with square channels. However these data are based on a theoretical film thickness, which is not known exactly for this system [9]. Several authors [36,45-46] have reported values of $d_{ch}/d_{F,eff}$ between 20 and 50, giving a broad range of values for Sh . It can therefore not be concluded from these data that the system is in the mass transfer limited regime, it is still possible that the calculated values for Sh are an underestimation of the theoretical values for the liquid phase system.

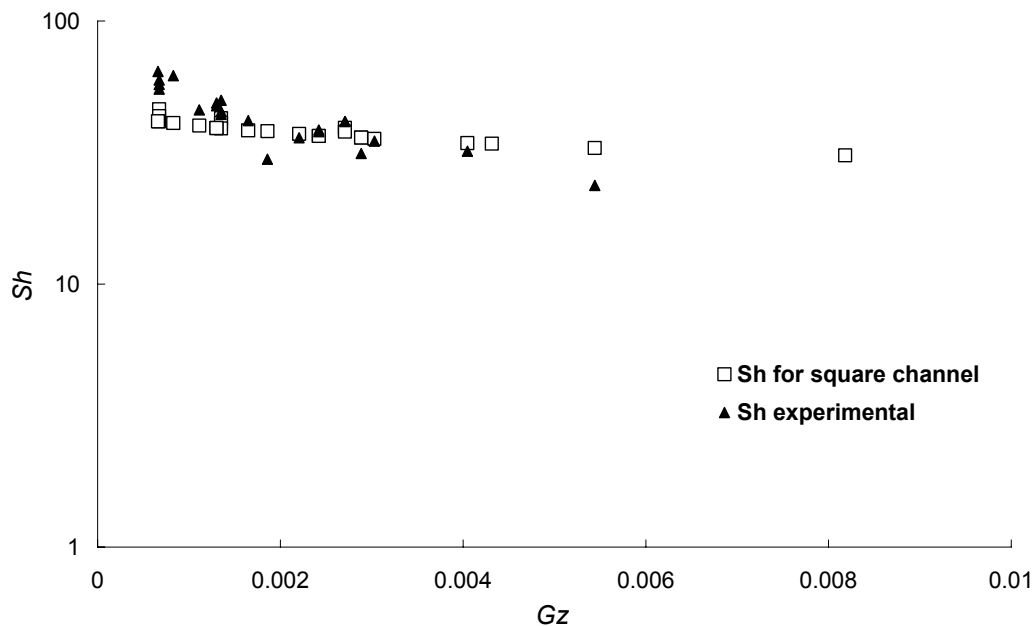


Figure 21. Experimental data and model values [44] for Sh as a function of Gz

This is illustrated by comparing the experimental values of Sh with values for mass transfer in circular channels in both film flow and Taylor flow (Figure 22) it can be seen that the present experiments are in an intermediate regime, with improved mass transfer compared to film flow, but not yet in the range of mass transfer in Taylor flow. Since it is not conclusive if the system is completely mass transfer limited, it is difficult to compare the data with previous experiments. The only conclusion that can be drawn is that the performance is better than single-phase flow.

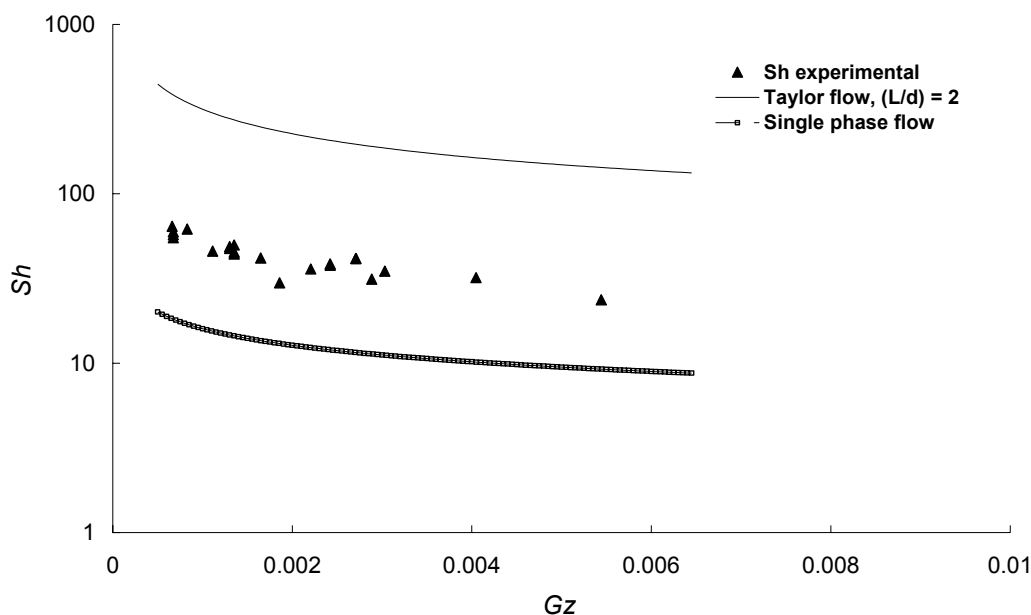


Figure 22. Comparison of experimental data with model values for single phase flow [9] and Taylor flow with [44]

The covalently bonded trypsin shows a clear trend in k_{eff} as a function of the liquid velocity and the cell density. k_{eff} increases with both increasing cell density and increasing v_L . The observed mass transfer coefficient for AM-ALD/IM is significantly higher, although it is a question whether the system is not kinetically limited under these conditions. For ACM monoliths more experiments should be performed to ensure operation in the mass transfer limited regime, either at higher trypsin loading or at lower v_L . But even under kinetic limitation, the ACM monolith has a significantly higher mass transfer coefficient. Based on the open structure of the monolith and the results of residence time distribution experiments [14] this could already be expected.

5 Conclusions

The trypsin-catalyzed hydrolysis of n-benzoyl-L-arginine ethyl ester (BAEE) was used to determine the liquid-solid mass transfer coefficient in the monolith loop reactor. Trypsin was immobilized by gel entrapment and by covalent bonding on monoliths with different cell density and microstructure. On the more porous ACM monoliths the carrier loading is higher, resulting in a higher total trypsin loading. The layer thickness of the gel-coated monoliths varies between 80 and 100 μm . The kinetics of the free trypsin can be described by a Michaelis-Menten expression with $V_{\text{max}} = 0.44 \text{ mmol s}^{-1} \text{ g}_{\text{enz}}^{-1}$, and $K_m = 55 \text{ mmol m}^{-3}$. For the immobilized trypsin V_{max} and K_m are $0.04 \text{ mmol s}^{-1} \text{ g}_{\text{enz}}^{-1}$ and 130 mmol m^{-3} respectively. An apparent activation energy, E_a , of 53 kJ mol^{-1} was found for the hydrolysis reaction. In the monolith loop reactor, operation in the mass transfer limited regime was approached by

operating at elevated temperature and with optimized enzyme loading. Also the Carberry number was calculated to be significantly larger than the threshold value of 0.05 for each experiment. The system is however not completely mass transfer limited ($Ca < 1$). For the ACM monoliths with a higher available surface area, the reaction is most likely (partially) kinetically limited. The conversion per pass varied between 0.05 and 0.4 for the different experiments. The observed mass transfer coefficient, k_{eff} , is not affected by the gas flow rate, but increases proportionally with liquid velocity. Also an increased surface area results in a higher k_{eff} . The use of catalysts under internal diffusion limitations leads to a large underestimation of k_{eff} and introduces several new parameters to consider such as catalyst loading, layer thickness and carrier distribution.

The use of fuzzy wall monoliths can be very advantageous, because of the very high enzyme loading that can be accomplished. For the determination of mass transfer parameters however, these catalysts are less suitable. This was already expected based on the layer thickness and gel distribution inside the monolith channels (Chapter 6). The gel is mainly present inside the corners, causing local high layer thickness and increased diffusion problems. If a very thin gel-layer could be applied on rounded channels (e.g. an alumina washcoat, see Chapter 3), the performance of this catalyst type could be improved significantly. Covalent immobilization via the ALD/IM protocol leads to a high enzyme loading in the absence of internal diffusion limitations. This catalyst is very suitable for the present application due to the strong enzyme-support bond and the high stability. The results are in good agreement with theoretical values for mass transfer in a square channel under the applied conditions.

For a maximal performance (based on conversion rate), AM-ALD/IM catalysts are recommended. These catalysts have a high activity in the absence of internal diffusion limitations, and provide a stable enzyme-support bond to resist the high shear forces at increased liquid flow rates.

6 Acknowledgements

Nico Hinskens and Ingrid Hoek are gratefully acknowledged for their valuable contribution to this work. Michiel Kreutzer is acknowledged for his contribution to this chapter, especially the mass transfer-related paragraphs. Corning Inc. is acknowledged for supplying the cordierite monoliths. The Dow Chemical Company is acknowledged for supplying the ACM monoliths and for funding part of this research.

7 Symbols

a'	specific surface area	$[\text{m}^2/\text{m}^3]$
A_m	geometric surface area	$[\text{m}^2]$
C_s	surface substrate concentration	$[\text{mol m}^{-3}]$
C_b	bulk substrate concentration	$[\text{mol m}^{-3}]$
C_{wet}	liquid meniscus in square channel	$[\text{m}^{-1}]$
Ca	Carberry number	$[-]$
Ca	Capillary number	$[-]$
d_{ch}	channel diameter	$[\text{m}]$
d_F	film thickness	$[\text{m}]$
$d_{F,eff}$	effective film thickness	$[\text{m}]$
D	diffusivity	$[\text{m}^2 \text{s}^{-1}]$
D_{eff}	effective diffusion coefficient	$[\text{m}^2 \text{s}^{-1}]$
e	total enzyme concentration	$[\text{mol l}^{-1}]$
E_a	activation energy	$[\text{kJ mol}^{-1}]$
g	gravitational constant	$[\text{m s}^{-2}]$
k	reaction rate constant	$[\text{s}^{-1}]$
k_0	reaction rate constant at 298 K	$[\text{s}^{-1}]$
k_{eff}	effective mass transfer coefficient	$[\text{s}^{-1}]$
$k_{r,obs}$	observed reaction rate constant	$[\text{s}^{-1}]$
k_s	mass transfer coefficient	$[\text{m s}^{-1}]$
K_m	Michaelis-Menten constant	$[\text{mol l}^{-1}]$
l_{wet}	distance between liquid solid contact points	$[\text{m}]$
L	layer thickness	$[\text{m}]$
L_{chit}	layer thickness chitosan layer	$[\text{m}]$
L_{hydro}	characteristic length for development of the velocity profile	$[\text{m}]$
L_m	monolith length	$[\text{m}]$
L_{mt}	characteristic length for development of mass transfer profile	$[\text{m}]$
n	reaction order	$[-]$
r_i	reaction rate of reaction i	$[\text{mol s}^{-1}]$
$r_{v,obs}$	observed reaction rate	$[\text{mol s}^{-1} \text{m}^{-3}_{cat}]$
Re	Reynolds number	$[-]$
Sc	Schmidt number	$[-]$
Sh	Sherwood number	$[-]$
v_g	superficial gas velocity	$[\text{m s}^{-1}]$
v_L	superficial liquid velocity	$[\text{m s}^{-1}]$
$\langle v_L \rangle$	mean liquid velocity	$[\text{m s}^{-1}]$
v_{Lm}	maximum superficial liquid velocity	$[\text{m s}^{-1}]$
V_L	liquid volume	$[\text{m}^3]$

V_{\max}	maximum rate for enzymatic conversion	[mol s ⁻¹ ge ⁻¹]
T	temperature	[K]

Greek symbols

α	liquid contact angle on channel	[°]
ε	porosity	[-]
η	liquid viscosity	[Pa s]
ρ	liquid density	[kg m ⁻³]
σ	surface tension	[N m ⁻¹]
σ_f	constriction factor	[-]
τ	tortuosity	[-]
ϕ	Thiele modulus	[-]
ϕ_{mol}	molar flow rate	[mol s ⁻¹]

Components

E	enzyme
ES	enzyme substrate complex
P	product
S	substrate

8 References

- [1] M.D. Mantle, A.J. Sederman, L.F. Gladden (2002) *AIChE Journal*; 48: 909-912
- [2] S. Irandoust, B. Andersson (1988) *Chemical Engineering Science*; 43: 1983-1988
- [3] M.T. Kreutzer, F. Kapteijn, J.A. Moulijn, J.J. Heiszwolf (2005) *Chemical Engineering Science*; 60: 5859-5916
- [4] J.J. Heiszwolf, L.B. Engelvaart, M.G. van den Einden, M.T. Kreutzer, F. Kapteijn, J.A. Moulijn (2001) *Chemical Engineering Science*; 56: 805-812
- [5] A.K. Heibel, T.W.J. Scheenen, J.J. Heiszwolf, H. van As, F. Kapteijn, J.A. Moulijn (2001) *Chemical engineering Science*; 56: 5935-5944
- [6] R. Lenormand, C. Zarcone, A. Sarr (1983) *Journal of Fluid Mechanics*; 135: 337-353
- [7] K. Spildo, J.S. Buckley (1999) *Journal of Petroleum Science and Engineering*; 24: 145-154
- [8] J.J. Heiszwolf, M.T. Kreutzer, M.G. van den Einden, F. Kapteijn, J.A. Moulijn (2001) *Catalysis Today*; 69: 51-55
- 9 M.T. Kreutzer, PhD thesis, Delft University of Technology, the Netherlands
- [10] A.K. Heibel F.J. Vergeldt, H. Van As, F. Kapteijn, J.A. Moulijn, T. Boger (2003) *AIChE Journal*; 49: 3007-3017
- [11] B. Andersson, S. Irandoust, A. Cybulski (1998), in *Structured Catalysts and Reactors*, Cybulski&Moulijn, Eds. Marcel Dekker, New York, United States

- [12] S.A. Wallin, A.R. Prunier, Jr, J.R. Moyer (2001) US Patent 6,306,335
- [13] J.M. Moyer, N.N. Hughes, *Journal of the American Ceramic Society*. 77 (1994) 1083
- [14] J.J.W. Bakker, M.T. Kreutzer, K. de Lathouder, F. Kapteijn, J.A. Moulijn, S.A. Wallin (2005) *Catalysis Today*; 105: 385-390
- [15] L.F. Gladden, M.H.M. Lim, M.D. Mantle A.J. Sederman, E.H. Stitt (2003) *Catalysis Today*; 79-80: 203-210
- [16] Y.F. Wang, Z.S. Mao, J. Chen (1998) *Chemical Engineering Science*; 53: 1153-1162
- [17] P. Marchot, D. Toye, M. Crine, A.M. Pelsser, G.L. L'Homme (1999) *Chemical Engineering Research and Design*; 77: 511-518
- [18] G. Dodson, A. Wlodawer (1998) *Trends in Biotechnology*; 23: 347-352
- [19] P.C. Engel (1977) *Enzyme Kinetics*, Chapman and Hall, London, Great Britain
- [20] M. Okubo, H. Ahmad (1999) *Colloids and Surfaces A: Physicochemical and Engineering Aspects*; 153: 429-433
- [21] M. Sardar, R. Agarwal, A. Kumar, M. N. Gupta (1997) *Enzyme and Microbial Technology*; 20: 361-367
- [22] J. M. Kisler, A. Dähler, G.W. Stevens, A. J. O'Connor (2001) *Microporous and Mesoporous Materials*; 44-45: 769-774
- [23] L. Geng, N. Li, M. Xiang, X. Wen, D. Xu, F. Zhao, K. Li (2003) *Colloids and Surfaces B: Biointerfaces*; 30: 99-109
- [24] J. Wu, M. Luan, J. Zhao (2006) *International Journal of Biological Macromolecules*; 39: 185-191
- [25] F. Xi, J. Wu, Z. Jia, X. Lin (2005) *Process Biochemistry*; 40: 2833-2840
- [26] C. Horvath, B.A. Solomon (1972) *Biotechnology and Bioengineering*; 14: 885-914
- [27] H. Wand (1978) *Acta Biologica et Medica Germanica*; 37: 501-502
- [28] E.A. Kulik, K. Kato, M.I. Ivanchenko, Y. Ikada (1993) *Biomaterials*; 14: 763-769
- [29] I. Hoek (2004) doctoral thesis, Delft University of Technology, the Netherlands
- [30] P. Lebens, PhD thesis (1999), Delft university of Technology, the Netherlands 75-89
- [31] J. Zhang, M. Giot (1995) *Proceedings of the First International Symposium on Two-Phase Flow Modelling and Experimentation*, Rome, Italy: 171
- [32] R.B. Bird, W.E. Stewart, E.N. Lightfoot (1960) *Transport phenomena*. John Wiley & Sons, New York, United States: 40-42
- [33] A. K. Heibel, F.J. Vergeldt, H. Van As, F. Kapteijn, J. A. Moulijn, T. Boger (2003) *AICHE Journal*; 49: 3007-3017
- [34] M. Dong, I. Chatzis (2004) *Journal of Colloid and Interface Science*; 273: 306-312
- [35] F.P. Bretherton (1961) *Journal of Fluid Mechanics*; 10: 166-188
- [36] W.B. Kolb, R.L. Cerro (1991) *Chemical Engineering Science*; 46: 2181-2195
- [37] A. van Miltenburg (2001) Master thesis, Delft University of Technology, the Netherlands
- [38] V. Balakotaiah, D.H. West (2002) *Chemical Engineering Science*; 57: 1269-1286
- [39] R.E. Hayes, S.T. Kolaczowski (1994) *Chemical Engineering Science*; 49: 3587-3599
- [40] K. Kang, C. Kan, A. Yeung, D. Liu (2005) *Macromolecular Bioscience*; 5: 344-351
- [41] S. Yamamoto, A. Imamura, I. Susanti, K. Hori, Y. Tanji, H. Unno (2005) *Food and*

- Bioproducts Processing; 83: 61-67
- [42] G. Ghadge, E thesis, ETN: A388T386, Microbial enzymes. National Chemical Laboratories (NCL), University of Pune, India
- [43] R.K. Shah, A.L. London (1978), Laminar flow force convection ducts. Advances in heat transfer, Volume 1, supplement 1, Academic Press, New York, United States
- [44] C. Horvath, B.A. Solomon, H.M. Engasser (1973) Industrial and Engineering Chemistry Fundamentals; 12: 431-439
- [45] S. Irandoust, B. Andersson (1989) Industrial and Engineering Chemical Research; 28: 1684-1688
- [46] A.L. Hazel, M. Heil (2002) Journal of Fluid Mechanics; 470: 91-114

Hydrolysis of penicillin G in a monolith loop reactor

Abstract

The objective of this work was to test a chitosan coated monolith for the immobilization of different commercial penicillin G acylases, Assemblase[®] (PGA I) and Separase[®] (PGA II). The monolithic biocatalyst was used in the Monolith Loop Reactor (MLR) in the hydrolysis of penicillin G, and compared to the current industrial immobilized enzyme and the free penicillin G acylase. Entrapment in combination with crosslinking was used for the immobilization of penicillin G acylase on cordierite monoliths. For 400 cpsi monoliths, the volumetric activity was $0.79 \text{ mol s}^{-1} \text{ m}^{-3}_{\text{monolith}}$. The storage stability is at least a month without loss of activity. Although the monolithic biocatalyst does not perform better than the current industrial catalyst ($4.5 \text{ mol s}^{-1} \text{ m}^{-3}_{\text{catalyst}}$), the rate per gel volume is slightly higher for monolithic catalysts. Good activity and improved mechanical strength make the monolithic bioreactor an interesting alternative that deserves further investigation for this application. The obtained results can be simulated by developing models for the different reactor configurations. Although moderate internal diffusion limitations have been observed inside the gel beads and in the gel layer on the monolith channel, this is not the main reason for the large differences in reactor performance that were observed. The pH drop over the reactor as a result of the chosen method for pH control results in a decreased performance of both the MLR and the packed bed reactor compared to the batch system. A different reactor configuration including an optimal pH profile is required to increase the reactor performance.

1 Introduction

In the previous chapter, the monolith loop reactor (MLR) was studied with respect to mass transport properties at different flow rates, and for different monoliths. In this chapter, the MLR is used to present an alternative reactor for the industrial hydrolysis of penicillin G. Antibiotics are secondary metabolites produced by (micro) organisms that kill or inhibit the growth of other microorganisms. The most important family of antibiotics, the β -lactam antibiotics, includes many of the most heavily used antibacterials in clinical medicine. These antibiotics are characterized by a β -lactam structure (a four-membered cyclic amide). This structure is the basis of the antimicrobial activity because it interferes in the cell wall synthesis of growing bacteria. Penicillin and its derivatives have become the most important class of antibiotics, because of their low toxicity and their effectiveness against bacterial infection. The commercial success of the semi-synthetic antibiotics has quickly resulted in a worldwide cost based market [1]. Presently Western-Europe, India and, especially, China are world leader in industrial production. Commercial success therefore, is governed by low cost processes preferably combined with technology leadership. Nowadays, at 7 \$/kg the penicillin price is still on a downward trend. The enzyme is one of the main drivers in the cost structure of 6-APA production. So, continuously improvements are being made to use the enzyme as efficiently as possible.

Gradually, chemical industry is replacing existing chemical transformations by cleaner (bio)catalytic steps. The need for so-called “green” transformations can be explained by regarding the amount of waste produced per kg product also known as the E factor [2]. Compared to the conventional chemical route ($E = 23$), E is around 0.1 for the enzymatic process.

1.1 Description of the reaction system

The current process utilizes immobilized penicillin G acylase, covalently immobilized in a chitosan gel. This carrier-enzyme combination has been shown to be very efficient; the enzyme generally has a very high immobilized activity. The commercially available immobilized acylases are immobilized on spherical carriers with a mean diameter of around 0.4 mm. The use of this catalyst requires fine-tuning of mechanical properties, enzyme distribution, and internal diffusion limitations. Due to the process requirements, the particles are relatively large, inducing problems with internal pH gradients and decreased selectivity. Coating of a carrier material on the walls of a monolithic structure combines the good mechanical and structural properties of a monolith with the efficient protein immobilization properties of the carrier. This reduces the adverse effect of internal diffusion limitations.

1.1.1 Pen G acylase

In 1928, Alexander Fleming discovered a compound with antibacterial action and gave it the name penicillin [3], after the fungi *Penicillium notatum* that it came from. Fleming studied its effectiveness against different bacterial infections but he was not able to isolate the active compound. This was eventually done by Chain and Florey and co-workers in 1940 [4]. In recognition of their efforts in the discovery of this “wonder drug” that has saved millions of lives, Fleming, Chain, and Florey received the Nobel Prize in 1945. The first report on the enzyme penicillin acylase was in 1950 by Sakaguchi and Murao [5] when they found the enzyme in mycelium of a *Penicillium sp.* capable of hydrolyzing penicillin G into phenylacetic acid and the then unknown 6-APA (named “penicin”). It is now well established that penicillin acylases are ubiquitous in bacteria, actinomycetes, fungi, and yeasts [6]. It is interesting to note that even today the biological function of the enzyme remains unknown. It is thought to have a function in the degradation of aromatics [7].

The introduction of semi-synthetic β -lactam antibiotics in the early 1960s initiated a development that would make the β -lactam nucleus in the form of 6-aminopenicillanic acid (6-APA) a major pharmaceutical intermediate [8]. Penicillin amidohydrolase (E.C. 3.5.1.11) is the official name for penicillin acylase or penicillin amidase [1,9]. Penicillin acylases catalyze the hydrolysis of an amide bond between a carboxylic acid and a β -lactam nucleus while leaving the β -lactam intact (Figure 1).

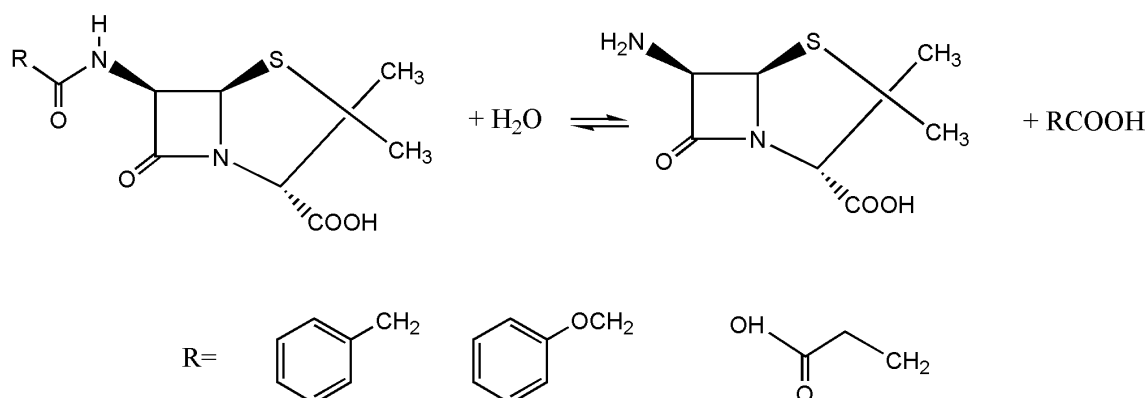


Figure 1. Reaction catalyzed by penicillin G acylases (R=benzyl), penicillin V acylases (R=phenoxyethyl) and glutaryl acylases (R=carboxypropyl). Also cephalosporin nuclei can be accepted in place of 6-APA

1.1.2 Catalytic activity of Pen G acylase

Penicillin acylase from *E. coli* is the best-studied penicillin acylase with respect to the synthesis of semi-synthetic antibiotics. The isoelectric point for *E. coli* penicillin acylase has been reported as pH 6.8 [9] and pH = 6.3 [10].

The crystal structure of *E. coli* penicillin G acylase was resolved by Duggleby *et al.* in 1995 [11]. The enzyme appeared to be a heterodimeric N-terminal serine hydrolase with a molecular mass of 86 kDa, with a 24 kDa (209 amino acids) α -subunit and a 62 kDa (566 amino acids) β -subunit. The enzyme is kidney-shaped (approximate dimensions are 7.5·5.5

nm) with a deep cup-shaped depression leading to the active site. It has a single-amino-acid catalytic centre, the β -chain N-terminal serine hydroxyl group.

From a structural point of view, penicillin acylase has two substrate binding pockets. The most specific one, S_1 (also known as the acyl donor binding pocket), consists of mainly hydrophobic residues. The enclosed structure and largely hydrophobic character of the S_1 pocket makes the enzyme very selective to the benzyl structure with some room for substitutions on the bridging C-atom or the aromatic ring. The S_2 pocket, or (β -lactam) nucleophile-binding pocket, is in reality the bottom of the cup-shaped depression mentioned before and therefore makes for a very broad substrate specificity of this pocket. In contrast to the S_1 pocket, the S_2 pocket is enantioselective and can therefore be used for *e.g.* amine resolution [12].

The catalytic mechanism of *E. coli* penicillin G acylase catalyzed amide hydrolysis is shown in Figure 2. The first step (a) in penicillin acylase catalysis is the nucleophilic attack of the active Ser on the electrophilic carbonyl carbon of the amide substrate. The transition-state intermediate is stabilised (b) by hydrogen bonding with two amino acids in the oxyanion hole (Ala β 69 and Asn β 241). Next (c), the product is released (6-Amino Penicillic Acid in case of pen G hydrolysis), and a covalent acyl-enzyme intermediate is formed to restore the carbonyl group. In the following step (d,e) the acyl moiety is transferred to a water molecule. Finally (f), the second product (Phenyl acetic acid) can be released.

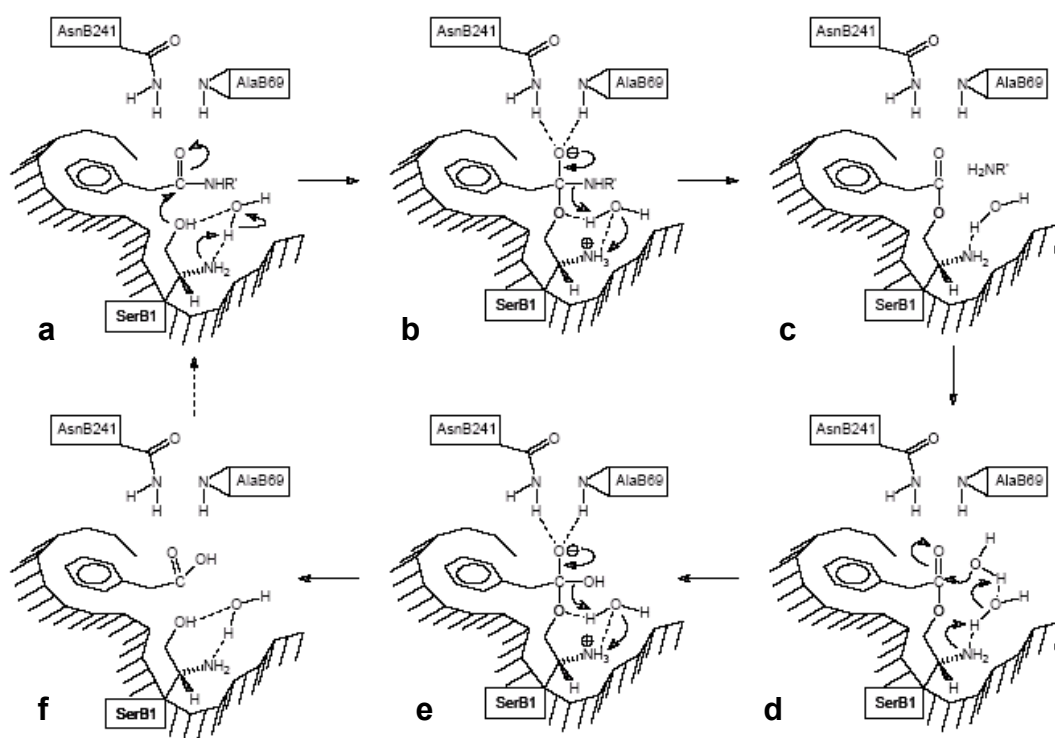


Figure 2. Catalytic mechanism of the penicillin G acylase catalyzed amide hydrolysis [from 13].

The activity of 2 different Pen G acylases (Assemblase[®] and Separase[®]) is investigated in the hydrolysis of Penicillin G to 6-aminopenicillanic acid (6-APA) and phenylacetic acid (PAA). The reaction scheme is given in Figure 3.

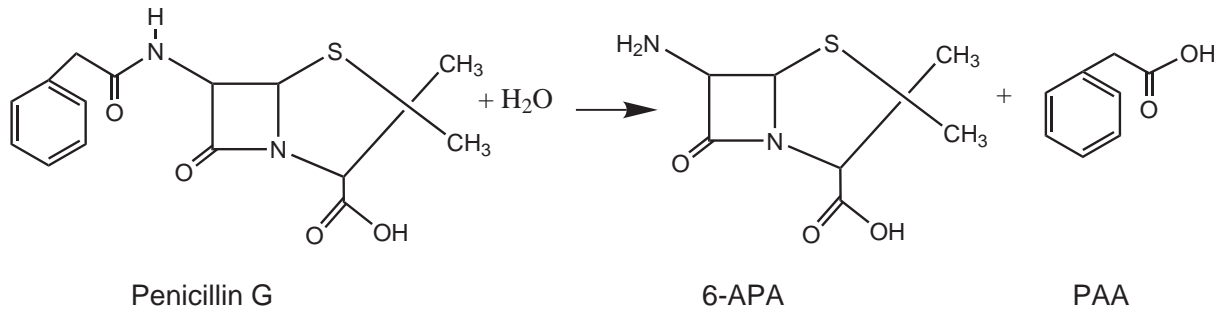
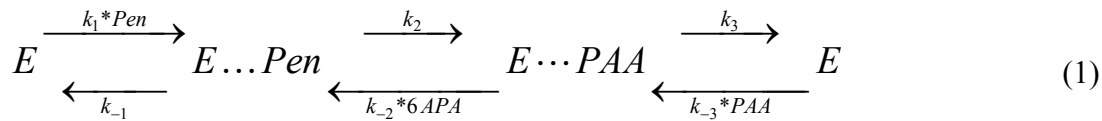


Figure 3. Reaction scheme of penicillin hydrolysis. The substrate is converted into phenylacetic acid (PAA) and 6-aminopenicillanic acid (6-APA)

The steady-state kinetics of the forward deacylation reaction of Pen G in the presence of penicillin acylase includes one substrate and two products, 6-APA and PAA [14,15]. The kinetics can be described by an ordered uni-bi mechanism, including the association of the substrate to the active site and formation of the acyl-enzyme complex and dissociation of 6-APA. This is followed by nucleophilic attack of water and dissociation of PAA. The third and fourth step are lumped ($[H_2O]$ is assumed constant) to a pseudo uni-bi mechanism [15]:



which yields an expression for the reaction rate:

$$r = \frac{\frac{k_{cat}}{K_{mPen}} * [E_0] * \left(C_{Pen} - \frac{C_{6APA} * C_{PAA}}{K_{app}^c} \right)}{1 + \frac{C_{Pen}}{K_{mPen}} + \frac{K_{iPen} * C_{6APA}}{K_{mPen} * K_{i6APA}} + \frac{C_{PAA}}{K_{iPAA}} + \frac{C_{Pen} * C_{PAA}}{K_{mPen} * K_{iPAA}} + \frac{K_{iPen} * C_{6APA} * C_{PAA}}{K_{mPen} * K_{i6APA} * K_{mPAA}}} \quad (2)$$

Where $k_{cat} \cdot [E_0]$ is the maximum reaction velocity, K_{mPen} , K_{m6APA} and K_{mPAA} are the Michaelis-Menten constants for Pen G, 6-APA and PAA. K_{iPen} , K_{i6APA} and K_{iPAA} are the inhibition constants for Pen G, 6-APA and PAA. K_{app}^c is the apparent equilibrium constant, which is expressed in terms of theoretical equilibrium constant and pH. The equation can be simplified by assuming that $K_{mPen} = K_{iPen}$, $K_{i6APA} = K_{m6APA}$ and $K_{iPAA} = K_{mPAA}$ [16], which yields:

$$r = \frac{\frac{k_{cat}}{K_{mPen}} * [E_0] * \left(C_{Pen} - \frac{C_{6APA} * C_{PAA}}{K_{app}^c} \right)}{1 + \frac{C_{Pen}}{K_{mPen}} + \frac{C_{6APA}}{K_{m6APA}} + \frac{C_{PAA}}{K_{mPAA}} + \frac{C_{Pen} * C_{PAA}}{K_{mPen} * K_{mPAA}} + \frac{C_{6APA} * C_{PAA}}{K_{m6APA} * K_{mPAA}}} \quad (3)$$

1.1.3 Penicillin G acylase immobilization

The technology of penicillin immobilization has had major success in improving the economics of the enzymatic production of 6-APA. Although other methods have been used for hydrolysis of penicillin to 6-APA, including the use of free suspension cells, soluble enzyme preparations, and immobilized whole cells, use of immobilized enzyme is preferred.

The various methods include adsorption, entrapment, micro encapsulation, cross-linking and covalent attachment. Penicillin G acylase has been immobilized on inorganic particulate carriers like silica [16] and Eupergit C [17-19]. Hydrogels like dextran [20], agarose [21, 22,19] and chitosan [23] are promising support materials for enzyme immobilization because they are cheap, hydrophilic, biocompatible, and biodegradable. The immobilization of penicillin acylase on chitosan powder, particles and beads was investigated in 1989 [23]. In the current system, mass transport problems are an important problem. The required stability of the carrier-enzyme system makes (ionic) adsorption and entrapment less suitable. The enzyme needs to be stabilized onto the carrier. Covalent immobilization generally leads to a low residual activity; in this respect a combination of entrapment with crosslinking could be better. This method has already been optimized for industrial application with gel-beads, the application of a monolithic structure coated with a hydrogel layer as a carrier for penicillin G acylase immobilization has not been used before.

1.2 Layout

The objective of this project is to apply a chitosan coating on the interior walls of a cordierite monolith¹ for the immobilization of penicillin G acylase. The prepared immobilized biocatalyst will be tested in the hydrolysis of penicillin G to yield phenylacetic acid and 6-aminopenicillanic acid. The kinetics of the reaction are studied by evaluating a set of initial rate experiments in a batch system. To compare the conventional system with the monolith reactor, a batch system, a packed bed, and a monolith loop reactor are employed. Possible mass transfer problems are evaluated for the different bioreactors by modeling the reactor systems with internal and external mass transport problems. The stability of the immobilized catalyst is tested and the activity is compared to a current industrial immobilized penicillin G acylase.

¹ ACM monoliths were not considered here, because the work was performed at the DSM facilities in Delft. The patent for ACM monoliths was still pending at this time.

2 Experimental

2.1 Materials

Colloidal silica solution (Ludox AS-40), low viscous chitosan with viscosity < 200 mPa s and (3-aminopropyl)triethoxysilane (APTES) were purchased from Fluka. Acetic acid and glutaraldehyde were purchased from Merck. Separase[®] (pen G acylase from *A. faecalis*), Assemblase[®] (from *E. coli*) are the penicillin G acylase that are employed in the present study, indicated with PGA I and PGA II respectively. Assemblase[®] stock solution (Batch nr: ASM 031302, 10 g l^{-1}), Assemblase[®] Immob (batch nr: D576010), Separase[®] solution (batch nr: SEP 032616) and Separase[®] Immob (batch nr: D572154) were all kindly supplied by DSM Anti-Infectives, Delft, The Netherlands. Cordierite monoliths (400 cpsi) were provided by Corning Inc.

2.2 Methods

Monoliths (400 cpsi, $L_m = 4 \text{ cm}$, $d_m = 2 \text{ cm}$) were coated with chitosan gel by dip-coating. Monoliths were held in a 1.0 % w/v chitosan solution containing 1.1 % w/v glutaraldehyde for 60 sec. After cleaning the channels, samples were air dried for 90 min. Optionally a second dipcoating step can be introduced, after the first round of dip coating. The monolith was air-dried for 60 min, then coated and dried for another 60 min. Some samples were washcoated (with colloidal silica, Ludox) and silanized (APTES) before chitosan application as described in Chapters 3 and 4.

2.2.1 Enzyme immobilization

Gels were suspended in 20-40 ml penicillin acylase solution. Immobilization was done at ambient temperature during 24 hours while gently stirring. After washing, 20 ml of phosphate buffer (25 mM pH 7.0) was added to the gel. Desorption of non-bound protein took place at ambient temperature during 24 hours, while gently stirring.

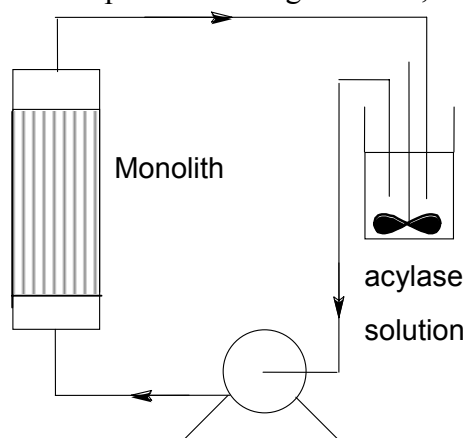


Figure 4. Continuous set-up for acylase immobilization

Immobilization on chitosan-coated monoliths was performed in a continuous set-up, consisting of a chromatography column with a diameter of 26 mm. Enzyme solution was pumped through the column in upflow (Figure 4).

Immobilization was performed by recycling a total volume of 30 ml through the monolith (flow rate 2 ml min^{-1}) at room temperature during 24 hours. The monolith was washed with demiwaterr to remove

unbound enzyme. During immobilization and washing the protein concentration in solution was determined by measuring the absorbance at 280 nm. Samples were analyzed on a Unicam UV300 UV/VIS Spectrophotometer. Biocatalysts were stored in a solution of 30 % w/w 1,2-propanediol at 277 K until further use.

2.3 Characterization

The average thickness of the chitosan gel layer was calculated by:

$$L_{chitosan} = \frac{m_{chitosan}}{\frac{\pi}{4} \cdot d_m^2 \cdot L_m \cdot a' \cdot \rho_{chitosan}} \quad (4)$$

Where $m_{chitosan}$ and $\rho_{chitosan}$ are the mass and density of chitosan filtrate, d_m and L_m are the diameter and height of the monolithic structure and a' is the specific surface area. The density of 1.0 % chitosan filtrate is assumed to be equal to the density of water.

2.3.1 Penicillin G decomposition

During storage at 277 K a slow decomposition of penicillin G in solution occurs. HPLC has been used to determine the penicillin concentration in the stock solution at the start of each conversion experiment. The decomposition of penicillin G appears to follow first-order decay. The inactivation rate constant k_{inact} was calculated at 0.009 day⁻¹, i.e. 9 ‰ penicillin decomposition per day.

2.3.2 Kinetics

Conversions with free enzyme and Immob were carried out in 80 ml penicillin solution (initial Pen G-ammonia salt concentration 250 mM), to which the equivalent of 50 mg enzyme ($[E_0] = 7.8 \times 10^{-3} \text{ mmol l}^{-1}$) was added. Conditions were pH = 8.50 and T= 304 K. The conversion was measured by titration with 1.0 M NaOH of released phenylacetic acid (PAA) by:

$$X_{PenG} = \frac{V_{NaOH} \cdot [NaOH]}{V_{L,t=0} \cdot [PenG_{t=0}]} \quad (5)$$

The initial Pen G concentration was determined by HPLC. The chromatographic experiments were performed on a Spectra Physics AS1000 HPLC with a Spectra Physics UV100 detector connected to a RP-18 column (5 μm particle diameter). The mobile phase used was water-acetonitril-phosphate buffer of pH 3.0, with the column flow rate set at 1.0 ml min⁻¹. The UV trace was followed at 214 nm. Retention times of 6-APA, PAA and Pen G are < 1 min, 2.84 and 3.91 minutes respectively. To validate the use of NaOH consumption to follow

conversion, samples were withdrawn at regular intervals to measure the Pen G and PAA concentrations by HPLC. Conversion was calculated by:

$$X = \frac{[PAA_{t=x}] - [PAA_{t=0}]}{[PenG_{t=x}] + [PAA_{t=x}] - [PAA_{t=0}]} \quad (6)$$

2.3.3 Catalyst performance

The continuous set up (Figure 4) was used to compare monoliths with a packed bed of Immob. Total enzyme loading on the monolithic structure (400 cpsi, $L_m = 4$ cm, $d_m = 1.9$ cm, $\varepsilon_m = 0.74$) was 50 mg (PGA II) or 120 mg (PGA I). To get an enzyme loading of 50/120 mg with Immob (PGA I/II, $d_p = 0.4$ mm and $\rho_{gel} = 1050$ kg m⁻³), a bed height of 1 cm was used ($d_b = 2.6$ cm, $\varepsilon_b = 0.448$) The flow rate of the circulating solution was set at 15 ml min⁻¹ to avoid pressure drop over the column. NaOH was added in order to reduce the negative effect of a pH gradient over the monolith/Immob. A different set-up with larger tubing was used to perform high-flow rate (52.5 ml min⁻¹) experiments. The total reaction volume was 120 ml (initial Pen G concentration 250 mM).

3 Results and Discussion

3.1 Immobilization on chitosan coated Monoliths

By weighing, and assuming a homogeneous gel layer throughout the channel, the average layer thickness of chitosan on a 400 cpsi monolith is 77 μ m (Table 1). This number varied between 95 μ m and 65 μ m for different samples. The chitosan layer thickness as calculated is an average over the entire monolith structure. In practice the gel film in a square channel will not be uniform. As a result of the surface tension during gelation, it will have a rounder shape. If a silane coating is applied on cordierite, the average gel layer thickness increases to 90 μ m. The silane-coated samples are used in the hydrolysis of penicillin G.

Table 1. Results monolith coating with chitosan layer, with and without pre-conditioning of the support

Carrier	Enzyme	$Y_{carrier}$ / layer thickness (L) [% / μ m]	Enzyme loading [mg ml ⁻¹ _{gel}]
C_Chit, (no Lx_APTES)	PGA II	25 / 80	12
C_Chit, (no Lx_APTES)	PGA I	24 / 77	32
C_Chit (Lx_APTES)	PGA II	29 / 93	14
C_Chit (Lx_APTES)	PGA I	28 / 89	36

The immobilization of pen G acylase was followed during 24 hours to establish the time necessary to reach “steady-state” loading. An immobilization time of 2 hours, in which 80 % of equilibrium is reached, matches reasonably well with the current industrial immobilization

process for Immob particles (with a similar diffusional distance $d_p/6$ as is observed for the gel coatings that are used in this study), which is also based on a loading time of two hours.

The results are in agreement with the expected values from the immobilization study in Chapter 6. Both layer thickness and total gel loading increase when the monolith is preconditioned (washcoated and silanized) before the gel is applied. The PGA II loading on chitosan-coated monoliths is significantly lower than for PGA I. This was already observed during the optimization of the immobilization method in Chapter 6, and no explanation can be offered (the enzymes are almost identical).

3.2 Hydrolysis of Pen G

Catalyst performance tests were used to compare the free enzyme, Immob and the monolithic biocatalysts under process conditions.

3.2.1 Catalyst performance

In a set of experiments in a batch reactor ($V_L = 80$ ml, $C_b = 250$ mM) the initial reaction rate of free and immobilized enzyme was determined. In Figure 5 the initial rates of free and immobilized (Immob) enzyme are compared with the initial rate of monolithic biocatalysts.

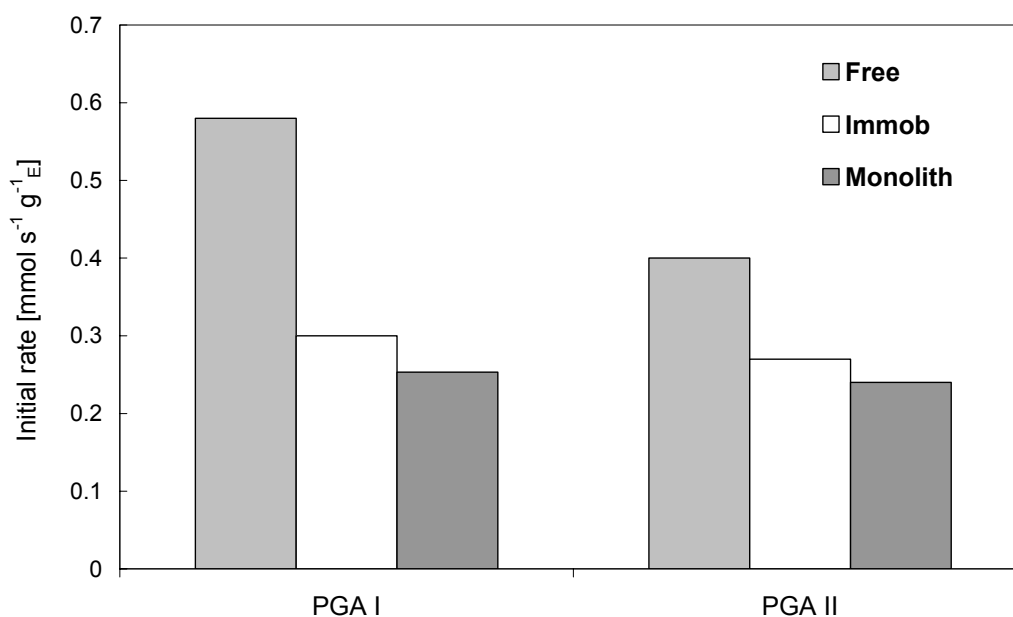


Figure 5. Initial rate of free enzyme, Chitosan beads and a monolith in the hydrolysis of Pen G at 304 K and pH = 8.50, normalized with respect to enzyme loading

The chitosan beads seem to suffer from internal mass transport problems (lower conversion compared to the free enzyme), as was already described by Schroën *et al.* [25]. If the Immob particles are crushed, the initial rate is identical to that of the free enzyme. The lower initial rate of Immob compared to that of the free enzyme is probably caused by diffusion limitation

in the gel matrix of the carrier. The reaction rate for fast reactions in carriers with high enzyme loading can become limited by diffusive transport of the reactive species. For this enzyme system an additional problem is present; in the hydrolysis of penicillin G an acid (PAA) is produced. This gives rise to pH gradients inside the gel matrix due to the coupling of reaction and diffusion of substrates and products within the carrier. If the initial rates of the Monolith, Immob and free enzyme are compared (Figure 5), it seems that the internal mass transport problems that are present inside the gel particles have slightly increased when the gel layer is applied on a monolith. This could have been expected from the difference in the respective diffusion distance, based on the layer thickness and the bead size ($d_p/6$) (90 μm vs 67 μm). The hydrodynamics of the different systems and the mass transport limitations will be discussed in more detail in the following paragraphs. The free PGA II is less stable with respect to local high concentrations of NaOH, as was already seen in Chapter 6. In immobilized form, the two acylases have a similar performance, although the PGA II loading is significantly lower. Because of the low stability of the free PGA II, only PGA I-biocatalysts were used for the simulations of reaction rate data. For 400 cpsi monoliths, the volumetric activity is around $0.79 \text{ mol s}^{-1} \text{ m}^{-3}_{\text{monolith}}$. Although the monolithic biocatalyst does not perform better than the current industrial catalyst ($4.5 \text{ mol s}^{-1} \text{ m}^{-3}_{\text{catalyst}}$), the intrinsic rates are comparable. This makes the monolithic biocatalyst an interesting alternative for gel beads, worth studying in more details.

3.2.2 Simulation of the experimental data of free PGA I

The hydrolysis of Penicillin G by free PGA I in batch ($V_1 = 80 \text{ ml}$, $\text{pH} = 8.5$) is presented in Figure 6 (symbols).

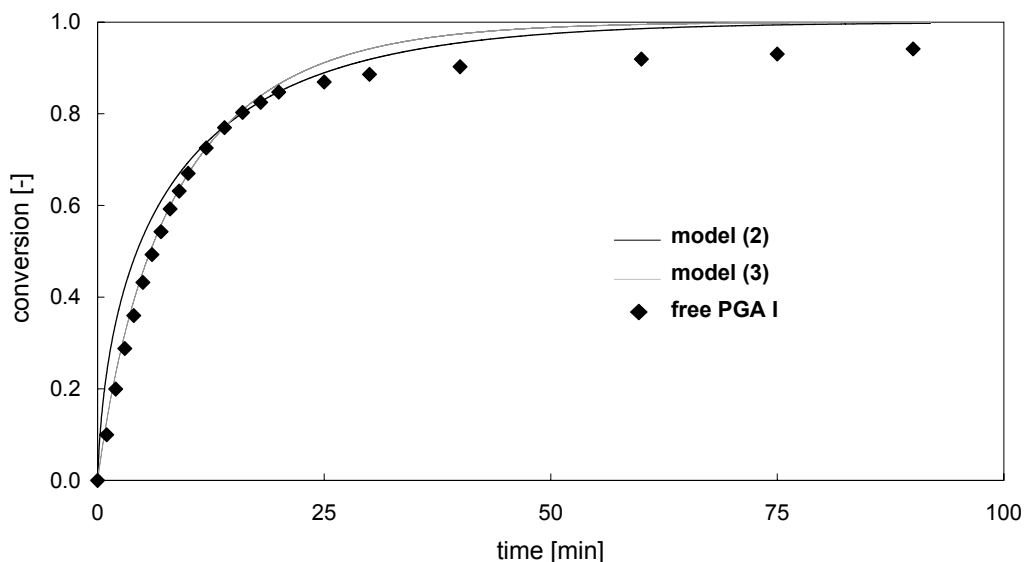


Figure 6. Fit of the experimental data of Peh G hydrolysis in the homogeneous system with PGA I, obtained using the kinetics from [15] (dashed curve) and after adaptation of the parameters k_{cat} and $K_{6\text{APA}}$ (bold curve); the symbols represent the experimental data

The kinetics of the hydrolysis of the test reaction can be described by equation 2 [15], which was simplified to yield equation 3:

$$r = \frac{\frac{k_{cat}}{K_{mPen}} * [E_0] * \left(C_{Pen} - \frac{C_{6APA} * C_{PAA}}{K_{app}^c} \right)}{1 + \frac{C_{Pen}}{K_{mPen}} + \frac{C_{6APA}}{K_{m6APA}} + \frac{C_{PAA}}{K_{mPAA}} + \frac{C_{Pen} * C_{PAA}}{K_{mPen} * K_{mPAA}} + \frac{C_{6APA} * C_{PAA}}{K_{m6APA} * K_{mPAA}}} \quad (3)$$

The parameters in this rate equation are a function of pH and were found to be [15]:

$$k_{cat} = \frac{50}{1 + \frac{10^{-pH}}{10^{-5}}} \quad (7)$$

$$K_{m6APA} = \frac{1}{1 + \frac{10^{-pH}}{10^{-6.4}}} \quad (9)$$

$$K_{mPenG} = 1 + 0.2 \cdot \frac{10^{-7}}{10^{-pH}} \quad (8)$$

$$K_{mPAA} = \frac{100}{1 + \frac{10^{-pH}}{10^{-6.15}}} \quad (10)$$

K_{app}^c was estimated at 31.4 [15]. The reaction itself affects the pH by means of product formation. The second reaction product PAA is weak acid, which reacts with the NaOH to its corresponding base. If PAA is indicated with HZ and its conjugated base with Z^- , the acid-base equilibrium is represented by:

$$K_Z = \frac{[H^+][Z^-]}{[HZ]} \quad (11)$$

with $K_Z = 10^{-pK_z}$. The $[H^+]$ is directly linked with the pH via

$$[H^+] = 10^{-pH} \quad (12)$$

Combining Eqs. (11) and (12) gives:

$$[HZ] = 10^{(pK_z - pH)} [Z^-] \quad (13)$$

When defining $[PAA] = [HZ] + [Z^-]$ it follows that:

$$[Z^-] = [PAA] \left(\frac{1}{1 + 10^{(pK_z - pH)}} \right) \quad (14)$$

and

$$[HZ] = [PAA] \left(\frac{10^{(pK_z - pH)}}{1 + 10^{(pK_z - pH)}} \right) \quad (15)$$

In the simulation the acid-base equilibrium reactions were represented by very fast reactions and it was verified that the arbitrarily chosen large value of the rate constant was high enough to obey the equilibrium equation at all places and at all times. These reactions are homogeneous non-catalyzed and thus also take place in absence of the enzyme. In order to avoid confusion, these very fast homogeneous reactions are not included in the reactor models in the following paragraphs.

With the kinetic parameters as stated above, the batch experiment was simulated (dashed curve in Figure 6). Unfortunately, it appeared that the experimental data could not be described well with the kinetic model; the simulated conversion was significantly lower than the experimental conversion. Since it appears that the absolute conversion rate may vary significantly, depending on pretreatment and possibly storage conditions, it was decided to adapt the kinetic parameters to obtain a better fit. A sensitivity analysis showed that the reaction rate constant k_{cat} and the adsorption constant K_{m6APA} have the largest influence on the reaction rate. k_{cat} influences the rate over the whole range whereas K_{m6APA} particularly influences the rate at higher conversion. By adaptation of the constants (by changing the numerator) in both parameters, a much better fit of the experimental data could be obtained, which is also shown by the bold curve in Figure 6. The adapted parameters are as follows:

$$k_{cat} = \frac{80}{1 + \frac{10^{-pH}}{10^{-5}}} \quad (7a) \quad K_{m6APA} = \frac{4.0}{1 + \frac{10^{-pH}}{10^{-6.4}}} \quad (9a)$$

$$K_{mPen} = 1 + \frac{0.2 \cdot 10^{-7}}{10^{-pH}} \quad (8) \quad K_{mPAA} = \frac{100}{1 + \frac{10^{-pH}}{10^{-6.15}}} \quad (10)$$

It was not attempted to fit the data at a conversion above 0.8 since it is known that the enzyme deactivates at very high pH, which occurs at the location in the liquid where the KOH droplets fall in the solution. And this deactivation effect will be most pronounced at long batch times, thus at high conversion. The numerical values of the kinetic parameters and initial literature values at pH 8.5 are summarized in Table 2.

Table 2. Parameter estimations from the adapted parameter equations to fit the kinetic data with Equation (3).

Parameter	Value	Initial value [15]
k_{cat}	79.9	49.9
K_{app}^c	31.4	31.4
Km_{Pen}	7.3	7.3
Km_{6APA}	3.99	0.99
Km_{PAA}	99.7	99.7

3.2.3 Hydrodynamic properties of different reactor configurations

To create comparable conversions in the MLR and the packed bed, analysis should be done at the same space-time. In Table 3, the selected flow rates are given with their characteristic times and liquid velocities.

Table 3. Calculation of space-time and superficial liquid velocity

ϕ [ml min ⁻¹]	MLR		Packed bed	
	τ [s]	v_L [cm s ⁻¹]	τ [s]	v_L [cm s ⁻¹]
	$\tau_m = \frac{L_m}{v_s}$	$v_s = \frac{\phi_l}{A_{m,open}}$	$\tau_i = \frac{L_b \cdot \varepsilon_b}{v_s}$	$v_s = \frac{\phi_l}{A_b}$
15.0	33.6	0.12	9.5	0.11
52.5	9.5	0.42	2.9	0.35

At equal flow rates the residence time in a packed bed of Immob is about 3.5 times shorter than in a monolith. For example, at a flow rate of 15 ml/min the residence time in a packed bed ($L_b = 1$ cm) is 9.5 seconds while residence time in the monolith ($L_m = 4$ cm) structure is 33.6 seconds.

The liquid-solid mass transfer for single-phase flow in a separate channel has been studied extensively in literature. Most equations are based on dimensionless analysis. An important mass transfer related dimensionless correlation is the Sherwood number, which describes the ratio between the actual mass transfer and the diffusion. The most widely used correlation for monoliths was developed by Hawthorn [26] (see Table 4). Some important dimensionless correlations that were already used in the previous chapter are summarized in Table 4.

Table 4. Dimensionless correlations to describe mass transfer in a monolith channel

$Sh_{wall,i} = Sh_{\infty} \left(1 + C \cdot Re \cdot Sc_i \frac{d_{ch}}{L_m} \right)^{0.45} \quad (16)$	$Ca = \frac{r_{reaction}}{r_{convection}} = \frac{r_{v,obs}}{a' \cdot k_s \cdot C_{b,i}} \quad (20)$
<p>for $Gz < 0.03$</p> $Re = \frac{\rho \cdot v_L \cdot d_{ch}}{\eta} \quad (17)$	$\Phi = \left(\frac{n+1}{2} \right) \cdot \frac{r_{v,obs} \cdot L^2}{D_{eff, chit} \cdot C_{b,i}} < 0.15 \quad (21)$
$Sc = \frac{\eta}{\rho_i \cdot D_i} \quad (18)$	$Gz = \frac{L_m}{Sc \cdot Re \cdot d_{ch}} \quad (22)$
$Sh = \frac{k_s \cdot d_{ch}}{D_i} \quad (19)$	$D_{eff,i} = \frac{D_i \cdot \varepsilon_{gel} \cdot \sigma}{\tau} \quad (23)$

For a packed bed of beads of Immob, the correlations 16-23 have to be adapted to describe the flow through the bed of particles. Equation 19 transforms to an equation for k_s over one particle:

$$Sh = \frac{k_s \cdot d_p}{D_i} \quad (24)$$

For packed beds, also the bed porosity must be taken into account and the shape of the particles. Thoenes and Kramer [31], developed the following equations to include bed geometry:

$$Sh' = \frac{Sh \cdot \varepsilon_b}{(1 - \varepsilon_b)\gamma} = 1.0(Re')^{1/2} Sc^{1/3} \quad \text{for } 0.25 < \varepsilon_b < 0.5, 40 < Re < 4000, Sc > 1 \quad (25)$$

in which γ is a shape factor that is 1 for spheres.

$$Re' = \frac{Re}{(1 - \varepsilon_b)\gamma} \quad (26)$$

where Re is first calculated over the particle with:

$$Re = \frac{\rho \cdot v_L \cdot d_p}{\eta} \quad (27)$$

The diffusivity in a liquid, D_i , was estimated using the correlation from Wilke and Chang (1955) [33]:

$$D_i = \frac{2.34 * 10^{-13} T \sqrt{\varphi M_{solv}}}{\eta V_m^{0.6}} \quad (28)$$

where φ = an association factor for the solvent (2.6 for water, 1.9 for methanol, 1.5 for ethanol, and 1.0 for unassociated solvents), and V_m = molar volume of the solute at its boiling point. For PAA (phenyl acetic acid, $C_8H_8O_2$) the molar volume was estimated at $172 \times 10^{-6} \text{ m}^3 \text{ mol}^{-1}$. Using water as solvent ($M = 0.01806 \text{ kg mol}^{-1}$ $\varphi = 2.6$), the diffusivity of PAA at 304 K was estimated at $9.0 \times 10^{-10} \text{ m}^2 \text{ s}^{-1}$. For Penicillin G and 6-APA it was estimated at $4.0 \times 10^{-10} \text{ m}^2 \text{ s}^{-1}$. For H^+ and OH^- , V_m is difficult to estimate and they also cause the 'drag' of water molecules. To simplify the calculations, the diffusivity for PAA was also used for OH^- and H^+ . From the derived correlations the mass transfer coefficient k_s was calculated for the monoliths at the two different flow rates, using the parameters listed in Table 5. Results are given in Table 6.

Table 5. Parameters and constants for the hydrolysis of penicillin G at 304 K

Parameter	Value	Reference
Asymptotic Sherwood, Sh_{∞}	3.53 for rounded corners	[27]
Surface roughness, C	0.095 [-]	[28]
Fluid viscosity, η	7.9×10^{-4} [Pa s ⁻¹]	[29]
Liquid density, ρ	995 [kg m ⁻³]	[30]

Table 6. Estimation of k_s for Pen G in a tubular reactor with Immob (packed bed) and in a monolith reactor

Flowrate [ml min ⁻¹]	Immob packed bed			Monolith reactor			
	$Re^?$ [-]	$Sh^?$ [-]	k_s [m s ⁻¹]	Re [-]	Gz [-]	Sh [-]	k_s [m s ⁻¹]
15	0.7	10	1.0×10^{-5}	1.6	9×10^{-3}	9.6	3.5×10^{-6}
52.5	2.8	20	1.9×10^{-5}	5.8	3×10^{-3}	16.5	6.1×10^{-6}

From the results in Table 6 it becomes clear that $Gz < 0.03$, it is therefore allowed to calculate Sh in the monolith channel from equation 16.

Mass transfer limitations

The diffusion of the reactant and products inside the chitosan is slower than in the reaction mixture. If equation 23 is used to estimate the effective diffusion coefficient in the same way as was done in chapter 10 ($\varepsilon = 0.8$, $\tau = 1.2$, $\sigma = 1$), D_{eff} for Pen G becomes 2.7×10^{-10} m² s⁻¹. If internal diffusion of the reactant is considered (inside the gel layer), a suitable criterion can be the Wheeler-Weisz criterion (equation 21). With $V_{\text{cat}} = 2.4$ ml ($L = 67$ μm) for 2.5 g beads, and 3.3 ml ($L = 90$ μm) for the monoliths, and assuming first order kinetics Φ is calculated for both reactor types (see Table 7).

The presence of external mass transfer problems can be deduced from the Carberry number (20). Since the maximum theoretical mass transfer coefficient is not exactly known, the values for k_s that were estimated in Table 6 are used here. With $a' = 2800$ m⁻¹ for 400 cpsi monoliths and $a' = 6/dp = 15000$ m⁻¹ for the beads, the values for Ca are reported in Table 7.

Table 7. Calculation of Ca and Φ for the reactant pen G in different reactors in the hydrolysis of PenG at 304 K

Reactor	$\phi = 15$ ml min ⁻¹			$\phi = 52$ ml min ⁻¹		
	r_{obs} [mmol s ⁻¹]	Φ [-]	Ca [-]	r_{obs} [mmol s ⁻¹]	Φ [-]	Ca [-]
Packed Bed upflow	2.9×10^{-3}	0.15	3.3×10^{-3}	-	-	-
Packed Bed downflow	4.2×10^{-3}	0.23	4.7×10^{-3}	-	-	-
MLR	3.3×10^{-3}	0.15	0.4	5.0×10^{-3}	0.2	0.35
Batch	8.5×10^{-3}	0.25	<<0.05	-	-	-

The initial rate of the packed bed in upflow operation is slightly lower than for downflow operation. The reason for this behavior will be discussed in more detail in paragraph 3.3.1. All systems are affected by internal diffusion due the use of the chitosan gel. The MLR is the best choice to decrease the internal diffusion limitations, especially if slightly thinner chitosan

coatings can be applied onto the monoliths. This reactor however is strongly externally limited at these low flow rates (see Table 6 for the large difference in estimated k_s). At increased flow rate, the reaction rate increases significantly in the MLR, while no improvement is observed in Ca and Φ . Apparently, the rate does not increase due to decreased mass transfer limitations. The most important difference between 15 and 52 ml min⁻¹ is the lower conversion per pass and therefore the significantly smaller decrease in pH. This observation introduces an extra difficulty in comparing the MLR with the packed bed; the bed is 4 times shorter than the monolith so the enzyme that is present at the outlet of the monolith reactor is most likely not used effectively or even deactivated by the low local pH. This large effect of local pH was already observed for free PGA II. When the reaction takes place in a batch reactor, as is the case for free enzyme and Immob, (almost) no local pH gradients are present due to instantaneous mixing. In the packed bed and monolith reactor, a local pH gradient will exist over the reactor because pH is not controlled in the reaction section. When the liquid flow is increased, the system will approach the behavior of a batch reactor, and local pH gradients will minimize. This effect will be described in the following section.

3.3 Pen G hydrolysis in different reactors with PGA I

To compare the different biocatalysts, different set-ups were used; a batch reactor, a packed bed reactor, and a monolith loop reactor. The set-ups are schematically depicted in Figure 7.

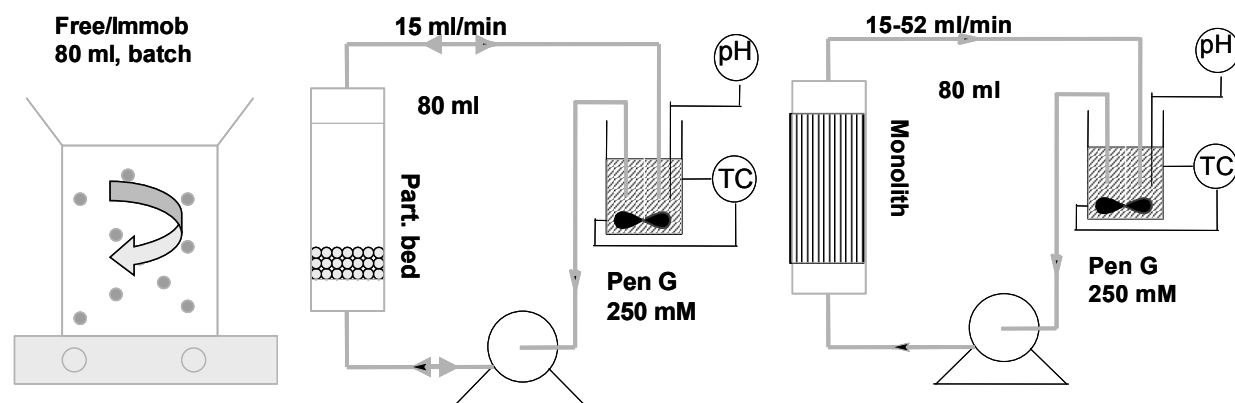


Figure 7. Different reactor configurations used in the enzymatic hydrolysis of Pen G at 304 K

Free and immobilized PGA I are used in the hydrolysis of penicillin G at 304 K and pH 8.5.

3.3.1 Comparison of the different reactor configurations

The performance of a monolithic structure is compared with the performance of a packed bed of Immob in the column at different flow rates. Hydrolysis of a 250 mM penicillin solution was done with PGA I/II Immob, equivalent to the enzyme loading on the monolith ($L_b \approx 1$ cm) and with monolithic structures loaded with PGA I/II. It was found that for PGA I Immob

the reaction rate is higher in downflow operation than in upflow operation. The performance of a monolith in upflow lies in between (Figure 8a).

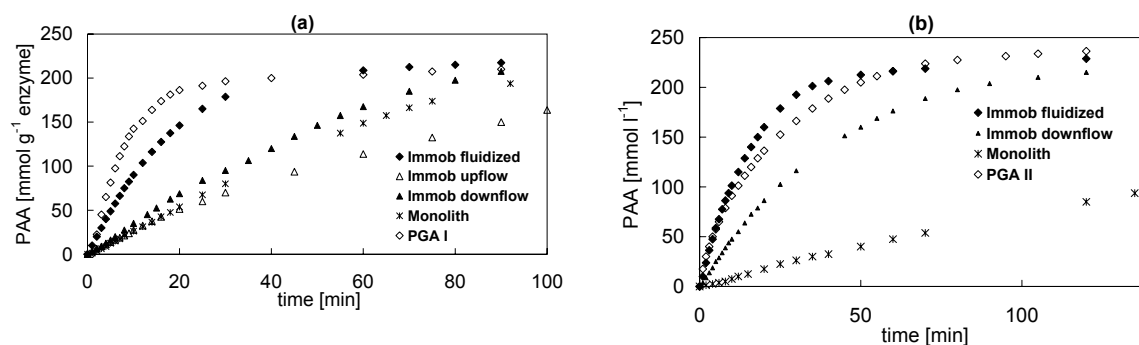


Figure 8. a) Product concentration of Free PGA I, Immob, and monolith equivalent to 120 mg enzyme at 304 K and pH=8.50 b) Product concentration of Free PGA II, Immob, and monolith equivalent to 50 mg enzyme at 304 K and pH=8.50

For PGA II, a larger difference in apparent reaction rate between Immob and monolith was found, when operated in downflow (Figure 8b) compared to PGA I (Figure 8a). The reason for this remains unclear. A possible explanation can be the different pH-sensitivity for both enzymes. As was observed before in the initial rate experiments (paragraph 3.2.1) PGA II is more sensitive for changes in pH. The difference between PGA II Immob and the PGA II monolith can probably be found in this low pH-stability. The reaction rate of PGA II Immob decreases with conversion. This is an indication that substrate is the limiting factor. In this system the pH is constant in the (well-mixed) batch reactor, so practically no deactivation is observed. The reaction rate for the PGA II-monolith remains constant throughout the reaction (0-order behavior). This suggests that the conversion is taking place at the maximum rate, without mass transfer limitations. The reason can be found in the sharp pH drop that is present over the reactor. The reaction rate is strongly influenced by local pH and decreases significantly at lower pH.

From the performance of Immob (Figure 8), it is evident that the flow direction and reactor configuration have a significant impact on the observed reaction rate. Since no pressure drop exists over the bed, rates of convective mass transfer can be assumed equal in both upflow and downflow operation. It is believed that the flow distribution in the radial direction in upflow operation is uneven compared to the downflow regime, leading to a lower observed reaction rate for the downflow-case.

Measurement of pH in the column effluent supports that the conversion rate is equal in a monolithic structure and a packed bed with Immob in the case of PGA I (Fig 8a). The pH gradient over the column is the same for both monolith and Immob packed bed, which indicates that an equal amount of acid is produced per unit time; hence a similar amount of substrate has been converted.

3.3.2 Effect of flow rate in the MLR

Increasing the flow rate from 15 to 52 ml min⁻¹ increased the apparent reaction rate by a factor 2 (Figure 9). Taking into account the estimated values for Ca and Φ (Table 7), this does not seem to be the result of decreased mass transfer limitations. The reaction rate has increased much more than could be expected based on the estimated mass transfer coefficient. The reason for the increase is the lower drop in pH over the reactor at higher flow rate. The kinetics of this reaction strongly depends on pH; a decrease in pH leads to a strong decrease in reaction rate. So the reaction rate over the monolith length is not constant. It would therefore be interesting to explore the effect of increase in flow rate further.

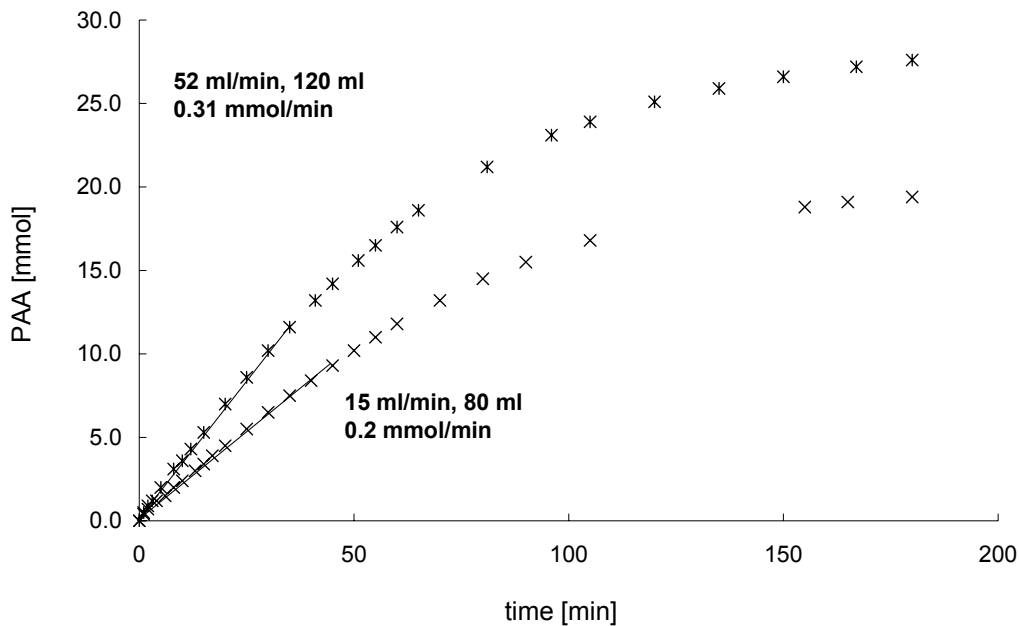


Figure 9. Product formation for a monolith with immobilized penicillin G acylase (PGA I) at flow rates of 15 and 52.5 ml min⁻¹ at 303 K in aqueous medium, pH 8

Increasing the liquid velocity would lead to an increase in k_s , and a decrease in the pH gradient. Another solution could be the use of smaller monolith pieces with intermediate NaOH addition to reduce the drop in pH over the total reactor volume. Possible, the use of a different reactor type could lead to better results. In the Monolith Stirrer Reactor (MSR), no pH gradients are present, because the vessel is well-mixed. Secondly, the channel velocities can be significantly increased compared to the MLR ([32] reports values of 1-5 cm s⁻¹, even at low stirrer rates, compared to the 0.5 cm s⁻¹ in the MLR).

3.4 Simulation of the experimental results

The simulation of the batch operation with free Separase was already discussed in paragraph 3.2.1.

3.4.1 Batch reactor with PGA I-Immobilized

Although it was found that the initial reaction rate for free enzyme is twice as high as the reaction rate for PGA I Immobilized (Figure 5), the total conversion proceeds much faster for the immobilized enzyme. This is depicted in Figure 10 for free PGA I (open symbols) and PGA I-Immobilized (closed symbols). The immobilized enzyme reaches full conversion after around 80 min, whereas the free enzyme reaches full conversion only after more than 350 min (not shown). It appears that the presence of transport limitations in and around the chitosan spheres significantly lowers the *initial* conversion rate. Particularly the transport of the formed PAA (a weak acid that leads to low local pH values) from the spheres is limiting. It causes the pH to decrease significantly, down to about 3 – 4, which significantly reduces the reaction rate via the pH dependencies of the kinetic parameters. The faster overall conversion of the immobilized enzyme compared to the free enzyme is caused by the pH sensitivity of the free enzyme. Inside the beads, the enzyme is protected against a pH-shock that can be caused by adding concentrated NaOH to the reactor.

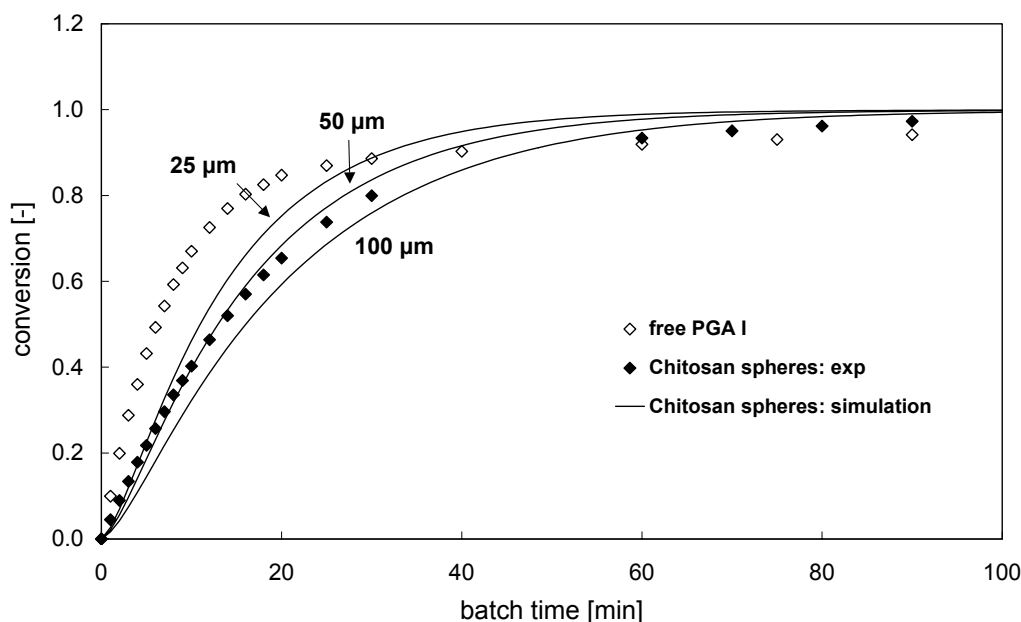


Figure 10. Fit of the experimental data from hydrolysis of Pen G with immobilized PGA I in chitosan spheres in batch obtained using the adapted kinetics and pH correction factors (as described in the next paragraph) and assuming different egg-shell thicknesses of 25, 50 and 100 micron; the symbols represent the experimental data

The diffusion coefficient for the PAA was estimated at $9.0 \times 10^{-10} \text{ m}^2 \text{ s}^{-1}$ using the Wilke & Chang method [33]. In a stirred reactor containing small solid spheres, the mass transfer coefficient for the mass transfer from the bulk liquid towards the edge of the catalyst particles, $k_{s,batch}$, follows from the Sherwood number (Sh) according to:

$$k_{s,batch,i} = \frac{Sh \cdot D_i}{d_p} \quad (29)$$

The value of the Sherwood number for component i in the liquid ($Sh_{i,l}$) is estimated according to the method described by Sano et al. [34]:

$$Sh_i = \varphi_C \left\{ 2.0 + 0.4 Re_K^{0.75} Sc_i^{1/3} \right\} \quad (30)$$

Where φ_C = the Carman correction factor for the shape of the particle: $\varphi_C = 6 V_p/A_p$ (this results in $\varphi_C = 1$ for a spherical particle). And with the Kolmogorov Reynolds number Re_K defined as:

$$Re_K = \frac{\rho d_p^{4/3} \bar{\varepsilon}^{1/3}}{\eta} \quad (31)$$

The energy dissipation rate per unit mass of liquid ($\bar{\varepsilon}$) can be measured, it can also be predicted using an empirical value of the power number according to:

$$\bar{\varepsilon} = \frac{N_{Pw} N_I^3 d_I^5}{V_L} \quad (32)$$

For turbulent flow, the Power number N_P is 4-6 for turbine impellers (Bates *et al.*, [35]), and 0.5-1.5 for propellers and inclined blade turbines. The Power number for a magnetic flea was estimated at 0.5. The stirring speed was 500 rpm and the length of the magnetic flea was 2.0 cm. The experiments were carried out in a 150 ml beaker. Following this approach, the external mass transfer coefficient in the batch reactor with PGA I Immob was estimated at $9.0 \times 10^{-5} \text{ m s}^{-1}$.

To simulate the conversion in the batch reactor, a mass balance over the reactor yields (Using: N_p = total number of catalyst particles in the CSTR):

accumulation = mass transfer to chitosan gel beads (all terms expressed in mol s⁻¹)

$$\begin{aligned} \frac{\partial C_{i,b}}{\partial t} V_L &= -k_{s,i} N_p \pi d_p^2 (C_{i,b} - C_{i,s}) \\ &= -k_{s,i} \frac{V_{cat}}{\frac{1}{6} \pi d_p^3} \pi d_p^2 (C_{i,b} - C_{i,s}) \\ &= -k_{s,i} \frac{6 V_{cat}}{d_p} (C_{i,b} - C_{i,s}) \end{aligned} \quad (33)$$

or:

$$\frac{\partial C_{i,b}}{\partial t} = -k_{s,i} \frac{6 V_{cat}}{d_p V_L} (C_{i,b} - C_{i,s}) \quad (34)$$

Initial estimates: $C_{i,b} = C_{i,0}$ and $C_{i,s} = C_{i,0}$

If it is assumed that the enzyme is homogeneously distributed in the chitosan gel spheres the mass balance inside the spheres is represented by (using: $\xi = r_p / \frac{1}{2} d_p$):

accumulation = radial diffusion + production/reaction (per unit of gel sphere volume)

$$\varepsilon_p \frac{\partial C_i}{\partial t} = \frac{4}{d_p^2} \frac{D_{i,eff}}{\xi^2} \frac{\partial}{\partial \xi} \left(\xi^2 \frac{C_i}{\partial \xi} \right) + \nu_i r_j \quad (35)$$

It is however more likely that the enzyme is not distributed homogeneously throughout the chitosan bead. If the catalyst is located in a thin layer at the surface (a so-called egg-shell distribution) a different model has to be used. If the egg-shell layer thickness is small compared to the particle size, the geometry can be approached with a flat-plate geometry (this is reasonably accurate up to a thickness of about 0.2 times the sphere diameter). This gives (using $\xi = r/d_{egg-shell-thickness}$):

accumulation = radial diffusion + production/reaction (per unit of gel sphere volume)

$$\varepsilon_p \frac{\partial C_i}{\partial t} = \frac{D_{i,eff}}{d_{egg-shell-thickness}^2} \frac{\partial^2 C_i}{\partial \xi^2} + \nu_i r_j \quad (36)$$

Initial values: $C_i=0$, left boundary equation (pellet center, $\xi = 0$): $\frac{\partial C_i}{\partial \xi} = 0$, right boundary equation (pellet edge, $\xi = 1$): $C_i = C_{i,s}$.

It is assumed that the enzyme is homogeneously distributed in the egg-shell layer of the chitosan gel spheres. Since in reality the enzyme concentration will gradually decrease when going deeper in the chitosan spheres, the model should be treated as a rough approximation. From literature data [36] follows that the egg-shell layer thickness of the enzyme and immobilization phase used in this study is in the order of 10 - 100 μm . In the simulations the accumulation term is neglected since it causes numerical problems in combination with the dynamic bulk mass balances and since its contribution is negligibly small.

If the enzyme distribution in the chitosan spheres is according to an egg-shell distribution, the concentration at the external surface of the pellets ($C_{i,s}$) follows from:

mass transfer to catalyst = diffusion into catalyst pellet (at the edge) (per unit of bed volume)

$$N_{pp} \pi d_p^2 k_{s,i} (C_{i,b} - C_{i,s}) = N_{pp} \pi d_p^2 D_{i,eff} \left. \frac{\partial C_i}{\partial \xi} \right|_{\xi=1} \frac{1}{d_{egg-shell-thickness}} \quad (37)$$

which leads to:

$$C_{i,b} - C_{i,s} = \frac{D_{i,eff}}{k_{s,i}} \frac{I}{d_{egg-shell-thickness}} \frac{\partial C_i}{\partial \xi} \Big|_{\xi=1} \quad (38)$$

$$C_{i,s} = C_{i,b} - \frac{D_{i,eff}}{k_{s,i}} \frac{I}{d_{egg-shell-thickness}} \frac{\partial C_i}{\partial \xi} \Big|_{\xi=1}$$

The balance for the particle is solved with Athena Visual Studio using orthogonal collocation using six interior collocation points. The particle mass balances and the reactor mass balances were solved sequentially. A sensitivity analysis showed that both the internal and the external transport resistance are of comparable importance, which implies that the optimal thickness of the egg-shell layer depends on the estimated diffusion coefficient and external mass transfer coefficient.

Using the kinetics with the adapted parameters (paragraph 3.2.1), the thickness of the egg-shell layer was varied (25-100 μm) in order to get the best fit with the experimental data (symbols in Figure 10). The conversion of component i (X_i) can be calculated with:

$$X_i = \frac{C_{i,feed}^{\circ} - C_{i,b,exit}^{\circ}}{C_{i,feed}^{\circ}} \quad (39)$$

The results (lines in Figure 10) indicate that the best fit was obtained with an egg-shell layer thickness of 50 μm , which falls well within the range indicated by Van Roon *et al.* [36]. It was not useful to try to adapt the pH dependencies of the kinetic parameters using these experimental data since also the egg-shell layer thickness is very uncertain. Therefore it was decided to use the experimental data obtained with the PFR of chitosan spheres in combination with a CSTR, which will be discussed in the next paragraph, to adapt the pH dependency of the rate parameters. These experimental data are much more suitable to fit the pH dependency of the parameters since these in these experiments the influence of transport limitations in and around the spheres is much smaller and thus only hardly dependent of the assumed egg-shell layer thickness.

3.4.2 PFR with PGA I Immob

The packed bed reactor was operated in both up- and downflow. The experimental data of the PGA I Immob in upflow operation (dark symbols) is given in Figure 11. The data for the batch reactor (light symbols) are given for comparison.

In a typical liquid-solid fixed bed, the mass transfer coefficient for the mass transfer from the bulk towards the edge of the catalyst particles ($k_{s,PFR}$) follows from the Sherwood number (Sh) according to:

$$k_{sPFR,i} = \frac{Sh_i \cdot D_i}{d_p} \quad (40)$$

The value of the Sherwood number for component i in a packed bed (Sh_i) is estimated from the empirical formula from Thoenes & Kramer *et al.* [31] (equation 25). At the present conditions, the mass transfer coefficient for PAA was found to be $1.4 \times 10^{-5} \text{ m s}^{-1}$. For comparison, the k_s of Pen G was estimated at 1.0×10^{-5} (see Table 6).

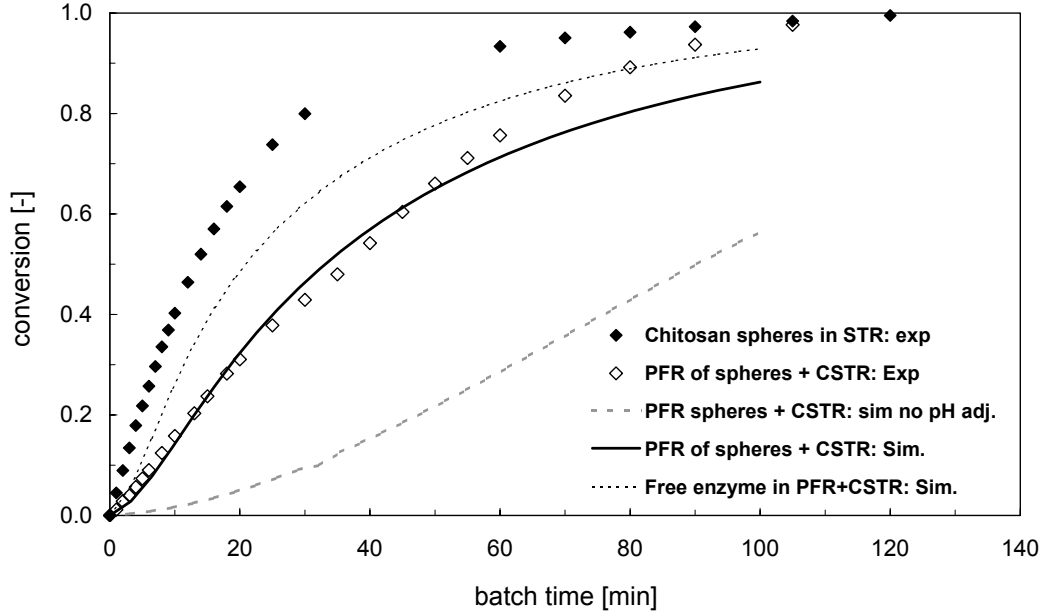


Figure 11. Fit of the experimental data obtained with the set-up consisting of a PFR of chitosan spheres in combination with a CSTR without catalyst using the reaction kinetics without adaptation of the pH influence (dashed gray curve), after adaptation of the pH influence (solid curve) and when transport limitations inside the chitosan spheres are neglected (black dashed curve). For the egg-shell thickness, a value of $100 \mu\text{m}$ was used

The reactor is modeled as a PFR, coupled to a CSTR where no catalyst is present, but where the pH value is re-adjusted to 8.5 by adding NaOH. The mass balance over the PFR reactor, using N_{pp} = total number of chitosan beads per unit of reactor volume yields:

$$\text{accumulation} = - (\text{axial convection} - \text{mass transfer to catalyst pellets})$$

(all expressed per unit of bed volume)

$$\begin{aligned} \varepsilon_b \frac{\partial C_{i,b}}{\partial t} &= - \frac{l}{L_b} \frac{\partial (u_0 C_{i,b})}{\partial z} - N_{pp} \pi d_p^2 k_{s,i} (C_{i,b} - C_{i,s}) \\ &= - \frac{l}{L_b} \frac{\partial (u_0 C_{i,b})}{\partial z} - \left(\frac{\frac{V_{cat}}{\frac{1}{6} \pi d_p^3}}{A_b L_b} \right) \pi d_p^2 k_{s,i} (C_{i,b} - C_{i,s}) \\ &= - \frac{u_0}{L_b} \frac{\partial C_{i,b}}{\partial z} - \frac{6 V_{cat}}{A_b L_b d_p} k_{s,i} (C_{i,b} - C_{i,s}) \end{aligned} \quad (41)$$

Using $L_b = \frac{V_{cat}}{(1 - \varepsilon_b) A_{bed}}$, or $\frac{V_{cat}}{A_b \cdot L_b} = (1 - \varepsilon_b)$ yields:

$$\varepsilon_b \frac{\partial C_{i,b}}{\partial t} = -\frac{u_0}{L_b} \frac{\partial C_{i,b}}{\partial z} - \frac{6(1-\varepsilon_b)}{d_p} k_{s,i} (C_{i,b} - C_{i,s}) \quad (42)$$

Boundary values $z = 0$: $C_{i,b} = C_{i,b,tank}$

Initial values: $C_{i,b} = C_{i,0}$ and $C_{i,s} = 0$

The mass balance over the chitosan layer and the liquid film surrounding the pellet are the same as for the batch system (Equations 36 and 38 in paragraph 3.4.1)

For the stirred tank without catalyst, the mass balance becomes:

$$\text{accumulation} = (\text{amount fed} - \text{amount withdrawn})$$

$$\frac{\partial C_{i,tank}}{\partial t} V_L = (F_v C_{i,in} - F_v C_{i,tank}) \quad (43)$$

Neglecting the dead time in the tubing between the bed and the stirred tank and with defining in the fixed bed at the outlet ($z = 1$): $C_{i,b} = C_{i,b,exit}$ gives:

$$C_{i,in} = C_{i,b,exit}$$

Initial estimates: $C_{i,tank} = C_{i,0}$

The conversion was calculated with Equation 39. The results of the first simulation are given in Figure 11 as the dashed gray curve. It appears that the simulated conversion using the new kinetic parameters is significantly lower than the experimental conversion indicated by the symbols. The major cause of the deviation is related with the decrease of the pH in the PFR due to the reaction. It appears that the pH very quickly decreases to values below 3.5 in the initial zone of the PFR thus decreasing the reaction rates strongly. This decrease of the reaction rate also results in a large decrease of the transport limitations inside and around the chitosan spheres, thus eliminating the possibility that the deviation is mainly due to transport limitations. The only way to get a better fit of the experimental data without influencing the conversion rate of the batch reactor with the free enzyme (the homogeneous system in which the pH is kept constant at 8.5) is to adapt the pH dependency of the reaction rate. This was done by adapting the pH dependency of the rate constant k_{cat} , the adsorption constant K_{6APA} , and the adsorption constant K_{PAA} in the following way:

$$k_{cat} = \frac{80}{1 + \frac{10^{-pH}}{C_1 \times 10^{-5}}} \times \frac{1 + \frac{10^{-3.5}}{C_1}}{1 + 10^{-3.5}} \quad (44)$$

$$K_{6,APA} = \frac{4}{1 + \frac{10^{-pH}}{C_1 \times 10^{-6.4}}} \times \frac{1 + \frac{10^{-2.1}}{C_2}}{1 + 10^{-2.1}} \quad (45)$$

$$K_{PAA} = \frac{100.0}{1 + \frac{10^{-pH}}{C_3 \times 10^{-6.15}}} \times \frac{1 + \frac{10^{-2.35}}{C_3}}{1 + 10^{-2.35}} \quad (46)$$

These rather complex equations were needed to achieve that the rate is not influenced by the modification factors C_1 , C_2 , and C_3 at pH = 8.5 at which a good fit was obtained. Since the number of available experimental data is insufficient to do thorough parameter estimation, it was only tried to find a reasonable estimate of the modification factors when using the same value for all three factors. It appeared that a value of 20 (i.e. using $C_1 = C_2 = C_3 = 20$) yielded a good fit, which is indicated by the solid curve in Figure 11.

At a closer look at the simulation curve it can be seen that the rate increases in the beginning of the experiment. This can be explained by the fact that the removal of the acid in the spheres is mainly taking place by diffusion of PAA out of the spheres since the concentration of H^+ and OH^- ions, the only other species that can achieve a removal of acid from the spheres, is relatively much lower. In the beginning of the experiment the concentration of PAA is still very low which results in a very low pH of about 3.5 and this value already increases to about 4.25 after a few percent conversion has occurred. The rate slows down quite strongly at high conversion, much stronger than for example in the free enzyme experiment (as shown in Figure 6). An analysis showed that this effect is due to the close approach to equilibrium inside the PFR. For achieving very high conversion this reactor set-up is thus not attractive, unless the flow rate is increased significantly. The reason for the deviation of the model from the experimental results at higher conversion can be a combination of the relatively large error in the estimated reaction rate (this parameter was only estimated until a conversion of 0.8) and a deviation from an ideal packed bed during real time operation. It is possible that some turbulence in the bed (the beads were not held in a confined space but could freely move in the tube) caused enhanced mixing, leading to faster conversion compared to the simulated data. In order to get an impression of the influence of mass transport limitations another simulation was performed of the imaginary experiment in which it is assumed that the enzyme was homogeneously distributed in the PFR. The result of this simulation is indicated by the black dashed curve. It appears that there is only a weak influence of transport limitations on the conversion rate.

3.4.3 Monolith reactor with immobilized PGA I

The results of the experiments with a MLR at different flow rates (triangles) are given in Figure 12.

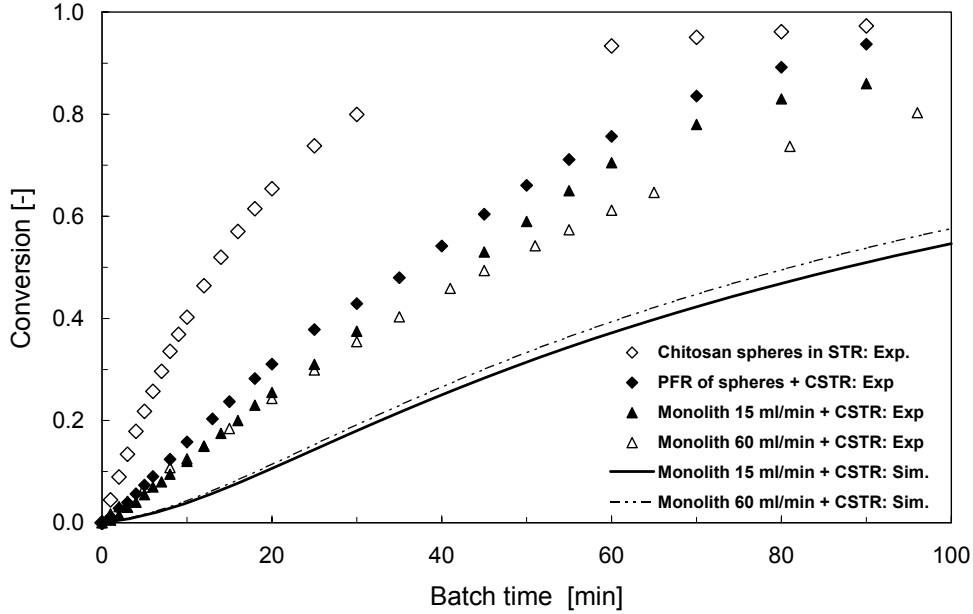


Figure 12. Fit of the experimental data obtained with the set-up consisting of a monolith reactor coated with a chitosan layer containing the enzyme in series with a CSTR without catalyst using the reaction kinetics after adaptation of the pH influence (bold curves) The thickness of the active layer, i.e. the layer containing the enzyme, was assumed to be 100 μm

The results of the PFR and the batch reactor are included for comparison. The MLR was modeled as a monolith section and a stirred tank with no catalyst present, where the pH was adjusted by adding concentrated NaOH. The mass balance over the monolith section is (using N_{ch} = total number of channels per unit of reactor volume):

accumulation = - (*axial*) *convection* - *mass transfer to channel wall*
(all expressed per unit of bed volume)

$$\begin{aligned} \frac{\partial C_{i,b}}{\partial t} &= - \frac{1}{L_m} \frac{\partial (u_0 C_{i,b})}{\partial z} - \frac{N_{ch} \pi d_{ch} L_m}{\varepsilon_b \frac{\pi}{4} d_m^2 L_m} k_{wall,i} (C_{i,b} - C_{i,s}) \\ &= - \frac{u_0}{L_m} \frac{\partial C_{i,b}}{\partial z} - \frac{4 N_{ch} d_{ch}}{\varepsilon_b d_m^2} k_{wall,i} (C_{i,b} - C_{i,s}) \end{aligned} \quad (47)$$

Boundary values $z = 0$: $C_{i,b} = C_{i,b,tank}$

Initial values: $C_{i,b} = C_{i,0}$, and: $C_{i,s} = 0$

It is assumed that the enzyme is homogeneously distributed in the egg-shell layer of the chitosan gel layer. Since in reality the enzyme concentration will gradually decrease when going deeper in the chitosan layer, the model should be treated as a rough approximation.

The concentration at the external surface of the gel layer ($C_{i,s}$) follows from (using: $\xi = r/d_{\text{egg-shell-thickness}}$):

accumulation = radial diffusion + production/reaction (per unit of chitosan volume)

$$\varepsilon_p \frac{\partial C_i}{\partial t} = D_{i,\text{eff}} \frac{\partial^2 C_i}{\partial \xi^2} + v_i r_j \quad (48)$$

Initial values: $C_i = 0$, left boundary equation (inside edge of egg-shell layer) ($\xi = 0$):

$$\frac{\partial C_i}{\partial \xi} = 0, \text{ right boundary equation (interface) } (\xi = 1): C_i = C_{i,s}.$$

The concentration at the external surface of the monolith ($C_{i,s}$) follows from:

mass transfer to catalyst = diffusion into pellet (at the edge) (per unit of bed volume)

$$N_{ch} \pi d_{ch}^2 k_{s,i} (C_{i,b} - C_{i,s}) = N_{ch} \pi d_{ch}^2 D_{i,\text{eff}} \frac{\partial C_i}{\partial \xi} \Big|_{\xi=1} \frac{1}{d_{\text{egg-shell-thickness}}} \quad (49)$$

$$C_{i,b} - C_{i,s} = \frac{D_{i,\text{eff}}}{k_{s,i}} \frac{1}{d_{\text{egg-shell-thickness}}} \frac{\partial C_i}{\partial \xi} \Big|_{\xi=1} \quad (50)$$

$$C_{i,s} = C_{i,b} - \frac{D_{i,\text{eff}}}{k_{s,i}} \frac{1}{d_{\text{egg-shell-thickness}}} \frac{\partial C_i}{\partial \xi} \Big|_{\xi=1}$$

The mass balance over the CSTR is given in Paragraph 3.4.2 by Equation 43.

The results of the simulation are presented in Figure 12 as solid lines. When using the adapted reaction kinetics including the adaptation of the pH influence on the kinetic parameters k_{cat} , K_{6APA} , and K_{PAA} , the experimental results could not be described well; the calculated conversion rate is about a factor 2 lower than the experimental conversion, see Figure 12. This is due to the stronger transport limitations when compared with the fixed bed. This is clearly expressed in the mass transfer coefficient k_s which amounts to 3.20×10^{-6} m/s in the monolith with 15 ml min^{-1} flow, whereas it amounts to $1.4 \times 10^{-5} \text{ m s}^{-1}$ in the fixed bed. Since the experimental conversion in the monolith is not much lower than with the fixed bed, the most likely cause of the deviation is in the correlations used for the mass transfer coefficients. E.g. the entrance effect may have enhanced the mass transfer in the monolith more than what is accounted for in the used Sherwood correlation. To address this effect an extra simulation of the monolith reactor was performed in which $k_{s,a}$ was increased compared to the initial estimations. The results are presented in Figure 13.

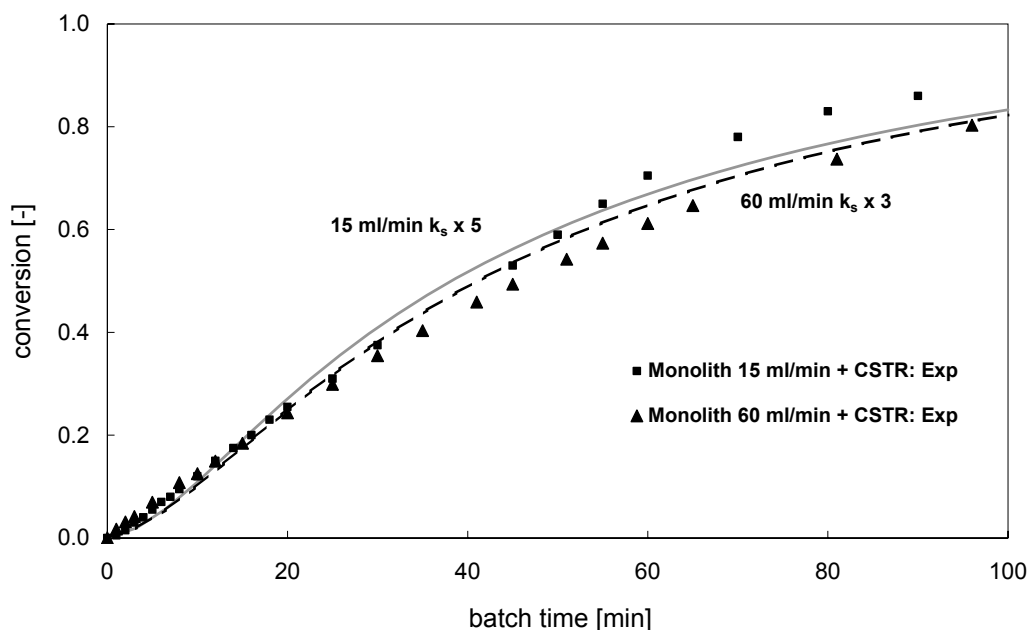


Figure 13. Fit of the experimental data obtained with the set-up consisting of a monolith reactor coated with a chitosan layer containing the enzyme in series with a CSTR without catalyst using the reaction kinetics after adaptation of the pH influence, with increased k_{sa} . The thickness of the active layer, i.e. the layer containing the enzyme, was assumed to be 100 μm

With an increased mass transfer coefficient, the simulation approaches the experimental data fairly well. In reality, the liquid solid mass transfer seems to be enhanced compared to the model. This can be caused by entrance effects or a partially undeveloped boundary layer for mass transfer over the monolith.

4 Conclusions

The covalent bonding of PGA I on chitosan-coated monoliths is 36 mg ml^{-1} gel. PGA II loading on the chitosan-coated monoliths is only 14 mg ml^{-1} gel. An immobilization time of two hours is sufficient to reach 80 % of the equilibrium loading, which was found to be comparable to current industrial carriers. It has been shown that the catalyst system is active in the hydrolysis of Penicillin G. The operational stability was tested in 5 reaction cycles. The catalyst lost 7% of its activity after the first cycle. The monolith system is stable for 35 days while stored in 1,2-propanediol at 277 K. For 400 cpsi monoliths, the volumetric activity was $0.79 \text{ mol s}^{-1} \text{ m}^{-3}_{\text{monolith}}$. Although the monolithic biocatalyst does not perform better than the current industrial catalyst ($4.5 \text{ mol s}^{-1} \text{ m}^{-3}_{\text{catalyst}}$), the rate per gel volume is slightly higher for monolithic catalysts in batch operation. In a continuous set-up (MLR), the reaction rate is limited by external mass transfer and a pH gradient over the length of the catalyst bed. An increase in flow rate reduces the external mass transfer limitations and suppresses the pH drop. A fair comparison between the monolith MLR-system and a packed bed of gel beads is difficult due to the existence of external mass transfer limitations. The performance of PGA II-Immob is superior to the performance of a PGA II monolith in the MLR. The reaction rate

is 5 times higher in the PGA II-Immob system than in the monolithic system. The reactor set-up has a large impact on the observed reaction rate. The apparent reaction rate is 2.5 times higher if Immob is fluidized in the reaction vessel than for the same amount of biocatalyst in a packed bed.

The observed reaction rate Immob is 50% lower than an equal amount of free enzyme, which is due to internal diffusion limitations imposed by immobilization in a gel network. This underlines the importance of realizing short diffusion lengths by control of the thickness of a gel layer coated on a monolithic structure. The effect of pH on the reaction rate was not in agreement with literature values, to simulate the conversion data, the kinetic parameters were adapted as a function of pH. With the new kinetic expression, the batch and fixed bed reactor with beads of immobilized pen G acylase could be simulated successfully. For the monolith reactor, the model predicted a much lower conversion than was experimentally observed. This effect was assumed to be due to a improved mass transfer in the experimental set-up. An increase in k_{sa} of 3-5 resulted in a good fit of the model values. The pH-dependence of the reaction is the main problem for the under-performance of the monolith reactor. To address this problem, other reactor configurations need to be explored.

5 Acknowledgements

Corning Inc. is acknowledged for supplying the cordierite monoliths. Rob Berger is gratefully acknowledged for his contribution to the simulations that are presented in this chapter. Mike Smeltink is acknowledged for performing the experimental part. Adrie Straathof (TU Delft), Emile van de Sandt and Marten Paasman (DSM Anti Infectives, Delft) are acknowledged for their contribution to the theoretical part and supervision. DSM Anti Infectives, Delft is gratefully acknowledged for financial support of this work.

6 Symbols

a'	specific surface area	$[\text{m}^2 \text{m}^{-3}]$
A_b	bed cross section	$[\text{m}^2]$
A_m	monolith cross section	$[\text{m}^2]$
A_p	particle surface area	$[\text{m}^2]$
C	surface roughness	$[-]$
Ca	Carberry number	$[-]$
C_i	concentration of component i	$[\text{mol m}^{-3}]$
$C_{i,b}$	reactant bulk concentration	$[\text{mol m}^{-3}]$
$C_{i,f}$	C_i in the feed	$[\text{mol m}^{-3}]$

$C_{i,s}$	C_i in the external catalyst surface	[mol m ⁻³]
d_b	bed diameter	[m]
d_l	magnetic flea length	[m]
d_p	particle diameter	[m]
d_m	monolith diameter	[m]
D_i	diffusivity component i	[m ² s ⁻¹]
$D_{eff,i}$	effective diffusion coefficient component i	[m ² s ⁻¹]
E	Amount of waste per amount of product	[-]
$[E_0]$	initial enzyme concentration	[mol m ⁻³]
$k_{s,i}$	solid liquid mass transfer coefficient component i	[m s ⁻¹]
k_{cat}	catalytic constant	[s ⁻¹]
K_{app}^c	apparent equilibrium constant	[mol m ⁻³]
$K_{i,j}$	inhibition constant component j	[mol m ⁻³]
$K_{m,j}$	Michaelis-Menten constant component j	[mol m ⁻³]
L	layer thickness	[m]
L_b	bed length	[m]
L_m	monolith length	[m]
m_i	mass component i	[kg]
$M_{w,SEP}$	mass Separase [®]	[Da]
n	reaction order	[-]
N_{Pw}	Power number	[-]
N_p	total amount of beads in the reactor	[-]
N_{pp}	total amount of beads per reactor volume	[-]
N_l	Stirrer speed	[s ⁻¹]
pKz	acid constant	[-]
Pe	Peclet number	[-]
r	radius	[m]
r_j	rate of formation of component i due to reaction	[mol·i m ⁻³ s ⁻¹]
$r_{v,obs}$	observed volumetric reaction rate	[mol s ⁻¹ m ⁻³]
Re	Reynolds number	[-]
Re_k	Kolmogorov- Reynolds number	[-]
Sh_i	Sherwood number component i	[-]
t	time	[s]
T	temperature	[K]
v_L	superficial velocity	[m s ⁻¹]
V_{cat}	catalyst volume	[m ³]
V_L	reaction volume	[m ³]
V_p	particle volume	[m ³]
W_{cat}	amount of Immob beads	[kg]
X_i	conversion of component i	[-]
Y	Yield	[%]

Greek symbols

ε_b	bed porosity	[-]
ε_{gel}	gel porosity	[-]
ε_{cat}	catalyst fraction (= $1 - \varepsilon_b$)	[m ³ -pellet m ⁻³ -bed]
ε_L	liquid holdup	[m ³ -liquid m ⁻³ -bed]
ε_m	monolith porosity	[-]
ε_p	catalyst particle porosity	[m ³ -void m ⁻³ -pellet]
$\bar{\varepsilon}$	energy dissipation rate per unit mass of liquid	[W kg ⁻¹]
γ	shape factor	[-]
ρ_i	density component i	[kg m ⁻³]
ρ_{gel}	gel density	[kg m ⁻³]
ϕ	Liquid flow rate	[m ³ s ⁻¹]
η	Fluid viscosity	[Pa s]
Φ	Wheeler Weiss modulus	[-]
τ	tortuosity	[-]
τ_s	residence time	[s]
ζ	dimensionless particle radius coordinate	[-]
φ	association factor for the solvent	[-]
φC	Carman correction factor	[-]
$\nu_{j,i}$	stoichiometric coefficient of component <i>i</i> in reaction <i>j</i>	[-]

Components

6-APA	6 amino penicillinic acid
HZ	acid component
PAA	phenyl acetic acid
PenG	Penicillin G
PGA I	Penicillin G acylase from <i>A. faecalis</i> , Separase [®]
PGA II	Penicillin G acylase from <i>E. coli</i> , Assemblase [®]
Z ⁻	conjugated base

7 References

- [1] A. Bruggink Ed. (2001) Synthesis of β -lactam Antibiotics, 1st ed., Dordrecht, the Netherlands: 13-54
- [2] R.A. Sheldon (1997) Chemistry & Industry; 1: 12-15
- [3] A. Fleming, (1929) British Journal of Experimental Pathology; 10: 226-236
- [5] E. Chain, H.W. Florey, A.D. Gardner, N.G. Heatley, M.A. Jennings, J. Orr-Ewing, A.G. Sanders (1940) Lancet; 2: 226-228
- [5] K. Sakaguchi, S. Murao (1950) Journal of Agricultural Chemistry Society Japan; 23:

- [6] A. Bruggink, E.C. Roos, E. De Vroom (1998) *Organic Process Research and Development*; 2: 128-133
- [7] M.A. Prieto, E. Diaz, J.L. Garcia (1996) *Journal of Bacteriology*; 178: 111-120
- [8] A. I. Kallenberg, F. van Rantwijk, R. A. Sheldon (2005) *Advanced Synthesis and Catalysis*; 347: 905– 926
- [9] A. Parmar, H. Kumar, S.S. Marwaha, J.F. Kennedy (2000) *Biotechnology Advances*; 18: 289-301
- [10] C.B. Patel, V.G. Gaikar, (2004) *Separation Science and Technology*; 39: 2655-2675
- [11] H.J. Duggleby, J.P. Tolley, C.P. Hill, E.J. Dodson, G. Dodson, P.C.E. Moody (1995) *Nature*; 373: 264-268
- [12] L.M. Van Langen, N.H.P. Oosthoek, D.T. Guranda, F. Van Rantwijk, V.K. Švedas, R.A. Sheldon (2000) *Tetrahedron: Asymmetry*; 11: 4593-4600
- [13] M. Janssen, PhD thesis, Delft University of Technology, Delft, the Netherlands
- [14] A. Kheirloom, M. Ardjmand, H. Fazelinia, A. Zakeri, (2001) *Process Biochemistry*; 36: 1095-1101
- [15] A. Spiess, R.C. Schlothauer, J. Hinrichs, B. Scheidat, V. Kasche (1999) *Biotechnology and Bioengineering*; 62: 267-277
- [16] E. Calleri, C. Temporini, G. Massolini, G. Caccialanza (2004) *Journal of Pharmaceutical and Biomedical Analysis*; 35: 243-258
- [17] M.H. Janssen, L.M. van Langen, S.R.M. Pereira, F. van Rantwijk, R.A. Sheldon (2002) *Biotechnology and Bioengineering*; 78: 425-432
- [18] C. Mateo, O. Abian, R. Fernandez-Lafuente, J.M. Guisan (2000) *Enzyme and Microbial Technology*; 26: 509-515
- [19] S. Rocchietti, A. San Vicente Urrutia, M. Pregnotato, A. Tagliani, J.M. Guisan, R. Fernandez-Lafuente, M. Terrini (2002) *Enzyme and Microbial Technology*; 31: 88-93
- [20] N. Burtreau, S. Burton R.R. Crichton (1989) *FEBS Letters*; 258: 185-189
- [21] Y.H. Guan, T.H. Lilley, A.H. Brook (2001) *Enzyme and Microbial Technology*; 28: 218-224
- [22] J.M. Guisan (1988) *Enzyme and Microbial Technology*; 10: 375-382
- [23] J. Braun, P. le Chanu, F. le Goffic (1989) *Biotechnology and Bioengineering*; 33: 242-246
- [24] V.K. Svedas, A.L. Margolin, I.V. Berezin (1980) *Enzyme and Microbial Technology*; 2: 138-144
- [25] C.G.P.H. Schroën, C.B. Fretz, V.H. de Bruin, W. Berendsen, H.M. Moody, E.C. Roos, J.L. van Roon, P.J. Kroon, M. Strubel, A.E.M. Janssen and J. Tramper (2002) *Biotechnology and Bioengineering*; 80: 331-340
- [26] R.D. Hawthorn (1974) *AIChE Symposium series*; 70: 428-438
- [27] A. Holmgren, B. Andersson (1998) *Chemical Engineering Science*; 53: 2285-2298
- [28] V. Balakotaiah, D.H. West (2002) *Chemical Engineering Science*; 57: 1269-1286
- [29] L.P.B.M. Janssen, M.M.C.G. Warmoeskerken (1991) *Transport Phenomena Data Companion*, 2nd edition, Delftse Uitgevers Maatschappij, Delft, the Netherlands

- [30] D.R. Lide Handbook of Chemistry and Physics (2002), 81st edition, CRC Press, Boca Raton, USA
- [31] D. Thoenes, H. Kramers (1958) Chemical Engineering Science; 8: 271-283
- [32] I. Hoek, PhD thesis (2004), Delft University of Technology, Delft, the Netherlands
- [33] R.K. Sinnott (1983) Coulson's and Richardson's chemical engineering. Vol. 6. An Introduction to chemical engineering design (SI units), Pergamon, Oxford
- [34] Y. Sano, N. Yamaguchi, T. Adachi, (1974) Journal of Chemical Engineering Japan; 7: 255
- [35] R.C. Bates, P.L. Fondy, R.R. Corpstein (1963) I.E.C.Proc.Dev; 3: 310
- [36] J.L. van Roon, R.M. Boom, M.A. Paasman, J. Tramper, C.G.P.H. Schroën and H.H. Beftink (2005) Journal of Biotechnology; 119: 400-415

Operation of the MSR with immobilized trypsin under mass transfer limited conditions

Abstract

The monolithic stirrer reactor (MSR) was used to study smooth wall monolithic biocatalysts and fuzzy-wall monoliths with different microstructure in the mass transfer limited regime. The trypsin-catalyzed hydrolysis of n-benzoyl-L-arginine ethylester (BAEE) was used as a model reaction. The monolithic stirrer reactor (MSR) was studied with respect to liquid solid mass transfer. The trypsin catalyzed hydrolysis of n-benzoyl-L-arginine ethyl ester (BAEE) was chosen as a model reaction. PEI-coated monoliths are not suitable for immobilization of trypsin; immobilization capacity and stability of these biocatalysts are low. Covalent immobilization and entrapment in a chitosan layer lead to active, stable biocatalysts. The use of ACM monoliths results in an additional increase in trypsin loading. The specific activity of the enzyme is not influenced by the monolith-microstructure. The catalysts show a slow deactivation when used over a longer period of time with intermediate storage at 278 K.

For all monoliths, the liquid solid mass transfer coefficient increased with increasing stirrer speed. The mass transfer coefficient decreased with increasing cell density (decreasing channel diameter), attributed to the decreasing channel velocity at higher cell density. The average channel velocity increases with increasing stirrer rate, but decreases at higher cell density. For the “fuzzy wall” catalysts, severe internal diffusion limitations exist, resulting in the underestimation of k_s . These catalysts are not suitable for the purpose of investigating hydrodynamics of the MSR. For the catalysts with covalently attached trypsin, the observed values for Sh agree well with theoretical values.

1 Introduction

In this study, the liquid solid mass transfer characteristics of the monolithic stirrer are determined. In this monolithic stirrer reactor, a catalyst is applied on the channel walls of monoliths mounted as stirrer blades on a rotating shaft. Under reaction conditions liquid-solid mass transfer takes place from the bulk flow in the monolith channels to the thin catalyst layer on the wall. Knowledge on the mass transport rate is important for the design of this reactor type and for checking the absence of transport limitations in kinetic studies. Trypsin is immobilized onto the monolith channels and used to hydrolyze n-benzoyl-L-arginine ethyl ester under different conditions. The advantage of this reaction is the high activity at moderate conditions, so that the reactants are converted immediately when they reach the catalyst surface. In this way, the reactant concentration at the catalyst surface approaches zero, so the reaction is completely externally mass transport limited. The observed reaction rate then represents the transport from the bulk to the catalyst layer. In chapter 10, the same approach was used to study the monolith loop reactor.

1.1 Description of the reaction system

1.1.1 The Monolithic Stirrer Reactor

In order to optimize the contact area and to minimize internal diffusion problems, catalysts are often applied in the form of a fine powder. With respect to the disadvantages of handling powdered catalysts (separation, attrition agglomeration, scale up), monolith reactors are an interesting alternative for conventional reactor types [1]. The open structure of the monoliths prevents plugging and allows for high flow rates. In combination with the thin layer of active material, diffusion problems can be minimized. The use of a novel type of monolith with a porous wall, developed by the DOW Chemical Company [2], efficiency and catalyst loading can be further enhanced [3]. An example of a monolith reactor is the monolithic stirrer reactor (MSR). The monolithic stirrer is a special type of catalytic stirrer that was presented as a possible alternative for the slurry reactor. The catalytic stirrer offers easy separation and minimized attrition or agglomeration of catalyst particles [4] compared to a conventional slurry reactor. In this reactor configuration, the catalyst is fixed to a stirrer. The first type of catalytic stirrer, the stirred basket reactor, was presented by Carberry [5] in 1964. This reactor was used as a lab tool to determine reaction kinetics under minimal external mass transfer limitations. The stirrer consists of two baskets that can be filled with catalyst pellets. In several studies however, severe internal diffusion limitations were observed inside the catalyst pellets [6-8]. These external diffusion limitations were overcome by using more permeable catalyst supports. Bennet *et al.* [9], used monolith pieces with a thin catalyst coating inside the baskets, and mounted monoliths on the stirrer shaft in different configuration. At sufficiently high stirrer rates, the reactor could now be operated without mass transfer limitations [10]. The new MSR has not yet received much attention in the chemical industry, although some

studies were performed on the possible application of spinning baskets filled with monolith pieces [11].

Since many biocatalytic processes employ particulate carrier materials, the combination of a monolith backbone with a suitable enzyme carrier is thought to be a versatile reactor with exchangeable monoliths for use in different reaction systems. The MSR is especially suited for small scale (fed)batch operation in biocatalytic processes.

At higher stirrer rates, in the absence of diffusion limitations, the MSR is a very useful tool for comparison of different monolithic (bio)catalysts [12]. At lower stirrer rates the presence of external mass transport limitations can be used to measure liquid-solid mass transfer in the MSR. The flow inside the monoliths is created by a pressure drop over the monolith due to the stirring action. The velocity of the liquid (the convection of reactants through the monolith channel) is therefore directly related to the stirrer speed. Liquid-solid mass transfer can further be influenced by the channel diameter and the monolith length [13].

1.1.2 Trypsin

Trypsin (E.C. 3.3.21.4) is produced in the pancreas as an inactive precursor (trypsinogen). After the enzyme arrives in the stomach, the N-terminal part of the pro-enzyme is split off, yielding the active enzyme. Bovine trypsin consists of 223 amino acids and has a molecular mass of 24 kDa. The natural function of the enzyme is to hydrolyze the peptide bonds next to lysine and arginine. Additionally the enzyme splits off the amide and ester groups (in case of a terminal position) of both amino acids. Reactivity increases in the order peptide<amide<ester. The enzyme has the highest activity around pH 8, but the highest stability around pH 2. Heavy metals, organic phosphates, and several natural inhibitors deactivate the enzyme [14]. The structure of the enzyme and the catalytic mechanism were already discussed in more detail in Chapter 10. A generally used assay to follow trypsin-activity is the hydrolysis of n-benzoyl-L-arginine ethyl ester (BAEE). The reaction scheme is presented in Figure 5. This reaction takes place in aqueous environment at pH 8 at 296 K, and can easily be followed by UV-VIS at 253 nm.

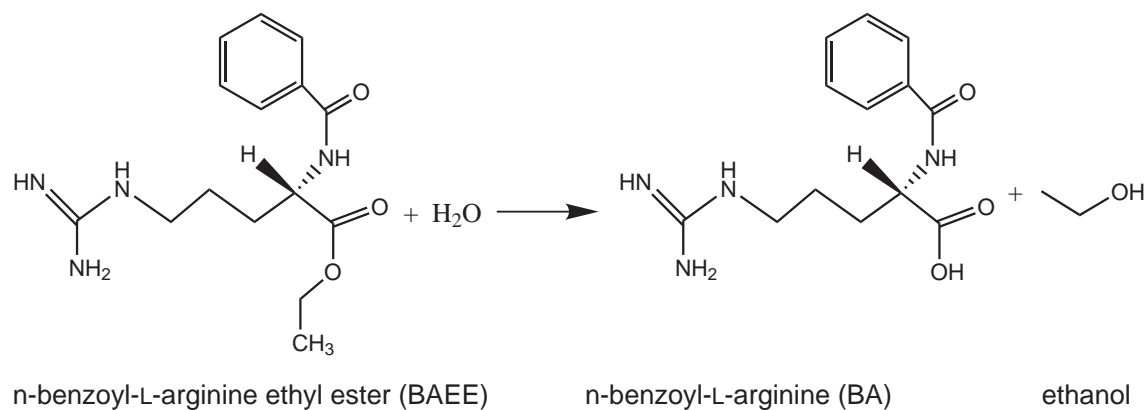


Figure 1. Hydrolysis of n-benzoyl-L-arginine ethyl ester (BAEE)

1.2 Immobilization of trypsin

Trypsin has been immobilized by adsorption on molecular sieves [15,16] and carbons [17]. Under dynamic conditions in aqueous environment however, desorption was found to increase. To increase the bond-strength, trypsin can also be crosslinked onto a support [18]. Also hydrogels or gel-derivatives can be used to stabilize or immobilize trypsin [19,20], but most applications use the covalent attachment of the enzyme onto a solid carrier [21-23]. For this application, a stable carrier is required that can withstand high shear forces and provide a sufficiently high activity to operate in the mass transfer limited regime. The carrier-enzyme system does not need to be reusable by means of reversible immobilization. A very important requirement for performing mass transport measurements is that internal mass transfer problems must be avoided. To avoid the generation of false data, the enzyme should preferably be attached directly onto the monolith surface.

Adsorption of trypsin for use in aqueous medium is not suitable to determine mass transfer characteristics, due to possible leaching of the catalyst. For other applications however, (drug/protein delivery), the carbon supports were found to be very effective for regulated desorption over a longer period of time [17].

A nice example of an immobilization method where the chemistry of the support and the chemistry of the enzyme are incompatible is ionic adsorption of trypsin. Although PEI has been shown to have a stabilizing effect on proteins, including trypsin [24], the high isoelectric point of the enzyme ($\text{pH} = 9$), makes ionic adsorption on PEI, combined with possible high shear forces in the monolithic stirrer, not very suitable. Possibly, adsorption can be done at $\text{pH} 10$ so that the enzyme will become negatively charged, but under alkaline conditions the stability of both PEI and enzyme is lower. Monolith-PEI composites will be included in this study to demonstrate the effect incompatible surface chemistry of carrier and enzyme.

The use of glutaraldehyde for crosslinking has been shown to result in a low activity; therefore this method cannot be used for this application where a high activity is required. Covalent immobilization has been shown to work for mass transport measurements [23]. This method provides a strong binding between enzyme and carrier, in combination with a sufficiently high loading. The use of glutaraldehyde-based covalent protocols is not recommended due to chemical deactivation of the enzyme. This leads to a limited window of operation in the MSR under mass transfer limited conditions [25]; at moderate stirrer speeds the system already enters the kinetically controlled regime due to a low enzyme loading and/or deactivation by glutaraldehyde. The covalent method that was optimized in Chapter 5, and was already successfully used in the MLR in Chapter 10, yields carriers with a higher enzyme loading and residual activity.

The monolith with “Fuzzy” walls [23], as introduced in Chapter 10, has a high enzyme loading capacity and strong enzyme-support bond, but also has fierce internal mass transport problems. This biocatalyst is included here to check if this problem can be recognized and distinguished from external mass transport limitation-only situations to prevent the generation of incorrect data.

1.3 Layout

The fast enzymatic hydrolysis of BAEE and the absence of internal diffusion limitations, make the monolithic bioreactor very suitable to operate in the mass transfer limited regime. In previous studies, enzyme coated monoliths were applied to determine mass transfer characteristics of monolith reactors [23,25]. The enzyme was covalently attached to the monolith support by the (APTES)-glutaraldehyde protocol. Initial hydrodynamics measurements in a monolith loop reactor and a monolithic stirrer [25], led to the conclusion that enzyme loading needed to be improved in order to remain in the mass transfer limited regime during measurement. After optimization of the covalent protocol (Chapter 5) and application of chitosan coatings for enzyme immobilization (Chapter 6), these monolith-carrier combinations were already applied to study mass transfer characteristics of the monolith loop reactor (MLR) in Chapter 10. The same enzyme carrier materials are now applied in the monolithic stirrer reactor in aqueous phase to measure L-S mass transfer coefficients at different stirrer rates. Further, chitosan coatings are applied on cordierite and ACM monoliths. Trypsin is subsequently immobilized on the chitosan layers and also chemically attached to washcoated monoliths. Polyethyleneimine coated monoliths are used as an alternative support material for ionic adsorption of the enzyme. All prepared biocatalysts are tested in the hydrolysis of n-benzoyl-L-arginine ethyl ester in the MSR.

2 Experimental

2.1 Materials

Glutaraldehyde (25% in water), low viscous chitosan (< 200 mPa s), n-benzoyl-L-arginine ethyl ester (BAEE), triethylamine, and NaCNBH₄ (purity >96%) were purchased from Fluka. (3-glycidoxypropyl)trimethoxysilane (GPTMS, 97%) was from Sigma. High molecular weight polyethyleneimine (MW = 60000-1000000), water free was from Aldrich. Buffer salts were of analytical grade and purchased at Baker. Acetic acid (>95%) was from Merck. Novo pancreatic trypsin, type 6 saltfree was kindly supplied by Novozymes. Honeycomb monoliths of ACM (200 and 400 cells inch⁻², 31 or 62 cells cm⁻²) were prepared by a proprietary Dow process. Cordierite monoliths with cell densities of 200 and 400 cells inch⁻² were supplied by Corning Inc. Monolith properties are given in Table 1.

Table 1. Properties of the monoliths

	ACM ("medium")	Cordierite
Cell density	200 / 400 cpsi	200 / 400 cpsi
Wall thickness	0.35 / 0.24 mm	0.3 / 0.18 mm
Wall porosity	60%	30%
Pore diameter	18 μm	7.5 μm
Specific surface area	> 10000	1945 / 2788 m ² m ⁻³

2.2 Catalyst preparation

2.2.1 Washcoating

Monoliths with a diameter of 4.3 cm (4.0 cm for ACM) and a length of 5 cm are used. The monoliths were calcined (10 K min^{-1} , 1273 K, 4 hrs) and washcoated with a colloidal silica solution (Ludox AS-40). Optimization of the washcoating with different silicas was described in Chapter 3. Cordierite samples were dipped in the Ludox solution as received. ACM monoliths were washcoated with a 4% silica (10 times diluted Ludox AS-40 in water) solution. After dipcoating the channels were cleaned with pressurized air and the monoliths were dried in a microwave oven for 20 min at 150 W. Samples were subsequently calcined at 673 K (5 K min^{-1} , 4 h).

2.2.2 Enzyme immobilization

Monoliths were functionalized following the different protocols. After enzyme immobilization and during stability tests, the catalysts were stored in a $1 \text{ g l}^{-1} \text{ NaN}_3$ solution in 10 mM phosphate buffer pH 8 at 278 K. This was done to prevent the growth of microorganisms on the biocatalysts.

2.2.3 Covalent binding via an indirect aldehyde group (ALD/IM)

The epoxy-group was reduced by treating 3 g GPTMS in 300 ml HNO_3 (pH 2) at 363 K for 1 h. The pH was raised to 7 by adding 0.5 M sodium acetate and a monolith was kept in this solution for 6 h. The product was then oxidized with 400 ml of a 70 mM NaIO_4 solution in 0.1 M acetate buffer pH 4.5 to form the aldehyde groups. Trypsin was immobilized on the carriers from a 3 g l^{-1} solution in 10 mM phosphate buffer pH 7.5. Cyanoborohydride (3 g l^{-1}) was added to reduce the imine bonds.

2.2.4 Entrapment in a chitosan layer

Washcoated monoliths were silanized in a 5 wt% solution of GPTMS in toluene with 1% ethylamine. Chitosan gel was applied by dip coating. Monoliths were held in a 1.0 % w/v chitosan solution containing 1.1 % w/v glutaraldehyde for 60 sec. After cleaning the channels, samples are air dried for 90 min. The average thickness of the chitosan gel layer was calculated by:

$$L_{chitosan} = \frac{m_{chitosan}}{\frac{\pi}{4} \cdot d_m^2 \cdot L_m \cdot \rho_{chitosan}} \quad (1)$$

Where $m_{chitosan}$ and $\rho_{chitosan}$ are the mass and density of chitosan filtrate, d_m and L_m are the diameter and height of the monolithic structure and a' is the specific surface area. Density of 1.0 % chitosan filtrate is assumed to be equal to the density of water. Trypsin was immobilized from a 3 g l^{-1} solution in a 10 mM phosphate buffer, pH 7.5.

2.2.5 PEI coating

Polyethylenimine-functionalized supports were prepared by using direct coupling through (3-glycidoxypropyl)trimethoxysilane (GPTMS). The monoliths were functionalized at room temperature for 24 h. in a 5wt% solution of GPTMS in toluene, containing 0.1% v/v triethylamine. After silanization the samples were washed with toluene and acetone and dried at 393 K (heating rate 2 K min^{-1}) for 2 h. The polymer was attached from a 10 wt% PEI solution in water (pH 10) under ambient conditions for 24 h. The carriers were washed with 1 M NaCl and water, and dried under vacuum. Trypsin was immobilized from a 3 g l^{-1} solution in 10 mM phosphate buffer, pH 8.

The enzyme concentration was followed by UV-VIS at 260 nm. Samples were measured in a 1 cm quartz cuvette on a Thermo Optek Unicam 540 spectrophotometer from Thermo Spectronic. After immobilization the samples were washed with 5 mM phosphate buffer pH 8 and stored in a 1 g l^{-1} sodium azide solution in phosphate buffer at 278 K.

2.3 Catalyst Characterization

The amount of coating, mass increase, and mass decrease were determined by measuring the sample weight before and after the various preparation steps. The carrier yield was calculated as:

$$Y_C = \left(\frac{w}{w_s + w} \right) * 100 \quad (2)$$

where w_s is the mass of the support and w is the carrier mass.

Thermogravimetric analysis (TGA) was performed on a Mettler Toledo TGA/SDTA851^e. The samples were heated in air (100 ml min^{-1}) to 1273 K (heating rate 10 K min^{-1}). Scanning Electron Microscopy was performed using a Philips XL-20 scanning electron microscope.

2.3.1 Catalyst performance in the MSR

The experiments to determine the liquid-solid mass transfer coefficient were done in the monolithic stirrer reactor as shown in Figure 2. To check mass transfer limitations during measurements of the kinetics, free trypsin and crushed catalyst were also used in the MSR.

The reactor had an internal diameter of 0.215 m (external diameter 0.25 m), a height of 0.16 m, and a working volume of 2.1 l. The stirrer diameter is 0.15 m from tip to tip. The vessel

was equipped with a double wall that was used to pass heating/cooling water to control the reaction temperature.

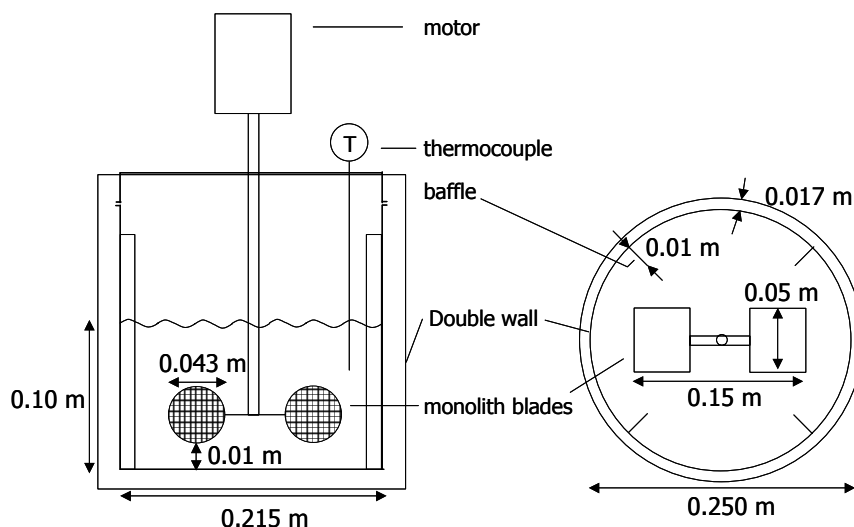


Figure 2. Schematic representation of the MSR used for the measurement of the liquid-solid mass transfer coefficient

A space of 1 cm was left between the stirrer and the bottom of the reactor. The temperature was varied from 290-318 K, and the stirrer rate between 10-250 rpm. The set-up was coupled to a UV-VIS system (Thermo Optek 540 from Thermo Spectronic) with a 1 cm quartz flowcell. The reaction was followed in-line, by recycling the reaction mixture through the spectrophotometer (volume < 5 ml) at a flow rate of 12 ml min⁻¹. The reaction rate was determined from the changes in absorption due to product formation. Calibration of the system was already presented in Chapter 5.

2.4 Nomenclature

Samples names are coded depending on the monolith type and the immobilization protocol. The first letter of the samples is used to distinguish the monolith type, “C” is used for cordierite, “A” for ACM. A second letter is used to express the microstructure of the ACM; “M” for medium needles. The methods are abbreviated with a third code. This is summarized in Table 2.

Table 2. Nomenclature

Position	Component	Code
1	Monolith type	C or A
2	Micro grain structure ACM	M
3	Method of immobilization:	
	<i>Indirect aldehyde/ indirect method</i>	ALD/IM
	<i>Chitosan</i>	Chit
	<i>GPTMS-PEI</i>	PEI

3 Results and Discussion

All immobilization protocols yielded active biocatalysts, but the differences in immobilization yield and activity were relatively large. In the following sections, the immobilization efficiency and catalyst performance of all prepared biocatalysts will be presented.

3.1 Catalyst preparation

The loading of the different carrier materials on the 200 and 400 cpsi monoliths is in the same order of magnitude as was seen before for the different methods. The mean yield and layer thickness on cordierite and ACM monoliths are presented in Table 3.

Table 3. Support preparation with different 200 and 400 cpsi monoliths.

	$Y_{\text{carrier}} (V_{\text{cat}})$		Layer thickness (L)
	200 / 400 cpsi		200 / 400 cpsi
AM-Chit	33 / 43 wt%	(14 ml / 18 ml)	110 μm / 100 μm
C-Chit	28 / 38.5 wt%	(13 ml / 17.75 ml)	93 μm / 88 μm
AM-PEI	12.2 / 15.9 wt%		-
C-PEI	8.6 / 14.0 wt%		-

For the PEI composites is assumed that the polymer layer is very thin and does not introduce a barrier for substrate/product diffusion towards the enzyme. The enzyme is assumed to be present directly on the monolith surface, just as is the case with the ALD/IM samples. The chitosan loading on the monoliths is in agreement with earlier results (see Chapter 6). The layer thickness on cordierite monoliths is the same as on the 2 cm monoliths that were used in Chapter 11 for the hydrolysis of PenG. It can be stated that the channel walls of the ACM monoliths are filled for around 60-80% by assuming that the layers present on each side of the wall (2x110 and 2x100 μm for 200 and 400 cpsi monoliths) are actually present inside the wall. It may be expected however, that part of the gel is also present as a thin layer on the individual micrograins.

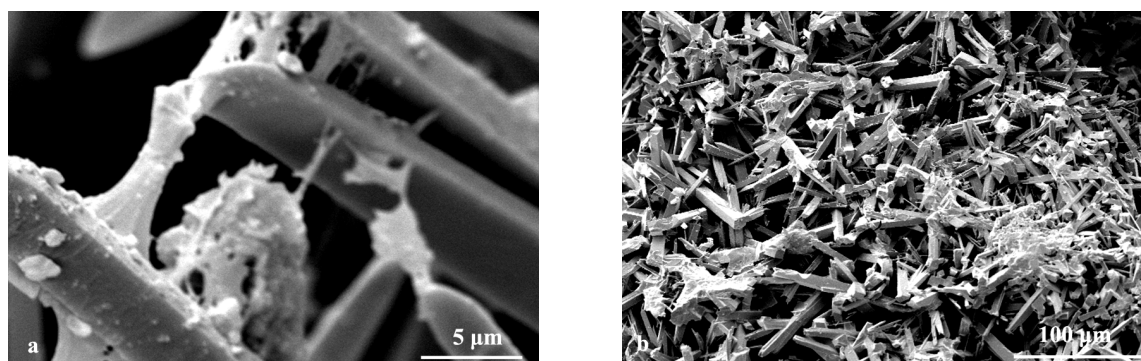


Figure 3. SEM micrographs of AM-Chit supports. a) close-up of the micrograins in the channel wall b) overview of a monolith wall.

To confirm the presence of the chitosan gel inside the porous ACM walls, SEM images were recorded (Figure 3). Due to the high-vacuum, only 1% of the gel volume remains inside the vacuum chamber. This technique can only be used to confirm the presence of the gel, no data on the exact position and dispersion in the wall can be obtained from these images. The dehydrated gel is clearly present throughout the open wall and on and between the micrograins. The SEM images of the C-Chit samples can be found in Chapter 6, paragraph 3.3.1.

3.2 Trypsin immobilization

The immobilization of trypsin via the proposed methods leads to carriers with different final enzyme yield. The used protein powder also contains other proteins and salts. The enzyme loading as determined by UV-VIS (including other proteins) is a measure for the trypsin loading, and will be indicated with ‘total trypsin loading’. The total trypsin loading is presented for the different carrier materials in Figure 4. Displayed values are corrected for a subsequent 90 min washing step to remove loosely bound enzyme.

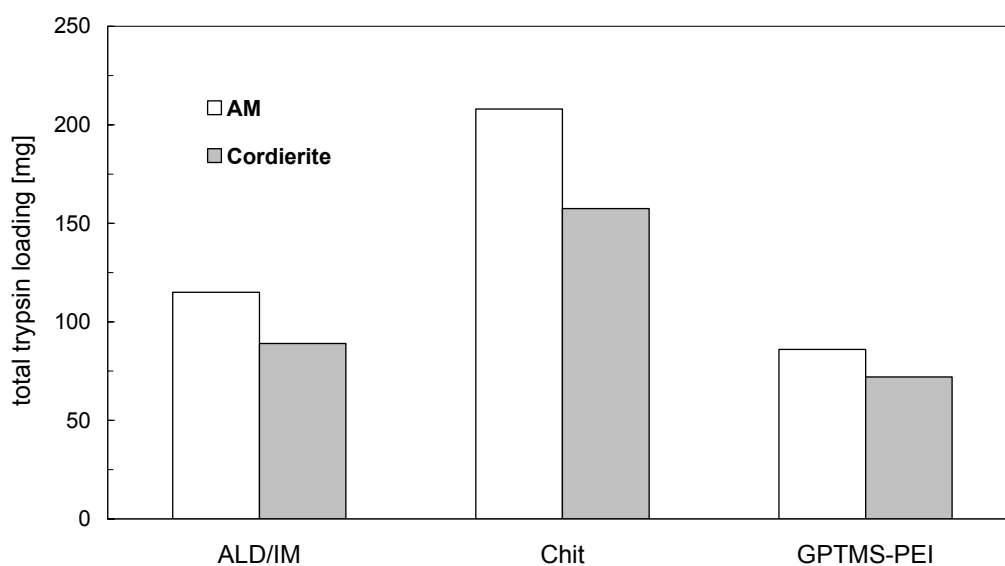


Figure 4. Trypsin loading on 200 cpsi monoliths of ACM and cordierite via different immobilization protocols. Immobilization was done from a 3 g l⁻¹ solution in 5 mM phosphate buffer pH 7.5 (pH 8 for PEI composites) at 295 K.

For all carriers, the use of ACM supports gives a higher total protein loading. This is consistent with the findings in the separate immobilization studies in Part II. The highest enzyme loading is obtained with the chitosan coating, but for this “Fuzzy wall” type coating, not all enzyme is accessible, as was already seen in Chapter 11. This leads to diffusion problems for product and reactant inside the gel layer. Covalent bonding via the ALD/IM protocol leads to a good enzyme loading, with a tight bond to prevent leaching at higher stirrer rates. As could be expected based on the iso-electric point of trypsin, the immobilization on PEI is not as high as with the other methods. Due to the different purities

of the used protein prepares, it is difficult to directly compare the exact enzyme loading (in mmol) on the PEI-coated monoliths. A rough estimation to compare the present results with the adsorption of lipase (see Chapter 7, total adsorption 220 mg, Mw = 55 kDa), leads to a slightly lower total adsorption. The trypsin loading is around 3 μmol , compared to 4 μmol lipase on C-PEI. Furthermore, in the case of trypsin-PEI, the enzyme-carrier bond is expected to be relatively weak, resulting in a quick desorption during use in buffered environment.

3.3 Catalyst performance in the MSR

3.3.1 Initial activity

In Table 4, the immobilization yield and the initial activity of the catalysts is presented for the 200 cpsi samples. These measurements were performed at high stirrer rates (150 rpm) to ensure operation in the kinetically controlled regime. Up to 50% conversion, the concentration-time plots show a linear dependence. At higher conversion, the substrate concentration becomes limited and the reaction rate decreases. The initial rate is determined over the 0-10% conversion interval (approximately 0-10 min). It is therefore assumed that the initial activity is measured in the kinetically controlled regime, and can be used to compare the catalyst performance.

Table 4. Yield and initial activity in the hydrolysis of BAEE at 306 K (150 rpm) for immobilized trypsin on 200 cpsi monoliths

Catalyst	Total adsorption mg	Initial activity $\text{mmol m}^{-3}_{\text{monolith}} \text{ s}^{-1}$	Specific activity $\text{mmol g}^{-1}_{\text{protein}} \text{ s}^{-1*}$
Free trypsin	-	-	42×10^{-2}
C-ALD/IM	89	57	3.8×10^{-2}
C-Chit	158	15	5.2×10^{-3}
C-PEI	72	7	5.8×10^{-3}
AM-ALD/IM	115	89	3.6×10^{-2}
AM-Chit	208	24	5.7×10^{-3}
AM-PEI	86	10	5.5×10^{-3}

* Trypsin content in the crude protein is estimated to be 10%

If a trypsin content of 10% is assumed in the protein powder, the specific activity of the free and immobilized enzyme can be used to calculate the turnover frequency (TOF), defined as the number of converted substrate molecules per second. For free trypsin, a TOF of 97 s^{-1} was found at this temperature, for covalently immobilized trypsin this number is 9 s^{-1} . These values are higher than the values that were found in Chapter 5 (55 s^{-1} measured for free trypsin at 298 K), and consistent with the expected value from the Arrhenius plot (for a more detailed description of the kinetic parameters of this enzyme, see Chapter 10). The retained activity of the ALD/IM catalysts is around 8-9% as was observed before in Chapter 5.

The residual activity of the PEI carriers is relatively low. This could be due to enzyme loss during washing, or deactivation due to the ionic interaction with the polyelectrolyte.

The immobilized activity of the enzyme on chitosan is much lower than the activity that was observed in Chapter 6. It is likely that there are severe internal transport problems due to the faster reaction. For the C-Chit samples, the Wheeler-Weisz modulus can be estimated to be around 2, assuming first order kinetics with:

$$\Phi = \frac{(n+1)}{2} \cdot \frac{r_{v,obs} \cdot L^2}{D_{eff} \cdot C_b} \quad (3)$$

(see Table 3 for L , and Table 8 for D_{eff}). The effect seems to be less however, for the more porous ACM carriers. Apparently the enzyme has a better accessibility in the open ACM monolith than in the gel layer on the cordierite monoliths. This means that the actual layer thickness is probably smaller than the value that was estimated assuming the same surface area for ACM and cordierite monoliths (Table 3). The relatively low specific activity of trypsin in chitosan gel could also be caused by sensitivity of the enzyme to the crosslinking agent (glutaraldehyde) that is used to form the gel-layer.

3.3.2 Kinetic parameters of the ALD/IM catalysts

Since the chitosan-based catalysts clearly suffer from internal diffusion limitations, the kinetic study of the immobilized enzyme was done with the ALD/IM monoliths. To check for possible mass transfer problems, the initial rate of monoliths and crushed monoliths was compared to that of the free enzyme at different substrate concentrations (Figure 5).

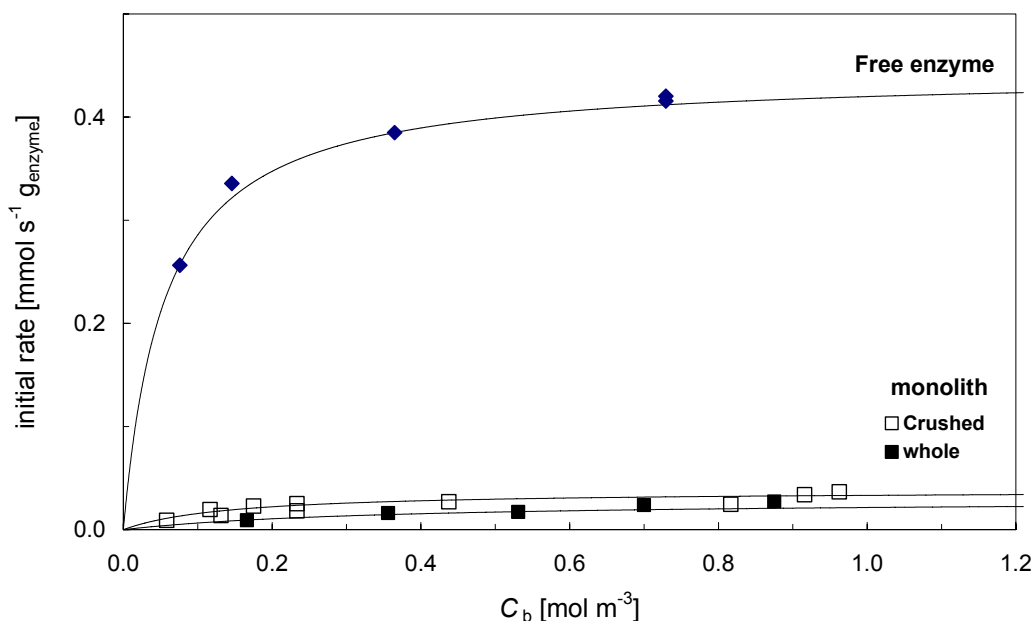


Figure 5. Michaelis-Menten plot for free trypsin, crushed monoliths and monolith on a stirrer axis in the MSR at 150 rpm, 306 K. Solid lines represent the simulations of the rate for free enzyme and crushed/whole monolith (see Table 5 for the model parameters)

From these data a Hofstee-plot can be constructed for the different catalysts, with a slope K_m and intersect V_{\max} (not shown, see Chapter 10). In Table 5, the values are presented for crushed monolith and whole monoliths compared to that of the free trypsin.

Table 5. Values of V_{\max} and K_m for free and immobilized (ALD/IM) trypsin in the MSR at 306 K

	Free trypsin	Crushed	Monolith
K_m [mol m ⁻³]	0.055	0.14	0.35
V_{\max} [mol s ⁻¹ g _{enz} ⁻¹]	4.6×10^{-4}	3.5×10^{-5}	2.8×10^{-5}

For whole monoliths in the MSR, a slight deviation from the crushed monolith was observed in Figure 5, indicating mass transport limitations at these high enzyme loadings.

To obtain indications that measurements are performed in the mass transfer limited regime, the temperature dependence of the reaction was studied and presented in an Arrheniusplot (Figure 6). Because the difference between internal diffusion and external mass transport limitations can easily be misinterpreted in Arrhenius-plot, only the catalysts with the enzyme directly attached to the monolith surface (AM/C-ALD/IM, no internal diffusion limitations) have been used to study the temperature dependence.

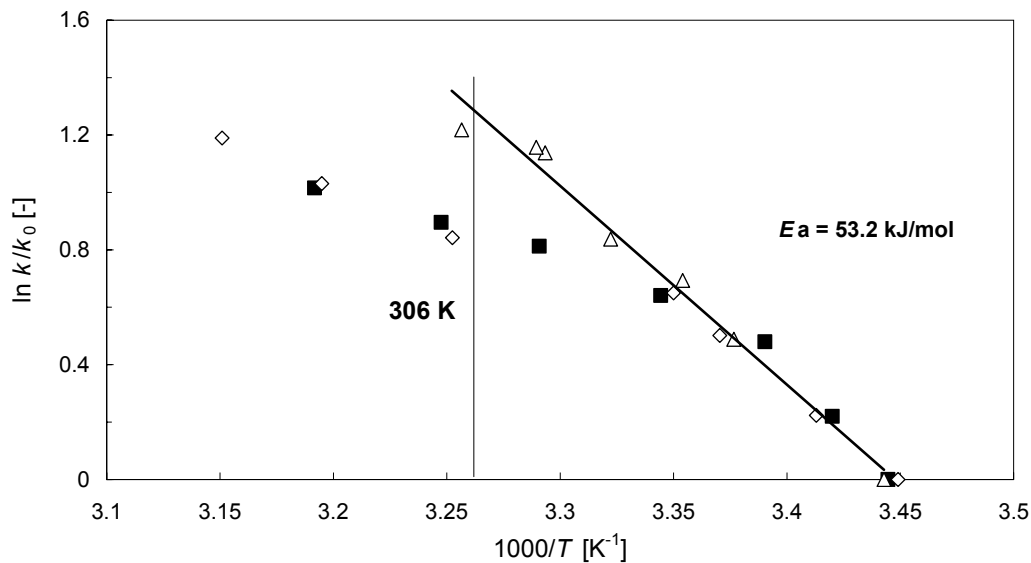


Figure 6. Arrhenius-plot for free and immobilized trypsin to calculate the apparent activation energy. Data are normalized for the observed reaction rate at 290 K (k_0) and plotted against $1000/T$. Free trypsin (Δ), AM-ALD/IM (\diamond) and C-ALD/IM (\blacksquare) at 150 rpm

From the slope of the trend line ($=-Ea/R$) in Figure 6, an apparent activation energy of 53 kJ mol⁻¹ can be calculated. The reaction was performed at different temperatures, in a range of 298-318 K. At temperatures above 299 K the immobilized enzyme starts to deviate, indicating the onset of mass transfer limitations. So the temperature at which the experiments at different substrate concentrations were performed with whole monoliths (306 K) is already in the (partly) mass transfer limited regime. This explains the increased Michaelis-Menten constant and lower maximum rate for whole monolith compared to the crushed enzyme (Table 5). The

apparent activation energy that was observed here is slightly higher than the 40 kJ mol^{-1} that was observed before [25]. It is possible that the previous measurements were actually performed in the transition region from the kinetically limited regime towards the mass transfer limited regime (see Figure 6), resulting in an underestimation of the apparent activation energy. This theory is supported by the observation that the enzyme loading in [25] was lower, resulting in a narrow window of operation in the MSR. Moreover, the experiments in [25] were performed at higher temperatures (310-320 K), where the enzyme already starts to deactivate. The combination of entering the mass transfer limited regime and higher temperature probably resulted in a lower observed E_a .

To check if the system enters the completely mass transfer limited regime at lower stirrer speeds, a second Arrhenius-plot was constructed at 50 rpm (Figure 7). At lower stirrer rate, the observed activation energy is indeed lower than at 150 rpm. Apparently the system is already in an intermediate regime. Above 304 K, the reaction becomes completely externally limited with an apparent activation energy of around 4 kJ mol^{-1} . This value is in agreement with earlier research [25], where a similar experiment was performed at 10 rpm. So from Figure 7 it can be concluded that for all experiments (performed at 306 K) at a stirrer rate lower than 50 rpm the reaction is externally limited, and k_s can be calculated from the observed reaction rate.

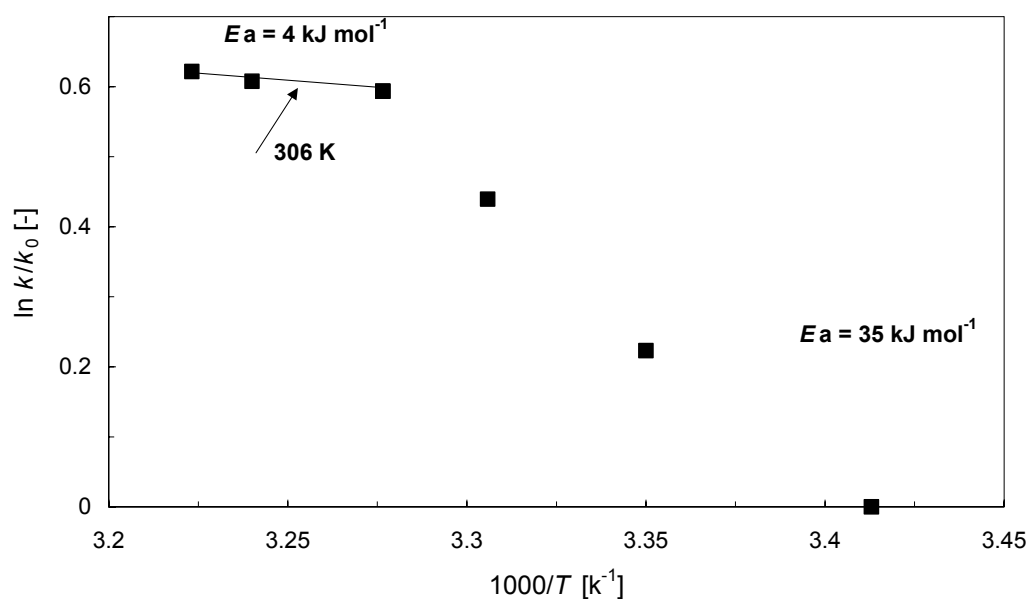


Figure 7. Arrhenius-plot for C-ALD/IM at 50 rpm, with $C_b = 0.3 \text{ g l}^{-1}$. The arrow indicates the experimental conditions for determination of the L-S mass transfer coefficient in the MSR.

3.4 Stability of the biocatalysts

The stability of the monolithic biocatalysts was studied with respect to storage for prolonged periods of time and activity tests in the MSR at 306 K. The operational stability of the

ALD/IM-based catalysts was already presented in Chapter 5. After 11 consecutive experiments, the activity had gradually decreased to 80%. In the present study, the biocatalysts are stored for five days at 278 K before repeating the experiment.

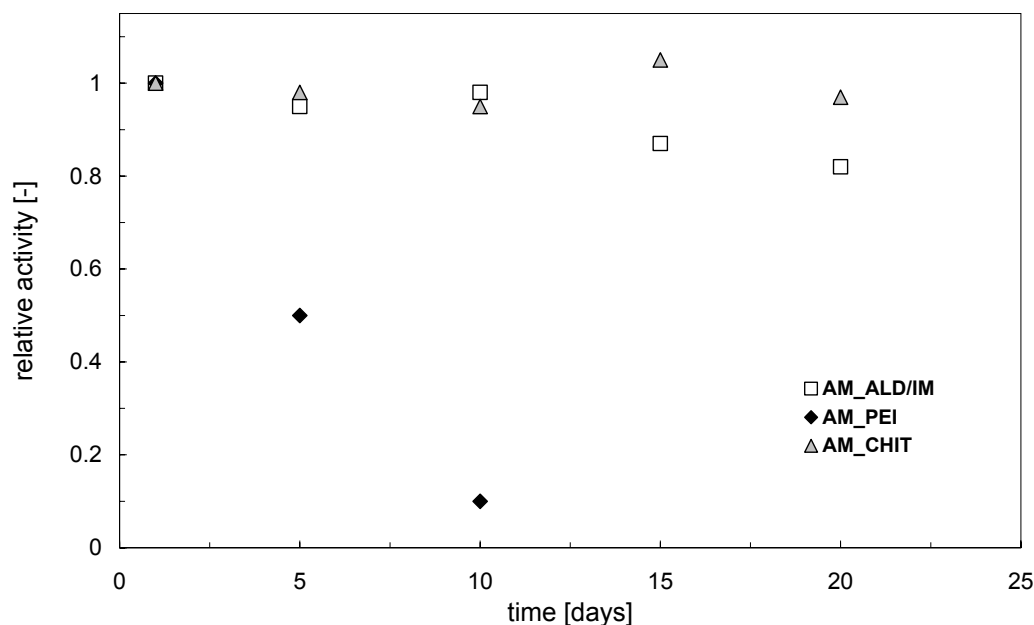


Figure 8. Stability of ACM monoliths with different carriers over a period of 20 days with intermediate storage at 278 K in a 5 mM phosphate buffer solution pH 8 with $1 \text{ g l}^{-1} \text{ NaN}_3$. Activity tests were performed at 306 K, $C_b = 0.3 \text{ g l}^{-1}$ BAEE

It can be seen (Figure 8) that the PEI-based catalysts deactivate very fast. This was already expected based on the chemistry of the enzyme and the adsorption results. The chitosan and ALD/IM catalysts are stable for a period of 20 days. In the mass transfer measurements, the catalysts were used over a period of 2 days, for 4-10 tests to minimize the effect of deactivation.

3.5 L-S mass transfer measurements in the MSR

After the stability experiments, PEI was not considered a suitable carrier material for use in the MSR under the present conditions. Only Chitosan and ALD/IM-based biocatalysts are used for performing mass transfer experiments. In Figure 5 it can be seen that the system enters the mass transfer limited regime above 298 K. Until around 305 K, the system is probably in an intermediate regime in which both kinetics and mass transfer control the reaction rate. At completely mass transfer controlled operation an apparent E_a of 4 kJ mol^{-1} was observed. This is however only shown for experiments at low stirrer rate ($<50 \text{ rpm}$). It is expected that the measurements at higher stirrer rate are performed in an intermediate regime. To ensure operation outside the kinetically controlled regime, all experiments to determine the effect of stirrer speed were performed at 306 K and relatively low stirrer rates (10-55 rpm). At higher temperature, the catalyst might show an increased deactivation, as was indicated in Chapter 5.

3.5.1 L-S Mass transfer coefficient

The experiments at different stirrer speed can be used to estimate the mass transfer coefficient. Although it was already observed that the chitosan-based composites have internal diffusion problems, they are also taken into account to study the effect on observed liquid-solid mass transfer coefficient. In Figure 9 the effect of stirrer rate on the activity of 200 cpsi chitosan-based catalysts is presented in a first order plot. The initial rate is a zero order dependency on substrate concentration; there is a relatively small difference between the experiments. This indicates that in the initial state the reaction is mainly kinetically controlled. As was already seen in Chapter 11, the first order reaction rate constant can be determined from the slope of the logarithmic concentration against time in a fixed concentration interval.

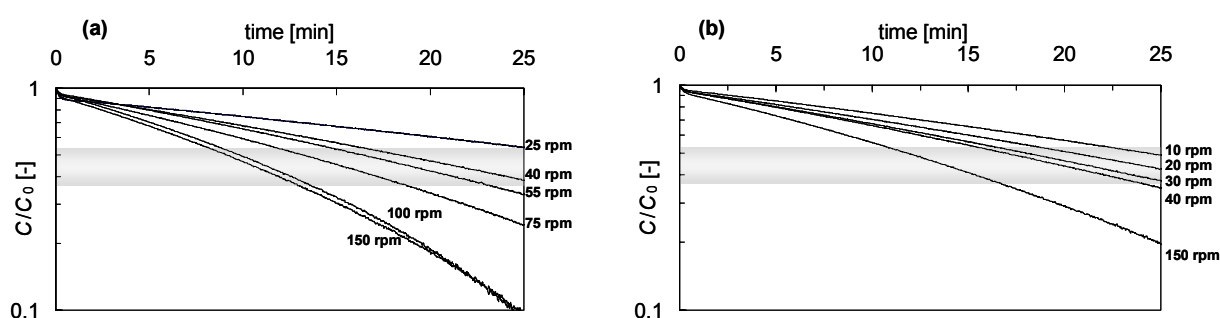


Figure 9. First order plot of the effect of stirrer speed on the activity of a) AM-Chit and b) C-Chit. The area of the logarithmic normalized concentration between 0.15 and 0.1 g l^{-1} is highlighted. Experiments were performed with 200 cpsi monoliths at 306 K, $C_b = 0.3 \text{ g l}^{-1}$.

In terms of Michaelis-Menten kinetics, this means that the active sites are all fully used in this region. At lower substrate concentrations, a larger effect of stirrer rate is observed in combination with a first order dependency. The effect of stirrer rate is most profound between 0.15 and 0.10 g l^{-1} . At lower stirrer rates the reaction rate is clearly affected by changing stirrer speed. Above a certain stirrer speed, the profiles start to coincide. For cordierite samples (Figure 9b) this seems to happen at lower stirrer speeds. This indicates that the ACM monoliths remain in the mass transfer limited regime at higher stirrer rates, possibly resulting in a higher mass transfer coefficient. It must be noted that for the chitosan based catalysts also internal diffusion limitations are present.

In Figure 10, the first order plots are given for 200 cpsi C-ALD/IM and AM-ALD/IM samples.

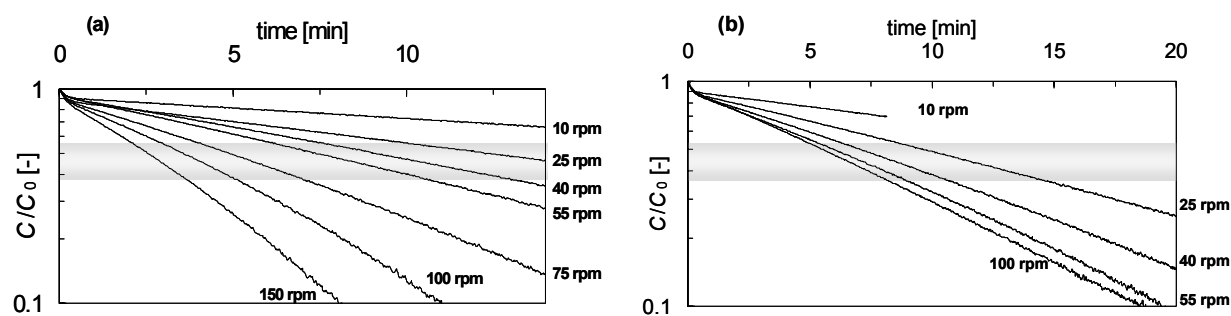


Figure 10. First order plot of the effect of stirrer speed on the activity of a) AM-ALD/IM and b) C-ALD/IM. The area of the logarithmic normalized concentration between 0.15 and 0.1 g l^{-1} is highlighted. Experiments were performed with 200 cpsi monoliths at 306 K, $C_b = 0.3 \text{ g l}^{-1}$.

The first order reaction rate constant ($k_{r,obs}$) in the mass transfer limited regime that is highlighted in Figure 9 and 10 ($0.1\text{-}0.15 \text{ g l}^{-1}$) can be used to determine the liquid-solid mass transfer coefficient k_s with:

$$k_s = k_{r,obs} \frac{V_L}{A_m} \quad (4)$$

In Table 6, the calculated values for k_s are given for different 200 and 400 cpsi samples.

Table 6. Liquid-solid mass transfer coefficient for cordierite monoliths at different stirrer speeds

Stirrer speed		C-ALD/IM		Stirrer speed		C-Chit	
rpm		$k_s \times 10^6$ m s^{-1}		rpm		$k_s \times 10^6$ m s^{-1}	
		200 cpsi	400 cpsi			200 cpsi	400 cpsi
10	4.31	2.23		10	4.05	2.23	
25	8.29	6.39		20	4.58	4.31	
40	11.4	9.66		30	5.14	4.44	
55	13.6	11.7		40	5.55	5.22	
75	15.5	14.4		150	7.97	7.18	

The observed liquid-solid mass transfer coefficient increases with increasing stirrer speed. For higher cell density (smaller channels) the mass transfer coefficient is lower. This is probably caused by a lower liquid velocity in the channels. Kritzinger *et al.* [26] show that the velocity in the monolith channels increases with increasing stirrer speed and with increasing channel diameter. The values for 10-20 rpm of C-ALD/IM samples are consistent with earlier work [25]. Above 20 rpm however, the presently observed k_s values are higher. This is another indication of the limiting enzyme loading in [25] that was already mentioned above. The k_s values for the chitosan-based samples are significantly lower. This means that careful catalyst selection is necessary to prevent an underestimation of the mass transfer coefficient due to internal diffusion limitations. This was already recognized in earlier research [7-9]. Only at the lowest stirring rates the two enzyme-monolith combinations show similar performance.

To compare ACM monoliths with the classical cordierite monoliths, an equal geometric surface area was assumed (this assumption implies that the walls of the ACM monoliths are completely plugged with carrier, which is a significant underestimation of the total available surface area). A significantly higher mass transfer coefficient was observed for the ACM samples (see Figures 11 and 12). Whereas k_s for the cordierite samples already approaches the maximum value (here the system seems to enter the kinetically controlled regime) at 50 rpm (see Figure 10a, the profiles start to coincide above 50 rpm), the maximum value of k_s for ACM monoliths is much higher (Figure 10b). This can be expected due to the more open structure and the higher enzyme loading. The open structure allows for a higher mass transfer rate and the higher enzyme loading keeps the system in the mass transfer controlled regime up to higher stirrer rates.

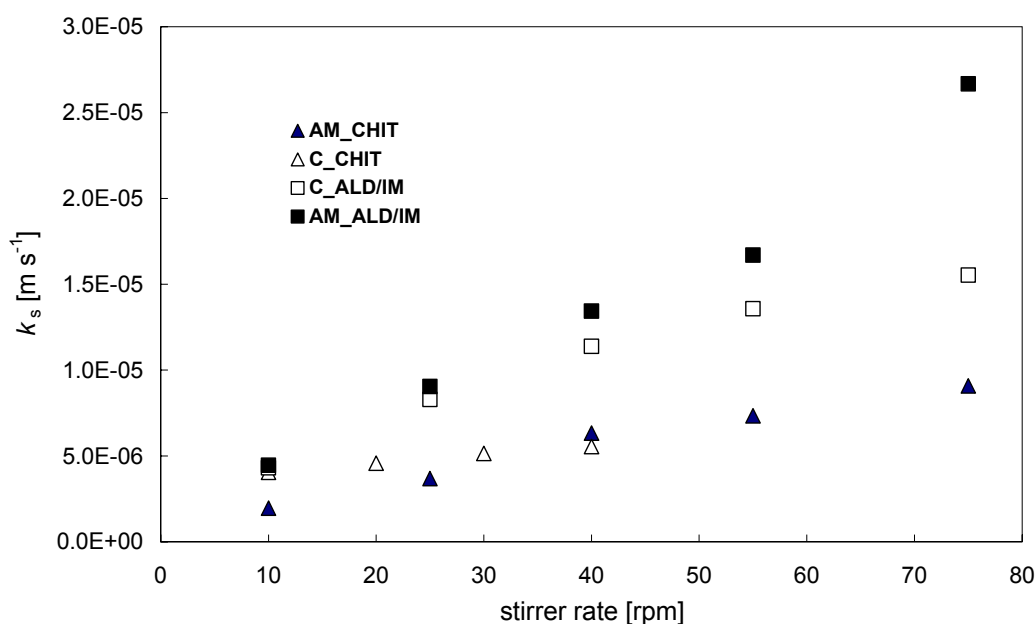


Figure 11. Liquid-solid mass transfer coefficient, k_s , at varying stirrer speed for 200 cpsi ACM and cordierite monoliths with immobilized trypsin. Experiments were performed at 306 K, and $C_b = 0.3 \text{ g l}^{-1}$ BAEE.

The data in Figure 11 only represent a real mass transfer coefficient outside the kinetically controlled regime. Above 55 rpm, the cordierite monoliths are assumed to be only partially mass transfer controlled. For the ACM monoliths the system seems to stay mass transfer controlled up to much higher stirrer speeds (75-100 rpm). For the chitosan-based composites, the observed values for k_s are the result of mixed internal and external diffusion limitations.

To study the effect of cell density on k_s , 400 cpsi ACM-ALD/IM and C-ALD/IM samples were tested under the same conditions (Figure 12). The closed symbols represent the 200 cpsi samples. For ACM monoliths the same trend is observed as can be seen in Table 6; at higher cell density the observed mass transfer coefficient decreases.

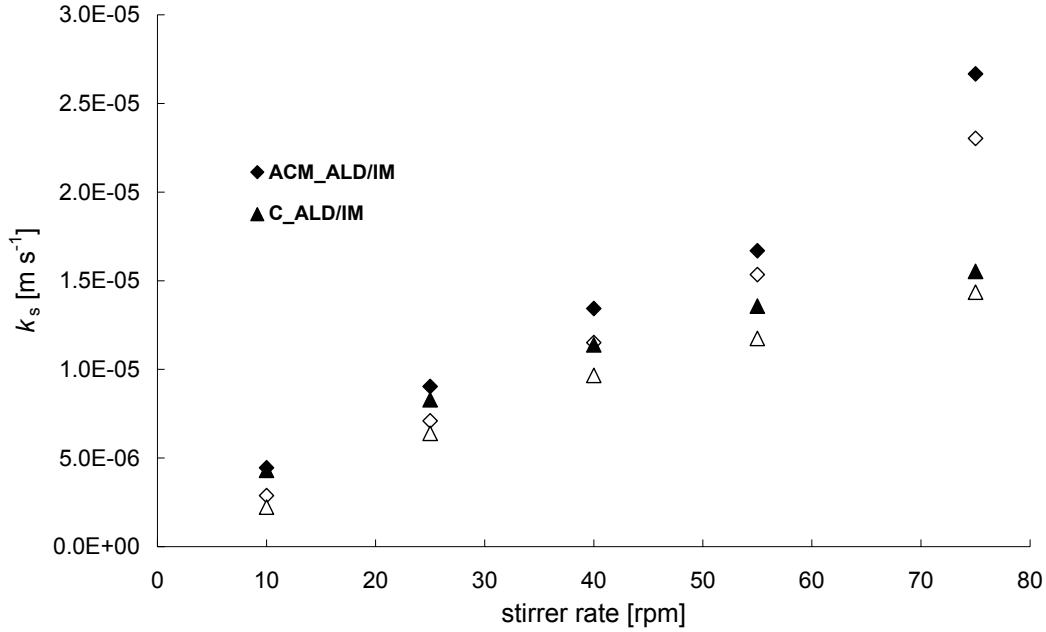


Figure 12. Liquid-solid mass transfer coefficient, k_s , at varying stirrer speed for 200 (closed symbols) and 400 rpm (open symbols) ACM and cordierite monoliths with covalently immobilized trypsin (-ALD.IM). Experiments were performed at 306 K, and $C_b = 0.3 \text{ g l}^{-1}$ BAEE.

3.5.2 Channel velocity

From the liquid-solid mass transfer coefficient, the channel velocity in the monolithic channels can be estimated. The liquid-solid mass transfer in liquid phase has been described extensively in literature. To effectively compare the experimental data with data from earlier work [25], the same set of correlations is used in here. In Table 7, the dimensionless equations that are used to describe mass transfer are summarized. The surface roughness, C , in the L ev eque equation was determined to be 1.16 for square channels [29]. Equation 5 can be used to describe developing mass transfer in case of a fully developed velocity profile.

Table 7. Dimensionless equations for describing single phase liquid-solid mass transport

Equation	Description
$Sh = \frac{k_s \cdot d_{ch}}{D_{eff}}$ (5)	The Sherwood number describes mass transfer. Ratio between the actual mass transfer and diffusion
$Sh = C \left(Re \cdot Sc \frac{d_{ch}}{L} \right)^{1/3}$ (6)	L�ev�eque [27,28] for heat transfer in a circular channel can be translated to mass transfer. Criterion: $Gz < 0.05$
$Re = \frac{\rho v_L d_{ch}}{\eta}$ (7)	The Reynolds number represents the ratio between convective and viscous transport
$Sc = \frac{\eta}{\rho \cdot D}$ (8)	The Schmidt number is the ratio between the hydrodynamic boundary layer and the mass transfer boundary layer
$Gz = \frac{L_m}{Sc \cdot Re \cdot d}$ (9)	The Graetz number characterises laminar flow in a channel

Some important properties of the reaction mixture at 306 K are given in Table 8.

Table 8. Used parameters

Parameter	Value
Density, ρ	995 kg m ⁻³
Viscosity, η	7.86 x 10 ⁻⁴ Pa s
Diffusivity, D	6 x 10 ⁻¹⁰ m ² s ⁻¹
Effective Diffusivity, D_{eff} in chitosan	4 x 10 ⁻¹⁰ m ² s ⁻¹

Two types of developing flow can be distinguished [13]: mass transfer and hydrodynamic (velocity profile). Mass transfer is in development as long as the boundary layer is changing with monolith length. The entrance length for developing mass transfer is the region in which the boundary layer for mass transfer builds up. The flow is in the hydrodynamic developing region when the local velocity depends on the position in the channel. At the entrance of the monolith the velocity profile is flat, but when it has developed it can be described as laminar. The two transport development-types are dependent (the developing flow at the entrance, influences the mass transfer) but have a different characteristic length. In general, the entrance length for the developing velocity profile is in the order of 10⁻³ m, and the entrance length for the developing mass transfer boundary layer is around 1 m. This means the L ev eque equation can only be used for systems with an undeveloped boundary layer for mass transfer, in other words when $Gz < 0.05$. This criterion gives the characteristic length for mass transfer development:

$$L_{mt} = 0.05 \cdot Sc \cdot Re \cdot d_{ch} \quad (10)$$

In addition, the velocity profile must be developed to justify the use of equation 6. The characteristic length for the development of laminar flow is given by [13]:

$$L_{hydro} = 0.05 \cdot Re \cdot d_{ch} \quad (11)$$

In order to apply equation 6, L_{mt} must be larger than 0.05 m, and L_{hydro} must be significantly smaller than 0.05 m. The characteristic length for development of hydrodynamic and mass transfer boundary layers as a function of stirrer rate are presented in Figure 13. From Figure 13a, it follows that under the present conditions the monolith is much shorter than the entrance length for mass transfer. At 10 rpm, the entrance length is around 20 cm, so the boundary layer for mass transfer is always undeveloped for the experiments performed in this study. The entrance length for the developing velocity profile is around 1 cm at 55 rpm, the highest stirrer rate that is used for measurement of the L-S mass transfer coefficient. At higher stirrer rates however, this criterion is not met and another Sherwood correlation would be needed. In all present experiments, the velocity profile is in the developed state, in other words the flow in the monolith channels is fully laminar.

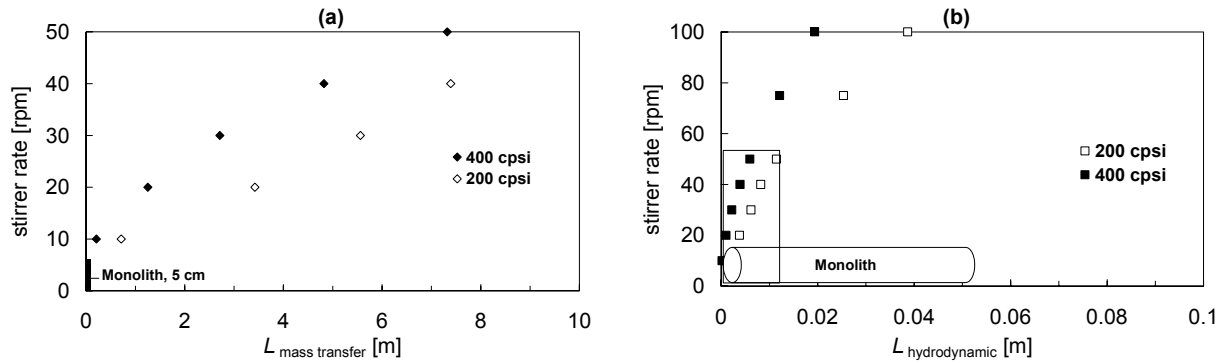


Figure 13. a) Developing mass transfer and b) developing velocity profiles as a function of stirrer rate. The monolith (5 cm) is added for comparison

For ACM monoliths, the same equations are used leading to values for L_{mt} in the range of 0.15-100 m. So for the AM-ALD/IM samples, the boundary layer for mass transfer is in the developing state. For L_{hydro} however, it can be expected that the irregular channel walls cause eddy's and local turbulent flow patterns, changing the velocity profile. For easy comparison, L_{hydro} is calculated in the same manner as for cordierite samples. ACM channels have a slightly smaller channel size, so the entrance length will be slightly lower than for cordierite monoliths.

From the data in Figure 11 and 12, the channel velocity was estimated by calculating Sh with equation 4, and subsequently calculating Re from equation 5.

In Figure 13 the estimated channel velocities are presented for C-ALD/IM and AM-ALD/IM monoliths. For comparison, the data from [25] is also included as -x-. The average channel velocity increases with stirrer speed. In Figure 14a the estimated channel velocity is slightly higher than was observed in the previous study. Apparently the system was partially limited due to the relatively low trypsin loading. If internal diffusion limitations are present, both channel velocity (Figure 14b) and mass transfer coefficient (Figure 11) will be underestimated.

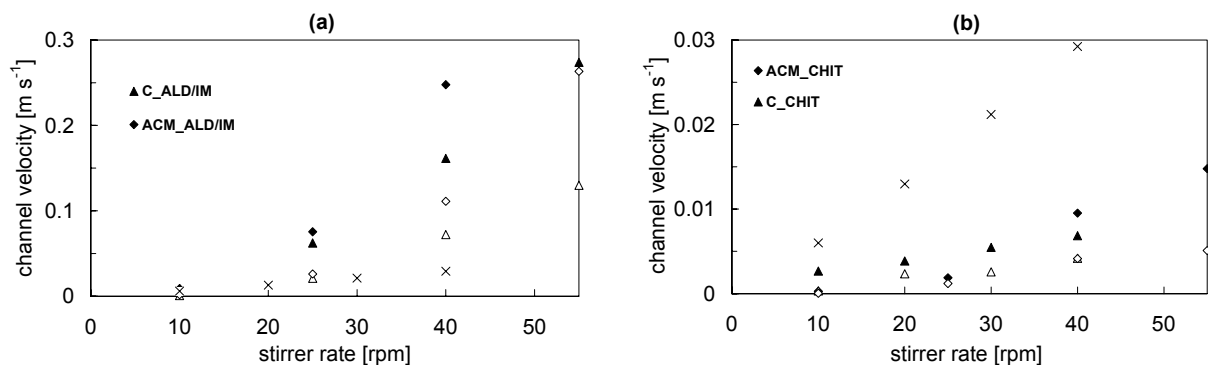


Figure 14. Estimated channel velocity of 200 (closed symbols) and 400 (open symbols) cpsi cordierite and ACM monoliths. a) trypsin on ALD/IM carrier, b) trypsin on chitosan carrier. Experiments were performed at 306 K with 0.3 g l^{-1} BAEE

3.5.3 Comparison with theoretical mass transfer

The channel velocity in the MSR under different conditions was also studied as a function of stirrer rate by Kritzing [26]. It was found that the channel velocity varies with the distance from the stirrer axis and with cell density. To effectively compare the data of Kritzing with the experimental values, a mean channel velocity (over the face of the monolith along a horizontal line at mid-blade height) was estimated for the different 400 cpsi monoliths. It is interesting to compare these calculated values for Sh with the values for Sh that were determined from k_s in the present work. In Figure 15, Sh_{exp} and Sh_{theory} are plotted as a function of the stirrer speed.

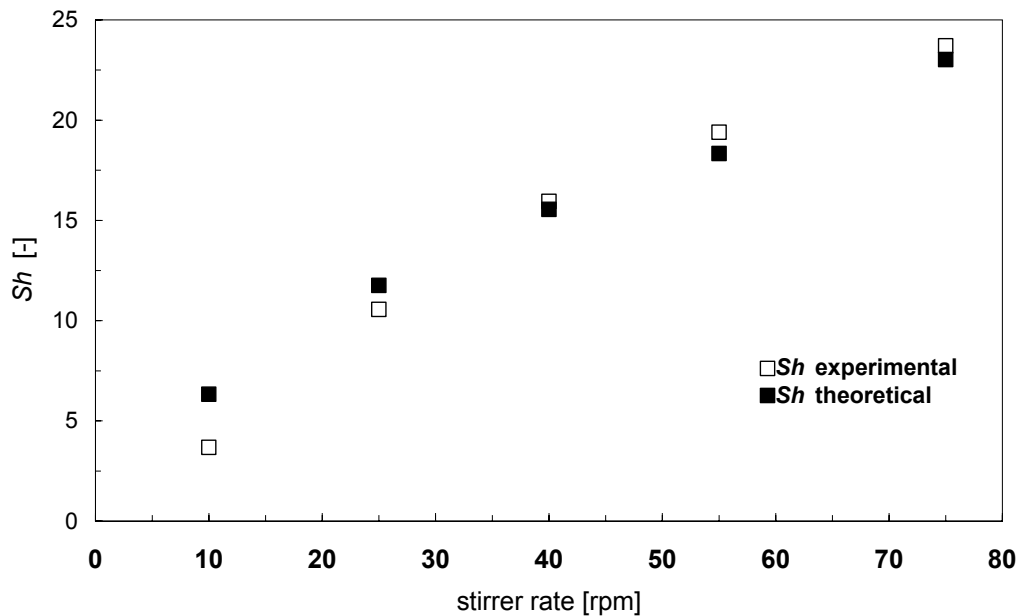


Figure 15. Experimental Sh values (open symbols) and theoretical values from [26] (closed symbols) for the MSR at different stirrer rates

The presence of external mass transfer limitations in the present experiments can now be confirmed by calculating the Carberry number Ca , defined as the ratio of the observed rate (in $\text{mol s}^{-1} \text{m}^{-3}_{\text{cat}}$) and the maximal mass transfer rate:

$$Ca = \frac{r_{v,obs}}{a' \cdot k_s \cdot C_b} \quad (12)$$

From the above it follows that $k_s \text{ theory} = k_s \text{ exp}$, so $k_s \text{ exp}$ can be used to estimate Ca . for the calculations the catalyst volume is $V_{\text{cat}} = 140 \text{ ml monolith}$ and a' is $1945 \text{ m}^2 \text{ m}^{-3}_{\text{monolith}}$.

For example: with a substrate concentration C_b of 0.5 mol m^{-3} (at the start of the chosen concentration interval), a k_s of $1.4 \times 10^{-5} \text{ s}^{-1}$ (from Figure 10), and $r_{\text{obs}} = 1.7 \times 10^{-6} \text{ mol s}^{-1}$, Ca becomes 0.9 for 200 cpsi C-ALD/IM catalysts at 55 rpm. So the system is close to being completely governed by external mass transport limitations. For the experiments performed at lower stirrer rate Ca was found to approach 1.

4 Conclusions

The monolithic stirrer reactor (MSR) was studied with respect to liquid solid mass transfer. The trypsin catalyzed hydrolysis of n-benzoyl-L-arginine ethyl ester (BAEE) was chosen as a model reaction. Based on an analysis of the reaction system, several immobilization protocols were proposed for application in the monolithic stirrer reactor.

Due to the surface chemistry of trypsin, ionic adsorption on polyethyleneimine is not suitable to prepare stable biocatalysts, as was predicted beforehand. Covalent immobilization and entrapment in a chitosan layer lead to active, stable biocatalysts. The use of ACM monoliths leads to an additional increase in trypsin loading. The specific activity of the enzyme is not influenced by the monolith-microstructure. The chitosan-based catalysts have a lower immobilized activity due to internal diffusion problems inside the gel layer. Here the ACM monolith outperforms the cordierite sample because of the higher accessibility inside the porous wall. The ALD/IM catalysts show a slow deactivation when they are used over a longer period of time with storage at 278 K. To minimize the effect of deactivation, catalysts should be used in no more than 10 subsequent tests over a maximum period of 5 days.

ALD/IM biocatalysts have a sufficient enzyme loading and activity to be successfully used in L-S mass transfer experiments in the monolithic stirrer reactor. At low stirrer rates the system enters the mass transfer controlled regime above 305 K.

For all monoliths, the liquid solid mass transfer coefficient increased with increasing stirrer speed. The mass transfer coefficient decreased with increasing cell density (with decreasing channel diameter). This can be attributed to the decreasing channel velocity at higher cell density.

The channel velocity was estimated by applying the L ev eque correlation. The average channel velocity increases with increasing stirrer rate, but decreases at higher cell density. Catalyst and reaction selection for mass transfer measurements is very important. If the reaction is too slow, the system remains kinetically limited. If internal diffusion limitations exist in the carrier material the mass transfer coefficient and the channel velocity will be underestimated. The hydrolysis of BAEE is a convenient model reaction for the measurement of liquid solid mass transfer coefficient in the MSR. The observed values for k_s are in good agreement with theoretical values for mass transfer and flow in the monolith channels in the MSR.

5 Acknowledgements

Nico Hinskens and Ingrid Hoek are gratefully acknowledged for their valuable contribution to this work. Corning Inc. is acknowledged for supplying the cordierite monoliths. The Dow Chemical Company is acknowledged for supplying the ACM monoliths and for funding part of this research.

6 Symbols

a'	specific surface area	$[\text{m}^2 \text{m}^{-3}]$
A_m	geometric surface area	$[\text{m}^2]$
C	surface roughness constant	$[-]$
C_b	reactant bulk concentration	$[\text{mol m}^{-3}]$
d_{ch}	channel diameter	$[\text{m}]$
D	diffusivity	$[\text{m}^2 \text{s}^{-1}]$
D_{eff}	effective diffusion coefficient	$[\text{m}^2 \text{s}^{-1}]$
$k_{r,\text{obs}}$	observed reaction rate constant	$[\text{s}^{-1}]$
k_s	mass transfer coefficient	$[\text{m s}^{-1}]$
K_m	Michaelis-Menten constant	mol l^{-1}
L	layer thickness	$[\text{m}]$
L_m	monolith length	$[\text{m}]$
m_i	mass component i	$[\text{kg}]$
n	reaction order	$[-]$
Re	Reynolds number	$[-]$
$r_{v,\text{obs}}$	observed reaction rate	$[\text{mol s}^{-1} \text{m}^{-3}]$
Sc	Schmidt number	$[-]$
Sh	Sherwood number	$[-]$
T	temperature	$[\text{K}]$
v_L	liquid velocity	$[\text{m s}^{-1}]$
V_L	liquid volume	$[\text{m}^3]$
V_{max}	maximum rate for enzymatic conversion	$[\text{mol s}^{-1} \text{g}^{-1}_{\text{enzyme}}]$
v_s	liquid velocity	$[\text{m s}^{-1}]$
w	mass support material	$[\text{kg}]$
w_s	mass coating	$[\text{kg}]$
Greek symbols		
η	liquid viscosity	$[\text{Pa s}]$
ρ	liquid density	$[\text{kg m}^{-3}]$
Φ	Wheeler-Weisz number	$[-]$

7 References

- [1] M.T. Kreutzer, F. Kapteijn, J.A. Moulijn, J.J. Heiszwolf (2005) Chemical Engineering Science; 60: 5859-5916
- [2] S.A. Wallin, A.R. Prunier, Jr, J.R. Moyer (2001) US Patent 6,306,335
- [3] K. M. de Lathouder, J. J. W. Bakker, M. T. Kreutzer, S. A. Wallin, F. Kapteijn, J. A.

- Moulijn (2006) *Chemical Engineering Research and Design*; 84(A5): 390–398
- [4] I. Hoek, T.A. Nijhuis, A.I. Stankiewicz, J.A. Moulijn, (2004) *Chemical Engineering Science*; 59: 4975-4981
- [5] J.J. Carberry (1964) *Industrial and Engineering Chemistry*; 56: 39-46
- [6] C.N. Kenney, W. Sedriks (1927) *Chemical Engineering Science*; 27: 2029-2040
- [7] K. Kawakami, S. Ura, K. Kusonoki (1976) *Journal of Chemical Engineering of Japan*; 9: 392-396
- [8] K. Kawakami, K. Kusonoki (1976) *Journal of Chemical Engineering of Japan*; 9: 469-474
- [9] C.J. Bennet, S.T. Kolaczkowski, W.J. Thomas (1991) *Chemical Engineering Research and Design*; 69: 209-220
- [10] C. Liakopoulos, S. Pouloupoulos, C. Philippopoulos (2001) *Industrial and Engineering Chemistry Research*; 40: 1476-1481
- [11] S.T. Kolaczkowski (1994) European patent, 605143A2 Assigned to Dow Corning Limited, Great Britain.
- [12] K.M. de Lathouder, T. Marques Flo', F. Kapteijn, J.A. Moulijn (2005) *Catalysis Today*; 105: 443–47
- [13] R.K. Shah, A.L. London (1978), *Laminar flow force convection ducts. Advances in heat transfer, Volume 1, Supplement 1*, Academic Press, New York, United States
- [14] H.P. Kasserra, K.J. Laidler (1969) *Canadian Journal of Chemistry* 47: 4031
- [15] R.N. Mukherjea, P. Bhattacharya, B.K. Gosh (1977) *Biotechnology and Bioengineering*; 19:1259-1268
- [16] D. Goradia, J. Cooney, B.K. Hodnett, E. Magner (2005) *Journal of Molecular Catalysis B: Enzymatic*; 32: 231–239
- [17] G.U. Ostrovidova, A.V. Makeev, A.V. Biryukov, S.K. Gordeev (2003) *Materials Science and Engineering*; C23: 377–381
- [18] I.P.G. Amaral, M.G. Carneiro-da-Cunha, L.B. Carvalho Jr., R.S. Bezerra (2006) *Process Biochemistry*; 41: 1213–1216
- [19] M. Malmsten, A. Larsson (2000) *Colloids and Surfaces B: Biointerfaces*; 18: 277–284
- [20] F. Xi, J. Wu, Z. Jia, X. Lin (2005) *Process Biochemistry*; 40: 2833–2840
- [21] H.H.P. Yiu, P.A. Wright, N.P. Botting (2001) *Journal of Molecular Catalysis B: Enzymatic*; 15: 81–92
- [22] H.H. Weetall, G. Baum (1970) *Biotechnology and Bioengineering*; 12: 399-407
- [23] C. Horvath, B.A. Solomon (1972) *Biotechnology and Bioengineering*; 14: 885-914
- [24] M.M. Andersson, R. Hatti-Kaul (1999) *Journal of Biotechnology*; 72: 21–31
- [25] I. Hoek (2004) PhD thesis, Delft University of Technology, the Netherlands
- [26] H.P. Kritzinger, B.C. Deelder, C.R. Kleijn, J.J. Derksen, H.E.A. van den Akker (2002) *Proceedings of. ASME Fluids Eng. Div., FEDSM2002-31360*.
- [27] M.A. Levêque (1928) *Annales des Mines*; 13: 276-289
- [28] H. Martin (2002) *Chemical Engineering Science*; 57: 3217-3223
- [29] S. Irandoust, B. Andersson (1998) *Catalysis Reviews- Science and Engineering*; 30: 341-392

Hydrolysis of lactose in the monolithic stirrer reactor

Abstract

Monolithic biocatalysts are used as support material for lactase from *Aspergillus oryzae* in the hydrolysis of lactose in the monolithic stirrer reactor (MSR). Polyethyleneimine (PEI) and chitosan have been applied on monoliths with a different microstructure. The volumetric hydrolysis rate at 308 K (pH 5) for lactase on 200 cpsi PEI- and chitosan-coated cordierite monoliths is 0.3 and 0.25 mol s⁻¹ m⁻³_{monolith} respectively. The porous wall of the ACM monoliths results in a higher enzyme loading capacity and a higher activity than for classical cordierite monoliths. (0.55 and 0.45 mol s⁻¹ m⁻³_{monolith} for PEI and chitosan respectively. If PEI is adsorbed onto the monolith without a chemical linker, the resulting biocatalysts are not stable due to desorption of the polymer. All other PEI and Chit-based catalysts are stable during operation at 308 K and prolonged storage at 278 K. The kinetics of the free enzyme is shown to follow Michaelis-Menten kinetics with competitive product inhibition. The hydrolysis of lactose in the MSR at 150 rpm was shown to be without external diffusion limitations. For the chitosan-catalysts internal diffusion limitations can be observed. The better accessibility of the catalysts in the open wall of the ACM monoliths minimizes the negative effect of possible internal transport problems. The monolithic stirrer reactor can be used as a lab scale tool to compare different monolithic biocatalysts in the absence of external mass transfer limitations.

1 Introduction

1.1 Description of the reaction system

Lactose is a disaccharide that occurs naturally in both human and cow milk, accounting for 40% of the milk solids. It is widely used in bakery and infant milk formulas. Lactose is the main carbohydrate in milk and whey (at a concentration between 50 and 100 g l⁻¹, depending on the source of milk) [1]. The amount of lactose produced annually from whey is about 3.3 million tons [2]. It is produced as cheese whey, which is the liquid, separated after milk coagulation. It represents around 90% of the milk-volume, this can be considered a serious pollution problem of the dairy industry. One alternative is the use of whey as the basic medium for various fermentation processes [3]. These processes are however still being explored at lab-scale. Direct fermentation of lactose into ethanol is possible with the appropriate yeast strains, but at the moment this process is industrially not viable [4]. The hydrolysis of lactose into its mono-saccharide components however, is a promising process in the food industry for the development of new products with no lactose in their composition.

The consumption of foods with a high lactose content is problematic for almost a 70% of the world population, as the enzyme that is naturally present in the human intestine loses its activity during lifetime [5]. Together with the relatively low solubility and sweetness of lactose, this has led to an increasing interest in the development of industrial processes to hydrolyze lactose. Hydrolysis of lactose is a way to recycle the whey, using it as a source to obtain additives for human or cattle feeding [6]. The reaction is presented in Figure 1.

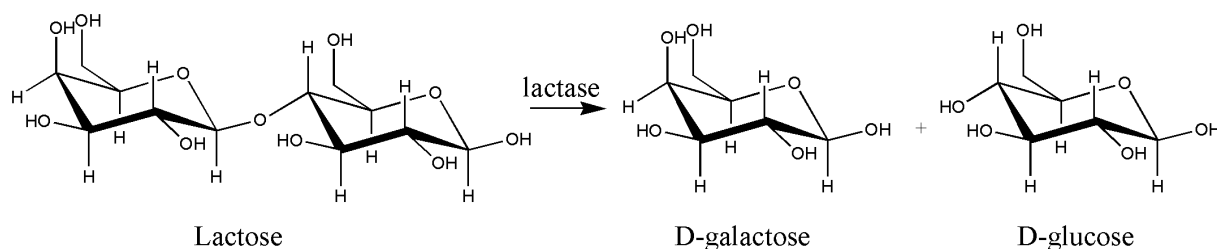


Figure 1. Lactose hydrolysis to form D-galactose and D-glucose

The hydrolysis of lactose can be performed by acids or acid resins or by enzymatic treatment. The use of acids is not adequate to hydrolyze lactose in milk and whey due to the generation of nasty flavors, odors, and colors during the process and the reduction in alimentary properties of milk. Lactase is commercially available and used in large-scale processes. When the enzymatic treatment is performed with β -galactosidases as catalyst, the taste of milk is only changed to a sweeter one (glucose and galactose are four times sweeter than lactose) and in the same time, the development of lactose crystals in refrigerated products is avoided. A second advantage is the occurrence of a side reaction: the synthesis of galacto-oligosaccharides, carbohydrates that promote the growth of beneficial bacteria in the intestine [8]. One problem associated with the use of lactase is that complete hydrolysis is difficult to

achieve because of product inhibition and production of larger saccharides and an isomer of lactose (allolactose) [2]. Also the low stability of these enzymes is a technical problem that is usually overcome by injecting an enzyme dose in milk brick and letting the hydrolysis proceed between the packing and the consumption of the milk.

Several microbial sources of β -galactosidase and reactor types have been used for the purpose of economic production of low lactose milk. Since the cost of the enzyme is the most important factor that determines process economy, only continuous systems that involve the reuse of enzyme can be considered. Thus enzymatic hydrolysis of lactose has been studied by using either immobilized enzyme reactors [10-14] or membrane reactors [15]. The major disadvantage of the membrane reactor is the increased risk of microbial contamination, especially during prolonged operation at ambient temperature, and the clogging of the ultrafiltration membranes with milk proteins. These drawbacks could be alleviated partially by operating the system at higher temperatures and by using deproteinated substrates. Lactose hydrolysis in plug-flow reactors gives a higher conversion compared to continuously stirred tank reactors, although the latter has good mixing and lower construction cost.

An efficient and economically feasible process for the hydrolysis of whey lactose strongly depends on the production cost of the enzyme in combination with favorable kinetic and stability properties. Continuous processes are still being studied and developed [6]. Large-scale hydrolysis is performed at different sites. Sumitomo, Snow Brand, and Central del Latte run a continuous process in a plug flow reactor. At 308 K, lactose is hydrolyzed by immobilized lactase to 70-80% conversion. The reactor volume can be as large as 250 m³. Central de Latte has a production capacity of 8000 l d⁻¹ [16].

1.1.1 Lactase

Galactosidases (EC 3.2.1.23) catalyze the enzymatic hydrolysis of lactose to glucose and galactose. These enzymes are widely distributed in nature, appearing in micro-organisms, plants and animal tissues [6]. The enzyme consists of four equal subunits, and has an approximate diameter of 10-15 nm. The size of enzyme varies depending on the source of the enzyme. *E. coli* lactase for instance is 464-kDa tetramer, while the lactase from *Aspergillus oryzae* is much smaller with around 106 kDa. Each chain consists of five domains, the third of which comprises much of the active site. This site does, however, include elements from other domains and other subunits. Catalytic activity proceeds via the formation of a covalent galactosyl intermediate with Glu537 (see Figure 2), and includes ‘shallow’ and ‘deep’ modes of substrate binding. The residues that form the active site are from different segments of the polypeptide chain.

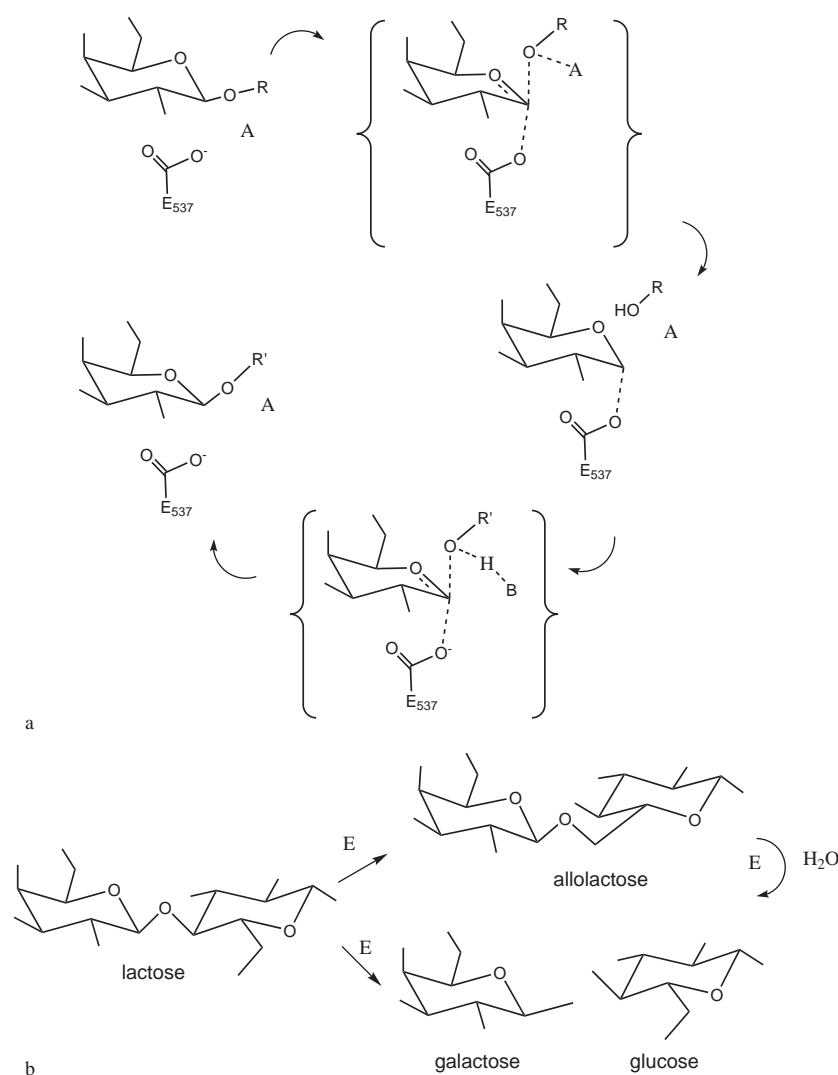


Figure 2. a) Generalized outline for a double-displacement reaction catalyzed by β -galactosidase. In the first step (top), the substrate, a β -D-galactopyranoside with OR as the aglycon, forms a covalent α -D-galactosyl enzyme intermediate with the nucleophile Glu537 and with assistance from an acid, A (either Glu461 or a magnesium ion). Galactosyl transfer to the nucleophile is shown here as concerted with glycosidic bond cleavage, although this is controversial and may depend on the nature of the leaving group. In the second step (bottom), release of the intermediate is facilitated by a base, B (probably Glu461), which abstracts a proton from the acceptor molecule, $\text{R}'\text{OH}$. **b)** General scheme for the action of β -galactosidase on the natural substrate, lactose. The enzyme can either perform hydrolysis (lower path) or transglycosylation (upper path). From [20]

Because it takes two monomers to complete an active site, individual monomers of the enzyme are inactive. Both Mg^{2+} and Na^+ are required for maximal activity of β -galactosidase [17]. In the human body, β -galactosidase has two catalytic activities; direct hydrolysis of the disaccharide lactose to galactose and glucose or via another disaccharide, allolactose. The latter route is aimed to regulate the enzyme production. Allolactose is the natural inducer for additional production of the enzyme in a living cell. The possibility of exploiting different substrates has allowed the introduction of a variety of commercially available substrates with useful chromogenic properties to easily follow conversion by UV-VIS and to quickly

compare different catalysts. These substrates include X-gal (5-bromo-4-chloro-3-indoyl- β -D-galactopyranoside) and oNPG (*o*-nitrophenyl- β -Dgalactopyranoside). β -Galactosidase is a retaining glycosidase, meaning that the product retains the same stereochemistry as the starting substrate. The two-step (double displacement) nature of the catalytic mechanism was first proposed by Koshland [18] and later demonstrated experimentally [19]. A generalized outline for the mechanism of action, is shown in Figure 2b.

1.1.2 Lactase kinetics

Several methods of determining the kinetics for enzymatic hydrolysis of lactose have been described previously [21-25]. The conventional methods of determining kinetic parameters for the Michaelis-Menten rate expression are to obtain the reaction rate as a function of substrate concentration and then perform a graphical method such as the Lineweaver-Burk, Hanes-Wolf, or the direct linear plot [26]. Other methods use integrated rate equations to fit the model with a set of values. In this study both methods are applied. The existing literature suggests that galactose is a competitive lactase inhibitor, while glucose does not inhibit enzyme activity [22-24]. A schematic illustration of the general kinetic model for reversible product inhibition is given in Figure 3 [24].

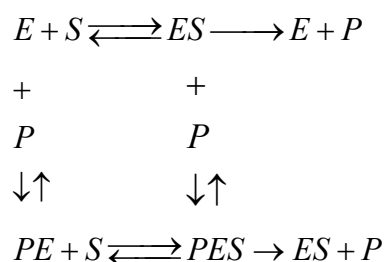


Figure 3. A schematic illustration of the general kinetic model for reversible product inhibition: E, enzyme; S, substrate; P, product

It also well known that glucose is the first released product, leaving an enzyme-galactosyl complex for further reaction. This complex is transferred to an acceptor containing a hydroxyl group. While in a diluted lactose solution water will be more competitive over other sugars to be an acceptor, in a more concentrated solution lactose molecules have a higher chance to interact with the enzyme complex to form trisaccharides [6,27,28]. Several forms of product inhibition exist. Non-competitive inhibition exists when a molecule (inhibitor) binds to part of the enzyme away from the active site and causes a conformational change in the active site of the enzyme, thereby inhibiting the binding of the appropriate substrate molecule. The enzyme will remain inhibited until the non-competitive inhibitor leaves this regulatory site. Acompetitive inhibition exists when the product can bind to the regulatory site and inhibit reaction of the ES complex. Competitive inhibition of enzyme activity occurs when an inhibitor resembling the structure of the substrate (this can also be the product) binds to the active site of the enzyme and blocks the binding of the substrate. The corresponding mechanisms are presented in Table 1. Model 4 is a variant of model 3, assuming that the

glucose molecule is the first to leave the active site of the enzyme and leaving the galactosyl group joined as an enzyme-galactosyl complex. This mechanism was postulated by Yang and Sokos [24].

Table 1. Proposed mechanisms for lactose hydrolysis with product inhibition

Kinetic model	Enzymatic mechanism	Rate equation
Michaelis-Menten with non competitive inhibition	$E + S \xrightleftharpoons[k_{-1}]{k_1} ES \xrightarrow{k_2} E + P$ $E + P \xrightleftharpoons[k_{-3}]{k_3} EP$ $ES + P \xrightleftharpoons[k_{-4}]{k_4} ESP$	$r = \frac{V_{\max} C_E C_S}{K_m \left(1 + \frac{C_P}{K_{i,1}}\right) + C_S \left(1 + \frac{C_P}{K_{i,2}}\right)} \quad (1)$
Michaelis-Menten with acompetitive inhibition	$E + S \xrightleftharpoons[k_{-1}]{k_1} ES \xrightarrow{k_2} E + P$ $ES + P \xrightleftharpoons[k_{-4}]{k_4} ESP$	$r = \frac{V_{\max} C_E C_S}{K_m + C_S \left(1 + \frac{C_P}{K_i}\right)} \quad (2)$
Michaelis-Menten with competitive inhibition	$E + S \xrightleftharpoons[k_{-1}]{k_1} ES \xrightarrow{k_2} E + P$ $E + P \xrightleftharpoons[k_{-3}]{k_3} EP$	$r = \frac{V_{\max} C_E C_S}{K_m \left(1 + \frac{C_P}{K_i}\right) + C_S} \quad (3)$
Michaelis-Menten with competitive inhibition, glucose leaves first	$E + S \xrightleftharpoons[k_{-1}]{k_1} ES \xrightarrow{k_5} EP + Gl$ $E + P \xrightleftharpoons[k_{-3}]{k_3} EP$	$r = \frac{V_{\max} C_E C_S}{K_m \left(1 + \frac{C_P}{K_i}\right) + (1 + K_p) C_S} \quad (4)$

By fitting the different model equations to the experimental data by nonlinear regression, the kinetic parameters can be determined and the most appropriate model can be selected.

1.1.3 Lactase immobilization

The use of free lactase is quite expensive, but when it is coupled to an adequate support matrix the enzyme can be reused several times. Lactase has been immobilized by using different methods such as physical adsorption, covalent bonding, and gel entrapment. However, despite the large interest in the β -galactosidase immobilization, it is difficult to obtain a catalyst showing high activity, stability and optimal mechanical properties. Even though special immobilized lactase reactors were developed for example by SNAM Progetti in Italy and Sumitomo Chemicals in Japan, free enzyme is still widely used in dairy industry around the world [29]. Some interesting improvements in the immobilization of lactase have been presented lately, including strong reversible immobilization on anionic exchangers [30], immobilization on acrylic resin to decrease product inhibition [31], and immobilization onto polymeric membranes [32]. Upon scale up or industrial application however, the problems concerning the mechanical strength of the polymeric beads and possible clogging or contamination of the membrane that were already stated above, are encountered. Also note

that diffusional limitations in enzyme-loaded beads often result in severely sub-optimal performance [33,34].

Monolithic catalyst supports, originally developed for use in automotive emission control systems where low pressure drop and high surface area are required, are an interesting alternative for conventional support materials in heterogeneous catalysis and biocatalysis. The honeycomb monolith support offers several advantages over particulate supports, including a high geometric external surface, structural durability, easy catalyst separation, a low pressure drop, and uniform flow distribution within the matrix [35]. Different immobilization methods that are traditionally used with particulate supports, can be translated for use with monolithic supports by applying the carrier material on the walls of the monolith. A thin layer of carrier material on a monolithic support could be an interesting alternative for these particulate carriers by increasing mechanical stability and decreasing diffusion distance.

1.1.4 The Monolithic Stirrer Reactor (MSR)

The Monolithic stirrer reactor consists of two monoliths that have the catalyst immobilized on the wall of their structure. These monoliths work like as stirrer blades that can easily be removed from the reaction medium, thereby eliminating the need for a filtration step after reaction. The set-up (Figure 3) was already discussed in more details in the previous chapter.

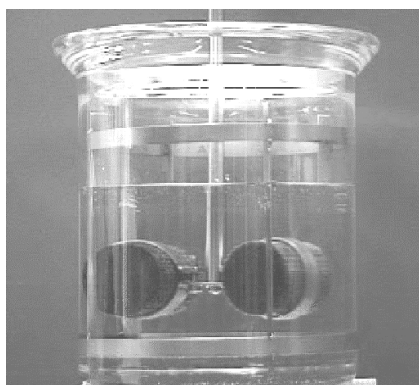


Figure 3. MSR set-up used for the hydrolysis of lactose

This reactor is thought to be especially useful in the production of fine chemicals and in biochemistry and biotechnology. In particular, the system has both characteristics of a fixed-bed, in the sense that the support with catalyst is a large structure that is readily separated from the liquid reaction medium, and of a stirred reactor, in the sense that it allows convenient batch operation and rapid mixing and contacting. The wide range of commercially available monolith geometries ensures that always a good compromise can be made between the stirring action of the blades and flow through the channels where the reaction occurs on the wall. Alternatively foam structures could be applied as stirrer blades. In this work, we use both cordierite monoliths and the open ACM support monoliths as stirrer blades for enzyme-catalyzed reactions. The potential of the latter combination is very attractive. The use of immobilized enzymes allows simpler and cleaner routes to many pharmaceutical

intermediates, and the ACM monolith stirrer is thought to give good performance and efficient enzyme use in these intensified processes.

1.2 Carrier selection

To select a suitable monolith-carrier combination to use in the hydrolysis of lactose, different parameters must be addressed. The reaction is performed in aqueous medium, so physical adsorption would be less suitable. The reaction shows product inhibition, but selection of specific carrier materials could have a positive influence on the reaction kinetics [31]. Regarding the enzyme-support interaction, the porosity of the carrier should match the use of the relatively large lactase. Furthermore, the enzyme is not extremely expensive. There is no need for complete reusability by means of covalent attachment. In this case, a reversible protocol can be a good choice. Reversible ionic adsorption on a polyelectrolyte (Chapter 7) and entrapment in a chitosan layer (Chapter 6) generally results in a stable biocatalyst with a high resulting activity, and are suitable for use in aqueous medium. These protocols are therefore selected to perform the lactose hydrolysis in the MSR. However, covalent immobilization could also be useful to ensure a good carrier-enzyme bond, but has been shown to result in a low immobilized activity (Chapter 5) and is therefore not considered in this study.

1.3 Layout

To maximize the conversion in the hydrolysis of lactose, the monolithic stirrer reactor is applied with different monolith-carrier combinations. Polyethylenimine and chitosan layers are applied on monoliths with different microstructure. These carriers provide adsorption sites for lactase from *Aspergillus oryzae*. ACM monolith materials are compared with classical cordierite monoliths with respect to carrier preparation, enzyme immobilization, and performance in the monolithic stirrer reactor for the hydrolysis of lactose. Free lactase is included in the study to address the kinetics of the enzyme.

2 Experimental

2.1 Materials

Ludox AS-40 colloidal silica solution, lactose, and PEI, water free; MW = 750000, 50% in water were from Aldrich. β -Galactosidase from *Aspergillus oryzae* (E.C. 3.1.2.23), o-nitrophenyl- β -galactopyranoside (oNPG), lactose, and (3-glycidoxypropyl)trimethoxysilane (GPTMS) were purchased from Sigma. All buffer salts were of analytical grade and from Baker. Glutaraldehyde (25% in water) and low viscous chitosan (< 200 mPa s) were from Fluka. Honeycomb monoliths of ACM with a cell density of 200 cpsi (31 cells cm⁻²) were

prepared by a proprietary Dow process to produce honeycombs. Cordierite monoliths of 200 cpsi were used for comparison. The key properties are given in Table 2.

Table 2. Geometric characteristics of the monoliths employed in this study.

	ACM ("medium")	Cordierite
Cell density	200 cpsi	200 cpsi
Wall thickness	0.35 mm	0.3 mm
Wall porosity	60%	35%
Pore diameter in the wall	18 μm	7.5 μm

2.2 Catalyst preparation

2.2.1 Washcoating

The monoliths were calcined (10 K min^{-1} , 1273 K, 4 hrs) and washcoated with a colloidal silica solution (Ludox AS-40). Optimization of the washcoating with different silicas was described in Chapter 3. Cordierite samples were dipped in the Ludox solution as received. ACM monoliths were washcoated with a 4% Silica (10 times diluted Ludox AS-40 in water) solution. The channels were cleaned with pressurized air and the monoliths were dried in a microwave oven for 20 min at 150 W. Samples were subsequently calcined at 673 K (5 K min^{-1} , 4 h).

2.2.2 Preparation of PEI-coated monoliths

Polyethylenimine-functionalized supports were prepared as described in Chapter 7, using a direct coupling through (3-glycidoxypropyl)trimethoxysilane (GPTMS). The monoliths were functionalized at room temperature for 24 h. in a 5wt% solution of silane in toluene, containing 0.1% v/v triethylamine. After silanization the samples were washed with toluene and acetone and dried at 393 K (heating rate 2 K min^{-1}) for 2 h. The polymer was attached from a 10 wt% PEI solution in water (pH 10) under ambient conditions for 24 h. GPTMS-based carriers were washed with 1 M NaCl and water, and dried under vacuum. After vacuum drying overnight, the supports were stored under air at 278 K. PEI was also adsorbed directly on the washcoated monoliths from a 10 wt% PEI solution for 24 h at ambient temperature.

2.2.3 Preparation of chitosan coatings

Washcoated monoliths were treated in 250 ml of a 2.5-10 wt% solution of silane in toluene with 0.1 % (v/v) tetraethyleamine. The monolith was mounted on glass pins that were present on the sides of the glass reactor to allow space for the magnetic stirrer. The mixture was stirred at 293 K for 24 h. Supports were washed with toluene and acetone and dried at 393 K for 4 h (2 K min^{-1}).

Chitosan-coatings were applied by dip-coating. Monoliths were held in a 1.0 % w/v chitosan solution containing 1.1 % w/v glutaraldehyde for 60 sec. After cleaning the channels, samples were air dried for 90 min. The average thickness of the chitosan gel layer was calculated by:

$$L_{chitosan} = \frac{m_{chitosan} / \rho_{chitosan}}{\frac{\pi}{4} \cdot d_m^2 \cdot L_m \cdot a'} \quad (5)$$

Where $m_{chitosan}$ and $\rho_{chitosan}$ are the mass and density of chitosan filtrate, d_m and L_m are the diameter and height of the monolithic structure and a' is the specific surface area. The density of 1.0 % chitosan filtrate is assumed to be equal to the density of water.

2.2.4 Enzyme adsorption

Lactase was adsorbed on the functionalized supports under ambient conditions, in a recycle reactor where the liquid was recycled over the support in upflow. A 10 mM phosphate buffer pH 7 was used as medium with a final lactase concentration of 4 g l⁻¹. The protein concentration was determined using UV-VIS (Thermo Optek Unicam 540) at 260 nm and checked with oNPG hydrolysis activity. After immobilization, the samples were washed with phosphate buffer pH 7 and excess distilled water, dried under vacuum overnight, and stored under air at 278 K.

2.3 Nomenclature

In this study, the samples are named depending on the monolith type, the carbon type, and the treatment. The first letter of the samples is used to distinguish the monolith type, “C” is used for cordierite, “A” for ACM. A second letter is used in the case of ACM to determine the microstructure of the ACM; The carrier is indicated with either PEI for polyethyleneimine, or Chit for chitosan. This is summarized in Table 3.

Table 3. Nomenclature

Position	Component	Code
1	Monolith type	C or A
2	Micro grain structure ACM	M
3	Spacer	GPTMS
4	Carrier	Chit or PEI

2.4 Characterization

The amount of coating, mass increase, and mass decrease were determined by measuring the sample weight before and after the various preparation steps.

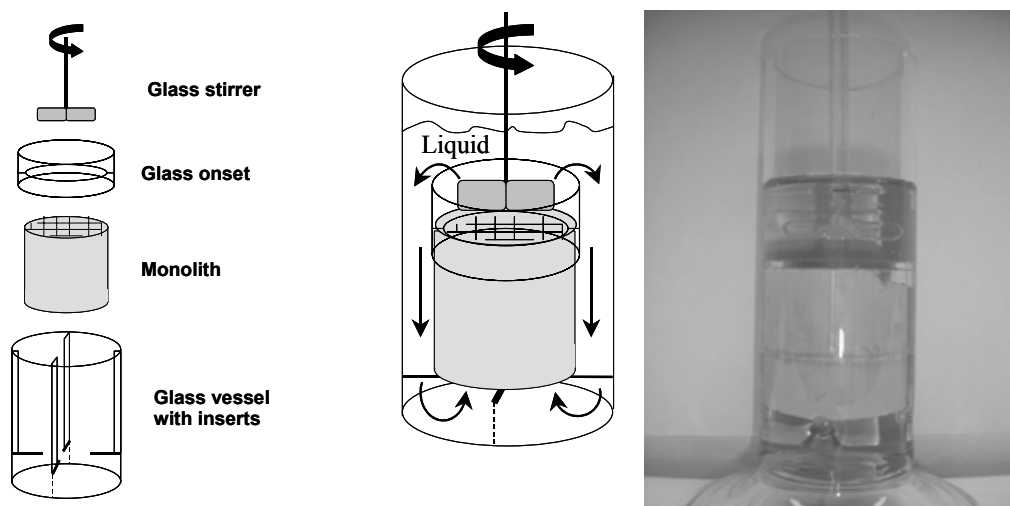


Figure 5. Experimental set-up with glass reactor, onset, and stirrer

2.5.2 Hydrolysis of lactose in the MSR

Catalytic tests were performed in a monolithic stirrer reactor consisting of a glass vessel equipped with a stirrer motor. The set-up is schematically drawn in Figure 6.

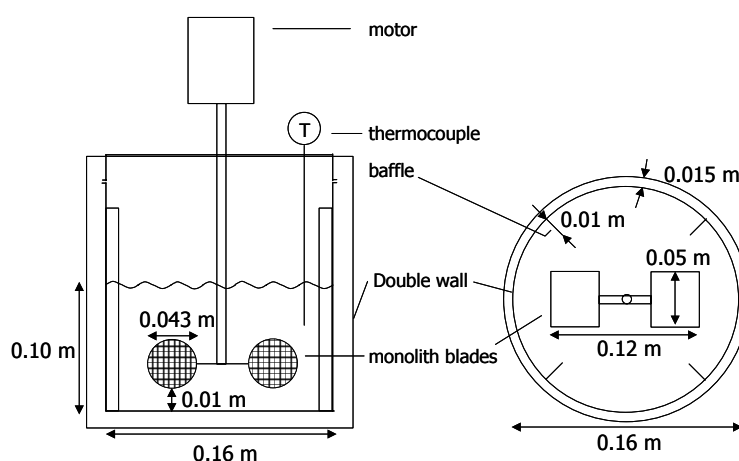


Figure 6. Schematic drawing of the MSR set-up. a) side view, b) top view

Two monoliths (length 5 cm) were mounted in plane on the stirrer axis. The total reaction volume was 2 l. Initial lactose concentration was 50 g l^{-1} . The reaction was followed by HPLC analysis on with a Rezex RCM monosaccharide column (8% Ca) with a Biorad Carbo C pre-column, coupled to an RI detector at 308 K. Elution was performed with milli-Q water (0.4 ml min^{-1}) as the mobile phase. Samples were diluted in water (100x) before HPLC analysis. The analysis results were processed with HP Chemstation software. The concentration of the reactants and products was calculated from the area of the peaks from the raw HPLC data. The calibration was done with standard solutions of the reactant and the products. In Figure 7, the calibration curves for lactose, glucose and, galactose are given.

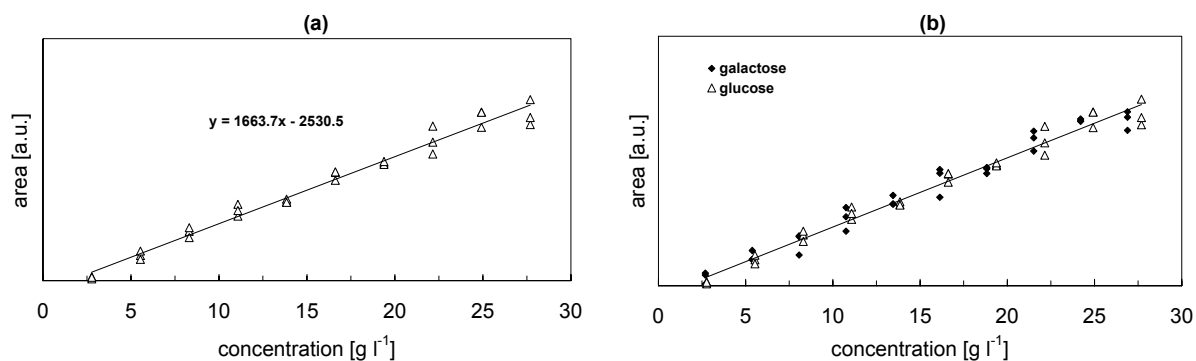


Figure 7. HPLC calibrations for a) lactose, b) glucose and galactose.

In the concentration range that is used in the performance tests, a linear dependency is observed between peak area and concentration. The slope of the lines in Figure 7 can therefore be used to quantify the HPLC data in terms of reactant concentration. Activity tests were performed at varying stirrer rate and temperature.

Possible desorption of the enzyme from the supports was checked by following oNPG hydrolysis activity of the supernatant after completion of the test. Stability was studied by storing the catalysts under vacuum for a longer period of time, by using the catalysts at elevated temperatures, and by consecutive testing under the same conditions. Free enzyme was used as a comparison.

3 Results and discussion

The results of functionalization of the monolithic supports with polyethyleneimine and chitosan are given in Table 4, where Y_c represents the carrier loading in wt% of the functionalized monolith.

Table 4. Carrier loading of the prepared monolithic supports

Method	Y_c wt%	Layer thickness (L) μm
C-PEI	2.6	-
C-GPTMS-PEI	9.7	-
C-CHIT	29.1	90
AM-GPTMS-PEI	13.1	-
AM-CHIT	32.2	102

All PEI yields are slightly higher than was observed before (see Chapter 7). The reason for this is unclear. The samples were made with a new batch of high molecular weight PEI, which could have been of influence on the final yield. With a mean loading of 0.37 and 0.48 g chitosan $\text{g}^{-1}_{\text{monolith}}$, for cordierite and ACM, the chitosan yields are in accordance with the values obtained in general for dipcoating different monoliths in chitosan gels (Chapters 6, 10-12). If we consider the total volume of the ACM channel walls (with a cell density of 30 cells

cm^{-2} , a wall thickness of 0.35 mm and a monolith length of 5 cm, this can be estimated to be 15 ml), the 10-12 ml of chitosan gel that is deposited fills the walls for 75-80%. This would give a layer thickness of 140 μm for a layer from the middle of the channel towards the center of that channel. The 100 μm that was calculated in Table 4, was estimated by assuming a solid layer on the geometric surface area of cordierite. Since the total amount of gel that is present inside the wall should yield a larger layer than is estimated based on flat channel wall, the gel is most likely present as a solid layer inside the centre of the wall and as a thin layer on the separate micrograins on the outside of the wall. This gel layer is assumed to present a significant diffusion barrier for both reactant and products.

For the PEI composites it is assumed that the very thin polymer layer does not form a barrier for internal diffusion. Since the exact size of the folded polymer is not known, no layer thickness was calculated.

3.1 Enzyme adsorption

Lactase was adsorbed onto the carriers from a 4 g l^{-1} solution in a 5 mM phosphate buffer pH 7.5. The results for the lactase immobilization are presented in Figure 8, expressed in total enzyme loading [mg] for every carrier. As could be expected based on the polymer/gel loading and the previous optimizations for the immobilization protocols, chitosan coatings have the highest lactase loading (20-30 $\text{mg lactase ml}^{-1}_{\text{gel}}$). The ACM monoliths have a higher lactase loading, due to their open channel walls.

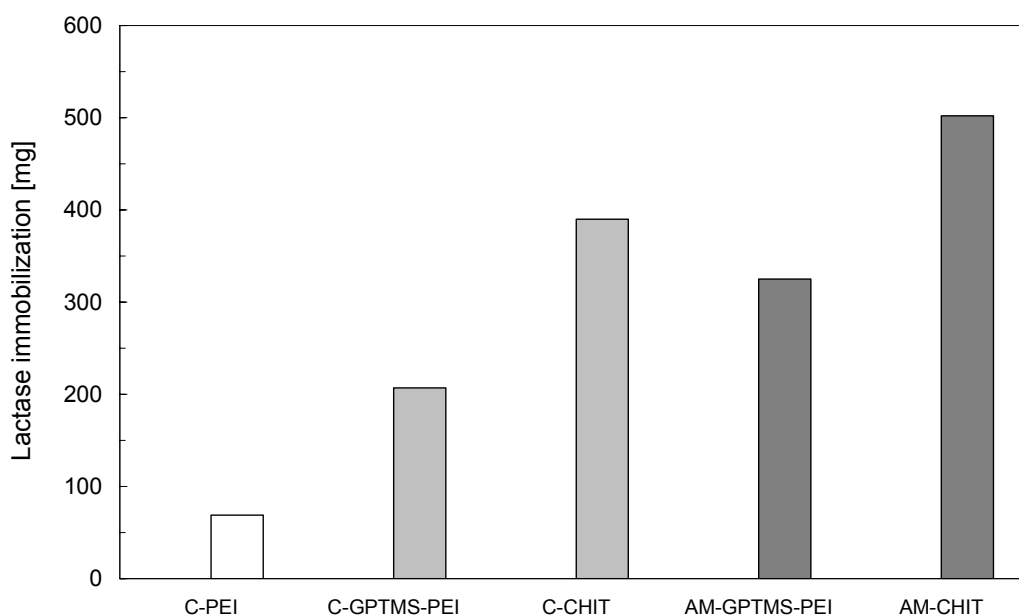


Figure 8. Lactase adsorption on the different monolith-carrier combinations

The low PEI loading that is obtained by adsorption of the polymer is reflected in the value for total enzyme loading, this value is also relatively low compared to that of the other catalysts.

3.2 Catalyst performance

To study the kinetics of this lactase, batch experiments were performed in a reactor at varying initial lactose concentrations (25-120 g l⁻¹). Also the effect of introducing a different substrate (oNPG) was included. The immobilized lactase was then used in the MSR at varying stirrer rates and temperatures. Operational and storage stability were investigated respectively by operating continuously, and by keeping the monoliths in phosphate buffer at 278 K for several weeks.

3.2.1 Kinetics of lactase from *Aspergillus oryzae*

In Table 5, the enzymatic mechanisms that were presented in the introduction are presented again, complemented with the Michaelis-Menten expression (7) without inhibition. The corresponding rate equation that was derived by assuming a steady state for the enzyme-lactose complex (ES) is given in the third column.

Table 5. Summary of the kinetic models that are used to describe the experimental data

Kinetic model	Enzymatic mechanism	Rate equation
Michaelis-Menten without inhibition	$E + S \xrightleftharpoons[k_{-1}]{k_1} ES \xrightarrow{k_2} E + P$	$r = \frac{V_{\max} C_E C_S}{K_m + C_S} \quad (7)$
Michaelis-Menten with non competitive inhibition	$E + S \xrightleftharpoons[k_{-1}]{k_1} ES \xrightarrow{k_2} E + P$ $E + P \xrightleftharpoons[k_{-3}]{k_3} EP$ $ES + P \xrightleftharpoons[k_{-4}]{k_4} ESP$	$r = \frac{V_{\max} C_E C_S}{K_m (1 + \frac{C_P}{K_{i,1}}) + C_S (1 + \frac{C_P}{K_{i,2}})} \quad (1)$
Michaelis-Menten with acompetitive inhibition	$E + S \xrightleftharpoons[k_{-1}]{k_1} ES \xrightarrow{k_2} E + P$ $ES + P \xrightleftharpoons[k_{-4}]{k_4} ESP$	$r = \frac{V_{\max} C_E C_S}{K_m + C_S (1 + \frac{C_P}{K_i})} \quad (2)$
Michaelis-Menten with competitive inhibition	$E + S \xrightleftharpoons[k_{-1}]{k_1} ES \xrightarrow{k_2} E + P$ $E + P \xrightleftharpoons[k_{-3}]{k_3} EP$	$r = \frac{V_{\max} C_E C_S}{K_m (1 + \frac{C_P}{K_i}) + C_S} \quad (3)$
Michaelis-Menten with competitive inhibition, glucose leaves first	$E + S \xrightleftharpoons[k_{-1}]{k_1} ES \xrightarrow{k_5} EP + Gl$ $E + P \xrightleftharpoons[k_{-3}]{k_3} EP$	$r = \frac{V_{\max} C_E C_S}{K_m (1 + \frac{C_P}{K_i}) + (1 + K_p) C_S} \quad (4)$

The experimental data points of the runs with free enzyme were fitted to the five kinetic models with Athena Visual Workbench version 8.2. The models were fitted with a non-linear Bayesian estimation method with two responses (lactose and the inhibiting component galactose). From literature it was already known that model 3 and 4 (competitive product inhibition) would probably give the best results [22-24]. At lower initial concentrations, the

rate of product formation is relatively slow, so at low concentration the initial rate will approach the rate calculated by a Michalis-Menten or Hofstee plot. To get good starting values for the parameters of the rate equations in Table 5, a Hofstee plot was constructed (not shown). From this plot the initial parameter starting values were $11 \text{ mmol g}_{\text{protein}}^{-1} \text{ min}^{-1}$ and 0.06 M for k and K_m respectively. After a first scan, models 1,2,5 were dismissed because no reasonable fit could be obtained, especially at higher conversion and at higher initial lactose concentrations. The obtained parameter values for model 3 and 4 are presented in Table 6.

Table 6. Results fitting models 4 and 5 to the experimental data obtained at 308 K, pH 4.5

Model	Parameter*	Value	95% confidence interval
3	$r = \frac{V_{\max} C_E C_S}{K_m \left(1 + \frac{C_P}{K_i}\right) + C_S}$	V_{\max}	1.1 ±0.66
		K_m	68 ±5.6
		K_i	15 ±1.4
4	$r = \frac{V_{\max} C_E C_S}{K_m \left(1 + \frac{C_P}{K_i}\right) + (1 + K_p) C_S}$	V_{\max}	9.2 ±0.98
		K_m	63 ±5.5
		K_i	13 ±1.4
		K_p	0.08 ±0.11

* $[k] = \text{mmol g}_{\text{protein}}^{-1} \text{ min}^{-1}$, $[K_m] = \text{mM}$, $[K_i] = \text{mM}$, $[K_p] = \text{mM}$

Model 3 and 4 seem to give the most accurate representation of the reaction rate at higher conversion. Based on the confidence interval of K_p in model 4, this parameter cannot be distinguished from 0. Secondly, the residuals-plot for model 3 as a function of concentration (not shown) indicates a better fit. From the limited set of kinetic data that is used in this study, it does not become clear that glucose is the first leaving product. The experimental concentration/time data are plotted with the model values of model 3 in Figure 9.

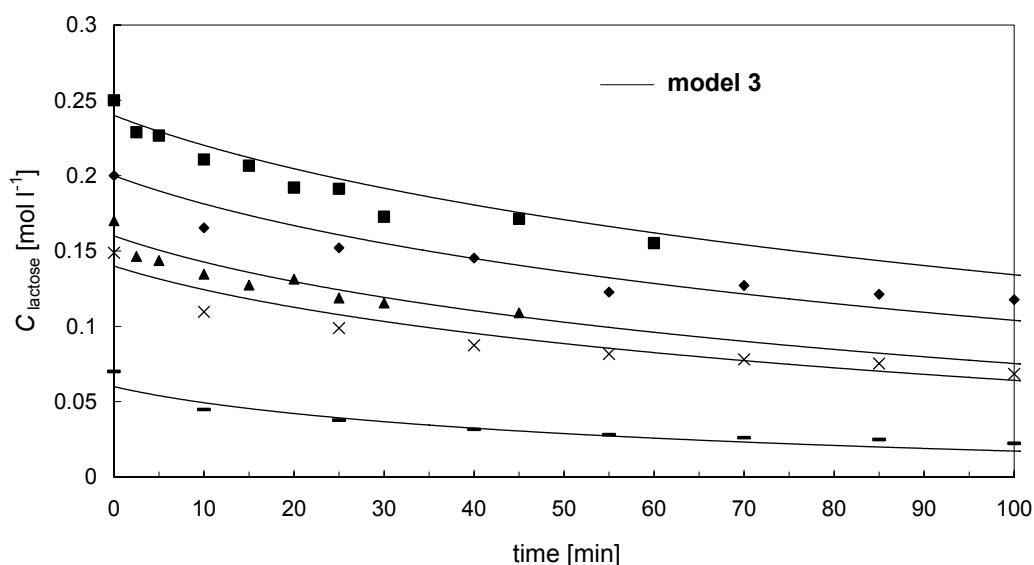


Figure 9. Lactose concentration as a function of time (markers) and model values (lines) of model 3, with $V_{\max} = 11 \text{ mmol g}_{\text{protein}}^{-1} \text{ min}^{-1}$, $K_m = 68 \text{ mM}$, and $K_i = 15 \text{ mM}$. Experimental data were collected in the hydrolysis of lactose at different substrate concentrations, $T = 308 \text{ K}$, 650 rpm .

3.2.2 Effect of substrate type

The hydrolysis of oNPG follows the same mechanism as the hydrolysis of lactose. Model 3 and 4 were also used to determine the initial rate constants for oNPG hydrolysis. The initial rate in the hydrolysis of oNPG as a function of substrate concentration is presented in a Hofstee plot (Figure 10a) and as a Michaelis-Menten plot in Figure 10b. From Figure 10a, V_{\max} and K_m can be determined as described in Chapter 10.

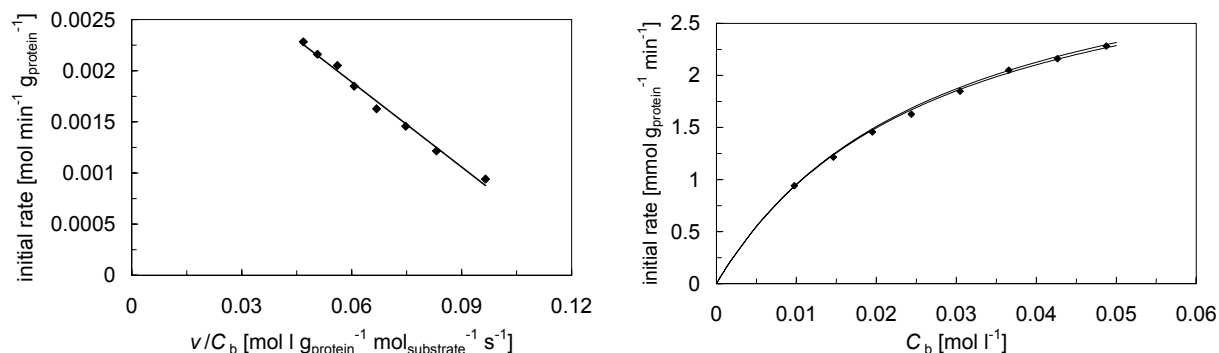


Figure 10. Hofstee-plot (left) and Michaelis-Menten plot (right) for lactase in the hydrolysis of oNPG at 295 K, 650 rpm at different substrate concentrations.

In Figure 10b the model values are given as a solid line. No distinction can be made between the two models at these negligible product concentrations. The kinetic parameters that were determined from the oNPG assay are presented in Table 7, in order to compare the different kinetic studies. Compared to the values that were calculated from the hydrolysis of lactose at 308 K, the values from Figure 10a are in the same order of magnitude. Differences can be caused by the different substrate or experimental parameters such as pH, temperature, and type of buffer.

3.2.3 Effect of immobilization

If the lactase is immobilized on a C_{PEI} carrier, the kinetic parameters are affected.

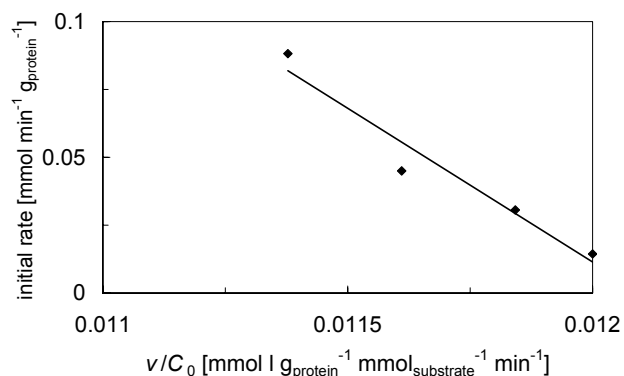


Figure 11. Hofstee plot for the immobilized enzyme. Tests were performed at 295 K, 500 rpm

The catalyst was tested in the same glass reactor as the free enzyme, at 650 rpm. From the Hofstee-plot (Figure 11), the kinetic parameters for lactose on a PEI carrier can be determined. For the immobilized lactase, $K_m = 0.12$ mM, and $V_{\max} = 1.4$ mmol g_{protein}⁻¹ min⁻¹. The increase in K_m after immobilization, combined with a decrease in V_{\max} after immobilization is generally observed.

This trend was also observed in Chapters 10 and 12 for immobilized trypsin. Upon immobilization the enzyme partly loses its conformational freedom and the affinity for the substrate is altered. This results in a lower

substrate affinity (a higher value for K_m) and a lower V_{max} . In Table 7, the results from the experiments with free and immobilized enzyme at varying substrate concentration and for the different substrates are summarized.

Table 7. Overview of the estimated parameters of model 3 and literature values

system	V_{max} [mmol g _{protein} ⁻¹ min ⁻¹]	K_m [M]	K_i [M]
Free oNPG, 295 K	3.6	0.028	-
C-GPTMS-PEI oNPG, 295 K	1.4	0.11	-
Free lactose 308 K	11	0.068	0.015
Literature values			
308 K, pH 6.5 [23]	225	4.6	3.6
298 K, pH 7 [36]	2.9	0.14	1.5
298 K, pH 5 [22]	2.0	0.044	0.052
323 K, pH 5 [7]	0.4	0.0052	-
303 K, pH 4 [24]	15	0.081	0.0053

Some values from literature that were obtained under comparable experimental conditions are also given in Table 7. The problem that arises with comparing data to literature values is that in general different lactases are used (fungal, bacterial or yeast) and that the modeling procedure is not transparent. Some authors even mention the effect of initial parameter estimation and note that they had to try several times to get to the final result [22]. A very detailed work on the kinetics of lactose and the effect of enzyme source was performed by Boon *et al.* [21,25]. In this work, the production of oligosaccharides is also included in the kinetics.

3.3 Catalyst performance in the MSR

The results of the lactase adsorption and the hydrolysis of lactose in the monolithic stirrer reactor are given in Table 8.

Table 8. Results lactase adsorption on 200 cpsi monoliths and hydrolysis of lactose at 150 rpm, 308 K, 50 g l⁻¹ lactose

Carrier type	Yield of Protein* mg	Initial rate 150 rpm, 308 K			
		mol s ⁻¹ m ⁻³ monolith	mol s ⁻¹ g _{protein} ⁻¹	Ca	Φ
Free lactase	-	-	0.096	-	-
C-PEI	69**	0.10	0.085	1*10 ⁻³	<<0.15
C-GPTMS-PEI	205	0.27	0.078	4*10 ⁻³	<<0.15
AM-GPTMS-PEI	325	0.53	0.081	<<0.05	<<0.15
C-CHIT	390	0.23	0.029	-	0.6
AM-CHIT	500	0.42	0.043	-	0.5

*Lactase content in the lyophilized powder is around 5 wt%

** UV signal was disturbed, probably by dissolved PEI

The activity of the free enzyme is around 65% of the maximal rate (V_{max} in Table 7, 11 mmol min⁻¹ g_{protein}⁻¹). This could be expected, because the MSR was operated at a substrate

concentration above K_m ($0.14 \text{ mol l}^{-1} > 0.068 \text{ mol l}^{-1}$). At $C_s = K_m$ the rate should be half the maximum rate (assuming Michaelis-Menten kinetics). For the PEI composites, the activity is proportional to the enzyme loading (Figure 12). This indicates effective use of all immobilized enzyme, in other words the absence of internal diffusion limitations. For the chitosan-based catalyst, a lower specific activity is observed. This is attributed to internal diffusion limitations inside the gel layer.

The immobilization efficiency on adsorbed PEI is high; the immobilized activity is around 90% of that of the free enzyme. For the other PEI-based catalysts this value is slightly lower, but constant, indicating effective use of all the immobilized lipase. For C-Chit, the immobilized activity is reduced significantly, indicating that the gel layer forms a barrier for diffusion of reactant and products. This could also enhance product inhibition, because the product is not removed effectively away from the enzyme. For AM-Chit, this internal diffusion component is less pronounced. Apparently the open structure of the walls allows for a better accessibility for substrate and products.

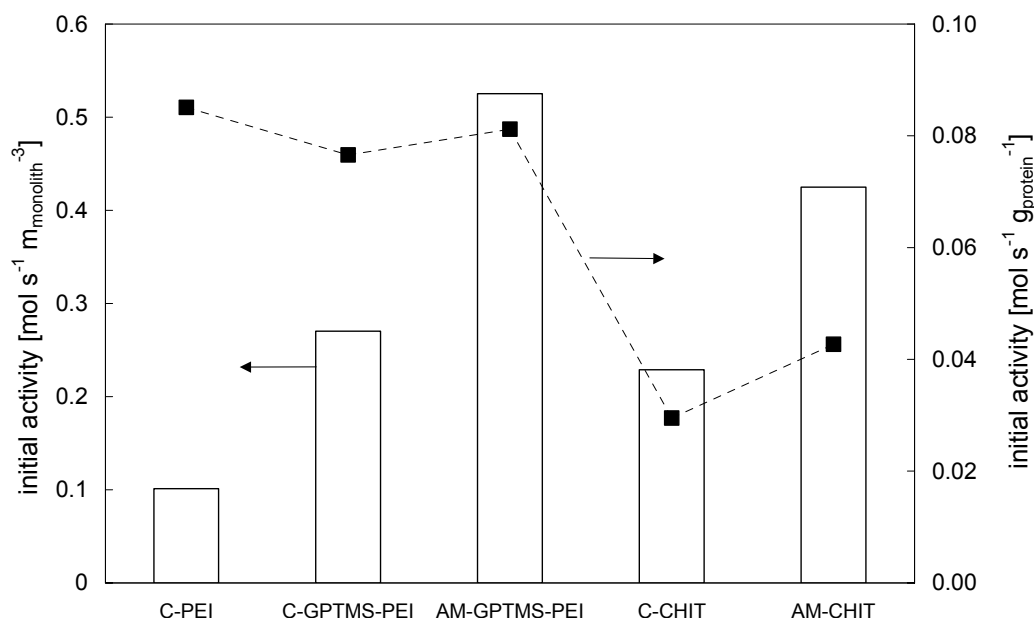


Figure 12. Initial activity per monolith volume (bars, left axis) and immobilized activity (markers, right axis) for lactase on different 200 cpsi monolith-carrier combinations in the MSR at 150 rpm and 303 K.

If a lactase content of 5wt% in the protein is assumed, the TOF becomes 160 s^{-1} for the free enzyme and $120\text{-}144 \text{ s}^{-1}$ for the PEI-based catalysts. These values are much higher than the values that were observed in Chapter 7 ($\text{TOF} = 8 \text{ s}^{-1}$). The present study is performed at pH 5, the optimum pH of this enzyme, and 303 K. The data in Chapter 7 was collected at room temperature and pH 7, resulting in a much lower intrinsic activity of the enzyme.

3.3.1 Mass transport in the MSR

To verify presence or absence of internal diffusion limitations in the catalyst coating under these conditions, the Wheeler-Weisz modulus was estimated for the chitosan-coated carriers (Table 8):

$$\Phi = \frac{(n+1)}{2} \cdot \frac{r_{v,obs} \cdot L^2}{D_{eff} \cdot C_s} < 0.15 \quad (8)$$

Using the observed reaction constant (in $\text{mol s}^{-1} \text{m}^{-3}_{\text{carrier}}$) of the experiments performed at 150 rpm and using 5×10^{-10} as an estimate for the effective diffusion coefficient [38], one finds $\Phi \approx 0.6$ for C-Chit, which is above the threshold value of 0.15 that indicates the onset of diffusion limitations.

For the Wheeler-Weisz modulus for AM-Chit carriers, L is estimated at 0.4 times the wall thickness (0.14 mm, assuming that the wall is 80% plugged), $\Phi \approx 2.0$. This high value is in contradiction with the intrinsic enzyme activity of the chitosan-carriers that can be seen in Figure 12. The specific activity of the AM-Chit carrier is higher than for the C-Chit catalyst. Based on this higher intrinsic activity, it was assumed that the internal diffusion limitations were less for AM-Chit monoliths compared to cordierite monoliths. This indicates that the assumption of the 80% plugged wall that was made before, is not completely correct. If part of the gel forms a thin layer on the needles of the mullite needles, the average layer thickness decreases significantly. When the layer thickness becomes smaller than 0.1 mm, $\Phi_{\text{AM-Chit}} < \Phi_{\text{C-Chit}}$, which can explain the higher intrinsic activity for AM-Chit. Apparently in practice the gel is also present as a thin film on the separate needles, leading to a mean layer thickness around 100 nm (which would give $\Phi = 0.5$).

For the PEI-coated carriers (with the SiO_2 -PEI coating taken as the carrier, layer thickness $\approx 1 \mu\text{m}$ [36]), $\Phi \ll 0.15$, indicating the absence of internal mass transport limitations.

To investigate the presence of external mass transfer limitations, the stirrer rate was varied between 50 and 400 rpm, see Figure 13. For these biocatalysts, no profound influence of stirrer rate could be detected. Apparently no external mass transfer limitations are present in the system above 50 rpm. In the short monolith channels, the contact time is too short for a mass transfer boundary layer to develop all the way to the axis of the channel. As a result, the Sherwood number is orders of magnitude higher than the lower limit of 3.66. The stirrer rate, and therefore the hydrodynamic entrance length are much larger than in the L-S mass transfer coefficient measurements of Chapter 10.

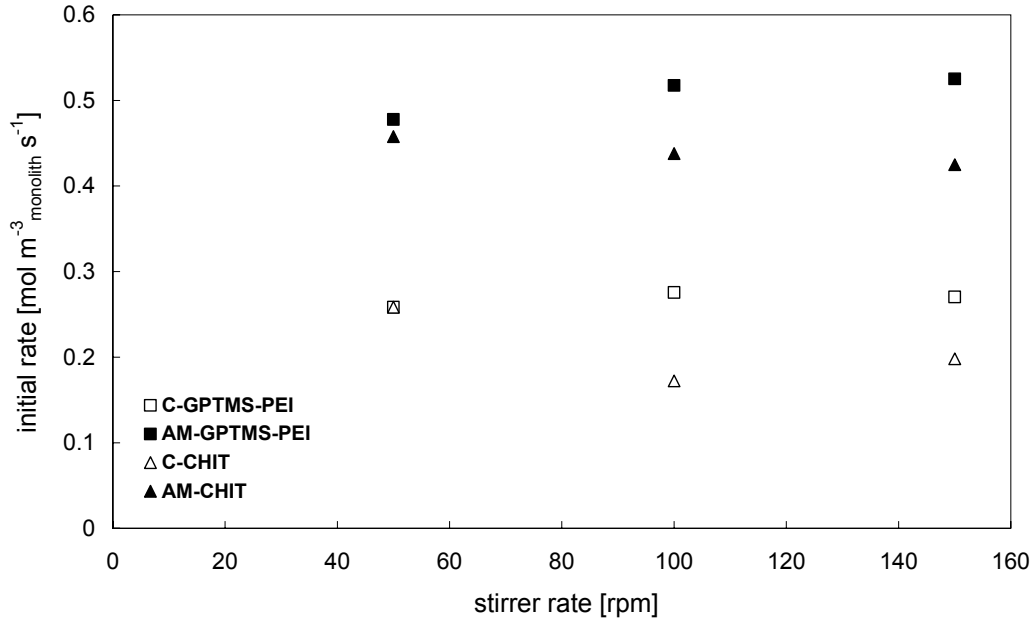


Figure 13. Effect of stirrer rate on the hydrolysis of lactose with 200 cpsi monoliths at 308 K, $C_s = 50 \text{ g l}^{-1}$

In the present study, the velocity profile is probably not developed. To check this assumption, the hydrodynamic and mass transfer entrance lengths (L_{mt} and L_{hydro}) are plotted as a function of stirrer rate in Figure 14.

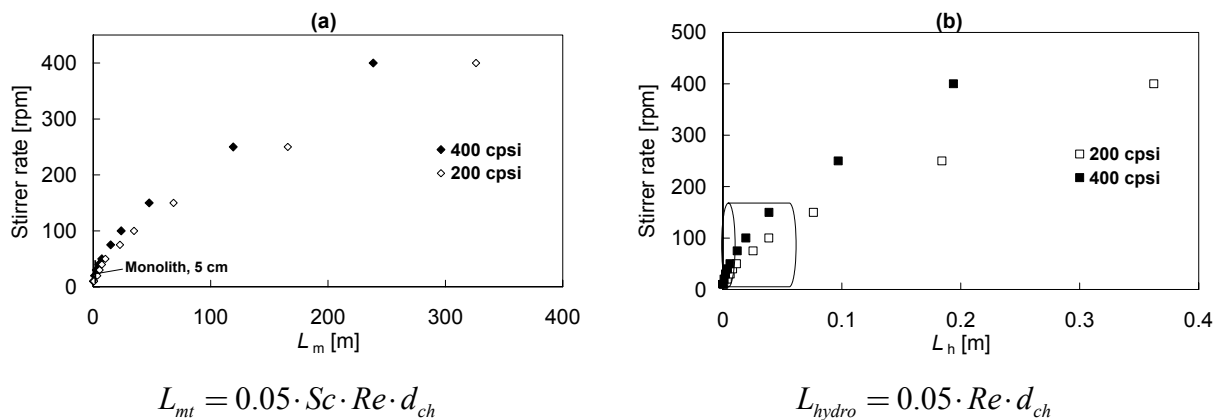


Figure 14. Characteristic entrance length as a function of stirrer rate for the development of a) the boundary layer for mass transfer, b) the velocity profile of along the monolith channel. a monolith of 5 cm length is added to the figures for comparison

In all experiments, the mass transfer profile is in the developing state. The velocity profile however, is not yet fully developed over the monolith length. The Sherwood correlations that were used in Chapter 12 to calculate the mass transfer coefficient cannot be used for this situation. Since the velocity profile is also not completely undeveloped, this intermediate situation is analyzed by calculating Sh from the thermally developing case and from the simultaneously developing case and taking the mean value. It was shown before that for rectangular ducts (with wall dimensions 1:2) the difference between the two cases is around a factor 2 for $0.001 < Gz < 0.01$ [39,42].

With the data supplied in Table 9, Sh was estimated for thermally developing flow with [39]:

$$Sh = Sh_{\infty} \left(1 + C \cdot Re \cdot Sc \frac{d_{ch}}{L_m} \right)^{0.45} \quad (9)$$

$$Re = \frac{\rho \cdot v_L \cdot d_{ch}}{\eta} \quad (10)$$

$$Sc = \frac{\eta}{\rho \cdot D} \quad (11)$$

At a stirrer speed of 150 rpm, liquid velocity (v_L) in the monolith channels is around 0.5 m s^{-1} [40]. With an estimated Sc of 1100, and Re of 940, Sh becomes 100.

Table 9. Used parameters

Parameter	Value
Density, ρ	990 kg m^{-3}
Viscosity, η	$7.86 \times 10^{-4} \text{ Pa s}$
Diffusivity, D	$7 \times 10^{-10} \text{ m}^2 \text{ s}^{-1}$
Asymptotic Sh , Sh_{∞}	2.96 [43]
Surface roughness, C	0.095 [44]

For simultaneously developing flow different models were developed, the majority for gas phase applications [43-45]. A model that can be extended to $Sc \rightarrow \infty$ without introducing large errors in the developing region [46] is used here to estimate Sh in simultaneously developing flow:

$$Sh = \frac{4}{\sqrt{\pi}} P^{1/2} \text{ for } P \rightarrow \infty \quad (12)$$

where P is:

$$P = \frac{d_{ch}}{4.25 \cdot L_m} \cdot Re \cdot Sc \quad (13)$$

A P of 7000 gives $Sh = 185$. This is in accordance with the assumption that there is a factor 2 difference between Sh in developed and in simultaneously developing flow. In the present experiments, Sh is probably somewhere in between. With $Sh = 140$, the mass transfer coefficient of lactose in water was estimated to be $6 \times 10^{-5} \text{ m s}^{-1}$, using [39]:

$$Sh = \frac{k_s \cdot d_{ch}}{D} \quad (14)$$

The absence of external mass transfer limitations could then be confirmed by calculating the Carberry number Ca , the ratio of the observed rate (in $\text{mol s}^{-1} \text{m}^{-3}$) and the maximal mass transfer rate [39]:

$$Ca = \frac{r_{v,obs}}{a' \cdot k_s \cdot C_b} \quad (15)$$

With a substrate concentration (C_b) of 140 mol m^{-3} for lactose and an a' of 1945 m^2 for 200 cpsi monoliths, Ca becomes 2×10^{-3} , which is below the boundary value of 0.05. For all other experiments with cordierite samples at 150 rpm, $Ca \ll 0.05$, so no external mass transfer limitations are present. For ACM monoliths, a' is assumed to be significantly larger, also leading to $Ca \ll 0.05$. With a conservative estimation that the surface area of the ACM monoliths is identical to that of the cordierite samples, all values for Ca of the experiments with ACM-based catalysts remained below the threshold value.

3.3.2 Operational and storage stability

The stability of the biocatalysts was tested by operating three 24-hour experiments (308 K, 150 rpm) consecutively, followed by a 20-day storage period at 278 K in sodium azide solution. After the final run at 308 K, an experiment was performed at 313 K. The results are presented in Figure 15.

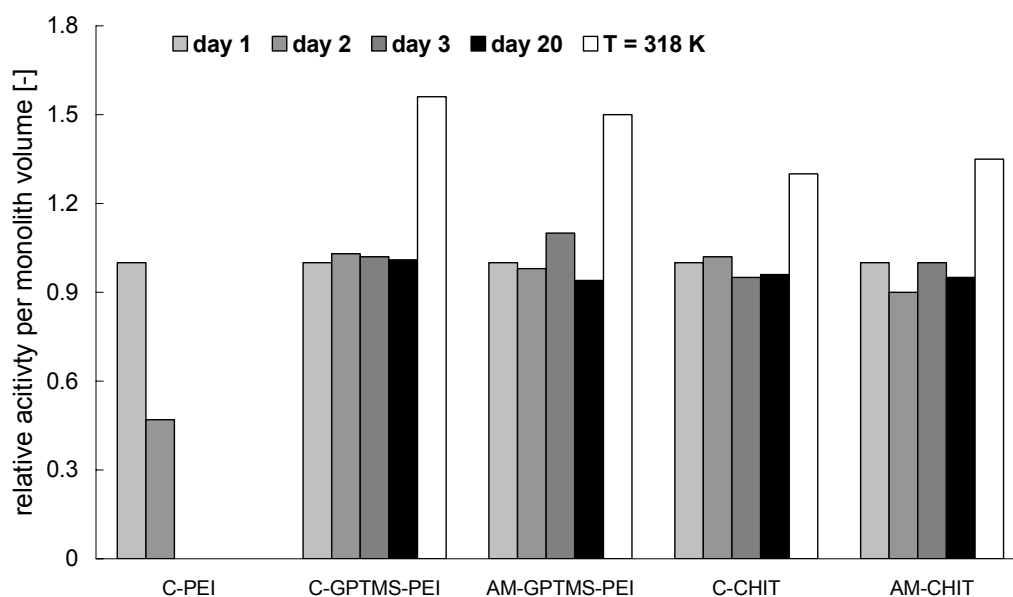


Figure 15. Operational and storage stability of 200 cpsi monolith carrier combinations in the hydrolysis of lactose at 308 K, 150 rpm. Continuous operation at 308 K on day 1-3, followed by 17 days of storage at 278 K in a $1 \text{ g l}^{-1} \text{ NaN}_3$ solution in 5 mM phosphate buffer pH 7. On day 21 a run at 313 K was performed.

C-PEI already lost part of the adsorbed carrier during the first run. As a result free enzyme activity was observed after oNPG addition to the supernatant. This catalyst is not stable and loses all activity after the second experiment. For the other carriers no enzyme leaching was detected during operation. The catalysts were stable during operation and storage, no decrease in activity was observed (Figure 15). At higher temperature, the observed reaction rate constant for the monolith-PEI carriers increases with about 50% from 0.032 mol s^{-1} to 0.049 mol s^{-1} . This corresponds to an observed activation energy (E_a) of around 35 kJ mol^{-1} . From [41] E_a was found to be 30 kJ mol^{-1} . The monolith-chitosan catalysts show a moderate increase in observed reaction rate of 30-40%. This can be attributed to internal diffusion limitations in the gel-layer, and supports the previous conclusion from the isothermal experiments.

After investigating the carriers that were selected for immobilization of lactase on monolithic supports, it can be concluded that both PEI and chitosan are both suitable for the present application. The presence of the internal diffusion limitations in the chitosan does not have to pose a problem. The chitosan-based carriers show the highest activity per monolith volume and would be the catalyst of choice to achieve a high conversion. The problem with this system is that the enzyme is not reversibly immobilized, and that the gel contains glutaraldehyde. Glutaraldehyde is in general an undesired component in food applications. Without a crosslinking agent however, chitosan gels usually do not hold the enzyme. The gel should be applied with a different crosslinker or the enzyme could be modified by attaching a larger protein or chemical group that would keep it inside the gel layer. The diffusion limitation can be overcome, especially for ACM monoliths, by optimizing the coating method. The use of a PEI carrier has the advantage of reversible immobilization. Especially for use at higher temperatures, the catalyst needs to be regenerated often. Although enzyme loading is slightly lower for the PEI catalysts, no internal diffusion limitations are present. Direct adsorption of PEI onto a washcoated monolith is not suitable to prepare a monolithic carrier, the polymer readily desorbs from the backbone upon use in the MSR.

The MSR has been shown to be useful to operate different biocatalysts in the absence of external diffusion limitations, at high reaction rates. The stirrer configuration makes the reactor very suitable for use with different monolith-carrier combination and reactions.

4 Conclusions

A suitable immobilization protocol was selected for the hydrolysis of lactose by immobilized lactase in a monolithic stirrer reactor (MSR). Based on the reaction conditions, the enzyme surface chemistry, compatibility with the monolithic support, and reactor performance, polyethyleneimine and chitosan were chosen as carrier materials. Different monolithic biocatalysts were prepared by applying PEI and chitosan layers on 200 cpsi classical cordierite monoliths and ACM monoliths with a more porous wall. 9.7 and 13.1 wt% of PEI was applied onto the cordierite and ACM supports respectively. Application of a chitosan

layer leads to a layer thickness of 90 μm on cordierite monoliths and a layer that theoretically fills 80% of the ACM wall.

The hydrolysis of lactose by free lactase from *Aspergillus oryzae* was studied by performing a set of experiments at different substrate concentration. From this set of experiments, a suitable model was selected to simulate the reaction rate. The model that gave the best results was a model for Michaelis-Menten kinetics with competitive substrate inhibition. Fitting the kinetic data to the model equation yielded values for the maximum rate ($11 \text{ mmol g}_{\text{protein}}^{-1} \text{ min}^{-1}$), the Michaelis-Menten constant (0.068 M), and the inhibition constant (0.015 M).

Application of the monolithic biocatalysts in the MSR at 150 rpm shows that no diffusion limitations are present for the PEI-based catalysts, and that for the chitosan-based catalysts some internal diffusion limitations are present. The volumetric hydrolysis rate at 308 K (pH 5) for lactase on 200 cpsi PEI- and chitosan-coated cordierite monoliths is 0.3 and 0.25 $\text{mol s}^{-1} \text{ m}^{-3}_{\text{monolith}}$ respectively. The porous wall of the ACM monoliths results in a higher enzyme loading capacity and a higher activity than for classical cordierite monoliths. (0.55 and 0.45 $\text{mol s}^{-1} \text{ m}^{-3}_{\text{monolith}}$ for PEI and chitosan respectively. The catalysts are stable during consecutive tests and after 17 days of storage at 278 K. The C_PEI carriers are not suitable for use in this reaction system; the polymer desorbs together with the enzyme, resulting in complete deactivation within three days. If the reaction temperature is increased, the observed reaction constant for monolith-PEI catalysts increases proportionally with temperature corresponding with an activation energy of 35 kJ mol^{-1} . Both chitosan and PEI carriers are suitable for application on a monolithic support and use in the MSR at high reaction rates.

5 Acknowledgements

The Netherlands Organization for Scientific Research (NWO) is acknowledged for funding part of this research by means of a grant, number R74-68. C. Mateo, R. Fernandez Lafuente, J.M. Guisan of the Biocatalysis group of the Spanish Research Counsel (CSIC-ICP) at the Univesidad Autonoma de Madrid are gratefully acknowledged for their contribution to this work. Corning Inc is acknowledged for the supply of the cordierite monoliths, The DOW Chemical Company is acknowledged for supplying the ACM monoliths. Marcel Bus of PAS&BR is acknowledged for performing the HPLC measurements.

6 Symbols

a'	surface area	$[\text{m}^2 \text{ m}^{-3}]$
A_m	geometric surface area	$[\text{m}^2]$
C_b	reactant bulk concentration	$[\text{mol m}^{-3}]$

Ca	Carberry number	[-]
d_{ch}	channel diameter	[m]
D	Diffusivity	[m ² s ⁻¹]
D_{eff}	effective diffusion coefficient	[m ² s ⁻¹]
E_a	activation energy	[kJ mol ⁻¹]
$k_{r,obs}$	observed reaction rate constant	[s ⁻¹]
k_s	mass transfer coefficient	[m s ⁻¹]
k_i	reaction constant for reaction i	[s ⁻¹]
$K_{m,i}$	Michaelis-Menten constant component i	[mol l ⁻¹]
L	layer thickness	[m]
L_m	monolith length	[m]
n	reaction order	[-]
r_i	reaction rate of reaction i	[mol s ⁻¹]
$r_{v,obs}$	observed reaction rate	[mol s ⁻¹ m ⁻³]
Re	Reynolds number	[-]
Sc	Schmidt number	[-]
Sh	Sherwood number	[-]
T	temperature	[K]
v_L	superficial liquid velocity	[m s ⁻¹]
V_{max}	maximum rate for enzymatic conversion	[mol s ⁻¹ ge ⁻¹]
w	weight carrier	[kg]
w_s	weight support	[kg]
Y_i	yield component i	[%]

Greek symbols

η	viscosity	[Pa s]
ρ	density	[kg m ⁻³]
Φ	Thiele modulus	[-]

Components

S	substrate
P	product
E	enzyme
Gl	glucose

7 References

- [1] I.M. Abu Reesh (2000) *Bioprocess Engineering*; 23: 709-713
- [2] A.E. Al-Muftah, I.M. Abu-Reesh (2005) *Biochemical Engineering Journal*; 27:167-178
- [3] D.G. Hatzinikolaou, E. Katsifas, D. Mamma, A.D. Karagouni, P. Christakopoulos, D. Kekos (2005) *Biochemical Engineering Journal*; 24: 161–172
- [4] A. Cote', W. A. Brown, D. Cameron, G. P. van Walsum (2004) *Journal of Dairy Science*; 87: 1608–1620
- [5] M. Richmond, J. Gray, C. Stime (1981) *Journal of Dairy science*; 64: 1759-1771
- [6] V. Gekas, M. Lopez-Leyva (1985) *Process Biochemistry*; 20: 2–12
- [7] S. Rejikumar, S. Devi (2001) *International Journal of Food Science and Technology*; 36: 91-98
- [8] R.R. Mahonay (1998) *Food Chemistry*; 63: 147-154
- [9] G. Mooser, in P.D. Boyer (ed) *The Enzymes* (1992), Academic Press, New York, United States: 187-233
- [10] M. Ladero, M.T. Perez, A. Santos, F. Garcia-Ochoa (2003) *Biotechnology and Bioengineering*; 81: 241-252
- [11] M. Ladero, A. Santos, F. Garcia-Ochoa (2000) *Enzyme and Microbial Technology* 27: 583-592
- [12] Q.Z. Zhou, X.D. Chen, X. Li (2003) *Biotechnology and Bioengineering*; 81:127-133
- [13] A. E. AL-Muftah, I.M. Abu-Reesh (2005) *Biochemical Engineering Journal*; 23: 139–153
- [14] A. Illanes, A. Ruiz, M.E. Zuriga, C. Agirre, S. Reilly, E. Curotto (1990) *Bioprocess Engineering*; 5: 257-262
- [15] I. Petzelbauer, B. Kuhn, B. Splechna, K.D. Kulbe, B. Nidetzky (2002) *Biotechnology and Bioengineering*; 77: 620-631
- [16] J.S. Dordick (1991) *Biocatalysts for Industry*, 1st ed., New York 193-213.
- [17] K. Wallenfels, R. Weil (1972) β -Galactosidase, Third ed., in: *The Enzymes*; 7, Academic Press, London, Great Britain 617–663.
- [18] D.E. Koshland Jr., (1953) *Biology Reviews*; 28: 416–436.
- [19] T.M. Stokes, I.B. Wilson (1972) *Biochemistry* 11 (1972) 1061–1064
- [20] D.H. Juers, T.D. Heightman, A. Vasella, J.D. McCarter, L. Mackenzie, S.G. Withers, B.W. Matthews (2001) *Biochemistry*; 40: 14781–14794.
- [21] M.A. Boon, A.E.M. Janssen, K. van 't Riet (2000) *Enzyme and Microbial Technology*; 26: 271–281
- [22] C.R. Carrara, A.C. Rubiolo (1996) *Process Biochemistry*; 31: 243-248
- [23] A. Santos, M. Ladero, F. Garcia-Ochoa, (1998) *Enzyme and Microbial Technology*; 22: 558-567
- [24] S.T. Yang, M.R. Okos (1989) *Biotechnology and Bioengineering*; 34: 763–773
- [25] M.A. Boon, A.E.M. Janssen, A. van der Padt (1999) *Biotechnology and Bioengineering*; 64: 558-567

- [26] D. Cavaille, D. Combes (1995) *Biotechnology and Applied Biochemistry*; 22:55–64
- [27] K.T. Huh, T. Toba, S. Adachi (1991) *Food Chemistry*; 39: 39–49
- [28] I.Y.S. Rustom, M.I. Foda, M.H. Lopez-Leiva (1998) *Food Chemistry*; 62:141–147
- [29] M. Di Serio, C. Maturo, E. De Alteriis, P. Parascandola, R. Tesser, E. Santacesaria (2003) *Catalysis Today*; 79–80: 333–339
- [30] B.C.C. Pessela, M. Fuentes, C. Mateo, R. Munilla, A.V. Carrascosa, R. Fernandez-Lafuente, J. M. Guisan (2006) *Enzyme and Microbial Technology*; 39: 909-915
- [31] B.C.Ch. Pessela, C. Mateo, M. Fuentes, A. Vian, J.L. Garcia, AV. Carrascosa, J.M. Guisán, R. Fernández-Lafuente (2003) *Enzyme and Microbial Technology*; 33: 199–205
- [32] E. Jurado, F. Camacho, G. Luzon, J.M. Vicaria (2006) *Enzyme and Microbial Technology*; in press
- [33] M.R. Benoit, J.T. Kohler (1975) *Biotechnology and Bioengineering*; 17: 1616-1626
- [34] T. Zhang, L. Yang, Z. Zhu, (2005) *Enzyme and Microbial Technology*; 36: 203-209
- [35] M.T. Kreutzer, F. Kapteijn, J.A. Moulijn, J.J. Heiszwolf (2005) *Chemical Engineering Science*; 60: 5859-5916
- [36] I. Hoek, T.A. Nijhuis, A.I. Stankiewicz, J.A. Moulijn, (2004) *Chemical Engineering Science*; 59: 4975-4981
- [37] D.T. Wadiak, R.G. Carbonell (1975) *Biotechnology and Bioengineering*; 17: 1157–1181
- [38] R. Dembczynski, T. Jankowski (2000) *Biochemical Engineering Journal*; 6: 41–44
- [39] R.K. Shah, A.L. London (1978), *Laminar flow force convection ducts. Advances in heat transfer, Volume 1, Supplement 1*, Academic Press, New York, United States
- [40] H.P. Kritzinger, B.C. Deelder, C.R. Kleijn, J.J. Derksen, H.E.A. van den Akker (2002) *Turbulent flow in a stirred tank with permeable impeller blades, proceedings of FEDSM 2002, Montreal, Canada: FEDSM2002-31360*
- [41] B.J. Macrist, P. Markakis (1981) *Applied and Environmental Microbiology*; 41: 956-958
- [42] P. Wilbulswas, PhD Thesis (1966), London University, London, Great Britain
- [43] M. Uberoi, C.J. Pereira (1996) *Industrial Engineering Chemistry Research*; 35: 113-116
- [44] A. Holmgren, B. Andersson (1998) *Chemical Engineering Science*; 53: 2285-2298
- [45] T. Kirchner, G. Eigenberger (1996) *Chemical Engineering Science*; 51: 2409-2418
- [46] V. Balakotaiah, D.H. West (2002) *Chemical Engineering Science*; 57: 1269-1286

Immobilized lipase in organic medium in the monolithic stirrer reactor

Abstract

The use of a monolithic stirrer reactor for carrying out enzyme-catalyzed reactions in organic media is presented. Monoliths are used as carriers for immobilizing a lipase from *Candida antarctica* (CALB). The enzyme-loaded monoliths are employed as stirrer blades in a monolithic stirrer reactor for the acylation of 1-butanol with vinyl acetate in toluene. This reaction follows a bi-bi-ping-pong mechanism with competitive inhibition by the alcohol. The kinetic parameters of the immobilized enzyme have been determined by modeling the effect of substrate concentrations on the initial reaction rate. Cordierite monoliths and a new high-porosity mullite advanced ceramic material (ACM), having an open pore structure on the micrometer scale, were functionalized with different carbons and with polyethylenimine (PEI). These monolith-carrier combinations were compared with integral activated carbon honeycombs. CNF-coated monoliths have the highest enzyme loading and therefore the highest volumetric activity. For cordierite and ACM monoliths, the initial rate is 4.4 and 4.7 mol s⁻¹ m⁻³_{monolith} respectively. For carbon-coated monoliths, internal and external mass transfer limitations were absent, and all immobilized enzyme is used effectively. The activity of the immobilized enzyme is 30-35% of that of the free enzyme. The observed conversion per monolith volume increases with monolith cell density, due to a higher enzyme loading.

1 Introduction

Most conventional enzyme carriers are inorganic particles or porous beads of synthetic polymers, or gel-like materials such as chitosan, agarose or alginate. Although they are very useful in many ways, a low mechanical strength and internal diffusion limitations are the most encountered problems. If large beads are used, intraparticle limitations of the often large molecules are bound to occur [1]. The advantage of using large beads is simple: the reliable workhorse fixed-bed reactor can be used. In enzymatic systems, this can lead to more than just substrate diffusion: intraparticle pH gradients or ionic strength gradients can be equally problematic. An alternative to large beads in a fixed-bed reactor is a stirred slurry of beads that can be as small as 100 μm [2]. However, the often soft support-material lacks the mechanical strength for high intensity contacting. Also, the density of the support material is often close to that of the solvent, which means that settling of the beads after completion of the reactions takes far too long and a separate filtering step is required. The use of structured support materials could be an interesting alternative for conventional particulate enzyme carriers. Monolith-supported enzyme systems present a low flow-resistance, leading to a decreased pressure drop compared to flow through conventional particulate systems. This low pressure drop allows the use of higher liquid velocities in order to reduce film diffusional effects. Also in case of more viscous media (e.g. starch hydrolysis), the monolithic support with a very thin layer of active material deposited on the walls, can be an interesting alternative in terms of pressure drop and internal diffusion in the carrier material. Finally in case of bed-plugging as can be observed in for example the hydrolysis of lactose in milk, the monolithic bioreactor can present a feasible alternative. Benoit and Kohler [1] used immobilized catalase on a ceramic monolith and compared this with particulate-supported systems. In 1989, Kawakami *et al.* [3] used ceramic monoliths in a three-phase system operating in both film flow and slug flow with immobilized glucose oxidase.

1.1 Description of the system

The explosive growth of drug discovery and the use of high throughput development of new potent pharmaceuticals have led to a high demand for effective stereoselective synthesis methods. Enzymes are frequently used for the production of fine chemicals. They are an attractive tool in asymmetric catalysis and efficiently complement traditional chemical methods [4,5]. The use of biocatalysts allows us to carry out chemical transformations without the need for laborious protection and deprotection steps [6]. The low solubility of reactants in aqueous medium can be overcome by using an organic solvent or a two-phase system. Recently, biocatalysis in nonaqueous media has been used for the resolution of alcohols, acids or lactones through transesterification with hydrolytic enzymes, especially lipases. Also the acylation of amines or alkoxycarbonylation of alcohols and amines can be useful for the resolution of amines and the preparation of chiral amides [6]. In addition, other biocatalysts such as lyases have emerged as an attractive alternative for chemical C-C bond

formation [7]. In the present study, an immobilized lipase is applied in a transesterification reaction in toluene.

1.1.1 Lipase catalysis

Lipases (triacylglycerol ester hydrolase, EC 3.1.1.3) catalyze the breakdown of fats and oils with subsequent release of free fatty acids, di-, and monoglycerides, and glycerol [8]. Different lipases are distributed among higher animals, microorganisms and plants in which they fulfill a key role in the biological turnover of lipids. Lipases have been traditionally defined as enzymes “capable of hydrolyzing esters of oleic acid” [9]. The definition of a lipase as a hydrolytic enzyme originated primarily from its physiological function of triglyceride hydrolysis. Later it was recognized that the enzymes are effective catalysts both for ester hydrolysis and the reverse synthesis reaction. This has resulted in many applications in synthetic organic chemistry. Additionally, lipases are capable of catalyzing transesterification (acidolysis, interesterification, alcoholysis), aminolysis, and thioesterification in anhydrous organic solvents and biphasic systems. The ability of lipases to accept not only water, but also other nucleophiles such as alcohols, amines, thiols, and more, implies a vast synthesis potential with these enzymes. The role of water in lipase catalysis is very important. Many studies were performed on controlling the thermodynamic activity of water [10-12]. However, it was found difficult to adapt the methods to a generally accepted technique for industrial biocatalysis.

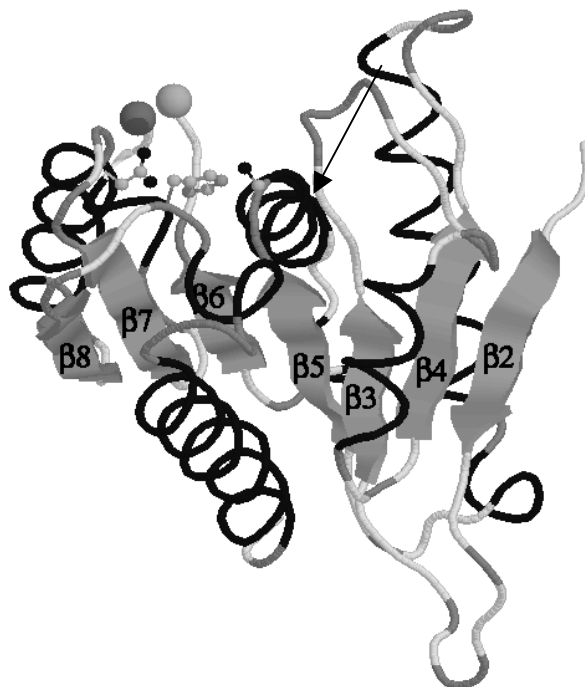


Figure 1. 3-D image of the lipase structure

Lipases are produced by virtually every living organism. Despite differences in size, sequence homology, substrates, activators, inhibitors, and other properties, most often adopt a similar

core topology, known as the α/β hydrolase fold. The interior topology of α/β hydrolase fold proteins is composed largely of parallel β -pleated strands (at least five in lipase), separated by stretches of α -helix, and forming an overall super helically twisted-pleated sheet. Helical peptide sections packed on both faces of this sheet form much of the outer surface of the protein. Figure 1 shows a 3-D image of this structure.

Despite widely varying degrees of sequence homology between the members of this family, one sequence is exceptionally highly conserved: the pentapeptide Gly-X-Ser-X-Gly. The conservation of the serine in this sequence, and the loss of catalytic activity upon its modification or replacement, argue that this amino acid is crucial to catalysis. Its topographic location is also conserved and significant: it sits at the apex of a tight bend (“nucleophilic elbow”) in the protein chain. This bend can only be formed when the amino acids at the -2 and $+2$ positions relative to the serine have small side chain groups – hence the predominance of glycine at this locations. In addition to the catalytic serine, the active centers of most lipases consist of a histidine and an acidic amino acid (Asp or Glu). The catalytic triad sits in a hydrophobic cleft or cavity in the enzyme. This may be a relatively shallow groove in the surface of the lipase. The fatty acyl chain of the substrate ester docks into this groove and aligns its ester bond with the catalytic triad sitting at the bottom of one end of the cleft.

1.1.2 Activation of lipase

In an aqueous medium an oil-water interface is necessary to activate the lipase. Lipase catalysis in such aqueous systems primarily concerns ester hydrolysis. Lipase catalyzed hydrolysis is mostly used for partial hydrolysis to the mono- and diglycerides in the food industry. The mono- and diglycerides serve as biocompatible emulsifiers and food additives.

In the past water seemed essential for an enzyme to maintain its conformation and it was believed that organic solvents would denature the enzyme. Although water is essential to maintain enzyme conformation, the real issue is the amount of water needed. Two methods of substrate-enzyme contact in limited-water environments are possible. The first is the concept of providing just sufficient water to hydrate the lipase and allow it to stay locked in an active conformation. The enzyme must be used in apolar organic solvents that do not remove the essential water of hydration. Such hydrated lipases are used directly or immobilized on inert supports. The second mode is that of encapsulating the lipase in water-oil micro emulsions, reversed micelles. The micro aqueous phase of reversed micelles provides a biomimetic environment for the lipase.

The enzyme has the ability to catalyze hydrolysis, ester synthesis or transesterifications acting only on selected positions of polyols. This offers the possibility of regioselective reactions. Lipase activation in organic solvents can be established using several methods, the simplest being to allow the enzyme to attain its optimal conformation in aqueous solution at optimal pH and then to remove excess water through lyophilization, which leaves the essential water of hydration intact. Lipase also displays a remarkable thermal stability in organic media. This is attributed to the fact that the minimal water content of the system is insufficient to cause

protein denaturation by hydrolysis at aspartic acid residues and breakage of disulfide bonds at higher temperatures.

1.1.3 Kinetics of the acylation of butanol with vinyl acetate in toluene

In organic medium, lipases can perform the cleavage and formation of ester bonds in a sequential form; this is known as transesterification. The transesterification reaction between vinyl acetate and butanol is schematically presented in Figure 2. This reaction takes place in toluene and is made irreversible by the use of vinyl acetate. The formed vinyl alcohol is unstable and will be converted into acetaldehyde.

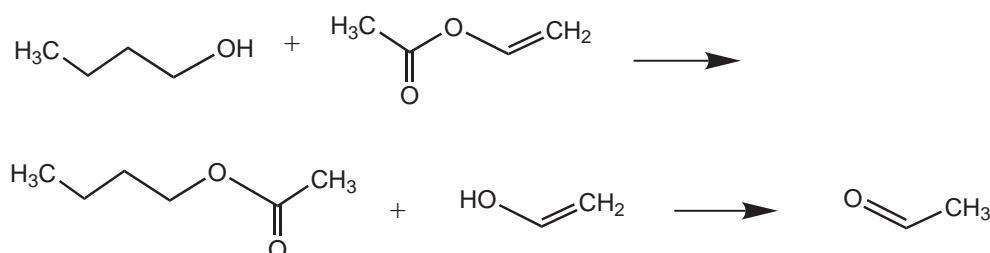


Figure 2. Reaction scheme of the acylation of 1-butanol with vinyl acetate

The kinetics of lipase-catalyzed reactions has been extensively reported in the open literature [13-17], and a variety of possible kinetic models have been collected by Segel [18]. In this study, two most probable mechanisms are evaluated for the acylation reaction; a bi-bi ping-pong mechanism [18], and a simplified bi-bi ping-pong mechanism [13] are used to fit the kinetic data. The rate expressions of these mechanisms are presented in Table 1.

Table 1. Proposed models for lipase-catalyzed transesterification reaction

Source	Rate Expression
[18]	$r = \frac{V_{\max}[A][B]}{K_{m,B}[A](1 + \frac{[A]}{K_{i,A}}) + K_{m,A}[B](1 + \frac{[B]}{K_{i,B}}) + [A][B]} \quad (1)$
[13]	$r = \frac{V_{\max}[A][B]}{K_{m,A}[B](1 + \frac{[B]}{K_{i,B}}) + K[A][A] + [A][B]} \quad , \text{ with } K = \frac{K_{m,B}}{K_{i,A}} \quad (2)$

1.1.4 Lipase immobilization for use in organic media

Immobilized lipases are very advantageous as catalysts in comparison with free lipases, due to the possibility of repeated or continuous use, the higher resistance to denaturing effects, easy separation, and the possibility of positively affecting the course of the reaction by selecting a suitable immobilization method. Most immobilized lipases exhibit higher optimum temperature values than their free counterparts. This is attributed to the fact that immobilized

enzymes are less sensitive to thermal deactivation since their structure is more rigid after immobilization. Enzymes in organic solutions are easily denatured by the action of the solvent, elevated temperature, or extremely low water activity. Irreversible changes in conformation, chemical changes of functional groups in side chains of amino acid units may occur. Immobilization provides long-term stability and high enzyme activity.

When lipases are used in organic medium, immobilization is not that important in terms of separation and reuse (enzymes are generally insoluble in organic solvents and will be present as suspended enzyme aggregates), but more in terms of stability and aggregation [2]. Suspended enzyme sometimes tends to form rather large aggregates or attach itself to the walls of the reactor. These systems must therefore be treated as heterogeneous systems [19]. Immobilization of the enzyme increases the stability in a hydrophobic medium and solves the problem by spreading the enzyme over a relatively large surface area [20]. Immobilization also increases mechanical strength and controls the particle size. For use in organic medium, no strong binding between enzyme and support is needed; the enzyme will not detach from the carrier due its insoluble nature. This makes physical adsorption a very suitable technique to prepare biocatalysts for use in organic solvents [19,21].

1.1.5 The Monolithic Stirrer Reactor

The Monolithic stirrer reactor consists of two monoliths that have the catalyst immobilized on the wall of their channels. These monoliths work like as stirrer blades that can easily be removed from the reaction medium, thereby eliminating the need for a filtration step after reaction. This reactor was already discussed in the previous chapters. A schematic overview of the MSR is given in Figure 3 [22]. The wide range of commercially available monolith geometries ensures that always a good compromise can be made between the stirring action of the blades and flow through the channels where the reaction occurs on the wall. In this work, we use both cordierite monoliths and the open ACM support monoliths as stirrer blades for enzyme-catalyzed reactions. The potential of the latter combination is very attractive (see Chapters 12 and 13).

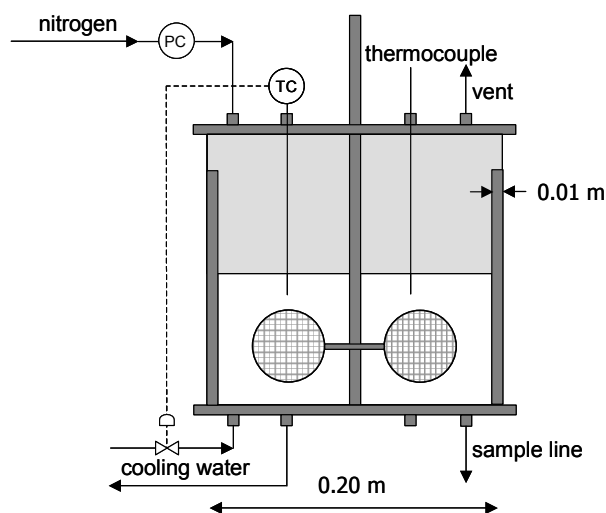


Figure 3. Schematic presentation of the MSR [22]

1.2 Carrier selection

It was already seen in the separate immobilization studies (Chapters 7-8) that lipase can be successfully immobilized by (ionic) adsorption. The enzyme is cheap, usually very robust and easy to handle, so no special requirements (extra stabilization, irreversible immobilization, etc.) are required. In this case an organic solvent is involved, and the most important requirement is the stability of the carrier with respect to the solvent, the reactants, and the products. Carbon materials are very advantageous in this respect.

Based on the results in Chapter 7, polyethyleneimine should also a good carrier for lipase, with a relatively high immobilized activity. But the polymer however is most likely not resistant to the solvent and/or the products (especially acetaldehyde is expected to degrade the carrier). PEI-based carriers would not be the matrix of choice. To verify this, PEI-coated monoliths were included in the study.

Entrapment in chitosan-layers, was shown to be very effective to get high enzyme loadings, but internal diffusion limitations can not be avoided when using this reaction system. Furthermore, it is probably not stable in the organic environment. This carrier material is not considered for use in this application.

To prevent catalyst leaching at high stirrer rates, covalent immobilization can provide stable biocatalysts, but, as was observed before, the activity is generally below 5% of the free enzyme activity. However, in this organic medium no leaching is expected since enzymes are virtually insoluble in organic solvents. This makes physical adsorption very suitable for use in organic solvents. In case of fast denaturation, the enzyme can easily be replaced. Because of the high adsorption yields that were observed in Chapter 8, and because no desorption is expected in the current system, carbon is suggested as a carrier material.

1.3 Layout

Polyethylenimine and different carbonaceous materials were used to functionalize ACM and cordierite monoliths for adsorption of a lipase from *Candida antarctica*. The catalysts are tested in the acylation of 1-butanol with vinyl acetate in toluene. This is an example of an enzymatic conversion in organic medium. ACM monolith materials are compared with classical cordierite monoliths with respect to carrier preparation, enzyme immobilization, and performance in the monolithic stirrer reactor for the acylation of butanol with vinyl acetate in toluene. Carbon monoliths of the integral type are used as a comparison. To address the kinetics of the reaction, a commercially available immobilized enzyme and the free enzyme were also included. The effect of substrate concentration was used to address the kinetics of the acylation reaction.

2 Experimental

2.1 Materials

Furfuryl alcohol (99%), pyrrole (98%), and Novozyme were purchased from Sigma. Nickel nitrate, urea, and toluene (99%) were purchased from Baker. Ludox AS-30 colloidal silica solution and vinyl acetate were from Aldrich. Sucrose, 1-butanol, and *n*-decane were from Merck. Honeycomb monoliths of ACM with cell densities of 200 and 400 cpsi (cells inch⁻², 31 and 62 cells cm⁻²) were prepared by a proprietary Dow process to produce honeycombs. Cordierite monoliths with cell densities of 200 and 400 cpsi were used for comparison. Lipase from *Candida antarctica* (Chirazyme L-2 lyophilized powder, >120 U mg⁻¹ lyo) was purchased from Roche. 200 Cpsi integral carbon monoliths with a loading of 30 wt% of microporous activated carbon were from Westvaco. The key properties are given in Table 2.

Table 2. Geometric characteristics of the monoliths employed in this study.

	ACM (“medium”)	Cordierite	Integral carbon
Cell density	200 / 400 cpsi	200 / 400 cpsi	200 cpsi
Wall thickness	0.35 / 0.24 mm	0.3 / 0.18 mm	0.3 mm
Specific surface area	> 10000 m ² m ⁻³	1945 / 2788 m ² m ⁻³	1945 m ² m ⁻³
Wall porosity	60%	30%	n.a.
Pore diameter in the wall	18 μm	7.5 μm	< 2 nm

2.2 Catalyst preparation

2.2.1 Washcoating

The ceramic monoliths were calcined (10 K min⁻¹, 1273 K, 4 hrs) and washcoated with a colloidal silica solution (Ludox AS-40). Optimization of the washcoating with different silicas was described in Chapter 3. Cordierite samples were dipped in the Ludox solution as received. ACM monoliths were washcoated with a 4% Silica (10 times diluted Ludox AS-40 in water) solution. The channels were cleaned with pressurized air and the monoliths were dried in a microwave oven for 20 min at 150 W. Samples were subsequently calcined at 673 K (5 K min⁻¹, 4 h).

2.2.2 Formation of carbon from a sucrose (SUC) coating [23, 24]

Monoliths were dipped for 5 min at room temperature in a 65% sucrose solution in water. After impregnation, excess solution was removed from the channels by blowing air through the channels. Samples were dried under continuous rotation for 24 h at room temperature, followed by drying at 393 K for 3 h. Subsequently they were carbonized in a tubular quartz reactor, placed in a horizontal furnace. The samples were heated (10 K min⁻¹) in a N₂ stream up to 823 K and carbonized for 2h under different N₂/H₂ mixtures (total flow 500 ml min⁻¹).

2.2.3 Carbonization of a polyfurfuryl alcohol (PFA) coating [25]

Furfuryl alcohol (90 ml) and pyrrole (27 ml) were stirred at 293 K. Acid catalyst (7 ml 65% HNO₃) was added stepwise over a period of 45 min. During this exothermic reaction, temperature was kept constant at 293 K by using an ice bath. Polymerization was continued for 1 h at 293 K. Monoliths were dip-coated for 5 min in the partially polymerized mixture. Excess liquid was blown out with nitrogen and the dip coating was repeated after 5 min. The polymer was solidified for 4 h at ambient conditions, and polymerization was continued overnight at 353 K. Carbonization of the polymer was performed in a quartz reactor at 823 K (heating rate 10 K min⁻¹, 300 ml min⁻¹, 100% Ar) for 2 h.

2.2.4 Growth of carbon nanofibers (CNF) over deposited nickel

Nickel was deposited from a 0.5 M urea solution by homogeneous deposition precipitation as described before [26]. For silica washcoated monoliths, the solution was acidified to pH 2 with nitric acid. For alumina a neutral environment was used. Monoliths were added to 300 ml 30 mM Ni(NO₃)₂ solution (to get a final Ni loading of 0.15 g g⁻¹_{washcoat} or 0.55 g g⁻¹_{monolith} = 2 wt%) and kept at 363 K for 6 h. After washing, the samples were dried at 393 K for 10 h (heating rate 2 K min⁻¹) followed by 673 for 2 h (heating rate 5 K min⁻¹).

Carbon fiber growth was carried out in a quartz reactor, placed in a horizontal furnace. The sample was heated (10 K min⁻¹) in a N₂ stream to 823-973 K. Then Ni was reduced for 1 h in 20% H₂ in N₂ (total flowrate 150 ml min⁻¹). After cooling to 773-873 K carbon fibers were grown in a flow of methane/propene (120 ml min⁻¹) and H₂ (10 ml min⁻¹) in N₂ (70 ml min⁻¹).

2.2.5 Preparation of PEI coated monoliths

Polyethylenimine-functionalized supports were prepared by the method of Mateo *et al.* (2000) [27], using a direct coupling through (3-glycidoxypropyl)trimethoxysilane (GPTMS). The monoliths were functionalized at room temperature for 24 h. in a 5wt% solution of silane in toluene, containing 0.1% v/v triethylamine. After silanization the samples were washed with toluene and acetone and dried at 393 K (heating rate 2 K min⁻¹) for 2 h. The polymer was attached from a 10 wt% PEI solution in water (pH 10) under ambient conditions for 24 h. GPTMS-based carriers were washed with 1 M NaCl and water, and dried under vacuum. After vacuum drying overnight, the supports were stored under air at 278 K.

2.2.6 Enzyme adsorption

Lipase was adsorbed on the monoliths under ambient conditions, in a recycle reactor where the liquid was recycled over the support in upflow. A 50 mM phosphate buffer pH 7 was used as medium. The protein concentration was followed by UV-VIS at 260 nm on a Thermo Optek Unicam 540. After immobilization, the samples were washed with phosphate buffer pH 7 and excess distilled water, dried under vacuum overnight, and stored under vacuum 298 K.

2.3 Nomenclature

In this study, the samples are named depending on the monolith type, the carbon type, and the treatment. The first letter of the samples is used to distinguish the monolith type, “C” is used for cordierite, “A” for ACM. The integral carbon monoliths are indicated with “I”. A second letter is used in the case of ACM to determine the microstructure of the ACM; “M” for medium needles. The carriers are added with “PEI” for polyethyleneimine, “A1” for the microporous carbon “SUC” for Sucrose, “PFA” for polyfurfuryl alcohol, and “CNF” for carbon nanofibers. This is summarized in Table 3.

Table 3. Nomenclature of the samples

Position	Component	Code
1	Monolith type	C, A, or I
2	Micro grain structure ACM, medium	M
3	Carrier type	PEI, A1, SUC, PFA, or CNF

2.4 Characterization

The amount of coating, mass increase, and mass decrease were determined by measuring the sample weight before and after the various preparation steps. The carrier amount was calculated as:

$$Y_C = \left(\frac{w}{w_s + w} \right) * 100 \quad (3)$$

where w_s is the mass of the support and w is the carrier mass.

Thermogravimetric analysis (TGA) was performed on a Mettler Toledo TGA/SDTA851^e. The samples were heated in air (100 ml min^{-1}) to 1273 K (heating rate 10 K min^{-1}).

2.4.1 Porosity

The texture of the prepared carriers was analyzed using N_2 (at 77 K) and CO_2 (at 273 K) adsorption on an AUTOSORB-6B. Samples were outgassed during 4 h at 523 K. Surface area was calculated from nitrogen adsorption using the BET equation (S_{BET}). Total pore volume was determined from N_2 adsorption isotherms at $P/P^0 = 0.95$ ($V_{\text{tot}} \text{ N}_2$). Total Micropore volume ($V_{\text{DR}} (\text{N}_2)$) and narrow micropore volume ($V_{\text{DR}} (\text{CO}_2)$) were calculated applying the Dubinin Radushkevich (DR) equation to the N_2 adsorption data at 77 K and the CO_2 adsorption data at 273 K, respectively.

2.4.2 Texture

To obtain qualitative information about the texture and distribution of the carbon in the monolith, Scanning Electron Microscopy was performed using a Philips XL-20 scanning electron microscope. Transmission electron microscopy (TEM) was performed using a Philips CM30T electron microscope with a LaB6 filament as the source of electrons operated at 300 kV. Bulk sample were grinded in a mortar. Ethanol was added in order to obtain a suspension. Samples were mounted on Quantifoil® microgrid carbon polymer supported on a copper grid by placing some drops of the suspension on the grid.

2.5 Catalyst performance

Catalytic tests were performed in a monolithic stirrer reactor (see Figure 3) consisting of a glass vessel equipped with a stirrer motor. During the catalytic tests, the vessel was flushed with nitrogen. Two monoliths (length 5 cm) were mounted in plane on the stirrer axis. The total reaction volume was 2.5 l. Butanol and vinyl acetate concentrations were 0.6 M and 1 M respectively. *n*-Decane was used as an internal standard. Since bubbling of nitrogen has proven to be a promising method [11], the reaction was performed under nitrogen atmosphere. Before testing, the reactants were equilibrated over a molecular sieve overnight. The reaction was followed by GC analysis of liquid samples on a Varian CP 3380 gas chromatograph, equipped with a 1177 FID detector and a CP-SIL-8 column (length 60 m, internal diameter 0.25 mm) and using H₂ as the carrier gas and a programmed temperature gradient of 10 K min⁻¹ from 323 to 523 K. Activity tests were performed at varying stirrer rate and temperature. Possible desorption of the lipase from the supports was checked by removing the monoliths after and adding fresh reactants after the completion of each test. Stability was studied by storing the catalysts under vacuum for a longer period of time, by using the catalysts at elevated temperatures, and by consecutive testing under the same conditions. The effect of water activity was studied by adding different amounts of water to the reaction mixture. Experiments with free enzyme and Novozyme to study the kinetics of the reaction were performed in a thermostated glass reactor ($V_L=100$ ml), equipped with a magnetic stirrer at 295-300 K.

3 Results and discussion

3.1 Catalyst preparation

Application of a PEI-coating, yielded carriers with a polymer loading of 7.5 wt% and 12.7 wt% for C_PEI and AM_PEI respectively. This is consistent with the values that were obtained in the different immobilization and application studies (Ch 7, 12, 13) and indicates the reproducibility of the methods. More PEI is deposited on the ACM supports than on cordierite monoliths. This is a result of the higher accessible surface area of ACM and

probably enhanced by the more homogeneous deposition of the colloidal silica coating. Depending on the preparation method, the properties of the carbon-ceramic composites could be varied, as was seen in Chapter 8. To summarize these results, SEM images of the different carriers are shown in Figure 4. As can be seen in Figure 4a and 4d, the sucrose-derived coating seems to consist of dense layers that form a 3-D network of carbon with an apparently hexagonal structure. The mainly microporous PFA coating (Figure 4b and 4e) forms a very dense layer, completely covering the cordierite surface and filling the porous walls of the ACM. Figure 4e shows a carrier prepared from PFA in which the porous wall is completely filled with carbon. Figure 4c and f show the CNF coating completely cover the surface, in the case of ACM maintaining the open structure of the channel walls. The CNF form a uniform layer of fibers up to 1 μm length.

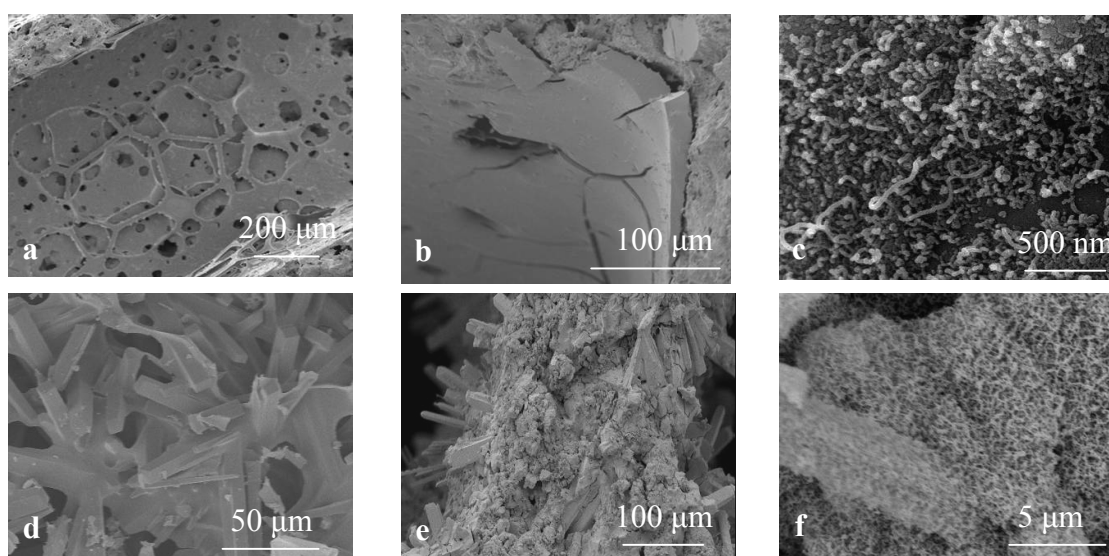


Figure 4. SEM micrographs of carbon ceramic composites a) C-SUC b) C-PFA c) C-CNF d) AM-SUC e) AM-PFA, and f) AM-CNF

The textural properties of the 200 cpsi carbon-ceramic composites are displayed in Table 4, complemented with the integral carbon monolith. Since the 400 cpsi monoliths are also included in the activity study, the data on these carbon composites is presented in Table 5.

Table 4. Textural properties of 200 cpsi carbon coated monoliths

Carbon / Support	Y_{Carrier} wt%	S_{BET} $\text{m}^2 \text{g}^{-1}$	S_{BET} $\text{m}^2 \text{g}^{-1}_{\text{Carbon}}$	Pore diameter nm	Pore volume $\text{cm}^3 \text{g}^{-1}$
C	-	<0.3	-	-	<0.001
AM	-	<0.3	-	-	<0.001
C-SUC	3.9	17	420	11	0.21
AM-SUC	14	64	454	11	0.23
C-PFA	12	0*	8	<1	0*
AM-PFA	29	0*	8	<1	0*
C-CNF	3.5	27	128	8	0.05
AM-CNF	3.2	56.2	131	9	0.11
I-A1	33.2	460	1095	n.a.	0.22

*very narrow pores, no equilibrium was reached during N_2 adsorption

Y_{carrier} represents the mean carbon content in wt%. For comparison, the S_{BET} of unsupported carbons prepared in the same manner as the supported carbons was 430, 350 and 70 $\text{m}^2 \text{g}^{-1}$ for the sucrose-derived carbon, the PFA derived carbon and CNFs, respectively. The carriers were prepared as supports for the globular α/β protein lipase, with approximate dimensions of 4.0•4.0•5.0 nm and relative mass of 33 kD (This is a slightly smaller lipase than the enzyme from *Candida rugosa* that was used in Chapter 8). The pore size of the carriers must be substantially larger than 5 nm for adequate enzyme adsorption inside the pores.

Table 5. Textural properties of 400 cpsi carbon coated monoliths

Carbon / Support	Y_{Carrier} wt%	S_{BET} $\text{m}^2 \text{g}^{-1}$	S_{BET} $\text{m}^2 \text{g}^{-1}_{\text{Carbon}}$	Pore diameter nm	Pore volume $\text{m}^3 \text{g}^{-1}$
C-SUC	4.5	20	442	12	0.30
AM-SUC	15	62	480	11	0.27
C-PFA	14	0*	8	<1	0*
AM-PFA	34	0*	8	<1	0*
C-CNF	4.4	27	120	8	0.06
AM-CNF	4.9	59	133	7	0.14

*very narrow pores, no equilibrium was reached during N_2 adsorption

For all carrier types, the carbon content of the ACM supports is higher than for the classical cordierite monoliths. This is not surprising, given the open structure of the channel walls of the ACM. The sucrose-based carriers have a moderate carbon yield, this can be increased by concentrating the precursor or perform two subsequent coating steps. The average pore diameter is around 10-12 nm; therefore this carrier type appears to be suitable for lipase adsorption.

The microporous PFA carriers have a high carbon content, a result of the high viscosity of the polymer precursor employed. For this carrier, both cell density and the preparation process (amount of samples, dip-time) can affect the yield to a high extent. The surface area that was determined from N_2 adsorption isotherms approached 0, but an estimation from the CO_2 adsorption isotherm reveals a large (narrow) microporous surface area. With a pore diameter < 1 nm, these carriers are not expected to be effective for lipase adsorption.

The loading of the CNFs on monoliths has proven to be very reproducible (4-5 wt%, see Chapter 8), although small local differences inside the monolith channels can be observed with TGA analysis. The moderate surface area of the fibers, combined with the open, network-like structure of the fibers and the large total pore volume, is expected to lead to a high lipase adsorption capacity.

3.2 Enzyme adsorption and catalyst performance in the MSR

The results of lipase adsorption on the PEI and carbon coated monoliths and subsequent application in the MSR are given in Table 6. The integral carbon monolith, I-A1 is also included. In general the ACM supports have a slightly higher adsorption capacity than the

similarly prepared cordierite supports, because the porous ACM supports allow more carrier to be deposited.

The I-A1 carrier has a high enzyme adsorption capacity but shows a decreased activity per monolith volume. Integral carbon monoliths are also very suitable as a support material for this lipase, but the activity is much lower than for the carbon-ceramic composites. For the latter, the observed activity corresponds to the amount of protein that was adsorbed. The activity per gram of enzyme (Table 6) is constant around a value of $\sim 0.9 \text{ mmol s}^{-1} \text{ g}_{\text{protein}}^{-1}$ for all types of carbon and with all supports.

Table 6. Results lipase adsorption and activity tests for 200 cpsi monoliths at 300 K, 150 rpm

Carrier type	Protein* mg monolith ⁻¹	Enzymatic activity at 150 rpm, 300 K				
		mol m _{monolith} ⁻³ s ⁻¹	mmol s ⁻¹ g _{protein} ⁻¹	Φ_m	Φ_L	Ca
C-SUC	75	0.98	0.95	0.84	0.02	$3 \cdot 10^{-3}$
AM-SUC	78	1.3	1.04	1.36	0.15	$1 \cdot 10^{-3}$
C-PFA	81	0.94	0.84	-	-	$2 \cdot 10^{-3}$
AM-PFA	98	1.3	0.86	-	-	$5 \cdot 10^{-4}$
C-CNF	380	4.4	0.84	1.18	0.05	$5 \cdot 10^{-3}$
AM-CNF	350	4.7	0.89	1.65	<0.05	$6 \cdot 10^{-3}$
C-PEI (GPTMS)	25	0.32	0.93	-	-	$5 \cdot 10^{-3}$
AM-PEI (GPTMS)	37	0.56	0.95	-	-	$1 \cdot 10^{-2}$
I-A1	330	1.5	0.32	1.31	-	$1 \cdot 10^{-4}$

*Lipase content in the lyophilized powder is around 20 wt%

For the I-A1 monoliths this value is significantly lower. This could indicate the presence of internal diffusion limitations. This will be discussed in the following paragraph.

If we assume a lipase content of 20% in the crude protein powder, this corresponds to a turnover frequency (TOF) value of 175 s^{-1} . The C-CNF and AM-CNF carriers have similar enzyme loading and display the same activity when used in the monolithic stirrer reactor; therefore the monolithic stirrer reactor is thought to be a useful reactor to perform biocatalytic reactions. To test the limits of the cordierite support and the ACM support, experiments should be performed outside the kinetically control regime by either increasing the enzyme loading or applying another, faster enzymatic reaction.

3.2.1 Mass transfer and dimensionless correlations

It is interesting to compare the catalyst effectiveness that is reported here with conventional catalyst systems. The characteristic length (L) for cordierite monoliths is of the order of a tenth of a millimeter in the worst case (wall thickness), which is comparable to the diffusional lengths in the smaller beads ($L = d_p/6$) [14,19,28]. For the open ACM structures with thin support coatings, the diffusional distance becomes at least an order of magnitude smaller, clearly outside of the range of what can realistically be achieved with beads. In the previous chapters a set of correlations was used to study mass transfer in the MSR. In Table 7, these correlations are summarized.

Table 7. Dimensionless correlations and formulas

$\Phi = \frac{(n+1)}{2} \cdot \frac{r_{v,obs} \cdot L^2}{D_{eff} \cdot C_b} < 0.15$	(4)	$Ca = \frac{r_{v,obs}}{a' \cdot k_s \cdot C_b}$	(9)
$Re = \frac{\rho \cdot v_L \cdot d_{ch}}{\eta}$	(5)	$Sc = \frac{\eta}{\rho \cdot D}$	(10)
$Sh = Sh_{\infty} [1 + C \cdot \frac{d_{ch}}{L_m} Re \cdot Sc]^{0.45}$	(6)	$Gz = \frac{L_m}{Sc \cdot Re \cdot d_{ch}}$	(11)
for $Gz < 0.03$			
$Sh = \frac{4}{\sqrt{\pi}} P^{1/2}$	(7)	$P = \frac{d_{ch}}{4.25 \cdot L_m} \cdot Re \cdot Sc$	(12)
for $P \rightarrow \infty$			
$Sh = \frac{k_s \cdot d_{ch}}{D}$	(8)	$D_{eff} = \frac{D \cdot \phi_p \cdot \sigma_f}{\tau}$	(13)

Internal diffusion limitations

To rule out possible internal diffusion limitations under these conditions the Wheeler-Weisz modulus Φ (equation 4) was estimated, assuming first order kinetics. For the microporous PFA and the PEI layer, all enzyme is assumed to be present on the outer surface, no internal diffusion problems exist for these catalysts.

Using the observed reaction rate (in $\text{mol s}^{-1} \text{m}^{-3}_{\text{catalyst}}$) of the experiments performed at 150 rpm, the Wheeler-Weisz modulus was calculated for all monoliths assuming a layer thickness (L) of half the monolith wall and a catalyst volume (V_{cat}) equal to the volume of the monolith walls (≈ 40 ml).

To estimate D_{eff} inside the carbon layers (equation 13), a tortuosity of 3.0 was assumed for the more closed carbon layers (sucrose and the integral monolith, with a porosity of 0.5), resulting in 80% decrease of the diffusion coefficient compared to the bulk diffusivity. For the more open CNFs, the tortuosity is assumed to be much lower. With a tortuosity of 1.5 (and a porosity of 0.8) D_{eff} decreases by a factor 0.5. This gives $1-3 \times 10^{-10} \text{ m}^2 \text{ s}^{-1}$ as an estimate for D_{eff} inside the different carbons.

The values for Φ_m (over $L = 0.5 \times d_w$) are presented in Table 6. These values indicate severe internal diffusion limitations. For I-A1, consisting mainly of macroporous carbon, it is likely that internal diffusion limitations are present inside the carbon walls (where the lipase is located). This is also indicated by the decreased activity per g of enzyme for these monoliths. For ceramic monoliths, the high values for Φ_m are in contradiction with the fact that activity was found to increase with enzyme loading (a constant turnover frequency for all carbon

types). The latter suggests that all adsorbed enzyme is used effectively. A more realistic approach would therefore be the determination of Φ_L (over $L = d_l$, see Figure 5).

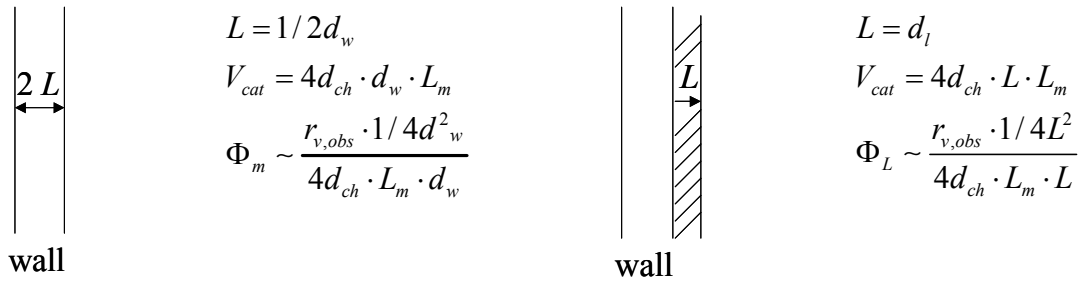


Figure 5. Comparison of different approaches to estimate the Wheeler-Weisz modulus in the carbon coatings

According to the calculation of Φ for both situations (Φ_L and Φ_m), this should give a 5 fold decrease if a layer thickness of around 15 μm is assumed.

$$\frac{\Phi_m}{\Phi_L} = \frac{1/4d_w}{L} = \frac{75\mu\text{m}}{15\mu\text{m}} = 5$$

The values for Φ_L are presented in Table 6. In the following paragraph the estimated parameters are discussed. For ACM catalysts the available surface area is much higher than for classical monoliths, leading to a decreased diffusion layer thickness. Since this layer thickness is not exactly known and is probably not the same throughout the sample (partly plugging the wall and partly present as a thin layer on the micrograins, as was stated in Chapter 13), the values for Φ_L in the ACM monoliths were estimated by assuming all catalyst is present in the center of the wall. By comparing the total wall volume of the monolith with the carbon volume, a layer thickness of the carbon inside the wall can be estimated. Half the thickness of this carbon layer is used to estimate Φ_L . For cordierite monoliths, the carrier is assumed to be homogeneously deposited onto the channel walls.

For C-SUC, 2 g of carbon per pair of monoliths has a volume of 1 ml ($\rho \approx 2000 \text{ kg m}^{-3}$). This gives a layer thickness L of 2 μm . This yields a Φ of 0.02, well below the threshold value for the onset of internal diffusion limitations. For AM-SUC, 8.5 g of carbon gives a total volume of 3.5 ml carrier material. Spread over the total channel wall volume, this would give a layer of 30 μm in each wall. With a layer thickness of 15 μm , Φ becomes 0.15. Since it is expected that the carbon is not solely present in the wall, but also as a thin layer on the separate micrograins, Φ is assumed to be significantly lower than 0.15.

For CNF, the density of the carbon fibers is significantly lower than for the solid carbon coatings. A layer thickness of 10 μm is assumed (from SEM, see Figure 6), which yields a total carbon volume of around 10 ml for a pair of monoliths. This gives a Φ_L of 0.05, also indicating that no severe internal diffusion limitations exist in the CNF-coating.

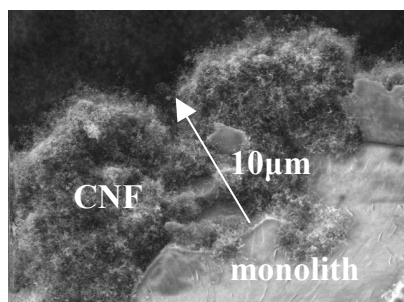


Figure 6. Estimation of L for C_CNF

For AM-CNF, Φ_L is calculated to be the same as for cordierite by assuming a 10 μm layer of CNF and using the specific surface area of cordierite. The SEM images showed a thin layer of CNFs over the needles. The carbon yield is only slightly higher than for cordierite, but this carbon is spread out over a larger surface area. The layer thickness will therefore be even smaller, resulting in an additional decrease of the Wheeler-Weisz modulus.

External mass transfer limitations

To investigate any external mass transfer limitations present in the system, the stirrer rate was varied between 50 and 400 rpm. The initial reaction rate for the different carrier materials is plotted as a function of stirrer speed in Figure 7. A lower initial activity was observed in the initial runs for the ACM monoliths, which were performed at 50 rpm. After testing at the higher stirrer speed, 50 rpm experiments were repeated and it was found that the activity had increased as is shown in Figure 7. These observations are attributed to some residual water in the porous ACM supports after preparation. This water, still present from the adsorption step, is gradually removed during the first runs. This removal can be enhanced by extensive washing with toluene and inverting the test sequence, starting at high stirrer rate working towards 50 rpm. This procedure was followed using sucrose-based carriers and no relatively low activity in the initial runs was found.

For these monolithic biocatalysts, no profound influence of stirrer rate could be detected (Figure 7). Apparently no external mass transfer limitations are present in the system. At these high stirrer rates, the contact time is too short for a mass transfer boundary layer to develop to the channel axis. Moreover, it can be expected that under these conditions, the velocity profile along the monolith length also hasn't completely developed.

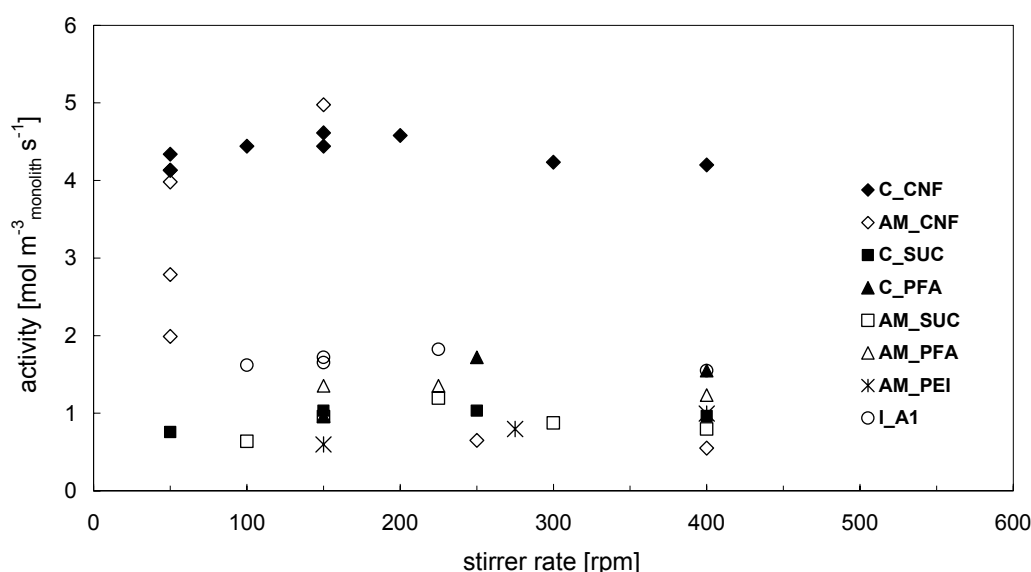


Figure 7. Effect of stirrer rate on the initial reaction rate at 300 K in the acylation of butanol with vinyl acetate with different 200 cpsi monoliths. $V_L = 3$ l, $C_{\text{but}} = 0.6$ M $C_{\text{VA}} = 1$ M

This was also observed in the hydrolysis of lactose in Chapter 13. In the following section, the hydrodynamics in the system will be analyzed in more detail.

Mass transfer in the MSR

Mass transfer can be quantified by calculating the Sherwood number, Sh (equation 6). In order to apply this equation, Gz must be smaller than 0.03. Under the present conditions, $Gz = 10^{-6}$, indicating that the boundary layer for mass transfer is in development. As a result, the Sherwood number is orders of magnitude higher than the lower limit of 2.96. A second requirement for the application of equation (6) is that the velocity profile must be developed, so the hydrodynamic entrance length must be small compared to the monolith length. To check whether the velocity profile is in the developed state, the hydrodynamic and mass transfer entrance lengths (L_{mt} and L_{hydro}) under the present conditions are plotted as a function of stirrer rate for 200 and 400 cpsi monoliths in Figure 8.

In all experiments, the mass transfer profile (Figure 8a) is in the developing state. The velocity profile however (Figure 8b), is not yet fully developed over the monolith length. Since the velocity profile is also not completely undeveloped, this intermediate situation is analyzed in the same way as was done in Chapter 13. Equation 6 holds for developing mass transfer in thin channels, with a developed velocity profile. Equation 7 [41] can be used for simultaneously developing flow. Sh is calculated in both the thermally developing case and the simultaneously developing case, with a resulting mean value for Sh . It was shown before that for rectangular ducts (with wall dimensions 1:2) the difference between the two cases is around a factor 2 for $0.001 < Gz < 0.01$ [30, 42].

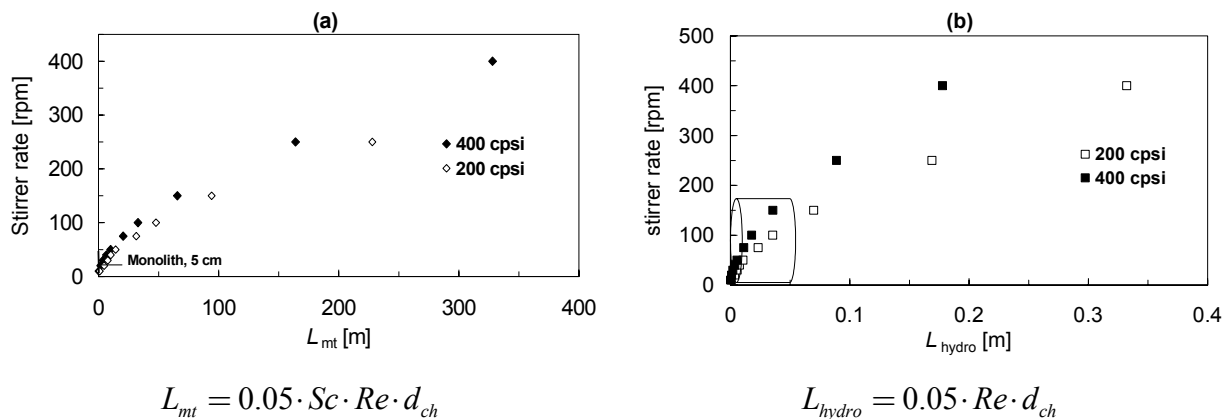


Figure 8. Characteristic entrance length as a function of stirrer rate for the development of a) the boundary layer for mass transfer, b) the velocity profile of along the monolith channel. a monolith of 5 cm length is added to the figures for comparison

Using the equations in Table 7 and the parameters from Table 8, Re , Sc , P , and Gz can be estimated. At a stirrer speed of 150 rpm, liquid velocity (v_L) in the monolith channels is around 0.5 m/s [31]. With an estimated Sc of 1350, and Re of 1150, Sh becomes 130 and 230 respectively for the developed and the undeveloped velocity profile (see Table 8 for some fluid properties).

Table 8. Used parameters

Parameter	Value
Density, ρ	858 kg m ⁻³
Viscosity, η	5.54 x 10 ⁻⁴ Pa s
Substrate concentration, C_b	600 mol m ⁻³
Diffusivity, D	5 x 10 ⁻¹⁰ m ² s ⁻¹
Asymptotic Sherwood, Sh_∞	2.96
Surface roughness, C	0.095

With the data supplied in Table 8 and a mean Sh of 180, the liquid solid mass transfer coefficient of the system at 150 rpm was estimated to be 5 x 10⁻⁵ m s⁻¹, using equation (8) [30].

From the data in Figure 7 it was concluded that no external mass transfer limitations are present. The absence of external mass transfer limitations can be confirmed by calculating the Carberry number Ca , the ratio of the observed rate (normalized for the catalyst volume) and the maximal mass transfer rate (see Table 6). Similar to the calculation of the Wheeler-Weisz number, the catalyst volume (V_{cat}) is defined as the volume of the deposited carbon carrier for the ceramic monoliths and the wall volume for I-A1. a' is defined as the surface area of the catalyst (the carbon coatings). Since this theoretical maximum mass transfer rate in the MSR is not known, the calculated k_s is used here to estimate Ca . This is justified by assuming the experiments were done under kinetically controlled conditions, so $r_{mass\ transfer} \gg r_{reaction}$.

The values for Ca are presented in Table 6 for the different experiments that were performed at 150 rpm. For 200 cpsi C-CNF-based supports, Ca becomes 0.005. This is below the boundary value of 0.05. For all other experiments with cordierite samples at 150 rpm, $Ca \ll 0.05$ (see Table 6), so no external mass transfer limitations are present. For ACM monoliths, a' is assumed to be significantly larger than for cordierite samples, also leading to $Ca \ll 0.05$.

3.2.2 Effect of cell density

Different 400 cpsi monoliths were used to immobilize the lipase and tested in the MSR under the same conditions. Based on the larger geometric surface area at higher cell density, theoretically more carrier can be deposited resulting in a higher enzyme loading per monolith. Therefore, the observed activity is expected to increase proportionally with the available surface area. As was already seen in Table 3, the carrier loading does not increase proportionally with surface area for carbon deposition. In general, only a slight increase in carrier loading was observed, this implies that the layer thickness L for internal diffusion will decrease, while the total catalyst volume will hardly be affected. The initial activity at 150 rpm, 300 K is presented in Figure 9 for different monolith carrier combinations. Numerical values are presented in Table 9. Due to the combination of the changing layer thickness (present as L^2 in equation 4), V_{cat} , and increased reaction rate, the values for Φ can be estimated from the values of the 200 cpsi samples.

Table 9. Results lipase adsorption and activity tests for 400 cpsi monoliths at 300 K, 150 rpm

Carrier type	Protein* mg monolith ⁻¹	Enzymatic activity at 150 rpm, 300 K			
		mol m _{monolith} ⁻³ s ⁻¹	mmol s ⁻¹ g _{protein} ⁻¹	Φ_L	Ca
C-SUC	113	1.4	0.93	0.02	5×10^{-3}
AM-SUC	125	2.1	0.99	0.15**	2×10^{-3} **
C-PFA	122	1.4	0.8	-	3×10^{-3}
AM-PFA	157	1.9	0.76	-	7×10^{-3} **
C-CNF	400	5.2	0.94	0.05	9×10^{-3}
AM-CNF	556	7.6	0.96	0.07	2×10^{-2} **

*Lipase content in the lyophilized powder is around 20 wt%

** Estimated with the wall-surface area of cordierite, assuming closed walls

For example, for C-CNF the available surface area increase by a factor 1.4 with a similar (+25%) carbon loading. In this case the estimated layer thickness decreases by a factor 1.1. The reaction rate per catalyst volume increases by a factor 1.2, so Φ_L remains constant. For AM-CNF the reaction rate increases almost by a factor 2, while the carbon loading increases by a factor 1.5. (50% higher CNF loading) This leaves the layer thickness L unchanged, but increases the Weisz-Prater number by a factor 1.3. Φ_L becomes 0.07. For the sucrose-based carriers the carbon loading increases slightly, this means that L will decrease by less than a factor 1.4. The activity of the sucrose-based carbons increases by a factor 1.4, assuming an unchanged V_{cat} . In this case the decrease in L is canceled out by the increase in reaction rate, and Φ_L remains unchanged compared to the 200 cpsi monoliths.

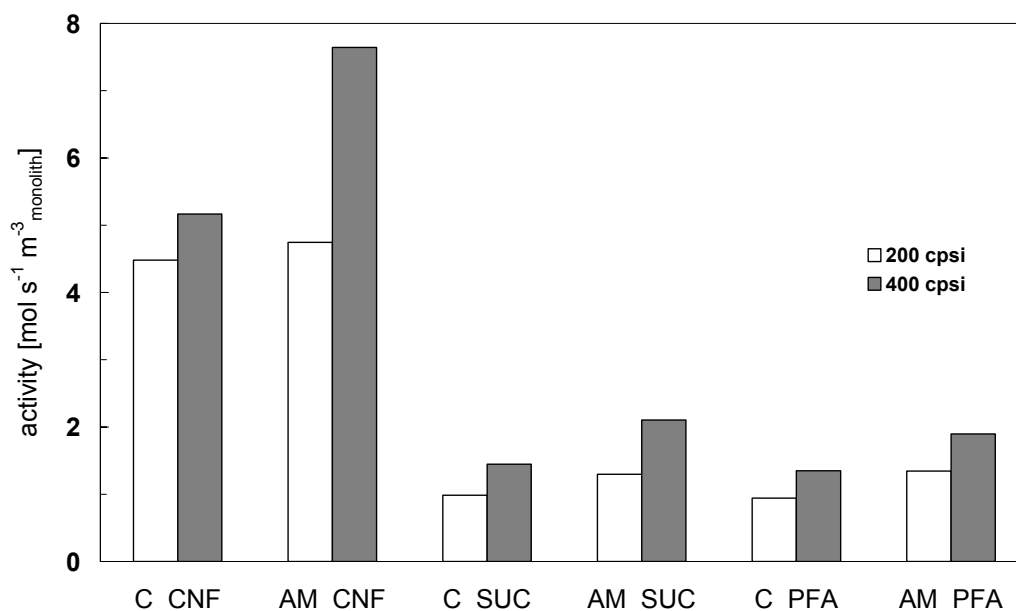


Figure 9. Effect of cell density on the activity in the acylation of butanol with vinyl acetate in organic medium at 150 rpm and 300 K.

To check whether the system enters the mass transport limited regime as a result of the higher enzyme loading, Ca was calculated for the 400 cpsi monoliths. For 400 cpsi, the channel

velocity at 150 rpm decreases to 0.3 m s^{-1} [31], which gives $Sh = 105$ and $k_s = 4.8 \times 10^{-5}$ after applying equations 5-12.

For all catalysts the same catalyst volume was assumed as was calculated for the 200 cpsi monoliths (actually a slight increase in carbon loading was observed, this leads to an overestimation of Ca), so $r_{v,obs}$ increases proportionally with the increase in reaction rate compared to the 200 cpsi monoliths (Figure 9). Secondly, k_s decreased by a factor 1.3 for the 400 cpsi monoliths at 150 rpm. So based on the lower observed k_s and the higher observed reaction rate, Ca slightly increases (by a factor 1.4-1.7) compared to the 200 cpsi monoliths. The values for Ca are presented in Table 9 for the 400 cpsi monoliths.

3.2.3 Stability

After each run, the monolithic stirrer was replaced by a normal stirrer, and fresh reactants were added to check if any enzyme had desorbed. No activity could be detected (Figure 10); apparently the lipase does not desorb from the support under the chosen reaction conditions.

To investigate catalyst storage stability, they were tested one more time after completing the series of varying stirrer rate. The time between the first and last test was approximately 1-2 weeks. The same initial conditions were applied. No decrease in activity could be detected. Hence the biocatalysts are stable for at least two weeks, under repeated catalytic testing up to 323 K.

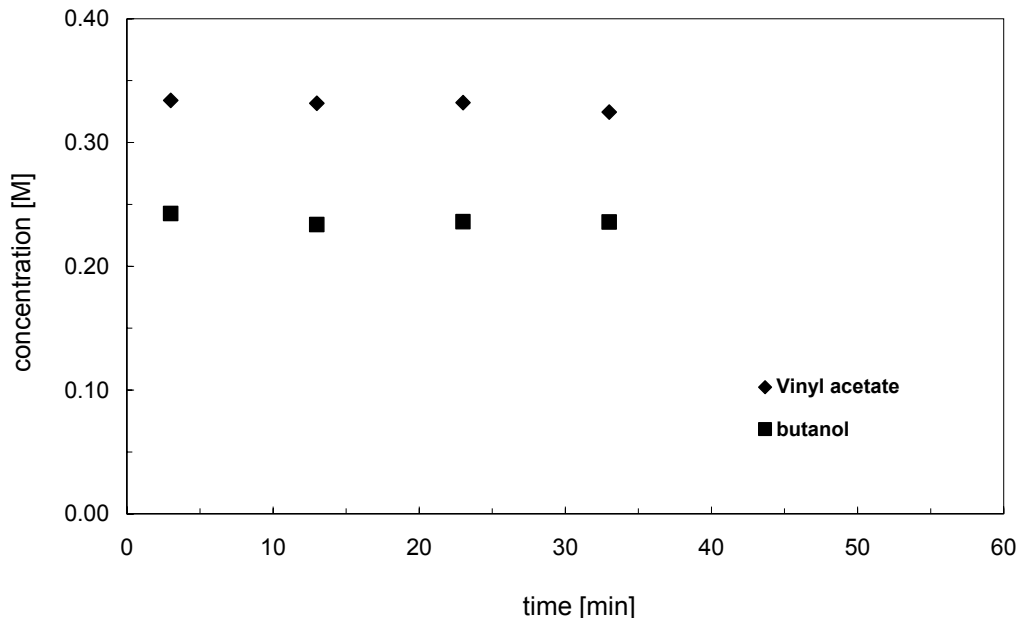


Figure 10. Leaching test for 200 cpsi AM-CNF in the MSR the acylation of butanol with vinyl acetate in organic medium, at 300 K, 150 rpm

3.2.4 Comparison with free lipase and Novozyme

To evaluate the catalyst performance, free lipase and a commercial immobilized lipase (Novozyme) were also tested. The results of the activity per g protein are plotted in Figure 11.

The specific activity of immobilized lipase is lower than that of the free enzyme. It is known that residual activity of an enzyme after immobilization usually decreases significantly. Also the carrier has a substantial influence on both residual activity and kinetic constants [32]. A decrease in the observed rate per g enzyme can usually be ascribed to conformational changes, steric effects or denaturation. Ayhan *et al.* [33], report a residual activity of 1% after coupling of urease via glutaraldehyde immobilization in polymer microbeads. Lee *et al.* [34] report a residual activity of 2% after covalent immobilization of glucoamylase onto controlled pore glass. When physical or ionic adsorption is employed, urease was found to maintain its natural configuration and the residual activity is around 30% of free enzyme activity [35]. For the monolithic biocatalysts, the immobilized activity was found to be 30-35%, and for Novozyme around 80% in the first run. This high value is not only a result of the immobilization procedure, but we must also bare in mind that the free enzyme tends to form aggregates and adheres to the reactor wall when used in organic media. The free enzyme aggregates probably have a decreased activity per g enzyme compared to free enzyme that is completely dissolved in aqueous medium. This behavior for lipase from CALB in organic solvent was also described by Dumitriu *et al.* [21]. Although a residual activity of 5-15% was reported, they also observed that immobilization leads to a more advantageous use of the enzyme.

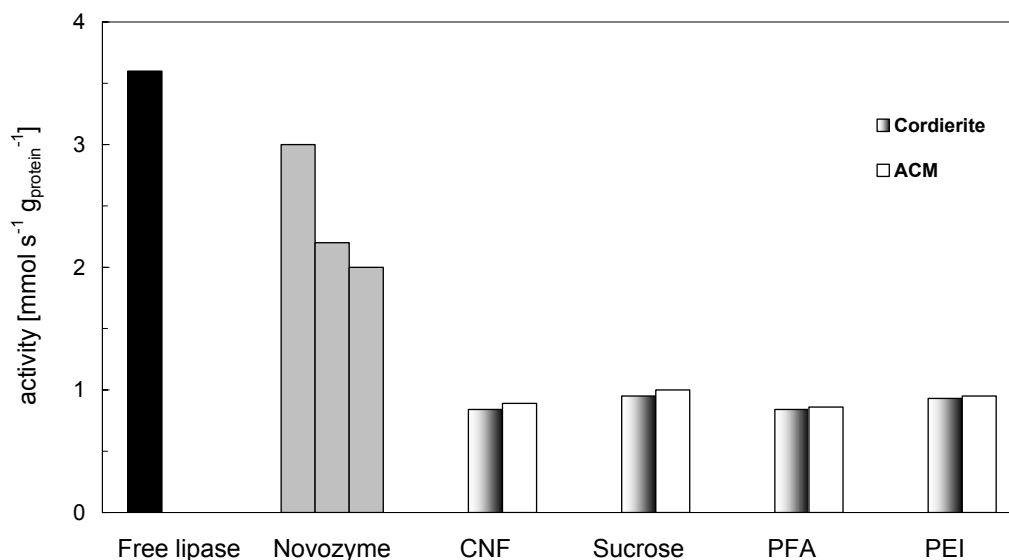


Figure 11. Initial reaction rate of free lipase, Novozyme, and 200 cpsi monoliths in the acylation of butanol with vinyl acetate in organic medium in different reactor systems, at 300 K

The deactivation of the commercial sample is probably due to the observed instability of the support matrix under reaction conditions [36,37]. The deactivation proved to be irreversible. Since no stability tests were performed with Novozyme catalyst, it is not known if the deactivation is caused by leaching. The same deactivation was also observed for the PEI composites (not shown). After 4 consecutive runs, the PEI-based catalysts had lost 50% of their original activity.

3.3 Kinetics of the acylation of 1-butanol with vinyl acetate

The kinetics of the acylation reaction were studied with a commercial immobilized lipase (Novozyme). Before the effect of substrate concentration can be investigated, the system must be checked for possible external mass transport problems (e.g. caused by ineffective mixing). This was done by varying the catalyst concentration.

3.3.1 Effect of catalyst concentration

Figure 12 shows the influence of the Novozyme concentration on the initial reaction rate of the transesterification reaction. No reaction takes place when there is no catalyst present. Furthermore, the straight line indicates that the reaction is first order in the enzyme concentration. This type of dependency is generally encountered in heterogeneous catalysis when the reactants/products do not poison the active sites. This linear fit also indicates the absence of diffusion limitations due to a high catalyst concentration or insufficient mixing (due to low stirrer rates). The kinetics study with the enzyme beads was made with a Novozyme concentration of 0.25 g l^{-1} at a stirrer rate of 650 rpm.

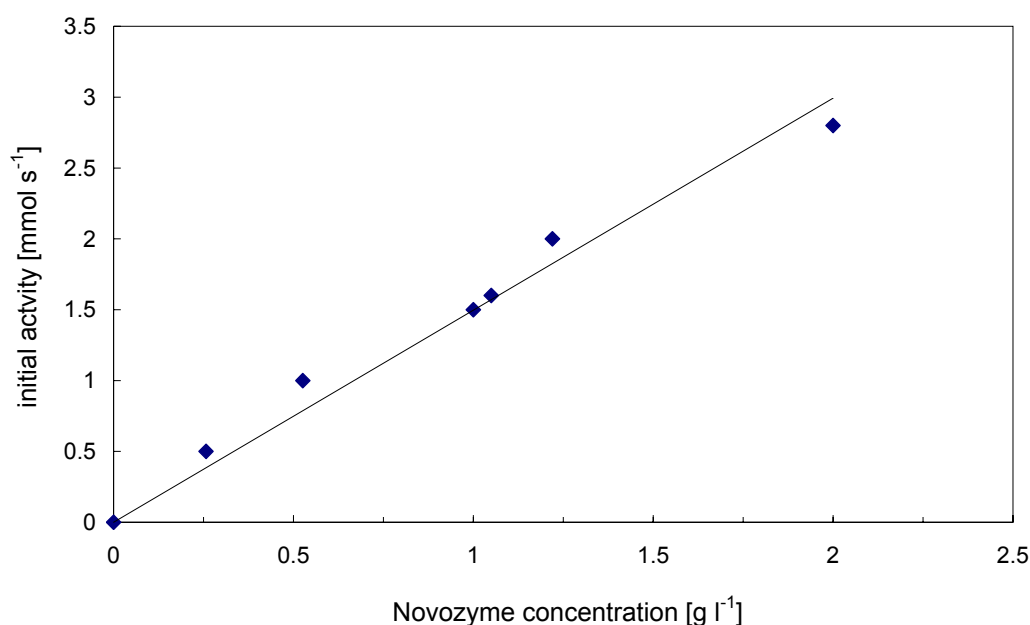


Figure 12. Effect of catalyst concentration in a slurry system on the initial reaction rate in the acylation of butanol with vinyl acetate in organic medium at 300 K, 650 rpm

3.3.2 Effect of temperature

The reaction was performed with different catalysts at temperatures in the range of 290-323 K. The results are presented in (Figure 13), to calculate the apparent activation energy. From the slope of the Arrhenius-plot ($=-E_a/R$) it follows that the apparent activation energy of the free enzyme is 47 kJ mol^{-1} . The values of E_a for Novozyme and C-CNF obtained in different

reactors are similar to this value, which supports earlier conclusions on the absence of internal and external mass transport problems for both reactor systems.

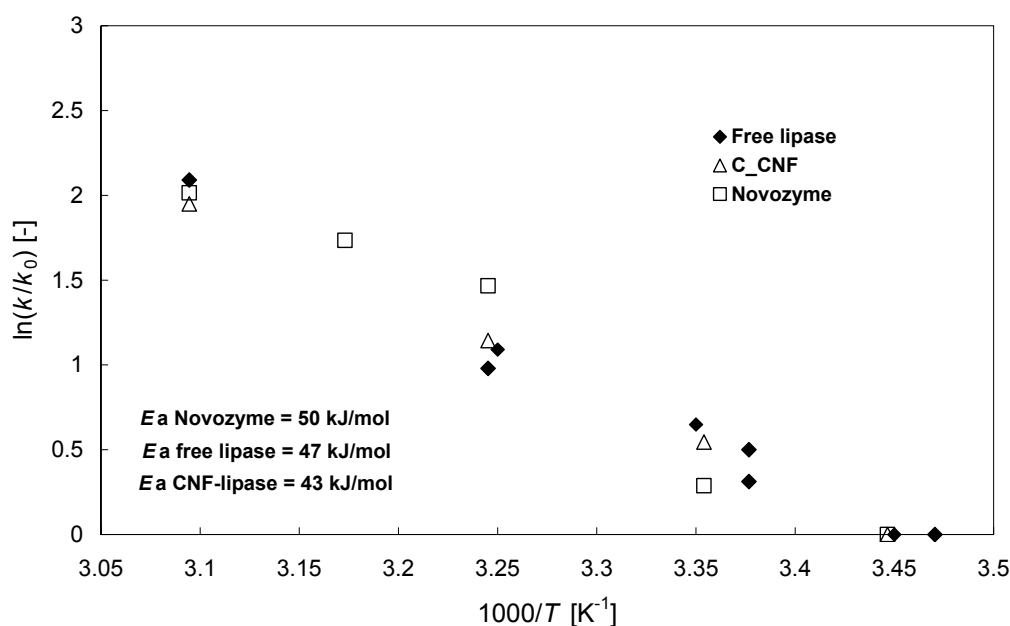


Figure 13. Arrhenius-plot of the acylation of vinyl acetate with butanol, catalyzed by lipase. Tests with free lipase and Novozyme were performed in a glass reactor (total volume 100 ml) with $C_{\text{butanol}} = 0.6$ M and $C_{\text{vinyl acetate}} = 1$ M at 650 rpm. C-CNF was tested in the MSR (total volume 3 l) at 150 rpm

3.3.3 Substrate concentration

Figure 14 shows the effect of the 1-butanol concentration at different vinyl acetate concentrations. The shape of the curves suggests an inhibition by butanol. At higher butanol concentrations, the observed activity decreases. In Table 10 the results are given for the two fitted models that were proposed. The best results were obtained for the bi-bi ping-pong equation (model 1). The fit of this model is presented in Figure 14 as the solid lines. The values for the parameters that were found are strongly dependent on the type of catalyst and the reactants. No values were found in literature for the kinetic parameters of this system with adsorbed lipase. The values are however in the same order of magnitude as values found for the free enzyme performing this reaction [15] (with model 1, values for $K_{m,B}$, $K_{m,A}$, $K_{i,A}$, $K_{i,B}$ of 0.04 M, 0.6 M, 3 M, and 0.5 M respectively were observed with A=vinyl acetate, B = 1-butanol). In this article the inhibiting effect of the reactant butanol was also observed.

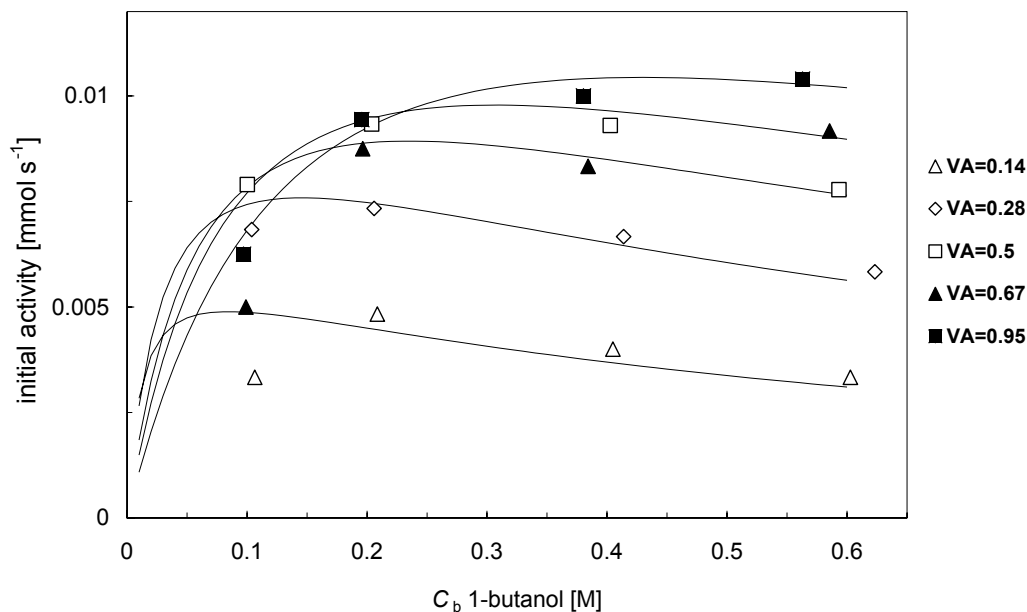


Figure 14. Effect of the 1-butanol concentration on the transesterification rate, catalyzed by Novozyme. Experiments were performed at 295 K, 0.25 g l⁻¹ Novozyme and 650 rpm. Experimental data points and curves from the theoretical rate expression with the best fitted parameters

The observed V_{\max} (Table 9) equals 2.2 mmol h⁻¹ mg_{cat}⁻¹, this is in the same order of magnitude as the value that was found by Maury *et al.* [14] (5 mmol h⁻¹ mg_{cat}⁻¹) for encapsulated lipase in a slightly different reaction.

Table 10. Results of parameter determination of the proposed kinetic expressions

Model	Rate Expression	Result
1	$r = \frac{V_{\max}[A][B]}{K_{m,B}[A](1 + \frac{[A]}{K_{i,A}}) + K_{m,A}[B](1 + \frac{[B]}{K_{i,B}}) + [A][B]}$	V_{\max} 0.78 mmol s ⁻¹ g _{cat} ⁻¹ $K_{M,B}$ 0.037 M $K_{m,A}$ 0.72 M $K_{i,B}$ 0.50 M $K_{i,A}$ 0.15 M $SSres$ 0.05
2	$r = \frac{V_{\max}[A][B]}{K_{m,A}[B](1 + \frac{[B]}{K_{i,B}}) + K[A][A] + [A][B]}$ <p>with $K = \frac{K_{m,B}}{K_{i,A}}$</p>	V_{\max} 0.53 mmol s ⁻¹ g _{cat} ⁻¹ $K_{m,A}$ 0.29 M $K_{i,B}$ 0.37 M K 1.49 (-) $SSres$ 0.83

3.3.4 Effect of water concentration in the reaction medium

It is important to control the quantity of water available for the enzyme in the reaction medium. To study the effect of water addition, small volumes of water were injected before starting the reaction. The results are presented in Figure 15.

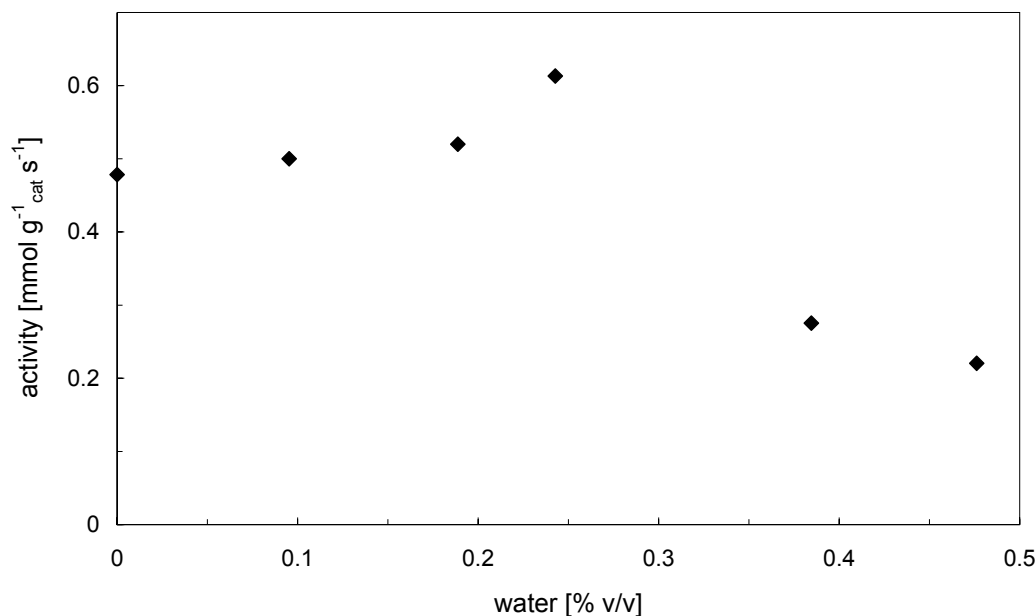


Figure 15. Effect of water concentration in the reaction medium (dried over molecular sieve, with different amounts of water added just before the experiment) on the initial reaction rate in the acylation of butanol with vinyl acetate in organic medium. The reaction was performed in a glass reactor ($V_L = 100$ ml) with 0.1 g l^{-1} Novozyme, at 300 K, 650 rpm

It seems from the data in Figure 15 that the reaction rate increases slightly with the addition of small amounts of water up to 0.3 % v/v. Above 0.3 % v/v water the activity clearly drops again. It has not been verified if this would also hold true for monolithic catalysts. At higher water content, also the hydrolysis reaction can occur, resulting in an adverse effect of water addition. Many authors have reported that the addition of small amounts of water was necessary to ensure activation of the enzyme, in particular to give the enzyme more conformational freedom [38-40]. It is generally accepted that a better control over the transformation kinetics can be achieved by working at a constant, optimal water activity [14].

4 Conclusions

Several monolithic enzyme biocatalysts were prepared and characterized. Carbon coatings consisting of carbonized sucrose, carbonized polyfurfuryl alcohol and carbon nanofibers were applied on monoliths with different microstructure. Additionally, polyethyleneimine (PEI) was used as a carrier material. The coated carbon monoliths were also compared with an

integral (composite) carbon monolith. A lipase from *Candida antarctica* was adsorbed on the monolithic supports. Adsorption on carbon coatings can be very effective, depending on the carbon microstructure. For a high lipase loading, mesoporous (I-A1) or open (CNF) carbon structures are preferred. The enzyme loading on ACM supports is generally higher than on cordierite supports. So the microstructure of the monolith is a relevant parameter for the enzyme adsorption capacity and catalytic activity. For all prepared biocatalysts, satisfactory immobilization and activity in the acylation of 1-butanol with vinyl acetate was observed. The CNF-based catalysts performed best, showing the highest activity per volume of catalyst. For cordierite and ACM monoliths, the initial rate is 4.4 and 4.7 mol s⁻¹ m⁻³_{monolith} respectively. The integral carbon monoliths have a high enzyme loading, but suffer from internal mass transfer limitations.

No enzyme leaching was detected from the prepared monolithic biocatalysts. The carbon-based catalysts were found stable for several weeks, without any significant loss of activity. PEI is less suitable as a carrier material in this system; initial activity is relatively low and significant deactivation was observed when the catalyst was reused several times.

We have demonstrated that ceramic monolith and carrier combinations offer significant practical advantages for the preparation of monolithic bioreactors. The use of a monolith stirrer reactor shows that immobilized enzymes can be used in an elegant construction that eliminates the use of powders or beads. This can offer significant advantages in reducing filling and cleaning between two runs in the same unit. Residual activity of the immobilized enzyme was 30-35% of the free enzyme activity. Compared to a commercially available immobilized lipase (Novozyme), the immobilized activity of the monolithic catalysts is slightly lower. The Novozyme however, shows significant deactivation in consecutive tests.

The present reactor configuration can be operated without any mass transport limitations, fully utilizing all adsorbed enzyme. Increasing the cell density of the monoliths leads to a higher lipase loading and hence a higher activity. Dimensionless correlations that are a measure for mass transfer were found to increase slightly with increasing cell density.

The kinetics of this the reaction were investigated for an immobilized enzyme (Novozyme) by varying the catalyst concentration, the substrate concentrations and the water activity. No diffusion problems were present in the system, and values for the Michaelis-Menten constants of the substrates ($K_{m,B} = 0.037$ M, $K_{m,A} = 0.72$ M), the inhibition constants ($K_{i,B} = 0.5$ M, $K_{i,A} = 0.15$ M), and the maximum rate (0.78 mmol s⁻¹ g_{cat}⁻¹) could be found. The apparent activation energy of the transesterification was found to be 47 kJ mol⁻¹ for free enzyme and 45-50 kJ mol⁻¹ for the immobilized enzyme (Novozyme and C_CNF). The optimum activity of Novozyme was observed at a water content of 0.3% v/v.

5 Acknowledgements

Toni Marquez Fló is gratefully acknowledged for performing all MSR experiments. Corning Inc. is acknowledged for the supply of the cordierite monoliths, The DOW Chemical

Company is acknowledged for supplying the ACM monoliths. Part of the work has been performed in the framework of the Network of Excellence 'Inside Pores'. The Netherlands Organization for Scientific Research (NWO) is acknowledged for funding part of this research by means of a grant, file number R74-68.

6 Symbols

a'	specific surface area	$[\text{m}^2 \text{m}^{-3}]$
A_m	geometric surface area	$[\text{m}^2]$
Ca	Carberry number	$[-]$
C_s	substrate concentration	$[\text{mol m}^{-3}]$
d_{ch}	channel diameter	$[\text{m}]$
D	diffusivity	$[\text{m}^2 \text{s}^{-1}]$
D_{eff}	effective diffusion coefficient	$[\text{m}^2 \text{s}^{-1}]$
E_a	apparent activation energy	$[\text{kJ mol}^{-1}]$
k	rate constant	$[\text{s}^{-1}]$
k_0	reaction rate constant at 298 K	$[\text{s}^{-1}]$
$K_{i,j}$	inhibition constant of component j	$[\text{mol l}^{-1}]$
$K_{m,j}$	Michaelis Menten constant of component j	$[\text{mol l}^{-1}]$
k_s	mass transfer coefficient	$[\text{m s}^{-1}]$
$k_{r,obs}$	observed reaction rate constant	$[\text{s}^{-1}]$
L	layer thickness	$[\text{m}]$
L_{hydro}	entrance length for development of the velocity profile	$[\text{m}]$
L_m	monolith length	$[\text{m}]$
L_{mt}	Entrance length for development of mass transfer boundary layer	$[\text{m}]$
n	reaction order	$[-]$
Re	Reynolds number	$[-]$
r_i	reaction rate of reaction i	$[\text{mol s}^{-1}]$
$r_{v,obs}$	observed reaction normalized for catalyst volume	$[\text{mol s}^{-1} \text{m}^{-3}_{cat}]$
Sc	Schmidt number	$[-]$
Sh	Sherwood number	$[-]$
T	temperature	$[\text{K}]$
V_{cat}	catalyst volume	$[\text{m}^3]$
v_L	liquid velocity	$[\text{m s}^{-1}]$
V_L	liquid volume	$[\text{m}^3]$
V_{max}	maximum rate for enzymatic conversion	$[\text{mol s}^{-1} \text{g}^{-1}]$
Greek symbols		
ε	porosity	$[-]$

η	liquid viscosity	[Pa s]
ρ	liquid density	[kg m ⁻³]
σ_f	constriction factor	[-]
τ	tortuosity	[-]
Φ	Wheeler-Weisz modulus	[-]

Components

A	vinyl acetate
B	1-butanol

7 References

- [1] M.R. Benoit, J.T. Kohler (1975) *Biotechnology and Bioengineering*; 17: 1616-1626
- [2] R.J. Barros, E. Wehtje, P. Adlercreutz (2001) *Journal of Molecular Catalysis B: Enzymatic*; 11: 841-850
- [3] K. Kawakami, K. Adachi, N. Minemura, K. Kusunoki (1989) *International Chemical Engineering*; 29: 320-327
- [4] A. Schmid, J.S. Dordick, B. Hauer, A. Kiener, M. Wubbolts, B. Witholt (2001) *Nature*; 409: 258-268
- [5] H.E. Schoemaker, D. Mink, M.G. Wubbolts (2003) *Science*; 299: 1694-1697
- [6] V. Gotor (2002) *Journal of Biotechnology*; 96: 35-42
- [7] F. Effenberger, J. Jager (1997) *Journal of Organic Chemistry*; 62: 3867-3873
- [8] P. Villeneuve, J.M. Muderhwa, J. Graille, and M.J. Haas (2000) *Journal of Molecular Catalysis B: Enzymatic*; 9: 113-148
- [9] J.S. Dordick (1991) *Biocatalysts for Industry*, 1st ed., New York, United States: 193-213
- [10] D. Pirozzi, G. Greco Jr. (2001) *Journal of Molecular Catalysis B: Enzymatic*; 11: 961-965
- [11] A.R.M. Yahya, W.A. Anderson, M. Moo-Young (1998) *Enzyme and Microbial Technology*; 23: 438-450
- [12] S.M. Kim, J.S. Rhee (1991) *Journal of the American Oil Chemists' Society*; 68: 499-503
- [13] S. Maury, P. Buisson, A. Perrard, A.C. Pierre (2005) *Journal of Molecular Catalysis B: Enzymatic*; 32: 193-203
- [14] T. Zhang, L. Yang, Z. Zhu (2005) *Enzyme and Microbial Technology*; 36: 203-209
- [15] L-R. Yang, H. Xu, S. Yao, Z-Q Zhu (1998) *Annual of the New York Academy of Science*; 864: 649-655
- [16] W. Chulalaksanukui, J.S. Condoret, D. Combes (1992) *Enzyme and Microbial Technology*; 14: 293-398
- [17] M. Rizzi, P. Stylos, A. Rick, M. Reuss (1992) *Enzyme and Microbial Technology*; 14: 709-714
- [18] I.H. Segel (1993) *Enzyme Kinetics behavior and Analysis of Rapid Equilibrium and Steady State Enzyme Systems*, Wiley, United States

- [19] R.J. Barros, E. Wehtje, P. Adlercreutz (1997) *Biotechnology and Bioengineering*; 59: 364-373
- [20] J.S. Dordick (1989) *Enzyme and Microbial Technology*; 11: 194-211
- [21] E. Dumitriu, F. Secundo, J. Patarin, I. Fechete (2003) *Journal of Molecular Catalysis B: Enzymatic*; 22: 119-133
- [22] I. Hoek, T.A. Nijhuis, A.I. Stankiewicz, J.A. Moulijn, (2004) *Chemical Engineering Science*; 59: 4975-4981
- [23] T. Valdés-Solís, G. Marbán, A.B. Fuertes (2001) *Microporous and Mesoporous Materials*; 43: 113-26
- [24] G.A. Kovalenko, O.V. Komova, A.V. Simakov, V.V. Khomov, N.A. Rudina (2002) *Journal of Molecular Catalysis A: Chemical*; 182-183: 73-80
- [25] Th. Vergunst, F. Kapteijn, J.A. Moulijn, (2002) *Carbon*; 40: 1891-1902
- [26] K.M. de Lathouder, D. Lozano-Castelló, A. Linares-Solano, F. Kapteijn and J.A. Moulijn (2006) *Carbon*; in Press
- [27] C. Mateo, O. Abain, R. Fernandez-Lafuente, J.M. Guisan (2000) *Biotechnology and Bioengineering*; 68: 98-105
- [28] F. Shiraishi, K. Kawakami, S. Kono, A. Tamura, S. Tsuruta, K. Kusunoki (1989) *Biotechnology and Bioengineering*; 33: 1413-1418
- [29] K.M. de Lathouder, J. Bakker, M.T. Kreutzer, F. Kapteijn, J.A. Moulijn, S.A. Wallin (2004) *Chemical Engineering Science*; 59: 5027-5033
- [30] R.K. Shah, A.L. London (1978), *Laminar flow force convection ducts. Advances in heat transfer, Volume 1, supplement 1*, Academic Press, New York, United States
- [31] H.P. Kritzinger, B.C. Deelder, C.R. Kleijn, J.J. Derksen, H.E.A. van den Akker (2002) *Turbulent flow in a stirred tank with permeable impeller blades, proceedings of. ASME Fluids Eng. Div., FEDSM2002-31360*.
- [32] C. Suan, M.R. Sarmidi (2004) *Journal of Molecular Catalysis B: Enzymatic*; 28: 111-119
- [33] F. Ayhan, H. Ayhan, E. Piskin, A. Tanyolac (2002) *Bioresource Technology*; 81: 131-140.
- [34] G.K. Lee, R.A. Lesch, P.J. Reilly (1981) *Biotechnology and Bioengineering*; 23: 487-497
- [35] C. Marzadori, S. Miletta, C. Gessa, S. Ciurli (1998) *Soil Biology and Biochemistry*; 30: 1485-1490
- [36] Z. Koszorz, N. Nemestothy, Z. Ziobrowski, K. Belafi-Bako and R. Krupiczka (2004) *Desalination*; 162: 307-313
- [37] D. Ganapati, D. Yadav, K. Manjula Devi (2002) *Biochemical Engineering Journal*; 10: 93-101
- [38] G. Pencreac'h, J.C. Baratti (1996) *Enzyme and Microbial Technology*; 18: 417-422
- [39] G. Pencreac'h, J.C. Baratti (1997) *Applied Microbiology and Biotechnology*; 47: 630-635
- [40] A. Zaks, A.M. Klibanov (1988) *Journal of Biological Chemistry*; 263: 8017-8021
- [41] P. Wilbulswas, PhD Thesis (1966), London University, London, Great Britain
- [42] V. Balakotaiah, D.H. West (2002) *Chemical Engineering Science*; 57: 1269-1286

15

Summary and evaluation

1 Background

In the 20th century, growing prosperity has led to a large industrial growth. As a result, the industrial pollution has also increased significantly. In Chemical industry, a great amount of energy is expended in the production, use, and disposal of chemicals. A large part of the total amount of industrial waste consists of unwanted by-products, especially in the fine chemical industry. To both conserve energy and avoid the unnecessary generation of hazardous wastes, the concept and benefits of Green Chemistry have already spread through industry and academia. Within the changing chemical industry, public awareness and nationwide agreements on emissions make way for sustainable technology and more environmentally friendly solutions. An example of this new approach is the implementation of one or more “green” reaction steps in both existing and future processes. Biocatalysis is such a “green” technology. Biocatalytic reactions can be carried out in water at ambient temperature and pressure and neutral pH, this means that valuable process energy is saved. Reactions that are not easily conducted by classical organic chemistry can be simplified by using a biocatalyst or several reaction steps can be replaced by a single enzymatic reaction step. Examples of common products that are made by biocatalysis include fructose, insulin, acrylamide, amino acids, and penicillin. Even though the selection of a biocatalyst and the design of the process present various problems and restrictions, biocatalysis is expected to play an important role in future technology.

In this respect, immobilized enzymes have a wide range of practical applications. Although the activity usually decreases upon immobilization, they possess important advantages over dissolved enzymes, e.g. the possibility of recovery and reuse, simple operation, and improved stability. Most conventional enzyme carriers are inorganic particles or porous beads of synthetic polymers, chitosan, agarose or alginate. These particulate supports generally have a low mechanical strength and low mass-transport efficiency. This can lead to attrition and deactivation upon use in stirred tanks or packed beds. When used in packed beds, a trade off must be made between particle size and pressure drop over the bed; to maintain a sufficiently low pressure drop over the bed, particle size usually has a certain minimum value.

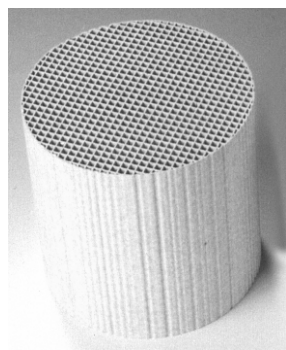


Figure 1. Cordierite monolith

This can cause internal mass transport problems [1]. Another frequently encountered problem with particulate carriers is the difficulty to scale-up. The use of a structured support of high mechanical strength, coated with a thin layer of active material can circumvent these problems. There are many types of structured bodies; in this study, ceramic monoliths with different microstructures are applied as structured carriers. Monolithic catalyst supports (Figure 1), originally developed for use in automotive emission control systems where low pressure drop and high surface area are required, are an interesting alternative for conventional support materials in heterogeneous catalysis and biocatalysis [2]. For liquid systems, the advantages of structured reactors compared to fixed-bed or slurry reactors include a high

available surface area, a low pressure drop over the reactor, ease of product separation, absence of maldistribution problems, and easy scale-up. The classical cordierite monolith has square parallel channels on which a washcoating can be applied. Here, the performance of a new type of structured monolithic support having the same macroscopic geometry as classical cordierite monoliths is studied. This material was developed by The Dow Chemical Company as a new catalyst support. This support is a highly porous acicular mullite. The support material will be indicated with Advanced Ceramic Material, ACM [3]. The unique open microstructure is shown in Figure 2.

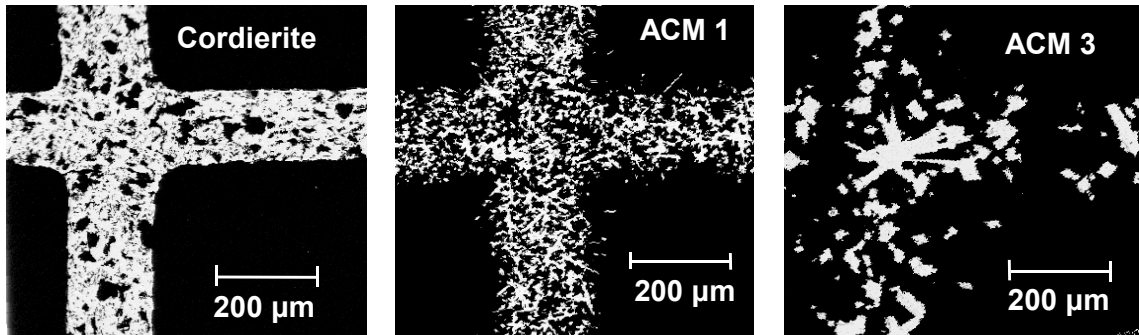


Figure 2. Backscatter images of cordierite, ACM small, and ACM large showing the open wall structure of ACM

By controlling the synthesis conditions, the mean pore size can be tailored on the micrometer length scale. The open pore structure allows excellent access of reactants to catalysts deposited within the monolith wall. In short, the new ACM supports allow us to further fine-tune the interplay of diffusion and reaction.

2 Monolith reactors

Monoliths are proven technology for single-phase processes, such as the catalytic converter in cars. But monoliths can also be applied in multi-phase operation. For co-current gas-liquid flow through a monolith channel, several flow regimes can occur. The preferred regimes for industrial application are film flow and slug flow (Taylor flow). In film flow operation (also possible in counter-current mode), the liquid moves as a thin film over the channel wall. The gas phase moves through the core of the channels. If the liquid velocity is increased or the gas velocity is decreased, the hydrodynamics will change towards Taylor flow, especially for small channels. In Taylor flow operation, gas and liquid move through the channels in separate slugs. The gas bubble fills the whole channel diameter and only a thin liquid film separates the gas from the active channel wall (Figure 3). Consequently a high gas-solid mass transfer rate through this film is possible. Inside the liquid slugs, an internal recirculation pattern is present. This internal flow increases radial mass transfer. The gas bubbles push the liquid slugs through the channels, yielding a type of plug flow.

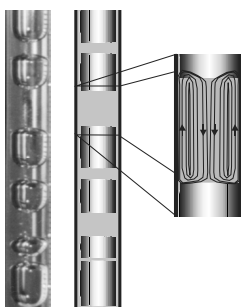


Figure 3. Taylor flow in a single channel

Compared to single-phase liquid flow, where the flow in small diameter channels will be laminar (no increased radial transport), mass transfer in multi phase operation is an order of magnitude larger. Slug flow conditions are easily realized under practical conditions. It can therefore be advantageous for single-phase liquid phase reactions to induce Taylor flow by adding an inert gas component.

To operate a monolith reactor, several configurations are possible. As an alternative for conventional three-phase reactors (slurry stirred tank reactors, trickle bed reactors and bubble columns), the monolith loop reactor (MLR) can be used [4]. The monolith is placed vertically in a recycle with a tank. The reactor can be operated in continuous or batch mode (Figure 4). The monolithic stirrer reactor (MSR) [5] is a novel reactor, utilizing existing reactor vessels. In the MSR (Figure 4), monolithic structures are used as stirrer blades. By rotating the monoliths through the liquid, both mixing of the reaction medium and contacting the catalyst with reactants by convection through the monolithic channels is facilitated. This reactor is thought to be useful in production of fine chemicals and biotechnology, because the stirrer configuration can be implemented relatively easy in existing stirred tanks.

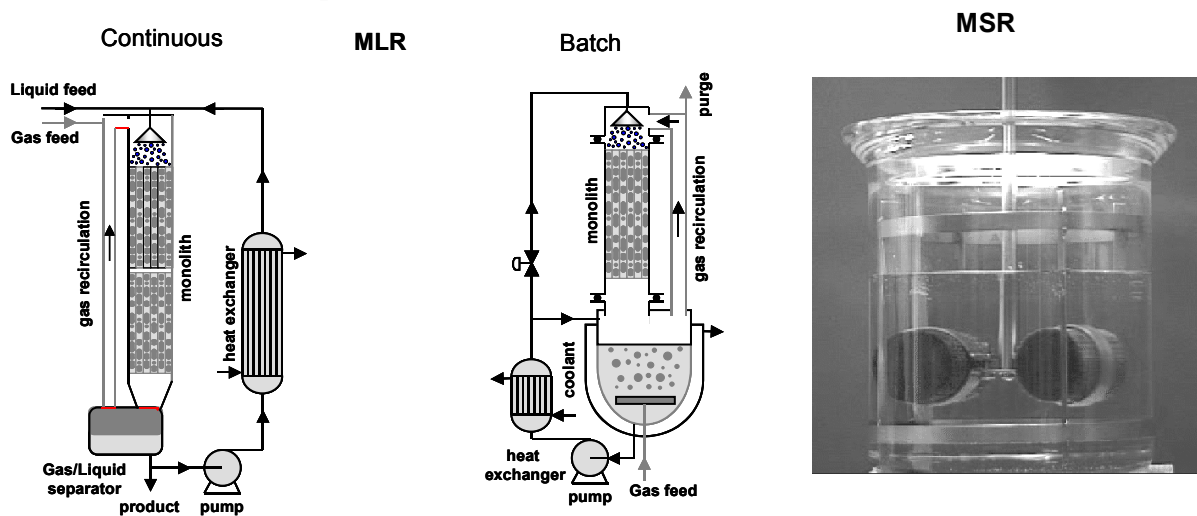


Figure 4. Configurations of different monolithic reactors

3 Objective

This work is concerned with the application of ceramic monoliths with different microstructures as catalyst support material in the field of biocatalysis. In order to apply a ceramic monolith as a suitable carrier material for different enzymes, some important questions need to be answered:

- Is it possible to attach different enzymes to the ceramic structure?
- If attached, within which window of operation will the enzyme stay attached?
- Does the catalyst maintain its original activity, or is there a decrease after immobilization?
- Is the monolithic bioreactor a feasible alternative for existing biocatalytic processes?

4 Approach

To systematically answer these questions, three main topics are distinguished in this study:

- Catalyst preparation; how to immobilize different enzymes to a ceramic support.
- Catalyst performance; how does immobilization affect activity and stability compared to the free enzyme?
- Application; how does the monolithic bioreactor perform compared to different (commercial) immobilized enzymes, is the monolith a viable alternative for conventional carriers?

Adsorption, ionic adsorption, entrapment and covalent binding have been selected as suitable immobilization protocols to be applied in combination with monolithic backbones. Different industrially relevant enzymes (lactase, lipase, penicillin acylase, and trypsin) are used in the catalyst performance study. By using the monolith-carrier-enzyme combinations in different reactor configurations for industrially relevant reactions, a feasibility study of possible application of a monolithic bioreactor can be performed. The results from the three main topics (preparation, performance, and application) can be combined into a general set of design rules for monolithic biocatalysts. The different topics and the approach are schematically depicted in Figure 5.

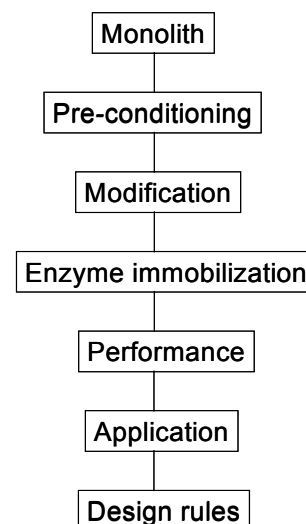


Figure 5. Project layout

The catalyst preparation consists of a comparison of cordierite and ACM monoliths in terms of enzyme immobilization. The monoliths are either washcoated directly with different enzyme carrier materials (hydrogels or carbon carriers) or washcoated with an inorganic carrier (Silica, Alumina) to provide additional surface area and anchor sites for attachment of enzymes or carriers. After application of the carrier, the immobilization conditions for different enzymes are optimized. The monolithic biocatalysts are then assessed in a lab scale set-up, to compare the different immobilization protocols and conditions. Also stability and immobilization efficiency are studied. Finally, the optimized immobilization protocols are applied for use in the monolithic stirrer and monolith loop reactor. With the obtained data, a set of design rules can be made that takes into account specific process requirements and conditions. A more detailed description of the separate steps and the results is presented in Figure 6. The results will be discussed on the basis of this scheme.

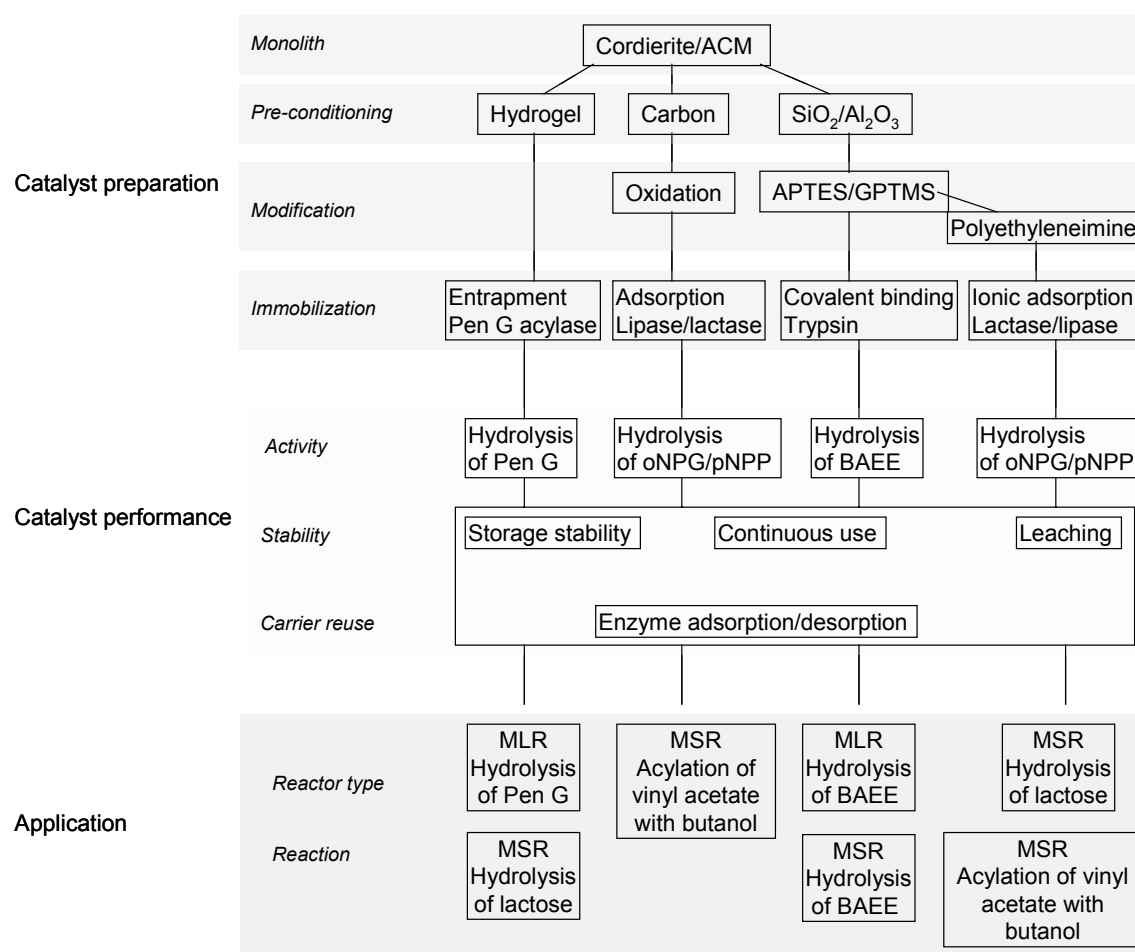


Figure 6. Detailed overview of the different topics and research approach of the project

5 Summary and evaluation

5.1 SiO₂ washcoating and functionalization of monoliths

In Chapter 3 and 4, the pre-conditioning of the monolith supports has been studied. In order to be able to pre-condition monolithic supports for covalent binding and ionic adsorption, a silica or alumina washcoat layer is needed. This layer provides both surface area and surface functionality for the successful binding of chemical linkers. By using α -alumina as a base layer, internal diffusion problems inside the washcoat layer can be prevented. The open frontal area however, decreases due to the higher total washcoat loading. If high catalyst loadings are required, washcoating of ACM samples with an active material yields significantly higher loadings than can be obtained for cordierite carriers, without increasing the pressure drop over the monolith. Although the open wall is partially plugged when using this washcoat procedure, the active material is much more accessible than if applied on cordierite.

Silanized silicas are among the most widely used backbones for enzyme immobilization via different routes. Therefore, two generally used organo silane compounds, (3-aminopropyl)triethoxysilane (APTES) and (3-glycidoxypropyl)trimethoxysilane (GPTMS), have been used to apply amino and epoxy-functionalities on silica-coated monoliths. Functionalization of the washcoated supports with APTES or GPTMS leads to a sharp decrease in available specific surface area and porosity. For ACM monoliths, the silanization yield per gram of silica is higher than for cordierite supports for both organo silanes. This is due to the higher accessibility of the silica in the open structure of the ACM monoliths. The silane loading only depends on the type of silane and on the microstructure of the monolith. DRIFT-IR was used to follow changes in the surface chemistry as a result of the chemical modification.

5.2 Covalent immobilization of trypsin

Preparation and characterization

Trypsin is a very suitable enzyme for hydrodynamics studies because of the straightforward, easy to follow enzyme assay; the hydrolysis of *n*-benzoyl-L-arginine ethyl ester (BAEE). The enzyme can be covalently attached to monolithic supports, following different protocols either via APTES or GPTMS. The immobilization protocols that use GPTMS generally result in a higher enzyme loading and a higher activity per g of enzyme. The best carrier material was obtained by immobilization via the ALD/IM protocol in which the epoxygroup of GPTMS is hydrolyzed before reaction of the silane with the silica support. The use of ACM monoliths leads to an additional increase in trypsin loading. For immobilized trypsin (ALD/IM) on cordierite and ACM monoliths, the initial activity in the hydrolysis of BAEE at 298 K is 21 and 27 mmol s⁻¹ m⁻³_{monolith} respectively. The specific activity of the immobilized enzyme is only 7% compared to the free enzyme and is not influenced by the monolith-microstructure. Reproducibility of monolithic biocatalysts, prepared via the ALD/IM method is high. Deactivation occurs during both storage and testing.

Application

ALD/IM-trypsin monoliths with different microstructure have been compared in a Monolith Loop Reactor (MLR) and a monolithic stirrer reactor (MSR) under external mass transfer limited conditions. An increased cell density, leads to a proportional increase in observed reaction rate. At increasing stirrer rate, mass transfer and channel velocity increase. The results of the experiments in the MSR were in good agreement with theoretical values for mass transfer in the monolith channels in the MSR.

The experiments in the MLR have been performed under Taylor flow conditions. Gas velocity in the MLR does not influence the observed reaction rate for cordierite monoliths. For ACM, a slight increase can be observed due to participation of catalysts that is deposited in the open wall. A higher liquid flow rate leads to a higher total reaction rate. The open structure of the ACM monoliths leads to an increased mass transfer. The results were in agreement with theoretical values for mass transfer in Taylor flow in square channels. Covalently bound

trypsin can be successfully applied to study mass transfer in a MLR or MSR under varying conditions.

5.3 Entrapment of penicillin G acylase in different hydrogels

Preparation and characterization

The scheme will be discussed from left to right, starting with the washcoating with hydrogels. Organic hydrogels can be directly applied onto the monolithic supports by washcoating. Penicillin G acylase has been immobilized in agarose, alginate, chitosan and gelatin coatings. Agarose, alginate and gelatin gels proved less successful in the immobilization of penicillin G acylase. Gel formation by pH shift, cross-linking and evaporation were compared for chitosan hydrogels. The cross-linking method yielded the best results; 36 mg ml⁻¹ penicillin G acylase can be immobilized on chitosan-coated monoliths. Scanning electron microscopy revealed that the gel is evenly distributed along the length of the monolith structures, but most of the chitosan has been accumulated in the corners of the channels. It has been shown that the monolith-chitosan-enzyme system is active in the hydrolysis of Penicillin G, with an initial rate of 0.79 mol s⁻¹ m⁻³_{monolith}. The operational stability was tested in 5 reaction cycles. The monolith system is stable for 35 days while stored in 1,2-propanediol at 277 K.

Application

In a continuous MLR set-up, reaction rate is limited by external mass transfer and a pH gradient over the length of the catalyst bed. Compared to the conventional catalyst particles, internal diffusion limitations are minimized, and mechanical strength has increased. The activity per catalyst volume of the commercial immobilized catalyst is around 4.5 mol s⁻¹ m⁻³_{cat}. Due to the thin catalyst coating the activity per monolith volume is only 20% of this value. Per volume of gel, the activity of the monolith-PGA combination equals that of the commercial beads. An increase in flow rate in the monolith reactor reduces the external mass transfer limitations and eliminates the pH gradient. The chitosan coatings were also successfully applied for the hydrolysis of lactose by immobilized lactase in the MSR. For this system, high enzyme loadings and activity can be observed, but the system suffers from internal diffusion limitations. In the hydrolysis of lactose at 308 K, the activity for cordierite and ACM monoliths is 0.25 and 0.45 mol s⁻¹ m⁻³_{monolith} respectively.

5.4 Ionic adsorption of lipase and lactase on polyethyleneimine

Preparation and characterization

Polyethyleneimine (PEI) can also be chemically attached via APTES or GPTMS. Lactase and lipase were immobilized via ionic adsorption on PEI coatings. The open structure of the ACM allows for a higher carrier deposition, and results in a higher protein loading. Immobilization via a GPTMS-functionalized ACM-monolith yields the best enzyme carrier. At pH 7, 200 mg lipase g⁻¹ SiO₂ and 150 mg lactase g⁻¹ SiO₂ can be deposited. These PEI systems provide an optimal environment for the lactase, 92% of the free enzyme activity is retained after

immobilization. For the more hydrophobic lipase, only 14% of the activity is retained. The initial reaction rate for a 200 cpsi PEI-lactase cordierite monolith in the hydrolysis of oNPG (at 293 K) is $4 \text{ mmol s}^{-1} \text{ m}^{-3}_{\text{monolith}}$. For lipase on the same carrier in the hydrolysis of pNPP, this number is $10 \text{ mmol s}^{-1} \text{ m}^{-3}_{\text{monolith}}$. For lactase and lipase on the equivalent ACM monoliths, this activity is 9 and $17 \text{ mmol s}^{-1} \text{ m}^{-3}_{\text{monolith}}$ respectively. The relatively low activities are caused by the elevated pH (optimum activity of both enzymes is usually seen around pH 5) at which the reaction was performed. Immobilization at varying pH influences both enzyme yield and specific activity. Immobilization at pH 5 was found to be optimal. The enzyme can be completely desorbed in consecutive adsorption-desorption cycles to facilitate reuse of the monolith-carrier combination. In general it can be concluded that a higher polymer loading provides a more stable environment for the enzyme and this stabilizing effect increases with polymer size. Therefore, the open walls of the ACM monoliths provide an important advantage when used in this immobilization protocol, because of the higher accessibility for larger polymer molecules.

Application

All PEI-based catalysts have been compared in the MSR. Monolith-PEI supports are not suitable for use with trypsin. The resulting enzyme loading is low and the stability is poor. PEI-monoliths have been shown to be very good supports for lactase immobilization and application in the hydrolysis of lactose. No enzyme leaching was detected and no profound effect of stirrer rate could be observed. The volumetric activity in the hydrolysis of lactose at 308 K (pH 5) is $0.55 \text{ mol s}^{-1} \text{ m}^{-3}_{\text{monolith}}$ for 200 cpsi ACM monoliths and $0.3 \text{ mol s}^{-1} \text{ m}^{-3}_{\text{monolith}}$ for 200 cpsi cordierite monoliths. It was confirmed that both external and internal mass transfer limitations were absent. The activity of the free enzyme is significantly higher than for the immobilized enzyme (30-60% was retained), but the use of free enzyme would require expensive downstream processing.

5.5 Adsorption of lactase and lipase on carbon-ceramic composites

Preparation and characterization

Carbon materials, deposited on monolithic supports have been used to adsorb lipase and lactase. Composites with different morphology, porosity, and surface chemistry have been prepared and compared in terms of immobilization capacity, activity, and stability. Mild treatment in air and subsequent treatment with HNO_3 did not affect the porosity of the carbons, but significantly improved enzyme adsorption capacity. Carbonized sucrose and polyfurfuryl alcohol (PFA) coated monoliths yielded enzyme carriers with a low enzyme adsorption capacity. This is attributed to the microporous nature of these carbons. The carbon nanofibers (CNF)-based supports show a large adsorption capacity due to the open structure between the fibers. Oxidation treatment was used to further improve enzyme adsorption of the CNFs, by increasing the amount of surface oxygen complexes. The adsorption capacity for lactase correlates well with the amount of oxygen containing surface groups. For lactase and

lipase, optimum loading was obtained at pH 5, from a 4 g l^{-1} enzyme solution. The open wall structure of ACM monoliths allows high and well-accessible catalyst loadings.

More carbon can be deposited per unit wall volume of ACM, thus more enzyme is immobilized. For immobilized lipase, the activity was 30% of the free activity, for lactase this value was slightly higher at 50-70%. The volumetric activity of lactase on 200 cpsi CNF-coated cordierite and ACM monoliths in the hydrolysis of oNPG at 298 K is 9 and $23 \text{ mmol s}^{-1} \text{ m}^{-3}_{\text{monolith}}$ respectively. For immobilized lipase on the same carriers the initial rates in the hydrolysis of pNPP are 39 and $154 \text{ mmol s}^{-1} \text{ m}^{-3}_{\text{monolith}}$ for cordierite and ACM respectively. Catalysts are stable for at least 10 days, stored at 278 K with intermediate testing. The enzyme can be completely desorbed, allowing for the reuse of both carbon carrier and monolith backbone.

Application

The Monolithic stirrer reactor (MSR) is a convenient tool to compare monolithic catalysts in the absence of external mass transfer limitations. The enzyme-loaded carbon-monoliths were employed as stirrer blades in a monolithic stirrer reactor for the acylation of 1-butanol with vinyl acetate in toluene. The initial rates of lipase on 200 cpsi CNF-coated cordierite and ACM monoliths in the acylation reaction at 300 K are 4.4 and $4.7 \text{ mol s}^{-1} \text{ m}^{-3}_{\text{monolith}}$ respectively. With higher cell density the catalyst loading increases, resulting in a higher volumetric activity. The results show that using the MSR, internal and external mass transfer limitations are absent, and that all of the immobilized enzyme is used effectively. If integral carbon monoliths are used, internal diffusion limitations inside the carbon-wall are observed and the activity per g of enzyme decreases significantly. The use of monoliths as stirrer blades allows easy reuse of both the enzyme and the supports-carrier combination.

6 Conclusions

Monoliths are suitable as enzyme support material, but a suitable carrier layer is required. The immobilization methods (physical and ionic adsorption, entrapment, and covalent binding) must first be translated for use with monolithic supports. Two types of monoliths are used; classical cordierite monoliths and a new material “Acicular Ceramic Monolith” (ACM), with a more open, porous nature of the channel walls. This open structure of the ACM monoliths allows for a higher enzyme loading for all employed methods and enzymes and can be exploited in two ways:

- If high catalyst loadings are desired (e.g. for reactions where mass transfer is not a limiting factor), the high porosity of the monolith wall allows the catalyst loading per unit volume to be maximized while still retaining a low pressure drop through the reactor and good accessibility of the catalyst inside the wall.
- When fast reactions impose diffusional limitations, the deposition of a thin conformal catalyst layer on the acicular grains minimizes diffusional limitations while permitting

significant catalyst loadings and ensuring bulk diffusional properties within the monolith wall.

The preparation of the catalyst can be generalized in a set of design rules that takes into account the various requirements of the system and the properties of the enzyme:

1. Choose the appropriate immobilization protocol based on the process parameters and conditions.

For high liquid flow rates, stronger binding (ionic/covalent) is recommended. For use in organic solvent, adsorption is usually sufficient. Is there a high extent of deactivation during reaction? In this case reversible immobilization is preferred.

2. Determine if the carrier material to be applied on the monolith, is stable depending on reaction conditions (solvent, reactants, temperature).

Hydrogels and polymeric carriers can be unstable under certain conditions, whereas inorganic carriers such as carbon and silica/alumina are usually more stable.

3. Consider the nature of the enzyme.

Size, shape and surface chemistry must be compatible with the carrier material. Also deactivation rate must be considered. For a fast deactivation of a cheap enzyme, the immobilization should be reversible, whereas for an expensive enzyme that deactivates fast, the carrier should offer increased stability.

These design rules were applied for the different reaction systems that could also be relevant with respect to industrial application. To check the design protocol, occasionally a less suitable reactor-carrier-enzyme combination was taken into account. In general these lesser options were also shown not to be optimal for the application under discussion.

The use of different monolith reactors shows that immobilized enzymes can be used in an elegant construction that eliminates the use of powders or beads. This could offer significant advantages in reducing filling and cleaning between two runs in the same unit. The potential of the latter combination is very attractive; the immobilization of enzymes allows simpler and cleaner routes to many pharmaceutical intermediates, and the ACM monolith system ensures good performance and high enzyme loading in these intensified routes. Covalently bound trypsin can be used to measure liquid solid mass transfer coefficients in different reactor systems. The results are in agreement with earlier studies on this topic.

It has been shown that the MSR is a versatile lab-tool that can be used to screen different catalysts or monolithic structures. But also industrially relevant reactions (lactose hydrolysis, transesterification in organic medium) could be performed at high volumetric rates ($0.5\text{--}1 \text{ mol m}^{-3}_{\text{monolith}} \text{ s}^{-1}$). The ease of changing the catalyst and the option to reversibly immobilize different enzymes, make this reactor an interesting alternative for small/medium scale batch processes. This system can be very useful for systems that currently operate in batch with

(expensive) free enzyme. With some modifications, the MSR could also be operated continuously.

The MLR is also suitable for implementation in existing systems and can be operated batch-wise or continuously. This reactor seems a promising alternative for the hydrolysis of penicillin G by immobilized pen G acylase, but the absence of axial pH control causes a steep decrease in pH over the monolith. This negatively affects the observed reaction rate. Adjusting the system with better pH control by using monolith sections could improve the performance. A better option would be to use the MSR, with much better mixing of the reaction medium.

In this thesis, different possibilities were explored to attach enzymes to monolithic supports. A first comparison with existing systems shows that the performance of the monolith reactors approaches that of conventional processes in terms of activity and stability. The use of a novel monolith resulted in an additional increase in catalyst loading and volumetric activity. A promising monolith-carrier combination for use in organic medium is the monolith-CNF support. This system also proved to work in unsupported form (without monolith), so the CNFs can also be applied in a different form (cloth or unsupported) as a support for different enzymes. An important advantage of a monolithic support for enzyme immobilization is that both the monolith (different carbon, gel, polymer-coatings can be applied) and the monolith-carrier system (different enzymes can be adsorbed/desorbed) can be reused and tuned for specific applications. If an optimization study would be performed for a specific application, the system might be able to compete with the existing process. A large drawback is that the preparation of the monolithic biocatalysts is time-consuming and expensive compared to conventional methods.

7 References

- [1] M.R. Benoit and J.T. Kohler (1975) *Biotechnology and Bioengineering*; 17: 1616-1626
- [2] A. Cybulski, J.A. Moulijn, ed. (2006), *Structured catalysts and reactors*. Second Edition. CRC Taylor & Francis, United States
- [3] S.A. Wallin, A.R. Prunier and J.R. Moyer (2001) US Patent 6,306,335
- [4] F. Kapteijn, J.J. Heiszwolf, T.A. Nijhuis and J.A. Moulijn (1999) *CATTECH*; 3:24-41
- [5] J.J. Heiszwolf, L.B. Engelvaart, M.G. vd Eijnden, M.T. Kreutzer, F. Kapteijn, J.A. Moulijn (2001) *Cemical Engineering Science*; 56: 805-812
- [6] I. Hoek, T.A. Nijhuis, A.I. Stankiewicz and J.A. Moulijn (2004) *Chemical Engineering Science*; 59: 4975-4981

Samenvatting

Het ontwikkelen van een monolithische bioreactor: ontwerp en toepassing

Biokatalyse, het hoe en waarom.

Een groot deel van het geproduceerde afval in de industriële chemie bestaat uit bijproducten, vooral in de fijnchemie en de farmaceutische industrie. Publieke opinie en internationale wetgeving zorgen voor een groeiende belangstelling voor milieuvriendelijke en duurzame productiemethoden. Een voorbeeld hiervan is de implementatie van zogenaamde “groene” technologieën. Biokatalyse is zo’n groene technologie. Biokatalytische reacties verlopen onder gematigde omstandigheden, en kunnen worden uitgevoerd in water bij neutrale pH. Op deze manier kan kostbare procesenergie bespaard worden. Ook reacties die moeilijk verlopen met behulp van chemische katalysatoren kunnen worden vereenvoudigd of zelfs geheel worden vervangen door een enkele enzymatische reactiestap. Producten die worden bereid met behulp van biokatalyse zijn bijvoorbeeld penicilline, fructose, insuline, acrylamide, en aminozuren. Ondanks praktische problemen zoals het selecteren van een geschikte katalysator, en het ontwerpen van het proces zal biokatalyse in de toekomst een steeds grotere rol gaan spelen.

Monoliet reactoren, waarom zo ingewikkeld?

In deze context kunnen geïmmobiliseerde enzym-systemen van grote waarde zijn. Hoewel de activiteit vaak lager wordt nadat een enzym is geïmmobiliseerd, heeft dit systeem een aantal belangrijke voordelen ten opzichte van het gebruik van vrij enzym zoals de mogelijkheid tot hergebruik, eenvoudige scheiding en procesvoering, en verhoogde stabiliteit. De meeste dragers zijn anorganische deeltjes of poreuze bolletjes van polymeer of organische gels. Deze deeltjes hebben vaak een lage mechanische sterkte en veel stoftransport problemen. Hierdoor kan tijdens het gebruik van deze dragers in geroerde tankreactors of gepakte bedden attritie of deactivering optreden. Bij gebruik in gepakte bedden, moet er een optimum gevonden worden tussen deeltjesgrootte en drukval over het bed. Om een acceptabele drukval te handhaven, is er een minimale deeltjesgrootte. Dit kan in sommige gevallen aanleiding geven tot interne stoftransport limiteringen. Ook het opschalen van systemen met kleine deeltjes kan soms moeilijkheden opleveren. Een mechanisch sterke, gestructureerde drager met een dunne laag actief materiaal kan dit soort problemen verminderen of voorkomen. Er zijn verschillende soorten gestructureerde dragers. In deze studie is gebruik gemaakt van keramische monolieten met verschillende microstructuur. Monolieten werden oorspronkelijk ontwikkeld voor het reinigen van auto-uitlaatgassen, omdat deze katalysatoren vrijwel geen drukval mogen vertonen en een groot oppervlak moeten hebben. Monolieten zijn ook een interessant alternatief voor conventionele dragers in heterogene (bio)katalyse.

In vloeistof (enkel fase) systemen hebben gestructureerde reactoren enkele belangrijke voordelen ten opzichte van vast-bed reactoren of geroerde tanks: een groot beschikbaar

oppervlak, een lage drukval over de reactor, makkelijke scheiding, afwezigheid van verdelingsproblemen, makkelijk(er) op te schalen.

De klassieke corderiet monoliet is een keramische structuur met duizenden rechte kanalen in de millimeterschaal. Op de wanden kan een laagje katalysator materiaal worden aangebracht. In dit onderzoek is ook het gedrag van een nieuw type monoliet, de ACM monoliet, onderzocht. Deze monoliet heeft dezelfde vorm als de klassieke monoliet, maar een veel poreuzere wand. Dit materiaal is ontwikkeld bij DOW. In het productieproces kan de microstructuur (de poriegrootte) van deze drager worden beïnvloed. In deze open structuur kan een veel hogere katalysatorbelading worden behaald dan met corderiet.

Welke mogelijkheden zijn er om monolieten toe te passen?

In enkel fase processen worden monolieten al toegepast, zoals in de katalysator onder de auto. Maar zeker in meer-fase processen zijn monolieten een veelbelovende technologie. Als er zowel gas als vloeistof door een monolietkanaal gaat, kunnen er verschillende stromingspatronen optreden. Voor industriële toepassing zijn vooral Taylor-stroming en filmstrooming van belang. Het verschil tussen de stromingspatronen zit in de manier waarop gas en vloeistof door het kanaal bewegen. Er kunnen belletjes gevormd worden (Taylor flow) of een dunne vloeistoffilm (filmflow). Het optreden van de verschillende patronen kan worden beïnvloed door de snelheid van gas en vloeistof en de stroomrichting (meestroom of tegenstroom, opwaarts of neerwaarts door de reactor)

De monolietreactor kan worden uitgevoerd in verschillende configuraties. In dit werk is er gebruik gemaakt van de monoliet 'loop'-reactor (MLR) en de monolitische roerder reactor (MSR). In de MLR is de monoliet verticaal geplaatst op een al dan niet bestaand reactorvat. De reactanten worden over de monoliet geleid door middel van rondpompen. De MSR is een nieuw soort reactor, waarin de monolieten gebruikt worden als roerbladen. Door het ronddraaien van de roeras worden de reactanten door de monolietkanalen gestuwd.

Wat is het doel van dit proefschrift?

In deze studie is het de bedoeling dat de twee verschillende monoliet structuren gebruikt worden als dragermateriaal voor enzymen en dat er gekeken wordt of er mogelijke toepassingen voor deze geïmmobiliseerd-enzym systemen zijn. Om dit te realiseren moeten enkele belangrijke vragen worden beantwoord:

- Kunnen enzymen makkelijk aan de monolieten worden 'vastgeplakt'?
- Blijven deze enzymen vervolgens zitten als we de reactor gaan gebruiken?
- Wat gebeurt er met het enzym als het wordt geïmmobiliseerd (activiteit, stabiliteit)?
- Kan de monolitische bioreactor een goed alternatief vormen voor bestaande processen?

Hoe is het probleem aangepakt?

Om deze vragen te kunnen beantwoorden is de studie verdeeld in drie onderdelen:

- Katalysator bereiding; hoe 'plak' je het enzym aan de monoliet?
- Prestatie; wat gebeurt er met het enzym na immobiliseren, kunnen we het hergebruiken?

- Toepassing; hoe presteert de monoliet-reactor ten opzichte van andere conventionele technieken en commerciële enzym-preparaten?

Adsorptie, ionische adsorptie, insluiting, en chemisch binden zijn gekozen als geschikte technieken om enzymen op monolieten te immobiliseren. Verschillende industrieel toegepaste enzymen (lactase, lipase, penicilline acylase, en trypsine) worden gebruikt om de toepasbaarheid van het systeem te toetsen.

De verschillende monolieten en reactor configuraties worden samengebracht in een haalbaarheids-studie van de monolitische bioreactor. Nadat de bereiding van het geïmmobiliseerde enzym is geoptimaliseerd kunnen de belangrijkste resultaten worden samengevat in een ‘handleiding’ voor het maken van enzym-monoliet combinaties.

De katalysatorbereiding bestaat uit het vergelijken van corderiet en ACM monolieten als drager voor enzym immobilisatie. Deze monolieten kunnen direct gecoat worden met het drager materiaal (gel of koolstof), of eerst worden voorzien van een laagje anorganisch materiaal (silica of alumina) dat dient om extra oppervlak en functionaliteit te creëren voor het aanbrengen van enzymen of dragermaterialen.

Nadat de drager op de monoliet is aangebracht, worden de immobilisatie condities geoptimaliseerd. De monolitische biokatalysatoren worden vervolgens gekarakteriseerd in een standaard opstelling om zodoende de verschillende immobilisatiemethoden en condities te kunnen vergelijken. Hierbij worden ook de stabiliteit en de efficiëntie van het immobilisatie proces bestudeerd. Aan de hand van de resultaten van de katalysatorbereiding en de prestatie kan een gegeneraliseerde set designregels worden opgesteld voor het maken van monolitische biokatalysatoren voor verschillende toepassingen.

Uiteindelijk worden deze ontwerpregels toegepast om industrieel relevante reacties uit te voeren in de monolitische roerder en de monoliet ‘loop’-reactor.

Wat zijn de resultaten?

De eerste stap van de bereiding omvat het aanbrengen van een silica of alumina laagje op de monoliet-kanalen. Dit laagje geeft zowel extra oppervlak als reactieve groepen voor verder behandeling. Om de poriën echt goed dicht te stoppen alvorens een katalysator aan te brengen kan α -alumina worden gebruikt. Deze behandeling verkleint echter wel het beschikbare open oppervlak voor doorstroming van de monoliet. Het gebruik van ACM-monolieten heeft hier juist weer een positieve invloed op omdat de coatings eerder *in* de wand dan *op* de wand zitten. De volgende stap is het functionaliseren van de aangebrachte laagjes. Twee veelgebruikte organo-silaan componenten, (3-aminopropyl)triethoxysilaan (APTES) en (3-glycidoxypropyl)trimethoxysilaan (GPTMS), zijn gebruikt om amino-groepen en epoxy-groepen op het oppervlak van deze silica en alumina laagjes aan te brengen. Dit heeft als gevolg dat de porositeit zeer sterk afneemt, met andere woorden de silanen vullen de poriën van silica en alumina bijna geheel op. Op ACM-monolieten kan meer silaan worden aangebracht per gram drager. Dit komt doordat de open structuur veel beter toegankelijk is.

De totale belading met silaan hangt af van het type silaan en de microstructuur van de monoliet.

Enzymen kunnen vervolgens **chemisch** worden gebonden aan deze silaan moleculen. Als GPTMS wordt gebruikt, dan is de totale enzym-belading en de rest-activiteit veel hoger dan voor APTES-monolieten. De optimale enzyme-monoliet combinatie met deze methode werd bereid met GPTMS door vóór de reactie van het silaan en de monoliet het silaan eerst te hydrolyseren in sterk zuur. Aan ACM-monolieten kan meer enzym worden gebonden dan aan cordieriet monolieten. De rest-activiteit van het geïmmobiliseerde trypsine is slechts 7% van de oorspronkelijke activiteit.

In plaats van een enzym, kan ook een andere drager aan de gefunctionaliseerde monolieten gebonden worden. Polyethyleneimine (PEI) kan zowel via APTES als GPTMS aan de monolieten worden vastgemaakt. Lactase and lipase kunnen dan worden geïmmobiliseerd door **ionische adsorptie** op het polymeer. In de open structuur van de ACM monolieten kan meer polymer worden aangebracht, dus ook meer enzym. Immobilizatie via GPTMS-gecoate ACM-monolieten levert de beste biokatalysator op. De rest-activiteit van deze katalysatoren is veel hoger dan voor chemisch gebonden enzym; lactase behoudt 92% van zijn originele activiteit en lipase ongeveer 14%. Het enzym kan geheel worden verwijderd en meerdere malen opnieuw worden aangebracht. De monoliet kan dus worden hergebruikt.

Het blijkt dat een hogere polymeer-belading in de praktijk leidt tot een sterkere enzym-polymeer binding. Dit effect wordt nog eens versterkt als een PEI met een hoger molecuulgewicht gebruikt wordt. Het gebruik van de meer open ACM monolieten kan dan een voordeel zijn om diffusie problemen van de visceuze polymeeroplossing in de monolietkanalen te voorkomen.

Gel materialen kunnen direct op de monolietkanalen worden aangebracht. Penicilline G acylase is **ingesloten** in verschillende gels, waaronder agarose, alginaat, chitosan and gelatine. Agarose, alginaat en gelatine gels bleken niet zo geschikt voor gebruik met monolieten en de enzymbelading bleef achter bij chitosan gels. De chitosan-monolieten werden getest in de hydrolyse van Penicillin G. Het systeem was stabiel gedurende meerdere testcycli en de monolieten konden gedurende 35 dagen bewaard worden zonder activiteit te verliezen.

Koolstofdragers zijn aangebracht op de wanden van de monolietkanalen om **adsorptie** van lipase en lactase mogelijk te maken. Composietmaterialen met verschillende porositeit en functionaliteit aan het oppervlak zijn vergeleken met betrekking tot enzymbelading, activiteit en stabiliteit. De monolieten met koolstoffibers (CNFs) hebben de hoogste beladingscapaciteit doordat er veel ruimte tussen en op de CNFs is. Voor lactase werd er een duidelijke positieve trend gezien van enzymadsorptie als functie van het aantal zuurstofhoudende groepen aan het oppervlak. Omdat de ACM monolieten poreuzer zijn dan de klassieke cordieriet monolieten, kan er meer dragermateriaal op aangebracht worden en zal de enzym belading dus hoger zijn.

Aan de hand van de studie naar de bereidingsmethoden is er een set ontwerpregels opgesteld, die nu toegepast kunnen worden voor het gebruik van monolitische biokatalysatoren onder verschillende condities. Vanwege de omzetsnelheid van enzymatische reacties, zijn deze bijzonder geschikt om de **hydrodynamica** van verschillende reactorssystemen te bestuderen. De ACM en corderiet monolieten met geïmmobiliseerd **trypsine** zijn vergeleken onder massa transportgelimiteerde omstandigheden in verschillende monolietreactoren. Een hogere celdichtheid leidt in het algemeen tot een hogere reactiesnelheid. Ook een hogere vloeistofsnelheid in de kanalen heeft een positief effect op de stofoverdracht. De resultaten van de monolitische roerder kwamen goed overeen met theoretische waarden voor stofoverdracht in geroerde systemen.

De experimenten in de monoliet 'loop'-reactor werden uitgevoerd in Taylor flow operatie; de resultaten kwamen goed overeen met de resultaten uit eerdere studies. Als ACM monolieten worden gebruikt, kan de reactiesnelheid iets verhoogd worden omdat ook de open kanaalwand meedoet en misschien zelfs zorgt voor extra stoftransport tussen de kanalen.

De **hydrolyse van Penicilline G** is uitgevoerd met geïmmobiliseerd penicilline hydrolase in een chitosan laagje. Verschillende reactorssystemen zijn met elkaar vergeleken. De reactiesnelheid in deze reactie wordt gelimiteerd door de diffusie van het gevormde zuur naar buiten, en de diffusie van OH⁻ naar binnen de gel in. De aanwezigheid van het zuur zorgt voor een grote daling van de pH over de lengte van de reactor. Vergeleken met de conventionele katalysatorbolletjes zijn de mechanische eigenschappen verbeterd, maar bestaan er nog steeds gelijksoortige diffusielimiteringen. De resultaten konden gesimuleerd worden aan de hand van opgestelde reactormodellen en kinetiek modellen uit de literatuur.

Deze chitosan-coatings op monolieten zijn ook gebruikt in de monolitische roerder met geïmmobiliseerd lactase. Doordat met dit systeem hoge enzymbelading kunnen worden gehaald is de totale **omzetting van lactose in glucose en galactose** relatief hoog, maar het systeem opereert wel met interne diffusie-limiteringen.

In dit systeem kunnen ook monolieten met ionisch geadsorbeerd lactase gebruikt worden. PEI is zeer geschikt als dragermateriaal voor lactase. De katalysator is stabiel, en het enzym spoelt niet van de drager af tijdens normale operatie.

De monolitische roerder is zeer geschikt om zonder externe massaoverdrachtsproblemen verschillende katalysatoren te vergelijken. Verschillende koolstof (gecoate) monolieten met geadsorbeerd lipase zijn in de MSR vergeleken in de **acylering van 1-butanol met vinyl acetaat** in toluen. In dit systeem zijn geen stofoverdrachtsproblemen aanwezig en al het geïmmobiliseerde enzym wordt effectief gebruikt. In organisch milieu vindt geen desorptie van het enzym plaats. Omdat de ACM monolieten een hogere enzymbelading hebben, is ook de totale omzetsnelheid in de reactor hoger voor deze monolieten. Het gebruik van monolieten als roerbladen biedt de mogelijkheid een breed scala aan verschillende enzymatische reacties uit te voeren in de MSR. Door verschillende enzymen reversibel aan te brengen op het dragermateriaal, kan ook de monoliet-drager combinatie worden hergebruikt.

Wat kan hieruit worden geconcludeerd?

Monolieten zijn geschikt om als enzym-drager te worden toegepast, zeker omdat ze extra stevigheid bieden en de operatie vergemakkelijken. Een vereiste is wel dat een geschikt drager-laagje wordt aangebracht op de kanaalwand. De verschillende immobilisatiemethoden die voorhanden zijn dienen eerst te worden vertaald naar gebruik in combinatie met monolieten. De meer poreuze ACM monolieten hebben een hogere immobilisatiecapaciteit voor alle gebruikte methoden. De open structuur van deze monolieten kan op twee manieren worden benut:

- Als hoge katalysatorbelading gewenst is (als stofoverdrachtsproblemen niet limiterend zijn), kan de open kanaalwand geheel benut worden om de drager-enzym combinatie aan te brengen. Op deze manier kan een maximale belading gehaald worden, terwijl de drukval over de reactor nog steeds laag blijft (de kanalen zelf blijven open) en het enzym goed toegankelijk blijft.
- Als snelle reacties leiden tot diffusieproblemen, kan een heel dun laagje drager worden aangebracht op de dunne naaldjes waaruit de wand is opgebouwd. Vergeleken met de klassieke monoliet is het beschikbare oppervlak aanzienlijk hoger en kan dus nog steeds een voldoende hoge belading gerealiseerd worden.

De activiteit van de geïmmobiliseerde enzymen is weliswaar lager dan van het vrije enzym, maar de mogelijkheid tot hergebruik en het wegvallen van extra scheidingsstappen in het proces maken de monoliet-enzym systemen toch tot een aantrekkelijk systeem voor biokatalytische processen.

Het gebruik van verschillende reactorconfiguraties toont aan dat de monoliet als enzym-drager een goed alternatief is voor de conventionele poeders en bolletjes. De katalysatorbereiding is echter tijdrovend en duurder dan voor de conventionele biokatalysatoren, maar kan worden vergemakkelijkt door de volgende ontwerpregels toe te passen alvorens het definitieve reactorconcept te kiezen.

1. Kies aan de hand van de condities en vereisten het juiste immobilisatieprotocol. Parameters als vloeistofsnelheid, bindingssterkte, milieu, etc. kunnen van grote invloed zijn op de prestaties van de biokatalysator.
2. Houdt rekening met de stabiliteit van de drager onder de gekozen condities (oplosmiddel, reactanten, temperatuur).
3. Let op de eigenschappen van het enzym zelf. Afmetingen, vorm en chemie van het enzym moeten overeenkomen met de gekozen drager. Een minder stabiel enzym kan waarschijnlijk beter reversibel worden geïmmobiliseerd, om eenvoudige verversing te garanderen.

De bovenstaande ontwerpregels werden toegepast op verschillende relevante reactie-systemen waarin tevens een aantal (bewust) minder goede keuzes naar voren kwamen. Chemisch

gebonden trypsine kan worden gebruikt om stofoverdrachtsmetingen te doen in verschillende monolietreactoren. De behaalde resultaten komen goed overeen met eerdere studies en met theoretische waarden voor stofoverdracht. De monolitische roerder is een veelzijdig laboratoriumgereedschap, waarin verschillende (meerfase) reacties kunnen worden uitgevoerd door drager-enzym combinaties en/of verschillende monolieten uit te wisselen. Het gemak van het verwisselen van de roerbladen maakt van deze reactor een goed alternatief voor kleine en grotere schaal batch-processen. Eventueel zou de MSR ook continu geopereerd kunnen worden. De monoliet 'loop'-reactor kan ook geïmplementeerd worden in bestaande systemen en kan zowel batch als continu worden bedreven. Voor hydrolyse van penicilline G, lijkt de MLR een aardig alternatief, maar het grote pH-verloop over de reactor is een groot nadeel. Een aangepaste pH regeling in of tussen de monolietsecties zou de prestatie aanzienlijk kunnen verbeteren. Vanwege de veel betere menging zou de MSR voor deze toepassing geschikt kunnen zijn.

In dit proefschrift zijn verschillende mogelijkheden onderzocht om enzymen aan monolieten te "plakken", als alternatief voor bestaande bioreactoren. Een eerste vergelijking met bestaande systemen laat zien dat de prestaties van de monolietreactoren in de buurt komen van conventionele proces in termen van stabiliteit en activiteit. Groot voordeel van de monoliet-drager is dat zowel de monoliet (koolstof, polymeer, gel) als monoliet-drager combinatie (verschillende enzymen kunnen worden uitgewisseld) hergebruikt kan worden. Als het systeem voor een bepaalde toepassing geoptimaliseerd zou worden, zou het kunnen concurreren met een conventionele aanpak. Als grote nadeel voor de monoliet-enzym systemen geldt wel dat de katalysator bereiding arbeidsintensief is en lang duurt, vergeleken met conventionele immobilisatiemethoden.

Een nieuw type monoliet, de ACM monoliet, is erg geschikt gebleken om een hoge enzym belading te halen. Op deze manier kan de volumetrische activiteit verder verhoogd worden. Een veelbelovend systeem voor toepassing in organisch milieu is de monoliet-koolstof nanobuisjes drager. Het koolstof-enzym systeem zou ook op een andere drager aangebracht kunnen worden of in een andere vorm gebruikt kunnen worden (bijvoorbeeld als koolstofdoek met enzymen erop).

Tevens is uit het onderzoek gebleken dat de MSR een veelbelovend, veelzijdig alternatief is voor bestaande batch reactoren. Daarbij kan deze reactor in een laboratorium omgeving zeer goed gebruikt worden om snel verschillende katalysatoren met elkaar te vergelijken.

Dankwoord

Op deze plek wil ik graag van de gelegenheid gebruik maken om de mensen te bedanken die hebben bijgedragen aan de totstandkoming van dit proefschrift. Allereerst mijn promotoren Freek Kapteijn en Jacob Moulijn. Ik heb van jullie alle vrijheid gekregen om dit onderzoek zelf in te vullen. Ik heb niet altijd de makkelijkste weg bewandeld, maar jullie stonden altijd aan de zijlijn met de nodige adviezen en hulp bij het bepalen van de richting. Verder wil ik jullie heel erg bedanken voor de kans om mijn werk over de hele wereld te presenteren, en ook een deel van het onderzoek in het buitenland uit te voeren. Tot mijn grote verbazing werden al mijn wilde plannen bijzonder positief ontvangen en met jullie hulp ook echt omgezet in toegekende beurzen en prijzen. Ik heb ook heel veel gehad aan de begeleiding en hulp van Michiel Kreutzer, zeker in de laatste fase van het schrijven. Michiel, ik vond het prettig om met je samen te werken onder andere in het DOW project. Rob Berger, heel erg bedankt voor de hulp met het simuleren van de penicilline G hydrolyse, zonder jou had ik dit niet van de grond gekregen. Adrie Straathof, bedankt voor de input en je voortdurende beschikbaarheid als “bio-helpdesk” en vraagbaak. John Nijenhuis en Ruud Monna, heel erg bedankt voor de hulp bij het uitvoeren van de monoliet experimenten in de proeffabriek, dat was zonder jullie niet gelukt in zo’n korte tijd! Sandy, thank you for the support and freedom I was given in the cooperation with the DOW Chemical Company. It was a pleasure working with you. Xander Nijhuis, bedankt voor de nuttige ideeën en het duwtje in de rug tijdens de eerste fase van mijn promotie. Daar heb ik heel erg veel aan gehad.

NWO wil ik bedanken voor de financiering van mijn tijd in Spanje. Dit heeft niet alleen veel bijgedragen aan de resultaten van het onderzoek, ook het werken en leven in een ander land is een hele goede ervaring voor mij geweest. Marten Paasman en Emiel van de Sandt van DSM Anti Infechtives Delft, bedankt voor de begeleiding van Mike en de prettige samenwerking. Hierbij wil ik ook graag ENGAS bedanken voor de financiering van mijn verblijf in Noorwegen, een mooie gelegenheid om in alle rust het nieuwe project te combineren met het proefschrift. Het PAS&BR lab (voorheen O&O) wil ik graag bedanken voor het uitvoeren van

een enorme hoeveelheid analyses. Johan Groen, Sander Brouwer, bedankt voor jullie geduld om de zoveelste stikstof adsorptie uit te voeren (het liefst gisteren!). Marcel Bus, heel erg bedankt voor de hulp bij de lactose experimenten...heb je toch je pipetteertechnieken weer even kunnen oefenen!

Verder wil ik alle (oud) collega's bedanken voor de fijne tijd in Delft. Ten eerste, Gerard, Bart en Harrie; bedankt voor de "technical support". Vervolgens onze "backoffice"....Sandra, Els en Elly bedankt voor alle ondersteuning en hulp als er weer eens wat vanuit het buitenland geregeld moest worden of een andere lastige situatie zich voordeed. Verder wil ik Annemarie Beers bedanken, tijdens mijn afstudeerproject heb je me de (goede) richting van het onderzoek doen opgestuurd. Jasper, bedankt voor alle wetenschappelijke discussies en vooral voor de "after work" praatjes. Nakul, bedankt voor je hulp met de alumina coatings, de gezellige etentjes, de "gebbetjes" en de tennis partijtjes. Mijn kamergenoten Gerben en Inkie, en de "Kamerjongste" Sander, bedankt voor de hulp, de gezellige tijd en jullie luisterend oor. Jullie relativerend vermogen in moeilijke tijden heeft achteraf onvergetelijke momenten en een heel eigenaardig taalgebruik in kamer 0.147A opgeleverd! Ingrid, wat heb ik het getroffen met een vriendin als jij, je bent een heel bijzonder mens en ik mis je heel erg. Zelfs onze 'werk' tripjes wisten we samen nog om te toveren in een waar feest...van het wegduiken voor opdringerige Italianen in Groningen tot het opslurpen van wanstaltige hoeveelheden Calixto in Granada! Ik hoop dat we nog veel van dat soort tripjes gaan maken....

Verder iedereen die nog niet genoemd is, bedankt voor de hulp met kleine praktische of theoretische problemen. Ook de gezamenlijke uitjes en borrels mogen niet onderschat worden in hun bijdrage aan dit proefschrift. Juist tijdens het karten, bowlen, zeilen, parachutespringen, en eten kun je ineens een grote stap voorwaarts maken in de wetenschap.

Natuurlijk is er ook een speciale plek voor de studenten die hebben bijgedragen aan dit werk. Mike, je bent bij alle fases van het proefschrift betrokken geweest; van "preparation" tot "application" en zelfs in de spin-offs. Heel erg bedankt voor je inzet en zelfstandige benadering van het onderzoek. Dirk, bedankt voor je inzet en de enorme hoeveelheid experimenten die je hebt uitgevoerd. Nico, heel erg bedankt voor de gezellige samenwerking en je studie naar covalent immobiliseren. Toni, gracias por todo...hiciste un gran trabajo!

A todos los companeros y amigos de Alicante y Madrid: Muchas gracias!! Fernando, Cesar, Roberto, Jose Manuel, gracias por todo, fue un placer trabajar en el departamento de biocatálisis! Gracias también las chicas de la planta baja (Consuelo, Gema, y MariCarmen). Como echo de menos la cocina mediterraneo! Justine, bedankt voor de super-tijd in Madrid, we hebben toch zeker de helft van de tijd pratend doorgebracht....Loli, Angel gracias por darme la oportunidad de hacer tantos experimentos en Alicante. Allí pude aprender todo sobre las técnicas de caracterización de materials carbonosos. Edu, gracias por tu ayuda con las isothermas y los (miles de) DTP's. Najlae, tantas fiestas en Alicante, Marruecos y La Haya...gracias por ayudarme a conocer la gente y salvarme de trabajar demasiado, eres el mejor (bio)catalizador del mundo! Juan Carlos, mi gran hombre pequeño preferido, gracias por estar ahí. No importa la distancia.... Y al final, al raco pequeño entero; Ale, Javi, Juanma, Qique, Raquel, Diana, Segundo, Yoshi, y los dueños del hotel Hermano. Me allegro de tener amigos como vosotros! I would also like to thank the people in Trondheim, Norway who

where there during the last stage of writing this thesis. Ingvar, thanks for your help, I enjoyed working with you. Esther, Øyvind, thanks for keeping me going and for all the nice dinners with good company. Ook mijn collega's van SSL in Leiden wil ik heel erg bedanken voor jullie steun en interesse. Af en toe even afstand nemen van het geheel heeft me veel goed gedaan.

Alle vrienden en familie, die zich jaren hebben afgevraagd of je enzymen met een pincet kunt pakken en wat het kuiken toch aan het doen was in het lab, bedankt dat jullie erin bleven geloven als ik het zelf niet meer zag zitten.

Tot slot wil ik nog wat mensen in het bijzonder bedanken. Pap, Mam, Hil, bedankt voor jullie steun en vertrouwen. Ik kan me niet anders herinneren dan dat jullie me hebben gesteund en aangemoedigd, ongeacht de wilde en onmogelijk plannen die ik tevoorschijn wist te toveren. Opa, bedankt voor de inspiratie, sorry dat je er zo lang op moest wachten. Jeannine, ik wil je bedanken voor je steun tijdens de eerste jaren van mijn promotie en de mooie foto op de voorkant. Richard, bedankt voor alle praktische hulp in het lab, wetenschappelijk discussies en vooral voor je vriendschap. Rob, bedankt voor onze eindeloze gesprekken over het leven en de wetenschap. Je hebt een bijzondere kijk op het leven, en je hebt op geheel eigen wijze een enorme bijdrage geleverd aan dit proefschrift. Brenda, bedankt voor alles. Ook het uitleggen van je werk aan niet-vakgenoten kan soms heel verhelderend werken! Simone, je gaf me het laatste duwtje in de goede richting. Bedankt voor je steun en liefde.

Karen

Delft, November 2006

List of publications and presentations

Publications

Jasper J.W. Bakker, Willem J. Groendijk, Karen M. de Lathouder, Freek Kapteijn, Jacob A. Moulijn, Michiel T. Kreutzer, S.A. Wallin “Enhancement of catalyst performance using pressure pulses on highly permeable structured catalysts” Submitted to Industrial and Engineering Chemistry Research

K.M. de Lathouder, D. Lozano-Castelló, A. Linares-Solano, F. Kapteijn, J.A. Moulijn. Carbon-ceramic composites for enzyme immobilization. Microporous and Mesoporous Materials (2006), in press

C. van Gulijk, K.M. de Lathouder and R. Haswell. Characterizing herring bone structures in carbon nanofibers using selected area electron diffraction and dark field. Carbon 44 (2006) 2950-2956

K.M. de Lathouder, D. Lozano-Castelló, A. Linares-Solano, F. Kapteijn, J.A. Moulijn. Carbon-coated monoliths as support material for a lactase from *Aspergillus oryzae*: Characterization of the carbon carriers. Carbon 44 (2006) 3053-3063

Karen M. de Lathouder, Freek Kapteijn, Jacob A. Moulijn. Development of a Monolithic Bioreactor: Tailor made functionalized carriers. Catalysis of Organic Reactions, Taylor & Francis, in press

K. M. de Lathouder; J.J.W. Bakker, M.T. Kreutzer, S. A. Wallin, F. Kapteijn J. A. Moulijn. Structured reactors for enzyme immobilization: a monolithic stirrer reactor for application in organic media. *Trans IChemE, Part A, Chemical Engineering Research and Design*, 84(A5) (2006) 390–398

J.J.W. Bakker, M.T. Kreutzer, K. de Lathouder, F. Kapteijn, J.A. Moulijn and S.A. Wallin. Hydrodynamic properties of a novel ‘open wall’ monolith reactor. *Catalysis Today*, 105 (2005) 385-390

K.M. de Lathouder, T. Marques Flo’, F. Kapteijn, J.A. Moulijn. A Novel Structured Bioreactor: Development of a Monolithic Stirrer Reactor with Immobilized Lipase. *Catalysis Today*, 105 (2005) 443–447

K.M. de Lathouder, J. Bakker, M.T. Kreutzer, F. Kapteijn, J.A. Moulijn, S.A.Wallin. Structured Reactors for Enzyme Immobilization: Advantages of tuning the wall morphology. *Chemical Engineering Science*, 59 (2004) 5027-5033

A. E. W. Beers, J. A. van Bokhoven, K. M. de Lathouder, F. Kapteijn and J. A. Moulijn. Optimization of zeolite Beta by steaming and acid leaching for the acylation of anisole with octanoic acid: a structure–activity relation. *Journal of Catalysis*, 218 (2003) 239-248

Publications in preparation

K.M. de Lathouder, S.A. Wallin, F. Kapteijn, J.A. Moulijn. Performance of the monolithic stirrer reactor: L-S mass transfer study with immobilized trypsin, in preparation

K.M. de Lathouder, S.A. Wallin, M.T. Kreutzer, F. Kapteijn, J.A. Moulijn. Characteristics of a gas-liquid-solid, three-phase monolith bioreactor; Hydrolysis of BAEE by immobilized Trypsin, in preparation

C. van Gulijk, K.M. de Lathouder, F. Kapteijn, J.A. Moulijn. Growth and characterization of carbon nanofibers on different support materials for application in respiratory filters, in preparation

K. M. de Lathouder, M.W. Smeltink, R. Berger, M. Paasman, E.A. vd Sandt, F. Kapteijn, J. A. Moulijn. Immobilization of penicillin G acylase on chitosan coated monoliths, in preparation

K. M. de Lathouder; D.T.J. van Benthem, C. Mateo, R. Fernandez-Lafuente, J.M. Guisan, S. A. Wallin, F. Kapteijn J. A. Moulijn. Polyethyleneimine (PEI) functionalized ceramic monoliths as enzyme carriers, in preparation

K. M. de Lathouder; J.J.W. Bakker, S. A. Wallin, F. Kapteijn J. A. Moulijn. Functionalization of washcoated monoliths with organosilane compounds, in preparation

Oral Presentations

Karen M. de Lathouder, Freek Kapteijn, Jacob A. Moulijn. Development of a Monolithic Bioreactor: Tailor made functionalized carriers. 21st ORCS Meeting. Orlando Florida, United States, April 2-6 2006

K. M. de Lathouder, M.W. Smeltink, M. Paasman, F. Kapteijn, J. A. Moulijn. Immobilization of penicillin G acylase on chitosan coated monoliths. 7th Netherlands Catalysis & Chemistry Conference (NCCC-VII). Noordwijkerhout, the Netherlands March 6-8, 2006

K.M. de Lathouder, T. Marques Flo, F. Kapteijn, J.A. Moulijn. "A novel structured bioreactor: development of a monolithic stirrer reactor with immobilized lipase" ICOSCAR. Delft, the Netherlands, October 17-19, 2005

K.M. de Lathouder, J.J.W. Bakker, M.T. Kreutzer, S.A. Wallin, F. Kapteijn, J.A. Moulijn. "Structured reactors for enzyme immobilization: application in a monolithic stirrer reactor" 6th Process Intensification Conference. Delft, the Netherlands, September 27 –29, 2005

K.M. de Lathouder, D.T.J. van Benthem, S.A. Wallin, F. Kapteijn, J.A.Moulijn. "Polyethyleneimine functionalized monoliths as enzyme carriers" 6th International congress of Chemical Engineering. Sofia, Romania, August 22-26, 2005

K.M. de Lathouder, P.J. Kooyman, U.L. Lafont, D. Lozano-Castello, A. Linares-Solano, F. Kapteijn, J.A. Moulijn. "Application of Carbon-Ceramic Composites in Biocatalysis: Characterization of the Carbon Carriers" Carbon 2005. Gyeongju, Korea, July 3-7, 2005

K.M. de Lathouder, P.J. Kooyman, F. Kapteijn, J.A. Moulijn. "Application of Carbon-Ceramic Composites in Biocatalysis: Enzyme distribution and Support-Enzyme Interaction" Carbon 2005. Gyeongju, Korea, July 3-7, 2005

K.M. de Lathouder, T. Marques Fló, F. Kapteijn, J.A. Moulijn "A Novel Structured Bioreactor: Development of a Monolithic Stirrer Reactor with Immobilized Lipase" 6th Netherlands Catalysis & Chemistry Conference (NCCC-VI). Noordwijkerhout, the Netherlands, March 7-9, 2005

K.M. de Lathouder, A.F. Perez Cadenas, J.J.W. Bakker, F. Kapteijn, J.A. Moulijn. "Carbon nanofibers for enzyme immobilization: Preparation and Application" Workshop on carbon nanofibers. TU Twente, Enschede, the Netherlands, November 22, 2004

K.M. de Lathouder, F. Kapteijn, J.A. Moulijn. “Carbon ceramic composites as carriers for lipase immobilization” Delft Centre for Sustainable Industrial Processes (SIP) Workshop. Delft, The Netherlands, September 7, 2004

K.M.de Lathouder, S.A. Wallin, F. Kapteijn, J.A. Moulijn. “Carbon ceramic composites as carriers for lipase immobilization” CHIZA 2004. Prague, Czech Republic, August 22-26, 2004

K.M. de Lathouder, F. Kapteijn, J.A. Moulijn “Carbon Coated Monoliths as carriers for Enzyme Immobilization” Carbon 2004. Providence, Rhode Island USA, July 11-16, 2004

S.A. Wallin, K.M. de Lathouder, J.J.W. Bakker, M.T. Kreutzer, F. Kapteijn, J.A. Moulijn “Structured Reactors for Enzyme Immobilization: Advantages of tuning the wall morphology” 18th International Symposium on Chemical Reaction Engineering. Chicago USA, June 6-9, 2004

K.M. de Lathouder, F. Kapteijn, J.A. Moulijn “Immobilization of β -Galactosidase via Adsorption onto Functionalized Monolithic Supports” EuropaCat-VI Conference. Innsbruck, Austria. August 31 - September 4, 2003

K.M. de Lathouder, F. Kapteijn, J.A. Moulijn. “Immobilization of β -Galactosidase via Adsorption onto Functionalized Monolithic Supports” 4th. European Congress of Chemical Engineering. Granada, Spain, September 21-25, 2003

K.M. de Lathouder, F. Kapteijn, J.A. Moulijn “Monolithic bioreactor for enzymatic reactions” 1st Congress on Bioreactor Technology in Cell, Tissue Culture and Biomedical Applications. Tampere, Finland, July 14 – 18, 2003

Poster presentations

D. van der Poel, K.M. de Lathouder, R.J. van Ommen, F. Kapteijn, M.O. Coppens. “Developing a large scale production method of Carbon Nanotubes” Carbon 2006. Aberdeen, Scotland, July 16-21, 2006

S. Cavenati, C.A. Grande, K.M. de Lathouder, J. Moulijn, A.E. Rodrigues. “Adsorption of CH₄ and CO₂ in Carbon-Coated Honeycomb Monolith” Carbon 2006. Aberdeen, Scotland, July 16-21, 2006

K.M. de Lathouder, D. Lozano-Castelló, A. Linares-Solano, F. Kapteijn, J.A. Moulijn. “CNF-coated monoliths for immobilization of *Aspergillus oryzae* lactase” 1st Workshop Inside pores. La Grande Motte, France, March 19-22 2006

K.M. de Lathouder, T.M. Fló, S.A. Wallin, F. Kapteijn, J.A. Moulijn “A novel structured bioreactor: development of a monolithic stirrer reactor with immobilized lipase” Netherlands Process Technology Symposium. Veldhoven, the Netherlands October 26-27 2004

K.M. de Lathouder, S.A. Wallin, F. Kapteijn, J.A. Moulijn “Carbon Ceramic Composites as Carriers for Enzyme Immobilization”, 13th International Congress on Catalysis ICC. Paris, France, July 11-16 2004

K.M. de Lathouder F.Kapteijn, J.A. Moulijn “Carbon Ceramic Composites as Carriers for Enzyme Immobilization”, 5th Netherlands Catalysis & Chemistry Conference (NCCC-V). Noordwijkerhout, the Netherlands, March 8-10, 2004

K.M. de Lathouder A. van Miltenburg J.A. Moulijn F. Kapteijn “Biocatalytic liquid phase hydrolysis in a monolith reactor”, 3rd Netherlands Catalysis & Chemistry Conference (NCCC-III). Noordwijkerhout, the Netherlands, March 4-6 2002

Curriculum Vitae

Karen de Lathouder werd op 18 februari 1977 geboren in Rotterdam. In 1995 behaalde zij haar VWO diploma aan het Segbroeck College in Den Haag. Hierna begon ze een studie Chemische Technologie aan de Technische Universiteit Delft. Daarnaast speelde ze van 1994 tot 1998 handbal voor jong oranje en het Nederlands team. Karen studeerde af in de vakgroep Industriële Katalyse onder begeleiding van prof. dr. Jacob Moulijn, prof. dr. Freek Kapteijn en dr. Annemarie Beers, op het onderwerp vaste zuren als katalysator in de Friedel-Crafts acylering van aromaten. In 2001 behaalde ze haar diploma met lof. Vanaf augustus 2001 werkte ze in de vakgroep Industriële Katalyse aan de Technische Universiteit Delft als promovendus onder begeleiding van prof. dr. Jacob Moulijn en prof. dr. Freek Kapteijn. Het onderzoek had als doel het bereiden, evalueren en toepassen van enzym gecoate monolieten. De resultaten van het onderzoek staan beschreven in dit proefschrift. In 2004 werd een NWO reisbeurs toegekend voor een kort verblijf in het buitenland. Met deze beurs werd een deel van het werk uitgevoerd in Alicante en Madrid. Een deel van het promotieonderzoek werd ook uitgevoerd in samenwerking met verschillende bedrijven, zoals DSM Anti-Infectives en The DOW Chemical Company. Tijdens haar promotie werkte Karen ook als docent scheikunde bij de Stichting Studiebegeleiding Leiden. Na een post-doc van 6 maanden in de groep Catalysis Engineering van de Technische Universiteit Delft aan de productie van koolstof nano-buisjes, werkt Karen sinds 1 september 2006 bij Shell Raffinaderij Nederland B.V. als technoloog.

